

Franzius-Institut für Wasserbau und Küsteningenieurwesen

Mitteilungen Heft 99



South Java Tsunami Model Using Highly Resolved Data And Probable
Tsunamigenic Sources

Widjo Kongko

This page is intentionally left blank

Mitteilung des Franzius-Instituts für Wasserbau und Küsteningenieurwesen, Heft 99

South Java Tsunami Model Using Highly Resolved Data
And Probable Tsunamigenic Sources

Dr.-Ing. Widjo Kongko

Dissertation, genehmigt von der
Fakultät für Bauingenieurwesen und Geodäsie
der Gottfried Wilhelm Leibniz Universität Hannover, 2011

Impressum

Leibniz Universität Hannover

Franzius-Institut für Wasserbau und Küsteningenieurwesen

Nienburger Str. 4, D-30167 Hannover

Tel.: +49 511 762-2573

Fax.: +49 511 762-4002

Mail: sekretariat@fi.uni-hannover.de

URL: <http://www.fi.uni-hannover.de>

ISSN: 0340-0077

Eigenverlag des Franzius-Instituts, 2012

Nachdruck und Vervielfältigung des Heftes – auch auszugsweise – bedarf der Genehmigung durch den Herausgeber und ist nur mit Quellenangabe gestattet.

Content

Widjo Kongko	South Java Tsunami Model Using Highly Resolved Data And Probable Tsunamigenic Sources	x
--------------	---	---

This page is intentionally left blank

Editorial Preface

As we've seen in our most recent past, mankind is becoming ever more susceptible to natural disasters, largely as a consequence of population growth and globalization, but also due to yet unidentified intrinsic geophysical processes often enforcing substantial natural extreme events that may then trigger a natural disaster. A sequence of devastating earthquakes and a large number of weather-related extremes caused severe losses of lives and had detrimental effects on livelihoods as well as it made 2011 the costliest year ever (US\$ 380bn) in terms of natural catastrophe losses as the global reinsurer MunichRe recently reported. Disastrous outcomes of extreme events can only increase unless better ways are found to mitigate the tentative effects of natural hazards through advancement of knowledge, improved forecasting and warning, together with more community preparedness and resilience.

Undeniably tsunamis are one of the most devastating geophysical hazards setting count-less coastal stretches worldwide at risk. This argument has not just been proven by the disastrous consequences of the great Sumatra-Andaman earthquake and succeeding tsunami of December 2004 which caused massive loss of life and property damage. Yet, our most recent experiences from Japan are still vividly present in our minds and pinpoint even stronger to advance knowledge on tsunamis and cascading effects by research and by taking action on preparation and countermeasures.

In regard of these aspects the present PhD thesis by Dr. Widjo Kongko denotes a substantial contribution to help filling this scientific gap by focusing on the 17 July, 2006 earthquake with a magnitude MW 7.7 that occurred near the trench of the Sunda subduction zone in an approximate distance of 100 miles south of Java Island, resulting in a large tsunami along the southern coast of Java killing more than 600 people with hundreds missing and more than 100,000 displaced as reported by official organizations. As Dr. Kongko clearly points out, the 2006 Java earthquake was characterized by a smooth rupture, indicating a compound frictional environment likely influenced by weak material properties related to sedi-

ment subduction or the presence of fluids that was almost not felt onshore. The rupture triggered a so-defined a tsunami earthquake as an abnormal, but known event that excites an unusually large tsunami in terms of its body and surface-wave magnitudes and exhibits a notable discrepancy between MS and MW.

It is Dr. Kongko's main objective to carry out a thorough validation of a numerical simulation for the 2006 Java tsunami that agrees well with the huge set of observed and self-collected run-up data by considering various tsunami sources and using high-resolution geometric data. The uniqueness of the present thesis is established on the numerical simulation of the 2006 Java tsunami by taking the combination of higher slip and lower rigidity at shallow depth into account. By these means the present study significantly contributes to the lack of the knowledge and analyzes the complex rupture effects of near-field tsunamis in terms of higher slip and slip concentration affecting the tsunami amplitudes and its distribution along the South Java Island coastline.

Additionally, by means of a novel hypothetical model for future tsunami hazard in the study area of Cilacap, Dr. Kongko unveils the effectiveness of greenbelts (mangroves) and sand dunes as locally proposed technical coastal defense structures in order to allegedly mitigate the detrimental effects of tsunami inundation onshore. This chapter effectively helps demystifying the legend that distinct soft coastal vegetation defense systems significantly reduce tsunami impacts in coastal areas and helps mitigating losses. Dr. Kongko also addresses further aspects to be investigated in ongoing research at-tempts, i.e. local topography and bathymetry refinements, additional ground investigation to distinguish various types of land covers and uses as well as numerical modeling in extreme run-up areas using a 3D numerical code. It is also recommended for any future research program to take into consideration a tsunamigenic combination of both a seismic and landslide source for the Java 2006 tsunami model.

Nonetheless, besides the essential advancement of knowledge on the Java 2006 tsunami, it is finally evaluated by the author that based on the modeling results and most reasonable insights about tentative future tsunami hazards on the South Java coastline, the proposed tsunami countermeasures (technological components) are all in all insufficient, and that thus prolonged disaster preparedness programs encompassing vertical and horizontal evacuation (shelters, training and drills) are - despite all other efforts - highly demanded to finally foster community preparedness and progress community resilience.

Hoping that you enjoy studying this thesis and obtain profitable new insights on tsunami earthquakes in order to advance scientific knowledge, stimulate new research approaches and constantly progress the exchange in between research institutions.

Hanover, January 2012

Prof. Dr. Torsten Schlurmann
(Franzius-Institute, Managing Director & Chair)

**SOUTH JAVA TSUNAMI MODEL USING HIGHLY RESOLVED DATA
AND PROBABLE TSUNAMIGENIC SOURCES**

Von der Fakultät für Bauingenieurwesen und Geodäsie
der
Gottfried Wilhelm Leibniz Universität Hannover

zur Erlangung des Grades eines
DOKTOR-INGENIEURS
Dr.-Ing.

genehmigte Dissertation

von

M.Eng. Widjo Kongko
geboren am 21.07.1967
in Banyumas-Indonesien

Hannover, Oktober 2011

SOUTH JAVA TSUNAMI MODEL USING HIGHLY RESOLVED DATA AND
PROBABLE TSUNAMIGENIC SOURCES

by

WIDJO KONGKO

M.Eng. Iwate University – Japan, 2004

A DISSERTATION

submitted in partial fulfillment of the requirements for the degree

DR.-ING.

Faculty of Civil Engineering and Geodetic Science

GOTTFRIED WILHELM LEIBNIZ UNIVERSITY OF HANNOVER

Hannover, Germany

Submitted : 25th October, 2011
Oral examination : 20th December 2011

PhD Committees:
Prof. Dr. –Ing. Habil. Torsten Schlurmann (Advisor & Supervisor)
Associate Prof. Hermann M. Fritz (co-Supervisor)
Prof. Dr.rer.nat. Insa Neuweiler (Commissioner)
Prof. Dr. –Ing. Uwe Haberlandt (Chair)

Abstract

The huge Sumatra-Andaman earthquake tsunami ($M_W > 9.2$) on 26 December, 2004 and the Nias earthquake tsunami ($M_W = 8.5$) on 28 March, 2005, which occurred off Sumatra Island were followed by another earthquake off Java Island ($M_W = 7.8$), which generated a tsunami in the Indian Ocean on 17 July, 2006. The epicenter of this earthquake was located near the trench of the Sunda subduction zone south of Java Island. Unlike the two previous tsunamis off Sumatera Island, this earthquake generated a sizable tsunami whose run-up were larger than expected based on the given seismic waves emanating from the slow-weak earthquake, and was classed as a tsunami earthquake.

Following this series of tragic events, which caused huge losses of life and enormous damage to infrastructure, initiatives and efforts were made by government and non-government institutions as well as scientists from a wide range of disciplines to gain a greater understanding of the earthquake-generating mechanisms along the Java Trench and increase the ability and knowledge required to identify hazards, impacts, and countermeasures.

The absence of accurate near-shore bathymetry and topography data poses a challenge for the tsunami model for the 17 July, 2006 Java is. Furthermore, the performances of the available models following such events, displayed inconsistencies when compared to the field observation data. In addition, the detailed analysis of tsunami models in terms of the variety of source models and their parameters affecting the tsunami run-up heights and their distribution along the coastline as well as model validations were limited.

In the present study, the tsunami of 17 July, 2006 is studied using a broad range of tsunami sources, highly resolved bathymetry and topography data, and extensive post-tsunami field observations for model validation. The numerical modeling of the tsunami was carried out using TUNAMI code, which is based on non-linear shallow water equations (NSWE). For the tsunami sources, the present study uses various fault models that were estimated using the empirical scaling laws and the inversion model from the tsunami mareograms as well as the finite fault model from broadband networks of seismic waveforms. The deformation model used the analytical expressions derived by Mansinha & Smylie (1971) and Okada (1985), while the GITEWS project established the RuptGen tool to determine seafloor displacement in the Sunda arc region.

The reconstruction of the 2006 Java tsunami model suggests that source models imposing low-rigidity material and higher slip are able to mimic field data and are more

comparable to the run-up heights than those using normal values. In addition, the comparison of tsunami amplitudes near-shore between numerical simulations and field observation shows that the distributed slip of the multi-fault model gives the better result than those from the uniform slip of the single-fault model. Furthermore, by evaluating the fitting curves' shape and the discriminant parameters estimated from the empirical formula, it suggests that the cause of the event was not so clear whether those due to solely seismic dislocations or associated with submarine landslides. The limitation of the NSWE model seems to have caused a deficiency of tsunami run-up in hilly areas where steep slopes exist.

Based on the proposed synthetic model for the effect of complex ruptures, the ratio between tsunami run-up resulting from uniform slip and distributed slip is in the range ~ 1 -2.5 along the coastline, whose length is four times that of the fault. While, the variation tsunami run-up normalized by average slip along the coastline follows Gaussian curves, with those at the center being the maximum with a ratio value varying in the range ~ 0.6 -1.55. The rigidity value ratio of 2, 3, and 4 times will reduce the tsunami amplitudes on average by 61%, 47%, and 37%, respectively. The significantly different geometric data input of about 27% only showed a negligible deviation in tsunami amplitudes of 2.4% and 1.5% for distributed and uniform slips. The tests for the 2006 Java tsunami source model using the proposed dimensionless graphs resulting from the present study, namely the ratio of rigidities, the ratio of uniformly distributed slips, and the variation of run-up, indicated that both display consistent trends.

To determine the level of future tsunami hazard in the study area, the hypothetical model based on several limited scenarios has been constructed. It revealed that the tsunami inundation concentrated in certain locations consists of four clusters. One of the farthest and biggest inundations is in the river mouth of the Serayu and its surrounding low-lying land up to ~ 15 km further east with the tsunami penetration reaching ~ 5 km inland. The other clusters, their tsunami inundation is varying less than ~ 1 km.

The effectiveness of the proposed mitigation measures varies by about ~ 7.5 -27% in terms of the inundation area. The greenbelt of "Waru" trees is able reducing tsunami $\sim 7.5\%$, while the sand dunes are of about 27%. These results suggest the mitigation measures by utilizing the artificial greenbelt and sand dunes are insufficient, hence the mitigation programs of vertical and horizontal evacuation in study area is highly demanded.

Zusammenfassung

Das große Sumatra-Andaman-Tsunami Erdbeben ($M_w > 9,2$) am 26. Dezember 2004 und der Nias Tsunami ($M_w = 8,5$) vor der Küste von Sumatra am 28. März 2005, wurde von einem weiteren Erdbeben vor der Insel Java ($M_w = 7.8$) gefolgt, das einen weiteren Tsunami im Indischen Ozean am 17. Juli 2006 erzeugte. Das Epizentrum des Bebens lag in der Nähe der Subduktionszone der Sunda-Grabens südlich von Java. Im Gegensatz zu den beiden vorherigen Tsunami vor Sumatra erzeugt dieses Erdbeben einen beträchtlichen Tsunami, dessen Wellenauflauf deutlich größer war, als aus den gegebenen seismischen Wellen des schwachen Erdbebens, das als Tsunami-Erdbeben klassifiziert werden kann, zu erwarten.

Im Anschluss an diese Reihe von tragischen Katastrophen, die große Verluste an Menschenleben und enorme Schäden an Infrastrukturen verursachten, wurden Initiativen und Bemühungen von staatlichen und nicht-staatlichen Institutionen sowie Wissenschaftler aus einem breiten Spektrum von Disziplinen gemacht, um mehr über den Erdbeben erzeugenden Mechanismus entlang des Java-Grabens zu verstehen und um die Fähigkeit und das Wissen zu mehren, die zur Identifizierung der Gefahren, Auswirkungen und Gegenmaßnahmen benötigt werden.

Die Herausforderung für die Tsunami-Modellierung des Ereignisses vom 17. Juli 2006 auf Java ist das Fehlen von genauen küstennahen Bathymetrie- und Topographie-Daten. Darüber hinaus stellten sich Inkonsistenzen mit Vergleichen der Modellergebnisse mit Feldmessungen heraus. Weiterhin wurde die detaillierte Analyse der Tsunami-Modelle in Bezug auf die Vielfalt der Anregungsmodelle sowie deren Parameter, die sowohl den Wellenauflauf als auch die Verteilung des Wellenaufbaus entlang der Küste betrifft, begrenzt.

In der vorliegenden Studie wird der Tsunami vom 17. Juli 2006 mit einer breiten Auswahl an Anregungsquellen sowie hoch aufgelösten Bathymetrie- und Topographie-Daten untersucht und es werden umfangreiche Post-Tsunami Feldbeobachtungen für Modellvalidierungen verwendet. Die numerische Modellierung der Tsunami-Katastrophe wird mit dem TUNAMI Code durchgeführt, der auf nicht-linearen Flachwassergleichungen (NSWE) basiert. Für die Anregungsquellen, verwendet die vorliegende Studie verschiedene Bruchmodelle, die unter Verwendung empirischer Skalierungsgesetze und Inversionsmodelle aus der Tsunami-Wasserstandszeitreihen und aus Finite-Bruch-Modellen von seismischen Breitbandnetzen abgeleitet wurden. Die Verformungsmodelle verwenden die analytischen

Ausdrücke von Mansinha & Smylie (1971) und Okada (1985). Darüber hinaus hat das GITEWS-Projekt das Werkzeug RuptGen etabliert, das die Verschiebungen des Meeresbodens in der Region des Sunda-Bogens bestimmen kann.

Die Rekonstruktion des 2006 Java Tsunami ergibt, dass die Anregungsmodelle, die geringe Materialsteifigkeiten und höhere Verwerfungswerte voraussetzen, in der Lage sind, die gemessenen Felddaten zu imitieren sowie besser vergleichbare Ergebnisse beim Wellenauflauf zu erzielen als mit Werten normaler Steifigkeiten. Desweiteren ergibt der Vergleich von standnahen Tsunami-Amplituden aus numerischen Modellrechnungen und Feldbeobachtungen, dass Modelle mit verteilten Verwerfungswerten bessere Ergebnisse liefern als mit homogener Verwerfungsverteilung. Eine Analyse der Form der Kurvenanpassung und der Diskriminanzparameter aus empirischen Formeln suggeriert darüber hinaus, dass die Gründe für das Ereignis nicht so konsistent sind und entweder auf ein seismisches Einzelereignis oder auf eine Kombination mit einem ausgelösten, submarinen Erdbeben hindeuten. Ebenfalls scheint die Begrenzung der NSWE Modell in hügeligen Gebieten mit steilen Geländegradienten zu geringen Wellenauflauf zu verursachen.

Basierend auf einem synthetischen Modell für die komplexen Bruchmechanismen ergibt sich, dass das Verhältnis des Wellenaufbaus infolge von homogener und räumlich verteilter Vertikalbewegung des Seebodens im Bereich von $\sim 1-2.5$ entlang der Küstenlinie ist, deren Länge der vierfachen Bruchlänge entspricht. Der variierende Wellenaufbau bezogen auf die durchschnittliche Vertikalbewegung des Seebodens entlang der Küste folgt Gauß-Kurven mit maximalen Werten im Zentrum, wobei das Verhältnis zwischen $\sim 0,6-1,55$ variiert. Das Verhältnis der Steifigkeiten von zwei, drei oder vier reduziert die Tsunami-Amplituden im Durchschnitt um 61%, 47%, bzw. 37%. Die erheblich unterschiedlichen geometrischen Daten von etwa 27% zeigten nur vernachlässigbare Abweichung der Tsunami-Amplituden von 2,4% und 1,5% für verteilte und gleichmäßig verteilte Vertikalbewegungen. Die Tests für den 2006 Java Tsunami-Anregungsmodell unter Verwendung vorgeschlagener dimensionsloser Diagramme zeigt konsistente Trends in der vorliegenden Studie, nämlich das Verhältnis der Steifigkeiten, das Verhältnis von gleichmäßig verteilter Vertikalbewegung und die Variation des Wellenaufbaus.

Um ein Maß für die zukünftige Gefährdung infolge von Tsunami für das Untersuchungsgebiet zu identifizieren wurde ein hypothetisches Modell und einer begrenzten Szenarioanzahl verwendet. Es zeigt sich, dass sich die Überflutung durch Tsunami in bestimmten Gebieten konzentriert, wobei vier spezifische Gruppen auszumachen sind. Eine

der weitesten und größten Überflutung tritt am Serayufluss und in den umgebenden tiefliegenden Gebieten bis ~15 km nach Osten auf, wobei in dieser Gruppe die größten Ausdehnung der Überflutung ins Inland von ~5 km zu verzeichnen ist. Bei den weiteren Gruppen liegt diese maximale Überflutungstiefe nur bei ~1 km und darunter. Die Effektivität der vorgeschlagenen Maßnahmen zur Reduzierung der Gefährdung variiert um rund ~7.5%-27% mit Hinblick auf die maximale Überflutung. Die Reduzierung, die aus einem Grüngürtel von „Waru“-Bäumen resultiert, beträgt ~7.5% und die Anordnung von Sanddünen erzielt eine Reduzierung von ~27%. Diese Ergebnisse bestätigen, dass die untersuchten Maßnahmen, wie etwa Grüngürtel oder Sanddünen alleine nicht ausreichen, sondern dass Vermeidungsstrategien wie vertikale und horizontale Evakuierung im Untersuchungsgebiet untersucht werden müssen.

Intisari

Mega gempa-tsunami di Sumatera-Andaman ($M_W > 9.2$) pada 26 Desember 2004 dan gempa-tsunami Nias ($M_W = 8.5$) pada 28 Maret 2005 yang terjadi di Pulau Sumatra diikuti oleh gempa di Pulau Jawa ($M_W = 7.8$) telah menimbulkan tsunami di Samudra Hindia pada 17 Juli 2006. Pusat gempa terletak di dekat palung di daerah subduksi Sunda di Selatan Pulau Jawa. Tidak seperti dua tsunami sebelumnya di Pulau Sumatera, gempa di Selatan Jawa menghasilkan tsunami yang cukup besar yang landaannya lebih besar dari perkiraan perhitungan melalui data seismik yang dihasilkan oleh gempa yang relatif lambat dan lemah, yang selama ini dikenal dan diklasifikasikan sebagai “tsunami-earthquake”.

Serangkaian bencana yang tragis tersebut di atas telah menyebabkan korban jiwa dan kerusakan infrastruktur. Inisiatif dan upaya-upaya kemudian dilakukan oleh institusi pemerintah dan non-pemerintah serta para ilmuwan dari berbagai disiplin ilmu untuk memahami lebih lanjut tentang mekanisme gempa di palung Jawa ini, yaitu dengan meningkatkan kemampuan dan pengetahuan untuk mengidentifikasi bahaya, dampak, beserta penanggulangannya.

Tantangan untuk membangun model tsunami Jawa 17 Juli 2006 adalah tidak tersedianya data batimetri dekat pantai dan data topografi yang lebih akurat. Sementara model yang ada yang dibuat segera setelah peristiwa ini, hasilnya tidak konsisten dibandingkan dengan data observasi lapangan. Selain itu, analisa detil model yang berkaitan dengan sumber-sumber tsunami, parameter-parameter gempa dan faktor-faktor lain yang mempengaruhi ketinggian landaan tsunami dan distribusinya di sepanjang pantai, berikut validasi modelnya, tersedia secara terbatas.

Dalam studi ini, tsunami Jawa 17 Juli 2006 dikaji menggunakan berbagai sumber tsunami secara mendalam, dengan data batimetri dan data topografi yang lebih detil, validasi model menggunakan data observasi lapangan paska-tsunami. Pemodelan numerik tsunami dilakukan dengan menggunakan TUNAMI, yang didasarkan pada persamaan non-linear air dangkal (NSWE). Untuk sumber-sumber tsunami, penelitian ini menggunakan model sesar yang dihitung menggunakan rumus empirik dan inversi dari tsunami “mareograms” serta model “finite fault” bersumber dari jaringan gelombang seismik global. Model deformasi memakai rumus analitik yang dikembangkan oleh Mansinha & Smylie (1971) dan Okada (1985), sementara proyek GITEWS menggunakan perangkat lunak model yang dikenal

sebagai RuptGen yaitu perangkat untuk memodelkan deformasi dasar laut di wilayah busur Sunda.

Hasil rekonstruksi model tsunami Java 2006 menunjukkan sumber tsunami yang menggunakan materi dengan kekakuan rendah dan “slip” yang lebih besar menghasilkan landaan tsunami mirip dengan data lapangan jika dibandingkan dengan model yang materinya menggunakan kekakuan normal. Sebagai tambahan, perbandingan landaan tsunami di dekat pantai hasil dari model numerik dan data lapangan menunjukkan bahwa model dengan sumber “slip” yang terdistribusi dan multi-sesar hasilnya lebih baik dibandingkan yang menggunakan model “slip” yang seragam dan sesar tunggal. Selanjutnya, dengan mengevaluasi bentuk kurva dan nilai-nilai pembeda dari rumus empirik yang telah ada, menunjukkan bahwa sumber penyebab peristiwa ini tidak begitu jelas apakah semata-mata hanya dari dislokasi seismik atau ada hubungannya dengan longsor bawah laut. Keterbatasan model NSWE tampaknya sebagai faktor penyebab defisiensi tingginya landaan tsunami di daerah perbukitan dengan lereng yang curam.

Berdasarkan model sintetik efek “rupture” yang kompleks yang diusulkan dalam studi ini, rasio landaan tsunami yang dihasilkan oleh slip yang seragam dan terdistribusi adalah berkisar $\sim 1-2,5$ terjadi di sepanjang pantai yang panjangnya empat kali lipat dari panjang sesar. Variasi landaan di sepanjang garis pantai mengikuti kurva Gaussian; dengan di pusatnya adalah bernilai maksimum dan memiliki rasio landaan tsunami dan rerata slip bervariasi antara $\sim 0,6-1,55$. Nilai kekakuan materi dengan rasio 2, 3 dan empat kali akan mengurangi amplitudo tsunami di daerah pantai rata-rata sebesar masing-masing 61%, 47%, dan 37%. Sementara itu, data geometri untuk input model yang secara signifikan berbeda sebesar kira-kira 27% hanya menunjukkan deviasi amplitudo tsunami di daerah pantai sebesar 2,4% dan 1,5% untuk masing-masing slip yang seragam dan terdistribusi. Tes model untuk tsunami Java 2006 dengan menggunakan grafik tak berdimensi yang dihasilkan dari penelitian ini yang berupa grafik rasio kekakuan, rasio slip seragam dan terdistribusi, dan variasi run-up menunjukkan bahwa keduanya tampil dalam tren yang konsisten.

Untuk menentukan tingkat bahaya tsunami di masa mendatang di wilayah studi Cilacap, model hipotetik berdasarkan beberapa skenario terbatas telah dibuat. Dengan hasil yang menunjukkan bahwa genangan tsunami terkonsentrasi di daerah tertentu terdiri dari empat kelompok lokasi. Salah satu genangan terjauh dan terbesar adalah di mulut sungai Serayu dan sekitarnya di daerah dataran rendah sampai sejauh ~ 15 km ke arah timur dengan

penetrasi tsunami mencapai ~5 km ke pedalaman. Sementara daerah lain, genangan tsunaminya adalah bervariasi kurang dari 1 km.

Efektivitas upaya mitigasi yang diusulkan bervariasi sekitar ~7.5-27% dalam hal luas daerah genangan. Jalur hijau pohon "Waru", mengurangi tsunami ~7,5%, sedangkan gumuk pasir efektivitasnya sekitar 27%. Hasil ini menunjukkan upaya mitigasi dengan memanfaatkan jalur hijau buatan dan gumuk pasir tidaklah mencukupi, program mitigasi dengan cara evakuasi vertikal dan horizontal di wilayah studi sangat diperlukan.

Table of Contents

Abstract	xii
Zusammenfassung.....	xiv
Intisari.....	xvii
Table of Contents.....	xx
List of Figures.....	xxv
List of Tables	xxviii
Acknowledgements.....	xxix
Dedication.....	xxxii
Chapter 1 - Introduction	1
1.1 Tectonics setting, seismicity, & its historical tsunami	1
1.2 Lesson learned and its initiatives	3
1.3 Background and motivation.....	7
1.4 Objectives and framework of study.....	10
1.5 Overview of the Study.....	10
Chapter 2 - The Problem	12
2.1 Significance of the Study.....	12
2.1.1 Potential hazard	13
2.1.2 Dense population and vast infrastructures	14
2.1.3 Flat topography.....	17
2.1.4 Contribution to knowledge & hazard mitigation program.....	18
2.2 The problem	19
2.2.1 Geo-data resolution.....	19
2.2.2 Numerical model performances.....	20
2.3 Theories, hypotheses, and questions	22
2.3.1 Theories.....	22
2.3.1.a Deformation model	22
2.3.1.b Earthquake Scaling Laws & fault Dimensions.....	30
2.3.1.c Numerical Model	38
2.3.2 Hypotheses	47
2.3.2.a Influence of the rigidity material	48
2.3.2.b Influence of the fault type and slip distribution.....	48

2.3.2.c Other tsunamigenic sources	49
2.3.3 Questions	49
2.4 Limitation of the Study	50
2.4.1 Scope of the study	50
2.4.2 Geo-data resolution	51
2.4.3 Tsunami source & seismic gap	51
2.5 Definition of Terms	51
2.6 Summary	52
Chapter 3 - Review of the Literature	53
3.1 Overview of the Researches	53
3.1.1 Quantification of earthquake & tsunami earthquake	53
3.1.1.a Quantification & its relations of earthquake	53
3.1.1.b Tsunami earthquake: definition & quantification	54
3.1.2 Tsunamigenic earthquakes in subduction zones & local tsunami	59
3.1.2.a Tsunamigenic earthquakes in subduction zones	59
3.1.2.b Local tsunami	62
3.1.3 Numerical model	65
3.1.3.a Java tsunami model	65
3.1.3.b Tsunami model development	67
3.2 Review & Critique of the Research	69
3.2.1 Characteristic of tsunami earthquake & rigidity variations	69
3.2.1.a Characteristic of tsunami earthquake	69
3.2.1.b Rigidity variations	71
3.2.2 Heterogeneous slip and fault dimension	72
3.2.2.a Heterogeneous slip	72
3.2.2.b Fault dimension	74
3.2.3 Tsunami model	76
3.2.3.a Java tsunami model	76
3.2.3.b Model performances	77
3.3 The Contribution of Study	79
3.3.1 Tsunami model reference & availability data in study area	79
3.3.2 Near-field tsunami & heterogeneous slip knowledge development	80
3.3.3 Supporting tsunami mitigation program	80

3.4 Summary.....	81
Chapter 4 - Research Procedures	83
4.1 Research Methodology.....	83
4.1.1 Types of methodology	83
4.1.2 Research design and business processes	84
4.1.2.a Research design.....	84
4.1.2.b Business process	86
4.2 Data Collection.....	88
4.2.1 Geo-data	88
4.2.1.a Data types, sources and scope area	88
4.2.1.b Field measurements.....	90
4.2.2 Observation data	93
4.2.2.a Historical events.....	93
4.2.2.b Field observations data.....	94
4.3 Data processing	97
4.3.1 Pre-processing	98
4.3.1.a Geo-data.....	98
4.3.1.b Field observation data	99
4.3.2 Data post-processing.....	100
4.3.2.a Types of output data.....	100
4.3.3 Specific treatment	101
4.4 Simulation model	105
4.4.1 Model tools.....	106
4.4.1.a Fault model	106
4.4.1.b Deformation model	107
4.4.1.c Tsunami model.....	107
4.4.2 Model set up	108
4.4.2.a Sources model.....	108
4.4.2.b Domains and model parameters.....	116
4.5 Summary.....	123
Chapter 5 - Findings.....	125
5.1 Procedures and Elements of Study.....	125
5.1.1 Geo-data assimilation.....	125

5.1.1.a	Data assimilation of numerical domains	125
5.1.1.b	Data assimilation in the study area (DSM/DTM).....	127
5.1.1.c	Data assimilation in Permisan-Nusakambangan Cilacap	128
5.1.2	Field observation data	129
5.1.2.a	Tsunami run-up along the coastline	129
5.1.2.b	Extreme tsunami run-up in Permisan Nusakambangan Cilacap	130
5.1.2.c	Points of maximum inundation in Cilacap Bay	132
5.2	Simulation model results	134
5.2.1	Model reconstruction of the 2006 Java tsunami.....	134
5.2.1.a	Tsunami run-up heights & its distribution along the coastline.....	134
5.2.1.b	Tsunami arrival time & its maximum inundation in Cilacap	137
5.2.1.c	Estimated discriminant values to predict tsunamigenic	145
5.2.2	Hypothetic model for future hazard.....	147
5.2.2.a	Tsunami inundation in study area	147
5.2.3	Synthetic model for the effect of complex ruptures	149
5.2.3.a	run-up heights and their distribution based on the distributed slip & various rigidities	149
5.2.3.b	Ratio run-up heights and their distribution based on fault type & source-coastline	151
5.2.3.c	run-up heights and their distribution based on the geometric data input	152
5.3	Hypotheses and Research Questions	152
5.3.1	Effect of the rigidity values on tsunami run-up heights.....	153
5.3.2	Effect of the fault types & slip distribution.....	154
5.3.3	Tsunamigenic associated with submarine landslide?	157
5.4	Summary.....	158
Chapter 6 - Conclusions & Recommendations.....		162
6.1	Conclusions.....	162
6.1.1	Procedures and elements of study.....	162
6.1.2	Simulation model results	163
6.1.3	Hypotheses and research questions	164
6.2	Recommendations	165
6.2.1	Recommendations for future research	165
6.2.2	Recommendations for practices.....	166

6.3 Summary.....	167
Bibliography	169
Appendix A – The deformation model	180
Appendix B – The scaling laws	192
Appendix C – Field measurements	193
Appendix D – Observation data.....	201
Appendix E – Tsunami sources	225
Appendix F – Parameters of the model.....	246
Appendix G – Data assimilation	248
Appendix H – Simulation results	264
Appendix I – Definition of Terms	280
Appendix J – The Flow-chart of Business Processes	288
Appendix K – Curriculum Vitae.....	292

List of Figures

Figure 1: Geography of Indonesia and surrounding regions	1
Figure 2: Different sensor systems utilized within the Indian Ocean warning system.....	6
Figure 3: Earthquake (dots), subsequent tsunami (stars), & seismic gap	13
Figure 4: 24 Sub-districts of Cilacap & the affected area during 2006 tsunami	16
Figure 5: Digital Terrain Model (DTM) of Cilacap incl. 14 lines normal to coastline	17
Figure 6: Geometry of the source model.....	23
Figure 7: Fault geometry & coordinate system	27
Figure 8: Comparison of frequency, magnitude, and energy release.....	31
Figure 9: Imperial Valley, 1979 of $M \sim 6$ & San Andreas, 1906 of $M \sim 8$	32
Figure 10: Relationship of the earthquake parameters S , D and M_o	33
Figure 11: Relationship of the earthquake parameters W , L , and M_o	33
Figure 12: Regression of rupture length, width, area, and earthquake magnitude (M)	35
Figure 13: Regression of rupture parameters (L & S) with moment magnitude (M) for dip-slip in subduction zone.....	36
Figure 14: Dataset plot of rupture parameters with (M_w) for interface events	37
Figure 15: Central difference.....	39
Figure 16: The arrangement of points' computation for the leap-frog scheme.....	40
Figure 17: The diagram of earthquake and fault parameters.....	45
Figure 18: Various moving boundary conditions at a wave front	46
Figure 19: M_l vs. M_s for a tsunami earthquake.....	56
Figure 20: The asperity model for subduction zones earthquakes.....	59
Figure 21: Schematic cross-section of the subduction zone.....	60
Figure 22: Plot of estimated rigidity variations along depth	71
Figure 23: Layout of the types of geo-data & its sources	90
Figure 24: Layout of data assimilation and its sources in Cilacap	91
Figure 25: Layout of the observation data & tsunami run-up heights	95
Figure 26: Marigram of tsunami recorded at three tide gauges station.....	95
Figure 27: Tsunami wave at shrimp basin at Keboncarik-Cilacap (16:16~16:20 WIB)	96
Figure 28: Video snapshot of tsunami waves at ship basin of PLTU-Cilacap	96
Figure 29: Two different tsunamigenic & discriminant curves.....	104

Figure 30: Slip distribution by Ammon et al. (2006) and 16 sub-faults (red boxes) proposed in the present study	110
Figure 31 : Epicenters of hypothetical model.....	114
Figure 32: Cross-section of the Java subduction zone	115
Figure 33: Slip distribution for the synthetic model #1	116
Figure 34: Layout of numerical domains for the 2006 Java tsunami model	117
Figure 35: Layout of numerical domains for hypothetical model of future tsunami hazard ...	119
Figure 36: Layout of the alignment of mitigation measures	120
Figure 37 Sketch of mitigation measures	120
Figure 38: Cross-lines of bathymetry of south Java	121
Figure 39: Seafloor profiles & its synthetic line	121
Figure 40: Numerical domain, tsunami source, and ground level for the synthetic model ..	122
Figure 41: Area of manually digitized data	126
Figure 42: Difference between DSM and DTM data.....	127
Figure 43: Topography survey in Permisan using Total Station instruments	128
Figure 44: Data assimilation of field measurements & SRTM-30	129
Figure 45: Entire vs. Selected field observation data of the 2006 Java tsunami	130
Figure 46: Points measurements of maximum tsunami run-up at Permisan	131
Figure 47: Bar chart of points' measurement at Permisan	132
Figure 48: Points' measurement of maximum inundation (interview)	133
Figure 49: Graph of field observation data vs. tsunami model based on multi-faults model by Ammon et al., 2006	135
Figure 50: Area of interest for model validation in Cilacap.....	137
Figure 51: Tsunami mareograms vs. water level resulting from the model.....	138
Figure 52: Tsunami mareogram vs. water level at eye witness points in Cilacap	139
Figure 53: Sequential video snapshot of tsunami waves at PLTU-Cilacap	140
Figure 54: Satellite imagery of SPOT-1 before and after event & its model comparison	141
Figure 55: Inundation model vs. field observation in tile 1, Cilacap.....	142
Figure 56: Inundation model vs. field observation in tile 2; DTM (top) and DSM (bottom)	143
Figure 57: Inundation model vs. field observation in tile 3; DTM (left) and DSM (right)...	144
Figure 58: Fitting curve for discriminant tsunamigenic (entire dataset of 394 points).....	146
Figure 59: Fitting curve for discriminant tsunamigenic (selected dataset of 114 points)	146
Figure 60: Hypothetic model (M_w 8.2 – without mitigation measures).....	148

Figure 61: Inundation area by using various mitigation measures	148
Figure 62: Tsunami run-up heights & its distribution for distributed slip ($\mu=10\text{GPa}$).....	149
Figure 63: Tsunami run-up heights & its distribution for uniform slip ($\mu=10\text{-}40\text{GPa}$).....	150
Figure 64: Ratio tsunami run-up for distributed & uniform slip ($\mu = 10\text{-}40 \text{ GPa}$).....	151
Figure 65: Ratio rigidity of the 2006 tsunami Java (red star).....	154
Figure 66: Ratio of run-up of uniform- distributed source of the 2006 Java tsunami (dots)	156
Figure 67: Ratio of run-up variation / average slip of the 2006 Java tsunami (dots)	157

List of Tables

Table 1: Source parameter of Java earthquake, 1978-2008 (USGS).....	15
Table 2: Published analytical expressions of the deformation due to shear and tensile faults in a half-space (after Okada, 1985)	26
Table 3: The fault dimension from various empirical relations	75
Table 4: Source model of the 2006 Java tsunami	109
Table 5: Source model of the 2006 Java tsunami (Fujii & Satake, 2006).....	109
Table 6: Source model of the 2006 Java tsunami (Ammon et al., 2006).....	111
Table 7: Source parameters of the 2006 Java tsunami (in the present study)	112
Table 8: K & k parameters of the model results	136
Table 9: Fitting curve for discriminants tsunamigenic	147
Table 10: Comparison of source parameters model & its run-up deviation.....	154

Acknowledgements

This study was partially a fulfillment of the requirements for a degree in doctoral engineering at the Faculty of Civil Engineering and Geodetic Science – Gottfried Wilhelm Leibniz University of Hannover, which is supported by the GITEWS Project (the German-Indonesia Tsunami Early Warning System Project) in collaboration with the United Nations University Institute for Environment and Human Security (UNU-EHS) under work package 6000 (WP 6000).

Firstly, I would like to express my heartfelt gratitude to Prof. Dr.-Ing Habil Torsten Schlurmann for his role as advisor and supervisor of my studies, for his patient guidance, our discussions on the ‘angle and direction’ of my dissertation, and for making a lot of corrections in the manuscript, and also his great encouragement, insight, and also support.

I would like to thank Prof. Dr. Hermann Fritz, my colleague during the 2006 Java tsunami post survey, for providing the complete processed tsunami run-up data and for all of the discussions on the data and related issues, as well as his dedication by serving as my second supervisor.

I also would like to thank Prof. Dr. rer.nat. Insa Neuweiler and Prof. Dr.-Ing. Uwe Haberlandt for their duties as a Commissioner and chairing the oral examination, for essential queries to my dissertation as well as pleasant atmosphere throughout the examination.

My thanks go to Prof. Dr. Eng. Fumihiko Imamura for providing me with the source code of TUNAMI and its tutorial documentation. He provided me with a lot of useful suggestions and comments related to modeling results, from the source tsunami generation to its run-up.

I had many fruitful discussions with Dr. Andrey Babeyko, to whom I am greatly thankful, especially in regard to the various tsunami source models for the Java 2006 event and the use of generation tools of RuptGen version 1.1, which have been used in this study. In addition, during ICCE 2010 in Shanghai I was fortunate enough to meet Prof. Hideo Matsutomi, with whom I am grateful for our discussion on the “tsunami earthquake” processes and their implications for the tsunami run-up heights. To all very fruitful discussions above, I would like to say thanks.

During my research, I was aided by Dr. Sascha Brune and Dr. Denys Dutykh in the sharing and providing of the landslide and Okada scripts. We also had many discussions, in particular on tsunami generation. I wish like to express many warmest thanks to them both.

To my Japanese colleagues, Prof. Kenji Harada and Prof. Tetsuya Hiraishi, I offer my thanks for supporting the articles and for their suggestions.

I also communicated via email with Dr. Vasily Titov, discussing with him the model performances, especially the tsunami during propagating the sea and its run-up. I had discussions with Prof. Steven N. Ward related to issues regarding the tsunami run-up distribution along the coastline, and how to deal with the sparse field observation data. Prof. Cheng Ji enlightened me on the behavior of the low rupture speed in accretionary prisms. All of the above discussions conducted via email were very fruitful and a great help for me in understanding seismic fields; I fully appreciate and thank my discussion partners for their kind help.

When I first arrived in Hannover, I had a lot of red tape to deal with including obtaining my residency permit, applying for a student apartment, and many other administrative matters. In addition, while conducting my research during day-to-day life at the institute I was also party to interesting and constructive discussions with colleagues related to my research topic as well as broader scientific issues. For this, I would like to thank my laboratory colleagues, especially Dr.-Ing Nils Goseberg and Dipl.-Ing Anna Zorndt.

Furthermore, I offer many thanks to the Ph.D. students were working on the GITEWS project, especially Dr.-Ing Widodo Pranowo for sharing his tips and tricks regarding the use of various software packages and for being ready to discuss all kinds of models and their performance. Thanks also must go to M.Sc. Ade Anggraini for sharing her knowledge and holding discussions with me related to seismic issues, particularly the “beach-ball” concept, and also to M.Sc. Pachoenchoke Jintasaeranee for extracting the newly GEBCO 2008 data and for being an important link in my communication with colleagues at the IfM-GEOMAR Kiel University when trying to obtain the ‘finer’ bathymetric data of South Java.

To my mom Mami T. Baskiwi whose endless support, energy, and prayers have been an enormous factor in helping me successfully pursue my studies, I offer my most heartfelt thanks. Finally, and most importantly, I would like to express a huge thank you to my wife, Evi Yuni, and my children for their patience and support during my research here and while this dissertation was being written.

Credits:

The Coordinating Agency for Surveys and Mapping of Indonesia (BAKOSURTAL) shared with me the bathymetric chart for South Central Java and also provided me with the tsunami marigram data for the Java 2006 event.

The dissertation proposal and writing structure were based on the following handbook: Guide to the Successful Thesis and Dissertation for Students and Faculty, third edition by James E. Mauch and Jack W. Birch University of Pittsburgh, Pennsylvania US.

The dissertation was written using Microsoft Office Word 2007 using the Electronic, Thesis, Dissertation, and Report (ETDR) Word template for Doctoral Dissertations produced by ITAC Kansas State University, which is available at: <http://www.k-state.edu/grad/etdr/template>, updated August 2009.

Regarding the bibliography, the author took advantage of the open-source Firefox plug-in Zotero from (<http://www.zotero.org/>), which together with the JabRef reference manager that can be downloaded for free at (<http://jabref.sourceforge.net/download.php>), enabled me to cite references and then have them written automatically at the end of document.

Dedication

This study is dedicated to the people who have never failed to give me moral support, especially my dearest wife, and children who wait patiently for me far away.

Chapter 1 - Introduction

“Although nature commences with reason and ends in experience, it is necessary for us to do the opposite; that is to commence with experience and from this to proceed to investigate the reason” (Leonardo da Vinci, 1452-1519 AD)

Indonesia is an enormous archipelago country consisting of more than 17,000 islands, around 6000 of which are inhabited. Its population of 238 million makes it the world’s fourth most populous country. With an area around 1,919,440 km², Indonesia is the world’s 16th largest country which an average population density of 124 people per km². Although as a country, it is ranked 79th in the world’s in terms of population density, Java Island itself has 940 people per km, and is the world’s most populous island¹ (See Figure 1).

Geographically, Indonesia lies on the equator, stretching over 5000 km from 6° N to 11° S and from east to west between 95° and 141° E. Its major islands, namely Sumatra, and partly Kalimantan (Borneo) share land borders with Malaysia, Java, Sulawesi, and West Papua of the island of Papua New Guinea¹.

1.1 Tectonics setting, seismicity, & its historical tsunami

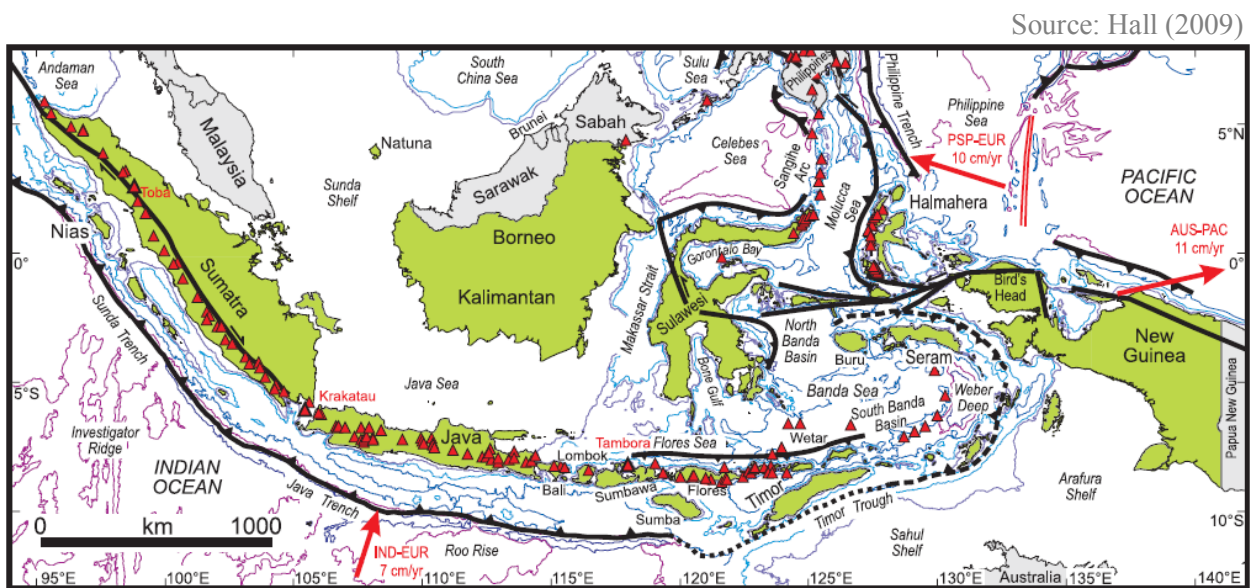


Figure 1: Geography of Indonesia and surrounding regions

Western Indonesia consists of the Sunda shelf, which includes the islands of Sumatra, Java, Bali, Borneo, and the southwestern part of Sulawesi. Tectonically, its

¹ <http://en.wikipedia.org/wiki/Indonesia>

activities are dominated by the convergence of the Australian plate with Java and Sumatra (Hall, 2009). In this region, along the Sumatra trench, the Australian plate subducts beneath the Sunda shelf with highly oblique convergence and is partitioned into nearly arc-perpendicular thrusting at the trench and an arc-parallel, right-lateral slip at the Sumatran fault (SF). Both faults are the source of strong and frequent earthquake activities in this region (Newcomb & McCann, 1987). It was suggested that these highly tectonic activities produced the two great ($M > 8$) earthquakes that occurred in 1833 and 1861.

In the central part of Indonesia, the oceanic part of the Australian plate is subducting beneath the Java trench. Bock et al. (2003) reported a convergence rate of 71 mm/year in an N20E direction at the longitude of 107°E at the Java trench as predicted by the NUVEL-1A model, and repeated (1989–1993) GPS measurements of a single trench-crossing baseline indicated a convergence rate of 67 ± 7 mm/year. The authors updated their estimate of the convergence rate by observing that the GPS velocity for the BAKO site relative to the Australia plate is 63.3 ± 0.4 mm/year at $N14.9 \pm 0.5E$.

In eastern Indonesia, the Australia plate collides obliquely with the oceanic Pacific plate in New Guinea at a rate of 110 mm/year ENE resulting in clear convergence signatures of the highlands thrust belt, namely a 1000-km-long and 4-km-high east-west-trending mountain belt, which covers much of the island (Bock et al., 2003).

Particularly in the Sunda arc, the complex tectonic setting has been the cause of significant changes in the characteristics along the strike direction, which extends over 5600 km between the Andaman Islands to the northwest and the Banda arc to the east. In the northwest of the Sunda Strait, earthquakes occurred in depths of less than 250 km, whereas those located in the east occurred at a maximum depth of 650 km with a gap in seismicity of 300–500 km. In Indonesia about 460 earthquakes of magnitudes greater than 4.0 occur every year, most of which happening beneath the sea along the seismic zones (Hamzah et al., 2000).

Newcomb & McCann (1987) evaluated the major earthquakes in the historical records with a magnitude $M_S > 6$ in Java and the Lesser Sunda Islands, and found that none are of the same magnitude as the great events near Sumatra. By interpreting the geophysical data of Roo Rise, a prominent bathymetric high appears, which was formed at a ridge crest and is more buoyant, and thus more difficult to subduct than the surrounding seafloor, the authors inferred that the majority of the slips on the plate interface near Java occur a-seismically.

Furthermore, according to the authors, Sumatra has a younger crust of 46 Ma than Java and the Lesser Sunda Islands, where the oldest crust is 152 Ma, which also implies that the entire length of Sumatra has the potential to produce great thrust earthquakes, while the plate interface near Java and the Lesser Sunda Islands should be considered as having a low seismic potential. They also added, for Java, based on historical records (< 1990) only three major events that suggest the submarine origins. These happened on June 10, 1867 causing massive damage to government and private buildings. The earliest instrumentally recorded shock occurred on February 27, 1903, which was reported by Richter (1958) for the Sunda arc and assigned a magnitude $M = 8.1$. Another event occurred on 11 September, 1921, to which Gutenberg and Richter (1954) assigned a magnitude of $M = 7.5$.

Hamzah et al. (2000) compiled the historical tsunami data for the period 1600 to 1999 and destructive earthquake data reported from 1800 to 1999. It was concluded that the number of tsunamis generated by earthquakes is 95 (90%), 9 (8%) by volcanic eruptions, and 1 (1%) tsunami by a landslide which caused 54,100 casualties, of which around 43,200 deaths were due to volcanic tsunamis. Furthermore, according to the authors there were 183 destructive earthquakes during the period mentioned above, which killed at least 10,600 people.

A recent cataloging of tsunamis in the Indian Ocean has been carried out. The data were taken from the National Geophysical Data Center (NGDC), the National Oceanic and Atmospheric Administration (NOAA), and the National Environmental Satellite Data and Information Service (NESDIS). About ninety tsunamis in the Indian Ocean were tabulated during the period 326 BC to 2005 AD, with the Sunda arc being the most active region having produced about seventy tsunamis (~80%) with magnitudes in the range M_S 5.4–7.2, and 14 events occurred in the Java's subduction region (Rastogi & Jaiswal, 2006).

1.2 Lesson learned and its initiatives

After the gigantic Sumatra-Andaman earthquake-tsunami of 26 December, 2004 ($M_W = 9.3$) and the Nias earthquake-tsunami of 28 March, 2005, which caused more than 220,000 deaths, another earthquake-generated tsunami with a large number of deaths and property loss happened. On 17 July, 2006 an earthquake with a magnitude M_W 7.7 occurred offshore near the trench of the Sunda subduction zone south of Java, resulting in a large tsunami along the southern coast of Java killing more than 600 people with hundreds missing and more than 100,000 displaced as reported by official organizations (WHO, 2006; RCS, 2006).

Following the series tragic disasters above, which caused huge losses of lives and enormous damage to infrastructure, efforts were made by government and non-government institutions as well as scientists from a wide range of disciplines to increase the ability and knowledge to identify the hazards, impacts, and countermeasures.

For instance, the ability to identify tsunami hazard zones provides at-risk coastal communities with the most basic tool for tsunami preparedness. Once a community has identified a tsunami hazard zone, the next step of evacuation maps can be developed enabling residents to safely and efficiently escape the dangers posed by tsunamis. To prevent disasters occurring from tsunamis, the concept of tsunami-resilient communities was created in order to provide direction and coordination for tsunami mitigation activities, and the mitigation effort should succeed as long as it has the involvement and support of local communities (Bernard, 2005).

The lessons learnt from recent tsunamis in the Sunda arc, especially the one on 17 July, 2006, were noted and assessed by several researchers and reported in papers and technical reports. Mori (2007) emphasized the need for seismic monitoring at low frequencies as well as the implementation of a robust public warning system in this region in the future. The 17 July, 2006 Java tsunami created a relatively low level of high-frequency radiation as reflected in the short-period magnitude estimates and the local field reports, caused no damage from shaking and the event was only felt slightly in coastal areas.

An analysis of why there were so many victims following the 17 July, 2006 earthquake was conducted. Several factors emerged, which can be summarized as follows: the earthquake and tsunami in the region were both unexpected; the earthquake was hardly felt by coastal communities, and no timely tsunami warnings were given to the affected area. In addition, in this area there was no clear precursory sign of rising sea level, the tsunami was relatively high at around 7–8 m, people faced with the tsunami acted in a spontaneous unsupervised manner, there were many inhabitants of the lowland coastal areas, and there was only a short warning period for the first emergency response (Abidin & Kato, 2007).

In anticipation of future hazards, the study proposed that a systematic and anticipative tsunami-related research and mitigation program should be properly prepared and conducted for the regions prone to tsunami earthquakes. Furthermore, the development of the Indonesian Tsunami Early Warning System (ITEWS) that is planned to be operational by 2009 should be made as reliable as possible. Land use planning along the beach should also be regulated and checked by the government and strictly enforced by in view of plausible

tsunami scenarios that might happen in the future. Other mitigation measures are also required in order to protect the region by using a greenbelt or artificial structures as well as educating coastal communities and enhancing the capacity of mitigation systems in all tsunami-prone coastal regions, which includes equipment, knowledge, and human skills.

The crustal deformation analysis following this event and its post-seismic horizontal deformation was estimated using GPS survey data (Abidin et al., 2009). During the period 2006 to 2007 after the earthquake, post-seismic deformation in general was less than 5 cm and in the following period of 2007 to 2008 it was less than 3 cm. Due to the vulnerability of Java Island to future earthquakes, the crustal deformation assessment using GPS surveys will be continued, and possibly newly established continuous GPS stations and other data sources will be incorporated and explored.

A collaboration team comprising scientists from Indonesia and New Zealand conducted the field survey to investigate the impact of the tsunami, especially run-up height, damage to infrastructure, and several related areas. DGPS-based surveying equipment was used to measure terrain profiles, tsunami flow depth and its impact on the various buildings; dozens of transect measurements normal to the coastline were made, concentrated around Cilacap and Pangandaran. The result is 2 to 4 m of flow depth causing serious damage to housing, of which 50% was newer buildings with rudimentary reinforced-concrete beams and columns, and 5–20% was engineered residential houses and multi-storey hotels with heavier Reinforced Concrete (RC) columns. The team also estimated the flow velocity by using the head loss formula, the results of which ranged from 1.8 to 4.5 m/s and were comparable with other authors as reported by (Reese et al., 2007).

Other researchers emphasized the importance of the use of satellite imagery and Geographic Information System (GIS) technology to estimate the density of population and the utilization of the land, especially the assessment of the coastal zone of central Java, which was recently suggested that the potential impact of future tsunamis is likely to be greater than those in the past (Marfai et al., 2008).

Several months after the 26 December, 2004 Aceh-Andaman earthquake-tsunami, German scientists started an initiative, supported by the German Minister for Education and Research (BMBF) and later in a joint declaration with Indonesia's government, establishing a roadmap for the installation of a tsunami early warning system in Indonesia, which was launched on 14 March, 2005. This marked the start of the GITEWS project (German-Indonesian Tsunami Early Warning System) with the main goal to design, develop and

implement the tsunami early warning system in Indonesia. Completely new technologies and scientific concepts were utilized to deliver a tsunami early warning within 5–10 minutes under the threshold of an average tsunami travel time of 30–40 minutes along the coastline in the Sunda arc region. GITEWS, therefore, integrates various modern and new scientific monitoring technologies and analysis methods as represented by a multi-sensor system installed in the Indian Ocean warning system (Lauterjung et al., 2010). Figure 2 shows the sensor systems used and their traffic communication in the GITEWS project, with all data packages being transmitted via satellite to the warning center.

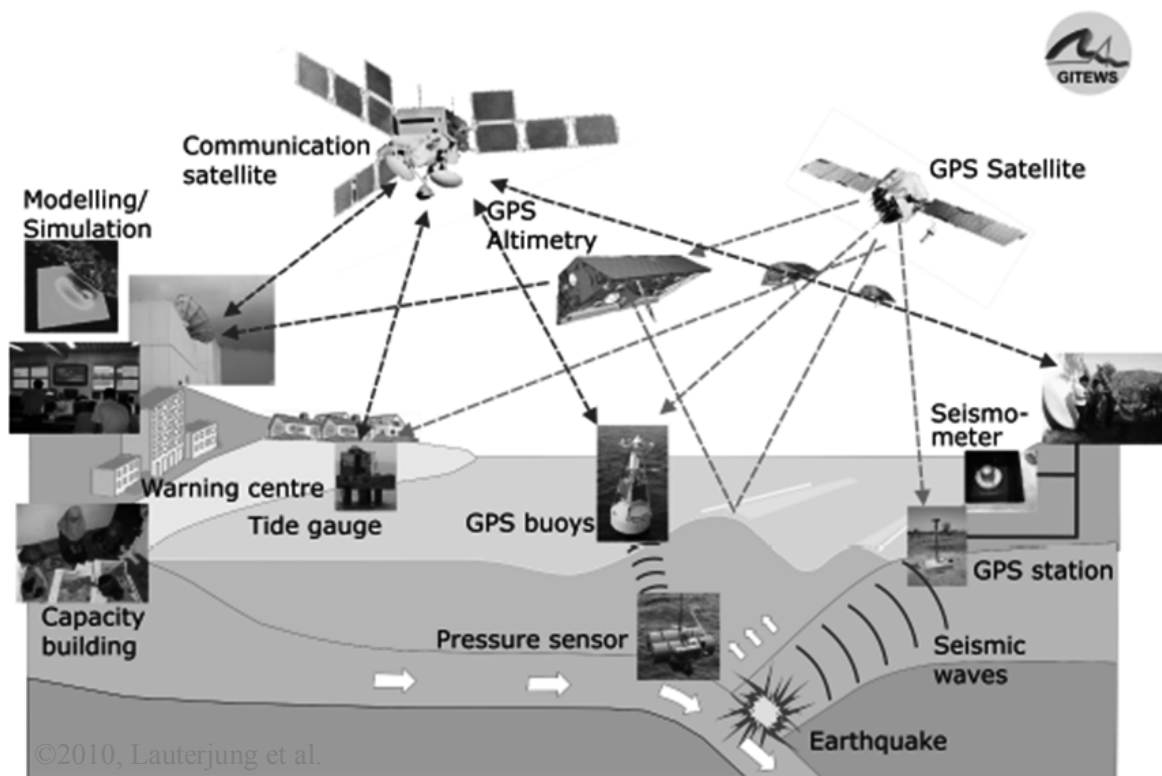


Figure 2: Different sensor systems utilized within the Indian Ocean warning system

In September 2007, the installed system was examined and successfully proved its capabilities to evaluate earthquake parameters of the Bengkulu earthquake that occurred on 12– 13 September. A stable solution for the main shock estimating a moment magnitude of 7.9 based on 25 stations was available and provided after 4 min and 20 s, leading to the first tsunami alert ever disseminated originally by the Indonesian Meteorological, Climatological and Geophysical Agency (BMKG) in less than 5 minutes (Rudloff et al., 2009).

Another initiative that was even established was an accomplishment of the official hazard and risk map of Padang, which was delivered in April 2009. The project, entitled Last Mile aims to maintain and update the local disaster preparedness management in the city of

Padang, which faces the real threat of tsunami hazards in the near future. This objective was achieved by collective multinational scientific effort with the participation of researchers from Indonesia, USA, Japan and Germany in collaboration with local scientists and municipal authorities from Padang. This official tsunami hazard map is greatly needed for further planning and preparedness processes in order to proceed with the development of a community-friendly evacuation plan by involving relevant stakeholders (Schlurmann et al., 2010).

Under the umbrella of the GITEWS project, the Capacity Building Unit (CBU) project was formed entitled Work-Package 6000 (WP 6000). This CBU project's main goal is to build the capacity to ensure that the early warning system is operated, maintained, and improved properly in space and time for coastal communities. Furthermore, this project is also ensuring that the local institutions and communities have adequate capacities (education, knowledge, and skill) through disaster awareness campaigns, technical training, and higher-level education programs. One of the CBU's programs is to strengthen the capabilities of individuals and academic scholars, who in this framework should be integrated into relevant research projects in order to gain useful practical insights and the basic conceptions of project management through continuing education (Schlurmann & Siebert, 2010).

1.3 Background and motivation

Within the last 12 years, two earthquake-generated tsunamis occurred in the Java subduction zone. The Java earthquakes, on 2 June, 1994 and 17 July, 2006, were of similar magnitude and located close to the Java trench (Bilek & Engdahl, 2007).

The epicenter of the 17 July, 2006 event was located 225 km off the coast of Pangandaran with a 7.7 magnitude (USGS, 2006; CEA-France, 2007). Inversion of tsunami waveforms based on six tide gauges also reveals that the tsunami source was about 200 km long, of which the largest slip was about 2.5 m for the instantaneous rupture model (Fujii & Satake, 2006). Polet & Kanamori (2000) categorized the similar events as a tsunami earthquake, which was originally defined by Kanamori (1972) as an event that excites an unusually large tsunami in terms of its body and surface-wave magnitudes and exhibits a notable discrepancy between M_S and M_W .

According to Ammon et al. (2006), the 2006 Java earthquake was characterized by a smooth rupture, indicating a compound frictional environment likely influenced by weak material properties related to sediment subduction or the presence of fluids. Their assumption

of $\mu = 10$ GPa is consistent with sedimentary material within the accretionary wedge as proposed by Kopp & Kukowski (2003), and gives an average slip of about 8 m and peak slip just under 14 m.

Twelve years ago, on 2 June, 1994, an earthquake of magnitude M_W 7.6 (M_S 7.2) occurred off the south-east coast of Java Island, Indonesia. A weak tremor and no damage were reported on land. In contrast, about 50 minutes after the main shock, a sizable tsunami hit the coast, causing considerable damage to several villages in the east Java province. One hundred people lost their lives and over a thousand buildings were destroyed, as reported by Maramai & Tinti (1997) and Tsuji et al. (1995).

Both Java tsunamis had extraordinary run-up heights as reported by the International Tsunami Survey Team (ITST), which was deployed a few days after the events. The team reported that the 17 July, 2006 event prompted a 5-to-7 m-high tsunami to sweep in 200 km off the southern coast of Java. A strange peak was noted by Fritz et al. (2007) on the south coast of Nusa Kambangan Island, where the tsunami impact carved a sharp trim line in a forest at an elevation up to 21 m located 1 km inland. Furthermore, for the 2 June, 1994 event, a high inundation of 13.9 m was measured at the east entrance road of the residential area of the village of Rajekwesi (Tsuji et al., 1995).

Several institutes attempted to model the 2006 Java tsunami. However, none of the comparable existing calculations mimic a tsunami run-up height such as the one resulting from field observation data. For instance, the tsunami model proposed by DCRC Tohoku University, Japan; TRT Bologna University, Italy; and CEA, France, yielded values ranging from 2 to 3.5 m, although with such results they argued and expected that its real run-up height could have reached 5 m due to amplifications of coastal features.

Another model proposed by Hanifa et al. (2007) follows the approach of nested grids with a bathymetric resolution of one and two minutes. These authors used low rigidity of 10 GPa as previously suggested by Ammon et al. (2006). The latter attempt resembles the best-fit model for the 2006 Java tsunami with maximum run-up heights of about 6.3 m in the relevant area.

All of the models proposed above, however, show strong discrepancies in comparison to the field observations of run-up heights along Java's coastline, which were jointly collected by several researchers in the aftermath of the disaster. Hitherto, the latter model proposed by Hanifa et al. (2007) is the only existing attempt which exposed similar run-up heights as it takes the larger slip due to low-rigidity material in the excitation zone into

account affected by a so-defined accretionary prism as introduced by Ammon et al. (2006) and Kopp & Kukowski (2003). However, due to the low resolution of the bathymetric and topographic data and the limited number of field observations used, an extensive model result comparison, i.e. tsunami run-up distribution along the coastline as well as its run-up onto land, which is significant for model validation, has not yet been carried out.

Recently acquired topography data from the German-Indonesia Tsunami Warning System (GITEWS) was assembled to set up a digital terrain model which clearly revealed the flat terrain slope in the area under study on the south coast of Java. One of the pilot project areas, namely the district of Cilacap, remarkably illustrates the extraordinary low topography of the region (Intermap Federal Services, 2007).

Furthermore, more than 1.7 million people reside in this particularly flat area. This denotes a population density of 760 inhabitants per km² and thus characterizes a densely urbanized coastal region with vast industrial production employing approximately 80,000 workers. Industrial installations in the area include a cement factory, an oil refinery plant, and a steam power plant, with the latter being one of the vital pillars of the electrical supply in Java-Bali (DPPK-Cilacap, 2007).

As mentioned in earlier paragraphs, the Sunda arc has a high potential tsunami hazard in the Indian Ocean rim, which is based on historical records showing that ~80% of all the events of this type occurred in this region. Furthermore, although from the geophysical data analysis the Java region can to be interpreted as an aseismic zone, and in terms of earthquake magnitude it tends to be lower than in the Sumatra region, the last two events that occurred in 1994 and 2006 caused high fatalities and severe damage. In addition, two events in Java were classified as tsunami earthquakes, which had low rupture speeds and caused ‘only’ slight tremors that could be felt by coastal communities, so there were no signs prior to the event that would have triggered a tsunami warning. On the other hand, the densely populated low-land coastal cities on the south coast Java as well as the presence of vital infrastructure like in Cilacap, which directly faces the Indian Ocean, put these cities at high risk from tsunamis.

By considering the above facts and the absence of the highly resolved geo-data as well as the reliable numerical model that can adequately reproduce the tsunami run-up height, this thesis attempts to provide a comprehensive study and analysis of the Java tsunami model, from the data collection and processing, through model validation, up to producing the hazard map for plausible scenarios of tsunamis in the respective area.

1.4 Objectives and framework of study

The main objective of this study is to carry out a validation of a numerical simulation for the 2006 Java tsunami that agrees with both, the observed run-up data along the south Java coastline and the maximum inundation in the respective area by considering various tsunami sources and using high-resolution geometric data. The achieved outcome, after undertaking an extensive study assessing the plausible maximum scenario affecting the study area, is to produce the estimation of the inundation for future tsunamis.

To fulfill the above goal, in the course of this study the author will:

- Conduct an historical study of the tsunamis in the Java subduction zone, including collecting extensive field observation data as well as geological records and their analysis.
- Collect topographic and bathymetric data as well as carry out bathymetric and topographic measurements to obtain a high-resolution data in the pilot study area.
- Validate the available tsunami model by using extensive field observation data of the Java 2006 event, and up-to-date assimilated geo-metric high-resolution data, coupled with various tsunami sources.
- Assess and propose plausible maximum scenarios and perform numerical simulations to produce tsunami inundation areas, examine the effectiveness of artificial countermeasures for the tsunami, and propose recommendations for study area.
- Assess the influence of the rigidity material in the subduction zone regarding its numerical model performance, including the sensitivity model of the slip distribution at the source zone.

1.5 Overview of the Study

Chapter 1: Introduction. This describes at a glance the overall thesis content, which includes the background, motivation, objective and study framework, as well as an overview of the study. **Chapter 2: The Problem.** This chapter outlines the significance of the study and the theoretical framework, and the problem statements and elements to be investigated. This chapter will also describe the theories, hypothesis, and research question, and end with a summary. The sub-chapters will discuss the limitations of the study and provide a definition of terms.

Chapter 3: Review of the Literature. This contains an historical review of the research literature specific and relevant to the topic. A critique on the validity of appropriate research, the contribution and outcome of this study to the literature, and a framework study will also be provided.

Chapter 4: The Research Procedures. In individual sub-chapters this chapter discusses the research methodology, the pilot study, data collection, pre-processing data and their treatment, model tools, model set-up runs, and post-processing data, and also provides a summary.

Chapter 5: Findings. This chapter discusses the findings procedures and elements of the study, the hypotheses and research questions, the evidence found, specific notes, and ends with a summary.

Conclusions and Recommendations are given in **Chapter 6** which is the final chapter. It describes the conclusions that can be drawn based on the findings. The recommendations are relevant to applied engineers, decision makers and local players who are at the frontline for applying the research results. The recommendations are also for further research or changing methodology, academic and engineering concepts or their modification in applied theory. This chapter ends with a summary.

The **Appendix** and **Bibliography** are at the end.

Chapter 2 - The Problem

“When the earth will be shaken to her utmost convulsion and the earth shall bring out all her inner burdens, man shall say: “What is happening to her?” On that Day she shall report whatever had happened on her”(the Quran, 099 the Earthquake: 1-3, ca.610-632 AD)

This chapter describes some aspects of the problems examined by the present study, which include the significance of the study, such as potential hazards threatening the study area, demography and infrastructure, as well as the terrain conditions. Furthermore, problems that appeared prior to this study and relevant issues are highlighted, especially regarding the geo-data resolution and numerical model available. The numerical model used in this study, and its scheme will be outlined in the sub-chapter on theories, which will include the basic scientific information on tsunami generation and the empirical study of scaling law to estimate the rupture’s dimensions. This chapter also presents the study hypothesis and several questions. At the end of the chapter, the limitation of the study is presented, and closes with a definition of the terms mostly used in the study.

2.1 Significance of the Study

Following the Boxing Day Sumatra-Andaman earthquake tsunami on 26 December, several countries started initiatives in relation to the improvement of the hazard mitigation systems in various regions. One of the initiatives came from the German government, i.e. the Federal Ministry of Education and Research (BMBF) in collaboration with Indonesia's government, which was to start installing a tsunami early warning system in Indonesia on 14 March, 2005 (Rudloff et al., 2009). Since then, the GITEWS project (German Indonesian Tsunami Early Warning System) was started with the main goal to design, develop and implement a tsunami early warning system in Indonesia. The target area is the coastal strip facing the Indian Ocean, from the islands of Sumatra, Java, Bali, and Lombok, where the three study areas of coastal front cities were determined, namely Padang west Sumatra, Cilacap south-central Java, and Kuta Bali.

The following’s sub-chapters discuss the significance of the study in Cilacap south-central Java as the focus of this study, in the aspects of potential hazard, demography and the presence of infrastructure, as well as the new digital terrain models (DTM), which were created in this project.

2.1.1 Potential hazard

Based on historical data, the number of earthquakes in Java's subduction zone that occurred within the time period 1977–2007 in bounding coordinates, as depicted in Figure 3, with magnitudes greater than M_S 5.0 and hypocenters shallower than 40 km, is about 419.

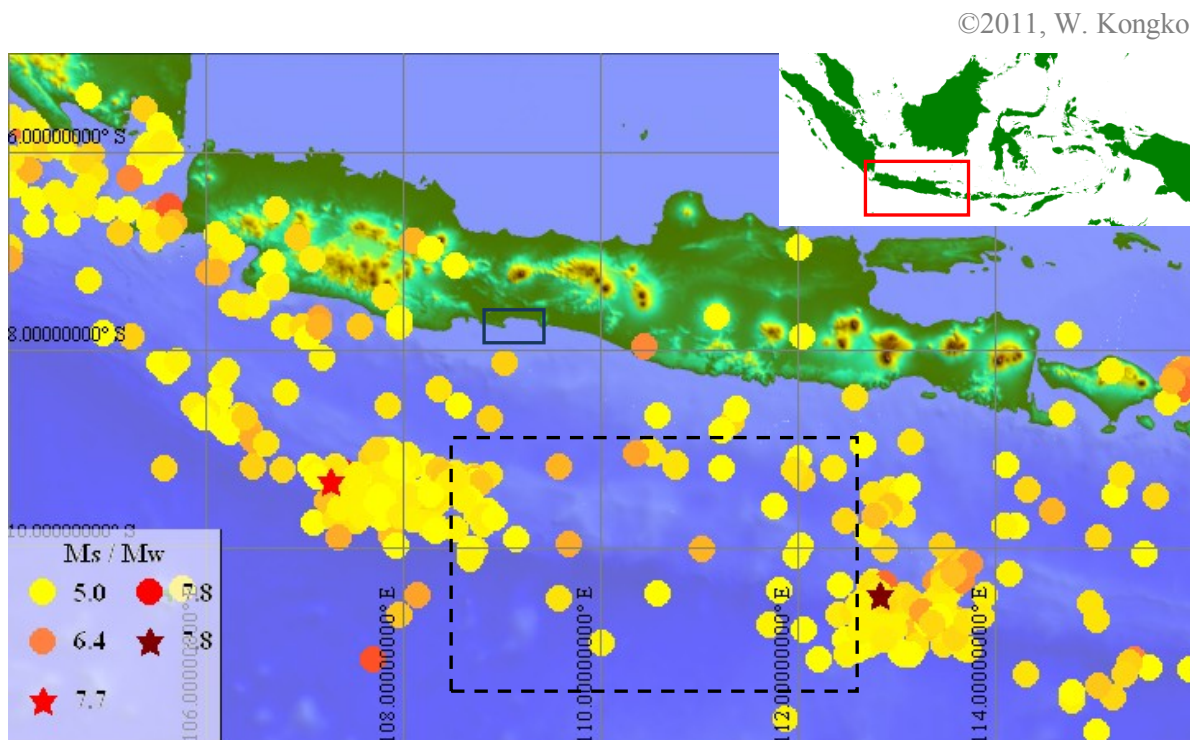


Figure 3: Earthquake (dots), subsequent tsunami (stars), & seismic gap

Among these candidates, two events of significant magnitude happened in 1994 and 2006. Each was followed by sizeable tsunamis causing damage and casualties along the South Java coastline (ITDB/WLD, 2007). According to USGS database for source parameters (USGS, 2010), there were 20 events with magnitudes above M_W 6.5 and depths less than 100 km within the period 1978–2008. Two earthquakes generated tsunamis that occurred at depths less than 20 km, which are depicted with black boxes in Table 1.

It is interesting to note, based on the above data, that the events that generated tsunamis have almost identical source parameters, namely strike, dip, and slip of $\theta \sim 278^\circ$ - 297° , $\delta \sim 10^\circ$, and $\lambda \sim 90^\circ$, respectively. Furthermore, according to historical data in the area between those events, from approx. 109°E to 112°E , as depicted with a black dashed box in Figure 3, no major events occurred, suggesting that this zone is categorized as a seismic gap. Although in terms of magnitude, the seismicity of Java's subduction zone is less than those in the Sumatra region and based on modern historical data, as compiled by Newcomb & McCann (1987), major earthquakes occurred in this region only three times, yet two

earthquake events generated tsunamis causing major damage and high fatalities in 1994 and 2006. In addition, the co-seismic wave analysis of those events, conducted by Ammon et al. (2006) and Polet & Kanamori (2000), suggested that the earthquakes caused large tsunamis with intensities relative to M_S indicating they should be classified as tsunami earthquakes as postulated by Kanamori (1972).

By considering the above conditions, it suggests that this area poses a high potential hazard and is prone to tsunamis, so for future disaster mitigation its assessment is greatly required.

2.1.2 Dense population and vast infrastructures

Cilacap is one of the regions in the south central Java province selected for a pilot study in the GITEWS project together with Padang in west Sumatra, and Kuta in the Bali islands (Strunz et al., 2011). In south Java, Cilacap is the only city with an international-level port that enables it to have access to trade with foreign countries, such as Australia. With its largest area and densely inhabited regions, as well as wide-ranging industries like fisheries, marine, mining, forestry, tourism, and the support infrastructures, this city is the vital urban area supporting other cities in Java.

Cilacap has an area of 225,361 hectares consist of 24 sub-districts and 284 villages occupied by more than 1.7 million people with a population density of 806 per km² (DPPK-Cilacap 2007). Six of its sub-districts face the Indian Ocean, namely Nusawungu, Binangun, Adipala, Kesugihan, Cilacap Utara, and Cilacap Selatan. In 2006, during the Java earthquake, these sub-districts were devastated by the tsunami with the farthest penetration being more than 450 m inland and at least 150 people were killed (Abidin & Kato, 2007; Cousins et al., 2006; Kongko et al., 2006). Figure 4 contains a map of the 24 sub-districts that is color-coded and shows the areas devastated by the tsunami.

Table 1: Source parameter of Java earthquake, 1978-2008 (USGS)

Tue May 12 13:35:59 UTC 2009
 FM Format
 Magnitude Range: 6.5 to 10
 Depth Range: 0 to 100
 Date Range: 1978 1 1 to 2008 1 1
 Latitude Range: -20 to -5
 Longitude Range: 100 to 115

DATE			TIME (UTC)			E P I C E N T E R			M O M E N T			P R I N C I P A L A X E S						N O D A L P L A N E S						SRC			
YR	MO	DA	HR	MN	SEC	LAT	LONG	SRC	DEPTH	VAL	EX	T	N	P	1	2	3	4	5	6	SRC						
deg	deg	km	Mw	Nm	VAL	PL	AZM	VAL	PL	AZM	VAL	PL	AZM	STK	DP	SLIP	STK	DP	SLIP	DC							
1979	07	24	19:31:28.30	-11.260	107.680	HRV	20.0	7.0	3.4	19	3.23	29	29	0.41	46	154	-3.65	29	280	65	46	-180	334	90	-44	78	HRV
1979	11	02	15:53: 7.80	-7.980	108.520	HRV	72.2	6.5	7.2	18	7.18	77	190	-0.01	12	34	-7.17	5	303	20	41	72	223	51	105	100	HRV
1985	12	27	05:38:53.45	-5.763	104.191	PDE	7.0	6.3	3.7	18	3.83	14	109	-0.23	45	4	-3.60	41	212	241	50	-22	346	73	-138	88	GS
1985	12	27	05:38:57.00	-5.910	103.960	HRV	19.9	6.5	6.2	18	5.92	11	292	0.53	69	54	-6.45	18	199	337	69	-175	245	86	-21	84	HRV
1994	06	02	18:17:34.02	-10.477	112.835	PDE	6.0	7.7	5.2	20	5.68	43	356	-0.93	11	96	-4.75	45	198	11	11	-175	276	89	-79	67	GS
1994	06	02	18:18:15.80	-11.030	113.040	HRV	15.0	7.8	5.3	20	5.43	52	9	-0.18	0	279	-5.26	38	189	278	7	89	99	83	90	93	HRV
1994	06	03	21:06:59.88	-10.362	112.892	PDE	29.0	6.3	3.4	18	3.43	3	185	0.03	16	94	-3.46	74	286	291	44	-67	81	50	-111	98	GS
1994	06	03	21:07: 7.30	-10.750	113.140	HRV	15.0	6.6	8.8	18	8.70	7	178	0.23	3	88	-8.93	82	337	271	38	-86	86	52	-93	95	HRV
1994	06	04	00:57:50.66	-10.777	113.366	PDE	18.0	6.1	2.1	18	2.14	4	14	-0.01	24	106	-2.14	65	274	80	46	-125	305	54	-60	99	GS
1994	06	04	00:57:59.50	-10.940	113.520	HRV	15.0	6.5	5.8	18	5.46	4	4	0.72	5	94	-6.18	83	236	88	41	-98	279	49	-83	77	HRV
1999	12	21	14:14:57.61	-6.845	105.555	PDE	45.0	6.4	5.4	18	5.90	41	31	-0.93	33	266	-4.97	31	153	189	33	11	90	84	123	68	GS
1999	12	21	14:15: 1.50	-7.060	105.540	HRV	56.0	6.5	5.5	18	5.54	36	45	-0.02	32	288	-5.52	37	169	197	32	-1	287	89	-122	99	HRV
2000	10	25	09:32:23.97	-6.549	105.630	PDE	37.0	6.7	1.6	19	1.59	74	4	-0.02	1	272	-1.57	16	181	270	29	89	92	61	91	97	GS
2000	10	25	09:32:32.10	-7.280	105.430	HRV	45.6	6.8	1.7	19	1.74	71	3	-0.04	5	108	-1.70	19	200	299	27	102	106	64	84	95	HRV
2002	06	27	05:50:35.11	-6.963	104.181	PDE	20.0	6.5	6.0	18	6.25	73	186	-0.51	11	315	-5.74	13	48	152	34	110	308	59	77	84	GS
2002	06	27	05:50:42.50	-7.230	103.760	HRV	15.0	6.5	6.6	18	6.64	82	335	-0.13	7	117	-6.51	5	208	305	40	100	112	50	81	96	HRV
2006	05	26	22:53:58.92	-7.961	110.446	PDE	37.0	6.3	4.2	18	3.90	11	105	0.59	79	268	-4.49	3	15	150	80	175	241	85	10	74	GS
2006	05	26	22:54: 5.30	-8.030	110.540	HRV	21.7	6.4	4.2	18	4.81	7	278	-1.19	76	36	-3.63	12	187	323	77	-176	232	86	-13	51	HRV
2006	07	17	08:19:26.68	-9.284	107.419	PDE	6.0	7.2	8.1	19	7.74	51	23	0.69	0	113	-8.43	39	204	297	6	93	113	84	90	84	GS
2006	07	17	08:20:38.40	-10.280	107.780	HRV	20.0	7.7	4.6	20	4.73	55	6	-0.24	2	98	-4.48	35	190	290	10	102	98	80	88	90	HRV

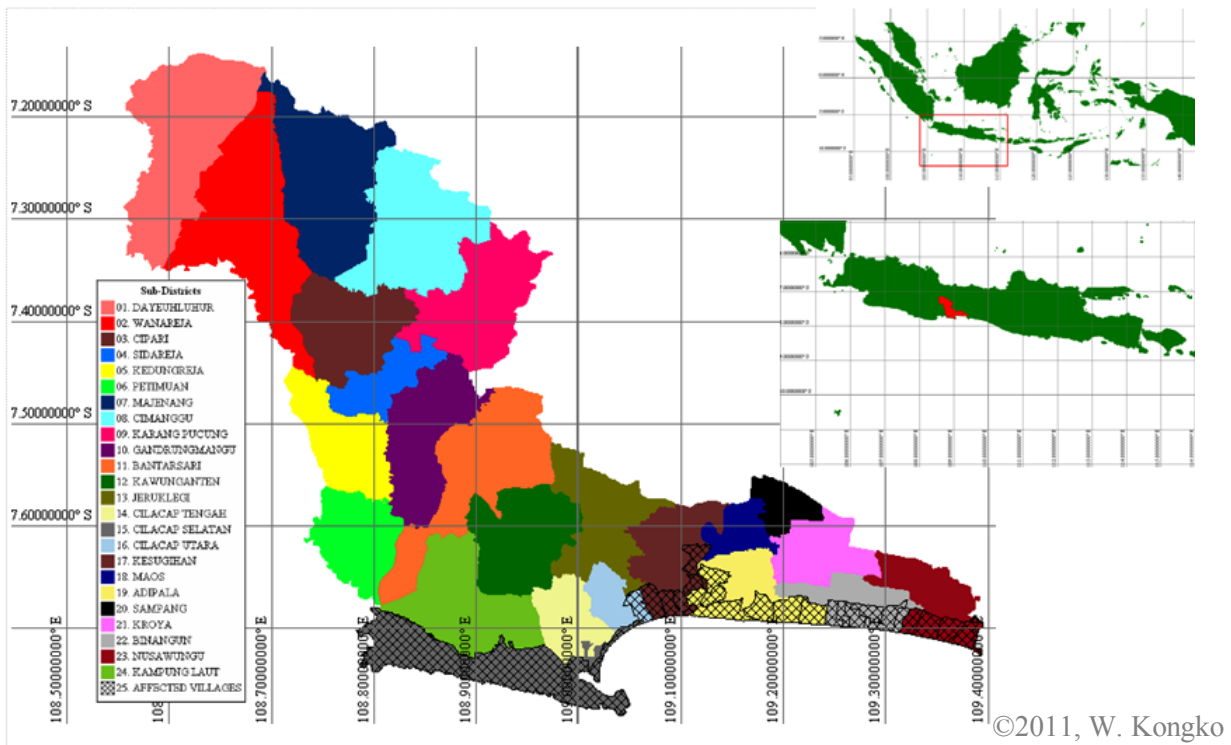


Figure 4: 24 Sub-districts of Cilacap & the affected area during 2006 tsunami

In this city, there are also several industries that support regional and domestic economic activities. These include oil refinery, cement, wood manufacturing, woven thread making, wheat-flour processing, fish canning, power generation, etc. According to the official statistical data published in 2006, all of the business units in various levels number 717 and employ more than 82,000 people, giving this region a high level of economic growth of 4.16%.

The presence of all the businesses and factories above can work successfully as they are fully supported by six infrastructure categories. These are a 6.7-million-km road network, a clean water network with a capacity of about 400 liters per second, an electricity network and a telephone network with an existing capacity of 165 MW and more than 23,000 lines, respectively, both of which are currently being expanded to meet increasing demand. In addition, other supporting infrastructures are 26 banking offices, an industrial area of more than 150 hectares existing area with a further 2,000 hectares under development, and international port facilities.

The dense population and its distribution as well as the presence of major industry led to economic activities to be concentrated mostly in the city, which is situated close to the beach, which is obviously a place vulnerable to tsunamis.

2.1.3 Flat topography

Recently acquired topography data from the German-Indonesia Tsunami Warning System (GITEWS) was assembled in order to set up a Digital Terrain Model (DTM). This dataset was generated using the Intermap STAR-4 airborne interferometric synthetic aperture radar (SAR) system mounted on a King Air 200T aircraft (Intermap Federal Services, 2007). It represents the cartographic information in a grid form at a 5-meter pixel resolution, and covers the area as depicted as a blue box in Figure 3. However, the data does not entirely cover the 24 of sub-districts of Cilacap, but only the places where a potential tsunami hazard may exist, and it needs to be assessed.

Figure 5 below is a blow-up of the area in the blue box in Figure 3, and shows the DTM data; its level of terrain is represented by a color bar scale on the left-hand side. The 14 cross-sections normal to the shoreline (indicated by thin black lines) were added in order to estimate the steepness of the topography of the area.

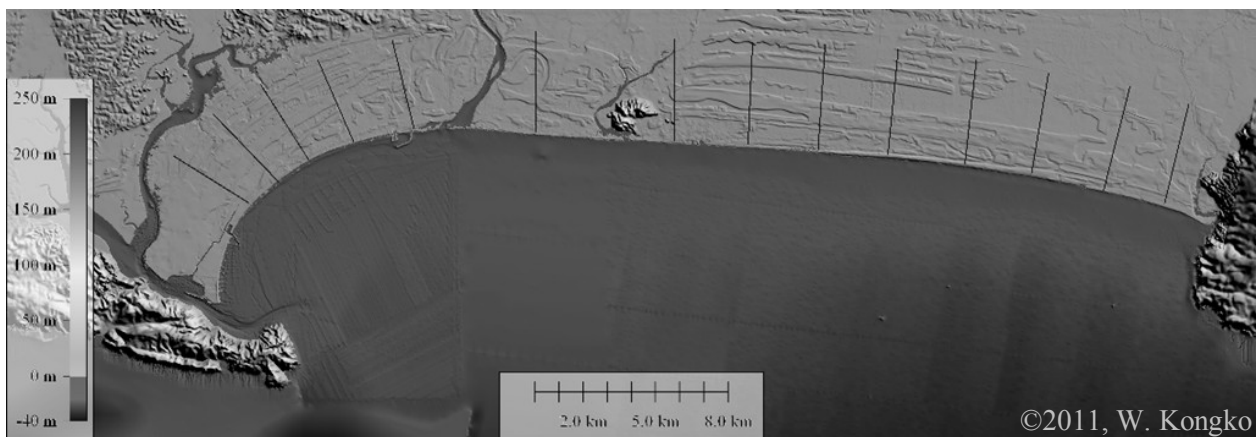


Figure 5: Digital Terrain Model (DTM) of Cilacap incl. 14 lines normal to coastline

Thousands of points were derived from 14 cross-sections with interval acquisition data of about 30 m, indicating an average topographic slope of less than 1%. The maximum ground-level data was found at approximately 9 m within a distance of about 4 km inland. Such an extraordinarily flat topographic terrain in the urban area of Cilacap causes this place to be one of the most vulnerable cities on the south coast of Java Island to tsunami hazards, as

happened at Wuhring Flores that tsunami hit in 1992 (Synolakis & Bernard, 2006; Yeh et al., 1993).

2.1.4 Contribution to knowledge & hazard mitigation program

The two tsunami events, which occurred in the Java subduction zone on June 3, 1994 and July 17, 2006, respectively, were categorized as tsunami earthquakes (Abercrombie et al., 2001; Polet & Kanamori, 2000; Polet & Thio, 2003; Ammon et al., 2006; Fujii & Satake, 2006; T. Kato et al., 2007). Tsunami earthquakes were originally defined by Kanamori (1972) as events that generate an extraordinarily large tsunami regarding their body and surface-wave magnitudes and show a remarkable discrepancy between M_S and M_W .

During the last four decades, researchers collected these kinds of events, distinguished them by studying and analyzing their seismic processes and tsunami impacts, and summarized their characteristics. Among these characteristics are a slow rupturing process and a long rupturing duration occurring at the plate boundaries where the plate coupling is weak, and a source area located within shallow sedimentary layers or on the plate boundary near the trenches (Pelayo & Wiens, 1992; Hanifa et al., 2007).

Although a tsunami earthquake is a rare event, the damage to infrastructure and the number of casualties are massive. Only a few occurred throughout the history of tsunami events, making it one of the reasons why this typical event is not well known. Since 1992 – the time where modern global networks of broadband equipment being initially introduced and deployed providing an opportunity to obtain improved seismological characteristic of their rupture processes – about 140 tsunami events occurred, among which only eleven (or about 8%) were classified as a tsunami earthquake (ITDB/WLD, 2007; Hanifa et al., 2007).

It is fortune that the GITEWS project has determined three pilot study areas, one of which is the district of Cilacap, which is situated in the south of Java and which was devastated by 2006 Java tsunami (Strunz et al., 2011). Through this project, the geo-data was made available for further assessment of hazard mitigation, not solely for this project but also for the numerical model analysis of the 2006 Java tsunami.

Furthermore, to complete the available figures above, supplemental fieldwork, such as bathymetric and topographic measurements in the area under study as well as collecting the dataset of tsunami run-up heights along the Java coastline and other data related to this event were conducted as reported in unpublished documents (Kongko & Leschka, 2009).

Utilizing such attainable data enabled the Java tsunami model analysis to be conducted. Through the numerical model, this study is attempting to analyze the influence of

the rigidity material in the source region to the tsunami run-up height and its distribution along the coastline. Both single and multi-fault tsunami source models as proposed by seismologists and a modification source model as a result of this study have also been constructed and evaluated. In addition, the variety source type of the available geo-data allows the sensitivity model analysis to be performed, in particular regarding the difference between near-shore bathymetric figures and those for the tsunami run-up. The other product of the study is the inundation map compiled from numerical simulations based on the plausible maximum scenario with variations in the magnitudes and the epicenters.

The aforementioned outcome will fill the gap regarding tsunami model analysis in Java, particularly for the most recent event and provide an alternative solution and explanation in answer to the foremost problem being voiced among scientists and engineers, namely the discrepancies of the tsunami model resulting and ‘in-situ’ field measurements. The proposed inundation map in Cilacap city and its vicinity derived from the numerical model for future hazards will also provide a significant contribution to the local authorities in conducting hazard assessment and support a public awareness and preparedness program regarding future tsunamis.

2.2 The problem

The fundamental problem in conducting tsunami assessment by utilizing numerical simulations for the south Java region, prior to 2007, is linked to the absence of accurate near-shore bathymetric and topographic data. Due to the absence of credible topographic data, there is not inundation model available before the present study. Furthermore, the performances of the available tsunami models following the 2006 Java tsunami have inconsistencies compared to the field observation data. In addition, the detailed analysis of the tsunami model in terms of the variety of source models affecting the tsunami run-up height’s distribution and the data used for model validation were very limited.

The following sub-sections describe and discuss the aspects of the problem related to the geo-data resolution and the model performances.

2.2.1 Geo-data resolution

Geometric data is essential for the numerical simulation. This type of data is derived from the assimilation of seafloor data, also known as bathymetric data, and terrain data or topographic data. By far, the most widely used bathymetric data among modelers is GEBCO (General Bathymetric Chart of the Oceans), which is publicly available and free to download

from the internet. The most recent resolution of such data is 30 arcseconds or approximately 925 m (GEBCO, 2008). The NASA Shuttle Radar Topographic Mission (SRTM) provides digital elevation data (DEM) for over 80% of the globe, which is available at a resolution of 3 arcseconds (approx. 90 m resolution), and a 1-arcsecond resolution (approx. 30 m) is available for limited countries. However, the vertical error of the DEM is reported as 16–20 m (CGIAR-CSI, 2008; Zielinski, 2007). The other global relief model of the Earth's surface is ETOPO which integrates land topography and ocean bathymetry. The latest version is ETOPO1 which has a resolution of 1 arcminute (Amante & Eakins, 2009).

Before this study, simulating a tsunami model in southern Java was using data of the resolution described above. A simulation of the tsunami propagation model is usually made and of course using the relatively coarse grid size, i.e. above 950 m. An inundation model, as far as is known, has never existed. If such a study exists, then the topographic data used would be SRTM data with the altitudes corrected using ground measurements. However, due to limited resources and time, the quantity and quality of corrections are very limited and lead to substantial errors.

2.2.2 Numerical model performances

After searching through the published articles, it was discovered that only a few tsunami model studies were conducted on the earthquake that occurred on June 3, 1994. The author found a tsunami model for the 1994 Java event, which was generated using a combination of horizontal and vertical displacement at the seafloor near the trenches (Tanioka & Satake, 1996). Such uncommon generation is typical for very steep sloping bathymetry ($>1/3$). The model was produced a tsunami run-up 30% higher than those using only vertical deformation. Due to the limited geometric and field observation data, the discussion of this model cannot be provided here.

The earthquake itself caused no land damage. However, about 40 minutes after the main shock, a sizable tsunami hit the coast killing more than 220 people and causing damage to several villages. The highest inundation of about 14 m was found at village of Rajekwesi (Tsuji et al., 1995). The most damage occurred at the pocket beaches area, suggesting that those areas and headlands may be more vulnerable to tsunami attack than previously thought (Synolakis et al., 1995). However, the absence of efforts to reconstruct such an event using a model, and the fact that extreme tsunamis have occurred than expected, means the event is still something of a mystery.

Twelve years later, on July 17, 2006, an earthquake with a magnitude of M_W 7.7 occurred in southern Java and was followed by a huge tsunami that attacked at least 200 km of coastline causing casualties of more than 600 coastal inhabitants (Abidin & Kato, 2007; RCS, 2006; Lavigne et al., 2007; Fritz et al., 2007; USGS, 2006; Mori et al., 2007; Kongko et al. 2006).

After this event, several institutions issued tsunami model assessments that were released through their official websites (DCRC - Univ. Tohoku – Japan, 2007; CEA-France, 2007; Italy, 2007; Latief et al., 2006). They used single-fault models, in which slip is estimated by assuming that the shear modulus or the rigidity is normal. Hanifa et al. (2007) conducted a tsunami simulation by using a system of multiple grids with one- and two-minute grid sizes, and included low-rigidity material leading to higher slip. However, the tsunami models produced average run-up height little different to field observation data.

The two main issues of the problem described above, namely geo-data resolution and the numerical model performances can be summarized as follows:

1. The geometric data used in the numerical simulation before the present study used a coarse resolution. Near-shore measurement bathymetric data were also not available, so an attempt to improve data in this area through assimilation with other data such as GEBCO cannot be conducted. In addition, medium-high-resolution topographic data such as LIDAR or IFSAR data, which have a vertical accuracy of less than one meter, were also absent; hence a reliable inundation model impossible needs to be achieved.
2. The average tsunami run-up heights along the coast south of Java resulting from the numerical simulation presented above still have major discrepancies compared to the field observations, thus further analysis to find solutions to the various problems is required. Numerous field observations made by several international tsunami survey teams (ITST) and tsunami mareograms were not used extensively to validate the tsunami model results. Such data can be used to validate tsunami run-up heights and its horizontal inundation as well as their distribution along the south coast of Java.
3. Java tsunamis occurred in the proximity of the Java trench; therefore, they are classified as near-field tsunamis. Hence, the tsunami run-up heights and their distributions are strongly affected by the tsunami source; rupture dimension, fault orientation, position as well as slip distribution as work conducted by previous

researchers showed (Behrens et al., 2010; Babeyko et al., 2010; Geist, 2002; Geist & Dmowska, 1999). Although, Hanifa et al. (2007) conducted a study that considered several of the aspects named above, they used limited data. Therefore, extensive numerical analysis by integrating the various tsunami source models, such as the single and multi-fault model, normal-low rigidity material, etc. is required.

2.3 Theories, hypotheses, and questions

In the sub-section below the theories, hypotheses, and questions related to the topic of this study will be elucidated. It consists of the classical analytical approach of the deformation model for the Earth's surface, several empirical formulas determining fault dimensions, and the hydraulic numerical model for tsunami propagation and its run-up. Furthermore, the hypotheses explain the elements as pre-assumptions may strongly influence the problems in this study. It comprises the heterogeneous source parameters, such as rigidity, fault orientation and dimension, and slip distribution, as well as the influence of geo-data on the model's performance, especially the tsunami run-up height along the coast. At the end of this sub-section several questions may arise in connection with the problems above, which are evaluated and assessed in this study.

2.3.1 Theories

2.3.1.a Deformation model

Earthquake processes originate beneath the earth floor; our basis of tsunami model source mimics the vertical sea-floor displacement. Therefore, the theoretical studies deriving expressions of the physical surface parameters are relevant to this study and will be presented here.

The dislocation theory, which has recently been widely used for deformation models in tsunami numerical simulation, was introduced into the discipline of seismology by Steketee in 1958. Since then, numerous theoretical formulations describing the deformation under a homogeneous medium were proposed with greater complexity in terms of parameters. The work accomplished in various papers dealing with the analytical expression of internal deformation fields due to shear faults in a half-space is summarized in Table 2 (Mansinha & Smylie, 1971; Okada, 1985). As our study is utilizing these expressions and they are also widely used among tsunami modelers, this study presents the deformation

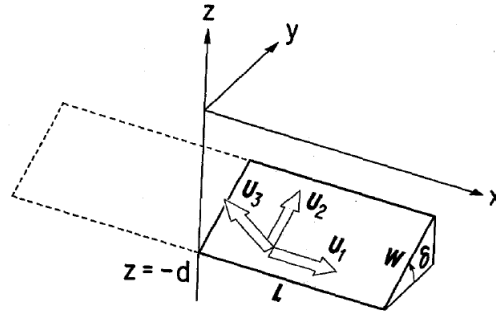
model, using the analytical expressions derived by Mansinha & Smylie (1971) and Okada (1985), which are shaded in Table 2.

The first formula for point source was proposed by Steketee (1958), which showed the displacement field $u_i(x_1, x_2, x_3)$ due to a dislocation $u_j(\xi_1, \xi_2, \xi_3)$ across a surface Σ in an isotropic medium is given by,

$$u_i = \frac{1}{F} \iint_{\Sigma} \Delta u_j \left[\lambda \delta_{jk} \frac{\partial u_i^n}{\partial \xi_n} + \mu \left(\frac{\partial u_i^j}{\partial \xi_k} + \frac{\partial u_i^k}{\partial \xi_j} \right) \right] v_k d\Sigma \quad (1)$$

where, δ_{jk} is the Kronecker delta, λ and μ are Lamé's constants; v_k is the cosine direction of the normal to the surface element $d\Sigma$. u_i^j is the i^{th} component of the displacement at (x_1, x_2, x_3) due to the j^{th} direction point force of magnitude F at (ξ_1, ξ_2, ξ_3) , whose expressions are in a homogeneous half-space.

Okada (1985) considered the Cartesian coordinate system as depicted in Figure 6. The strike direction of the fault is taken to be parallel to x-axis, and the medium in the region of $z \leq 0$ is assumed elastic. U_1 , U_2 , and U_3 is the component of dislocations corresponding to the strike-slip, dip-slip, and tensile, respectively. Then u_i^j at the ground surface are expressed as follows:



©1985, Y. Okada

Figure 6: Geometry of the source model

$$\begin{cases} u_1^1 = \frac{F}{4\pi\mu} \left\{ \frac{1}{R} + \frac{(x_1 - \xi_1)^2}{R^3} + \frac{\mu}{\lambda + \mu} \left[\frac{1}{R - \xi_3} - \frac{(x_1 - \xi_1)^2}{R(R - \xi_3)^2} \right] \right\} \\ u_2^1 = \frac{F}{4\pi\mu} (x_1 - \xi_1)(x_2 - \xi_2) \left\{ \frac{1}{R^3} - \frac{\mu}{\lambda + \mu} \frac{1}{R(R - \xi_3)^2} \right\} \\ u_3^1 = \frac{F}{4\pi\mu} (x_1 - \xi_1) \left\{ -\frac{\xi_3}{R^3} - \frac{\mu}{\lambda + \mu} \frac{1}{R(R - \xi_3)} \right\} \end{cases} \quad (2)$$

$$\begin{cases} u_1^2 = \frac{F}{4\pi\mu} (x_1 - \xi_1)(x_2 - \xi_2) \left\{ \frac{1}{R^3} - \frac{\mu}{\lambda + \mu} \frac{1}{R(R - \xi_3)^2} \right\} \\ u_2^2 = \frac{F}{4\pi\mu} \left\{ \frac{1}{R} + \frac{(x_2 - \xi_2)^2}{R^3} + \frac{\mu}{\lambda + \mu} \left[\frac{1}{R - \xi_3} - \frac{(x_2 - \xi_2)^2}{R(R - \xi_3)^2} \right] \right\} \\ u_3^2 = \frac{F}{4\pi\mu} (x_2 - \xi_2) \left\{ -\frac{\xi_3}{R^3} - \frac{\mu}{\lambda + \mu} \frac{1}{R(R - \xi_3)} \right\} \end{cases} \quad (3)$$

$$\begin{cases} u_1^3 = \frac{F}{4\pi\mu} (x_1 - \xi_1) \left\{ -\frac{\xi_3}{R^3} + \frac{\mu}{\lambda+\mu} \frac{1}{R(R-\xi_3)} \right\} \\ u_2^3 = \frac{F}{4\pi\mu} (x_2 - \xi_2) \left\{ -\frac{\xi_3}{R^3} - \frac{\mu}{\lambda+\mu} \frac{1}{R(R-\xi_3)} \right\} \\ u_3^3 = \frac{F}{4\pi\mu} \left\{ \frac{1}{R} + \frac{\xi_3^2}{R^3} + \frac{\mu}{\lambda+\mu} \frac{1}{R} \right\} \end{cases} \quad (4)$$

where $R^2 = (x_1 - \xi_1)^2 + (x_2 - \xi_2)^2 + \xi_3^2$.

By using Equation (1), the followings are the contributions from surface elements $\Delta\Sigma$ of each component dislocation:

Strike-slip

$$\frac{1}{F} \mu U_1 \Delta\Sigma \left[-\left(\frac{\partial u_i^1}{\partial \xi_2} + \frac{\partial u_i^2}{\partial \xi_1} \right) \sin \delta + \left(\frac{\partial u_i^1}{\partial \xi_3} + \frac{\partial u_i^3}{\partial \xi_1} \right) \cos \delta \right] \quad (5)$$

Dip-slip

$$\frac{1}{F} \mu U_2 \Delta\Sigma \left[\left(\frac{\partial u_i^2}{\partial \xi_3} + \frac{\partial u_i^3}{\partial \xi_2} \right) \cos 2\delta + \left(\frac{\partial u_i^3}{\partial \xi_3} - \frac{\partial u_i^2}{\partial \xi_2} \right) \sin 2\delta \right] \quad (6)$$

Tensile

$$\frac{1}{F} U_3 \Delta\Sigma \left[\lambda \frac{\partial u_i^n}{\partial \xi_n} + 2\mu \left(\frac{\partial u_i^2}{\partial \xi_2} \sin^2 \delta + \frac{\partial u_i^3}{\partial \xi_3} \cos^2 \delta \right) - \mu \left(\frac{\partial u_i^2}{\partial \xi_3} + \frac{\partial u_i^3}{\partial \xi_2} \right) \sin 2\delta \right] \quad (7)$$

Further, for the point source, by setting $\xi_1 = \xi_2 = 0$, $\xi_3 = -d$ and substituting Equations (2), (3), and (4) into (5), (6), and (7), the surface displacements will be obtained from a point source at $(0, 0, -d)$. The set of expressions of the surface displacements, strains, and tilts applied by point source were discussed in detail and presented in Okada (1985). Here, however, the expressions for a finite rectangular fault source will be presented.

In Figure 6, for a finite rectangular fault with length L and width W , its deformation field may be derived by taking $x - \xi'$, $y - \eta' \cos \delta$, and $d - \eta' \sin \delta$ and replacing x , y , and d , which were obtained after solving the differentiation equations above. And after manipulating the parameters by using techniques proposed by Sato and Matsu'ura (1974) and finally condensing the expression form using Chinnery's notation as quoted by Okada (1985), the expressions for surface displacements are then expressed as shown below:

For strike-slip:

$$\begin{cases} u_x = -\frac{U_1}{2\pi} \left[\frac{\xi q}{R(R+\eta)} + \tan^{-1} \frac{\xi \eta}{qR} + I_1 \sin \delta \right] \\ u_y = -\frac{U_1}{2\pi} \left[\frac{\tilde{y} q}{R(R+\eta)} + \frac{q \cos \delta}{R+\eta} + I_2 \sin \delta \right] \\ u_z = -\frac{U_1}{2\pi} \left[\frac{\tilde{d} q}{R(R+\eta)} + \frac{q \sin \delta}{R+\eta} + I_4 \sin \delta \right] \end{cases} \quad (8)$$

For dip-slip:

$$\begin{cases} u_x = -\frac{U_2}{2\pi} \left[\frac{q}{R} - I_3 \sin \delta \cos \delta \right] \\ u_y = -\frac{U_2}{2\pi} \left[\frac{\tilde{y} q}{R(R+\xi)} + \cos \delta \tan^{-1} \frac{\xi \eta}{qR} - I_1 \sin \delta \cos \delta \right] \\ u_z = -\frac{U_2}{2\pi} \left[\frac{\tilde{d} q}{R(R+\xi)} + \sin \delta \tan^{-1} \frac{\xi \eta}{qR} - I_5 \sin \delta \cos \delta \right] \end{cases} \quad (9)$$

For tensile-fault:

$$\begin{cases} u_x = \frac{U_3}{2\pi} \left[\frac{q^2}{R(R+\eta)} - I_3 \sin^2 \delta \right] \\ u_y = \frac{U_3}{2\pi} \left[\frac{-\tilde{d} q}{R(R+\xi)} - \sin \delta \left\{ \frac{\xi q}{R(R+\eta)} - \tan^{-1} \frac{\xi \eta}{qR} \right\} - I_1 \sin^2 \delta \right] \\ u_z = \frac{U_3}{2\pi} \left[\frac{\tilde{y} q}{R(R+\xi)} + \cos \delta \left\{ \frac{\xi q}{R(R+\eta)} - \tan^{-1} \frac{\xi \eta}{qR} \right\} - I_5 \sin^2 \delta \right] \end{cases} \quad (10)$$

where

$$\begin{aligned} I_1 &= \frac{\mu}{\lambda+\mu} \left[\frac{-1}{\cos \delta} \frac{\xi}{R+\tilde{d}} \right] - \frac{\sin \delta}{\cos \delta} I_5 \\ I_2 &= \frac{\mu}{\lambda+\mu} [-\ln(R+\eta)] - I_3 \\ I_3 &= \frac{\mu}{\lambda+\mu} \left[\frac{1}{\cos \delta} \frac{\tilde{y}}{R+\tilde{d}} - \ln(R+\eta) \right] + \frac{\sin \delta}{\cos \delta} I_4 \\ I_4 &= \frac{\mu}{\lambda+\mu} \frac{1}{\cos \delta} [\ln(R+\tilde{d}) - \sin \delta \ln(R+\eta)] \\ I_5 &= \frac{\mu}{\lambda+\mu} \frac{2}{\cos \delta} \tan^{-1} \frac{\eta(X+q \cos \delta) + X(R+X) \sin \delta}{\xi(R+X) \cos \delta} \end{aligned} \quad (11)$$

If $\cos \delta = 0$,

$$\begin{aligned} I_1 &= -\frac{\mu}{2(\lambda+\mu)} \frac{\xi q}{(R+\tilde{d})^2} \\ I_3 &= -\frac{\mu}{2(\lambda+\mu)} \left[\frac{\eta}{R+\tilde{d}} + \frac{\tilde{y} q}{(R+\tilde{d})^2} - \ln(R+\eta) \right] \\ I_4 &= -\frac{\mu}{\lambda+\mu} \frac{q}{R+\tilde{d}} \\ I_5 &= -\frac{\mu}{\lambda+\mu} \frac{\xi \sin \delta}{R+\tilde{d}} \end{aligned} \quad (12)$$

Table 2: Published analytical expressions of the deformation due to shear and tensile faults in a half-space (after Okada, 1985)

SOURCE TYPE	ORIENTATION			FAULT			MEDIUM		SURFACE DEFORMATION								DEFORMATION AT DEPTH													
	vertical	horizontal	inclined	strike	dip	tensile	$\lambda = \mu$	$\lambda > \mu$	U_x	U_y	U_z	$\frac{\partial U_x}{\partial x}$	$\frac{\partial U_x}{\partial y}$	$\frac{\partial U_y}{\partial x}$	$\frac{\partial U_y}{\partial y}$	$\frac{\partial U_z}{\partial x}$	$\frac{\partial U_z}{\partial y}$	U_x	U_y	U_z	$\frac{\partial U_x}{\partial x}$	$\frac{\partial U_y}{\partial x}$	$\frac{\partial U_z}{\partial x}$	$\frac{\partial U_x}{\partial y}$	$\frac{\partial U_y}{\partial y}$	$\frac{\partial U_z}{\partial y}$	$\frac{\partial U_x}{\partial z}$	$\frac{\partial U_y}{\partial z}$	$\frac{\partial U_z}{\partial z}$	
POINT SOURCE																														
Steketee (1958)	0			0			0		0	0	0							0	0	0										
Maruyama (1964)	0	0		0	0	0	0		0	0	0							0	0	0										
Okada (1975)	0	0	0	0	0		0	0	0	0	0	0	0	0	0	0	0													
Yamazaki (1978)		0				0	0	0										0	0	0										
Iwasaki & Sato (1979)	0	0	0	0	0		0	0										0	0	0										
Okada (1985)	0	0	0	0	0	0	0	0	0	0	0	0	0	0	0	0	0													
FINITE FAULT																														
Chinnery (1961)	0			0			0		0	0	0																			
Chinnery (1961, 1963)	0			0			0	0										0	0	0										
Maruyama (1964)	0	0		0	0	0	0		0	0	0																			
Press (1965)	0			0	0		0		0	0	0		0	0	0	0	0													
Savage & Hastie (1966)			0		0		0				0																			
Mansinha & Smylie (1967)	0			0	0		0											0	0	0										
Mansinha & Smylie (1971)		0	0	0	0		0											0	0	0										
Alewine (1974)		0	0	0	0		0														0	0	0	0	0	0	0			
Sato & Matsu'ura (1974)	0	0	0	0	0		0	0				0	0	0	0	0	0													
Yamazaki (1975)		0	0	0	0		0					0	0	0	0	0	0													
Matsu'ura (1977)	0	0	0	0	0		0	0	0	0	0		0	0	0	0	0													
Iwasaki & Sato (1979)	0	0	0	0	0		0	0													0	0	0	0	0	0	0	0	0	0
Matsu'ura & Tanimoto (1980)	0	0	0	0	0		0	0	0	0	0		0	0	0	0	0													
Davis (1983)	0	0	0			0	0	0			0																			
Okada (1985)	0	0	0	0	0	0	0	0	0	0	0		0	0	0	0	0													

$$u_i = \mu U \int_d^D \int_{-L}^L \left[2 \left(\sin \theta \frac{\partial u_i^2}{\partial \xi} - \cos \theta \frac{\partial u_i^3}{\partial \xi} \right) + \left(\frac{\partial u_i^3}{\partial \xi_2} - \frac{\partial u_i^2}{\partial \xi_3} \right) \right] d\xi_1 d\xi \quad (14)$$

where θ is the dip angle of the fault, μ is the 2nd of Lamé constant, and u_i^j is the i^{th} component of the displacement at (x_1, x_2, x_3) due to a force of unit magnitude at (ξ_1, ξ_2, ξ_3) applied in the j -direction, and the rectangular fault surface has an area between $-L \leq \xi_1 \leq L$ and $d \leq \xi \leq D$.

It is convenient to manipulate expressions by using several abbreviations to shorten long terms by introducing parameters R , Q , r_2 , r_3 , q_2 , and q_3 , which were discussed in detail by Mansinha & Smylie (1971). They represent the distances of the field points from the source points on the fault plane, and the field coordinates were measured normal to and in the down direction from the dip to the fault plane and its image as discussed a detail in the paper mentioned above.

Furthermore, the results of the integrations by assuming a Lamé constant are equal ($\lambda = \mu$), which for the strike-slip displacements are

$$\begin{aligned} 12\pi \frac{u_1}{U_1} = & (x_1 - \xi_1) \left[\frac{2r_2}{R(R+r_3-\xi)} - \frac{4q_2-2x_3 \cos \theta}{Q(Q+q_3+\xi)} - \frac{3 \tan \theta}{Q+x_3+\xi_3} + \frac{4q_2 x_3 \sin \theta}{Q^2} - 4q_2 q_3 \sin \theta \frac{(2Q+q_3+\xi)}{Q^3(Q+q_3+\xi)^2} \right] - \\ & 6 \tan^2 \theta \tan^{-1} \left[\frac{(k-q_2 \cos \theta)(Q-k)+(q_3+\xi)k \sin \theta}{(x_1-\xi_1)(q_3+\xi) \cos \theta} \right] + 3 \tan^{-1} \frac{(x_1-\xi_1)(r_3-\xi)}{r_2 R} - \\ & 3 \tan^{-1} \frac{(x_1-\xi_1)(q_3-\xi)}{q_2 Q} \\ 12\pi \frac{u_2}{U_1} = & \sin \theta 3 \tan \theta \sec \theta \ln(Q + x_3 + \xi_3) - \ln(R + r_3 - \xi) - (1 + 3 \tan^2 \theta) \ln(Q + q_3 + \xi) + \\ & \frac{2r_2^2 \sin \theta}{R(R+r_3-\xi)} + \frac{2r_2 \cos \theta}{R} - 2 \sin \theta \frac{[2x_3(q_2 \cos \theta - q_3 \sin \theta) + q_2(q_2 + x_2 \sin \theta)]}{Q(Q+q_3+\xi)} - 3 \tan \theta \frac{(x_2-\xi_2)}{Q+x_3+\xi_3} + \\ & 2 \frac{(q_2 \cos \theta - q_3 \sin \theta - x_3 \sin^2 \theta)}{Q} + 4q_2 x_3 \sin \theta \frac{[(x_2-\xi_2) + q_3 \cos \theta]}{Q^3} - 4q_2^2 q_3 x_3 \sin^2 \theta \frac{(2Q+q_3+\xi)}{Q^3(Q+q_3+\xi)^2} \\ 12\pi \frac{u_3}{U_1} = & \cos \theta [\ln(R + r_3 - \xi) + (1 + 3 \tan^2 \theta) \ln(Q + q_3 + \xi) - 3 \tan \theta \sec \theta \ln(Q + x_3 + \xi_3) + \\ & \frac{2r_2 \sin \theta}{R} + 2 \sin \theta \frac{(q_2 + x_2 \sin \theta)}{Q} - \frac{2r_2^2 \cos \theta}{R(R+r_3-\xi)} + \frac{4q_2 \sin^2 \theta - 2(q_2 + x_2 \sin \theta)(x_3 + q_3 \sin \theta)}{Q(Q+q_3+\xi)} + \\ & 4q_2 x_3 \sin \theta \frac{[(x_3+\xi_3) - q_3 \sin \theta]}{Q^3} - 4q_2^2 q_3 x_3 \cos \theta \sin \theta \frac{(2Q+q_3+\xi)}{Q^3(Q+q_3+\xi)^2}] \end{aligned} \quad (15)$$

And for the dip-slip displacements,

$$12\pi \frac{u_1}{U} = (x_2 - \xi_2) \sin\theta \left[\frac{2}{R} + \frac{4}{Q} - 4 \frac{\xi_3 x_3}{Q^3} - \frac{3}{Q+x_3+\xi_3} \right] - \cos\theta [3 \ln(Q + x_3 + \xi_3) + 2 \frac{(x_3 - \xi_3)}{R} + 3 \ln(Q + x_3 + \xi_3) + 2 \frac{(x_3 - \xi_3)}{R}] + \frac{3}{\cos\theta} [\ln(Q + x_3 + \xi_3) - \sin\theta \ln(Q + q_3 + \xi)] + 6x_3 \left[\frac{\cos\theta}{Q} - \frac{q_2 \sin\theta}{Q(Q+q_3+\xi)} \right]$$

$$12\pi \frac{u_2}{U} = \sin\theta [-\ln(R + x_1 - \xi_1) + \ln(Q + x_1 - \xi_1) + \frac{4\xi_3 x_3}{Q(Q+x_1-\xi_1)} + \frac{3(x_1-\xi_1)}{Q+x_3+\xi_3} + (x_2 - \xi_2)^2 \left\{ \frac{2}{R(R+x_1-\xi_1)} + \frac{4}{Q(Q+x_1-\xi_1)} - 4\xi_3 x_3 \left(\frac{2Q+x_1-\xi_1}{Q^3(Q+x_1-\xi_1)^2} \right) \right\}] - \cos\theta [(x_2 - \xi_2) \left\{ \frac{2}{R(R+x_1-\xi_1)} + \frac{4}{Q(Q+x_1-\xi_1)} - 4\xi_3 x_3 \left(\frac{2Q+x_1-\xi_1}{Q^3(Q+x_1-\xi_1)^2} \right) \right\}] - \cos\theta [(x_2 - \xi_2) \left\{ \frac{2(x_3-\xi_3)}{R(R+x_1-\xi_1)} + \frac{4(x_3-\xi_3)}{Q(Q+x_1-\xi_1)} + 4\xi_3 x_3 \left(\frac{2Q+x_1-\xi_1}{Q^3(Q+x_1-\xi_1)^2} \right) \right\}] + 6 \tan^{-1} \left\{ \frac{(x_1-\xi_1)(x_2-\xi_2)}{(h+x_3+\xi_3)(Q+h)} \right\} - 3 \tan^{-1} \left\{ \frac{(x_1-\xi_1)(r_3-\xi)}{r_2 R} \right\} + 6 \tan^{-1} \left\{ \frac{(x_1-\xi_1)(q_3-\xi)}{q_2 Q} \right\}] + 6 \left[\frac{1}{\cos\theta} \tan^{-1} \left\{ \frac{(k-q_2 \cos\theta)(Q-k) + (\pm\xi)k \sin\theta}{(x_1-\xi_1)(q_3+\xi) \cos\theta} \right\} + x_3 \left\{ \frac{(\sin^2\theta - \cos^2\theta)(q_3-\xi) + 2q_2 \cos\theta \sin\theta}{Q(Q+x_1-\xi_1)} + \frac{(x_1-\xi_1) \sin^2\theta}{Q(Q+q_3+\xi)} \right\} \right]$$

$$12\pi \frac{u_3}{U} = \sin\theta [(x_2 - \xi_2) \left\{ \frac{2(x_3-\xi_3)}{R(R+x_1-\xi_1)} + 4 \frac{(x_3-\xi_3)}{Q(Q+x_1-\xi_1)} - 4\xi_3 x_3 (x_3 + \xi_3) \left(\frac{2Q+x_1-\xi_1}{Q^3(Q+x_1-\xi_1)^2} \right) \right\}] \left[-6 \tan^{-1} \left\{ \frac{(x_1-\xi_1)(x_2-\xi_2)}{(h+x_3+\xi_3)(Q+h)} \right\} + 3 \tan^{-1} \left\{ \frac{(x_1-\xi_1)(r_3-\xi)}{r_2 R} \right\} - 6 \tan^{-1} \left\{ \frac{(x_1-\xi_1)(q_3-\xi)}{q_2 Q} \right\} \right] + \cos\theta [\ln(R + x_1 - \xi_1) - \ln(Q + x_1 - \xi_1) - 2 \frac{(x_3-\xi_3)^2}{R(R+x_1-\xi_1)} + 4 \frac{(x_3-\xi_3)}{Q} - 4 \frac{\{(x_3-\xi_3)^2 - x_3 \xi_3\}}{Q(Q+x_1-\xi_1)} - 4\xi_3 x_3 (x_3 + \xi_3)^2 \left(\frac{2Q+x_1-\xi_1}{Q^3(Q+x_1-\xi_1)^2} \right)] + 6x_3 [\cos\theta \sin\theta \left\{ \frac{2(q_3+\xi)}{Q(Q+x_1-\xi_1)} + \frac{x_1-\xi_1}{Q(Q+q_3+\xi)} - q_2 \frac{\sin^2\theta - \cos^2\theta}{Q(Q+x_1-\xi_1)} \right\}] \quad (16)$$

It is important to note that these expressions are unable to evaluate a vertical dipping fault, which an angle value of $\theta = \frac{\pi}{2}$. In addition, there were some discussions about the conditions of terms and the limit, i.e. the expression gives the singular value, which was discussion in detailed by Mansinha & Smylie (1971).

For practical use, the script codes of Okada (1985) and Mansinha & Smylie (1971) are available in the FORTRAN programming language, and can be easily coupled to any tsunami numerical program. The Okada (1985) program is available and free to download via the link quoted by Wang et al. (2003), while Mansinha & Smylie's (1971) source code is available in the TUNAMI code.

The GITEWS project established the deformation model known as RuptGen. It was created in order to achieve a seafloor deformation model due to co-seismic slip at the Sunda trench. This tool employs the concept of 15 x 150 patches in the proximity of the trench, for both single- and multiple-rupture scenarios. It performs output for slip and surface deformation in various formats with an easy and flexible program input. It is used in particular for the initial tsunami source of the tsunami propagation model of TsunAWI (Babeyko, 2007).

2.3.1.b Earthquake Scaling Laws & fault Dimensions

The tsunami parent is located in sea areas by its excitation associated with catastrophic geophysical events, such as earthquakes, landslides and volcanic eruptions. And to model the respective tsunamigenic events, there are several unique parameters and processes that correspond to the related causes, i.e. earthquakes have generally been modeled successfully by double couples as mathematical representations derived from moment tensor. Other tsunamigenic events, such as submarine landslides could be mimicked by a long-period single horizontal force, and marine volcanic eruptions are even induced by more complex phenomena (Okal, 1988).

This study emphasizes tsunami numerical modeling generated by an earthquake; hence in this section the relevant issues related to the earthquake properties and the so-called earthquake scaling law are presented. In addition, for the demands of the deformation model input, which in turn will set the initial conditions for the numerical model, the empirical study relating to earthquakes and their characteristics, such as magnitude and rupture dimensions, will also be presented.

The earthquakes are a geophysical phenomenon causing a lot of damage and casualties; for this reason researchers have for a long time made tireless attempts to better understand their characteristics, particularly for large-scale earthquakes. However, this wish is yet to be achieved, since earthquakes of a sizeable scale are rare. Accordingly, researchers were more focused on evaluating the growth pattern of earthquakes, and examining and correlating the parameters relationship associated with the sources.

Figure 8 shows a comparison of the number of earthquakes with their magnitudes and energy releases, including those classified as major earthquake of $7 < M < 8$ which in general occur once or twice every year (Stein & Wyssession, 2003). An earthquake of such a magnitude occurring in the sea might inflict a low-to-medium-level tsunami, which happen on average once of a year, according to the recent historical tsunami records (Synolakis & Bernard, 2006)

The geophysical phenomena induced by earthquakes in terrain sometimes appeared, for instance, the earthquake in Imperial Valley in 1979 and in San Andreas in 1906 as depicted in Figure 9. Following that, their geometry dimensions, i.e. surface ruptures, can be measured; researchers then use these dimensions to correlate with other various parameters, especially the magnitude as recorded in seismographs.

Nowadays, sophisticated methods using real-time data derived from geodetic GPS arrays are able to provide precise crustal deformation measurements. It gives vertical and horizontal motion to cm or even mm accuracy during the inter- and co-seismic process of the earthquakes.

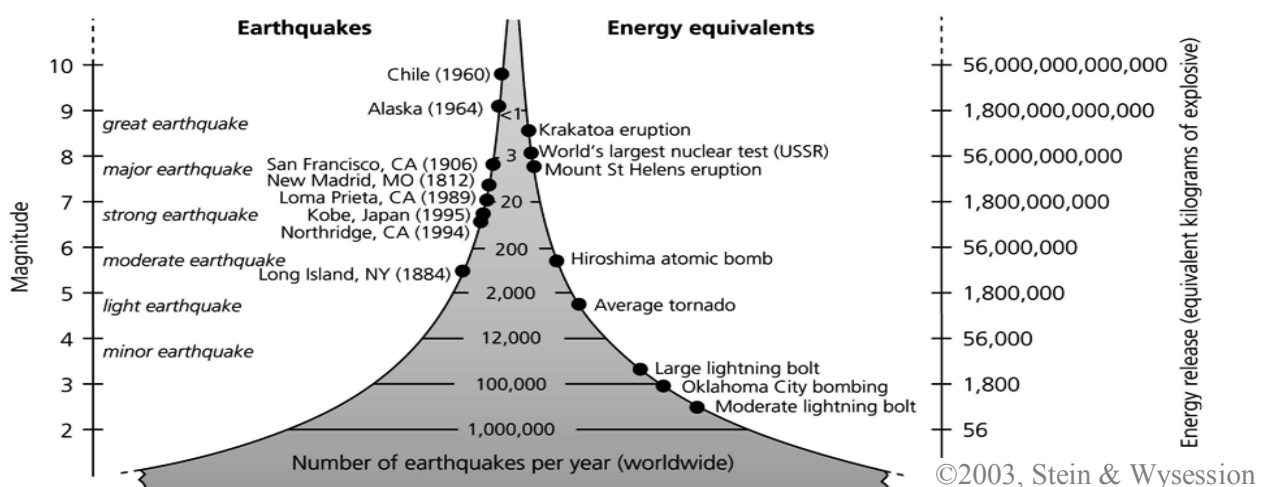


Figure 8: Comparison of frequency, magnitude, and energy release

An earthquake fault is expressed by a shear dislocation applied across a surface Σ in an elastic substance. This dislocation is equal to a double-couple distribution on the surface whose total seismic moment M_O is,

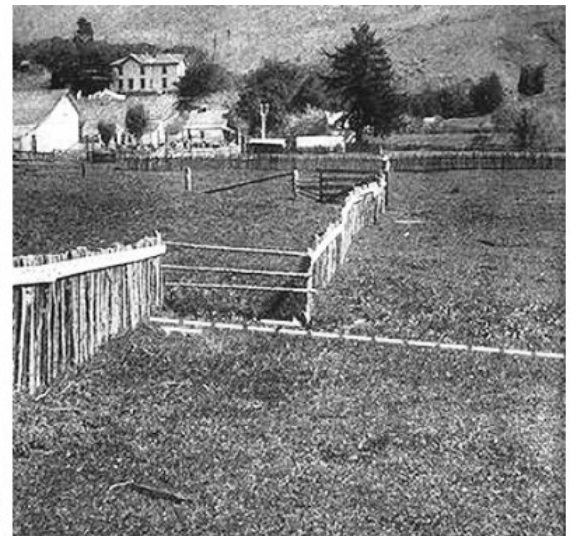
$$M_O = \mu S \Delta u = \mu L W \Delta u \quad (17)$$

where μ is the rigidity of the material, S is the area of Σ , and Δu is the average dislocation. Here, S can also be represented by L and W , which denote rupture length and width, respectively (Brune, 1968; Aki, 1966; Kanamori & Anderson, 1975; Wyss, 1979). Obtaining fault length L is sometimes possible following an earthquake rupture in the field, thus an estimation of rupture length can be achieved. The distribution of aftershocks is generally used to determine the extent of the rupture area of a major earthquake. These approaches also yield an estimate of the transverse dimension of width W (Okal, 2006).

Empirical evidence showed that the aforementioned parameters, namely S , Δu , L , and also W grow with earthquake size as represented by its seismic moment, M_O . Kanamori & Anderson (1975) summarized the data of 41 earthquakes, which are classified into two groups related to hypocenter, inter-plate and intra-plate, and plotted the relation between fault surface area of S and seismic moment of M_O . Beroza, G. in Okal (2006) proposed the relationship between Δu or D against the seismic moment of M_O and differentiated them by following the mechanism of events. The relationships between such parameters are plotted and depicted in Figure 10.



Source: <http://www.smate.wvu.edu/teched/geology/eq-CA-south.html>



Source: E. Okal, UNESCO-IOC Course, Oostende-Belgium, 2006

Figure 9: Imperial Valley, 1979 of $M \sim 6$ & San Andreas, 1906 of $M \sim 8$

Geller (1976), on the other hand, proposed an empirical relationship between fault length of L against fault width of W . A dataset of 41 moderate and large earthquakes was plotted with a considerable scatter result. He found an empirical relationship of fault rupture dimension of $L = 2W$ based on a dataset where earthquakes mainly occurred in the Pacific area.

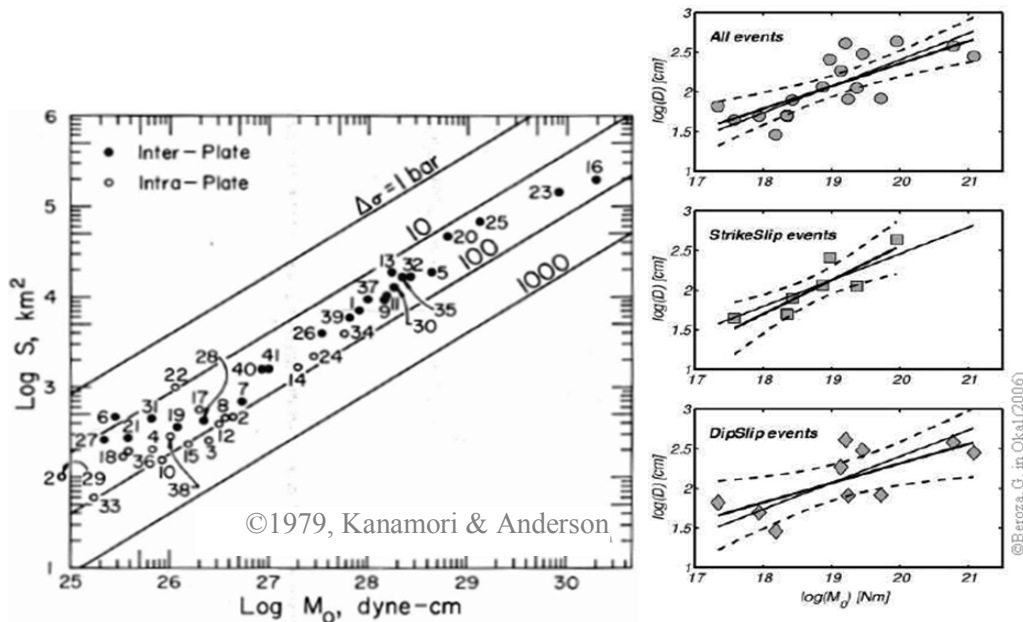


Figure 10: Relationship of the earthquake parameters S , D and M_o

Stein & Wyession (2003) provided the estimate of $M_o \sim L^3$ based on a plot dataset, which comprised events that occurred in inter-plate and strike-slip mechanisms. The plots from the studies by Geller (1976, left) and Stein & Wyession (2003, right) are shown in Figure 11.

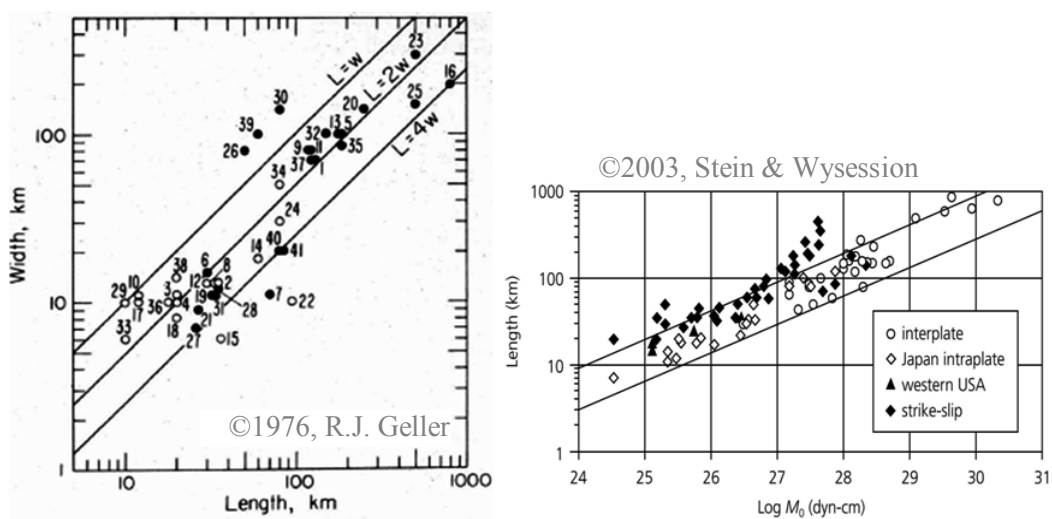


Figure 11: Relationship of the earthquake parameters W , L , and M_o

An extensive dataset of the seismic moment M_o and the other fault properties, such as fault surface area S , length L , and width W as compiled and plotted in several figures above, demonstrates remarkable relations between them, which verify that the parameters grow with the size of the earthquake. Hence, several simple ideas regarding earthquake scaling laws were summarized by Okal (2006) as follows:

1. As the source grows, the μ as the rigidity of the material should remain invariant,
2. As long as one of the parameters does not reach the physical limits of the seismic zone, the “shape” of the fault may remain constant. And the rupture can grow in all directions on the fault plane,
3. The rock cracks due to that have too-much accumulated strain ε , which is measured by the ratio of $\Delta u/L$ or $\Delta u/W$. Such ratios should also be invariants, and related to the strength of the rock, which ruptures at a certain, and might be the universal value of ε_{max} ,
4. Therefore, one predicts that the seismic moment M_o should grow as the cube of the linear size of the earthquake, which follows $M_o \sim L^3$ as its relation proposed by Stein and Wysession (2003).

Furthermore, in relation to an earthquake magnitude scale, Hanks & Kanamori (1979) introduced a moment magnitude scale M . The expression of the moment magnitude M may then be written as follows:

$$M = \frac{2}{3} \log M_o - 10.7 \quad (18)$$

where M is moment magnitude (or simply considered as M_w), and M_o is the seismic moment (in dyne.cm).

For practical use in tsunami modeling generated by earthquakes, relations between the fault parameters (L , W , and D), and the amount of energy released as represented by seismic moment M_o are essential. These parameters will be used as input in the deformation aforementioned model in the sub-section above to estimate earth surface displacement; the latter will be used for the initial condition of the tsunami model.

The most widely used empirical relationship among earthquake magnitudes and their fault parameters are the scaling relations developed by Wells & Coppersmith (1994). Through regression analysis, they used a worldwide database of source parameters for 244 earthquakes to derive relations between moment magnitudes M and rupture length L , rupture width W , rupture area A , and displacement D . They proposed three regressions tables of such

relations and producing nine pairs figures of log-log graphs that plotting moment magnitude versus each component of the rupture parameter above. For practical use in this study, however, the entire tables and graphs are not presented here; as required for this study, the author presents the table regression of rupture parameters (L , W , and A) and moment magnitude (M) in Appendix B – The scaling laws. Three figures of logarithmic graphs for relations between magnitude (M) and rupture parameters (L , W , and A) are presented here as shown in Figure 12.

Based on relations of rupture parameters and moment magnitude (M) such as the figures depicted in Figure 12, the empirical relationship for all events of earthquakes for respective geometric rupture parameters developed by Wells & Coppersmith (1994) may be written,

$$\begin{cases} M = 4.38 + 1.49 \log(RLD) \\ M = 4.06 + 2.25 \log(WID) \\ M = 4.07 + 0.98 \log(RA) \end{cases} \quad (19)$$

where RLD is subsurface rupture length (in km), WID is subsurface rupture width (in km), and RA is subsurface rupture area (in km^2).

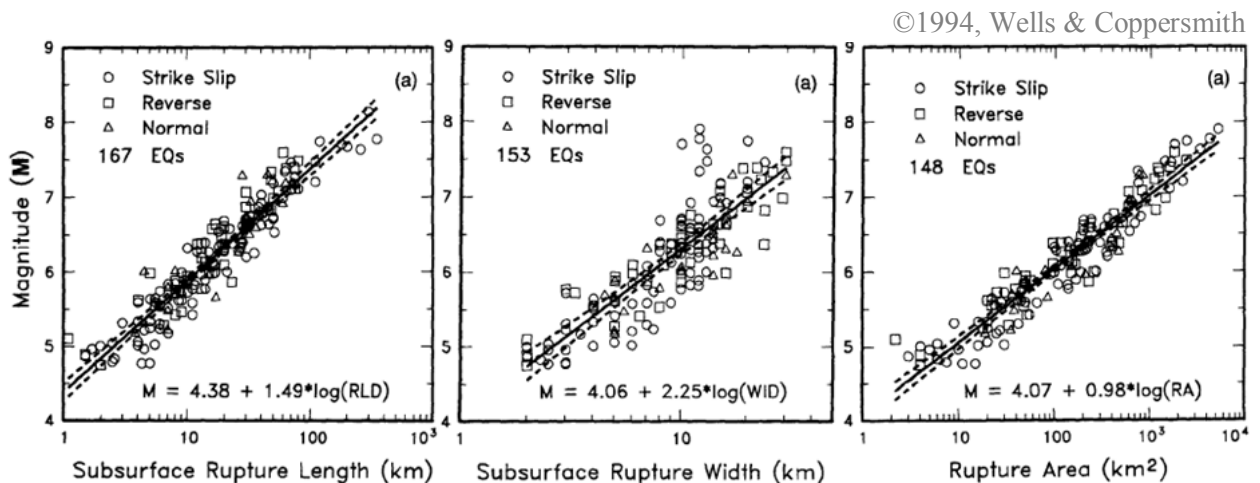


Figure 12: Regression of rupture length, width, area, and earthquake magnitude (M)

Papazachos et al. (2004) presented a paper dealing with global relations between fault parameters and moment magnitude of earthquakes that occurred in three seismotectonic regimes, namely strike-slip faults, dip-slip faults in continental regions, and dip-slip faults in regions of lithospheric subduction.

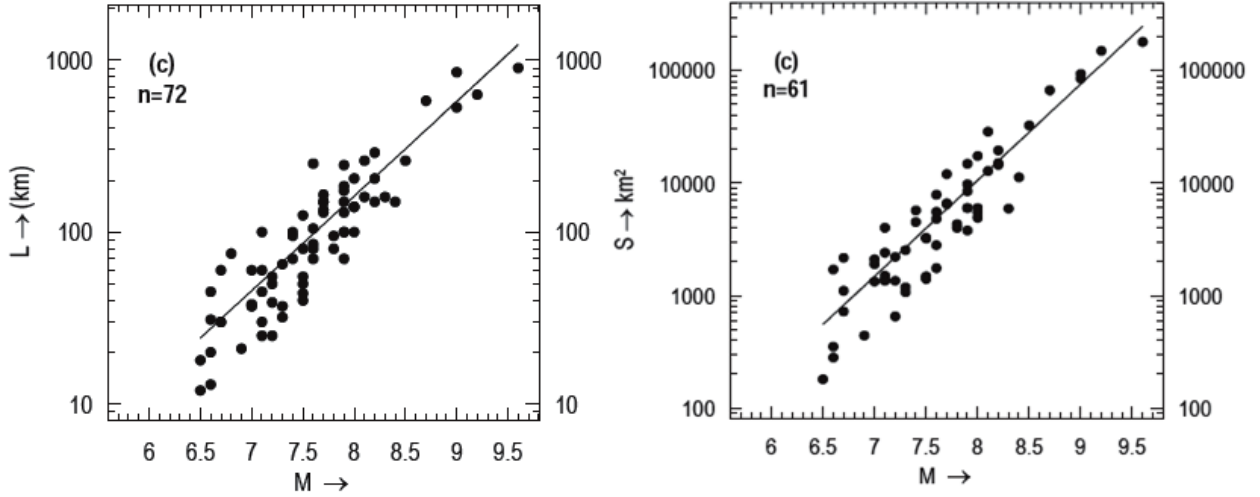


Figure 13: Regression of rupture parameters (L & S) with moment magnitude (M) for dip-slip in subduction zone

They classified 265 earthquakes into three classes: 116 strike-slip faults, 77 dip-slip faults in continental regions, and 72 dip-slip faults in subduction regions, which all correspond to strong earthquakes ($M \geq 5.8$). The author only presents here their regression graphs for earthquakes of dip-slip type in the subduction zones, which are of interest to this study, as shown in Figure 13.

The expressions that fit the data above are the following:

$$\begin{cases} \text{Log } L = 0.55M - 2.19, \sigma = 0.18, 6.7 \leq M \leq 9.3 \\ \text{Log } S = 0.86M - 2.82, \sigma = 0.25, 6.7 \leq M \leq 9.2 \\ \text{Log } W = 0.31M - 0.63 \\ \text{Log } u = 0.64M - 2.78 \end{cases} \quad (20)$$

where L is fault length (in km), S is fault area (in km²), M is moment magnitude, W is fault width that attained from S/L (in km), and u is average displacement (in cm) derived from Equations 17, 18, and 20.

Okal (2006) in his unpublished works as a handout delivered in UNUESCO-IOC Training in Oostende, Belgium proposed the relations between earthquake seismic moment and rupture dimensions for practical use in initial conditions for tsunami modeling. The relations are expressed below:

$$\begin{cases} L = \frac{M_O^{1/3}}{1.935 \cdot 10^7} \\ W = \frac{M_O^{1/3}}{3.87 \cdot 10^7} \\ D_u = \frac{M_O^{1/3}}{6.68 \cdot 10^8} \end{cases} \quad (21)$$

where L is faulting length (in km), W is faulting width (in km), M_O is the seismic moment (in N.m), and D_u is the average displacement (in m). For practical use, however, no further direction is given as to whether such expressions are suitable for earthquakes that occurred in certain conditions, such as the continental crust or subduction zone.

The most recent work related to the empirical relations between earthquake moment magnitude and their fault dimension parameters was conducted by Strasser et al. (2010). They derived regression relations based primarily on a database compiled by previous researchers, by separating them into two seismotectonic regimes: earthquakes that occurred in the interface and intraslab subduction zone. They classified the earthquakes that occurred at the contact between the subducting and the overriding plate into interface subduction zone earthquakes, and those that occurred within the subducting slab as intraslab events.

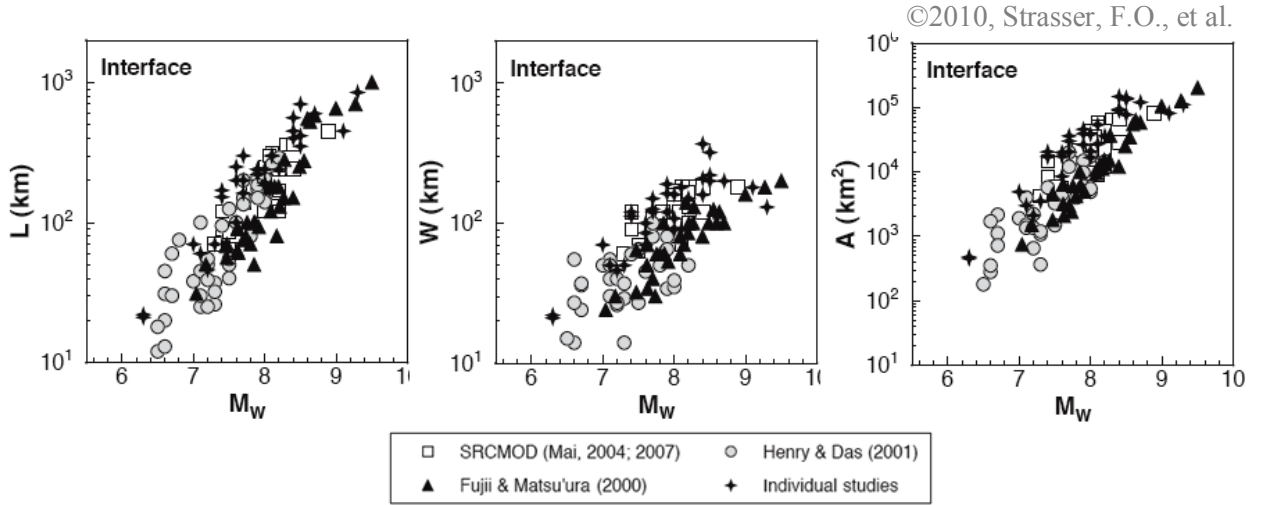


Figure 14: Dataset plot of rupture parameters with (M_w) for interface events

Figure 14 shows the plot of the dataset of earthquakes for all events that occurred in the interface subduction zone. The regressions derived from Figure 14 are expressed in Equation (22).

$$\begin{cases} M_W = 4.868 + 1.392 \text{ Log } L, \sigma = 0.28, N = 95 \\ M_W = 4.410 + 1.805 \text{ Log } W, \sigma = 0.39, N = 85 \\ M_W = 4.441 + 0.846 \text{ Log } A, \sigma = 0.29, N = 85 \end{cases} \quad (22)$$

where L is faulting length (in km), W is faulting width (in km), and M_w is earthquake moment magnitude. σ and N is the standard deviation and samples amount, respectively.

2.3.1.c Numerical Model

The numerical model of TUNAMI (Tohoku University's Numerical Analysis Model for Inundation) was initially developed in the late 1970s in Japan and was adopted in the 1990s by IOC-UNESCO under the TIME (Tsunami Inundation Modeling Exchange) project. Its source code, which had already been transferred to and applied in 43 institutions in 22 countries (Shuto & Fujima 2009), has been used in the present study. Therefore, this section briefly presents the governing equations, numerical scheme, initial and boundary conditions. The extensive discussion regarding to the TUNAMI model are provided in its manual (Imamura et al., 2006).

Tsunami is classified as a long wave due to the ratio of water depth to wave length being relatively small, whereby the vertical acceleration of water particles is negligible and the curvature of trajectories of water particle is small. Additionally, the horizontal velocity of water particles is vertically almost uniform. Based on those approximations, the motion of long waves is expressed well by shallow water theory, which is used as a governing equation in the numerical simulation.

The following shows the two-dimensional expression of the continuity equation and momentum equation in terms of discharge flux.

$$\left\{ \begin{array}{l} \frac{\partial \eta}{\partial t} + \frac{\partial M}{\partial x} + \frac{\partial N}{\partial y} = 0 \\ \frac{\partial M}{\partial t} + \frac{\partial}{\partial x} \left(\frac{M^2}{D} \right) + \frac{\partial}{\partial y} \left(\frac{MN}{D} \right) + gD \frac{\partial \eta}{\partial x} + \frac{gn^2}{D^{7/3}} M \sqrt{M^2 + N^2} = 0 \\ \frac{\partial N}{\partial t} + \frac{\partial}{\partial x} \left(\frac{MN}{D} \right) + \frac{\partial}{\partial y} \left(\frac{N^2}{D} \right) + gD \frac{\partial \eta}{\partial y} + \frac{gn^2}{D^{7/3}} N \sqrt{M^2 + N^2} = 0 \end{array} \right. \quad (23)$$

The above equations are the fundamental equations for shallow water motion used in this study, where η is the vertical displacement of water surface above still water level. $M = u(h + \eta)$ and $N = v(h + \eta)$ is the discharge fluxes for the x- and y-directions, u and v are the water particle velocities in the x and y direction respectively. The notation D is equal $(h + \eta)$ and the water depth is represented by h , and g is the gravitation acceleration.

The friction coefficient used is the Manning roughness as denoted by n , which is familiar to civil engineers'. The value of n is estimated by using the previous studies for channel (Arcement & Schneider 1984) and tsunami numerical models (Kotani et al. 1998),

assuming that the terrain in the simulation domain is farm land with the n value approximately 0.020. This value is smaller than those of study conducted by Harig et al. (2009) for the 2004 Sumatra-Andaman earthquake-tsunami, which is $n = 0.025$.

In this numerical simulation, the leap-frog scheme is used with a central difference scheme of the second-order truncation error to discrete the governing equations. The Cartesian diagram of the central difference is shown in Figure 15 below.

The central difference of the first-order derivative with the second-order truncation error $O(\Delta x^2)$ may be obtained from the difference between the two Taylor series expressions for F_{i-1} and F_{i+1} as the following:

$$\frac{\partial F}{\partial x} = \frac{1}{2\Delta x} [F_{i+1} - F_{i-1}] + O(\Delta x^2) \quad (24)$$

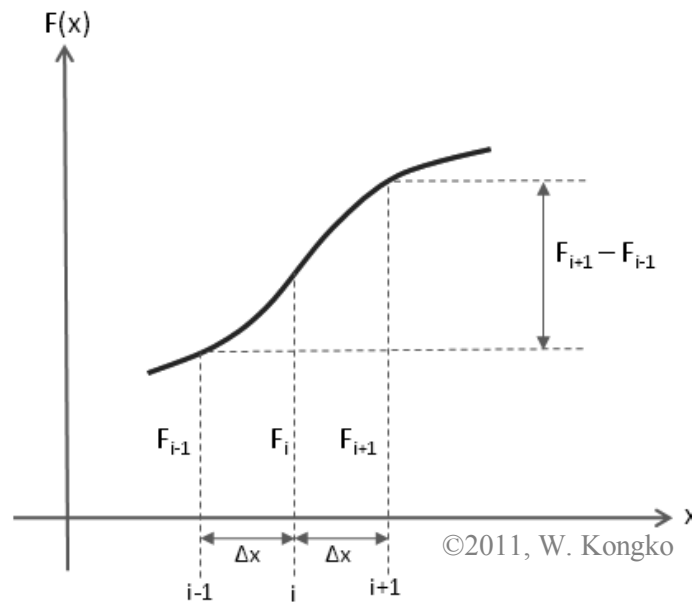


Figure 15: Central difference

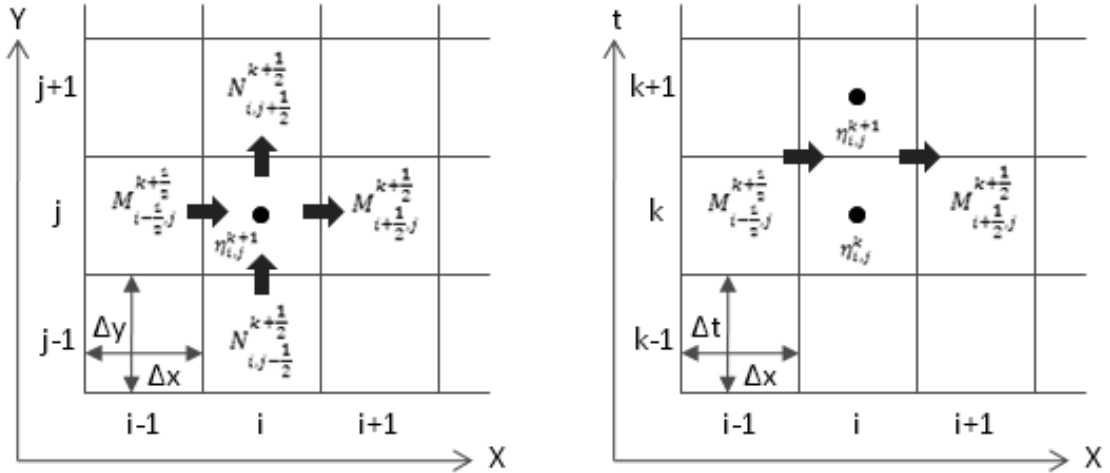
The leap-frog scheme is used in order to easily set the boundary conditions for η , M , and N as written in the first row of the continuity equation in (23). It assumes that the computation point for η does not coincide with M and N . The arrangement of points' computation for the leap-frog scheme is depicted in Figure 16.

The continuity equation in the first row in Equation (23) may be expressed as a difference equation using the central difference scheme as the following:

$$\begin{cases} \frac{\partial \eta}{\partial x} = \frac{1}{\Delta x} [\eta_{i,j}^{k+1} - \eta_{i,j}^k] \\ \frac{\partial M}{\partial x} = \frac{1}{\Delta x} \left[M_{i+\frac{1}{2},j}^{k+\frac{1}{2}} - M_{i-\frac{1}{2},j}^{k+\frac{1}{2}} \right] \\ \frac{\partial N}{\partial y} = \frac{1}{\Delta y} \left[N_{i,j+\frac{1}{2}}^{k+\frac{1}{2}} - N_{i,j-\frac{1}{2}}^{k+\frac{1}{2}} \right] \end{cases} \quad (25)$$

The values at the time step of k and $k + \frac{1}{2}$ are known; the unknown value of the difference equation in (25) is only $\eta_{i,j}^{k+1}$. Then solving the continuity equation by applying Equation (25) to the first row of Equation (23) yields

$$\eta_{i,j}^{k+1} = \eta_{i,j}^k - \frac{\Delta t}{\Delta x} \left[M_{i+\frac{1}{2},j}^{k+\frac{1}{2}} - M_{i-\frac{1}{2},j}^{k+\frac{1}{2}} \right] - \frac{\Delta t}{\Delta y} \left[N_{i,j+\frac{1}{2}}^{k+\frac{1}{2}} - N_{i,j-\frac{1}{2}}^{k+\frac{1}{2}} \right] \quad (26)$$



©2011, W. Kongko

Figure 16: The arrangement of points' computation for the leap-frog scheme

For the momentum equation in the second and third row in (23), their linear terms may be reduced to become,

$$\begin{cases} \frac{\partial M}{\partial t} + gD \frac{\partial \eta}{\partial x} = 0 \\ \frac{\partial N}{\partial t} + gD \frac{\partial \eta}{\partial y} = 0 \end{cases} \quad (27)$$

Furthermore, the momentum $M_{i+\frac{1}{2},j}^{k+\frac{1}{2}}$ and $N_{i,j+\frac{1}{2}}^{k+\frac{1}{2}}$ may be solved as the following:

$$\begin{cases} M_{i+\frac{1}{2},j}^{k+\frac{1}{2}} = M_{i+\frac{1}{2},j}^{k-\frac{1}{2}} - gD_{i+\frac{1}{2},j}^k \frac{\Delta t}{\Delta x} [\eta_{i+1,j}^k - \eta_{i,j}^k] \\ D_{i+\frac{1}{2},j}^k = h_{i+\frac{1}{2},j} + \eta_{i+\frac{1}{2},j}^k = h_{i+\frac{1}{2},j} + \frac{1}{2} [\eta_{i+1,j}^k + \eta_{i,j}^k] \end{cases} \quad (28)$$

$$\begin{cases} N_{i,j+\frac{1}{2}}^{k+\frac{1}{2}} = N_{i,j+\frac{1}{2}}^{k-\frac{1}{2}} - gD_{i,j+\frac{1}{2}}^k \frac{\Delta t}{\Delta y} [\eta_{i,j+1}^k - \eta_{i,j}^k] \\ D_{i,j+\frac{1}{2}}^k = h_{i,j+\frac{1}{2}} + \eta_{i,j+\frac{1}{2}}^k = h_{i,j+\frac{1}{2}} + \frac{1}{2} [\eta_{i,j+1}^k + \eta_{i,j}^k] \end{cases} \quad (29)$$

where h is the initial water depth below datum. Equations (26), (28), and (29) are the solutions for the linear long waves as usually applied for the tsunami propagation, excluding the run-up.

In order to keep the computation stable, the leap-frog scheme utilizes an upwind scheme in the convection terms. In the upwind scheme, the difference should be taken in the direction of flow. By doing so, the convection equation is always kept positive; this condition means the computation should be conducted in two ways, namely forward difference and backward difference. Therefore, the convection term as expressed in (23) will become,

$$\begin{cases} \frac{\partial}{\partial x} \left(\frac{M^2}{D} \right) = \frac{1}{\Delta x} \left[\lambda_{11} \frac{\left(M_{i+\frac{3}{2},j}^{k-\frac{1}{2}} \right)^2}{D_{i+\frac{3}{2},j}^{k-\frac{1}{2}}} + \lambda_{21} \frac{\left(M_{i+\frac{1}{2},j}^{k-\frac{1}{2}} \right)^2}{D_{i+\frac{1}{2},j}^{k-\frac{1}{2}}} + \lambda_{31} \frac{\left(M_{i-\frac{1}{2},j}^{k-\frac{1}{2}} \right)^2}{D_{i-\frac{1}{2},j}^{k-\frac{1}{2}}} \right] \\ \frac{\partial}{\partial y} \left(\frac{MN}{D} \right) = \frac{1}{\Delta y} \left[\nu_{11} \frac{M_{i+\frac{1}{2},j+1}^{k-\frac{1}{2}} N_{i+\frac{1}{2},j+1}^{k-\frac{1}{2}}}{D_{i+\frac{1}{2},j+1}^{k-\frac{1}{2}}} + \nu_{21} \frac{M_{i+\frac{1}{2},j}^{k-\frac{1}{2}} N_{i+\frac{1}{2},j}^{k-\frac{1}{2}}}{D_{i+\frac{1}{2},j}^{k-\frac{1}{2}}} + \nu_{31} \frac{M_{i+\frac{1}{2},j-1}^{k-\frac{1}{2}} N_{i+\frac{1}{2},j-1}^{k-\frac{1}{2}}}{D_{i+\frac{1}{2},j-1}^{k-\frac{1}{2}}} \right] \\ \frac{\partial}{\partial x} \left(\frac{MN}{D} \right) = \frac{1}{\Delta x} \left[\lambda_{12} \frac{M_{i+1,j+\frac{1}{2}}^{k-\frac{1}{2}} N_{i+1,j+\frac{1}{2}}^{k-\frac{1}{2}}}{D_{i+1,j+\frac{1}{2}}^{k-\frac{1}{2}}} + \lambda_{22} \frac{M_{i,j+\frac{1}{2}}^{k-\frac{1}{2}} N_{i,j+\frac{1}{2}}^{k-\frac{1}{2}}}{D_{i,j+\frac{1}{2}}^{k-\frac{1}{2}}} + \lambda_{32} \frac{M_{i-1,j+\frac{1}{2}}^{k-\frac{1}{2}} N_{i-1,j+\frac{1}{2}}^{k-\frac{1}{2}}}{D_{i-1,j+\frac{1}{2}}^{k-\frac{1}{2}}} \right] \\ \frac{\partial}{\partial y} \left(\frac{N^2}{D} \right) = \frac{1}{\Delta y} \left[\nu_{12} \frac{\left(N_{i,j+\frac{3}{2}}^{k-\frac{1}{2}} \right)^2}{D_{i,j+\frac{3}{2}}^{k-\frac{1}{2}}} + \nu_{22} \frac{\left(N_{i,j+\frac{1}{2}}^{k-\frac{1}{2}} \right)^2}{D_{i,j+\frac{1}{2}}^{k-\frac{1}{2}}} + \nu_{32} \frac{\left(N_{i,j-\frac{1}{2}}^{k-\frac{1}{2}} \right)^2}{D_{i,j-\frac{1}{2}}^{k-\frac{1}{2}}} \right] \end{cases} \quad (30)$$

Where,

$$\left\{ \begin{array}{l} M_{i+\frac{1}{2},j}^{k-\frac{1}{2}} \geq 0, \lambda_{11} = 0, \lambda_{21} = 1, \lambda_{31} = -1 \\ M_{i+\frac{1}{2},j}^{k-\frac{1}{2}} < 0, \lambda_{11} = 1, \lambda_{21} = -1, \lambda_{31} = 0 \\ N_{i+\frac{1}{2},j}^{k-\frac{1}{2}} \geq 0, \nu_{11} = 0, \nu_{21} = 1, \nu_{31} = -1 \\ N_{i+\frac{1}{2},j}^{k-\frac{1}{2}} < 0, \nu_{11} = 1, \nu_{21} = -1, \nu_{31} = 0 \end{array} \right. \quad (31)$$

$$\left\{ \begin{array}{l} M_{i,j+\frac{1}{2}}^{k-\frac{1}{2}} \geq 0, \lambda_{12} = 0, \lambda_{22} = 1, \lambda_{32} = -1 \\ M_{i,j+\frac{1}{2}}^{k-\frac{1}{2}} < 0, \lambda_{12} = 1, \lambda_{22} = -1, \lambda_{32} = 0 \\ N_{i,j+\frac{1}{2}}^{k-\frac{1}{2}} \geq 0, \nu_{12} = 0, \nu_{22} = 1, \nu_{32} = -1 \\ N_{i,j+\frac{1}{2}}^{k-\frac{1}{2}} < 0, \nu_{12} = 1, \nu_{22} = -1, \nu_{32} = 0 \end{array} \right. \quad (32)$$

Regarding to friction terms, they are discretized as follows:

$$\left\{ \begin{array}{l} \frac{gn^2}{D^{7/3}} M \sqrt{M^2 + N^2} = \frac{gn^2}{\left(D_{i+\frac{1}{2},j}^{k-\frac{1}{2}}\right)^{7/3}} \frac{1}{2} \left(M_{i+\frac{1}{2},j}^{k+\frac{1}{2}} + M_{i+\frac{1}{2},j}^{k-\frac{1}{2}} \right) \sqrt{\left(M_{i+\frac{1}{2},j}^{k-\frac{1}{2}} \right)^2 \left(N_{i+\frac{1}{2},j}^{k-\frac{1}{2}} \right)^2} \\ \frac{gn^2}{D^{7/3}} N \sqrt{M^2 + N^2} = \frac{gn^2}{\left(D_{i,j+\frac{1}{2}}^{k-\frac{1}{2}}\right)^{7/3}} \frac{1}{2} \left(N_{i,j+\frac{1}{2}}^{k+\frac{1}{2}} + N_{i,j+\frac{1}{2}}^{k-\frac{1}{2}} \right) \sqrt{\left(M_{i,j+\frac{1}{2}}^{k-\frac{1}{2}} \right)^2 \left(N_{i,j+\frac{1}{2}}^{k-\frac{1}{2}} \right)^2} \end{array} \right. \quad (33)$$

The differential equations in (23), can further be summarized as

$$\eta_{i,j}^{k+1} = \eta_{i,j}^k - \frac{\Delta t}{\Delta x} \left[M_{i+\frac{1}{2},j}^{k+\frac{1}{2}} - M_{i-\frac{1}{2},j}^{k+\frac{1}{2}} \right] - \frac{\Delta t}{\Delta y} \left[N_{i,j+\frac{1}{2}}^{k+\frac{1}{2}} - N_{i,j-\frac{1}{2}}^{k+\frac{1}{2}} \right] \quad (34)$$

$$\begin{aligned}
M_{i+\frac{1}{2},j}^{k+\frac{1}{2}} &= \frac{1}{1+\mu x_{i+\frac{1}{2},j}^{k-\frac{1}{2}}} \left[\left(1 - \mu x_{i+\frac{1}{2},j}^{k-\frac{1}{2}} \right) M_{i+\frac{1}{2},j}^{k-\frac{1}{2}} - \frac{\Delta t}{\Delta x} \left\{ \lambda_{11} \frac{\left(M_{i+\frac{3}{2},j}^{k-\frac{1}{2}} \right)^2}{D_{i+\frac{3}{2},j}^{k-\frac{1}{2}}} + \lambda_{21} \frac{\left(M_{i+\frac{1}{2},j}^{k-\frac{1}{2}} \right)^2}{D_{i+\frac{1}{2},j}^{k-\frac{1}{2}}} + \lambda_{31} \frac{\left(M_{i-\frac{1}{2},j}^{k-\frac{1}{2}} \right)^2}{D_{i-\frac{1}{2},j}^{k-\frac{1}{2}}} \right\} - \right. \\
&\quad \left. \frac{\Delta t}{\Delta y} \left\{ \nu_{11} \frac{M_{i+\frac{1}{2},j+1}^{k-\frac{1}{2}} N_{i+\frac{1}{2},j+1}^{k-\frac{1}{2}}}{D_{i+\frac{1}{2},j+1}^{k-\frac{1}{2}}} + \nu_{21} \frac{M_{i+\frac{1}{2},j}^{k-\frac{1}{2}} N_{i+\frac{1}{2},j}^{k-\frac{1}{2}}}{D_{i+\frac{1}{2},j}^{k-\frac{1}{2}}} + \nu_{31} \frac{M_{i+\frac{1}{2},j-1}^{k-\frac{1}{2}} N_{i+\frac{1}{2},j-1}^{k-\frac{1}{2}}}{D_{i+\frac{1}{2},j-1}^{k-\frac{1}{2}}} \right\} - g D_{i+\frac{1}{2},j}^k \frac{\Delta t}{\Delta x} \{ \eta_{i+1,j}^k - \eta_{i,j}^k \} \right]
\end{aligned} \tag{35}$$

$$\begin{aligned}
N_{i,j+\frac{1}{2}}^{k+\frac{1}{2}} &= \frac{1}{1+\mu y_{i,j+\frac{1}{2}}^{k-\frac{1}{2}}} \left[\left(1 - \mu y_{i,j+\frac{1}{2}}^{k-\frac{1}{2}} \right) N_{i,j+\frac{1}{2}}^{k-\frac{1}{2}} - \frac{\Delta t}{\Delta y} \left\{ \nu_{12} \frac{\left(N_{i,j+\frac{3}{2}}^{k-\frac{1}{2}} \right)^2}{D_{i,j+\frac{3}{2}}^{k-\frac{1}{2}}} + \nu_{22} \frac{\left(N_{i,j+\frac{1}{2}}^{k-\frac{1}{2}} \right)^2}{D_{i,j+\frac{1}{2}}^{k-\frac{1}{2}}} + \nu_{32} \frac{\left(N_{i,j-\frac{1}{2}}^{k-\frac{1}{2}} \right)^2}{D_{i,j-\frac{1}{2}}^{k-\frac{1}{2}}} \right\} - \right. \\
&\quad \left. \frac{\Delta t}{\Delta x} \left\{ \lambda_{12} \frac{M_{i+1,j+\frac{1}{2}}^{k-\frac{1}{2}} N_{i+1,j+\frac{1}{2}}^{k-\frac{1}{2}}}{D_{i+1,j+\frac{1}{2}}^{k-\frac{1}{2}}} + \lambda_{22} \frac{M_{i,j+\frac{1}{2}}^{k-\frac{1}{2}} N_{i,j+\frac{1}{2}}^{k-\frac{1}{2}}}{D_{i,j+\frac{1}{2}}^{k-\frac{1}{2}}} + \lambda_{32} \frac{M_{i-1,j+\frac{1}{2}}^{k-\frac{1}{2}} N_{i-1,j+\frac{1}{2}}^{k-\frac{1}{2}}}{D_{i-1,j+\frac{1}{2}}^{k-\frac{1}{2}}} \right\} - g D_{i,j+\frac{1}{2}}^k \frac{\Delta t}{\Delta y} \{ \eta_{i,j+1}^k - \eta_{i,j}^k \} \right]
\end{aligned} \tag{36}$$

where,

$$\begin{cases} \mu x_{i+\frac{1}{2},j}^{k-\frac{1}{2}} = \frac{\Delta t}{2} \frac{gn^2}{\left(D_{i+\frac{1}{2},j}^{k-\frac{1}{2}} \right)^{7/3}} \sqrt{\left(M_{i+\frac{1}{2},j}^{k-\frac{1}{2}} \right)^2 \left(N_{i+\frac{1}{2},j}^{k-\frac{1}{2}} \right)^2} \\ \mu y_{i,j+\frac{1}{2}}^{k-\frac{1}{2}} = \frac{\Delta t}{2} \frac{gn^2}{\left(D_{i,j+\frac{1}{2}}^{k-\frac{1}{2}} \right)^{7/3}} \sqrt{\left(M_{i,j+\frac{1}{2}}^{k-\frac{1}{2}} \right)^2 \left(N_{i,j+\frac{1}{2}}^{k-\frac{1}{2}} \right)^2} \end{cases} \tag{37}$$

$$\begin{cases} D_{i+\frac{1}{2},j}^k = \frac{1}{2} (D_{i+1,j}^k + D_{i,j}^k) = \frac{1}{2} (\eta_{i+1,j}^k + \eta_{i,j}^k) + h_{i+\frac{1}{2},j} \\ D_{i,j+\frac{1}{2}}^k = \frac{1}{2} (D_{i,j+1}^k + D_{i,j}^k) = \frac{1}{2} (\eta_{i,j+1}^k + \eta_{i,j}^k) + h_{i,j+\frac{1}{2}} \\ D_{i+\frac{1}{2},j}^{k-\frac{1}{2}} = \frac{1}{4} (D_{i+1,j}^k + D_{i+1,j}^{k-1} + D_{i,j}^k + D_{i,j}^{k-1}) = \frac{1}{4} (\eta_{i+1,j}^k + \eta_{i+1,j}^{k-1} + \eta_{i,j}^k + \eta_{i,j}^{k-1}) + h_{i+\frac{1}{2},j} \\ D_{i,j+\frac{1}{2}}^{k-\frac{1}{2}} = \frac{1}{4} (D_{i,j+1}^k + D_{i,j+1}^{k-1} + D_{i,j}^k + D_{i,j}^{k-1}) = \frac{1}{4} (\eta_{i,j+1}^k + \eta_{i,j+1}^{k-1} + \eta_{i,j}^k + \eta_{i,j}^{k-1}) + h_{i,j+\frac{1}{2}} \end{cases} \tag{38}$$

The values of λ and ν are given as equations in (31) and (32).

For practical use in tsunami mitigation, the numerical model has been used to estimate the influence of coastal vegetation on reducing the impact of tsunamis. In the present study, the author adopts the experimental study on the resistance by mangroves under unsteady flow conducted by Harada & Imamura (2000). The Morison equation in (39) initially used to estimate the force distribution exerted on piles due to surface waves, has been coupled with the momentum equation in (23).

$$F = F_D + F_I = C_D \frac{\rho}{2} A_O u |u| + C_M \rho \frac{\partial u}{\partial t} \quad (39)$$

where F is the total force, F_D is the drag force, and F_I is the inertia force. C_D is the drag coefficient, and C_M is the mass coefficient. The fluid density is represented by ρ , and A_O is the projected area of the resistance medium in the flow direction, V_O is the volume of the resistance medium and u is the particle velocity. By applying such an expression in (39), the momentum equation in the second and third row in (23) is then expressed as,

$$\begin{cases} \frac{\partial M}{\partial t} + \frac{\partial}{\partial x} \left(\frac{M^2}{D} \right) + \frac{\partial}{\partial y} \left(\frac{MN}{D} \right) + gD \frac{\partial \eta}{\partial x} + \frac{gn^2}{D^{7/3}} M \sqrt{M^2 + N^2} + \frac{C_D}{2} \frac{A_O}{\Delta x \Delta y} \frac{M|M|}{D^2} + C_M \frac{V_O}{V} \frac{\partial M}{\partial t} = 0 \\ \frac{\partial N}{\partial t} + \frac{\partial}{\partial x} \left(\frac{MN}{D} \right) + \frac{\partial}{\partial y} \left(\frac{N^2}{D} \right) + gD \frac{\partial \eta}{\partial y} + \frac{gn^2}{D^{7/3}} N \sqrt{M^2 + N^2} + \frac{C_D}{2} \frac{A_O}{\Delta x \Delta y} \frac{N|N|}{D^2} + C_M \frac{V_O}{V} \frac{\partial N}{\partial t} = 0 \end{cases} \quad (40)$$

Furthermore, Equations (34), (35), and (36) remain similar. However Equation (37) should impose the Morison term and become,

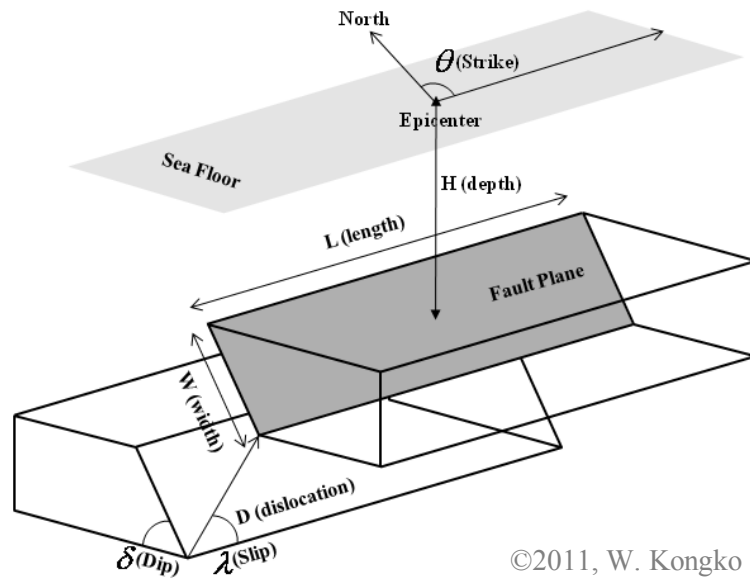
$$\begin{cases} \mu x_{i+\frac{1}{2},j}^{k-\frac{1}{2}} = \frac{\Delta t}{2} \left[\frac{gn^2}{\left(D_{i+\frac{1}{2},j}^{k-\frac{1}{2}} \right)^{7/3}} + \frac{C_D A}{2 \left(D_{i+\frac{1}{2},j}^{k-\frac{1}{2}} \right)^2} \right] \sqrt{\left(M_{i+\frac{1}{2},j}^{k-\frac{1}{2}} \right)^2 \left(N_{i+\frac{1}{2},j}^{k-\frac{1}{2}} \right)^2} + C_M \frac{V_O}{V} \Delta t \\ \mu y_{i,j+\frac{1}{2}}^{k-\frac{1}{2}} = \frac{\Delta t}{2} \left[\frac{gn^2}{\left(D_{i,j+\frac{1}{2}}^{k-\frac{1}{2}} \right)^{7/3}} + \frac{C_D A}{2 \left(D_{i,j+\frac{1}{2}}^{k-\frac{1}{2}} \right)^2} \right] \sqrt{\left(M_{i,j+\frac{1}{2}}^{k-\frac{1}{2}} \right)^2 \left(N_{i,j+\frac{1}{2}}^{k-\frac{1}{2}} \right)^2} + C_M \frac{V_O}{V} \Delta t \end{cases} \quad (41)$$

The initial conditions are given for momentum fluxes M , N , and water level η . Since only a tsunami is considered in this present model, no wind waves and tides are included. However, when tides are applied, a constant value for them is imposed throughout the entire time simulation. The initial conditions in the wet region is,

$$\begin{cases} \eta_{i,j}^{k-1} = 0 \\ M_{i+\frac{1}{2},j}^{k-\frac{1}{2}} = 0 \\ N_{i,j+\frac{1}{2}}^{k-\frac{1}{2}} = 0 \end{cases} \quad (42)$$

while in the dry area, the initial water level η is set equal to ground level $h_{i,j}$, the sign of whose value is negative.

The tsunami source in the TUNAMI model uses a static source by simply putting the co-seismic vertical displacement at the ground surface produced from the deformation model into the sea surface. Figure 17 is a simplified diagram of subducting and overriding slab, fault plane and their parameters, which are required as input for the deformation model mentioned above.



©2011, W. Kongko

Figure 17: The diagram of earthquake and fault parameters

The earthquake parameters consist of angle parameters, such as the dip δ , slip λ , and strike θ , and the fault parameters are fault length L , width W , dislocation D , and the focal depth H . These seven parameters are required as input for the deformation model.

The boundary conditions are divided into open boundary conditions and run-up front boundary conditions. There are three types of open boundary conditions offshore, namely

those for the simple harmonic wave's train, forced input and free transmission. The run-up front boundary has two types: the boundary conditions at run-up fronts and those when water overflow structures also well known as moving boundary conditions.

The present study will only provide the run-up front boundary conditions. The other boundary conditions, however, were extensively discussed in the tsunami modeling manual by Imamura et al. (2006).

The run-up modeling is carried out through nonlinear computations and the judgment of the computational domain, regardless of whether a cell is dry or submerged, by evaluating the value of parameter D . The logical condition is, when $D = h + \eta > 0$, then the cell is submerged, otherwise the cell is dry.

The wave front is situated at the boundaries between the dry and submerged cells (see Figure 18), and the water discharges are applied if the ground level in the dry cell is lower than the water level in the submerged cell. Inversely, the water discharge is considered nil.

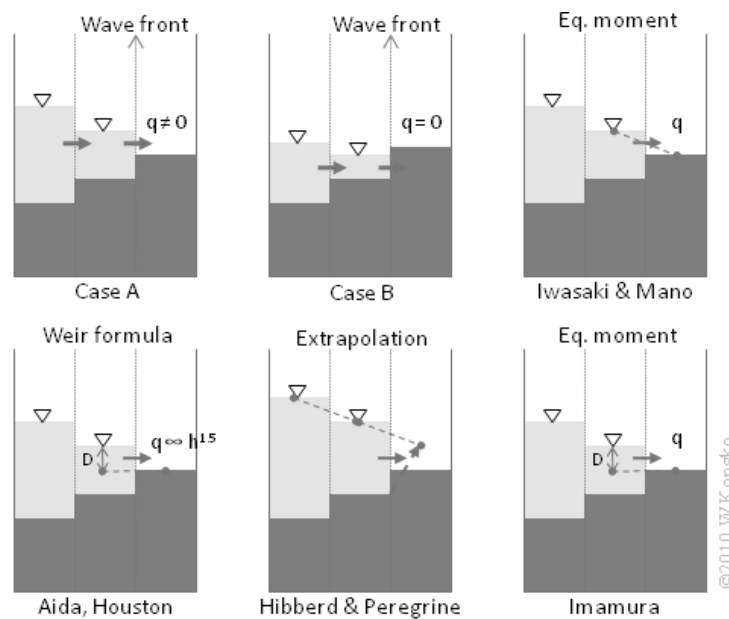


Figure 18: Various moving boundary conditions at a wave front

Referring to the tsunami model manual by Imamura (2006) and Imamura (2009), there are several approximations for moving boundary condition such as those in the diagrams shown in Figure 18. Iwasaki & Mano (1979) assumed that the line connecting the water and ground surface at the wave front gives its slope a first-order approximation, while Hibberd & Peregrine (1979) proposed the provisional water level in the dry cell derived from the extrapolation of the backward water surface. Aida (1977) and Houston & Butler (1979)

approximated the water discharge onto the dry cell with broad-crested weir formulas, and Imamura (1996) evaluated directly by applying the momentum equation, keeping the total depth on the “first” dry cell at zero.

The tsunami source is located offshore in the deep and open sea, where the boundary conditions can accurately and easily be set up. Furthermore, to be more economic and save CPU time, proper computations are strongly recommended by utilizing the linear and non-linear theories in accordance with the applied physical phenomena. Hence, the coarse grids may be applied in the open and deep sea and the finer grids in the near-shore zone; this method is called the nested grid computational domain. This requires the continuation of computation at the boundary of regions of different spatial grid lengths.

It should be noted that to maintain stability of the two-dimensional numerical computation, the C.F.L condition should be satisfied like in the expression below:

$$\sqrt{2gh} < \frac{\Delta x}{\Delta t} \quad (43)$$

where g is gravity acceleration, h is water depth, Δx and Δt is the temporal and spatial grids respectively.

In the deep and open sea, where the linear theory is used, the continuation of computation at boundaries between domains that have different spatial grid lengths can be achieved by adjusting Δx and keeping Δt constant, so that the C.F.L condition in (43) is still fulfilled. However, approaching the near-shore zone where the water depth h becomes smaller, inevitably requires setting the temporal grids Δt properly.

The extensive discussion on the continuation of regions for both the different temporal and spatial grids in the nested computational domain in the TUNAMI model were provided in the manual by Imamura (2006) and will not be given in this document.

2.3.2 Hypotheses

This section describes the hypotheses, which explain the facts or observations conducted by the author and previous researchers related to the aforementioned problems and all related aspects that have important roles in the focus of this study.

It includes the influence of the rigidity as a material property that controls behavior in the source zone, and the geometric source such as fault dimension, orientation, and slip distribution. Two other pre-assumption will also be proposed that may have links to the extraordinary tsunami run-up being highlighted in this study, namely the sensitivity model

due to geometric data uncertainties, and other tsunamigenic events associated with the earthquake, such as submarine landslides.

2.3.2.a Influence of the rigidity material

The Java tsunami is classified as tsunami earthquakes characterized mainly by a large slip for a given seismic moment and slow rupture speed. It occurred at shallow depths in regions of low rigidity in the subduction zone (Hanifa et al., 2007; Bilek & Engdahl, 2007; Kopp et al., 2006; Ammon et al., 2006; Polet & Thio 2003; Abercrombie et al. 2001).

According to Scholtz, C. (1990) in Bilek & Lay (1999), Bilek & Lay (1999), and Lay & Bilek (2007), the rock and sediment properties in the proximity of the plate interface play an important role in controlling the frictional fault's behavior and its rupture dynamics. One of the important properties here is the rigidity material, which has variations in depth.

By looking at the standard definitions of the seismic moment (M_0) as the expression in (17), the relations among the parameters can obviously be qualitatively estimated, where by reducing the value of the rigidity (μ) will be increasing the average displacement (Δu) or D , assuming that the other parameters remain constant.

Since only a few tsunami earthquakes have occurred, extensive studies of such types of event by varying the fault dimension and its rigidity and comparing the model results with field observations are rare. The author found such a study conducted by Satake (1994) evaluating the Nicaragua tsunami earthquake that happened in 1992. The Nicaragua tsunami is likely comparable to the 2006 Java tsunami in terms of tsunami class, i.e. tsunami earthquake, the level of a seismic moment, the low rigidity may be involved in the seismic process, and so on.

Therefore, this study proposes the pre-assumption that the Java tsunami is most likely similar to such an event as described above, and thus the low-rigidity material in the subduction zone has an important role in this seismic rupture process, manifested by an around threefold bigger tsunami run-up along the coastline than a normal tsunami.

2.3.2.b Influence of the fault type and slip distribution

The 2006 Java tsunami was originated in the Java subduction zone, offshore of Java Island with a distance from the epicenter of about 180 km. Hence, it may be classified as a near-field tsunami or local tsunami.

Several previous studies discussing the far-near field tsunami in relation to the seismic moment, focal mechanism, depth, fault parameters, and tsunami size were conducted. In

general their findings in regard to far-field tsunamis were that the primary parameter is the seismic moment M_0 , which grows directly proportional to M_0 , and has little influence on the focal mechanism and depth (Okal, 1988). In contrast, for near-field tsunami, the rupture complexity such as the fault dimension, slip distribution patterns, and low shear modulus or rigidity has an important effect on the tsunami waveform along the coast (Geist & Dmowska, 1999; Geist, 2002; Behrens et al., 2010).

In this study, the author has made a pre-assumption that the correlation between the tsunami waveform along the coast and the variation of fault types as well as the slip distribution in the source zone is significant. Especially, the slip distribution along the strike direction at source has a strong influence on the distribution of tsunami run-up height along the coastline. However, the precise sensitivity of the variability tsunami amplitudes with the distance of the epicenter to the coastline is still unknown. In general, a greater distance is less sensitive to the tsunami waveforms and its amplitudes.

2.3.2.c Other tsunamigenic sources

The Java tsunami still poses opens question to scientists. It qualified as a tsunami earthquake and had signs comparable to those that occurred in other places, such as in Nicaragua in 1992, showed characteristics of slow rupture duration like those that occurred in the subduction zone, and generated a higher tsunami for the given seismic moment. However, the 2006 Java tsunami had extraordinary run-up heights along a short segment as reported by ITST as mentioned earlier in section 1.3, which led to a speculation among researchers as to whether it was triggered by a landslide.

In discriminating whether a landslide or seismic activity induced the extreme run-up for the near-field tsunami in Java, the present study uses a method developed by Okal & Synolakis (2004). By evaluating the physical nature of the distribution of run-up amplitudes along a coastline our pre-assumption for the Java event is not triggered solely by a single source of landslides. Yet, it is possible that an earthquake occurred and was subsequently followed by the landslide.

2.3.3 Questions

This study has two main questions: By using the available geo-data and the established tsunami model tool, is the numerical simulation for the Java tsunami resulting from the model capable of producing the run-up heights along the coastline that are comparable to and agree with the field observation data collected? What are the factors as

well as the parameter inputs that play a significant role adjusting the model above and how can they be applied for similar events in future?

The following questions are derived from the above hypotheses:

1. If rigidity has a significant role in the tsunami run-up along the south coast of Java, what is the approximation value of the shear modulus in the source zone that gives a suitable average co-seismic slip that fits to the field data?
2. Among the source parameters, i.e. the fault dimensions, single-fault model, multi-fault model, and finite-fault model, which one of the tsunami run-up resulting from the model has a good agreement with the field observation data and what is the relation between the relevant factors mentioned above?
3. In regard to discriminating whether seismic dislocations or landslides induced the Java tsunami, what are the quantities of the discriminant values and what do the curves look like? What interpretation can be concluded from the data plotting? What is the cause of the extraordinary run-up that occurred in a short segment in Cilacap?

2.4 Limitation of the Study

In this sub-chapter, the limitation of the study is given. It includes the scope of the study, the geo-data resolution, and the tsunami source and seismic gap.

2.4.1 Scope of the study

The Java tsunami model uses highly resolved data and probable tsunamigenic events to estimate and validate the run-up and distribution along the coastline, which include the tsunami generation, propagation, and run-up. Therefore, this study will describe the earthquake scaling laws, the deformation model, the NLSW numerical model, the techniques for model validation, and the data collection of topography and bathymetry. Due to time and space constraints, this study will not discuss in detail each element above. Although the fundamental theories and empirical approaches are briefly provided and used, for further details the reader may refer to the corresponding references.

This study emphasizes the model validation for the 2006 Java tsunami, and the probable significant factors that may be involved in the seismic process that led to the extraordinary run-up heights. The findings may proof and support the assumptions by previous researchers in regard to the seismic process in the subduction zone and the behavior

of near-field tsunamis. Further, the significant factors at source that influence the tsunami run-up and its distribution along the coastline are also assessed.

2.4.2 Geo-data resolution

In this study, the geo-data for the numerical model are prepared by assimilating various data with different resolutions. Highly resolved bathymetric and topography data are present for the study area, i.e. Cilacap, while beyond this boundary, data of low-medium resolution are the only data available. Therefore, only in this study area can the inundation model validation be conducted.

Furthermore, to validate the model for the travel time of the 2006 Java tsunami, three tsunami mareograms available from the tide gauge network on the south coast of Java have been used. However, all the datasets were acquired in semi-closed channel ports or bays leading to unpredictable tsunami amplitudes due to local oscillations. Thus, only the first or second wave of the incoming tsunami will be considered.

2.4.3 Tsunami source & seismic gap

The tsunami sources are earthquakes whose double-couple force is considered, thus other tsunamigenic events for generating a source for initial conditions, i.e. submarine landslides, are beyond the scope of the present study. The tsunami source is generated using empirical scaling law models, an inversion model from tide gauges and a broadband seismic network of finite-fault models, multi-faults models proposed by other researchers, and a combination of both by adjusting the dominant factor involved in the seismic process as proposed by the author.

There is seismic gap in the Java subduction zone, the location of which is between the two seismicity clusters of the earthquakes that happened in 1994 and 2006. However, in the present study which attempts to model the tsunami that originated from this area, a detailed discussion has not been made due to an absence of the relevant data.

2.5 Definition of Terms

The definition of terms contains an alphabetical listing of terms includes abbreviations, acronyms, and a glossary containing only initial letters or a combination of names of letters, and a word at the initial paragraph followed by the definitions.

The terms listed are those that are mostly used in coastal engineering, geology, oceanography, and applied mathematics. This definition of terms refers to the tsunami

glossary by the UNESCO-IOC (2006), the glossary of geology by the American Geological Institute², and various other internet-based sources, such as Wikipedia³.

The detailed listing of terms used in this study is listed in Appendix I.

2.6 Summary

The study of the Java tsunami is greatly demanded given that this area poses a high potential hazard due to its proximity to the subduction zone. The deadly 2006 Java tsunami dealt out a harsh lesson that dense habitations in low-lying coastal zones, e.g., Cilacap, are the area most vulnerable from a tsunami.

The Java tsunami is qualified as a tsunami earthquake and its behaviors have been documented and identified through previous studies, yet it remains something of a puzzle, primarily due to the disparities of the impact in land between the run-up height along the coastline and numerical simulation result.

Particular problems are the absence of high-resolution geo-data and the complex tsunami source; the latter is associated with the fault parameters, seismic processes and its material. Furthermore, a near-field tsunami, like those in the Java subduction zone, leads to the run-up heights along the coastline that are strongly affected by the fault parameters and slip distribution.

Solving the aforementioned problems and discussing relevant issues, for instance like in the present study by a numerical simulation that was validated using extensive data, would make a great contribution to the knowledge of tsunamis, particularly in fields of seismology and coastal engineering, and moreover for practical use, namely supporting the tsunami mitigation program by determining a reliable inundation map for the affected area for use for similar events in the future.

² <http://www.agiweb.org/pubs/glossary/#>

³ http://en.wikipedia.org/wiki/Main_Page

Chapter 3 - Review of the Literature

*“Scientists still do not appear to understand sufficiently that all earth sciences must contribute evidence toward unveiling the state of our planet in earlier times, and that the truth of the matter can only be reached by combing all this evidence. ... It is only by combing the information furnished by all the earth sciences that we can hope to determine 'truth' here, that is to say, to find the picture that sets out all the known facts in the best arrangement and that therefore has the highest degree of probability. Further, we have to be prepared always for the possibility that each new discovery, no matter what science furnishes it, may modify the conclusions we draw” (Alfred L. Wegener, 1880-1930 AD, *The Origins of Continents and Oceans*).*

This chapter reviews the literature that is relevant to this study, and is divided into four sub-chapters, namely the overview of the past research, the review & critique of the research, the contribution of the present study, and summary. The overview of the research will encompass the quantification of earthquakes and tsunami earthquakes, tsunamigenic events in the subduction zone and local tsunamis, and a numerical model. Before closing with the contribution of the study and a summary, the sub-chapter for the review & critique of the research be address the characteristic tsunami earthquake and rigidity variations, the heterogeneous slip and fault dimension, and the tsunami model.

3.1 Overview of the Researches

This sub-chapter describes the overview of the relevant researches, which consist of the issues relating to the quantification of the earthquake and their relations. Further, the topics of tsunamigenic events in the subduction zone and local tsunamis are also presented. The numerical model will be described briefly at the end of this sub-chapter.

3.1.1 Quantification of earthquake & tsunami earthquake

3.1.1.a Quantification & its relations of earthquake

The magnitude scales are fundamental parameters in seismology engineering for quantifying earthquakes. Due to there being various types of measurement apparatus, earthquake focal mechanisms, and levels of seismicity, several magnitude scales inevitably exist which are used in different regions.

Richter (1935) defined a M_L , which is basically a local magnitude for southern California using the maximum amplitude of seismic waves with the period of 0.1 to 2 s as recorded by the Wood-Anderson seismograph. This is an empirical scale without any correlation with the physical parameters of the earthquake source. However, this scale is

defined in the period range where its effect of seismic waves on infrastructures is most pronounced; therefore, it is good for measuring the strength of ground shaking at a given distance and is very useful for practical engineering purposes (Richter, 1935; Kanamori, 1978; Gutenberg & Richter, 1955).

Further, to measure far-field earthquakes, whose seismic surface waves have a period of 20 s and are often dominant on seismograms, Gutenberg (1945b) developed the magnitude scale for surface waves, so-called M_S . He also extended another scale using seismic body waves, whose period is usually from 1 to 10 s, so-called body wave magnitude, m_b Gutenberg (1945a). The studies conducted by Gutenberg and Richter in 1956 suggested that M_S and m_b seem have a relationship and could be used to represent the energy of seismic waves, E , and they proposed the empirical expression of E to be $\text{Log}E_S = 1.5M_S + 11.8$, where E in ergs (Kanamori 1978).

The aforementioned earthquake magnitude scale of M_L , M_S , and m_b suffered saturation when the dimension of an earthquake rupture exceeds the wavelength of the seismic wave used for their magnitude determination, i.e. 5 to 50 km. To cope with such a problem, for huge earthquake a new magnitude scale was invented, which is estimated from the seismic moment M_O (Kanamori, 1977). As a result of their efforts at substituting empirical expressions, Hanks & Kanamori (1979) proposed the represented magnitude of $M = \frac{2}{3} \log M_O - 10.7$, where M_O is a seismic moment in Ergs. The advantages of the last scale magnitude of M are that it will not saturate in great earthquakes and acts similar to M_S for a number of earthquakes with a magnitude less than 8. Furthermore, it is very useful for practical purposes, since a lot of prior works related to the earthquake scaling law that depend on rupture dimensions used the magnitude of M .

3.1.1.b Tsunami earthquake: definition & quantification

The term tsunami earthquake was introduced by Kanamori (1972) to be used for an anomalous tsunami, whose run-up heights are larger than those expected from the given seismic waves. He was interpreting the obtained seismic wave period of the Aleutian Islands earthquake in 1946 and the Sanriku earthquake in 1896, and concluded that the source deformation of this event in the rupture process had a time of about 100 s and was longer than the usual ones. He suggested that the slow deformation in the excitation area was influenced by the visco-elasticity of the weak zone in the trench's margin. The oceanic and continental lithospheres at the inner trench's margins may be responsible for such a process. Despite

slow deformation in the rupture process, the tsunami run-up heights onshore are higher compared to those from the usual tsunamigenic earthquake with similar magnitudes.

Fukao (1979) investigated two events of tsunami earthquakes in the Kurile Islands and Hokkaido that occurred in 1963 and 1975, respectively. He suggested that, despite the process time being relatively slow, i.e. about 100 s, such earthquakes occurred at extremely shallow depths. Although the wedge portion of the subduction zone – the place that these earthquakes originated – is usually experiencing low seismic activity presumably due to the ductile sediment, he added that the fracture process of these events was brittle. He postulated that the wedge portion consists of thick sediments causing low elastic wave velocities and densities where in the mechanism of tsunami earthquakes, fracturing through the sediments produces large displacement. Thus, it plays an important role in the earthquake process and its activities.

A comprehensive study identifying various characteristics of tsunami earthquakes was conducted by Pelayo & Wiens (1992). They analyzed four earthquake events that happened in Peru, Kurile, Philippine, and again Kurile in 1960, 1963, 1968, and 1975, respectively. The Peru and Kurile earthquakes were classified as tsunami earthquakes, based on long-period wave analysis indicating double-couple fault mechanisms rather than the single-force process as results from the tsunamigenic events of submarine landslides. Other findings were that the events occurred near the trench axis at a shallow depth of less than 15 km. Further, body waveform inversion indicates a shallow dipping thrust faulting mechanism of 6° – 8° with a slow moment release duration 60 s – 85 s and an estimated rupture speed of about 1 km/s or less; the latter may result from rupturing through the sedimentary rock along the base of the accretionary prism. In addition, the authors also attempted to form a relation between the magnitudes of M_S and M_O . The tsunami earthquake has the value of M_S , which is about half-to-one unit lower than ordinary earthquakes using a similar moment magnitude.

To discriminate between tsunami earthquakes and usual tsunamis, Abe (1989) proposed the tsunami magnitude of M_t . This is principally based on the tsunami amplitude as recorded in the tide gauges and the distance from the epicenter. The M_t may be expressed as:

$$M_t = \log H + a \log \Delta + D \quad (44)$$

where H is the maximum single tsunami amplitude wave (in m) as recorded by tide gauges, Δ is the distance (in km) from the epicenter to the tide station along the shortest

oceanic path, and a and D are constants, which are assumed to be 1.0 and 5.80, respectively Abe (1989).

By using such magnitudes of M_t and M_S , where the latter is one of the magnitude scales determined from surface waves with a period of 20 s, he then proposed a diagram showing an M_t - M_S relation. This diagram quantifies the tsunamigenic earthquake, distinguishing between tsunami earthquakes and ordinary ones. He suggested the value of 0.5 higher in M_t scale than M_S as a threshold to classify the event as a tsunami earthquake. Figure 19 shows the relation between M_S and M_t as Satake & Tanioka (1999) updated the plot from Abe (1989) by adding data for tsunami earthquake events since 1979.

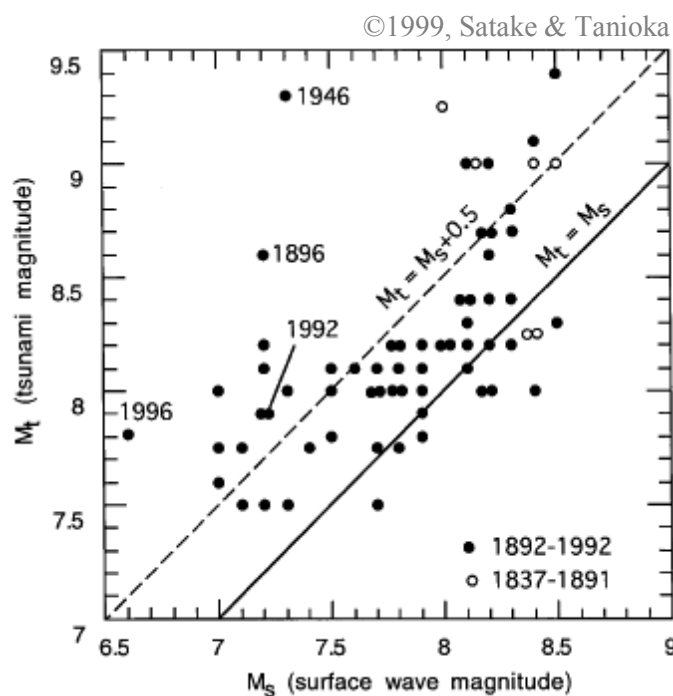


Figure 19: M_t vs. M_S for a tsunami earthquake

After an absence of more than a decade, from 1992 to 2006, tsunami earthquake events again occurred, as documented and identified in several published papers. According to Hanifa et al. (2007), Bilek (2002), and Satake & Tanioka (2003) six events were categorized as the tsunami earthquakes within this period. Two happened two 1992 in Nicaragua and Flores, one in 1994 in Java, one 1996 in Peru, one in 1998 in Papua New Guinea and the last in 2006 in Java. The following paragraphs briefly present the overview of subsequent events that occurred during the above period.

In 1992 two earthquakes that generated tsunamis occurred in Nicaragua and Flores. Satake (1994) classified the 1992 Nicaragua event as a tsunami earthquake since it had the

discrepancies' relation between M_S and M_W , and the slow duration process of 100 s. He proposed fault dimension by comparing the tsunami waveform from the numerical model with tide records. The estimated fault dimensions were achieved; however, the tsunami run-up observed were still larger than those from the model results, by an average amplification factor of three. The assumption was then that this earthquake occurred presumably in the subducted sediments, where the average rigidity for the top 10 km of crust was relatively lower than normal. Following that, Ide et al. (1993) investigated in more detail the source characteristics of the 1992 Nicaraguan earthquake. The focal mechanism of this event was also proposed, with the main shock interpreted as a low-angle thrust fault of 16° and the rupture velocity as low as 1.5 km/s with a rupture duration time of about 100 s. Further, Imamura et al. (1993) conducted a numerical simulation. They found the strike direction that gives the best agreement for the distribution tsunami heights between the model and field data. The fault dimension was adjusted to increase the slip value, yet the model result was still far from mimicking the measured tsunami heights by a factor 5.6 to 10.

In the 1992 Flores events, Tsuji et al. (1995) in field work along the north coast of the eastern part of the island found an extraordinary tsunami run-up height that reached 26.2 m. This was also confirmed by Yeh et al. (1993) who reported the run-up heights varying in the range 19-25 m in the mainland and 5–7 m in Babi Island. Beckers & Lay (1995) carried out a very broadband seismic analysis to reveal the anomalously high tsunami run-up measured. They inferred that the seismic source is unlikely to be responsible for such an event. They referred to the other study conducted by Hidayat et al. (1995) that was able to explain the anomalous run-up heights by involving the slumping events in the model as also suggested earlier by Tsuji et al. (1995). Another model was proposed by Satake (1995) with the findings that the computed tsunami amplitudes along the coastline are three times smaller than the observed tsunami run-up heights, although this case might be influenced by the coarse grid size used.

In 1994, the south coast of east Java was devastated by a tsunami with a maximum documented run-up height of about 13.9 m. The seismic intensity was estimated to be below MMIV (Tsuji et al., 1995; Polet & Thio, 2003; Abercrombie et al., 2001) suggesting that this event occurred as slip over a subducting seamount, since the source is situated in the bathymetry that has been identified as a subduction seamount. Furthermore, there is no evidence for slow and thrust faulting aftershocks. However, they interpreted this as being

similar to the 1992 Nicaragua earthquake through having a shallow rupture of 16 km near the trench and having a dip of 12° .

An earthquake of magnitude $M_W 7.5$ occurred in 1996 at a shallow depth of 7–10 km at the interface between the South American plates and Nazca generating a tsunami that attacked the coast of Peru with run-up heights varying 1–5 m as reported by Bourgeois et al. (1997) in Ihmle et al. (1998). They investigated the moment release of this event and inverted their surface wave source spectrum that reveals the rupture velocities to be about 1.5–2.0 km/s with average rupture duration of about 50s. They concluded that this event was not quite in the class of slow earthquakes.

The 1998 Papua New Guinea earthquake was also followed by an unusual tsunami that had run-up heights of 10 m that were found along a 25-km-stretch of coastline with a maximum of about 15 m and killed more than 2000 people (Kawata et al. 1999). Joku et al. (2007) even reported in a recent paper that this event caused damage at several points as far as 230 km to the northwest; eyewitnesses saw the surging wave of about 2 m. In Satake & Tanioka (2003), Kikuchi et al. (1999) estimated this event to have a magnitude M_t of 7.5, and the difference with the surface wave magnitude M_S is 0.4 suggested that this event might be classified as a tsunami earthquake (Abe, 1989). Based on a comprehensive dataset of high-resolution seismic reflection combined with photographic and bathymetric measurements, confirmed that the generation of tsunamis was by a submarine slump (Tappin et al., 2008). Furthermore, Okal (2003) analyzed an anomalous wave recorded at hydrophone and seismic stations, which showed high frequencies suggesting its spectrum can only be explained by the model of a submarine slump. Tanioka (1999), on the other hand, was able to model and explain the tsunami waveforms observed in Japan by using an ordinary seismic model without any additional source, i.e. submarine slump. Matsuyama et al. (1999) demonstrated the significance role of the offshore bathymetry. The new high-resolution bathymetry is used to run the model, and the seismic source could explain the concentrated of tsunami distribution into study area.

The south coast of Java was again devastated by a deadly tsunami in 2006, causing more than 600 fatalities and damage to thousands of coastal houses (WHO, 2006; Abidin & T. Kato, 2007). The average tsunami run-up height was 5 ~ 8 m and stretched 400 km along the Java coastline. However, the maximum run-up of 15 ~ 21 m was found in the short segment of Nuskambangan Island (Ammon et al., 2006; Fritz et al., 2007; Lavigne et al., 2007; Kongko et al., 2006). The event had a $M_W 7.8 - M_S 7.2$, dip of 10° , and depth of 10 km

(USGS, 2006; Ammon et al., 2006). Furthermore, it was barely felt along the Java coastline with as it had an estimated peak intensity of MMIV, and an unusually low rupture speed of 1.5 km/s with a rupture duration of ~185 s.

3.1.2 Tsunamigenic earthquakes in subduction zones & local tsunami

3.1.2.a Tsunamigenic earthquakes in subduction zones

The subducting oceanic to the continental lithosphere forms contact surfaces between the overriding and underthrusting plates in the convergent margins. Such a zone is called a megathrust zone, which accommodates the convergent motions with different portions of seismic and aseismic slip in various geometries and levels of earthquake in all spatial regions. And about 90% of the seismicity activities manifested by earthquakes occurs in the proximity of the subduction zones, where its upper and lower fault bounds are approximately on the interplate seismic slip at a depth of ~5-10 and ~25-55 km below the seafloor, respectively (after Lay & Bilek, 2007).

Since heterogeneity is attributed to earthquakes of all tectonic levels, it has long been a concern for seismologists to observe them in the rupture processes. This is done primarily by evaluating the earthquake locations and recurrence patterns that yield the estimate of heterogeneity. Furthermore, seismologists, by utilizing models to conduct the analysis of the source time function that provides seismic moment release history and estimates of the effect of the Earth's structure on seismic wave propagations. By doing so, the earthquake slips and its distribution of the fault can be determined (Bilek, 2007).

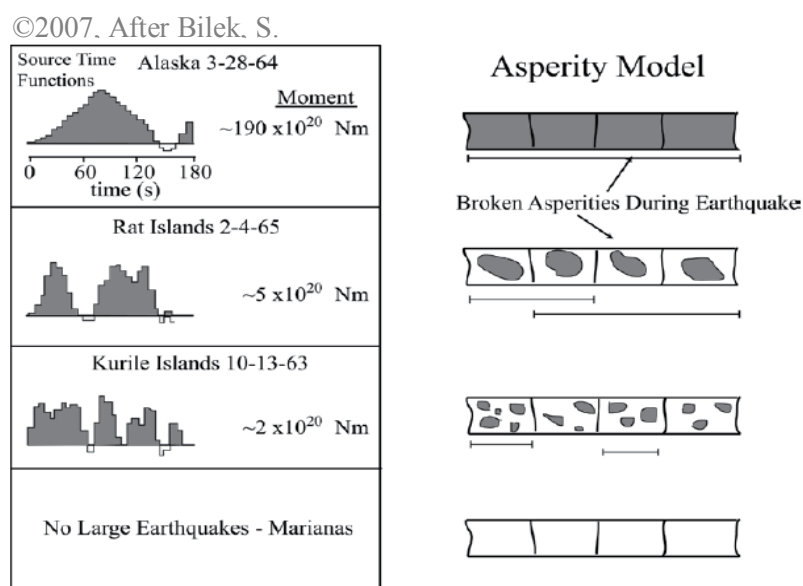


Figure 20: The asperity model for subduction zones earthquakes

Figure 20 is an example of the source time function model known as the Asperity model for subduction zone earthquakes as modified from Ruff and Kanamori (1980) and Lay et al. (1982) in Bilek (2007). Two panels in Figure 20 show the time function of the moment release during an earthquake rupture (left) that may be represented by the asperity classes (right). This model suggests that the form of moment release is linked to the heterogeneously slip asperities, whose distribution varies from one to another subduction zone related to the geological nature (Lay & Kanamori, 1981) in Satake & Tanioka (1999).

It is common knowledge that the shallowest large earthquakes in the shallow subduction zone may trigger a tsunami. A tsunamigenic earthquake is an earthquake capable of generating a tsunami, and a so-called tsunami earthquake is one that generates a tsunami larger than those expected from its given seismic waves (Kanamori, 1972). In regard to tsunamigenic earthquakes in the subduction zone, depending on the source location, Satake & Tanioka (1999) classified them into three types: earthquakes in the plate interface (interplate events), earthquakes at the outer rise (intraplate events), and tsunami earthquakes that trigger a tsunami considerably larger than expected from the seismic waves.

Figure 21 shows the schematic cross-section of the subduction zone, which clearly depicts the classification of tsunamigenic earthquakes related to the source location. Interplate earthquakes happen at the boundary between the subducting and overlying plates. Intraplate earthquakes are outer rise, crustal, and slab earthquakes. Tsunami earthquakes occur beneath the most trenchward part of the accretionary wedge (Satake & Tanioka, 1999).

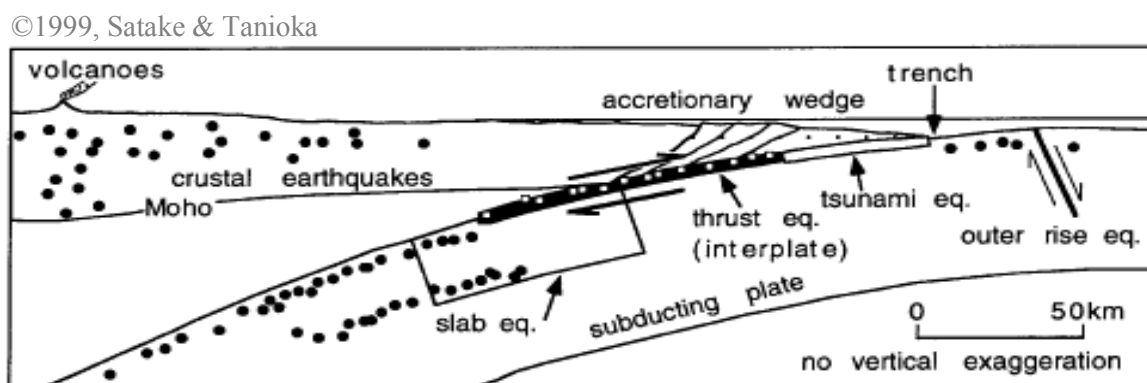


Figure 21: Schematic cross-section of the subduction zone

According to Satake & Tanioka (1999), the source area of an interplate earthquake typically extends ~ 10 to 40 km below the seafloor located in the proximity of the contact between the subducting and overriding outer plate of the base of the accretionary wedge.

Furthermore, the source region of tsunami earthquakes is in the shallower region near to the trench axis beneath the accretionary prism as depicted in Figure 21.

A comparative study for the two events of tsunami earthquakes occurring in 1963 in Kurile, and 1975 in Hokkaido was conducted by Fukao (1979). The results show that the duration of the rupture process was long and these events were generated in the wedge portion characterized by low seismic activity due to ductile deformation of sediments. They suggested that the sedimentary wedge plays an important role in the generation process of earthquakes of high magnitude. The tsunami earthquakes' mechanism is seismic slip fracturing through the thick sediments producing huge seafloor displacement.

In 1992, the modern broadband seismic networks were established, which coincided with the tsunami earthquake event in Nicaragua. This allowed scientists to obtain high-quality seismic data and to conduct detailed analysis of the mechanism of the rupture process. Kanamori & Kikuchi (1993) conducted the analysis of the long seismic waves of this event, and concluded that the Nicaragua earthquake was a slow-thrust earthquake that occurred in the subduction zones. Since in this area was already known to have no sediment on the trench floor offshore, the slip propagation reached to the seafloor and created a huge tsunami. By learning lessons from this, the two types of tsunamigenic earthquakes for the class of tsunami earthquake may then be suggested. The first is that the event occurs in trenches with a large amount of sediment and an accretionary prism. Although the rupture of the earthquake does not reach the seafloor, the slumping associated with the event may occur and cause large tsunami earthquakes. The second is that the event occurs in subduction zones without a large amount of sediment. The sediments are completely subducted and fill the plate interface. The earthquake slip reaches the surface and breaks through a relatively weak plate interface (Kanamori & Kikuchi, 1993).

Extended studies on the shallow subduction zone and its tsunamigenic by examining the source spectra of all events from 1992 to 1996 with $M_W > 7.0$ were conducted by Polet & Kanamori (2000). They identified and proposed another sub-class of tsunami earthquake, the so-called slow tsunami earthquakes for the event which has an anomalous energy release in the 1–20 s frequency bands. This sub-class consists of the 1992 Nicaragua, the 1994 Java, and the 1996 Peru earthquakes.

The Java subduction zone is part of the Sunda arc, whose trenches extend over 5600 km from the Andaman Islands to west off Sumatra and the Banda arc to the east. The convergence across the Java trench was estimated from annual GPS measurements

commencing in 1989, which the result that Christmas Island moves from west Java by 67 ± 7 mm/yr in a direction $N11^\circ E \pm 4^\circ$ (Tregoning et al., 1994). The update to the estimate of the convergence rate by extending the time series measurements conducted by Bock et al. (2003) gave a slightly slower rate of 63.3 ± 0.4 mm/yr with a direction $N14.09^\circ E \pm 0.5^\circ$.

Furthermore, based on the interpretation of seismic reflection data and velocity information, the convergent Sunda margin showed all geological features characteristic of an accretion-dominated subduction zone (Kopp & Kukowski, 2003). However, at the eastern Sunda margin running from central Java to Sumba Island, the subduction erosion process coincides with the presence of the oceanic Roo Rise and numerous seamounts on a steeping seafloor (Masson et al., 1990; Kopp et al., 2006). The change of the nature process from accretion to erosion in the subduction regime confirmed with the dataset analysis of MERAMEX network that the gap is about $\sim 110^\circ E$ off Java Island (Manzanares, 2008).

According to Spicak et al. (2007), analyzing the global seismic data in the Sunda arc revealed that the seismicity off Java Island is not laterally continuous but segmented. This zone consists of segment 1 as a cluster of the 2006 earthquake and segment 2 as a cluster of the 1994 earthquakes, with the seismic gap in between. The analysis also revealed the existence of a strip of distributed earthquakes along the Java trench, separated by a trench-parallel of a 50–150-km-wide aseismic zone.

3.1.2.b Local tsunami

The tsunami run-up heights and their distributions on shore are not only affected by the source parameters but also on the propagation distance. Therefore, scientists and engineers made a distinction between teleseismic tsunamis or far-field tsunamis and local tsunamis or near-field tsunamis.

According to a study conducted by Okal (1988), in far-field tsunamis the depth of source and focal mechanism play the only marginal role in tsunami excitation. The variation depth from 20 to 100 km only reduces the far-field tsunami amplitudes by a factor of two. Furthermore, various types of slips of the focal mechanism were also investigated with results showing that dip and tilt-slip only cause slightly bigger excitation than dip-slip, even the dip and tilt-slip at a depth of about 30 km, and that there is practically no difference in excitation. Hence, the average tsunami amplitude of teleseismic tsunamis depends mainly on the level of the scalar seismic moment of M_0 .

Tanioka (1999) investigated the far-field tsunami generated by the 1998 Papua New Guinea earthquake by analyzing several tide gauges and ocean bottom pressure gauges in

Japan. However, four years later it was confirmed that anomalous run-up heights are caused by submarine mass failure as reported by Synolakis et al. (2002) and Okal (2003); the numerical simulation conducted by Tanioka (1999) using a seismic dislocation source was comparable to the tide gauge recordings. He did not use any additional sources, e.g., slumping mass representing the submarine landslide. It appears that the far-field tsunami amplitude is also insensitive to the tsunamigenic types.

If the far-field tsunami amplitudes are primarily influenced by the size of the scalar seismic moment, in contrast the local tsunami is dependent on the complexity of the source parameters. The extensive studies related to local tsunamis and the complex earthquake source parameters, such as the heterogeneity slip were carried out by Geist (1998), Geist & Dmowska (1999), again Geist (2002), and McCloskey et al (2007). While, Schlurmann et al. (2010), by using newly highly-resolved geo-data, studied the near-field tsunami propagation both in shallow-water environments and bore-like wave propagation on land to obtain fundamental knowledge on the tsunami hazard potential in the city of Padang Indonesia.

In local tsunamis generated by earthquakes, if the source area covers the land, the co-seismic vertical displacement near the coastline is commonly observed. Since most large-scale events occur in the interplate boundary subduction zones, the seafloor experiences uplift while land subsides. This phenomenon was obviously observed for the 1960 Chilean earthquake and for the 1964 Alaskan earthquake as reported by Linde and Silver (1989) and Hwang & Divoky (1970) in Geist (1998). Other instances of co-seismic land-uplift and subsidence were also reported for recent events, such as for the 1993 Hokkaido earthquake (Satake & Tanioka, 1995), the 2004 Indian Ocean earthquake tsunami (Jaffe et al., 2006), and the 2005 Nias-Simuelue earthquake and tsunami (Borrero et al., 2010).

The local tsunami amplitude is also influenced by the types of subduction zone faulting, such as outer rise fault, interplate thrust, deep intra-slab, and back arc thrust. The interplate thrust is the most frequent of the tsunamigenic earthquakes; on the other hand, infrequent events occur in the very shallow front along the interplate thrust within the overriding accretionary wedge, which are often classified as tsunami earthquakes (Geist, 1998).

Among the source parameters studied by Geist (1998), such as the focal depth, rupture area, dip, and slip, the magnitude of slip and the spatial slip variations are the dominant effect on the excitation of local tsunamis. The study conducted by Geist & Dmowska (1999) also demonstrated the significance of utilizing heterogeneous rupture

models to accurately model the local tsunami waveforms. They also stressed that in most cases, slip distribution derived from a body wave seismic inversions model of broadband data can be used to model the local tsunami.

Based on a global tsunami catalog of tsunami run-up observations, the greatest variability of local tsunami run-up due to tsunamigenic earthquakes in subduction zones are of the magnitude range $7 < M_w < 8.5$. This variability in local tsunami run-up according to Geist (2002) depends on the source parameters that are independent of seismic moment M_0 , such as the water depth variations in the source region, the combination of higher slip and lower shear modulus at shallow depth, and rupture complexity in the form of heterogeneous distribution's slip patterns. Among them, the latter has been extensively investigated with results showing that for shallow subduction zone earthquakes, the irregularities of the slip distribution are significant for local tsunami amplitudes; on the other hand, the other source parameters such as focal depth and steep dip angles are less pronounced (Geist, 2002).

McCloskey et al. (2007) investigated controls on the tsunami excitation and its propagation in the local tsunami for large megathrust earthquakes. The 100 complex earthquake ruptures as hypothetical scenarios derived from geodetic and stress accumulation studies were examined. The remarkable results are that the timing of the inundation of the tsunami is independent of the slip distribution on the earthquake as well as its magnitude. Further, the maximum tsunami amplitudes are directly proportional to the vertical co-seismic displacement at the source. They also suggested that the single estimate of vertical co-seismic displacement may provide a robust short-term forecast of the maximum tsunami run-up heights.

Schlurmann et al. (2010) by utilizing hydro-numerical model conducted the analysis on the most reasonable seismic sources and possibly triggered near-shore tsunamis in order to develop upgraded disaster mitigation programs in Padang Indonesia. The observations of continuous Global Positioning Satellite (cGPS) systems and supplemental coral growth investigations verify a greater likelihood of occurrence that a great earthquake and following tsunami are likely to hit the region in the near future. The newly surveyed and processed sets of geo-data have been collected and used to progress towards most credible rupture scenarios to approximate the extent and magnitudes of a further earthquake.

With local tsunamis, there is an intriguing issue related to the extraordinary run-up that triggers the event, where in a short time in the aftermath of the disaster, it is difficult to confirm whether the tsunamigenic event was caused by seismic dislocation or submarine

landslide and this has led to controversy among researchers. The issue is related to the tsunamigenic event and whether its parent is an earthquake or submarine mass failure as happened in the 1998 Papua New Guinea earthquake (Tanioka, 1999; Synolakis et al., 2002; Lynett et al., 2003; Okal, 2003; Satake & Tanioka, 2003), and in 2006 Java tsunami (Fritz et al., 2007; Lavigne et al., 2007).

Okal & Synolakis (2004) developed robust discriminants to identify the physical nature of the tsunami source based on the distribution of run-up amplitudes along the coastline for local tsunami. They conducted the numerical simulation of local tsunami for a dataset of 72 source models involving both tsunamigenic earthquakes and landslides. They are able to separate the individual influence on the tsunami run-up amplitude and its distribution by characterizing the dimensionless parameters. The threshold value as a discriminant was achieved and tested for the 1998 Papua New Guinea earthquake and the 1946 Aleutian earthquake.

3.1.3 Numerical model

3.1.3.a Java tsunami model

In the preceding chapter and section mentioned the 2006 Java tsunami earthquake in relation to the focal mechanism, characteristics, and the relevant impacts following the disaster. This sub-section will elucidate more details compiled from Java tsunami models proposed by several institutions for a rapid assessment in the aftermath of an event as well as in further detailed studies.

The Disaster Control Research Center (DCRC), Tohoku University released a numerical modeling of the 2006 Java tsunami. They used TUNAMI code, which is based on the linear shallow water theory in the spherical co-ordinate system. The computational grid size is approximately 2 minutes of ETOPO2, and the seismic deformation modeling is based on the theory of Mansinha & Smylie (1971). Four fault parameter models were used. Two were based on USGS Moment Tensor, and the others on the CMT Solution of Harvard University. The fault dimension for the parameter model of USGS Moment Tensor and CMT Solution of Harvard University is 40 x 20 km and 84.8 x 42.4 km, respectively. Moreover, its dislocations were 2.3 m for the first two and 3.71 m for the others, while depths were 40 km, 10 km, 10 km, and 10 km for the respective fault parameters. By using these parameters, the maximum tsunami run-up height at near-shore along the coastline of south Java was approximate as 3.0 to 3.5 m.

Another tsunami model for the July 17, 2006 Java earthquake was suggested by Earth and Environmental Science, Military Application Division (CEA/DAM), France. The preliminary rapid estimation for the earthquake magnitude was M_W 7.5, but this subsequently corrected following a further detailed analysis of records conducted by Harvard to be M_W 7.7. They resolved the source parameters as derived from the first seismological inversions, which correspond to the earthquake magnitude stated above, yielding the fault dimension of 130 x 30 km with a co-seismic slip of 2.7 m. The simulation results from the CEA/DAM confirm the maximum sea surface height (SSH) in deep water to be about 50 cm, which is shown in two figures displayed on their official website. They estimated that with a tsunami source in deep water of about 50 cm combined with the coastal configurations, the model may have resulted in water heights of between 3 and 5 m along the coastline. The greatest energy is expected to be in the perpendicular orientation to the subduction trench. Hence, the tsunami effectively generates the highest amplitudes that occurred in Pengandaran, west Java.

Preliminary numerical simulation was also conducted by the Tsunami Research Team Department of Physics University of Bologna Italy. They proposed four cases of fault parameters; the focal mechanisms were provided by the Harvard Moment Tensor Solution. The angle parameters and their depth in all cases were identical, namely for strike = 289° , dip = 10° , rake = 95° , and hypocenter = 5 km. The numerical simulations were carried out by finite difference code, by solving the linear Navier-Stokes equations in the shallow-water approximation and in spherical coordinates. Two fault dimensions and co-seismic slips were used: cases 1, 2, and 4 used 127 x 28 km with slip 3.3 m for the first two and 2.35 m for the last one. For case 3, the fault dimension was 100 x 50 km with its slip 2.35 m. The bathymetric data was ETOPO2, and in all cases the initial sea surface height was taken to coincide with the vertical co-seismic displacement of the seafloor induced by the earthquake, which was computed by an analytical solution of Okada's formula (1992). This preliminary numerical simulation resulted in maximum run-up heights at the coastline of close to 2 m.

The Department of Oceanography, ITB released preliminary results of simulation of the tsunami in West Java 2006 (Latief et al., 2006). The source parameters used were obtained from the USGS Moment Tensor Solution, which were similar to those used in the previous model. Based on their rapid assessment, the proposed fault dimension was 80 x 40 km; yet, the co-seismic slip as well as the numerical code used was not explained. However, vertical dislocation of about 1.7 m was depicted in the graph and a 3 to 4 m high tsunami run-up along the coast was produced numerically.

The last model provided in the present study was proposed by Hanifa et al. (2007), who utilized the approach of nested grids with one (GEBCO) and two minutes (ETOPO2) of arc of bathymetric resolution. The initial sea surface height was taken from co-seismic vertical displacement calculated with Okada Formula (1992). The authors conducted both the crustal motion analysis as well as numerical model simulations, with the latter attempt obtaining its source parameters from several sources (USGS, 2006; Fujii & Satake, 2006; Ammon et al., 2006). Both seismic moment and the rigidity vary from M_W 7.2 to 8.1, 10 GPa, and 30 GPa, respectively. The fault dimensions corresponding to the sources model above, namely 200 x 40 km and 200 x 70 km. Using the low rigidity of 10 GPa as previously suggested by Ammon et al. (2006), results in maximum run-up heights of ~ 6.0 m in the relevant area being obtained. They also stressed that the variation of fault depth (6 – 8 km) does not give a significant difference to the tsunami run-up heights, by contrast the increasing slip leads to a large effect.

3.1.3.b Tsunami model development

The vast developing tsunami hydrodynamics was initiated in the early 1980s, which was still focusing on the solitary waves as an initial condition (Synolakis & Bernard, 2006). In the late 1980s, Synolakis (1987) solved the initial value problem (IVP) of non-linear shallow water (NSW) for solitary waves by propagating at constant water depth to the run-up on a sloping beach. He derived the equation – currently known as “the run-up law” – for solitary waves climbing up a certain sloping beach and comparing the result to the series' laboratory experiment.

In Japan, the tsunami numerical method was initially proposed by Goto & Ogawa in 1982 to solve a near-field tsunami propagating from the source and run-up onto land. However, the development itself had already started in the late 1970s following progress in computer technology. During the International Decade for Natural Disaster Reduction (IDNDR) in the 1990s, the IUGG in collaboration with IOC/UNESCO carried out the project of TIME (Tsunami Inundation Modeling Exchange). In this project, Goto-Ogawa's tsunami numerical model code, known as TUNAMI (Tohoku University's Numerical Analysis Model for Inundation), was adopted and transferred to institutions and countries (already 43 institutions and 22 countries) with a demand for tsunami numerical analysis (Shuto & Fujima, 2009).

To enhance the knowledge on the hydraulic modeling engineering and sciences, researchers hold serial long-wave run-up workshops. And since 1990 up to the present day,

the three long-wave run-up workshops have been held. The first workshop took place on Catalina Island, U.S.A., in which several institutions, including the Novosibirsk's Computing Center, NOAA, Tohoku University, presented tsunami numerical models for propagation and inundation. This workshop established the following conclusions: the run-up of a single non-breaking wave could be computed analytically and numerically, and the NSW model was adequate for the applications of the geophysical problem in long-wave.

The 2nd workshop was held in 1995 in Washington, U.S.A., during which several 1D and 2D numerical computations were presented for predicting the benchmark problems prepared by the workshop organizers. Three models were able to reproduce more than one of the problems proposed by the workshop committee: TUNAMI-N2, Liu et al.'s code (1995) (currently well known as COMCOT), and MOST (Synolakis & Bernard, 2006).

The 3rd workshop for long-wave code validation took place in 2004 again on Catalina Island, U.S.A. It was just before the Boxing Day 26 December Indian Ocean tsunami event. In this workshop the four benchmark problems were delivered and the novel meshless models using smooth particle hydrodynamics (SPH) was presented. The MOST, TUNAMI-N2, and Lynett et al.'s (2003) model had an edge over the rest through involving the Boussinesq solution that led to greater numerical cost. The presented models attempted to predict the Okushiri tsunami run-up problems with varying degrees of success (Synolakis & Bernard, 2006).

The lesson learned from the 1993 Hokkaido Nansei-Oki earthquake tsunami, was that the maximum run-up of 31 m that occurred in the valley on the west coast of Okushiri Island was not able to be explained using the primitive model. Shuto & Fujima (2009) assumed that the long-wave-based numerical model no longer had the capability to model such an event and this led to accelerating the introduction of the new 2D/3D hybrid simulation model, known as STOC (Storm surge and tsunami in Oceans and Coastal area), whose code was developed by Tomita et al. (2004) in Shuto & Fujima (2009).

Further, the most recent tsunami model development is the new method for real-time tsunami forecasting by integrating tsunameter recordings and seismic data. This was developed and successfully tested for the 17 November, 2003 tsunami in evaluating the leading wave height off Hilo, Hawaii (Titov et al., 2005; Synolakis & Bernard, 2006). Meanwhile, for local tsunamis, by considering the uncertainty of the tsunami run-up heights due to heterogeneity slip, the new tsunami forecasting method involving multi sensors was proposed. This method was tested for the minor tsunami following the 30 September, 2009

Padang earthquake. It employed a synthetic pre-calculated event and evaluated independent sensors simultaneously to achieve an accurate tsunami run-up height and their arrival time along the coastline (Behrens et al., 2010). It marked substantial progress in the field of tsunami science during the last few decades.

3.2 Review & Critique of the Research

This sub-chapter reviews the research that was carried out by grouping it into three sections: the characteristic tsunami earthquake and rigidity variations, the heterogeneous slip and fault dimension, and the tsunami model.

3.2.1 Characteristic of tsunami earthquake & rigidity variations

3.2.1.a Characteristic of tsunami earthquake

The tsunami earthquake and its mechanism for past events were compiled in the preceding sub-section; its co-seismic process is associated with several characteristics. They include the following:

- A long duration in the rupture process and slow rupture speed,
- the source is located within a shallow depth in the sedimentary layers and near the trenches,
- the tsunami has extraordinary run-up amplitudes along the coastline.

The rupture durations of tsunami earthquakes observed range from 60 s to several hundred seconds. The events in Sanriku in 1896, the Aleutian Islands in 1946, the Kuriles in 1963 and 1975, Nicaragua in 1992, and Java in 1994 and 2006 had rupture duration from 60 s to 185 s (Kanamori, 1972; Fukao, 1979; Pelayo & Wiens, 1992; Abercrombie, 2001; Ammon et al., 2006; Satake, 1994; Ide et al., 1993). The 1996 Peru earthquake had 50 s of rupture duration and 1.5–2.0 km/s of rupture speed. Bourgeois et al. (1997) and Ihmle et al. (1998) suggested that this event was not quite in the class of slow earthquakes. The tsunami earthquake also has slow rupture speeds of 1–1.5 km/s, such as events for the 1992 Nicaragua and 2006 Java earthquakes (Pelayo & Wiens, 1992; Kanamori & Kikuchi, 1993; Ide et al., 1993; and Ammon et al., 2006).

The source of a tsunami earthquake is located within shallow depths of about 5–16 km, with a dipping thrust angle of about 6°–16° and near trenches, as occurred in Peru in 1960, the Kuriles in 1963 and 1975, Nicaragua in 1992, and Java in 2006 (Fukao, 1979;

Pelayo & Wiens, 1992; Satake, 1994; Kanamori & Kikuchi, 1993; Satake & Tanioka, 1999; Ammon et al., 2006; Bilek & Lay, 2002).

Previous research also reported that all events classified as tsunami earthquakes have extraordinary run-up heights in coastal areas. The events in Sanriku in 1896 and the Aleutian Islands extraordinary 1946 had higher run-up than the given seismic waves (Kanamori, 1972). The 1994 and 2006 Java tsunamis also had maximum run-up heights of about 14 m and 20 m, respectively (Tsuji et al., 1995; Fritz et al., 2007; Lavigne et al., 2007; Kongko et al., 2007).

By using such characteristics above, the events that fulfill characteristics of the tsunami earthquake are listed below:

1. 1896 Meiji-Sanriku, Japan
2. 1946 Aleutian, Alaska US
3. 1960 Peru
4. 1963 Kurile Islands, Russia
5. 1975 Kurile Islands, Russia
6. 1992 Nicaragua
7. 1992 Flores, Indonesia
8. 1994 Java, Indonesia
9. 2006 Java, Indonesia

The list above is slightly different to those proposed by Hanifa et al. (2007), who included the events that occurred in Peru 1996 and Papua New Guinea 1998. In the present study, however, such events have been excluded, since they do not entirely satisfy the characteristics of tsunami earthquakes mentioned above.

The 1996 Peru earthquake was excluded due to is not having an assertive character like that observed for the other tsunami earthquakes. The co-seismic rupture duration and speed are 50 s and 1.5–2.0 km/s, respectively. These values are not as slow as those of other tsunami earthquakes. In addition, the tsunami amplitudes in coastal zones vary across the range 1–5 m, which may not be classified as extraordinary heights produced by a given seismic moment. Bourgeois et al., (1997) and Ihmle et al., (1998) also suggested that this event was not quite in the class of slow earthquakes.

Furthermore, the 1998 Papua New Guinea tsunami has also been omitted as a tsunamigenic earthquake as it has been classed as a tsunami earthquake. It has been identified through the extensive marine surveys that the extra tsunami run-up heights are due to submarine landslides. It was also successfully modeled using submarine mass failure or slumping mass (Synolakis et al., 2002; Tappin et al., 2008; Okal, 2003; Lynett et al., 2003).

However, the detailed process attributed to this event, namely the earthquake-triggering landslides, remains unclear.

3.2.1.b Rigidity variations

Since tsunami earthquakes are situated in shallow depths near to the trenches, the rock and sediment properties in this plate interface have a significant role in controlling the frictional behavior of faults and the earthquake rupture process. The essential material property is rigidity, which affects the level of slip in the rupture process of earthquakes (Bilek & Lay, 1999).

Bilek & Lay (1999) plotted the entire 291 events, and the estimated rigidity of the seismogenic zone between depth ranges of 5 and 50 km increases as shown in Figure 22. Further, at depths between 20 and 40 km, the average rigidity values are comparable to those estimated by the Preliminary Reference Earth Model (PREM). The PREM is a mathematical abstraction model of the inner parts of structures based on regions or layers within the Earth. This model uses three principal subsets of data, namely astronomic-geodetic data, free oscillation and long-period surface wave data, and body wave data (Dziewonski & Anderson, 1981).

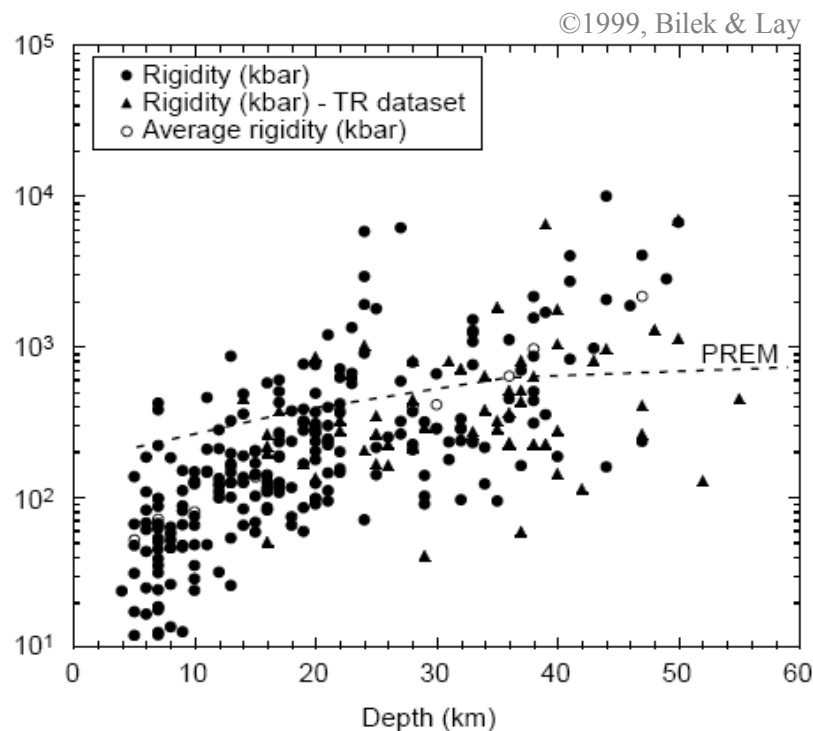


Figure 22: Plot of estimated rigidity variations along depth

The average rigidity is more pronounced at shallow depths (< 20 km) than those estimated by PREM (Dziewonski & Anderson, 1981). In depths of about 5 and 20 km, the increasing rigidity is following a factor of ~ 5 . This trend is also consistent with the prior hypothesis that tsunami earthquakes that occurred in the shallow depth region caused by low rigidity (Kanamori, 1972; Fukao, 1979; Pelayo & Wiens, 1992; and Bilek & Lay, 1999).

The results indicate that such analysis can provide more flexibility in the use of low rigidity at shallow depths and improve the estimation of accurate slip in the tsunami excitation model. However, almost all tsunami models, which have their tsunamigenic earthquakes located near to trenches, did not take into account the above condition and still use normal rigidity. Only a limited number of models took into account low rigidity, such as the tsunami model for the 1992 Nicaragua and the 2006 Java earthquakes.

Satake (1994) suggested low rigidity for the 1992 Nicaragua tsunami. He estimated the rigidity 3–4 times lower than PREM and close to that shown in Figure 22. Other similar efforts were carried out for the 2006 Java tsunami, such as the low rigidity of 10 GPa (10^2 kbar) proposed by Ammon et al. (2006) and the numerical model created by Hanifa et al. (2007).

3.2.2 Heterogeneous slip and fault dimension

3.2.2.a Heterogeneous slip

The epicenters of the two events of Java tsunamis that occurred in 1994 and 2006 were very near to the Java trenches, namely of about 15 km and 40 km, respectively. However, the shortest dip-directed distance from each epicenter to the south coast of Java is about 245 km for the 1994 event and 180 km for the 2006 event. The distance of the epicenters from the nearest land was less than 80 km for the tsunami earthquakes listed in the preceding sub-section, except the first two, namely the 1896 Meiji-Sanriku and 1946 Aleutian Alaska earthquake and both events above. Therefore, the Java tsunami earthquakes were rather remote in terms of distance from the land.

The previous studies of the source mechanism of the Java tsunamis suggested that the utmost fault width is not more than 100 km; hence Java Island is located out of the fault area and did not experience land displacement. This was also confirmed by the GPS data recordings during the co-seismic and post-seismic period. As for the 2006 event, the ‘tiny’ co-seismic rebound to the southward was observed at BAKO station in West Java of about 4 mm (Hanifa et al, 2007). Furthermore, the post-seismic horizontal deformation estimated

from more than 20 GPS survey points carried out within one month after the event, in general was less than 5 cm with a direction to the south (Abidin et al., 2009).

Based on the above data, it is also assumed that the co-seismic vertical displacements near the coastline for both events were almost meaningless. Thus, following the criteria for local tsunamis set out by Geist (1998) that the earthquake is associated with vertical land deformation, it is still questionable whether the Java tsunami earthquakes can really be classified as such.

According to Geist (2002), based on historical data the greatest variability of tsunami run-up frequently occurred in the subduction zone with the magnitude range of $7.0 < M_W < 8.5$. He added that there are three factors that affect the variability of local tsunamis that originated from source parameters that are independent of the seismic moment M_0 . They are the variations in the water depth in the source region, the combination of higher slip and lower rigidity at shallow depth, and rupture complexity of the heterogeneous slip distribution pattern.

The variations of the water depth in the source region influence the variability in local tsunamis. Geist et al. (2006) compared and examined the source parameters of both the 26 December, 2004 and the 28 March, 2005 earthquake to explain the difference in tsunami observations. Both tsunamis were local tsunamis; for the December 2004 earthquake the tsunami amplitudes in the coastal zone are similar to other tsunamigenic earthquakes of comparable magnitude. In contrast, the tsunami amplitudes of the March 2005 earthquake were far lower than those being expected from the relative given magnitude. The significant factor causing the deficiency of the March 2005 tsunami appears to be related to concentration of slip distribution at the down-dip part and by the fact that the portion of vertical displacement occurred in very shallow water or even in land (Geist et al., 2006).

The rupture complexity of the heterogeneous slip distribution pattern is a significant factor to the variability of local tsunami. For this topic, Geist (2002) conducted extensive studies and demonstrated that the irregularities of the slip distribution are essential factors. Yet, the influence of the rupture complexities at deeper depths with steep dip angles is less pronounced. Furthermore, the analysis of a case study for the Pacific coast of central Mexico using fixed location and similar geometry and seismic moment also indicated that the variability in local tsunamis can vary by a factor of 3 (Geist, 2002).

McCloskey et al. (2007) also investigated the controls on the excitation and its propagation for the near-field tsunami due to large megathrust earthquakes. By using a series

numerical simulation tests of about 100 complex earthquakes, ruptures derived from geodetic data for stress accumulation studies at the Sunda megathrust, the remarkable results for near-field tsunamis came to two conclusions: first, the travel time of tsunami inundation is independent of slip distribution of the tsunami source or even of its earthquake magnitude; second, the utmost tsunami amplitude is directly proportional to the vertical co-seismic displacement experienced at the source zone.

From the three significant factors of source parameters that are independent of seismic moment M_0 affecting the variability in local tsunamis as proposed by Geist (2002) and the second conclusion postulated by McCloskey et al. (2007), among them the combination of higher slip with low rigidity at shallow depth, has not been assessed yet.

Furthermore, for Java events that have a source that is rather remote compared to the other tsunami earthquake events and thus is not really classified as a local tsunami, may have interesting issues requiring further analysis. Such a distance of the fault area from the coastal zone might also have significant effects on the variability of run-up heights and their distribution.

3.2.2.b Fault dimension

The preceding chapter presented several empirical relations scaling the fault dimensions of length, width, slip (L , W , D), and the moment magnitude of the earthquakes. The most widely used of the relations were developed by Wells & Coppersmith (1994). Since then, scientific work related to these issues was conducted by several researchers. However, their work could be differentiated into the seismotectonic regimes until a recent study was conducted by Somerville et al. (2002) in Strasser et al. (2010). They proposed approaches that distinguished scaling relations between large crustal and large subduction zone earthquakes. The main finding was of the rupture area of subduction earthquakes being larger by a factor of two or more than those of crustal earthquakes produced by similar seismic moments.

Several scaling relations by separating the event mechanism process and their source locations were also proposed by Papazachos et al. (2004) and Strasser et al. (2010). The first authors introduced the scaling relations based on the seismotectonic regimes. They made distinct relations for the events whose different focal mechanisms and source regions, such as the strike-slip faults, dip-slip faults in continental regions, and slip faults in regions of lithospheric subduction. Furthermore, the second authors derived regression relations by

separating the dataset into two seismotectonic regimes, namely earthquakes that occurred in the interface and those that occurred in the intraslab subduction zone.

Okal (2006) in unpublished works proposed the scaling relations to estimate the fault dimensions by omitting the tectonic environments. The fault dimension ratio of L/W was adopted from the relationship proposed by Geller (1976) for moderate trend, where the ratio value is equal to ~ 2 .

The scaling relations discussed above utilize empirical logarithmic regressions, while those for fault dimensions use scalar unit, which leads to variability values resulting from each expression. Table 3 depicts the fault dimensions of L , W , and D resulting from the scaling relations proposed by the researchers mentioned above. Since there are many variation conditions for the scaling relations, the present study selects the conditions that are suitable for tsunami excitation. These occur in the interplate regime and in the shallow subduction zone, differentiated in terms of type of earthquake mechanisms, i.e. reverse or all events. Here, as an example, the magnitude of M_w 7.8 or equal to $6.31E+20$ Nm in seismic moment of M_o has been used to produce fault dimensions.

Table 3: The fault dimension from various empirical relations

Magnitude	Wells & Coppersmith (1994)			Papazachos et al. (2004)			E. Okal (2006)			Strasser et al. (2010)			
$M_w / M_o(\text{Nm})$	Event	L (Km)	W (Km)	Slip (m)	L (Km)	W (Km)	Slip (m)	L (Km)	W (Km)	Slip (m)	L (Km)	W (Km)	Slip (m)
7.8	All	197.4	45.9	2.32	125.9	61.4	2.70	95.5	47.7	2.77	127.7	75.5	2.18
6.31E+20	Reverse	127.1	38.7	4.27									

The results in Table 3 show that the comparable scaling relations are among the length of reverse by Wells & Coppersmith (1994), Papazachos et al. (2004), and Strasser et al. (2010), namely $L \sim 126\text{-}128$ km. The widths from Papazachos et al. (2004) and Strasser et al. (2010) are also in a comparable value ($W \sim 61\text{-}76$ km), yet they are nearly twice as big as those of Wells & Coppersmith (1994) ($W \sim 39$ km) for the reverse event. This disparity value caused by the expressions was used derived from the dataset of crustal regions. This difference is consistent with the findings of Somerville et al. (2002) in Strasser et al. (2010), who stated that the fault area in the subduction zones has a slip that is at least two times larger than those in crustal regions. However, it is important to note here that for the length of fault, the Wells & Coppersmith (1994) relations for all events are the longest.

Except for Okal's (2006), the other slip values above were obtained by assuming the rigidity of $\mu \sim 30$ GPa. However, in the expressions of Okal (2006), the rigidity is inherently

set to be of ~ 50 GPa. Such a difference in value of the rigidity used in Okal's (2006) expressions is also manifested in different values in the fault length and width.

However, overall the relations excluded the reverse events by Wells & Coppersmith (1994). The slip, which according to McCloskey et al. (2007) is also proportional to the vertical displacement at source and is sensitive to the tsunami amplitudes for local field, has comparable values. The selection of the reverse and all event regression as proposed by Wells & Coppersmith (1994) gives a significant difference in dimension of fault; this issue will be assessed in the present study.

3.2.3 Tsunami model

3.2.3.a Java tsunami model

In the previous sub-section the tsunami model for the 2006 Java earthquake was elucidated. So far, five tsunami models have been proposed. Among them the first four were the preliminary tsunami models reconstructed quickly in the aftermath of the event (DCRC - Univ. Tohoku – Japan, 2007; CEA-France, 2007; Italy, 2007; Latief et al., 2006). The last was an extensive study conducted by Hanifa et al. (2007), where tsunami sources were developed from model inversions using tide gauges recordings (Fujii & Satake, 2006) as well as from the seismic body waves (Ammon et al., 2006).

The hydrodynamic numerical model used for all models above was based on the Non-linear Shallow Water Equation (NSWE) equations with coarse grid spatial geometric data derived from GEBCO and ETOPO2, which have one and two minutes of arc resolution, respectively. Furthermore, for the first four preliminary tsunami models, the tsunami source use the USGS Moment Tensor and the CMT Solution of Hazard University, while the last model proposed by Hanifa et al. (2007) used several tsunami sources. Hanifa et al. (2007) used tsunami sources from the USGS Moment Tensor and model proposed by Fujii & Satake (2006) and Ammon et al. (2006). They modified the magnitudes from M_W 7.2 – 8.1 and used both normal and low rigidities of 30 GPa and 10 GPa, respectively.

The initial conditions of the tsunami models above use deformation models with the analytical solution was proposed by Mansinha & Smylie (1971) and Okada (1985). In addition, the fault dimensions greatly vary depending on the model. The fault length varies in the range 40–200 km and 20–70 km for fault width, while the slips range between 1.7–3.7 m for normal rigidity and a maximum of 15 m for low rigidity. By using coarse spatial grid and such initial conditions, the tsunami run-up heights at shoreline are calculated as being

between 2–5 m. However, the last model with low rigidity was able to produce a tsunami run-up height of about 6 m.

3.2.3.b Model performances

Within the last two decades, more than ten numerical methods suitable for simulation of tsunami waves from propagation to run-up were produced. They range from primitive code based on NSWE, such as that proposed by Goto and Ogawa in 1982 (Shuto, 1991) to the most recent method of the 3D computational water dynamic by solving 3D Navier-Stokes equations (Nicolosky et al., 2010). Regardless of what method is used in the numerical models, the essential areas are subjected to validation and verification. Moreover, after the tsunami on 26 December 2004, increasing numbers of tsunami-prone countries began developing tsunami mitigation plans (Synolakis et al., 2008).

To verify a model, whether the assumed initial condition of the tsunami is satisfied or not to represent its amplitude at the coastline, Aida (1978) introduced two parameters K and k . K is an average of the ratio of the observed and computed amplitudes of the tsunami, and k is the corresponding standard deviation. The complete expressions are given as below:

$$\begin{cases} K_i = \frac{x_i}{y_i} \\ \text{Log } K = \frac{1}{n} \sum_{i=1}^n \text{Log } K_i \\ \text{Log } k = \left[\frac{1}{n} \sum_{i=1}^n (\text{Log } K_i)^2 - (\text{Log } K)^2 \right]^{1/2} \end{cases} \quad (45)$$

where, x_i and y_i are the observed and computed amplitudes of the tsunami, and n is the number of samples.

For practical purposes, the numerical model is evaluated as giving satisfactory results if K is between 1.2 and 0.8, and k is less than 1.4 (e.g., Aida & Hatori, 1984; Hasegawa, 1986; Shuto et al., 1987) in Shuto (1991). Suppasri et al. (2008) used such methods for their study comparison of the eight source models available following the 26 December, 2004 Indian Ocean tsunami.

Shuto (1991) conducted a model comparison among three long wave theories in deep water, namely linear long wave theory, linear Boussinesq equation, and Boussinesq equation. He pointed out that the linear Boussinesq and Boussinesq equations almost coincide with the true solution as given by the linear surface theory. This suggests that the nonlinear term is not important in the propagation of a tsunami in the deep ocean. He added that the linear long wave theory gives a satisfactory result in the sea with a depth more than 50 m. However, at

shallower depths, the shallow water theory with bottom friction should be used. Overall, according to Shuto (1991), by taking the numerical scheme error with appropriate selection of the linear and non-linear equations, the final error is usually within 15% as far as the maximum run-up height is considered.

Dao & Tkalich (2007) conducted a sensitivity study of tsunami propagation modeling by taking into account additional parameters, such as astronomic tide, sea bottom friction, dispersion, Coriolis force, and spherical curvature. The 2004 tsunami event was selected as one of the scenarios to examine the sensitivity of numerical simulations to the variation phenomena above. The results suggest that the astronomic tide and bottom frictions may have a major effect on tsunami propagation in shallow water. The bottom frictions of Manning's coefficient terms of 0.025 and 0.015 may have the effect of increasing by 0.5 m near-shore. The effect of Coriolis should be larger at higher latitudes and could give a variation of the maximum tsunami between 10% and 15%. Furthermore, the dispersion can have a remarkable effect on the tsunami amplitudes that propagate at a far distance in deep water, such as in trans-oceanic tsunami simulation.

In connection with the performance tsunami model with the geo-data used, there are recent studies of sensitivity of the model with varying bathymetry data. Based on these studies, the tsunami run-up heights are less sensitive despite varying near-shore bathymetry data (Kongko, 2008; Leschka et al., 2009a; Leschka et al., 2009b). However, already prevalent among modelers, when using rough data, the grid size used in the simulation model is also coarse. The grid-size used has a significant effect on the tsunami run-up, as studies conducted by Satake & Tanioka (1995) and Gusman et al. (2009) showed. The comparison of the tsunami inundation model using different grid sizes shows that the average tsunami height on the coastline using a 2-second grid is about 2 times larger than using a 1-minute grid system.

The discrepancies of run-up heights of tsunamis as predicted by numerical models and field observations may also be caused by the tsunamigenic mechanism. The 2006 Java tsunami, for instance, has been considered as having been triggered by an earthquake associated with a submarine landslide (Fritz et al., 2007 and Lavigne et al., 2007). This phenomenon occurred in the 1998 Papua New Guinea (PNG) earthquake based on various evidence collected. Acquired high-resolution seismic reflection data yielding new images of a large underwater slump, and a reconstruction model result was consistent with the field observation data (Lynett et al., 2003; Okal, 2003; Synolakis et al., 2002). They suggested that

submarine mass failure was the cause of this event. The 2006 Java tsunami, however, has not been confirmed as the cause of the extreme tsunami run-up as reported at a very short-segment coastline at Nusakambangan Island.

Furthermore, the extensive tsunami hazard analysis of submarine landslide in the Indonesian Sunda Arc had been conducted by Brune et al. (2009a), Brune et al. (2009b), and Brune et al. (2010). By using newly series' bathymetry data, they found some novel mass movements of 12 locations that stretched from off the tip of North Sumatra until off Sumbawa Islands. The volume of the landslides is varying from 1-20 km³ with seafloor slope of 3-15°. In Java subduction zone, by far, it was one candidate event being found.

3.3 The Contribution of Study

The contribution of study is described in the three sections below. It consists of the contribution of the availability of data in the study area and references the Java tsunami model. Further, the present study is expected to contribute to the knowledge of the near-field tsunami and heterogeneous slip. Finally, the result of this study also contributes to the mitigation program through a tsunami model using hypothetical scenarios for future tsunamis in the study area.

3.3.1 Tsunami model reference & availability data in study area

In the present study, the author collected and prepared the materials related to the geometric-geological data, and evidence of the 2006 Java tsunami. Additional surveys have also been conducted to fill the 'blanks' in terms of available data. The data was collected from many sources, but mainly from the GITEWS project and its partner institutions. Further, the additional bathymetry and topography survey in the study area have been made to complete the data above. The to-date current data are the most detailed data available in this area and is adequate for carrying out model analysis for the present study. The data are also essential and useful for any parties who will conduct further detailed analysis in the future.

The Java tsunami earthquake model used highly resolved data and is validated with extensive field observations and tsunami mareograms. The tsunami sources use both empirical and inversion models from tide gauges and global broadband seismic networks. It also attempts to combine the low rigidity at sources and heterogeneous slip of the finite-fault model from seismic networks. Thus, the present study is expected to provide a reliable outcome, and its result becomes a reference for a Java tsunami model.

3.3.2 Near-field tsunami & heterogeneous slip knowledge development

As mentioned in the preceding section, based on the analysis of global seismic data for major earthquakes at subduction zones conducted in previous research, the heterogeneous slip of the complex rupture has a significant role in the variability amplitudes of local tsunami. One of the three factors regarding source parameters, which is independent of the seismic moment and has not been assessed yet, is the combination of higher slip and lower rigidity at shallow depth. In addition, the analysis of prior work showed that the far-field and near-field tsunamis, as physically represented by the distance between epicenters to the coastal zone, have a significant role in the level of variability of tsunami amplitudes near-shore.

The present study conducts analysis of a tsunami model using both the 2006 Java tsunami earthquake as a case study and the hypothetical model with various sources. In the 2006 Java tsunami model, its epicenter and magnitude are fixed. However, the tsunami sources vary to accommodate the slip distributions as well as slip magnitudes. The slip distributions are derived from the inversion model of tide gauge recordings and the broadband seismic network, and the slip magnitudes are estimated from the low rigidity at shallow depths near trenches. The hypothetical model uses synthetic initial conditions, which accommodate the uniform and various slip distribution as well as varying vertical displacement. Such a study is expected to contribute to the lack of the analysis of complex rupture effects of near-field tsunamis in terms of higher slip and slip concentration affecting the tsunami amplitudes and its distribution along the coastline.

3.3.3 Supporting tsunami mitigation program

Cilacap in central Java is one of the pilot study areas of the GITEWS project together with Padang West-Sumatra and Kuta-Bali, Indonesia. The end goal of the project is setting-up domestic and local stakeholders to create and establish the mitigation tsunami program through several elements, one of which is the availability of a reliable tsunami hazard map.

Based on the lesson learned from the 2006 Java tsunami event and the most recent studies conducted by several researchers by interpreting the seismic and bathymetric data suggested that the tsunamigenic at Java subduction zones is strongly influenced by the accretion-erosion subducting process in the complex regimes. Thus, for future tsunamis by involving broad tsunamigenic such as the tsunamigenic tsunami earthquake are unable to be ruled out. On the other hand, the studies available in this area are still using tsunamigenic events of 'normal' earthquakes. Therefore, the present study will model future tsunami

hazard in the study area using limited plausible scenario tsunami sources involving higher slip, and shallow depth with the epicenter near the trench as typical tsunamigenic tsunami earthquakes are expected to make a significant contribution to the tsunami mitigation program.

3.4 Summary

The magnitude scales are fundamental parameters to quantify earthquakes in seismology engineering, among those widely used is the moment magnitude M_W , which is easily converted to the seismic moment M_O . The M_O represents the physical nature of fault dimensions, which in turn can be estimated using various empirical scaling relations. Although, researchers proposed several approaches which depend on fault mechanism and tectonic environment, their scaling relations gave comparable results.

The tsunami earthquake is the sub-class of the tsunami; its amplitudes are higher than those expected from the given seismic waves. Although such events are rare, since they occur at shallow depths in the subduction zone near the trench where in the most cases the prism sediment is present, they lead to slow ruptures in the co-seismic process. They provide false security for the coastal inhabitants and in many cases inflict huge casualties.

The Java tsunami is classified as a tsunami earthquake; its sources originated in the Java subduction zone and the seismic process is strongly influenced by the morphology features of accretion-erosion subducting plates in complex regimes. The model and field data analysis showed that the rigidity material has a variation dependence depth. The depth, which is as shallow as 5–20 km, has a deficiency of rigidity of a factor of ~ 5 and might be closely correlated with the slow ruptures speed in the tsunami earthquake process.

Tsunami earthquakes are situated in the proximity of the trench, which is located near to the respective land, and thus is classified as a local tsunami. The complex rupture of slip concentration, the higher slip due to low rigidity, as well as the epicenter distance are the M_O -independent factors that have significant roles in controlling the variability of tsunami amplitudes near-shore. However, such studies of this topic are of less concern here.

Due to the absence of highly resolved geometric data, the available Java tsunami models use data of a coarse resolution. Moreover, the model validations using field observation data as well as tsunami mareograms have not been conducted yet. The numerical methods suitable for tsunamis in the last two decades dramatically increased in terms of quantity and quality, with a level of acceptable error.

The present study deals with a tsunami model using highly resolved geometric data in the study area of Java, with broad tsunami sources and validated by extensive field observations. The present study is expected to contribute to the availability of high-resolution geometric data in the pilot area and the reference of the reliable Java tsunami model. Further, the complex rupture of slip concentration as well as the low rigidity of material will also be assessed by using a synthetic model test to comprehend the significance of the relevant factors. This will contribute to the knowledge of the complex rupture effects on the tsunami amplitudes in the local field. The present study also proposes the inundation hazard map based on a limited scenario that might support the tsunami mitigation program in a pilot study.

Chapter 4 - Research Procedures

“Smong dumek-dumekmu, linon uwak-uwakmu, elai kedang-kedangmu, kilek sulusulumu...Nga linon fesang Smong. (the tsunami is your water-bath, the earthquake is your cradle, thunder is your percussion, and flash is your lantern...after earthquake followed by tsunami” (Poetry and indigenous knowledge of Simeulue Island of Indonesia-anonymous).

The research procedures of the present study are outlined in this chapter. It consists of five sub-chapters; the first three are the research methodology, data collection, and data processing. The simulation model follows before the chapter concludes with a summary.

4.1 Research Methodology

The research methodology is the method of undertaking the research, which generally means the method of the process of collecting, analyzing, interpreting information to answer the problems and questions⁴.

The following sub-chapter describes the research methodology, which consists of two sections, namely the types of methodology, and the research design & business processes. It provides the used research types and shows the total plan of the relevant elements' research in the present study. The step-by-step tasks of the business process as a conceptual framework of research methodology is also delivered.

4.1.1 Types of methodology

There are at least fifteen common types of research according to the literature. However, there is no standardization in the terminology of research methodology across professional or academic fields. Each is a valuable method when linked to appropriate problems (Mauch & Birch, 1993).

The types of research can also be classified from three perspectives, namely from the application of the study, the objectives in undertaking the research, and the inquiry methods approaches⁴. The first perspectives consist of the pure and applied research, and the second cover the descriptive, correlational, explanatory, and exploratory research. The last are adopted from the process when finding the answer to the research questions, which consist of two approaches; structured or quantitative and unstructured or qualitative approaches.

⁴ http://www.ihmctan.edu/PDF/notess/Research_Methodology.pdf

The present study is categorized as applied research, where the specific and practical questions related to the phenomenon of the 2006 Java tsunami are addressed. It is also classified as a correlational and quantitative study, since it attempts to discover and establish the interdependence among parameters that play roles in the events.

The present study also collects the primary and secondary data related to the 2006 Java tsunami, conducts a bathymetric-topographic survey as well as documents survivor interviews in the study area. In addition, hundreds of numerical model simulations have been carried out to validate the past event and to predict future tsunami hazard in the area considered. Therefore, to accommodate such element tasks above, the present study utilizes the combined types of methodology, namely the case study, historical, correlation-predictive, and experimental types of methodology.

The type of case study used in this research was chosen for the reason that the available highly resolved data as well as other data collected is only present in the limited area of Cilacap and surroundings. Furthermore, the correlation-predictive type is used due to the fact that the similar geological tectonic environment in the Java subduction zone may provide recurrence events for future hazards. In addition, to validate and examine the tsunami source parameters as well as their run-up along the coastline, the numerical model experiment of hundreds of simulations has been conducted.

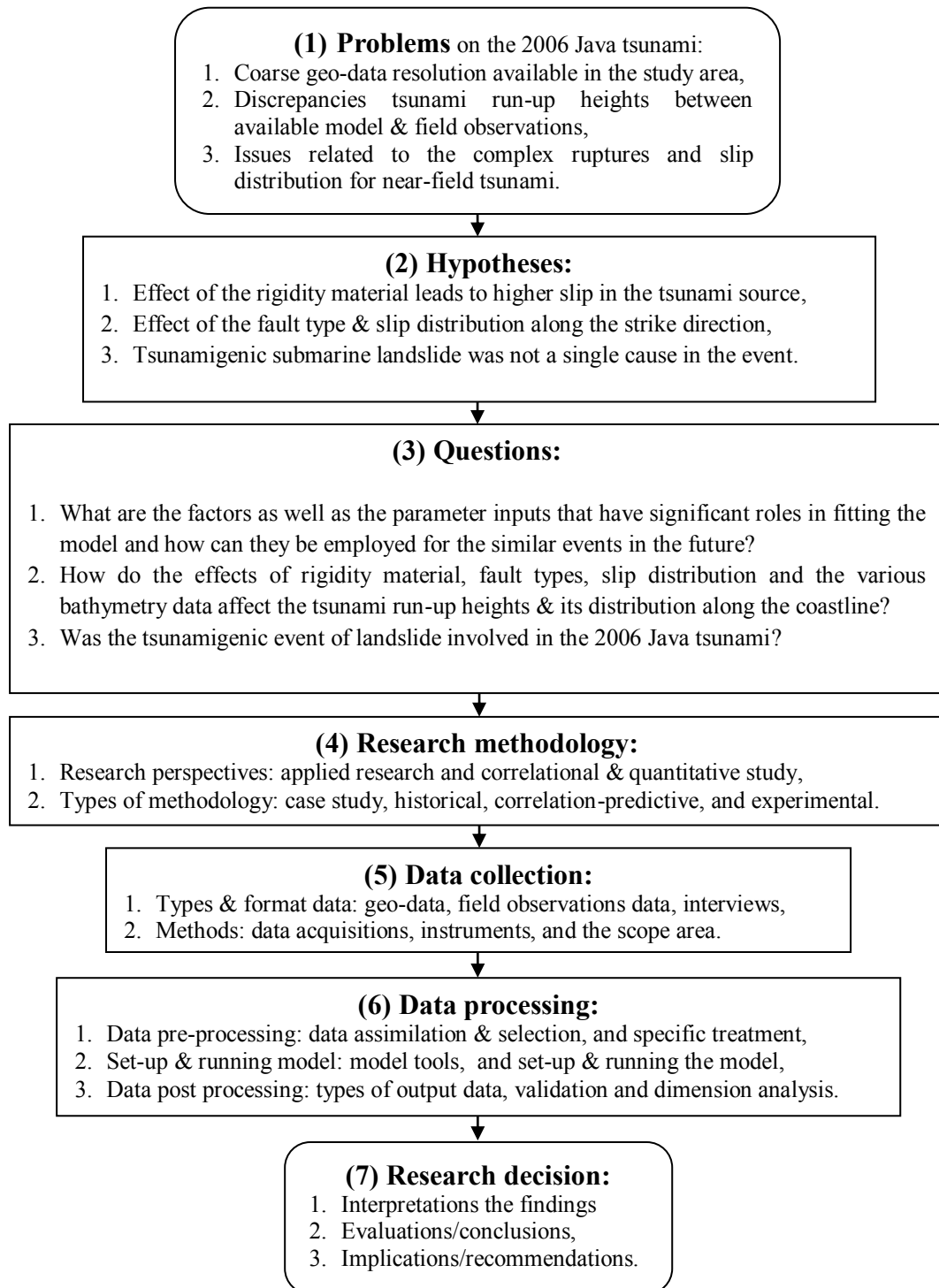
4.1.2 Research design and business processes

4.1.2.a Research design

The research design of the present study is depicted by a flowchart in order to show the flow and sequence of tasks as well as their processes, each of which is a separate scientific investigation. The total step-by-step plan of group tasks limits the scope of the study and guides it along the path towards achieving the research objectives.

It is also intended to map the problems of the relevant research elements and obtain objective, reliable and valid information. This indicates how the available resultant objectives' information should be used to determine the conclusions and their processes to proof the hypotheses and answer the questions of this study (Mauch & Birch, 1993).

The following is the research design of the present study.



4.1.2.b Business process

The task group of the present study as depicted in a flowchart of (1), (2), and (3) in the research design as given in the preceding sub-section may be classified into four groups as follows:

- A. Geo-data improvement from data collection and field survey,
- B. Reconstruction of the 2006 Java tsunami model using highly resolved data and various tsunami sources,
- C. Hypothetic model for future tsunami hazard by using plausible maximum scenario for similar event,
- D. Synthetic model for examining the effect of higher slip & its distribution (complex ruptures) to the run-up heights along the coastline for local tsunami.

Each task group above is conveniently represented visually by a flowchart. The flowchart is an ideal diagram for representing the business process. It has various forms and conventional meanings and shows the steps and their order connected by arrows. It was first introduced by Frank Gilbreth in his presentation for the members of American Society of Mechanical Engineers (ASME) in 1921⁵.

Here, however, the author adopts the eight standard flowchart symbols with conventional meanings to represent the task groups above, which the descriptions are elucidated in the link in the footnote below⁶. The flowcharts of each task group above are presented in Appendix J – The Flow-chart of the Business Process in section A-D.

By looking at the flowcharts of the business processes in Appendix J, task groups A, B, and C have direct dependencies that are interconnected by connector diagrams (shown as circle diagrams). For instance, the task group of geo-data improvement (A) produces improved geo-data, which will be used for further process of the task group of reconstruction of the 2006 Java tsunami model (B). Further, in task group B, through the looping process of examining the various tsunami sources to attempt to fit the model with field observations and marigram data. The tsunami source parameters from the best-fitting model of the 2006 Java tsunami are selected and associated with other assumptions to determine the plausible maximum scenario of certain magnitudes. These scenarios then are used in the hypothetic model for future tsunami hazard of the Java tsunami in the study area as depicted in task group C.

⁵ <http://en.wikipedia.org/wiki/Flowchart>

⁶ <http://www.edrawsoft.com/flowchart-symbols.php>

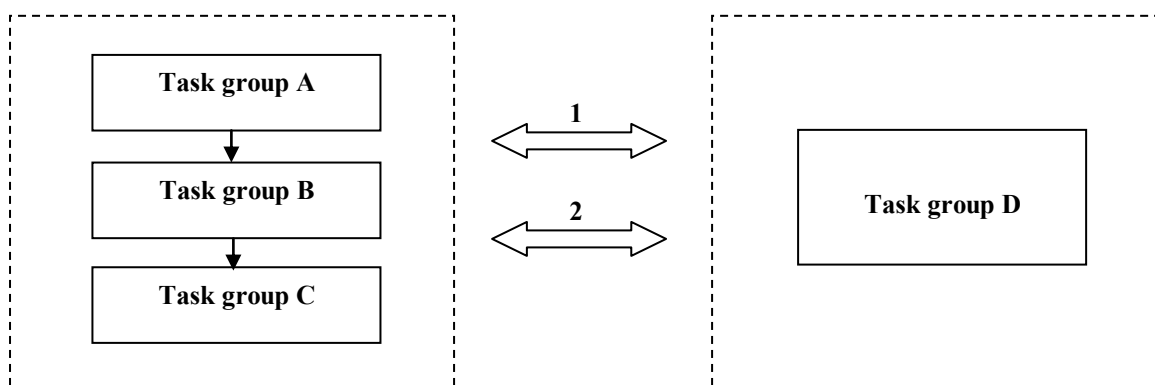
Task groups A, B, and C have a sequential dependency in terms of geo-data improvement, the 2006 Java tsunami model validation, and the selected tsunami sources for plausible scenarios for future hazards. However, task group D is the synthetic model intended to examine the effect of the complex ruptures that are independent unlike the previous three task groups in terms of the geometric data and tsunami sources. Task group D focuses especially on the sensitivity model of the tsunami amplitudes along the coastline due to the uniform-distributed slip effects as well as the higher slip of the low-rigidity material.

This task group, the geometric data for the numerical simulation, uses synthetic data resulting from generalized bathymetric data of south Java. The model results are dimensionless graphs, which include significant parameters such as fault lengths, tsunami run-up heights, length of the distribution along the coastline, and vertical dislocation values.

Task groups A, B, and C on one side and D on the other, in general have relations in the following matters:

1. Each examines whether the higher slip / low rigidity has a significant role in the tsunami amplitudes along the coastline and estimates the consistency of the amplification ratio between the rigidity values and tsunami run-up heights.
2. Each examines the effects of the type of tsunami sources in terms of the uniform and distributed slip to the tsunami run-up heights and to estimate the ratio of uniformly distributed slip to the run-up variation and its distribution along the coastline.

The relations above are depicted in the diagram below.



4.2 Data Collection

One of the issues addressed in the present study and mentioned in research design in the preceding sub-chapter is the absence of high-resolution data for the study area. Furthermore, to reconstruct the 2006 Java tsunami model and its further analysis, such as model validation of tsunami run-up heights and its distribution along the coastline, reliable geometric and field observation data are inevitably needed.

This sub-chapter describes the data collection, which consists of the primary data acquisition carried out through field measurement campaigns, and secondary data collection undertaken by previous researchers as well as those derived from the earthquake-tsunami database and tide gauge stations.

4.2.1 Geo-data

4.2.1.a Data types, sources and scope area

The geo-data are one of the basic requirements and must be present before performing the numerical simulation, and are thus deemed essential. This refers to data assimilation from both bathymetry data and topography data, where the latter is simply ground-level data.

The present study undertakes the model simulation, whereby the numerical domain covers the Java subduction zone and Java Island. This domain stretches from $\sim 104^{\circ}$ - 116° E and $\sim 5^{\circ}$ - 12° S occupies an area of over 1.03×10^6 km²; therefore, in the most areas only coarse bathymetry data are available. In land, where the tsunami run-up heights were observed, medium topography data has been used. In the study area of Cilacap and its vicinity, however, high-resolution geo-data has been made available through the GITEWS project.

The types of geo-data that have been used in the present study and its sources are as follows:

1. Bathymetry data:

-GEBCO (General Bathymetric Chart of the Oceans) provides data that is publicly available and free to download via the internet. The GEBCO is a continuous terrain model for ocean and land with a grid spatial resolution of 30 arcseconds or approximately 925 m in the place near to the equator (GEBCO 2008).

-BAKOSURTANAL stands for Badan Koordinasi Survei dan Pemetaan Nasional or the Coordinating Agency for Surveys and Mapping of Indonesia. In July to September 2007, it conducted a bathymetric measurement campaign using single-beam echo-sounder equipment. The survey covered an area within of 109° - 110° E

and 7.4°-8°S off south central Java with its track spacing normal to the coastline of about 250–500 m and points data acquisition along the track of about 30–90 m. -Field measurement campaigns within the framework of the GITEWS (German-Indonesia Tsunami Early Warning Systems) project were conducted three times during the period of 2008 to 2009. The first was conducted in March 2008 using multi-beam echo-sounder equipment mounted at ~20x6 m on the survey vessel. The coverage area of the survey is about 70 km² located within the bay of Cilacap. The second and third bathymetric surveys were carried out in November 2008 and July 2009, respectively. The survey area was the river and channel in the main city, and near-shore zone with water depth less than 5 m. These surveys were also intended to fill the area that had not been measured in the first survey due to time and equipment constraints. The explanation of the bathymetry survey is briefly provided in the next sub-section of this sub-chapter.

2. Topography data:

-NASA Shuttle Radar Topographic Mission (SRTM) provides digital elevation data (DEM) for over 80% of the globe. It is available at a resolution of 3 arcseconds (approx. 90 m resolution, and thus called SRTM-90), and 1-arcsecond resolution (approx. 30 m, also known as SRTM-30) for limited countries. The vertical error of the SRTM-30 is reported between 16–20 m (CGIAR-CSI, 2008; Zielinski, 2007).

-DEM (Digital Elevation Model) was collected within the framework of the GITEWS project. It uses Intermap Technologies STAR-4 airborne interferometric SAR, whose available ground sampling data is 5 m (Intermap Federal Services 2007). The data covers the land area of the district of Cilacap from 108.94°-109.41°E and 7.64°-7.8°S. There are two types of DEM data, namely DSM (Digital Surface Model) and DTM (Digital Terrain Model). DSM is the data in which the land cover is included, such as buildings, vegetation, etc., while DTM is the data containing solely terrain or bare soil, and land cover such as buildings and vegetation by using certain methods are removed.

-Field measurement for topography has also been used to compensate for the absence of DEM data especially in the area of Permisan – Nusakambangan Cilacap, the place where previous researchers reported extreme run-up heights

during the 2006 Java tsunami (Fritz et al, 2007; Lavigne et al, 2007). The explanation of the topography survey is briefly provided in the next sub-section of this sub-chapter.

The layout of the types of geo-data and its sources that have been collected and used in the present study is shown in Figure 23.

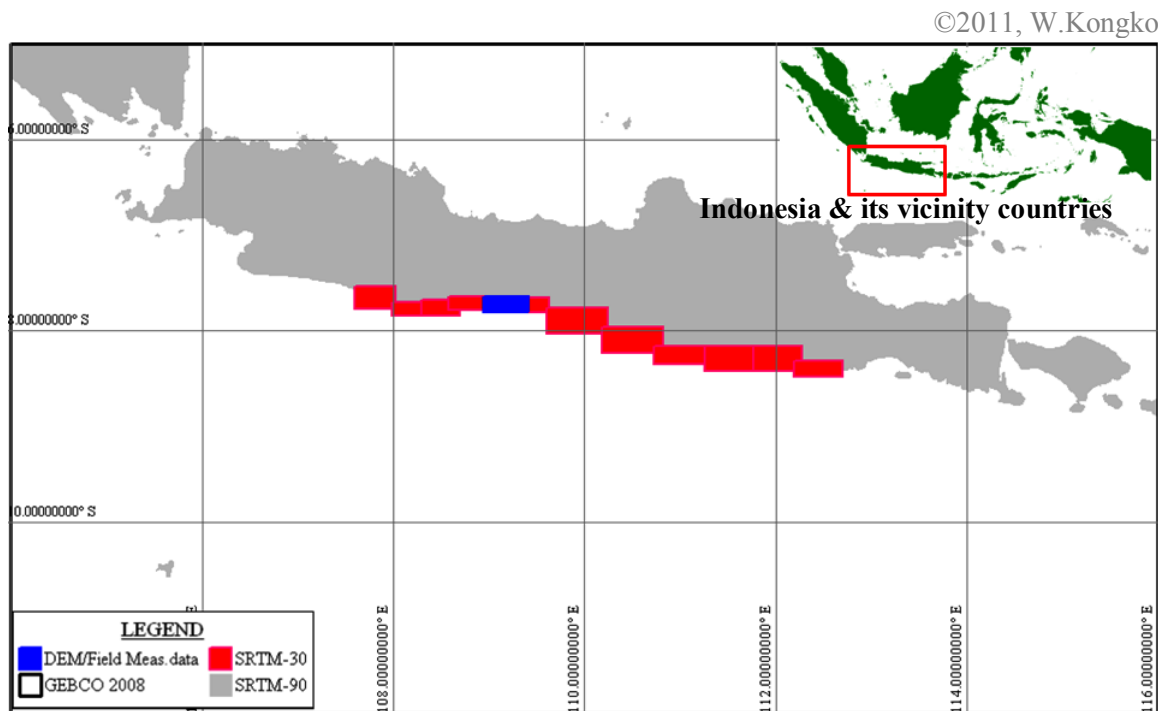


Figure 23: Layout of the types of geo-data & its sources

4.2.1.b Field measurements

Within the framework of the GITEWS project, series field measurements were conducted in the study area of Cilacap. It consists of three phases: bathymetry survey, topography survey and ground check in Permisan-Nusakambangan, and survivor interviews in the area affected by the 2006 Java tsunami.

Figure 24 is a blow-up of the blue box depicted in Figure 23. It shows the layout of the various data collected through field measurements, which were provided by many sources during this study.

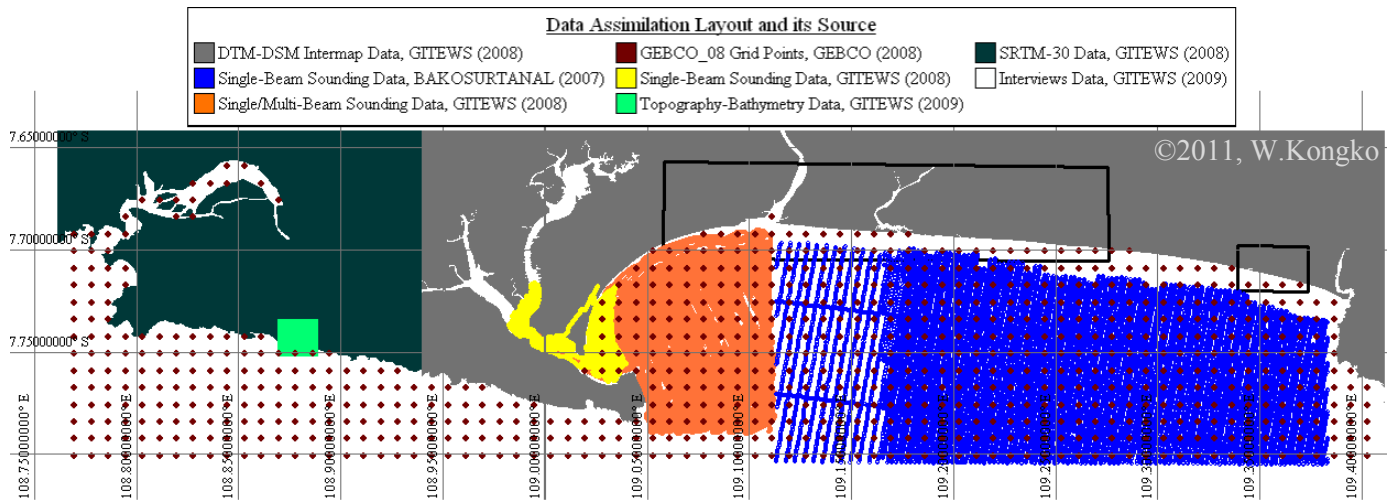


Figure 24: Layout of data assimilation and its sources in Cilacap

The first two phases of the bathymetry survey were conducted in Penyuu Bay of Cilacap, the river and city channels, and the near-shore zone with water depth less than 5 m altogether covering more than 70 km² (see the areas marked yellow and orange in Figure 24). The other bathymetry survey was done off Nusakambangan Island and indicated by a light-green box in Figure 24. Although the last survey could not be completed due to bad weather, several transects of point measurements normal to the coastline were attained.

The detailed field measurements include the scope area, equipment, and survey methods provided in the series reports by Kongko & Leschka (2009), Ahmad & Kongko (2008), and Ahmad & Harmiawan (2009). Here, however, the project's brief info and technical specifications are given in Appendix C – Field's measurements in sections A, B, and C.

To conduct further analysis on the extraordinary tsunami run-up following the 2006 Java tsunami, the topography survey and ground check were also carried out on Permisian-Nusakambangan Island off Cilacap (light-green box in Figure 24). This survey performs two tasks: first, data collection of coastal features surrounding the 39 points of maximum run-up and flow depth of the 2006 Java tsunami as conducted by previous tsunami survey teams (Fritz et al., 2007 and Lavigne et al., 2007); second, measurement of the ground level in this area, since DEM data as provided by the GITEWS project are only available for the dense population area in Cilacap city (colored gray in Figure 24) and do not cover Permisian; therefore, additional field work is required.

The ground-checking survey used a handheld GPS device to track the points that had been investigated and documented by teams previously. Ground features were also recorded, such as steepness, vegetation, etc.

The topography survey campaigns were equipped with high-accuracy Total Station instruments for measuring the ground level at more than 1,200 points. The survey points are located within the area of about 1.5 km² with its spacing ranging from 10–40 m in a transect fashion normal to the coastline. The ground-level measurements were made from the coastline by climbing onto some surroundings steep hilly areas inland to reaching the location of the maximum run-up heights of the 2006 tsunami.

The detailed topography and ground check survey was provided in the survey report by Ahmad et al. (2009) and the project's brief info and technical specifications are given in Appendix C – Field's measurements in section D.

Furthermore, for inundation's modeling validation purposes, the estimation of the maximum inundation points during the 2006 Java tsunami is required. Hence, local people living in the Bay of Cilacap and who have experienced such events were interviewed. The survey locations were concentrated in two places as depicted by two black empty boxes in Figure 24. The big box (in the western part) is situated by the riverside of Serayu and Bengawan and includes the low-land of four sub-districts (17 villages), the places where the farthest tsunami penetration occurred, and the most victims were found. And the small box (in the eastern part) that includes one sub-district (3 villages) is also the place that the 2006 tsunami reportedly penetrated far inland, implying many casualties.

Due to time constraints, only 23 point locations of estimated maximum tsunami run-up in 11 villages were investigated. The survey method is a direct interview with survivors instead of delivering questionnaires. To minimize information uncertain from survivors, blind-cross interviews were conducted in the same locations. The respondent data and the variety of information attributed to the tsunami event, such as the points of maximum inundation, earthquake tremors, the tsunami's time arrival, wave counts, incident direction, land cover, and victims were collected and documented. The detailed information of the tsunami run-up survey is provided in the survey report by Kongko (2010), and the summary report is given in Appendix C – Field's measurements in section E.

4.2.2 Observation data

4.2.2.a Historical events

The present study utilizes two sources of the earthquake-tsunami historical data, namely the Integrated Tsunami Database for the World Ocean (ITDB/WLD, 2007) and the United States Geological Surveys (USGS) source parameter database (USGS, 2010). Both databases provide information related to the earthquake's parameters. Although, the given information in both datasets is not exactly similar in terms of parameters and format, they function as complementary sources. The first database is delivered in compact disc (CD), which is available with a Window-based software interface package giving the historical event information related to the earthquake and tsunami. The data were compiled and assembled from a wide variety of both published and unpublished sources, so that they represent the most complete historical tsunami dataset in digital format ever (ITDB/WLD, 2007).

The second one, on the other hand, is an internet-based database, offering a wide choice of data sources and output formats in the required parameters as well as the optional parameters, such as the range of magnitude, scope area, and period of time and is available in the source parameters' submission search applet. The USGS source parameter database provides detailed information of the earthquake's parameters, such as time of event, epicenter, depth, magnitude (in M_W and M_O), and nodal planes (or angle parameters of strike, dip, and slip).

The area of the present study is within the geographic coordinates 104.0°–116.0°E and 5.0°–12.0°S, which cover an area of about 1.03×10^6 km². According to ITDB/WLD (2007), 419 earthquakes occurred in Java's subduction zone in the time period 1977–2007 within these bounding coordinates with magnitudes greater than M_S 5.0 and hypocenters shallower than 40 km. Among these events, the two most significant earthquakes in terms of magnitude happened in 1994 and 2006 and generated sizeable tsunamis causing damage and casualties along the south Java coastline. The plot of earthquake and tsunami dataset on the map of Java is depicted in Figure 3 in Chapter 2. The list of events compiled from ITDB/WLD (2007) is re-tabulated and provided in Appendix D – Observation data in section A.

To obtain the source parameters of tsunami candidates and past tsunami events, the author retrieved data from the USGS database with similar bounding coordinates to those

given above. Since its purpose is to obtain the source parameters attributed to the tsunamigenic earthquake, thus present study limits the retrieving data values, i.e. for magnitude $M_W > 6.5$ and depth < 100 km within the time period of 1978–2008. 20 events were compiled; two events that generated tsunamis in 1994 and 2006 had source parameters by Harvard (HRV source) that were nearly similar, namely the strike, dip, and slip are $\theta \sim 278^\circ\text{-}297^\circ$, $\delta \sim 10^\circ$, and $\lambda \sim 90^\circ$, respectively. The table of source parameters of Java earthquakes within the period 1978–2008 by USGS is provided in Appendix D – Observation data in section B.

4.2.2.b Field observations data

The present study collects field observation data related to the 2006 Java tsunami, which consists of two numerical types of data and one sequence of photos and video snapshots capturing the tsunami waves recorded by a survivor. The first data types are field observations of tsunami run-up heights conducted by several international tsunami survey teams (ITST) and the three tsunami marigrams that were collected from the tide gauge network installed along the south Java coastline. The second is the secondary data of the sequence of photos and video snapshots that were documented and published by previous researchers. The layout of the field observation data as well as the location of tide gauge stations is shown on the map in Figure 25.

The observation data of tsunami run-up heights used in the present study have been collected from five sources of published and unpublished reports, namely Fritz et al. (2007), Fujima & Matsutomi (PARI team, personal communication), Tsuji et al. (personal communication), Lavigne et al. (2007), and Kongko et al. (2007). The data were taken along the south Java coastline from west Java at a point approximately 107.68°E to east Java at a point about 112.68°E , which is has a straight length of more than 550 km. Even though the data collected have different formats, in general they contain the location's name, geographic coordinates (or position), tsunami run-up heights, flow depth, ground level, horizontal distance from the coastline, and descriptions of the points measured, such as trim-lines, debris, broken branches, water marks on walls, etc. 394 data points were collected. However, not all data contain all of the information of the tsunami parameters as mentioned above. Figure 25 shows the overlay of the run-up height points on the map and for this study the numeric data were re-edited and re-tabulated into a common format as provided in Appendix D – Observation data in section C.

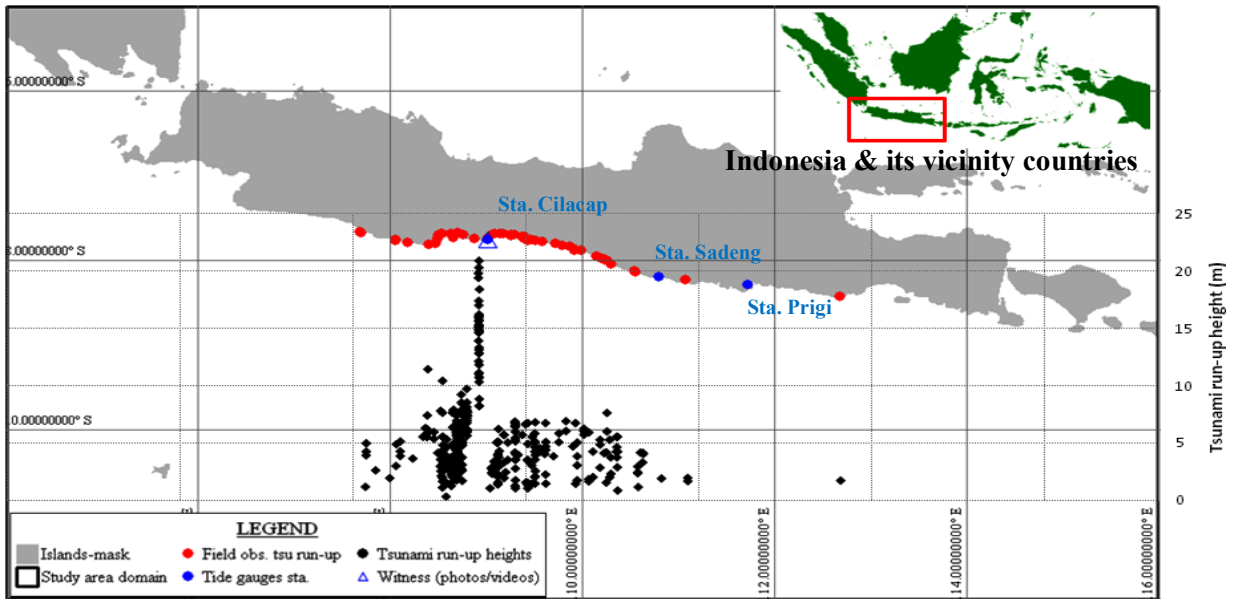


Figure 25: Layout of the observation data & tsunami run-up heights

The present study also collected tsunami marigram data from three locations of tide gauge stations operated by BAKOSURTANAL, namely the stations at Cilacap (108.89°E / 7.75°S), Sadeng (110.798°E / 8.190°S), and Prigi (111.733°E / 8.283°S) (see Figure 26). For this study, real-time tsunami marigram data were selected and taken four hours after the earthquake.

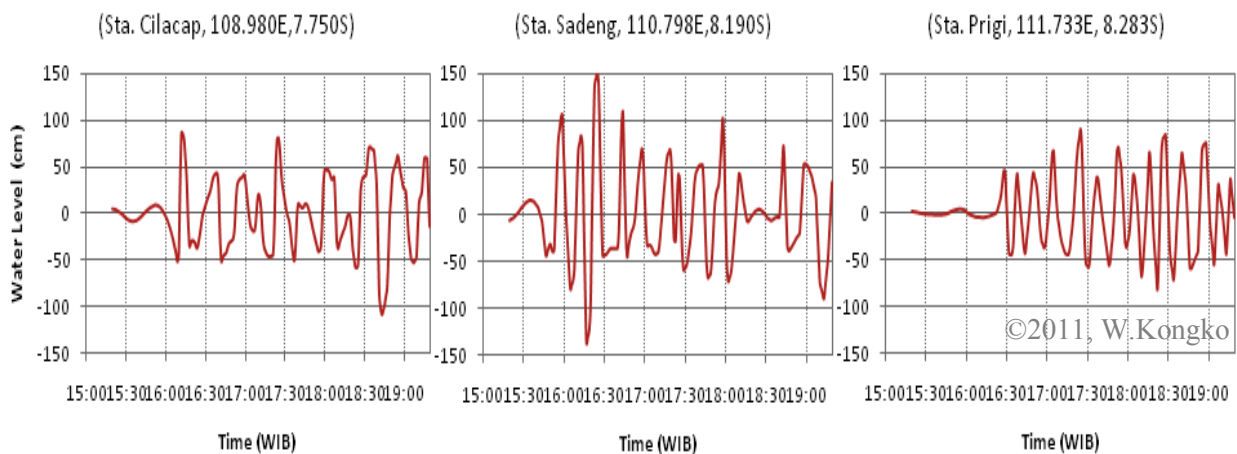


Figure 26: Marigram of tsunami recorded at three tide gauges station



Figure 27: Tsunami wave at shrimp basin at Keboncarik-Cilacap (16:16~16:20 WIB)

The secondary data of photos and sequence of video snapshots of the tsunami incident in Cilacap were collected from a paper published by Lavigne et al. (2007). Photos A and B in Figure 27 show the tsunami waves entering the shrimp basin (local language is “Tambak”) located in Keboncarik-Cilacap, showing the inundating waves between 16:16 and 16:20 WIB. Photo C is the same location as A and shot from approximately the same angle; it was taken one and a half months after the disaster.

©2007, Lavigne et al., courtesy of Ir. Chandra Dwi Putra, MM, PLTU Cilacap

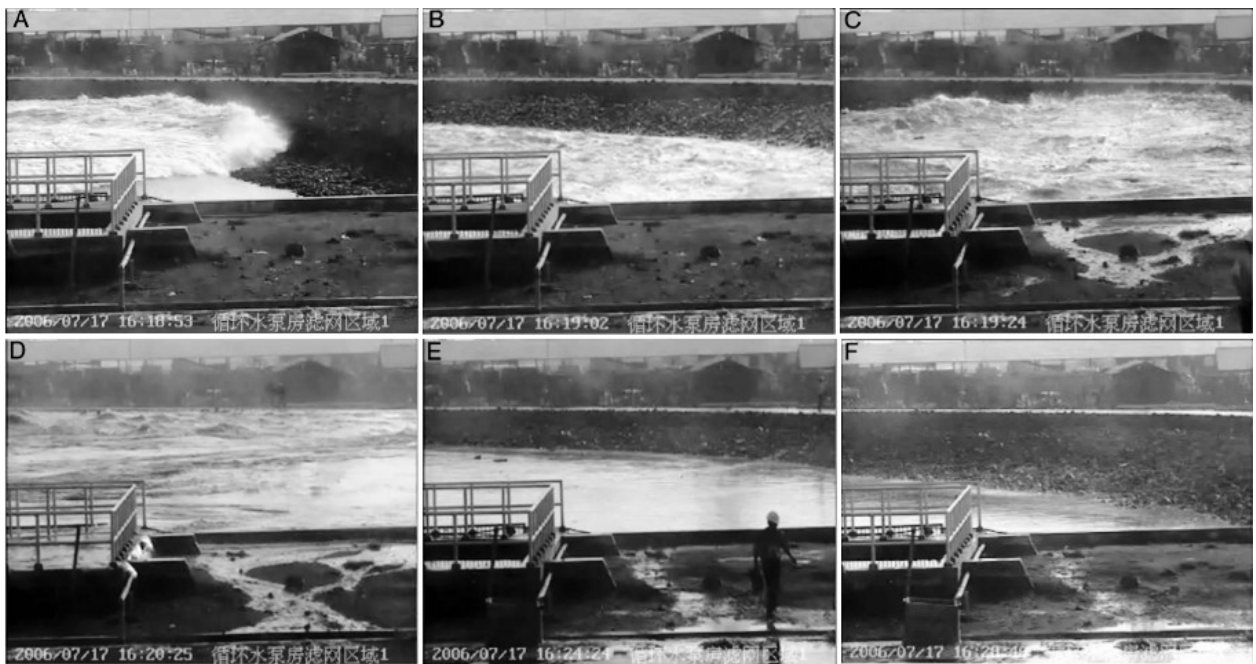


Figure 28: Video snapshot of tsunami waves at ship basin of PLTU-Cilacap

Furthermore, further data come from the sequence of video snapshots taken by a survivor in the ship basin of PLTU (Steam Power Plant). This is the best evidence of the tsunami’s arrival time and its wave evolutions for the 2006 Java event in Cilacap. They comprise six frames of video snapshots shown in Figure 28; each frame has a time tag at the

bottom allowing the evolution of the tsunami to be interpreted in terms of time. Snapshot A at 16:18:53 shows the tsunami bore leading the wave; snapshot B at 16:19:02 then shows the wave in a second receding. Further, a sizable long-period wave is rushing onto the beach and reaching the top of the breakwater in snapshots C and D at 16:19:24 and 16:20:25, respectively. And the water level is again going down in snapshots E at 16:24:24 and F at 16:28:48.

The whole data collection described in this sub-chapter that consists of field measurements and provided geo-data, combined with historical events and field observations, have been used for further analysis in this study, namely to validate the tsunami model of the 2006 Java tsunami and other relevant issues.

4.3 Data processing

The data used in the present study as mentioned in the preceding sub-chapter can generally be classified into three data categories in terms of data type, data source, and the data format.

The types of data consist of bathymetry, topography, and observation data. The first two are simply the level of sea bed and land against the certain reference respectively, and the latter includes the historical events of the tsunami earthquake and the evidence of the 2006 Java tsunami. It comprises the tsunami run-up heights along the coastline, tsunami marigram data at tide stations; a collection of photos and video snapshots from a survivor, and survivor interviews in the study area.

Furthermore, data sources may be differentiated in terms of where the data originated, i.e. primary and secondary data. Both data types were made available within the project's framework, thus the measurement campaigns and interviews were fully supported and funded by GITEWS. In addition, since the present study is one of the capacity-building programs in the project, the collecting secondary data from the project's partner in this framework was also possible.

The variety of types and sources of data led to many kinds of format being attributed to both numeric (i.e. geo-data and observation data) and non-numeric (i.e. interviews and pictures) data. These formats include, for instance, the kinds of data projection and their references (UTM/Geographic coordinates, WGS84), and the data format such as the XYZ, ASCII grid data, *.ASC, *.SHP, *.BIL, etc. However, the most important of all above is the data resolution.

This sub-chapter describes the data processing and its specific treatment, which consists of pre-processing for geo-data as well as field observations, and post-processing of numerical results and their validation.

4.3.1 Pre-processing

4.3.1.a Geo-data

The bathymetry and topography data from both field measurements and data collection available in this project are merged and processed to create a structured continuous dataset, and then used for the geometric data input in the numerical simulation as well as for further analysis. Meanwhile, the data type and sources as depicted in Figure 23 and Figure 24 in the preceding sub-chapter are unstructured with different resolution.

The GEBCO data, which covers the whole numerical domain (the whole box in Figure 23), has the lowest resolution of ~925 m, and the higher is the SRTM-90 data with its resolution of around 90 m (the land shaded gray in Figure 23). Further, the medium resolution of ~30 m of SRTM-30 are made available in the area where the 2006 Java tsunami run-up heights were observed as depicted by red boxes in Figure 23. And the highest resolution data are in the study area of Cilacap as shown by the blue box in Figure 23. The data is assimilated from both field measurements and data collection within this project. It consists of eight types of data from three sources. The layout of data assimilation and its sources in Cilacap and the surrounding area is depicted in Figure 24.

To process the many kinds of types, resolutions, and sources of data above and for the numerical simulation purposes, in which due to the use of the nested grid system requires different grid-spacing depends on the domain level, thus the steps of data preprocessing might be taken in the following way:

- Sorting the bathymetry and topography data from the highest to the lowest resolutions, regardless of data sources.
- By using GIS software, overlying the data in one coordinate system domain and making *.SHP files for each data source. These files are useful for further processes of blanking and filling the data, due to the fact that in the merged data inevitably any overlapping data or data gap within the whole domain is considered.
- In the case of overlapping data, the data with highest resolution will be selected and the lower data de-selected. On the other hand, in the case of any data gaps,

data interpolation using surrounding data available will be needed to fill the gap. If necessary, the blank area will be filled using manual digitizing data.

- The last step is interpolating the merged data based on the requirements of the grid-spacing for each numerical model's domain, a detailed discussion of which is provided in the next section.

4.3.1.b Field observation data

The field observation data that has been collected for present study includes the 2006 Java tsunami run-up heights, tsunami marigram data, and the sequence of photo and video snapshots. The data preprocessing here, however, is carried out only for the first two. For the latter, i.e. the sequence of the photos and video snapshots, preprocessing is not required, since for model validation purposes the author only interprets the pictures of the incoming tsunami wave and their real-time evolution that is clearly indicated at the bottom of the picture frames or those adopted from corresponding papers.

There are three tsunami marigram datasets as mentioned in the preceding sub-chapter as their locations plotted on map of Java in Figure 25. The raw marigram data provided by BAKOSURTANAL still includes the astronomical tides in the respective location. The data has been filtered using FFT (Fast Fourier Transform) band-pass filters by passing the component of tsunami waves, whose period varies in the range 100–2000 seconds (Wiegel, 1964 & 1970 in Bryant, 2008). The de-tide marigram tsunami graphs for three tide stations are shown in Figure 26.

The tsunami run-up heights along the south Java coastline are plotted as a dataset in Figure 25 in the preceding sub-chapter; the run-up heights were observed by several international tsunami survey teams which were formed a few days or weeks after the tsunami. The entire dataset contains 394 points stretching more than 550 km along the coastline and was collected by five teams (Fritz et al., 2007 – 124 points; Tsuji team – 32 points; Fujima & Matsutomi/PARI team – 76 points; Lavigne et al., 2007 – 133 points, and Kongko et al., 2006 – 29 points). However, for model validation of tsunami run-up heights and their distribution, to reduce uncertainties caused by topographic artifacts in the surrounding area, the author selects the dataset according to the following criteria:

- The distance of acquisition points is less than approximately 150 m from the coastline, by assuming the existence of a typical beach profile and the absent coastal vegetation have been considered.

- The dataset without any horizontal distance information from the coastline or its beach slope is relatively steep, i.e. bigger than 1/10 being excluded. The reason is the steeper beach slope then the higher effects on the vertical component of water particles, which are not taken into account in the numerical model of NSW E leading to numerical error predictions.
- The author separated the data of the extraordinary tsunami run-up at Permisan and the maximum run-up collected from interviews with the dataset above. However, both are used for model validation of tsunami inundation onto land.

These approaches enabled a total of 114 pre-selected points of tsunami reference. These datasets have a mean beach slope of 1/32.5, an average horizontal distance of 93.8 m, and tsunami run-up heights varying between 1.1 – 14.7 m. The datasets are available in Appendix D – Observation data in section D.

Following the above criteria, the separation data of the extraordinary tsunami run-up at Permisan from the other data was done with the purpose that they will be used for validation of the inundation model onto land. In addition, they are meant for further analysis by comparing them with topography measurements in the area. The datasets and their comparison with topography measurements are provided in Appendix D – Observation data in section E, F and G.

4.3.2 Data post-processing

4.3.2.a Types of output data

As elucidated at the beginning of this chapter, i.e. in the research design and its business processes, there are four group tasks in the present study, namely geo-data improvement, reconstruction of the 2006 Java tsunami, formulation of a hypothetic model for future hazards, and of a synthetic model for the effect of complex ruptures. The types of output data, therefore, follow and represent each of the business processes above.

The type of geo-data improvement is the structured continuous ground level data as the result of the assimilation and interpolation process of various data sources and resolution. The data format is in three columns: an XYZ format, a gridded matrix of ASCII format, and a gridded matrix of ASC format. Since the study domain covers approximately 1.03×10^6 km², to minimize the geo-data size, their grid resolution follows the nested grid system in the numerical models. Hence, the data post-processing simply synchronizes the grid spacing data during the interpolation process that follows the grid spacing in the nested grid system of the

numerical models. The layout, bounding coordinates, and grid spacing of each domain are provided in the next sub-chapter.

The reconstruction of the 2006 Java tsunami produces three types of data output, namely the tsunami run-up heights along the south Java coastline, the tsunami inundation from selected scenarios (based on selected parameters) in the study area, and the tsunami time series at the points of the tide stations and witness' positions. These outputs are used for validating the model by comparing them with the tsunami observation data, maximum tsunami run-up in Permisan and Cilacap Bay (Serayu and Bengawan river & surroundings; eastern part of Cilacap), and tsunami marigram recorded in the tide gauge stations as well as interpretation of photos and video snapshots. For the first two, the post-processing for model validation is provided in the section of the specific treatment. The latter simply interprets the time series data and compares them with tsunami marigram as recorded at tide gauges as well as photos and a sequence of video snapshots.

The study on the hypothetical model for future tsunamis in the study area proposes the inundation map based on limited multi-scenarios of plausible maximum of certain magnitudes with several assumptions. The number of inundation maps is equal to the combination of parameters, namely magnitude scenario of earthquakes, epicenters, and kinds of mitigation measures. The inundation map, however, was set up based on epicenters by taking the envelope of each maximum inundation of each epicenter considered.

The last task group in the present study is the synthetic model for the effect of complex ruptures, whose business process and outcome are independent unlike the three sequential task groups above. The results for this task group are dimensionless graphs that include significant parameters of the process, such as fault lengths, tsunami run-up heights and its distribution, etc. The dimension analysis of the synthetic model is provided in the next section.

4.3.3 Specific treatment

This section discusses the specific treatment of the data processing that is related to three issues addressed in previous sections. They are the data assimilation process in the boundary areas near the coastline, the model validation resulting from the reconstruction of the 2006 Java tsunami, and the dimension analysis of the synthetic model.

When dealing with the data assimilation in which their resolutions are very different, such as the GEBCO data that has a resolution of ~925 m compared to the SRTM-30 data with a resolution of ~30 m, a specific treatment is needed to fill both blank and overlapping data in

these boundaries near the coastline. In many cases, such a problem can only be resolved by manual digitization, which occurs in the present study. As mentioned in the previous section, to resolve such a problem, the first step is to determine and select which one has the highest resolution. The second step is to discard the coarser data, which in this case is the GEBCO data, up to a certain water depth. The strip blanking data area near the coastline is then filled by using manual digitizing data. The present study conducted such a treatment along the coastline of more than 550 km following the SRTM-30 data as depicted with red boxes in Figure 23, except in the area of Cilacap where high-resolution data are available.

Model validation of tsunami run-up heights along the south Java coastline is conducted by comparing the field observations with the model results. As pointed out previously, validation is applied to 114 points of pre-selected data from the total of 394 points of tsunami run-up stretching more than 550 km along the coastline. For the tsunami model, the run-up data are collected from the maximum wave excursion in the numerical domain's level that occupies the near-shore zone in the water depth of ~ 1-3 m with spatial acquisition ~205 m. Therefore, all the numerical domains are situated near-shore with data comprising 2910–3020 points. To validate the model of tsunami run-up heights, the present study using two criteria. The first is using the method of two parameters K and k proposed by Aida (1978), where the expression and satisfactory factor for practical purposes were provided in the previous chapter in the sub-section of model performances. The second is model validation by using moving average analysis to filter underlying datasets. The fact that the south Java coastline is partially characterized by beach sections with fringing coral reefs and complex bathymetry formations means model validation by comparing point-to-point data is not recommended (personal communication by Prof. Steven N. Ward).

For validation of the inundation model, the present study compares the results from the best fit of the selected source model above with the collected maximum tsunami run-up in 29 points (in Permisan), 23 points (in Serayu & Bengawan river and eastern part of Cilacap bay) on the basis of testimonies of the survivors' interview, and 1 transect located between the Serayu and Bengawan river as conducted by Moore et al. (2011). The first method of the validation model provides a quantity number; however, the second method and the last of the validation methods of the inundation model only provide the trend and interpretative approaches.

In the task group of for the reconstruction of the 2006 Java tsunami, there is a process to testify the tsunamigenic submarine landslide that may be associated with the earthquake.

This phenomenon was considered by Fritz et al. (2007) and Lavigne et al. (2007) who conducted field observations in the short segment of Permisan-Cilacap. Okal & Synolakis (2004) developed discriminants to identify the physical nature of the tsunami source based on the distribution of run-up amplitudes along the coastline for local tsunamis. They proposed to characterize the shape of tsunami run-up distribution by empirically fitting a formula expressed as:

$$\zeta(y) = \frac{b}{[(y-c)/a]^2+1} \quad (46)$$

where the parameters a , b , and c are optimized by trial and error.

They then differentiated three dimensionless quantities of I_1 , I_2 , and I_3 . I_1 scales of the maximum run-up on the beach (b) to the amplitude of seismic slip on the fault (Δu), I_2 characterizes the aspect ratio of the distribution of run-up on the beach, and I_3 scales the maximum run-up on the beach (b) to the amplitude of the initial depression on the ocean surface (η -). The first two are for the case of seismic dislocations and the third for tsunamigenic landslide. Each of the dimensionless quantities above has the following expression:

$$I_1 = \frac{b}{\Delta u}; I_2 = \frac{b}{a}; I_3 = \frac{b}{\eta-} \quad (47)$$

Furthermore, they proposed the dimensionless quantity of I_2 with the threshold value of less than 10^{-4} for seismic dislocation sources, and inversely are for all physically realistic models of underwater landslides.

By using such expressions as (46) and (47), the present study testifies the tsunami run-up heights and its distribution along the coastline estimating the parameters a , b , and c above through trial and error. Further, they have been used to predict the discriminant of the threshold value and to investigate the probable factors causing the extreme run-up.

Figure 29 shows the examples of the two different tsunamigenic events employed by using the above expression to attain the discriminant curve and threshold value differentiating its source. The top panel in Figure 29 shows the Nicaragua event in 1992 as generated by the tsunami earthquake, thus it was caused by the seismic dislocation source with $I_2 = 4.15 \times 10^{-5}$ or less than the threshold value of 10^{-4} . The bottom panel, however, shows the 1998 PNG

earthquake and here the tsunami source remained a puzzle for several years after the event until 2002–2003 when extensive studies revealed the submarine landslide as the most likely cause of the extraordinary run-up. The discriminant curve was then plotted and the I_2 of 4.74×10^{-4} was achieved bigger than the threshold value indicating the landslide sources of the tsunamigenic event.

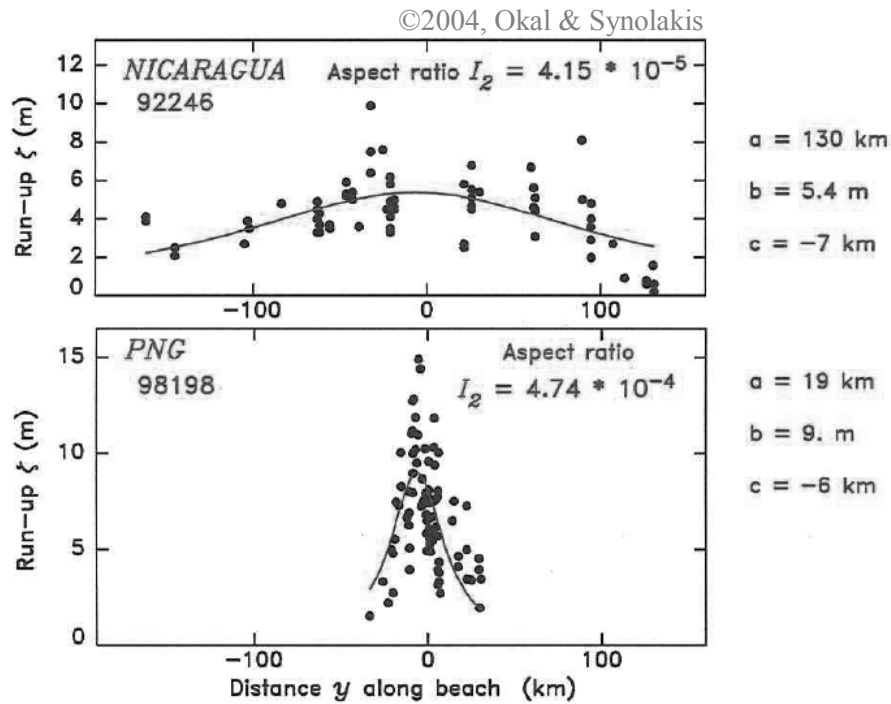


Figure 29: Two different tsunamigenic & discriminant curves

The last specific treatment deals with the task group of the synthetic model for the effect of complex ruptures. It produces both dimensional and dimensionless graphs of the combination of relevant parameters. Prior works through both empirical and analytical studies mentioned earlier in preceding sections conducted by Okal (1988), Satake & Tanioka (1995), Geist (1998), Tanioka (1999), Geist & Dmowska (1999), Geist (2002), Jaffe et al. (2006), Geist et al. (2006), and McCloskey et al. (2007), and Borrero et al. (2010) suggested that local tsunamis are sensitive to the complex ruptures in the source zone as well as the factors that are independent of the magnitude M_0 , such as the higher slip (or low rigidity) and slip distribution. Therefore, the tsunami amplitudes and its distribution with the parameter sources above are closely linked and addressed in the present study. Hence, parameters such as the tsunami amplitudes and its distribution in the strike direction at source as well as near-shore, the variation of the rigidity value varying from 10–40 GPa, the fault dimension, and the uniform-distributed slip effect are used to compose the graphs.

The eleven graphs of the combination parameters are as follows:

1. The four dimension graphs for the tsunami amplitudes near-shore and its distribution along the coastline for the distributed slip fault under the variety of rigidity value,
2. The one dimension graph for the tsunami amplitudes near-shore and its distribution along the coastline for the rectangular fault under the variety of rigidity value,
3. The one dimensionless graph for the ratio of difference tsunami amplitudes and maximum amplitudes for distributed versus the ratio of coastal length to the fault length under the variety of rigidity value,
4. The one dimensionless graph for the ratio of tsunami amplitudes for distributed and rectangular fault versus the ratio of coastal length to the fault length under the variety of rigidity value,
5. The one dimensionless graph for the ratio of tsunami amplitudes of various rigidity values versus the ratio of the rigidity value, where one is selected as a control value,
6. The one dimensionless graph for the ratio of tsunami amplitudes at source and near-shore versus the ratio of coastal length to the fault length for distributed and uniformly slip,
7. The two dimension graphs for the tsunami amplitudes along the coastline by using three different synthetic geometric data input for distributed and uniform slip.

4.4 Simulation model

This sub-chapter provides the simulation model that consists of two sections, namely the model tools and set up of the model. The model tools that have been used in the present study included those for estimating the fault slip, the deformation model in the source zone for initial condition of the numerical simulation, and the hydraulic model for propagating and tsunami run-up. The model set up describes the tsunami sources with its scenarios, the numerical domains and the model parameters, as well as types of mitigation measures.

4.4.1 Model tools

4.4.1.a Fault model

In the aftermath of the earthquakes, the seismological agencies, such as the USGS, GFZ, JMA, BMKG, and so, announce the source parameters that at least commonly consist of the earthquake magnitude, focal depth, and its epicenter. To estimate the spatial distribution, dimension, and its values of earthquake slip, which are usually assumed to occur in the fault plane, several methods have been used. The present study utilized two methods, i.e. the empirical scaling law and the inversion model, with the latter being derived from the tsunami waveform recorded at tide gauges and the finite-fault model determined by teleseismic body waveform.

The empirical scaling law, whose expressions were given in the preceding chapter, is used to estimate the geometric fault dimension of L , W , and D . The comparison results of the proposed empirical formula as developed by Wells & Coppersmith (1994), Papazachos et al. (2004), Okal (2006), and Strasser et al. (2010), gave comparable values under similar rigidity. These expressions are used to estimate the fault dimension for the present study.

The second method is the slip distribution of the inversion model derived from tsunami waveforms recorded at tide gauges and the finite fault of the body seismic waveform. Fujii & Satake (2006) proposed the source of the 2006 Java tsunami by using the tsunami waveforms method which those recorded at six tide gauges. The number of faults, dimensions and slips were estimated. Ji (2006) and Ammon et al. (2006) proposed the tsunami source by inversion model derived from teleseismic body waveforms. The sub-fault format data by Ji (2006) were published on the USGS website⁷. It consists of 147 sub-faults, with each fault having dimensions of 15 km (strike direction) x 11 km (dip direction). Ammon et al. (2006) proposed six slip distributions derived from the finite-fault inversion model by assuming the ruptures to be located in the so-called accretionary prism, which has low-rigidity material of 10 GPa.

All of the source parameters and their slip distribution for reconstruction of the 2006 Java tsunami, the plausible maximum scenario for future hazard, and synthetic model are provided in the next section.

⁷ http://neic.usgs.gov/neis/eq_depot/2006/eq_060717_qgaf/neic_qgaf_ff.html

4.4.1.b Deformation model

The analytical expressions for displacement fields derived by both Mansinha & Smylie (1971) and Okada (1985) were provided in the preceding chapter. The script codes are available in the FORTRAN programming language, and for practical use they must be coupled with tsunami numerical programs. Wang et al. (2003) provided the URL address that serves the Okada (1985) script, while Mansinha & Smylie's (1971) is available in the TUNAMI code.

Since the author uses both the scripts of Mansinha & Smylie (1971) and Okada (1985), whose available codes use different coordinates systems, i.e. Cartesian and spherical coordinates, a comparison is needed to ensure that their results are still in an acceptable deviation.

The model comparison for both of the scripts above has been performed using single-fault and multi-faults models. For this purpose, the author took the slip model's sample for the tsunami hazard map for Padang when Schlurmann et al.'s (2010) paper was published. The source parameter list and the comparison results are provided in Appendix A – The deformation model in Figure 1-3. The statistical analysis using root mean squared deviation (RMSD) and normalized root mean squared deviation (NRMSD) for the sampling data of $n = 260,604$ cells of single and multi-faults model gives 0.05 m and 0.29 m and 0.8% and 5.2%, respectively.

Within the GITEWS project, the deformation model called RuptGen was developed for the requirements of the tsunami source model due to co-seismic slips at the Sunda trench. The concept employs 15 x 150 patches to represent the slip, each having dimensions of 40 km x 15 km and situated in the proximity of the trench. The tool was prepared especially for the tsunami source of the tsunami propagation model of TsunAWI (Babeyko, 2007).

The tsunami sources in the present study use all of the above tools for the reconstruction of the 2006 Java tsunami model, for the plausible maximum scenario of future tsunami hazard in study area, and for the synthetic model.

4.4.1.c Tsunami model

The numerical model of TUNAMI, which stands for Tohoku University's Numerical Analysis Model for Inundation, has been used in the present study. It was initially developed in the late 1970s in Japan, and in the 1990s a joint collaboration between IUGG and IOC-UNESCO was formed for the TIME (Tsunami Inundation Modeling Exchange) project,

which facilitated the transfer of the tsunami code to the countries prone to tsunami disaster. So far this code has been distributed to and been applied in 43 institutions in 22 countries (Shuto & Fujima, 2009).

The TUNAMI is a primitive generation of the tsunami model using a non-linear shallow water equation (or abbreviated as NSW). The governing equations, numerical schemes, and boundary conditions were briefly given in the preceding chapter; an extensive discussion regarding the above features and script code is provided in the TUNAMI manual (Imamura et al., 2006).

As mentioned in the introduction to the program manual (Imamura et al., 2006), officially there are five types of TUNAMI code: TUNAMI-N1, TUNAMI-N2, TUNAMI-N3, TUNAMI-F1, and TUNAMI-F2. The N and F in the suffix of TUNAMI mean the coordinate system used, namely Cartesian and Spherical coordinates, respectively. The denotation of 1, 2, or 3 involve linear theory, linear and non-linear theory, and for varying grids, respectively. Beyond such types, dozens of variants of TUNAMI have been developed under specific requirements.

For the present study the author uses TUNAMI code with linear theory in deep sea, non-linear shallow water theory in shallow sea, and run-up onto land with varying grids. To accommodate the hydraulic roughness, the Morison equation has been coupled to the momentum equation, in which the drag coefficient of the C_D and mass coefficient of the C_M are estimated based on the laboratory study by Harada & Imamura (2000).

4.4.2 Model set up

4.4.2.a Sources model

According to research design and its task groups in the business process mentioned at the beginning of this chapter, three numerical simulations have been performed in this study, i.e. a model reconstruction of the 2006 Java tsunami, a hypothetical model for future hazards, and a synthetic model for the effect of complex ruptures.

4.4.2. a.1 Model reconstruction of the 2006 Java tsunami

Six source models for the reconstruction of the 2006 Java tsunami are applied in the present study. The first three were proposed by previous researchers and the remaining models and their dimensions are estimated using the scaling law incorporated with both normal and low-rigidity material. The fault types, source, and its description of the whole source model of the 2006 Java tsunami are listed in Table 4.

Table 4: Source model of the 2006 Java tsunami

No.	Fault Type	Authors/Source	Description
1	Multi-faults	Fujii & Satake (2006)	The tsunami source was derived from tsunami waveforms recorded at six tide gauges.
2	Multi-faults	Cheng-Ji (2006)	Fault rupture model was determined by the inversion of teleseismic body waveform.
3	Multi-faults	Ammon et al. (2006) – with modification in the present study	The slip distribution from finite-fault inversion model assuming low rigidity of $\mu=10$ GPa and rupture speed of 1.25 km/s.
4	Single-fault	RuptGen ver.1.1-GITEWS (2010)	The single-fault model was generated by using the RuptGen model (ver.1.1) – GITEWS Project using rigidity normal of $\mu=30$ GPa.
5	Single-fault	RuptGen ver.1.1-GITEWS (2010)	The single-fault model was generated by using the RuptGen model (ver.1.1) – GITEWS Project using low rigidity of $\mu=10$ GPa.
6	Single-fault	Present Study (2011)	The single-fault model whose dimension was estimated empirical studies. The slip was calculated by using low rigidity of $\mu=10$ GPa.

Each of the proposed source models above provides an estimate of the magnitude and extent of the underlying rupture dimension and co-seismic slip. To attain ground vertical displacement, both analytical solutions of Mansinha & Smylie (1971) and Okada (1985) have been used. Source models 1, 2, 3, and 6 use the deformation model whose solution was developed by Mansinha & Smylie (1971), and the remaining models have applied RuptGen ver.1.1, whose solution was developed by Okada (1985). The ground vertical displacements, in turn, are used as the initial conditions for the numerical simulation.

Table 5: Source model of the 2006 Java tsunami (Fujii & Satake, 2006)

No	Epicenter of sub-fault		Depth (km)	Area (km ²)	Slip (m)	M_o (Nm) ($\mu=10$ GPa)	M_w
	Lon (deg)	Lat(deg)					
1	107.125	-9.211	3.0	2500	1.59	3.975E+19	7.0
2	107.286	-8.805	11.7	2500	0.45	1.125E+19	6.6
3	107.554	-9.357	3.0	2500	1.53	3.825E+19	7.0
4	107.708	-8.958	11.7	2500	0.00	0.000E+00	0.0
5	107.991	-9.495	3.0	2500	4.14	1.035E+20	7.3
6	108.136	-9.112	11.7	2500	2.37	5.925E+19	7.1
7	108.427	-9.655	3.0	2500	4.29	1.073E+20	7.3
8	108.581	-9.257	11.7	2500	0.00	0.000E+00	0.0
9	108.856	-9.809	3.0	2500	7.41	1.853E+20	7.4
10	109.002	-9.395	11.7	2500	6.36	1.590E+20	7.4
				25000		7.04E+20	7.8

Note: strike, dip, and slip angle are 289°, 10°, and 95° respectively.

Source model 1 was derived by Fujii & Satake (2006) based on the inversion model of the tsunami waveforms method, which was recorded at six tides gauges. The length of

source is 200 km with the largest slip being 2.5 m for the instantaneous rupture model. To represent the tsunami source and its distribution, 10 sub-faults of size 50 km x 50 km have been proposed. The source parameters are listed in Table 5.

Source model 2 refers to the USGS official website⁸. It was proposed by Ji (2006) based on the finite-fault model, which consists of $21 \times 7 = 147$ patches with each patch having the dimensions 15 km (strike direction) x 11 km (dip direction). The source parameters are provided in Appendix E – Tsunami source in section A.

Source model 3 is derived from the slip distribution proposed by Ammon et al. (2006) using the finite-fault inversion model. The source was situated in the proximity of the trench, which is where the so-called accretionary prism exists, and thus its rigidity material is assumed to be of 10 GPa.

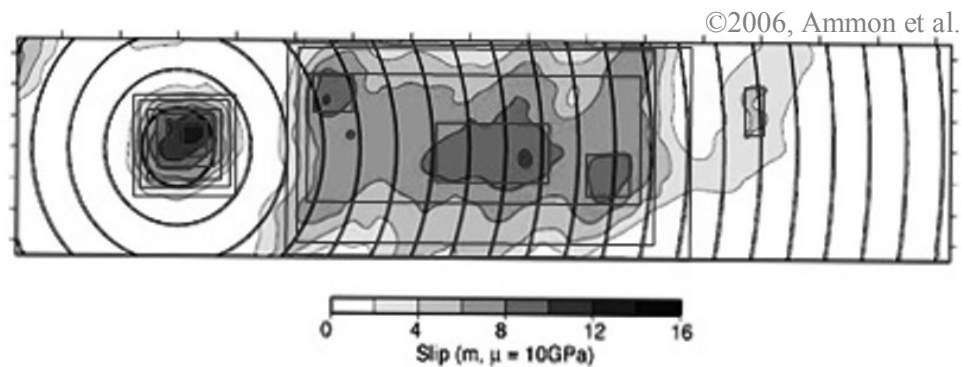


Figure 30: Slip distribution by Ammon et al. (2006) and 16 sub-faults (red boxes) proposed in the present study

They suggested six non-uniform slip distributions, with a maximum slip of about 13.5 m. For this study the author proposes decomposition of un-uniform slip distribution and to regenerate 16 rectangular sub-fault areas (red boxes) to resemble slip distribution, where each value was interpreted through the color scale and the total moment being kept constant.

The inspiration to decompose the source model proposed by Ammon et al. (2006) was based on similar techniques where the slip distribution can be estimated by taking the benefit of the inversion model from broadband seismic networks as well as cGPS measurements (Satake & Kanamori, 1991; Geist, 2005; Schlurmann et al., 2010; also personal communication with Prof. Imamura and Dr. Dutykh).

⁸ http://neic.usgs.gov/neis/eq_depot/2006/eq_060717_qgaf/neic_qgaf_ff.html

The slip distribution and the sub-faults are depicted in Figure 30. The source parameters of this model, i.e. epicenters, depths, fault dimensions, and their given moments as well as proposed patches parameters are provided in Table 6.

Table 6: Source model of the 2006 Java tsunami (Ammon et al., 2006)

Decomposed un-uniform slip distribution							Proposed rectangular patches									
No	Depth (km)	Polygon Area (km ²)	Slip (m)	M_0 ($\mu=10$ GPa)		M_w	Epicenter of sub-fault (deg)		Fault Dim. (km)		Fault Area (km ²)	Slip (m)	Overlaid Slip (m)	M_0 (Nm) ($\mu=10$ GPa)	M_w	
				Overlaid	Residual		Lon.	Lat.	W	L						
1	10	36.0	13.5	4.86E+18	7.20E+17	6.4	107.431	-9.242	6.0	6.0	36.0	2.0	13.5	7.20E+17	5.8	
2	10	168.0	11.5	1.93E+19	3.36E+18	6.8	107.398	-9.239	13.0	13.0	169.0	2.0	11.5	3.38E+18	6.3	
3	10	358.7	9.5	3.41E+19	7.17E+18	7.0	107.396	-9.244	19.0	19.0	361.0	2.0	9.5	7.22E+18	6.5	
4	10	584.0	7.5	4.38E+19	1.17E+19	7.0	107.403	-9.262	24.0	24.0	576.0	2.0	7.5	1.15E+19	6.6	
5	10	817.0	5.5	4.49E+19	1.63E+19	7.0	107.406	-9.264	28.5	28.5	812.3	2.0	5.5	1.62E+19	6.7	
6	10	1102.0	3.5	3.86E+19	3.86E+19	7.0	107.416	-9.267	33.0	33.0	1089.0	3.5	3.5	3.81E+19	7.0	
7	8	3.5	11.5	4.03E+17	7.00E+16	5.7	107.845	-9.276	1.9	1.9	3.6	2.0	11.5	7.22E+16	5.2	
8	8	3.9	9.5	3.71E+17	7.80E+16	5.6	107.897	-9.409	1.9	1.9	3.6	2.0	9.5	7.22E+16	5.2	
9	8	17.3	11.5	1.99E+18	3.46E+17	6.1	108.394	-9.633	4.1	4.1	16.8	2.0	11.5	3.36E+17	5.6	
10	8	149.5	9.5	1.42E+19	2.99E+18	6.7	108.598	-9.757	12.2	12.2	148.8	2.0	9.5	2.98E+18	6.2	
11	8	789.0	9.5	7.50E+19	1.58E+19	7.2	108.294	-9.542	17.5	45.0	787.5	2.0	9.5	1.58E+19	6.7	
12	8	174.6	9.5	1.66E+19	3.49E+18	6.7	108.240	-9.572	13.0	13.0	169.0	2.0	9.5	3.38E+18	6.3	
13	8	4645.0	7.5	3.48E+20	9.29E+19	7.6	108.221	-9.587	45.0	100.0	4500.0	2.0	7.5	9.00E+19	7.2	
14	8	7440.0	5.5	4.09E+20	1.49E+20	7.7	108.184	-9.542	60.0	125.0	7500.0	2.0	5.5	1.50E+20	7.4	
15	8	80.7	5.5	4.44E+18	1.61E+18	6.4	109.101	-9.727	9.0	9.0	81.0	2.0	5.5	1.62E+18	6.1	
16	8	10011	3.5	3.50E+20	3.50E+20	7.6	108.317	-9.578	75.0	135.0	10125	3.5	3.5	3.54E+20	7.6	
				6.94E+20		7.8									6.96E+20	7.8

Notes:

-All sub-faults, strike, dip, and slip angle is 289°, 10°, and 95°, respectively

-Conversion formula M_0 to M_w using Kanamori & Hank (1979)

Source models 4 and 5 were attained from version 1.1 of the rupture generation tool RuptGen. It was developed within the GITEWS project to support the establishment of the tsunami hazard map in the coastal strip facing the Sunda arc (Babeyko, 2007). RuptGen employs the concepts of patches at the subduction plate interface, where regular meshing of the rectangular patch of size of 40 km x 15 km represents seismogenic activity at depths of around 0–60 km. The present study applies the derived magnitude and epicenter as given in Table 4 with two conditions of the rigidity value, namely 30 GPa and 10 GPa. The summaries of tsunami source are provided in Appendix E – Tsunami source in section B and C.

The source parameters of model 6 proposed in the present study is depicted in Table 7. The one segment single-rectangular dimension is to be assumed by considering the results of the scaling laws and the other proposed models above. However, the present study applied only the low rigidity of 10 GPa.

Table 7: Source parameters of the 2006 Java tsunami (in the present study)

Segment	Epicenter of sub-fault		Depth (km)	Fault Dimension		Slip (m)	M_o (Nm) ($\mu=10\text{GPa}$)	M_w
	Lon.(deg)	Lat.(deg)		L(km)	W(km)			
Single	107.989	-9.405	10.0	200.0	80.0	3.95	6.33E+20	7.8

The six source models mentioned above have several fault types, rupture dimensions, and the assumption of rigidity values, which leads to diverse slips and, of course, produces various seafloor vertical deformations. These deformations are the initial conditions offshore that represent the tsunami source in the numerical models. The picture of tsunami sources is provided in Appendix E – Tsunami source in section D to I.

4.4.2. a.2 Hypothetic model for future tsunami hazard

The main assumptions of the source parameters of the hypothetic model for future hazards are selected from the prior process of the model reconstruction of the 2006 Java tsunami. Such a process suggests that the epicenters are located in the accretionary prism with a low rigidity giving a bigger tsunami source, and thus it is assumed that it will provide larger run-up.

In addition, the multi-faults model can only be reconstructed through the inversion model from either the teleseismic body waveform or mareograms from tide gauges after the event. Therefore, for future hazards, the single-fault model is inevitably imposed also by assuming that the study area has a relatively short coastline, i.e. about 50 km with presumably less effects from single-multi fault types.

The present study proposes a limited multi-scenario hypothetic tsunami model, which focuses on the plausible maximum of the specific magnitude given in the Java subduction zone when a tsunami exerts maximum impact on the study area of the Cilacap region. To accommodate this, several assumptions have been made as follows:

1. Scenarios of the hypothetic model are the expected events that give a plausible maximum impact to the study area. Hence, the epicenters' coordinates are located in a way so that the major section of the virtual rectangular rupture faces or is normal to the study area.
2. The epicenters are close to the Java trench (< 70 km) and their hypocenters are shallow (< 25 km), thus the ruptures can be assumed to occur in the accretionary prism and its tsunami excitation is influenced by low-rigidity material, e.g., 10 GPa.

3. The scenario magnitudes are estimated based on historical data on tsunamis that happened in the Java subduction zone, namely between M_W 7.8 to M_W 8.2. For the present study, the increment magnitude was set to 0.2.
4. Other source parameters based on historical data (1994 & 2006 tsunami), strike (278° - 297°), dip (7° - 11°), slip (89° - 102°), and focal depth (< 25 km).
5. Fault dimensions are proposed by considering empirical studies conducted by Wells & Coppersmith (1994), Papazachos et al. (2004), Okal (2006), Strasser et al. (2010), and model reconstructions of the 2006 Java tsunami. The single-fault type of source model is applied.

Following such assumptions above, the present study proposes 16 locations of the epicenter off the coast of south Java. Among them, 12 epicenters are located in the south of the Cilacap region, in which from these locations the normal direction is projected to the study area of Cilacap as illustrated in the 5th domain in Figure 31. Two others represent the 1994 and 2006 Java tsunami, and the two remaining sources are placed in the area between the group of 12 epicenters above and the 1994 Java tsunami. The configuration of the epicenters plotted on the map is depicted in Figure 31.

In regards to magnitude scenarios, the present study refers to the historical data for tsunamis that occurred in the Sunda trench, namely in 2006 (USGS, 2006 and others), 1994 (Tsuji et al., 1995), and 1977 (Gusman et al., 2009), with magnitudes ranging from M_W 7.6 to M_W 8.2. For the hypothetical model study, however, M_W 7.8, M_W 8.0, and M_W 8.2 are selected.

According to the historical data, the angle parameters of the major earthquakes ($M_W > 7.0$) and tsunamis in Java's subduction zone were almost identical. The strike angles are nearly parallel to the Java trench within 278° - 297° , which the longitude regime being approximately 110° E. In the present study, the epicenters situated in the west of such a regime are set to 289° and in the eastern regime to 280° . For the dip angle an estimated generally follows the depth in the interplate zone, further to the north it is steeper with values of 10° - 15° , while slip angles are set at a constant value of 95° .

Furthermore, rupture dimensions of the hypothetical model of corresponding magnitudes are estimated by using previous empirical studies conducted by Wells & Coppersmith (1994), Papazachos et al. (2004), Okal (2006), and Strasser et al. (2010). For rupture length, the author prefers using Wells & Coppersmith's (1994) estimation for all events since the dataset used to obtain the regressions was the largest and a good estimate for

the 2006 Java tsunami. For rupture width, however, other expressions of Papazachos et al. (2004) and Strasser et al. (2010) have been considered. Except Okal's (2006), other slips based on the low rigidity of 10 GPa. The datasets of epicenters, focal depths, and angle parameters of 16 scenarios are provided in Appendix E – Tsunami source in section J and K. The pictures of the source models of M_W 7.8, M_W 8.0, and M_W 8.2 with epicenters at point 11 as examples are provided in Appendix E – Tsunami source in section L, M, and N.

©2011, W.Kongko

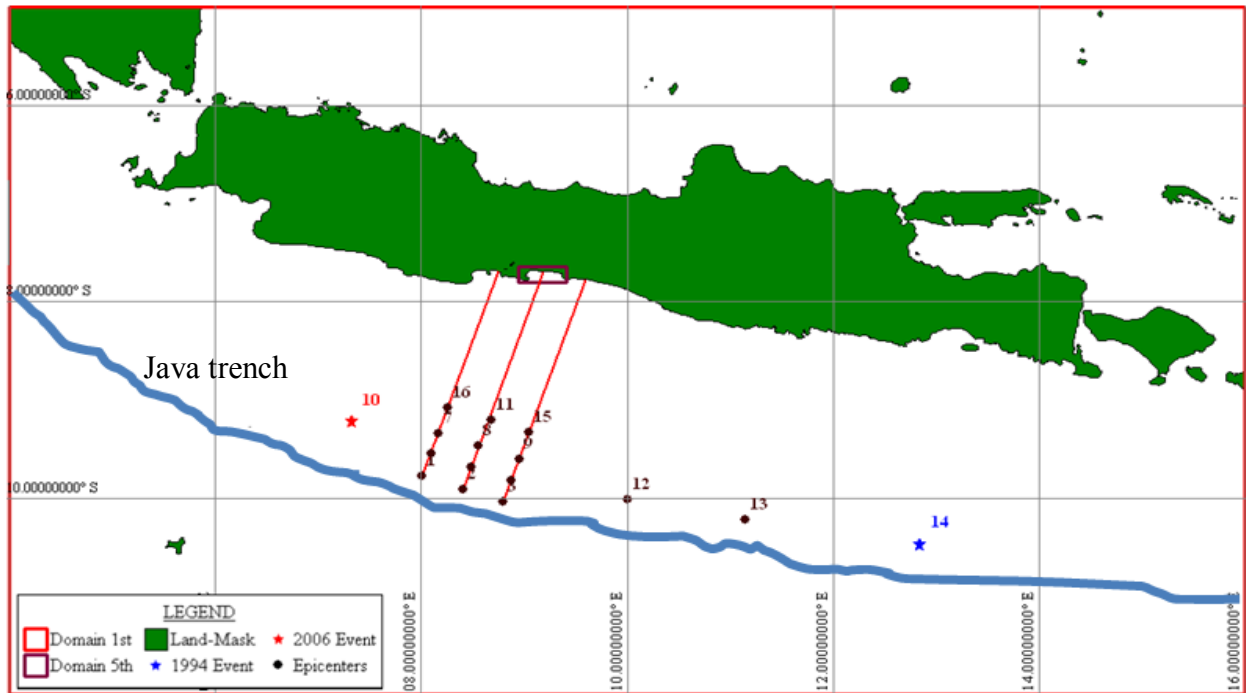


Figure 31 : Epicenters of hypothetical model

4.4.2. a.3 Synthetic model for complex rupture

As discussed in the preceding chapter, the combination factors of higher slip with low rigidity at shallow depth and uniformly distributed slip affecting the tsunami amplitudes and their distribution in the coastal zone has not been assessed yet. Furthermore, the distance of the tsunami sources in the Java subduction zone is rather remote compared to those of the other tsunami earthquake events. Hence, the present study performs a parametric analysis using the series synthetic model involving relevant factors such as those mentioned above.

The earthquake magnitude in this simulation is selected as M_W 7.8. Such a magnitude, by using empirical scaling laws has fault dimensions of L and W , varying from ~126 km – 198 km and ~39 km – 76 km, respectively. The present study proposes the moderate fault dimension of $L = 150$ km and $W = 60$ km.

To accommodate the combination of the higher slips/low rigidity to normal slips/normal rigidity in the source zone, various values of 10 GPa – 40 GPa are imposed. The average slips are then calculated using expression (17) from the preceding chapter for four of the rigidity values, namely 10 GPa, 20 GPa, 30 GPa, and 40 GPa producing 6.3 m, 3.47 m, 2.35 m, and 1.76 m, respectively.

The other source parameters, such as strike, dip, and slip angle are determined by considering general trend of earthquakes that occur near the trench and characterized by a thrust-faulting focal mechanism and symmetrical orientation of source coastline in the numerical domain. The present study applies angles of the strike and slip at $\sim 270^\circ$ and $\sim 90^\circ$, respectively. For the dip angle, by following the typical shallow earthquakes near trenches (<70 km from the trench) it is estimated to be $\sim 10^\circ$.

For the source hypocenter or depth, the fault zone is assumed to be in the interplate boundary underlying the accretionary prism and oceanic crust and shown as a solid red line in Figure 32. The synthetic model of the present study uses both single-fault for uniform slip and multi-faults for distributed slip. For the former, the average depth of 9.4 km has been used, and for multi-faults, depths depend on the horizontal distance from the trench (from 10 km to 60 km) classified into six rows, namely 5 km, 6.8 km, 8.5 km, 10.3 km, 12 km, and 13.7 km.

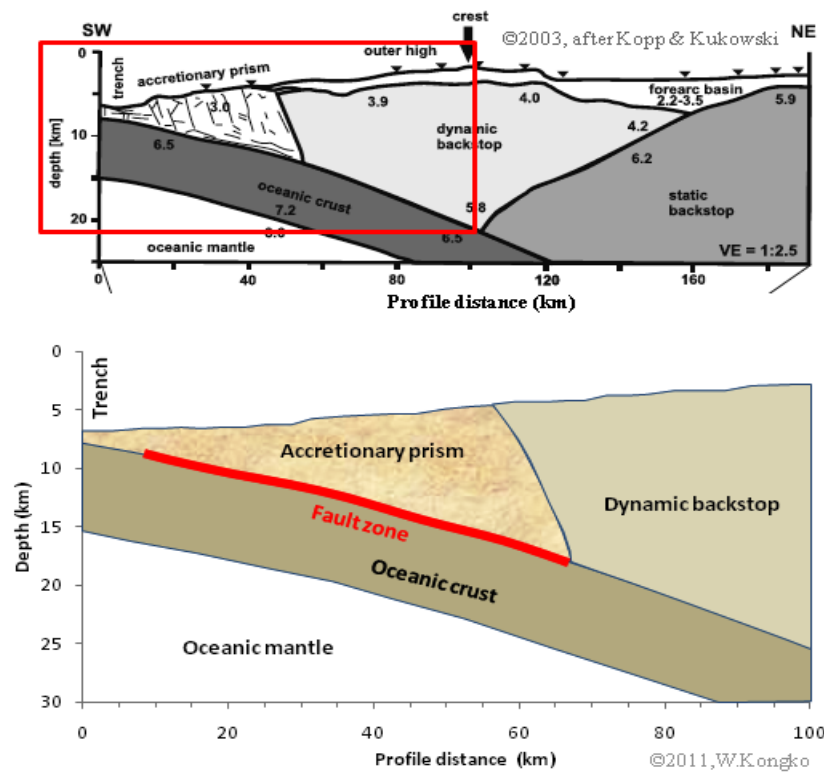


Figure 32: Cross-section of the Java subduction zone

The synthetic model uses both single-fault for uniform slip with dimension $L = 150$ km and $W = 60$ km and multi-faults of 15×6 patches with each patch is $10 \text{ km} \times 10 \text{ km}$ in dimension. Their slip distribution is assumed in an ideal shape with extreme conditions in terms of the slip differences between patches at the given earthquake magnitude. It varies along the strike direction by shifting the peak of slip in the area of $10 \text{ km} \times 10 \text{ km}$ to the right with an interval of 10 km , so that there are 11 distribution slips for one series of rigidity. An exemplary picture is given in Figure 33.

The source parameters of single-faults (uniform slip) and multi-faults (distributed slip for $\mu = 10 \text{ GPa}$) are provided in Appendix E – Tsunami source in section O and P. The datasets of the slip distribution of the synthetic model for $\mu = 10 \text{ GPa}$ and its deformations result for both uniformly and distributed slip are given in Appendix E – Tsunami source in section Q and R, and Appendix F – Parameters of the model in section C.

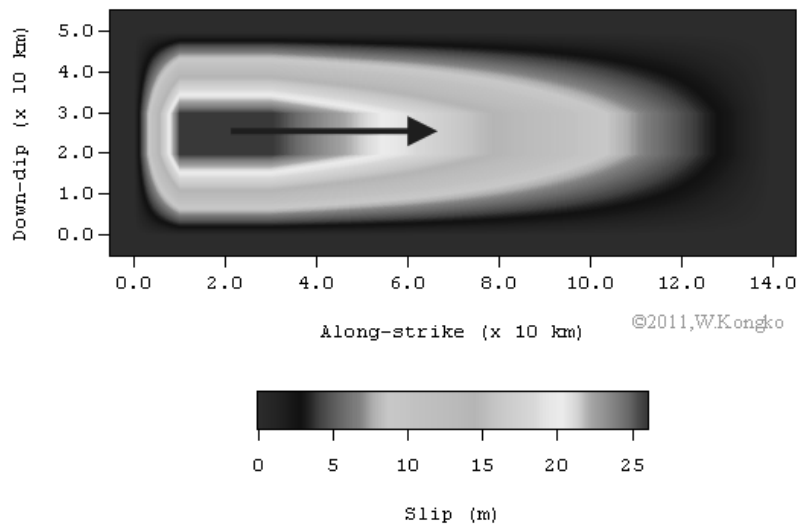


Figure 33: Slip distribution for the synthetic model #1

4.4.2.b Domains and model parameters

This sub-section mentions the numerical domains and model parameters as part of the model set-up that has been used for three task groups elucidated in the process of the present study. It includes the number and bounding coordinates of the numerical domains and the model parameters, such as grid spacing, time step, and relevant properties in the numerical simulation processes.

4.4.2. b.1 Model reconstruction of the 2006 Java tsunami

In order to numerically model the 2006 Java tsunami, the region considered is treated as multi-nested-grid sub-systems, in which the inner domain always has a finer spatial grid

and in many cases using better-resolution data. The present study proposes a numerical domain up to a level of 7, such that levels 1st (1), 2nd (2), 3rd (2), 4th (4), 5th (12), 6th (2), and 7th (2) represent the grid level, while the number in the brackets corresponds to the domain number. The layout of numerical domain of the 2006 Java tsunami model is shown in Figure 34.

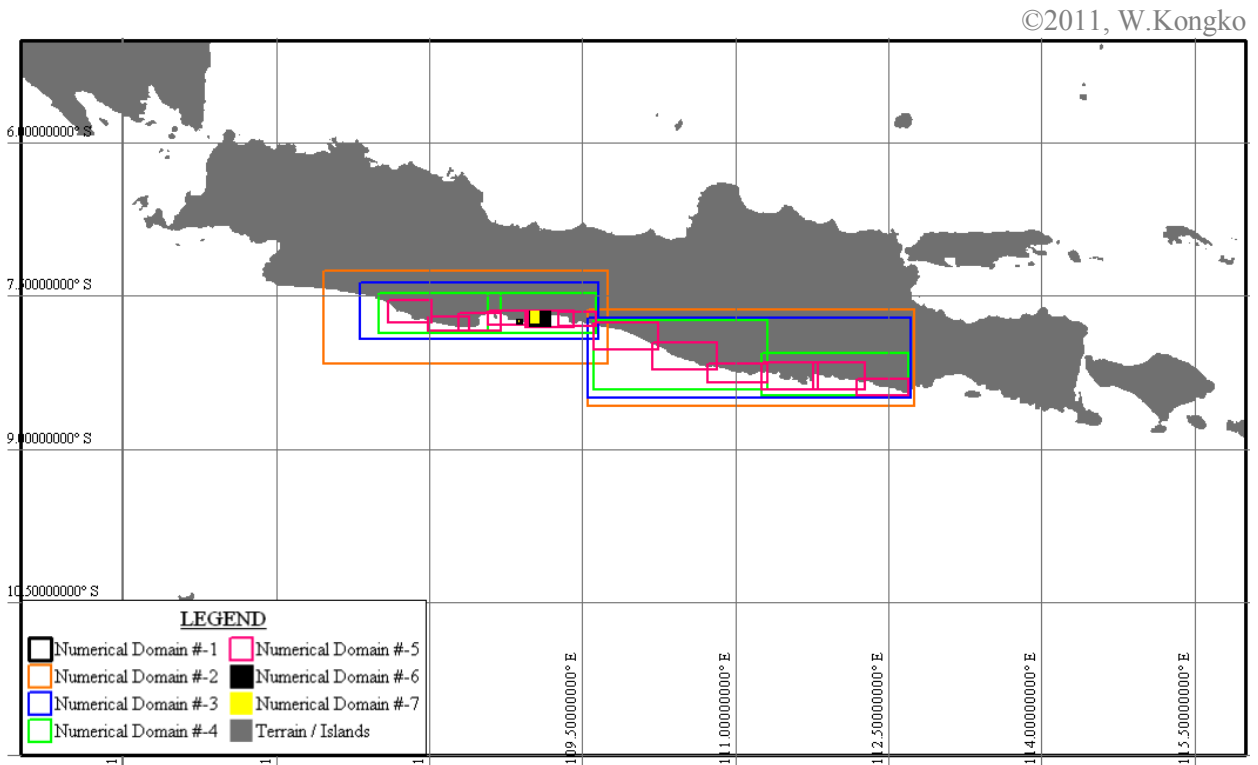


Figure 34: Layout of numerical domains for the 2006 Java tsunami model

The entire region, therefore, has a total of 25 sub-system domains, which are the spatial grid by order of 1st to 7th set to be ~1850 m, ~616 m, ~205 m, ~68 m, ~23 m, ~7.6 m, and ~2.5 m respectively. In order to ensure robust and stable numerical computations, the C.F.L. condition should be satisfied by giving a time step that is small in comparison to the spatial grid, hence for the corresponding spatial grid above by order of 1st to 7th is set to be 1s, 1s, 0.5s, 0.3s, 0.2s, 0.1s, and 0.05s. Furthermore, the total time simulation for the 2006 Java tsunami is estimated to be about 5400 seconds (1.5 hours), assuming that such a duration includes the whole processes from its the original source, propagation, and 3–5 waves reaching the coastline. The longer time simulation is not recommended for reducing the unexpected wave reflection due to the domain’s boundaries in the smallest domain near to the shore.

The TUNAMI model allows the linear term or non-linear term calculations to be used depending on the consideration of the nested-grid system applied and its water depth, thus economical computing times can be achieved. The 2006 Java tsunami simulation model applies the linear model computation for the 1st to 4th domain, and the non-linear one for the remaining domains.

The non-linear model computation employs a uniformly distributed Manning's value of 1/50 (or 0.020), assuming that in the run-up area, the terrain is farm land or firm soil of moderate roughness (Arcement & Schneider, 1984; Kotani, et al., 1998; Imamura et al, 1997; Imamura et al., 2006; Imamura, 2009).

For validation purposes of the maximum horizontal tsunami run-up heights, i.e. in Penyu Bay of Cilacap and Permisan (as depicted with two empty boxes and one solid green box in Figure 24), two different versions of the Digital Elevation Model (DEM) are employed, namely a Digital Terrain Model (DTM) and a Digital Surface Model (DSM). This selection allows to distinguish between different land cover characteristics and land use types, i.e. vegetation, urban infrastructure, etc. which have been sampled and interpreted during field surveys.

The parameters of the model of the 2006 Java tsunami that include the geometric sources, domain names, bounding coordinates, grid sizes, grid spacing, and time steps are tabulated in the table provided in Appendix F – Parameters of the model in section A.

4.4.2. b.2 Hypothetic model for future tsunami hazard

The numerical domain of the hypothetic model for future tsunami hazard consists of five sub-domains. It is similar to the previous model in that the largest domain one, the 1st, occupies Java Island and its surroundings including the subduction zone, while the smallest domain, the 5th, covers the district of Cilacap. The layout of the numerical domains for the hypothetic model for future tsunami hazard is depicted in Figure 35.

The spatial grids and their time step are set up analogous to the previous model for the 2006 Java tsunami, as well as its Manning's roughness, which is imposed only in the smallest domain. The total simulation time is also set at 5400 seconds (1.5 hours), assuming that during this time, the tsunami waves propagate, reach the coastline, and run-up onto Cilacap terrain with subsequently 3–4 tsunami waves.

As mentioned in the preceding sub-section, the hypothetic model for future tsunami hazard is proposed to accommodate varying magnitudes from M_W 7.8 to M_W 8.2, which are set to be the three scenarios of M_W 7.8, M_W 8.0, and M_W 8.2. Further, there are 16 epicenter

sources situated in the locations where their impacts will have maximum inundation in the study area. In addition, the three conditions of natural beach and mitigation measures are imposed, namely without mitigation measure, with greenbelt and sand dunes. All of the combinations of such conditions result in 144 runs of the numerical model.

©2011, W.Kongko

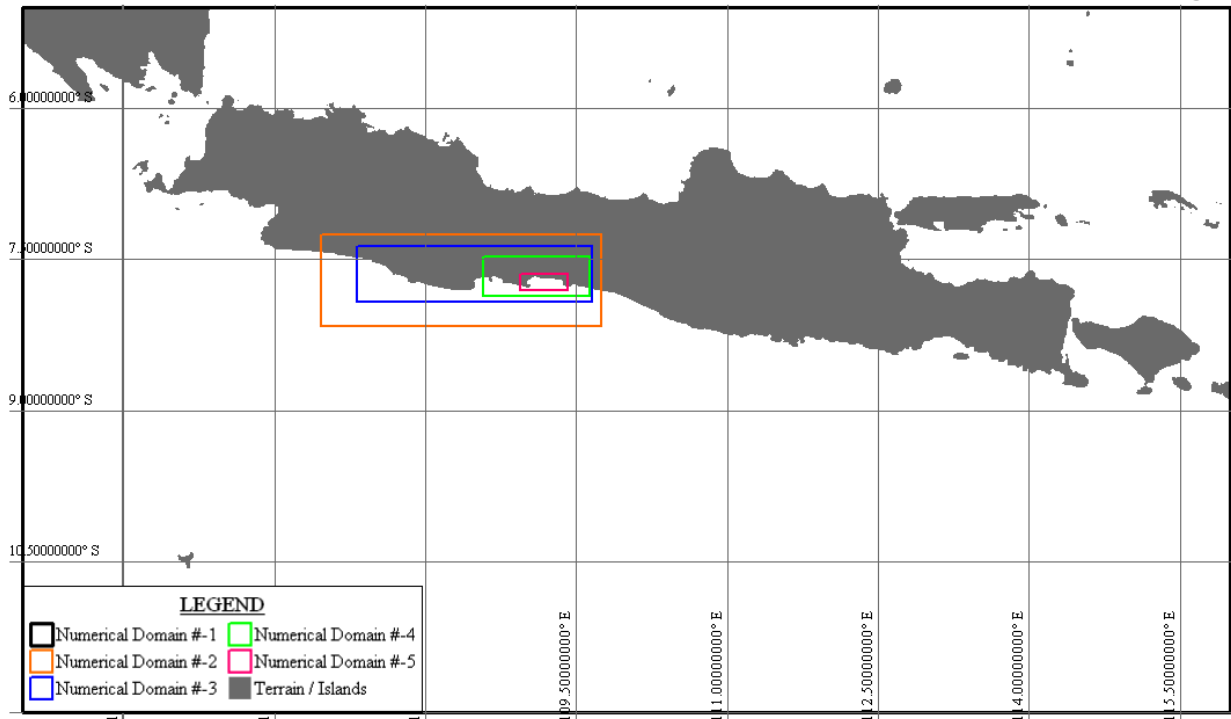


Figure 35: Layout of numerical domains for hypothetical model of future tsunami hazard

The hypothetical model for future tsunami hazard uses similar geometric data of the 2006 Java tsunami model. The GEBCO is used for the 1st to 4th domains, and the assimilating data from various sources (data collection as well as field measurements of bathymetry and topography) for the 5th domain. In the run-up study area, however, the DTM was used instead of DSM data, as the former have the advantage that vegetation and infrastructure have been removed, which leads to larger inundation and thus greater safety. This model also imposes an astronomical tide at the highest water level state as well as an additional estimated wave set-up during the burst, which together are assumed to be 1.5 m.

For tsunami mitigation purposes, the artificial sand dunes and greenbelt of “Waru” trees (*Hibiscus tiliaceus*) protecting against tsunamis are examined. Figure 36 shows the map of the district of Cilacap with the proposed alignment of the mitigation measures (red strips) as located in the low-level beach.

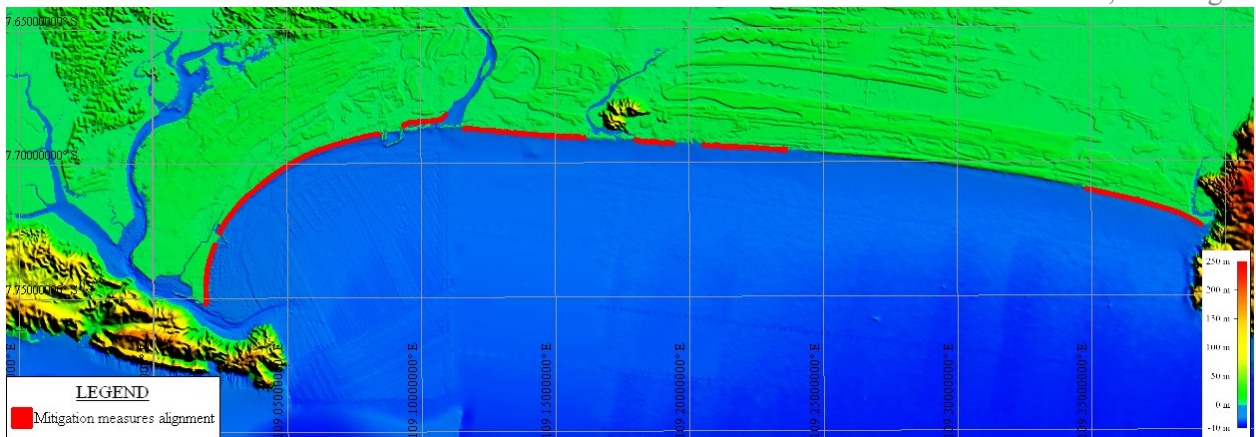


Figure 36: Layout of the alignment of mitigation measures

The first, a natural beach (without mitigation measures) is examined, and further the mitigation measure of 100 m width of the sand dunes with its height 7.5 m is included in the design. The last attempt, a width of 200 m of “Waru” trees with a density of 16 trees/100 m² is applied as a greenbelt coastal protection. The other tree parameters are trunk height H_T of 3.5 m with diameter D_T of 0.35 m, branch height of H_L 1.5 m with diameter D_L of 2.5 m, and branch occupancy ratio S_L of 0.20. A detailed sketch is shown in Figure 37.

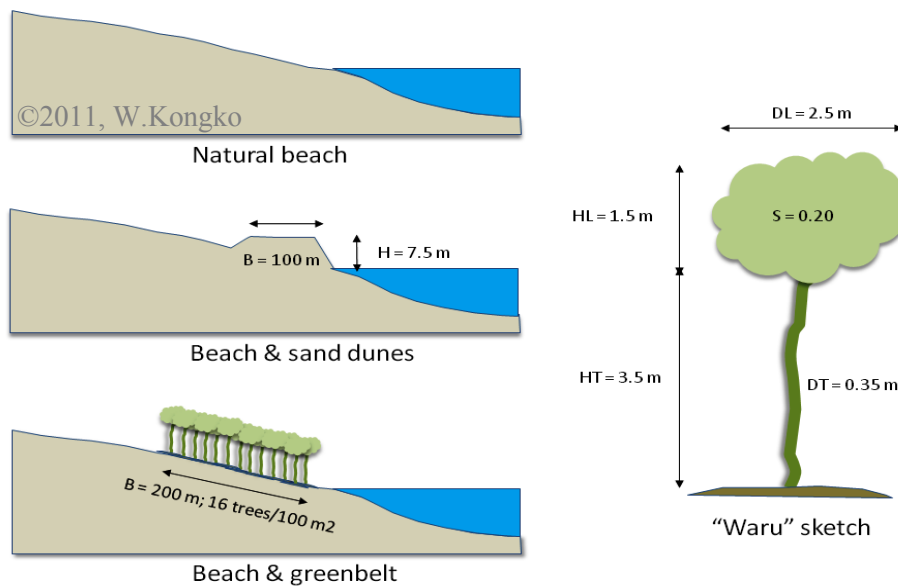


Figure 37 Sketch of mitigation measures

4.4.2. b.3 Synthetic model of complex rupture

The geometric data for the synthetic model of complex ruptures are derived from generalization of the bathymetry data on the south Java Island. The seafloor data following

the normal direction of five cross-sections from the coastline to the trench as shown in Figure 38 has been considered as simplifying the complex bathymetry for the synthetic model.

©2011, W.Kongko

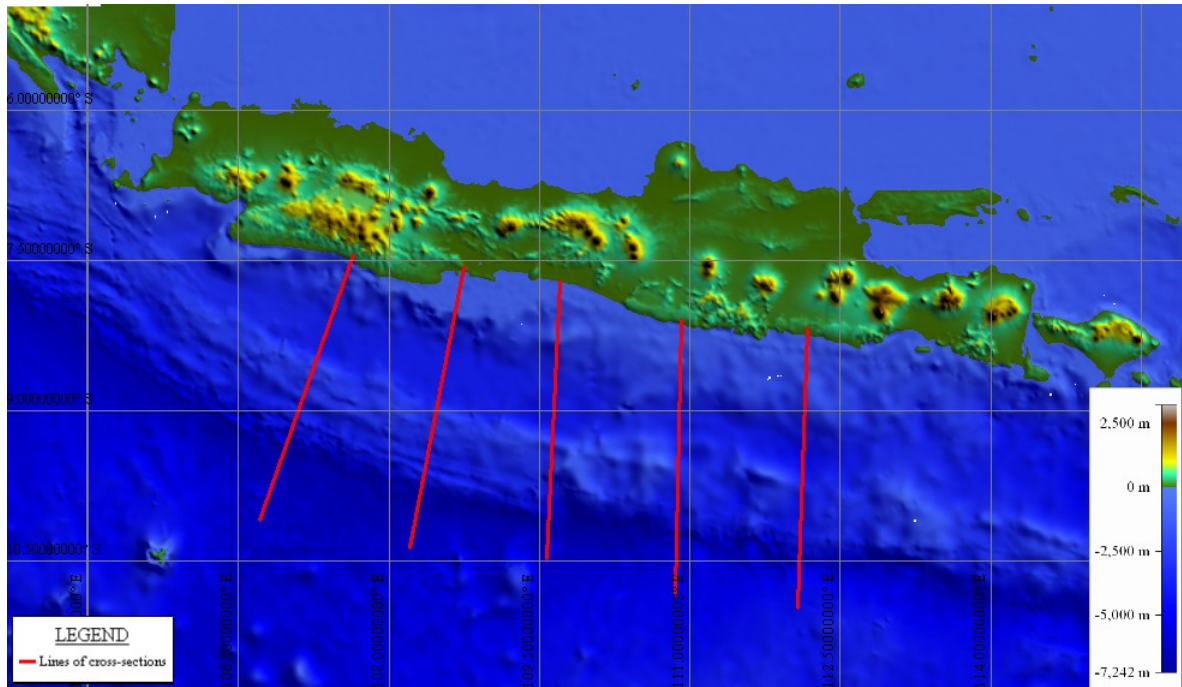


Figure 38: Cross-lines of bathymetry of south Java

The seafloor profiles of cross-lines as shown in Figure 38 and its three proposed synthetic lines (green, red, and dark blue solid line) to represent irregularities of Java bathymetry are depicted in Figure 39. These synthetic lines are then laterally imposed on the entire numerical domain for the geometric data input in the synthetic model.

©2011, W.Kongko

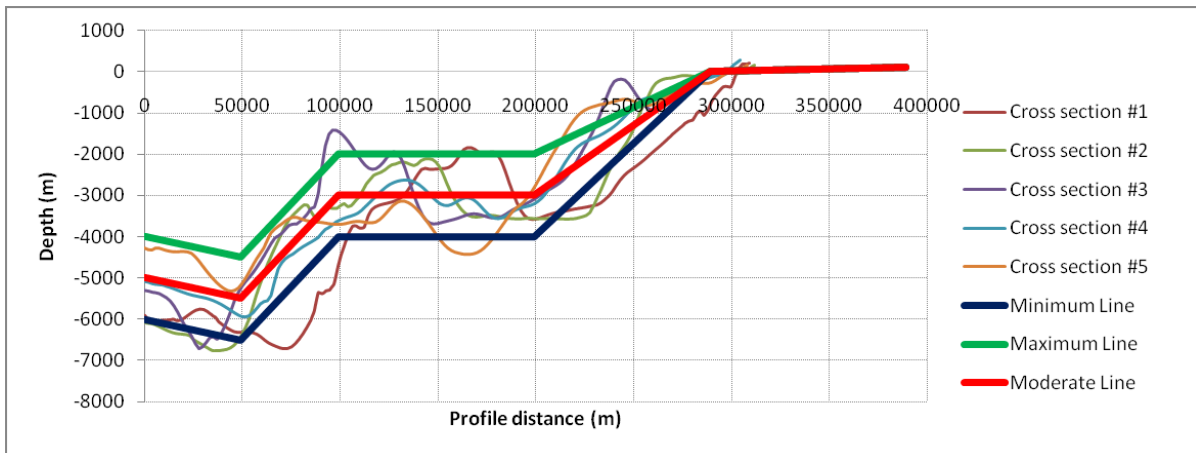


Figure 39: Seafloor profiles & its synthetic line

Figure 40 shows the layout of the numerical domain, tsunami source, and its ground level for the synthetic model of moderate bathymetry. The numerical domain consists of only one grid system, with a grid size of 1000 x 750 and grid spacing determined to be 1000 m. The time step is 2 seconds and the total time for the simulation is 5400 seconds (1.5 hours). As mentioned in the previous sub-section, the tsunami source for the synthetic model uses both uniform and distributed slip by accommodating the variety of rigidity and slip distribution of 11 variations. The synthetic model using minimum and maximum bathymetry data, however, is designed only for one selected tsunami source, i.e. the uniform tsunami source and centered distributed source, respectively.

The tsunami source zone is depicted as a yellow rectangle with sub-fault epicenters represented by 90 red dots in Figure 40. It is located in the proximity of the trench and the fault zone is assumed in the interplate boundary underlying the accretionary prism and oceanic crust shown as a solid red line in Figure 32.

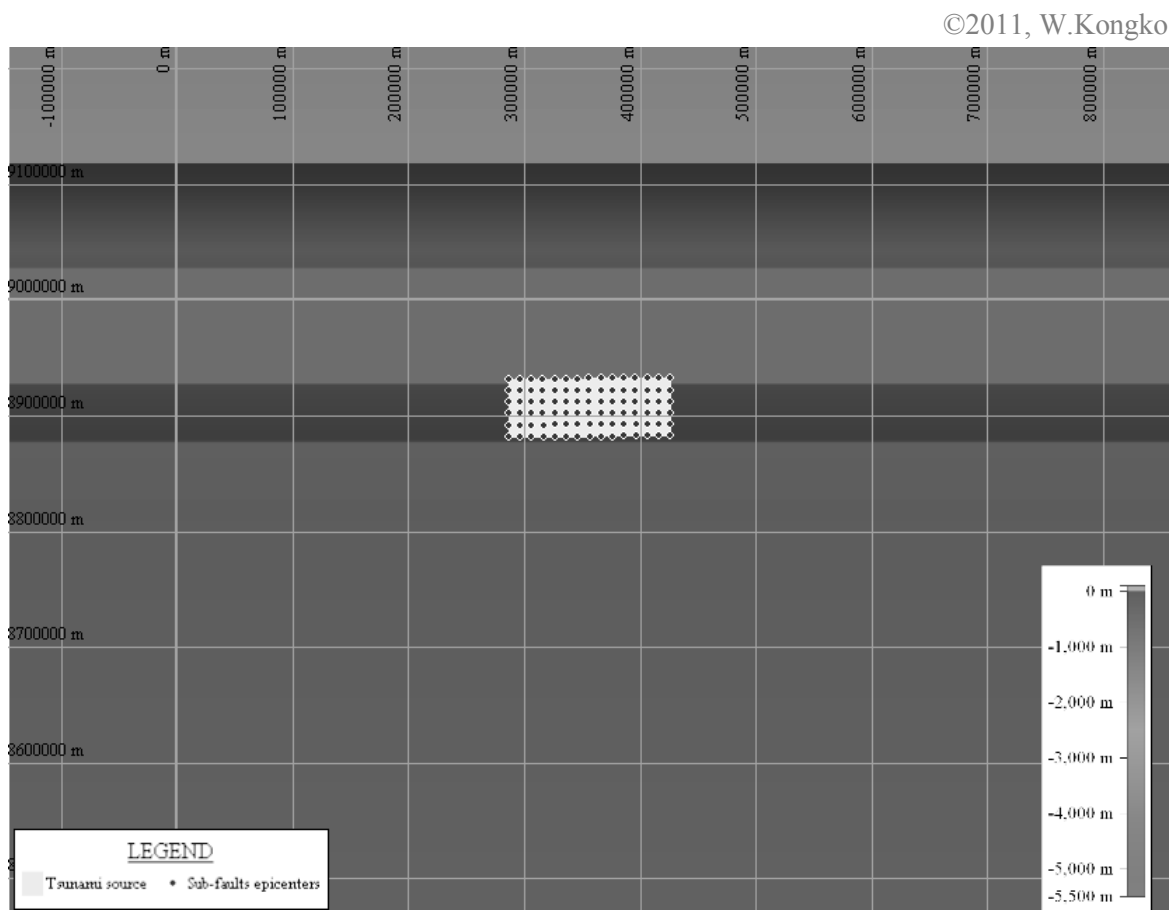


Figure 40: Numerical domain, tsunami source, and ground level for the synthetic model

4.5 Summary

The present study is categorized as applied research, which through correlational and quantitative study attempts to discover and establish the interdependence among parameters that play a role in the events. To accommodate the element tasks, the study combines different types of methodology, namely the case study, historical, correlation-predictive, and the numerical models.

The research design and its business processes as represented by a flowchart showing the step-by-step sequence of the task groups proposed to limit the scope of the study and guide it along the path to achieving the objectives of the research. They are also intended for mapping the problems and the resultant objectives' information available for determining the conclusions, proofing the hypotheses, and answering the questions in this study. The four task groups in this study encompass the geo-data improvement, reconstruction of the 2006 Java tsunami model, hypothetical model for future hazard, and the synthetic model for the effect of complex ruptures.

To ensure the reliability of the research and to make up for the absence of data, which is essential for further analysis and geometric data input in the numerical model, a wide variety of both primary and secondary data with diverse resolutions, formats, and sources has been collected, processed, and assembled. They consist of the data of bathymetry, topography, historical events, and other additional field measurement campaigns.

In the simulation model process, several tools, which comprise the fault slip estimators, deformation models, and hydraulic model for propagation and tsunami run-up, have been utilized. The fault model is estimated using the empirical scaling laws and inversion model derived from the tsunami and seismic waveforms. The deformation model is based on the analytical expressions derived by Mansinha & Smylie (1971) and Okada (1985), while the GITEWS project established the RuptGen tool to attain seafloor displacement in the Sunda arc region. Further, for propagation and run-up simulation, the present study uses TUNAMI code based on the primitive generation of a 2D model utilizing non-linear shallow water equation (NSWE).

For tsunami source, however, several fault types accommodating the slip values and its distribution have been proposed, and the various model parameters of the nested-grid system, spatial grids, and time step are determined as being robust and stable during numerical simulation processes.

For tsunami mitigation purposes, the artificial sand dunes and a greenbelt protecting against tsunamis have been suggested. Their dimensions and layout have been considered suitable for the study area of Cilacap. These mitigation measures have been numerically coupled in the tsunami model for future hazard.

The synthetic model has been created to examine the consistency of the amplification ratio of the rigidity values and tsunami run-up heights as well as to interpret the effects of the uniform-distributed slip at tsunami source on the tsunami amplitudes and its distribution along the coastline. This is conducted in the three task groups listed above. The geometric data input is using generalized bathymetry of south Java in three conditions, and the model sources are situated near trenches, which accommodating the combination of low-normal rigidity and uniform-distributed slips.

Chapter 5 - Findings

“And you see the mountains, thinking them rigid, while they will pass as the passing of clouds. [It is] the work of Allah, who perfected all things. Indeed, He is acquainted with that which you do” (the Quran, 027 the Ant: 88, ca.610-632 AD)

The findings of the present study are provided in this chapter. It comprises the procedures and elements of the study, simulation model results, hypotheses and research questions, and concludes with a summary.

In the sub-chapter on procedures and elements of the study, the findings are mainly related to the processing of the geo-data and field observations. Further, the simulation model provides the dataset of numerical simulation results, model validation, and other evidence interpretations. Finally there is a summary of the findings, a discussion on the hypotheses and then the research questions are addressed.

5.1 Procedures and Elements of Study

In the previous chapter the procedures and elements of study were elucidated, the items of which were represented by a flowchart of research design and the task groups, as well as further descriptions. The major findings from such processes that will be delivered here include geo-data assimilation and field observation data. The first is the data assimilation results at seven levels comprising of 25 numerical domains, of which two are situated in the study area, i.e. the 5th level Cilacap and the 7th level Permisan. The second is the field observation data that deal with the data selection of the tsunami run-up heights, which have been collected in previous works, the comparison field measurements in Permisan, and the interpretation of maximum inundation of past events as documented from interviews in Cilacap.

5.1.1 Geo-data assimilation

5.1.1.a Data assimilation of numerical domains

As mentioned in preceding chapters, the geometric data input for numerical simulations is data assimilation many data resolutions and sources, mainly through an interpolation process. The specific treatment for data assimilation was carried out, in which the data has very different resolutions, such as GEBCO and SRTM-30, which causes problems at the boundaries of both datasets. In the present study, it was found that this can only be resolved by using manually digitized data instead of using the options available in the

GIS software properties, i.e. TIN (Triangulated Irregular Network) interpolation, and so. TIN interpolation is a very convenient and effective way of filling blank data between two contour lines that have smoothed curves. However, it has disadvantages when meeting fringe contours or sharply bending lines leading to flattened triangles with zero values being produced. Furthermore, this technique does not consider whether the bordered data are topography or bathymetry, leading to difficulties promoting which data have priority due to resolution. However, there are methods for avoiding such problems, e.g., by adding break lines or adding more mass points; however, for huge number data, this is not an economical solution⁹.

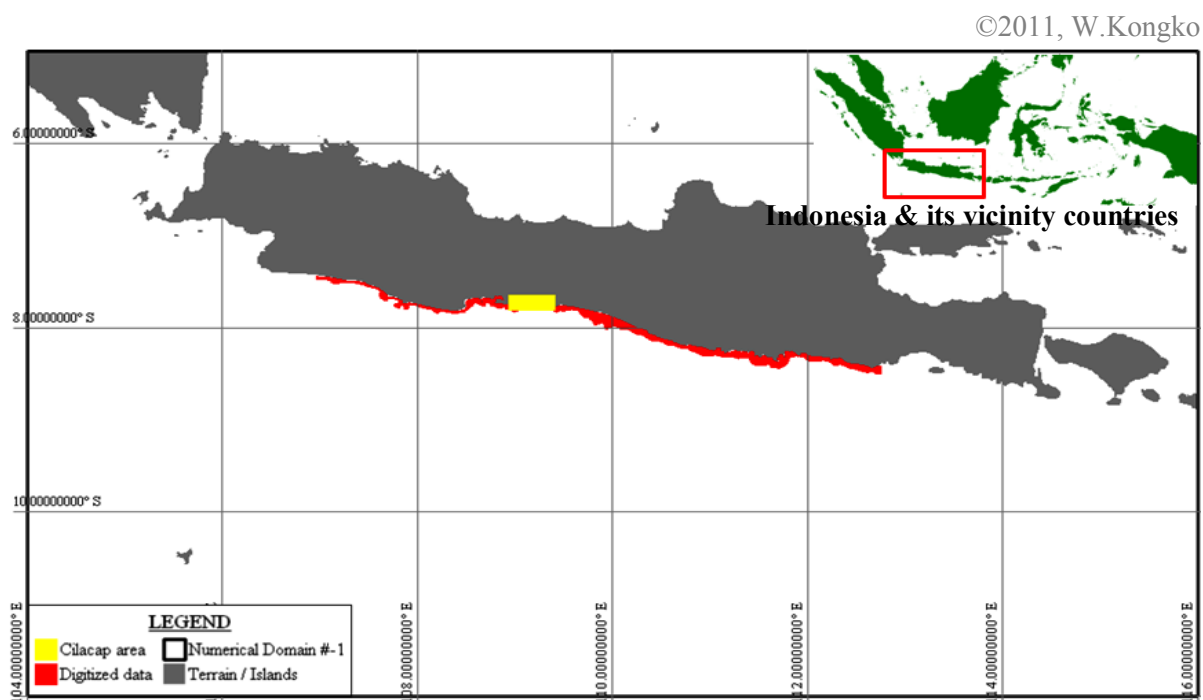


Figure 41: Area of manually digitized data

Figure 41 shows the area of digitized data of about $70 \times 10^3 \text{ km}^2$ shaded red. This area should be filled using manual digitizing data after those of low resolution of GEBCO have been removed. In the study area of Cilacap (yellow box), however, the highly resolved data from both field measurements as well as collected data are available, thus negating such a process.

The digitized data are made linear between the coastlines derived from the SRTM-30 to a distance near-shore with a water depth of 50–200 m or should bigger than several times

⁹ http://www.ian-ko.com/resources/triangulated_irregular_network.htm

of grid-spacing data of GEBCO. The results of data assimilation for seven levels, which consist of 25 domains, are provided in Appendix G – Data assimilation in section A to O.

5.1.1.b Data assimilation in the study area (DSM/DTM)

In the study area of Cilacap, the various data that have been collected through field measurement campaigns and those provided by other sources within the framework of the project has been merged as depicted in Figure 24 in the preceding chapter.

©2011, W.Kongko

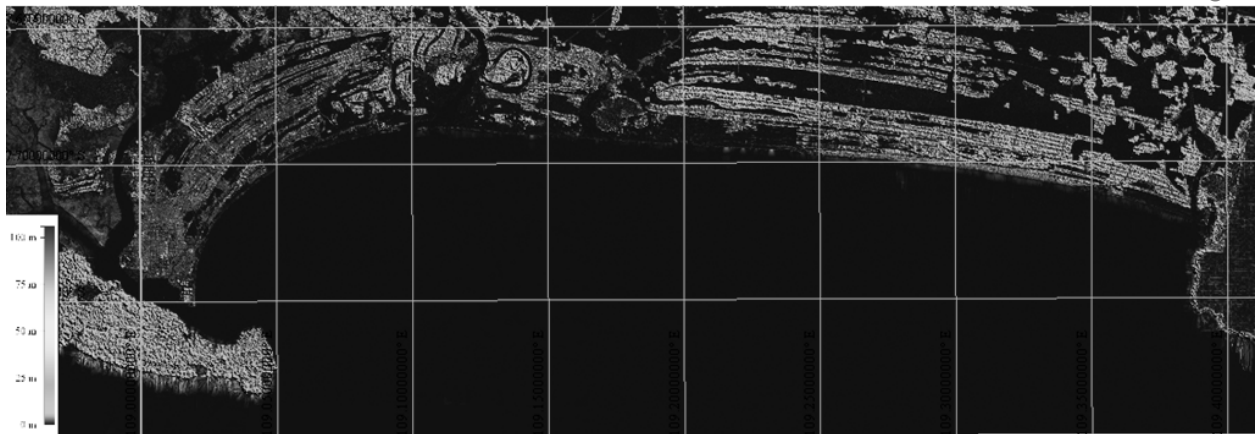


Figure 42: Difference between DSM and DTM data

There are eight data types and sources that have been collected and used in the study area. However, in terms of tsunami run-up modeling, the significant issue is the DEM (digital elevation model) data that consists of DSM (digital surface model) and DTM (digital terrain model). DSM is the elevation model data, in which the land cover is included, such as buildings and vegetation, while DTM is the data containing solely terrain or bare soil after its land cover has been removed by certain techniques. The difference between both data types is illustrated in Figure 42.

To compare the difference between DSM and DTM data, simple statistical methods have been used, namely the root mean squared deviation (RMSD) and normalized root mean squared deviation (NRMSD). The entire number of cell areas considered of n is 1,778,976. The RMSD and NRMSD are 2.76 m and 0.9%, respectively. The maximum value of both datasets is 250.7 m, and their minimum values are -54.2 m.

For model validation purposes, especially of the maximum horizontal tsunami run-up heights in Cilacap's Penyu Bay, the geometric data input in numerical simulation considers the two datasets above. This selection allows distinguishing between two major

characteristics of land cover and land use types, which can only be interpreted during field surveys.

5.1.1.c Data assimilation in Permisan-Nusakambangan Cilacap

The topography survey campaigns were equipped with high-accuracy Total Station instruments for measuring the ground level in more than 1,200 points. The survey points are located within an area of about 1.5 km² with spacing in the range 10–40 m in the transect fashion that is mainly normal to the coastline. The measurement points are indicated by yellow dots overlaid on an IKONOS image depicted in Figure 43.

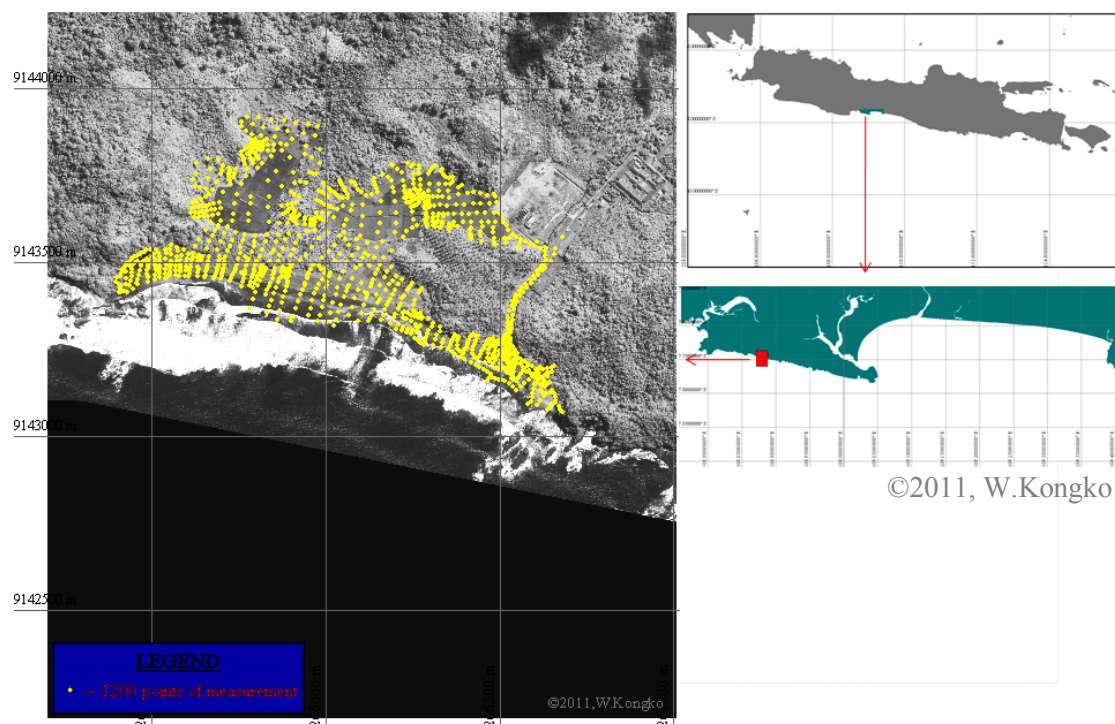


Figure 43: Topography survey in Permisan using Total Station instruments

The ground-level measurements were conducted from the coastline and climbed as far as possible to some surrounding hilly areas inland, reaching the location of the 2006 Java's maximum tsunami run-up heights. However, due to dense trees and bushes as well as steep hills in some places, the measurements at ground level could not be performed. Therefore, some blank inaccessible areas are inevitably present, and filled with the medium-resolution SRTM-30 data using a technique to remove the inclusion of the unnecessary land cover, such as trees.

Within the framework of the GITEWS project, the author collected images from the IKONOS satellite of Permisan as shown in Figure 43. This allows the shape and location of the prison area to be interpreted, and thus it was also gathered in the terrain model derived from the field measurements and SRTM-30 data. The data assimilation results gathered with bathymetry measurements as well as digitized data are shown in Figure 44.

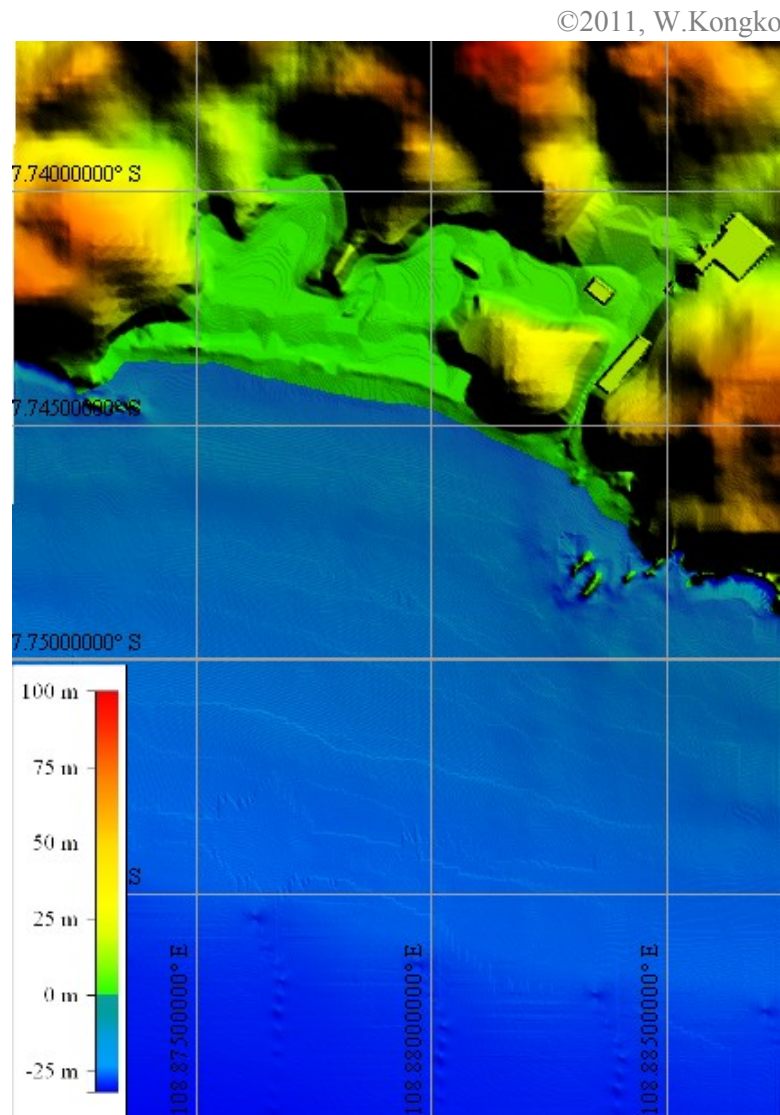


Figure 44: Data assimilation of field measurements & SRTM-30

5.1.2 Field observation data

5.1.2.a Tsunami run-up along the coastline

In the preceding chapter, to reduce uncertainties due to topography features, three criteria were outlined for selecting and deselecting the tsunami observation data collected during the 2006 Java tsunami. One is the horizontal distance from the coastline linked to absent coastal vegetation. Further, the dataset that has no slope information or steep slope has

also been excluded to reduce numerical error prediction. The last is the division dataset between the extreme run-up in Permisan Nusakambangan Cilacap with other data. These approaches select a total of 114 points from the entire data collected.

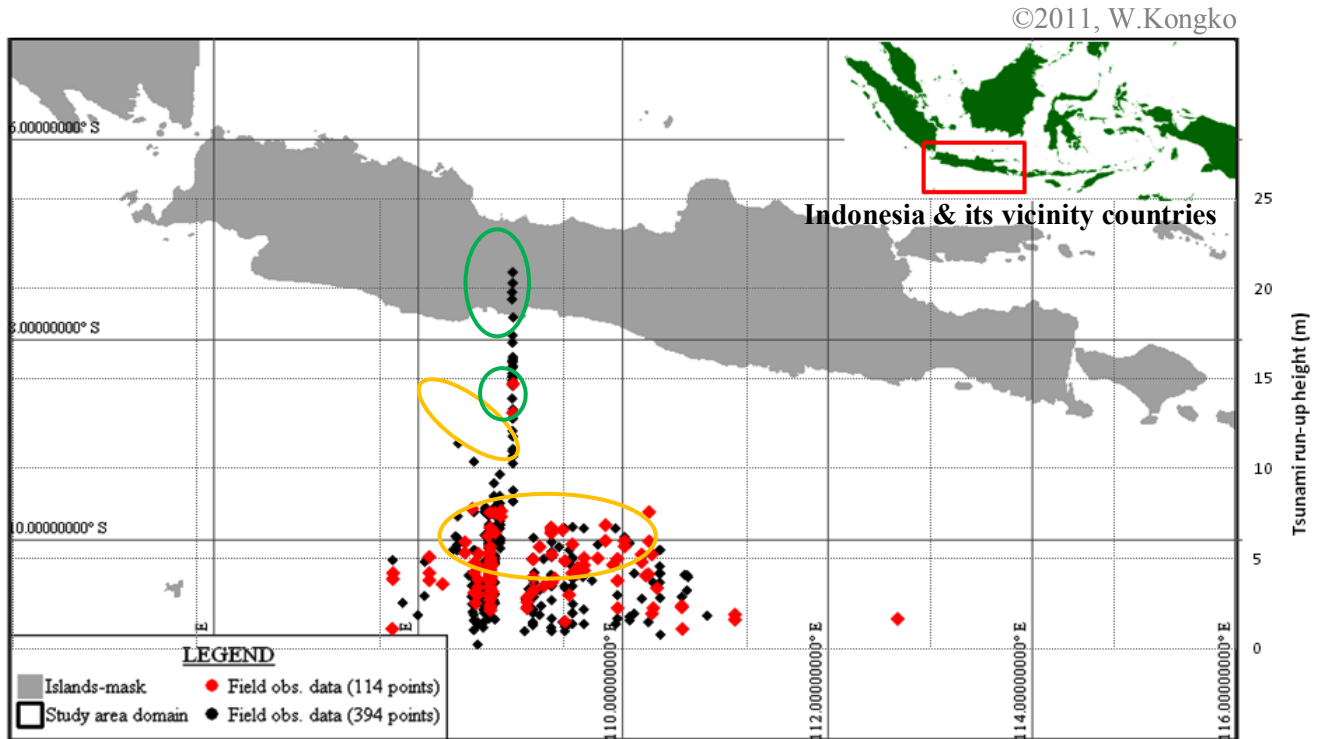


Figure 45: Entire vs. Selected field observation data of the 2006 Java tsunami

Figure 45 shows the data plotting of both the entire and also selected field observation data of the 2006 Java tsunami run-up heights overlaid on a Java Island map and differentiated by colored dots. It is clearly shown in Figure 45 that the extreme run-up data at Permisan-Cilacap are absent (as indicated by two green ovals), and the points' measurement of run-up heights below 3–4 m and between 7–13 m stretched from Pangandaran to Kebumen (as depicted by two amber ovals) also disappear. This indicates that the aforementioned uncertainties factors are sufficiently significant. However, the scattering data still exist and the expected convergent points following a Gaussian curve are not clearly pronounced.

5.1.2.b Extreme tsunami run-up in Permisan Nusakambangan Cilacap

There are 39 points of tsunami run-up in Permisan-Nusakambangan as documented in prior works (Fritz et al., 2007, and Lavigne et al., 2007). The present study performs re-marking of the points above then uses them for further analysis, namely measuring ground

level, estimating the 2006 tsunami run-up heights, and collecting the coastal features in the surrounding area.

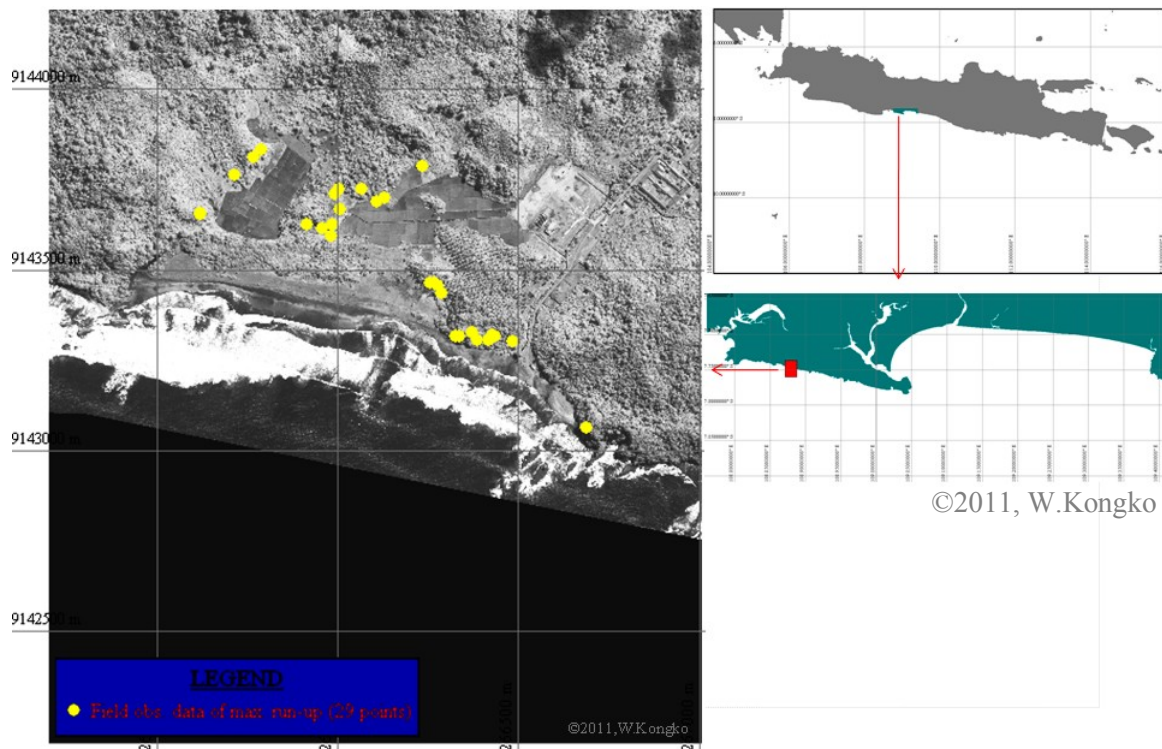


Figure 46: Points measurements of maximum tsunami run-up at Permisan

29 of the 39 points are the maximum tsunami run-up data, whose flow depth is equal to zero and thus are to be assumed as being similar to the ground level. Figure 46 shows the locations of the points, all of which are situated in the steep hilly area (see also the brief survey report and technical specification in Appendix C – Field’s measurements in section D).

The topography survey in Permisan measures the ground level by using Total Station instruments. The results are then combined with the SRTM-30 and bathymetry measurement near-shore data to generate continuous geometric topography-bathymetry data.

The 29 points of maximum run-up heights are taken by overlying the re-marking points of the field survey, where the positions were estimated using a handheld GPS device, onto the merged geometric data above. The points are further compared with the rapid survey results from the studies conducted by previous researchers (Fritz et al., 2007, and Lavigne et al., 2007).

Figure 47 shows the bar chart of points' measurement at Permisan, both from prior field observation data and those derived from merged geometric data resulting from field measurements. The difference in the rapid survey of field observations and topography measurements is 25.5% on average. This average difference assumes that the re-marking points are using positions estimated by a handheld GPS device, whose horizontal accuracy is about 10 m¹⁰ and without any horizontal corrections. The data are available in Appendix D – Observation data in section F.

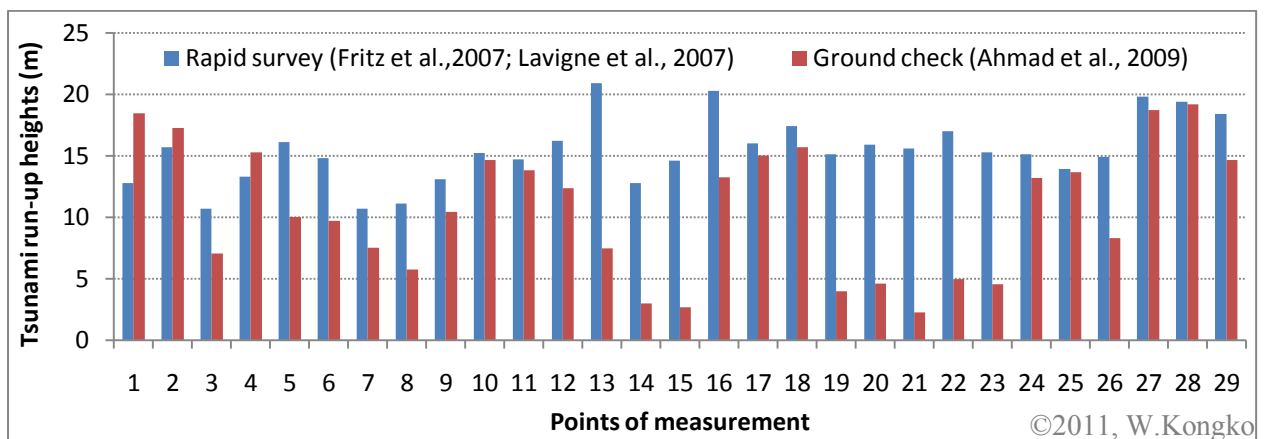


Figure 47: Bar chart of points' measurement at Permisan

However, when the data are corrected following the run-up heights from the field observation data, the re-marking points should be horizontally shifted a few dozen meters. Appendix D – Observation data in section G provides the horizontal distances from origin points when the run-up heights are adjusted to follow the field observations. 14 of the 29 data points have a shifting distance greater than 10 m, which is the value of the GPS horizontal error. This indicates that the performance of the handheld GPS device used by both prior survey team and topography teams of the current study might have deficient accuracies in areas with dense tree coverage.

5.1.2.c Points of maximum inundation in Cilacap Bay

To validate the inundation of the 2006 Java tsunami, the estimation of the maximum run-up during the event is inevitably required. Hence, the present study conducted interviews with the residents who had experienced the tsunami. Its locations were concentrated in the

¹⁰ http://www8.garmin.com/manuals/eTrexLegendHCx_OwnersManual.pdf

riverside of Serayu and Bengawan, where the topography is flat and experienced far tsunami penetration. In the eastern part the interviews were also held; many report stated that the 2006 Java tsunami inundated hundred meters of farm fields. The whole of the interview area includes five sub-districts comprising 20 villages. However, only 23 point locations of estimated maximum tsunami run-up in 11 villages have been investigated due to time and weather constraints.

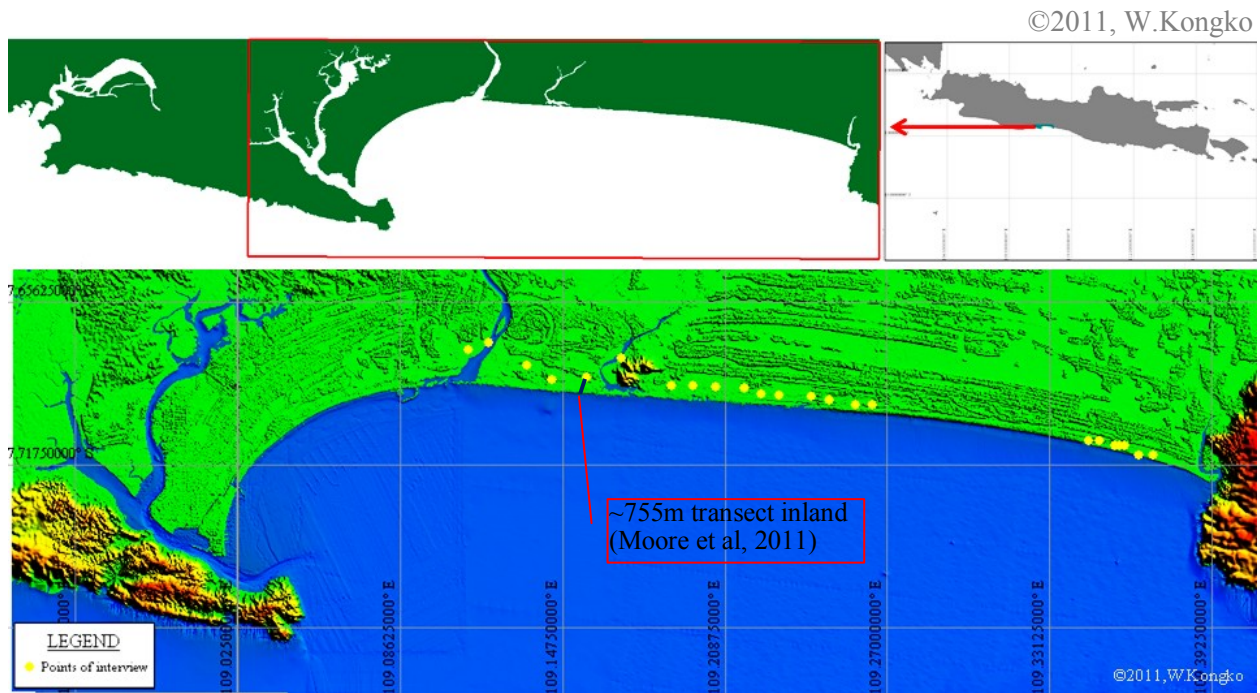


Figure 48: Points' measurement of maximum inundation (interview)

Figure 48 shows the points' measurement of maximum inundation during the 2006 Java tsunami. The farthest points of tsunami penetrations have been investigated, with distances of about 1.8 km from the coastline located on the riverside of Serayu and Bengawan. In the western part, this includes four sub-districts, the tsunami penetrations range from 350 m – 1.8 km, while in the eastern part consisting of only one sub-district, the tsunami inundation according to witnesses varied from 50–350 m.

At Adipala, the sub-district which is located between Serayu and Bengawan rivers, the maximum tsunami inundation and its direction were represented by the ~755m transect of coring tsunami deposits that has been made by Moore et al. (2011). It was intended to study the tsunami impact through its deposits by characterizing the thickness, deposit stratigraphy, and analyzing other sediment properties. The end of transect also coincides with estimated

maximum inundation point from interview that being made in this study (indicated with blue line in Fig. 48).

It is interesting to note that in the city of Cilacap there were no reports of the tsunami penetrating inland more than 50 m. The presence of the Nusakambangan peninsula or the headland seems to have functioned as an effective protection against the incoming tsunami wave from the south-west direction.

5.2 Simulation model results

As mentioned in the research design in Chapter 4, the present study performs three model simulations, namely the reconstruction of the 2006 Java tsunami, a hypothetical model for future hazard, and a synthetic model for the effect of complex ruptures. The model tools and their set up used in the present study were described in the preceding chapter. Here, however, the simulation model results of the three issues named above will be provided.

The reconstruction of the 2006 Java tsunami provides the model results and its validation for the run-up heights along the coastline, the maximum inundation onto land in the study area of Cilacap as well as the arrival time and the interpretation of the tsunami evolution approaching the shore. The hypothetical model for future tsunami hazard produces the hazard maps resulting from the hundreds of maximum plausible scenarios for the Cilacap area, while the synthetic model delivers the results of the tsunami amplitudes along the coastline due to the variety of data input of both tsunami source and geometric data.

5.2.1 Model reconstruction of the 2006 Java tsunami

5.2.1.a Tsunami run-up heights & its distribution along the coastline

Model validation of the tsunami run-up along the south Java coastline has been conducted by comparing the field observation data and the model results. As discussed in previous chapters, there are only 114 of 394 data points of tsunami run-up that have been selected to validate the model. These will be compared with the run-up data from the maximum wave excursion in the 5th numerical domain, which has ~23 m grid-spacing within water depths varying between ~1-3 m and ~205 m at interval acquisition points along the coastline.

To validate the model of tsunami run-up heights and its distribution along the south Java coastline, the present study uses two criteria of moving average analysis to filter underlying datasets and the parameters K and k proposed by Aida (1978). Another additional

validation model uses graphs as well as image interpretations of the data from the three mareograms and video snapshots/photos documented by an eye witness.

The use of the first criterion produces graphs showing the comparison of the field observation data with the model results for each fault model proposed in Table 4 in Chapter 4. Since the south Java coastline is partially characterized by vast beach sections with fringing coastal morphology and complex bathymetry formations, a statistical approach of trend line of moving average was recommended (personal communication by Prof. Steven N. Ward).

The subsequent graphs are provided in Appendix H – Simulation results in section A (A.1. – A.6); here, however, one of them is given in order to show exemplary results of the multi-faults model by Ammon et al. (2006) in Figure 49.

The model results from the six fault models in comparison to field observations as shown in the subsequent graphs (see in Appendix H – Simulation results in section A: A.1– A.6) reveal remarkable variations. Although the evaluation using statistical moving average only gives trend curves, this approach clearly shows that tsunami sources of 3, 5, and 6 in Table 4 have more reasonable agreement than others.

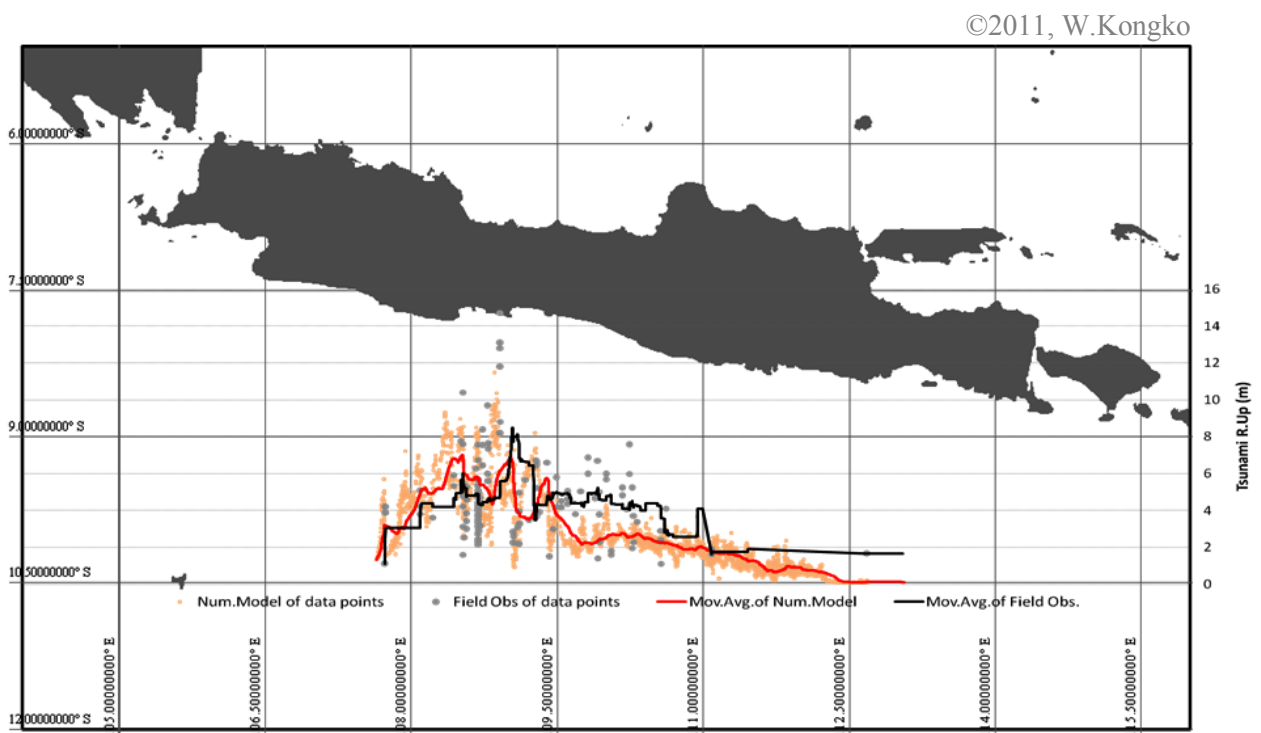


Figure 49: Graph of field observation data vs. tsunami model based on multi-faults model by Ammon et al., 2006

If the first approach of the validation model using moving average analysis provides trend curves and thus the justification can only be made qualitatively by interpreting the two curves of field data and the model results, the second one that calculates the parameters K and k as proposed by Aida (1978) provides quantitative values. This method is recommended by Prof. Imamura (personal communication) for reducing an error interpretation of the tsunami run-up' data due to coastal features if a trend line is used. Furthermore, such a method gives quantitative values, which can be further evaluated for specific purposes.

Each source model in Table 4 produces tsunami run-up heights along the coastline. Further, in the corresponding location of the 114 points, the wave excursions are taken out and using the expressions in (45); the parameters K and k are then calculated. Table 8 below shows the parameters K , k , root mean squared deviation (RMSD), and % error ($n=114$ samples) of each source model result.

Table 8 shows the four parameters K , k , RMSD, and % error for each source model, whereby the K value being near to 1.0 and the lower value of k , RMSD, and % error represent a better model result in the field data being mimicked. The best three results might be selected; they are in descending order source models 3, 5, and 6 (based on K – or the average of the ratio between the observed and computed tsunami amplitudes) and 3, 6, and 5 (based on k , RMSD, % Error – or the standard deviation of samples considered).

Table 8: K & k parameters of the model results

No	Source models	K	k	RMSD (m)	Error (%)
1	Fujii & Satake (2006)	3.632	1.904	3.82	28.1%
2	Cheng-Ji (2006)	5.808	2.267	4.19	30.8%
3	Ammon et al. (2006) – with modification in the present study	1.010	1.707	2.23	16.4%
4	RuptGen ver. 1.1-GITEWS (2010), normal rigidity ($\mu=30$ GPa)	3.426	2.225	3.62	26.6%
5	RuptGen ver. 1.1-GITEWS (2010), low rigidity ($\mu=10$ GPa)	1.326	2.081	2.77	20.4%
6	Present study (2011)	1.496	1.730	2.54	18.7%

According to the results in Table 8, the source model proposed by Ammon et al. (2006) – with a modification for the present study – has $K=1.01$ and $k=1.71$, which is able to fulfill the satisfactory criteria of K ($K=0.8-1.2$) proposed by Aida & Hatori (1984), Hasegawa (1986), Shuto et al. (1987) in Shuto (1991), and Suppasri et al., (2008), yet the k value is out

of the criteria ($k < 1.4$). However, the best three results above are consistent with the moving average analysis mentioned in previous paragraphs.

These findings indicate that source models 3, 5, and 6 which imposed the low rigidity of $\mu = 10$ GPa enable field observation data to be mimicked better than those using a normal rigidity. This phenomenon is reasonably justified since by applying low rigidity the initial sea surface heights are larger, leading to an amplified tsunami run-up along the coastline. Furthermore, in terms of the tsunami run-up distribution depicted in the subsequent graphs in Appendix H – Simulation results in section A (A.1 – A.6), those that use multi-faults models are better than the single-fault model. This is because the multi-faults model more realistically reflects the co-seismic slip distribution than the simple single-fault model.

5.2.1.b Tsunami arrival time & its maximum inundation in Cilacap

To obtain the model validation of the arrival time and the maximum inundation of the tsunami, a comparison model was constructed based on the evidence collected along the Java coastline and from the study area of Cilacap. This validation model also has the benefit of the available high resolved geometric data with the additional field survey as well as three mareogram recordings and videos/pictures captured by an eye witness in study area.



Figure 50: Area of interest for model validation in Cilacap

Figure 25 in Chapter 4 and Figure 50 above depict the area of interest, where data for model validation of the 2006 Java tsunami have been collected. The data for model validation consists of three mareogram recordings in the stations at Cilacap ($108.89^{\circ}\text{E} / 7.75^{\circ}\text{S}$), Sadeng ($110.798^{\circ}\text{E} / 8.190^{\circ}\text{S}$), and Prigi ($111.733^{\circ}\text{E} / 8.283^{\circ}\text{S}$), shown on the graphs provided in

Figure 26. Further, additional field surveys of maximum inundation have also been conducted in the Cilacap area as shown in tiles 1, 2, and 3 in Figure 50. To interpret the tsunami time arrival and its wave evolution, the present study also uses sequential videos/pictures collected by an eye witness at the ship basin of the steam power plant (PLTU, 109.089°E, 7.691°S) as published by Lavigne et al. (2007).

The tsunami mareograms of the 2006 Java tsunami from the tide station at Cilacap can be downloaded from internet for free¹¹, while two other mareograms, i.e. from the stations at Sadeng and Prigi were provided by BAKOSURTANAL. Further, these particular data sources were compared to the corresponding water levels of the numerical simulation resulting from six source models in Table 4. The graphs of the comparison between tsunami mareograms and the tsunami model are shown in Figure 51.

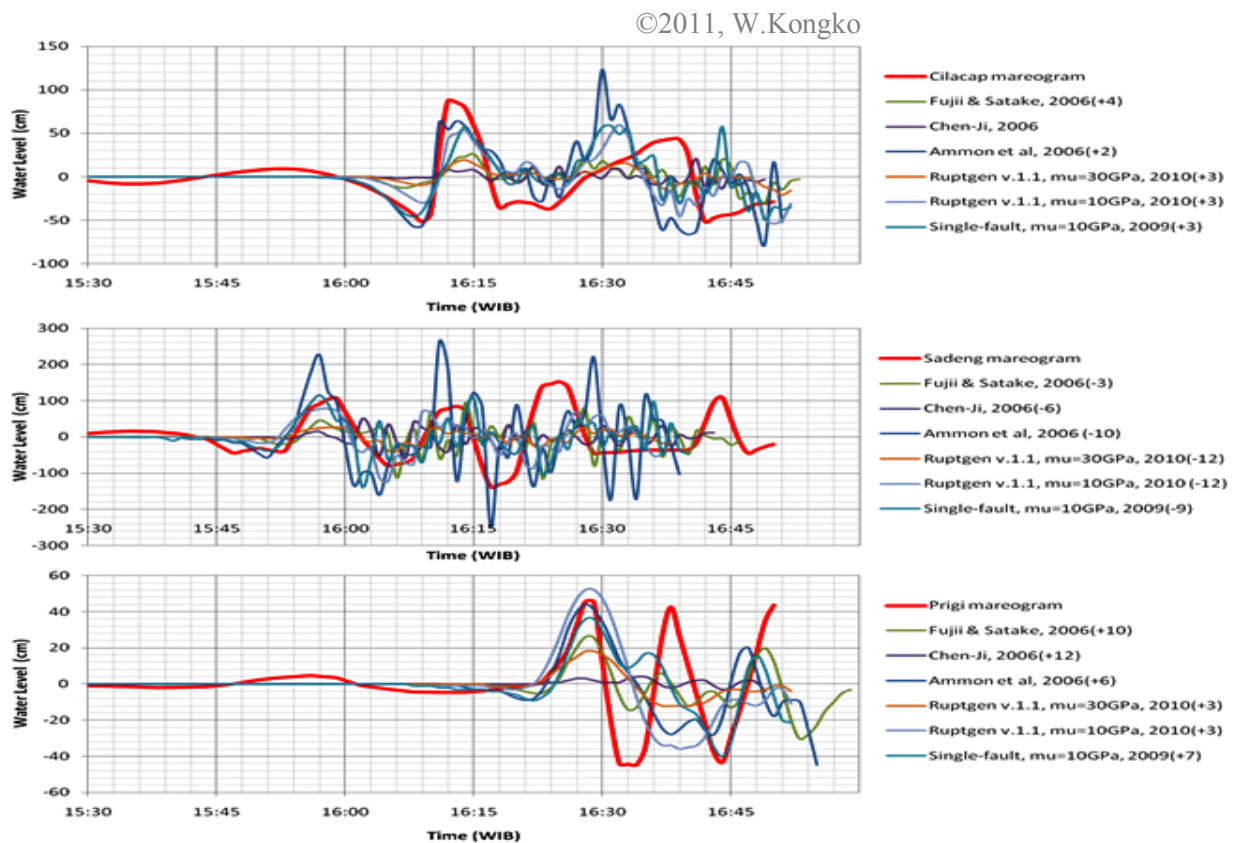


Figure 51: Tsunami mareograms vs. water level resulting from the model

The top of three panels in Figure shows the Cilacap tsunami mareogram; its location is Cilacap's Penyu Bay and depicted by a blue triangle in Figure 50. The middle and bottom

¹¹ <http://www.vliz.be/vmcddata/iode/>

panels show the tsunami mareograms from the stations at Sadeng and Prigi as shown in Figure 25 in Chapter 4. By evaluating graphs of the comparison of the mareograms and tsunami model results in three tide stations in Figure 51, some conclusions can be drawn.

First, in all graphs, the time arrival of the simulation model results should be adjusted from 2 to 12 minutes to fit the corresponding mareogram, including for the Cilacap station where highly resolved data have been employed. This shows that the near-shore bathymetry has a remarkable effect on the tsunami arrival time within the approximate time shift above. This is also caused by the bathymetry data gap very near to the coastline where the location of the tide station is. The fact that there are portions of the area in the bay as well as channels where the bottom profiles was not covered in the surveys and led to data inaccuracies.

Second, the waveforms of both mareograms and models can only be compared in terms of their first or second wave, showing that the coastal topography features create a lot of wave perturbation from the third wave on. This may also be due to the harbor or bay's resonance, so that the new waves being excited or amplified if the periods of incoming waves are approximate some harmonic of the natural frequency of the basin (Aida, 1978; Wiegel, 1964, 1970; Bryant, 2008).

Third, all simulation results show leading depression waveforms and thus this is consistent with the mareograms as well as the typical tsunami waveforms in the dip direction due to tsunamigenic earthquakes (Synolakis & Bernard, 2006). It can be noted that the first wave amplitudes that give comparable values with mareograms are also from simulations run using source models 3, 5, and 6.

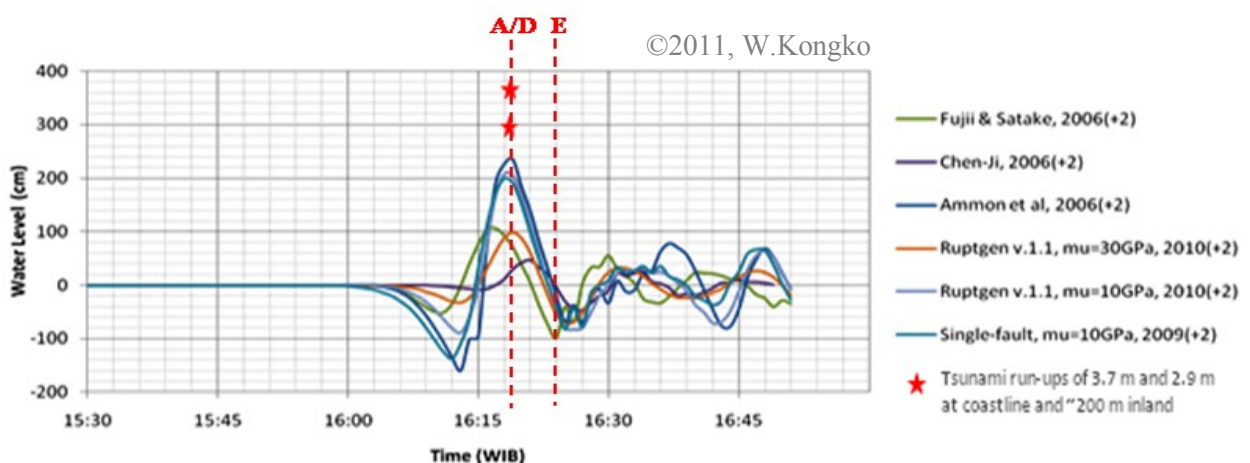


Figure 52: Tsunami mareogram vs. water level at eye witness points in Cilacap

The model validation for time arrival and amplitudes of the tsunami also benefits from the sequential video snapshots and photos captured by an eye witness and published by Lavigne et al. (2007). They visualize the evolution of the incoming tsunami located near the ship basin of the steam power plant (PLTU), which clearly resembles a tsunami rushing towards the shore or receding backwards away from it. Other pictures of the presence of the tsunami also documented by Lavigne et al., (2007) at Shrimp basin (or well-known as “Tambak” in local language) are located in Keboncarik Cilacap (see Figure 27 in Chapter 4).

©2007, Lavigne et al



Figure 53: Sequential video snapshot of tsunami waves at PLTU-Cilacap

Figure 53 shows selected pictures taken from Figure 28 in Chapter 4. It reveals the evolution of the 2006 Java tsunami in PLTU Cilacap (shown by a red triangle in Figure 50) with the re-edited time tag stamped on the bottom left of each frame. For model validation, the water-level time series data was taken at a virtual point at depth 5 m located within a ship basin approximately 300 m from the eye witness. The tsunami travel time from such a point reaches the coastline in about 1–2 minutes, thus the time series data is shifted by that value. The water-level time series data are plotted in a graph in Figure 52.

The tsunami evolution is displayed in real-time in Figure 53 (A), (D), and (E), and if it is plotted on the graph in Figure 52 it provides a suitable comparison of the tsunami rushing towards the shore (A), in a maximum state (D), and when it is in a receding phase (E). The nearest tsunami run-up data taken from field observations was also plotted, which are 3.7 m and 2.8 m located near to the coastline, approximately 200 m inland (as denoted by red stars in Figure 52). Furthermore, in Figure 27, pictures (A) and (B) show the presence of the tsunami at the shrimp basin (or local language is “Tambak”), which was taken between 16:16~16:20 WIB (Lavigne et al., 2007). The presence of the tsunami and its given time also matches the water level of the tsunami resulting from the model simulation as plotted in Figure 52.

Even though the model validation using three tsunami mareograms and video snapshots as well as pictures in the Cilacap area give some variation of arrival time and, thus, the time shift should be imposed, nevertheless, source models 3, 5, and 6 again give comparable amplitudes, from which it can be concluded that the higher slip gives results comparable to the field observation data.

For the three approaches to model validation shown above – where the first two were delivered in the previous sub-section, i.e. tsunami run-up heights and its distribution along the south Java coastline by using analysis of moving average and parameters K and k (Aida, 1978) and the third is the arrival time of model validation utilizing the mareograms recordings as well as videos/pictures – all of the results suggest that source models 3, 5, and 6 give a result comparable with the observation data of the 2006 Java tsunami.

For inundation model validation of the 2006 Java tsunami, the study area of Cilacap is selected, in which investigations are concentrated on tiles 1, 2, and 3 in Figure 50. The reason behind the selection of this particular area is the availability of highly resolved data and the additional field survey of maximum inundation points of such events that has been conducted.

The model validation compares the maximum inundation of the 2006 Java tsunami resulting from numerical simulation and field observation data as collected from previous works as well as those documented in the additional field measurements in the study area of Cilacap. For this purpose, the present study selects the best three source models above for the initial conditions of the further model validation, namely source model 3.

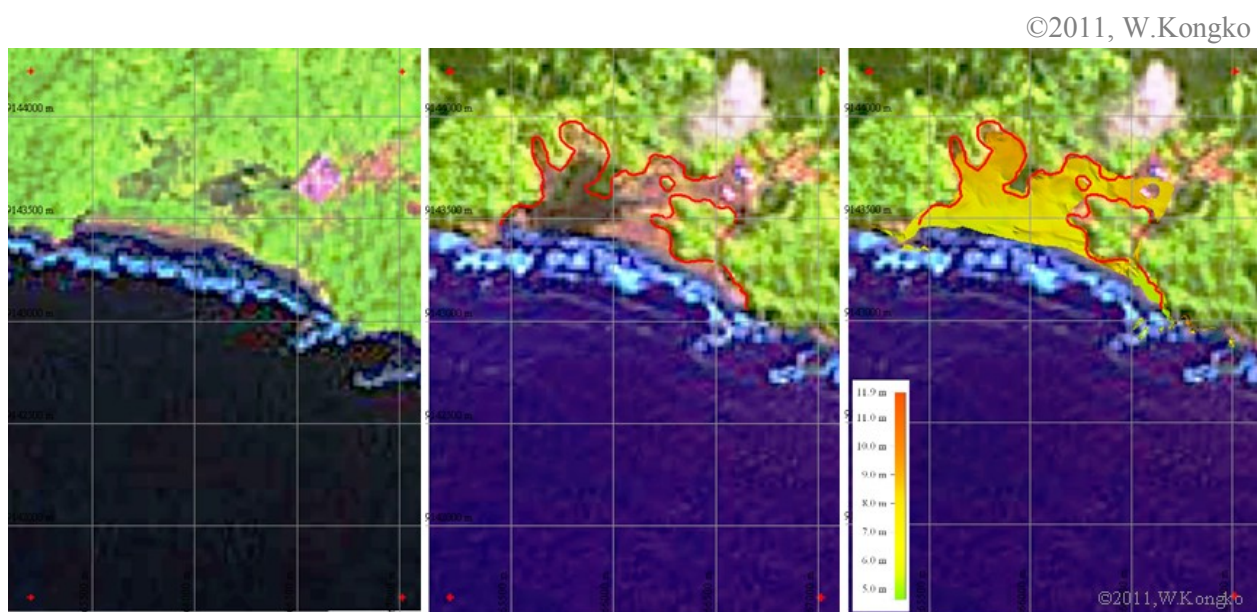


Figure 54: Satellite imagery of SPOT-1 before and after event & its model comparison

Figure 54 shows the satellite images of SPOT¹² before and after the event in Permisan Nusakambangan Cilacap Java Island located in tile 1 in Figure 50. The left-hand picture is the image that was taken on 22 January, 2006, and the middle picture was taken on 18 July, 2006, one day after the event. Since only the low-resolution version is freely available in the internet, a coarse interpretation of the maximum tsunami inundation was made by drawing red lines on the image based on the contrast-level color, which has a high possibility of having been formed by tsunami debris or transported land cover. The right-hand picture is the SPOT image with the interpreted maximum tsunami inundation (shown by red lines) and overlaid with the tsunami model result (color mask), whose its comparison is fairly good.

Figure 55 shows IKONOS-based images whose location is similar to that of Figure 54, and depicts the inundation model result with 29 points of maximum tsunami run-up (excluding the seven points of flow-depth data) conducted by Fritz et al. (2007) and Lavigne et al. (2007). The tsunami penetration went further inland from hundreds of meters to a km, except in the eastern part where the cliff and hill exist. The tsunami climbed and reached the hills surrounding Permisan and a small portion inundated the surrounding prison area, flooding the sewer system, which was confirmed by local people who were interviewed during a ground survey.

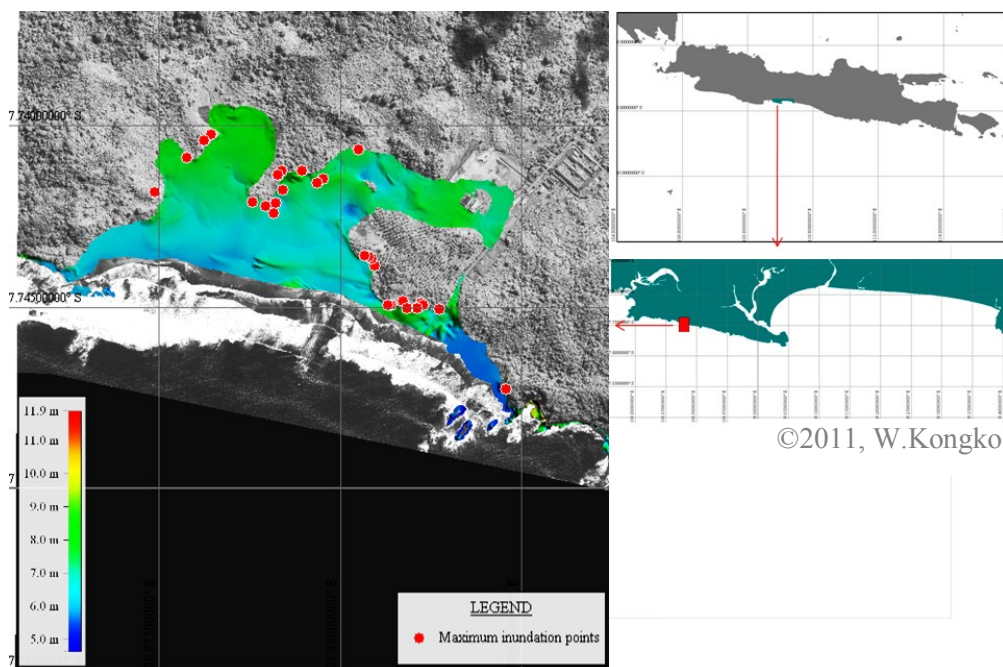


Figure 55: Inundation model vs. field observation in tile 1, Cilacap

¹² <http://www.crisp.nus.edu.sg/coverages/tsunami20060717/view20060718.html>

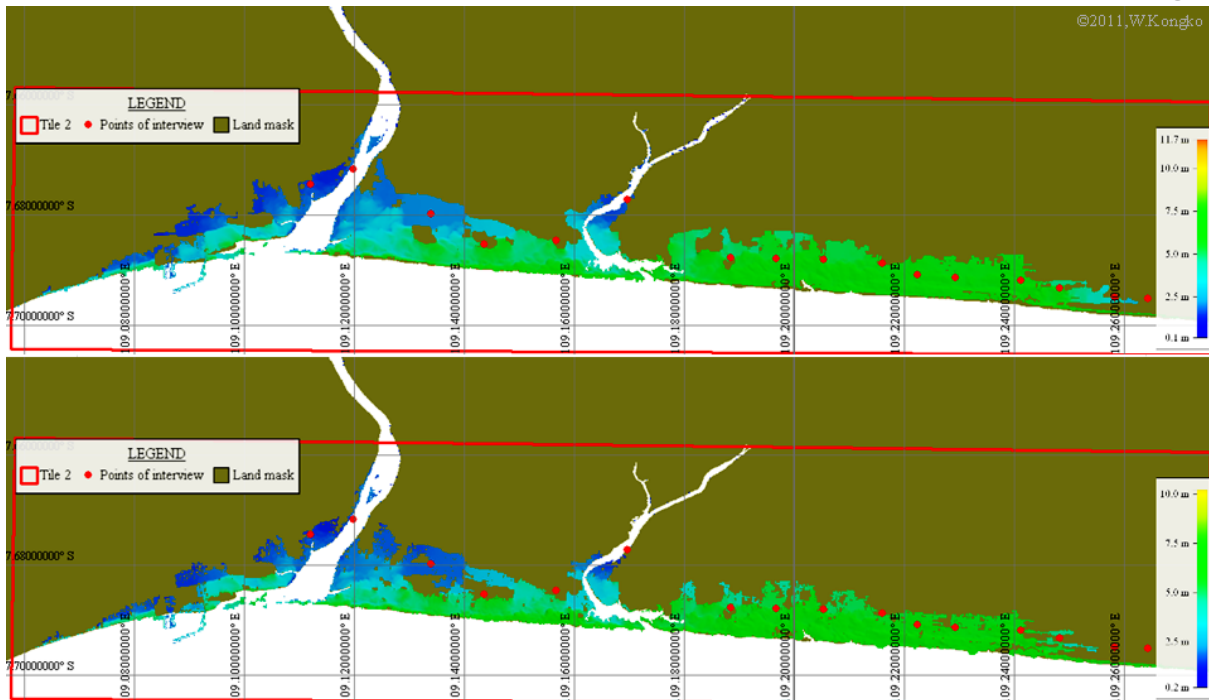


Figure 56: Inundation model vs. field observation in tile 2; DTM (top) and DSM (bottom)

Figure 55 also shows that the tsunami run-up points from the field observations (indicated by red dots) are more or less located at the tip of the inundation mask resulting from the simulation model, indicating that horizontally the model validation gives a good result. In contrast, vertically, the comparison of the tsunami run-up heights for both the model result and field observations shows discrepancies. The model result gave only the tsunami run-up an average fit of 57% to the field observation data. Such discrepancies seem to have been caused by both the inaccuracies of the assimilated terrain model, which includes the low-resolution SRTM data and the limitations of the NSWE model, which is unable to represent the vertical component flux due to the steep slopes ($>1/10$). The whole area in the numerical domain was not covered by field measurement, especially parts located on steep slopes and in inaccessible densely covered areas of trees and bushes. To fill such blank data, the rough resolution of SRTM-30 or SRTM-90 were used, leading to a lower accuracy at ground level and thus inaccuracies of geometric data input in the model.

For model validation purposes, the present study also compared the inundation model results with the estimates of the horizontal maximum run-up in two distinct locations: in the Penyu Bay of Cilacap as shown in tile 2 and tile 3 in Figure 50. The comparison of the model

validation in tile 2 is provided in Figure 56. In the top panel, the geometric model used is the Digital Terrain Model (DTM), while in the bottom panel it is the Digital Surface Model (DSM). Both geometric datasets give different results in the inundation model. At the riversides of Serayu and Bengawan, the difference is less pronounced since less vegetation exists in this area.

East of the Bengawan river, however, the difference appears to follow the typical land cover characterized by coastal vegetation, such as coconut trees, etc. The results, therefore, in the riversides of both rivers are comparable when using both geometric data, while in the eastern part of the Bengawan River; the DSM data are more suitable and give a better result compared to the model, although 1–2 data points are located in dry places. Nevertheless, by using both of the above geometric datasets the model results are still comparable to the field observation data.

Tile 3 as shown in Figure 57 above, however, gives different results using both DSM and DTM geometric data input in the model. By using the DTM data, the model results seem to be better than the DSM data.

Of the four model validations, three, namely the tsunami run-up heights, the tsunami distributions along the coastline, and tsunami travel time, which use six model sources, and one model validation of maximum inundation using selected model sources have been conducted and give qualitative and quantitative model performances.

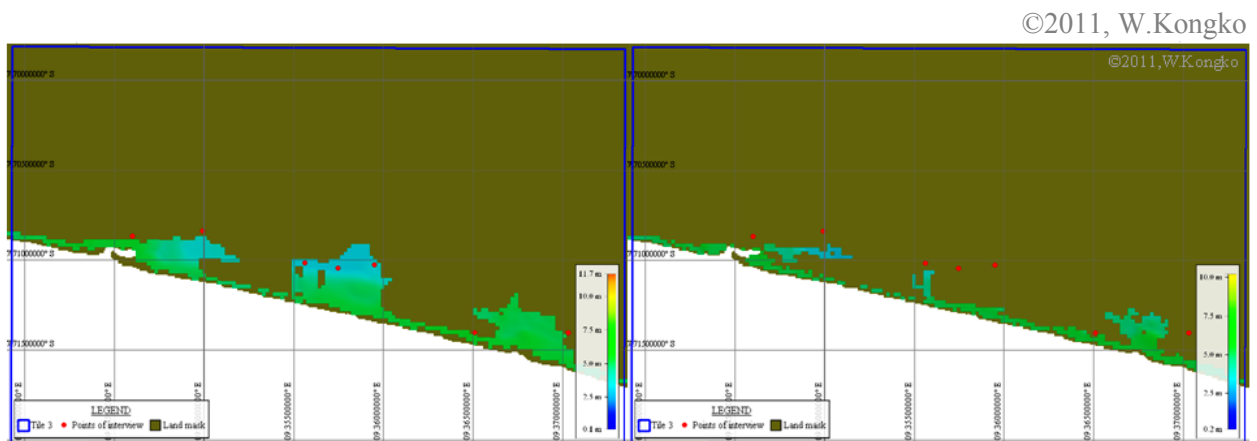


Figure 57: Inundation model vs. field observation in tile 3; DTM (left) and DSM (right)

In regard to the model validation of the tsunami run-up distribution as well as their travel time, it is clearly shown that the 2006 Java tsunami can be mimicked by a model that imposes low-rigidity material at excitation zone as represented by source models 3, 5, and 6. And the best source model, model 3, of a multi-fault type was selected to have further model

validations in tiles 1, 2, and 3, which also show reasonable agreement with field observation data.

5.2.1.c Estimated discriminant values to predict tsunamigenic

This sub-section delivers the result of the test for the tsunamigenic submarine landslide that may be associated with the earthquake following the 2006 Java tsunami. As mentioned in the previous chapter, a robust and simple method was developed by Okal & Synolakis (2004) to characterize the shape of near-field tsunami run-up distribution by empirically fitting a formula as expressed in (46), in which the parameters are optimized by trial and error.

Since, for fitting curves on the data points of tsunami run-up by using such an empirical expression of 46 above can only be done with visual evaluation, to check the equality and reliability of the goodness of fit of the obtained curve-fittings, this study uses a tool so-called *XLfit*. It is a curve-fitting and data analysis package that integrates with Microsoft Excel that offers a fit and statistics models as well as charts and graphs to visualize, interpret and present experimental data¹³.

The data points of tsunami run-up that have been examined consists of two conditions, namely the entire dataset contains 394 points and 114 pre-selected points of tsunami run-ups according to the criteria as mentioned in preceding Chapter.

Figure 58 and 59 show the fitting curve for discriminant tsunamigenic events plotted on the entire dataset of 394 and 114 points, respectively. The curves are obtained by adjusting parameters a , b , and c as written in expression 46 superimposed with the curve-fittings produced by the *XLfit*, which their statistical parameters are summarized in Tables in Appendix H – Simulation results in Section A (A7-A8).

The both curve-fittings show the low square of the correlation coefficient of R^2 , indicating that the high goodness of fit could not be achieved since the scattered data is clearly presence. The parameters a , b , and c as well as the parameters I_1 , I_2 , and I_3 are summarized in Table 9 below.

¹³ <http://www.excelcurvefitting.com/productinformation.html>

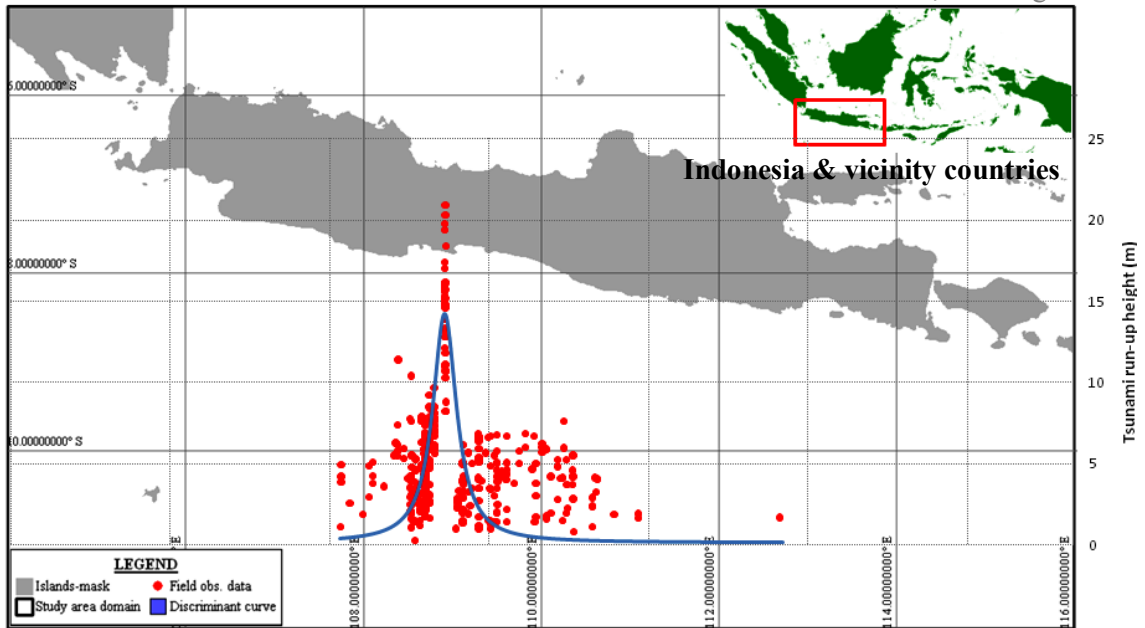


Figure 58: Fitting curve for discriminant tsunamigenic (entire dataset of 394 points)

The conclusion can be drawn from the efforts made above is that in general the tsunami run-up data are scattered and do not convergent along the coastline following the Gaussian curve, which leads to failure in trying to find a better-fitting curve for the discriminant tsunamigenics.

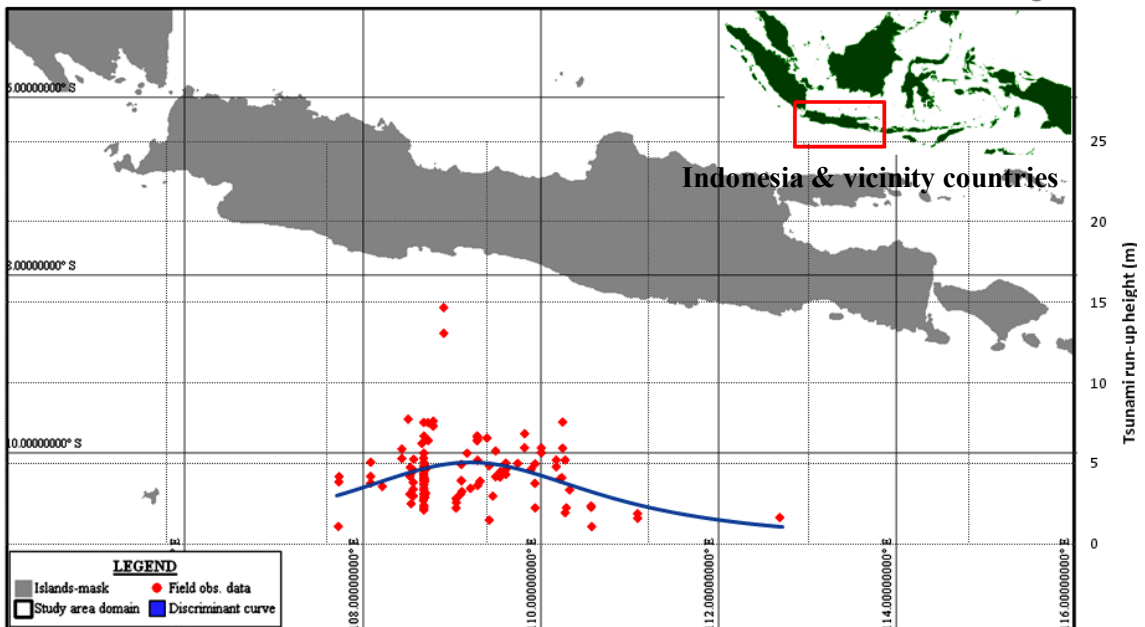


Figure 59: Fitting curve for discriminant tsunamigenic (selected dataset of 114 points)

Table 9: Fitting curve for discriminants tsunamigenic

Fitting curve	a	b	c	I_1	I_2	I_3	Remarks
	(km)	(m)	(km)				
1	17	13.7	265	2.63	8.06E-04	8.56	entire data (394 points)
2	209	5.1	306	0.98	2.44E-05	3.19	selected data (114 points)

By visual evaluation of curve-fitting shape in Figure 58 – where the entire dataset included – the curve’s peak at the center and those flat in both sides that all in one fitting-curve seem likely different to those what Okal & Synolakis (2004) produced in Figure 29 as shown in preceding Chapter. Furthermore, the parameter I_2 for both Figures as summarized in Table 9 are rather close to the threshold of 10^{-4} . Both factors suggest that the cause of the event does not clearly display whether those solely from the seismic dislocation source or associated with the submarine landslide.

There was the possibility the combination of both seismic dislocation and submarine landslide sources are associated with this event. However, this gets a challenge due to the absence of the tsunami run-up height along Nusakambangan Islands and detail near-shore bathymetry that enable proving the submarine landslide.

5.2.2 Hypothetic model for future hazard

5.2.2.a Tsunami inundation in study area

The assumption of the tsunami sources, numerical domains, and model parameters for the hypothetic model of future tsunami hazard in the study area of Cilacap were mentioned in Chapter 4. There were 144 model runs in total, using three magnitudes (M_W 7.8, M_W 8.0, and M_W 8.2), three mitigation measure types (without mitigation measures – natural beach, using sand dunes, and applying the greenbelt), and generated from 16 epicenters. An inundation map as a product of the hypothetic model was set up on the basis of 16 epicenters by taking the envelope of each maximum inundation of each epicenter, yielding a total of nine inundation maps.

Figure 60 shows one of the exemplary inundation model results of the hypothetic tsunami model under the condition of an earthquake of magnitude M_W 8.2. Without any mitigation measures imposed on the model, the inundated area is 50.45.km². All of the entire inundation maps are provided in Appendix H – Simulation results in section B for future tsunami hazard (B.1 – B.9).

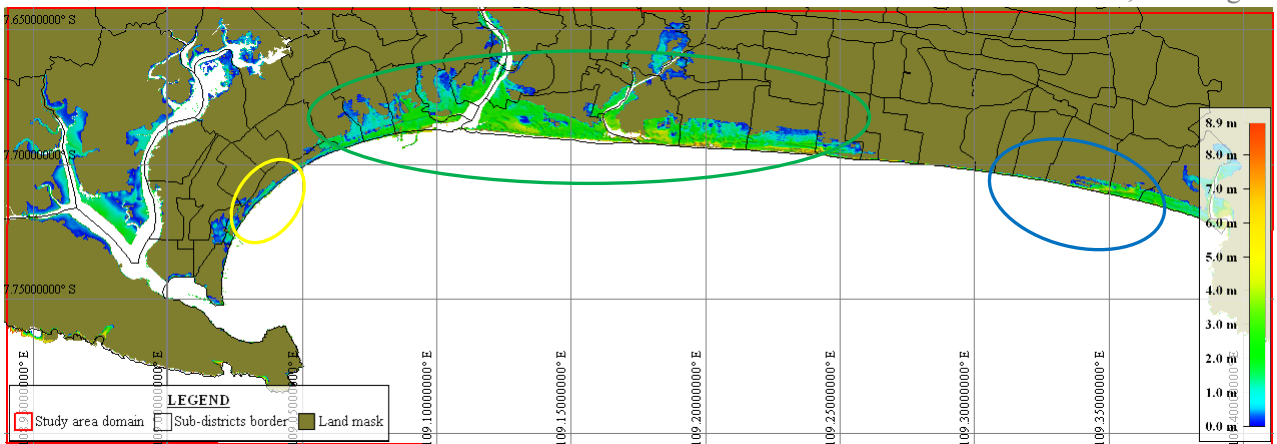


Figure 60: Hypothetic model (M_W 8.2 – without mitigation measures)

By evaluating the hypothetic model results, in general the tsunami inundation is concentrated in four regions (see Figure 60). They are in the upstream river of Donan (marked by a red oval), in the surroundings of the fishing port (yellow oval), in the river mouth of Serayu and its surroundings (up to ~15 km further east, including river of Bengawan –green oval), and the river of Jetis (blue oval).

Figure 61 shows bar charts of the whole inundated area resulting from the hypothetic model classified by magnitudes and the types of mitigation measures. The model results reveal that the sand dunes are more effective at reducing the tsunami than the greenbelt, with an average effectiveness of ~27% for sand dunes and ~7% for greenbelt.

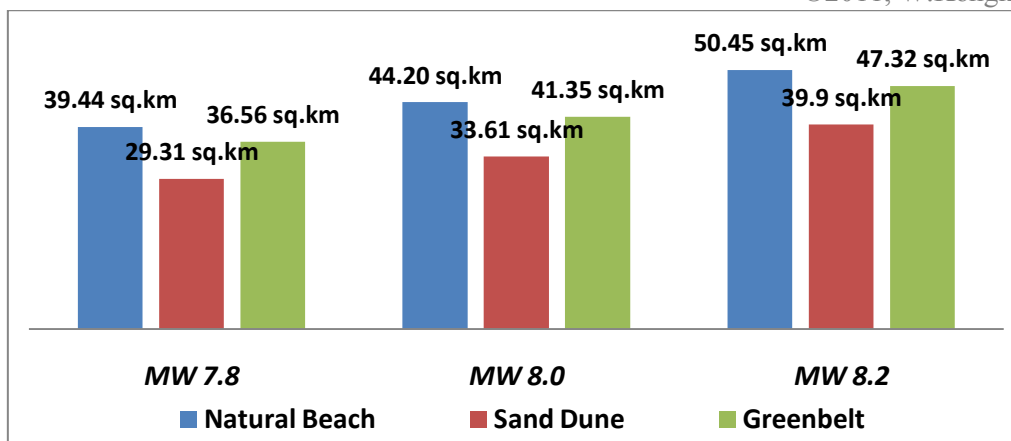


Figure 61: Inundation area by using various mitigation measures

It is also observed that the higher the magnitude, the lower the average percentage of effectiveness; at M_W 7.8, the highest average percentage effectiveness is ~27% for sand dunes and ~7.5% for greenbelt.

5.2.3 Synthetic model for the effect of complex ruptures

Previous chapters showed that based on relevant prior works and hypotheses, the effect of fault models and its slip distribution along the strike may have a significant role in the tsunami amplitudes and distribution along the coastline. Hence, in Chapter 4 in the research design, this issue has been addressed and its task group representing the business process was arranged with its task focuses on the tsunami amplitudes and distribution near-shore by using various geometric data input and tsunami sources.

This section shows the synthetic model results represented by several dimension and dimensionless graphs consisting of relevant factors, namely the fault types of distributed and uniform slip, the various rigidity values of four categories (from 10 GPa - 40 GPa), and the geometric data inputs (minimum/shallow, moderate, and maximum/deeper of water depth).

5.2.3.a run-up heights and their distribution based on the distributed slip & various rigidities

The eleven synthetic distribution slips and one uniform slip are provided in Appendix E – Tsunami source in section Q and R. The tsunami amplitudes along the coastline are given in graphs in Appendix H – Simulation results in section C (C.1-C.5). Here, two exemplary graphs are shown in Figure 62 and Figure 63.

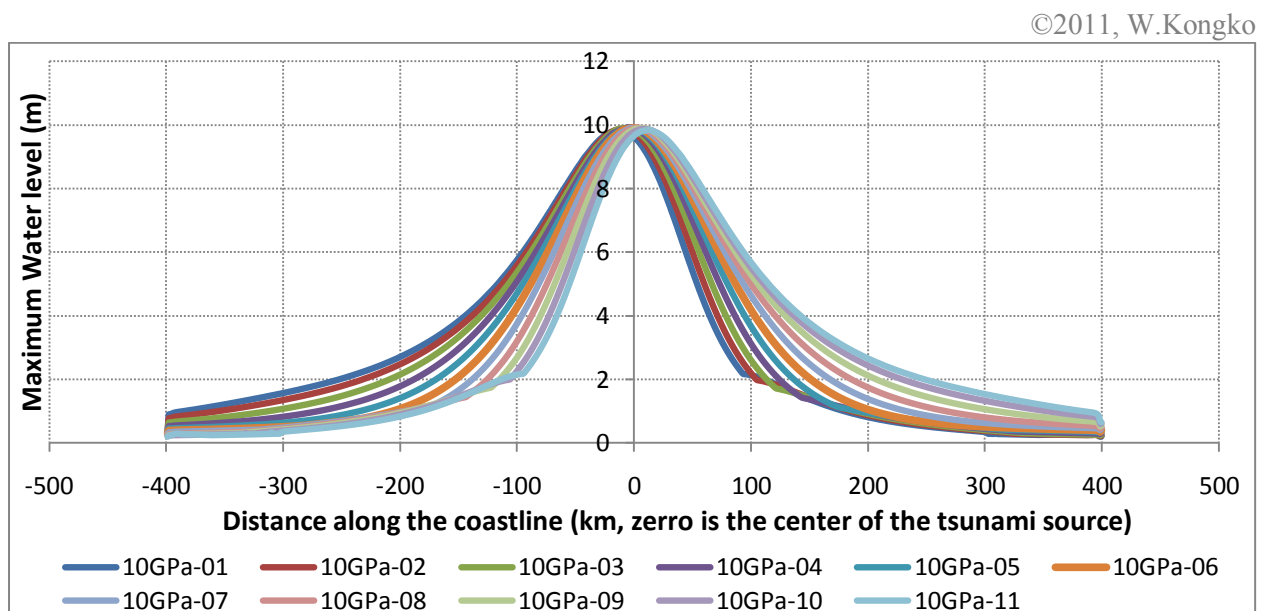


Figure 62: Tsunami run-up heights & its distribution for distributed slip ($\mu=10\text{GPa}$)

Figure 62 is a graph of the model results based on the distributed slip model with rigidity value of $\mu = 10$ GPa. Figure 63 shows the model results with the uniform slip model under rigidity values from $\mu = 10$ -40 GPa.

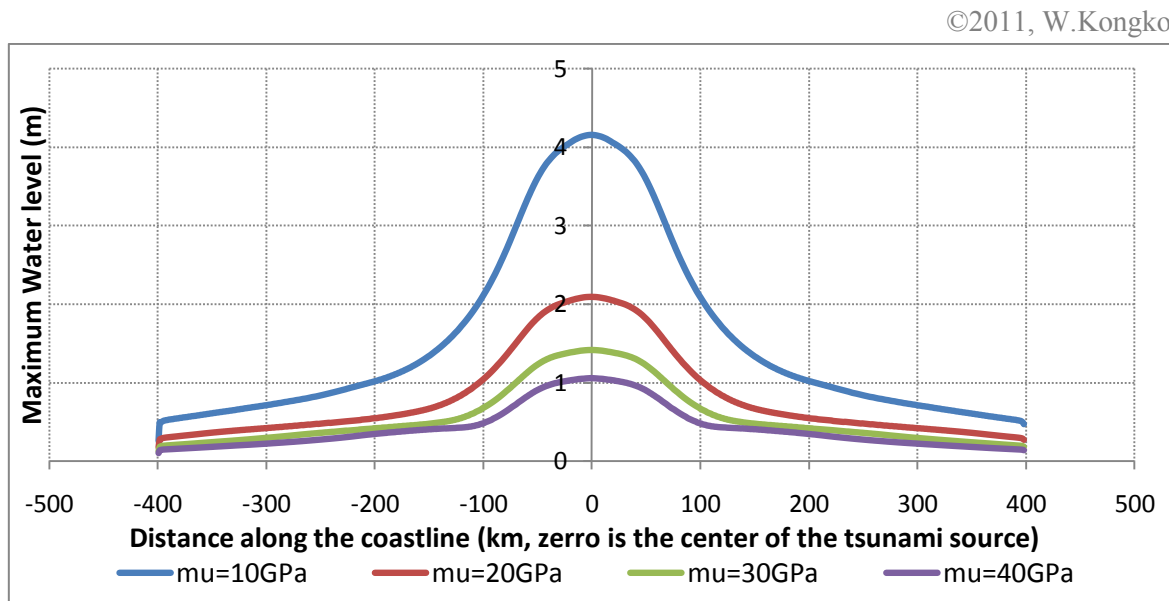


Figure 63: Tsunami run-up heights & its distribution for uniform slip ($\mu=10$ -40GPa)

From the six graphs, the two graphs in Figure 62 and Figure 63 together with those in Appendix H – Simulation results in section C (C.1-C.5), two things can be concluded: First, distributed slip at tsunami source has a significant role in tsunami run-up heights and its distribution along the coastline. The slip distribution is from 1 to 11 and its peak moves from left to right along the strike direction with an interval of 10 km producing the corresponding skewed curves of vertical deformation on the earth. The tsunami run-up distribution along the coastline follows the shape of this initial condition. If the tsunami run-up from both distributed and uniform slip are overlaid and their envelope values, i.e. minimum and maximum tsunami amplitudes are taken, the variation of tsunami run-up heights due to the slip distribution at the point considered, the so-called variation run-up threshold, can be assumed and estimated. The dimensionless graph of the distribution slip threshold normalized by average slip versus coast length divided by fault length for all rigidity values is provided in Appendix H – Simulation results in section C.6. This graph clearly shows the maximum and minimum thresholds as the variety of the tsunami amplitudes along the coastline due to the effect of the uniformly distributed slip.

Second, the rigidity value has a significant role in the tsunami amplitudes along the coastline. By evaluating the graphs from 48,000 data points of tsunami amplitudes along the

coastline under various rigidity values for both distributed and uniformly slip, it can be concluded that the lower rigidity value or the higher slip, then the greater tsunami amplitudes. The dimensionless graph of the ratio of tsunami run-up of certain rigidity to the reference rigidity (10 GPa) versus the rigidity ratio is provided in Appendix H – Simulation results in section C.8. This graph shows that the rigidity value ratio of 2, 3, and 4 times will reduce the tsunami amplitudes of 48-74%, 33-60%, and 25-50% or in average percent is 61%, 47%, and 37%, respectively.

5.2.3.b Ratio run-up heights and their distribution based on fault type & source-coastline

The two dimensionless graphs of the ratio tsunami run-up of the distributed slip to the uniform slip versus the coast length divided by the fault length are provided in Appendix H – Simulation results in section C.7 and C.9, and the first is also shown here in Figure 64 below.

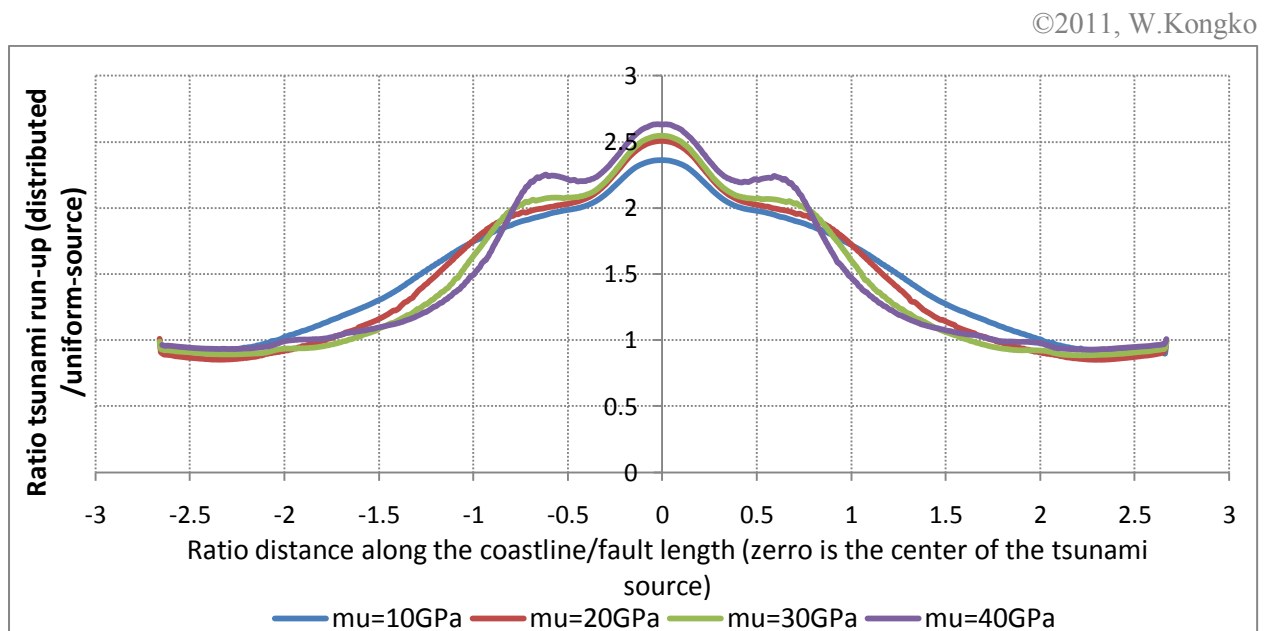


Figure 64: Ratio tsunami run-up for distributed & uniform slip ($\mu = 10\text{-}40$ GPa)

The graph in Figure 64 shows that in all rigidity values, the tsunami amplitude of average distributed slip has an amplification factor of $\sim 1\text{-}2.5$ times than the uniform slip within approximately four times the fault length of the coastline. The peak amplification factor of $2\text{-}2.5$ is in the coastline segment, whose length is equal to the fault's and is symmetrical at the center of the fault area along the strike direction.

Another graph is depicted in Appendix H – Simulation results in section C.9. It provides the ratio tsunami amplitudes at source and along the coastline for both distributed

and uniform slip sources. The graph shows that coinciding curves for both fault types occurred within the coastline segment that is approximately equal to the fault length, with the varying factor of 0.6-1. This means that regardless of whether distributed or uniformly slip, the ratio tsunami amplitudes at source and near-shore are similar within the coastline length that is approximately similar to the fault dimension of L .

5.2.3.c run-up heights and their distribution based on the geometric data input

In the synthetic model, the geometric data are derived from generalization bathymetry of the south Java Island. This is because bathymetry is significantly different in Java's cross-profiles as shown in Figure 38 and Figure 39. To simplify such conditions, the present study proposed three synthetic lines that represent sea bottom profiles, i.e. minimum, moderate, and maximum state (see Figure 39). The synthetic model, therefore, examines the three different geometric data inputs above with distributed and uniform slip as a tsunami source. In this study, however, the synthetic model for sensitivity test of various geometric data input using only one type of distributed slip and rigidity value, i.e. slip source of number 6 and under rigidity of $\mu=10$ GPa.

The model results are two graphs as provided in Appendix H – Simulation results in sections C.10 and C.11. Even though they are based on statistical analysis the geometric data inputs have significant deviations of RMSD 1,773.1 m and NRMSD 27% ($n=750,000$), with minimum and maximum values of -6500 m and 100 m; the tsunami amplitudes resulting from the model using such data have tiny deviations, i.e. 2.36% and 1.53% for distributed and uniform slips, respectively.

5.3 Hypotheses and Research Questions

Three main problems in the present study were written in the research design, i.e. coarse geo-data resolution, discrepancy tsunami run-up heights between model and field data, and the effect of complex rupture on local tsunamis. To assess such issues, this study proposes some hypotheses followed by several questions.

This sub-chapter discusses the hypotheses and research questions as well as the findings after conducting the investigations utilizing all of the data collected and elaborating the analysis of the results model, all the task group processes of which and their flowchart diagrams were given in preceding chapter. It includes the effect of the rigidity values on

tsunami run-up heights, the effect of fault types and slip distribution, and the association of the submarine landslide to the 2006 Java tsunami.

5.3.1 Effect of the rigidity values on tsunami run-up heights

The discussion of the effect rigidity material to tsunami amplitudes was given in the preceding chapters. It suggests that the material property in the seismic zone, i.e. rigidity has a significant role in controlling the rupture dynamics. By plotting the huge number of events occurring at depths of 5–50 km, previous researchers demonstrated that the average rigidity values are comparable to the Preliminary Reference Earth Model (PREM). And in shallow depths less than 20 km, they are more pronounced and increase by a factor of ~ 5.

The results of the 2006 Java tsunami simulation also suggested that low-rigidity material has an important role in the tsunami run-up heights along the coastline. The rigidity of 10 GPa, which is 3–4 times lower than the normal value (30 – 40 GPa) being imposed in source models 3, 5, and 6, gives results comparable to both the selected tsunami run-up datasets at 114 points and for three tsunami marigrams. Further, source model 3 is selected based on the evaluation using parameters K and k (Aida, 1978) and moving average analysis. The model validation is again carried out on the selected source model above in three locations located in the study area of Cilacap. By using the estimate of the 52 points of the maximum inundation in Permisan and Cilacap Bay and one interpretation of the video snapshots and pictures taken by the eye witness, the model validation shows a fairly good result.

Such findings above are consistent with the most recent papers discussing about the presence of the tsunami earthquake in Sunda arc by Kanamori et al (2010) for the 1907 Sumatra earthquake, and Bilek (2011), Newman et al (2011), Lay et al (2011) for the 25 October 2010 Sumatra earthquake.

The dimensionless graph of the rigidity ratio vs. tsunami run-up resulting from the synthetic model as depicted in Figure 65 has been used for checking the consistency of the rigidity ratio of the four source models of the 2006 Java tsunami. The average ratio of tsunami run-up from three pairs as the combination of source models 3, 4, 5, and 6 is 0.40 or 40%. This value is consistent with the synthetic model results and falls within the range of 33–60% as plotted with a red star in Figure 65.

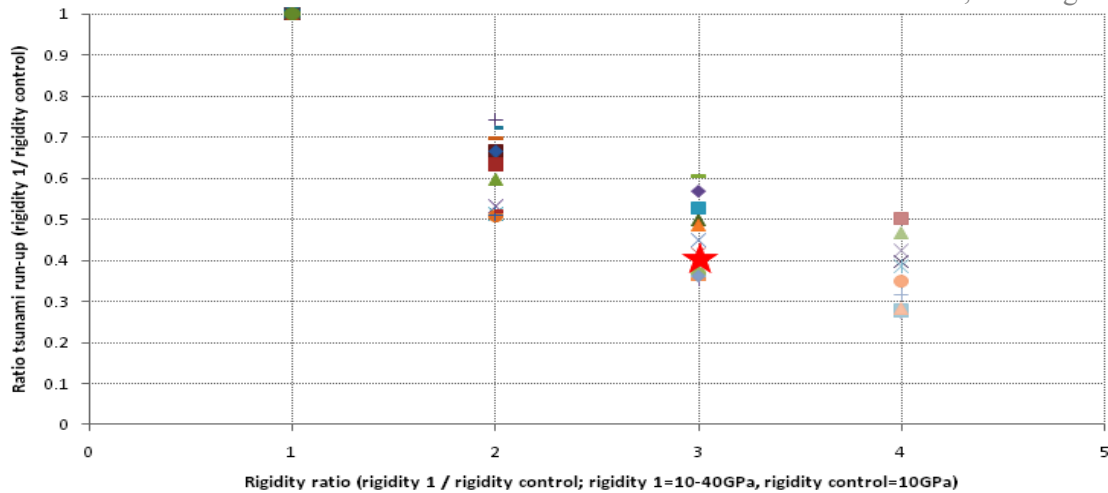


Figure 65: Ratio rigidity of the 2006 tsunami Java (red star)

These findings confirm the hypotheses in the present study and support the prior investigations that the rigidity material has an important role in the tsunami run-up heights along the coastline.

5.3.2 Effect of the fault types & slip distribution

Several previous studies suggested that the tsunami amplitudes and its distribution along the coastline are sensitive to the rupture complexity, such as the fault dimension and its types, and slip distribution patterns.

Aside from the study conducted by Okal & Synolakis (2004), other researchers carried out such studies, in which considered tsunami sources very near to coastal areas. In the Java subduction zone, however, the tsunamigenic events generally originated at a distance from the coastal area of more than 150 km. Such a distance is farther than other tsunami earthquakes that previous researchers categorized as local tsunamis.

This section delivers the analysis of the four factors above by using the results of the 2006 Java tsunami model, especially for the source models that their results are comparable to the field data, i.e. source models 3, 5, and 6.

Table 10: Comparison of source parameters model & its run-up deviation

No.	Source model	Fault dimension		Slip	Fault difference		Tsunami run-up difference			
		L (km)	W (km)	Du (m)	Area (%)	Δu (%)	RMSD	NRMSD	min (m)	max (m)
1	5	127	39	6.03	44.6%	41.7%	1.45	18.8%	0.71	8.43
2	6	200	80	3.95						

First, to examine the fault dimension effect on the tsunami amplitudes and distribution near-shore, the present study uses source models 5 and 6 of the 2006 Java, since only they meet the criteria, i.e. they are of single-fault type and have similar rigidity. The results are tabulated in Table 10, which consist of the fault parameters and their deviations. The deviations both of the source parameters model represented by fault area and average slip of Δu , are 44.6% and 41.7%, respectively. Even though the fault's source parameter deviations are significant, the tsunami run-up shows far less of a difference, i.e. 18.8%. This suggests that by selecting a different scaling law formula in terms of focal mechanisms, i.e. reverse or all events that lead to different fault dimensions, the tsunami run-up would only have a moderate effect.

Furthermore, dealing with the effect of the fault types, i.e. single-multi fault, the present study utilizes source models 3, 5, and 6. Source model 3 is composed of 16 sub-faults, while two others are of single-fault type. The ratio of tsunami run-up resulting from the model in 114 points of source model 3 divided by 5 and source model 3 divided by 6 are plotted together and overlaid on the graph of a ratio of tsunami run-up (distributed/uniformly source) as provided in Appendix H – Simulation results in section C.7.

Figure 66 is similar to the graph mentioned above in that it takes the average value of the ratio of tsunami run-up from the source models with a rigidity value of 10-40GPa. The 228 points of ratio tsunami run-up from two pairs of the source model above have been plotted on this graph as shown in Figure 66 below. About 83% of the 228 points are under the ratio of the uniformly distributed curve, whose factor ratio varies from 0.5–2.2. This means that source model 3 for the 2006 Java tsunami has a more homogeneous slip in terms of slip difference than the proposed distributed slip in the present study.

Evaluating the data plots under the curve and the rough trend line indicated by black dashed breaking line in Figure 66 also shows the consistency between the synthetic model results and the selected source model 3 for the 2006 Java tsunami. It shows the heterogeneity slip at source followed by the tsunami run-up distribution along the coastline, in which at the center of the fault length in the strike direction there is a higher ratio following more or less the curve's shape. However, its trend line's peak is rather shifted to the right than synthetic curve due to the distribution of tsunami amplitudes of uniformly slip along the coastline.

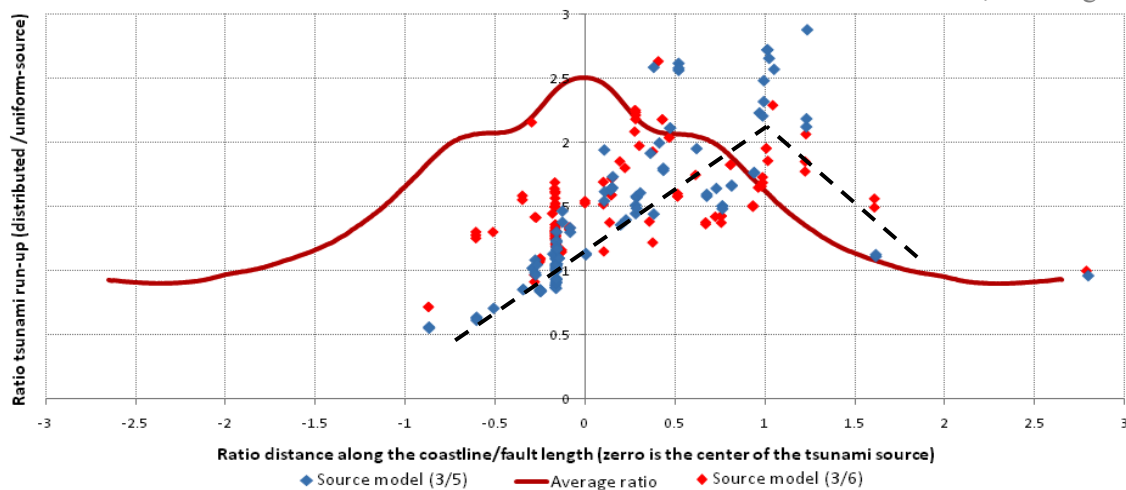


Figure 66: Ratio of run-up of uniform- distributed source of the 2006 Java tsunami (dots)

The knowledge of the trend and ratio value of the tsunami run-up and its distribution along the coastline as a function of the uniform- distributed source is essential, since for practical purposes to design the tsunami hazard its source is made up of uniform- rectangular faults, which in reality are absent.

To check the variety of the tsunami run-up heights and its distribution along the coastline due to the distributed slip, the present study again uses source model 3 for the 2006 Java tsunami and the graph of the ratio of run-up variation as given in Appendix H – Simulation results in Section C.6. This graph proposed two curves, i.e. the maximum threshold that has its source in the proposed distributed slip (assumed as the most heterogeneous slip in terms of difference slip) and the minimum threshold that has its source in the uniform rectangular fault.

Figure 67 is similar to the graph mentioned in the previous paragraph with overlying the data points of tsunami run-up heights resulting from source model 3. Based on this graph, the maximum variety of tsunami run-up heights is at the center of the fault length with the ratio value varying from 0.6–1.55 with the minimum occurring at both edges of the curves with a ratio value less than 0.2.

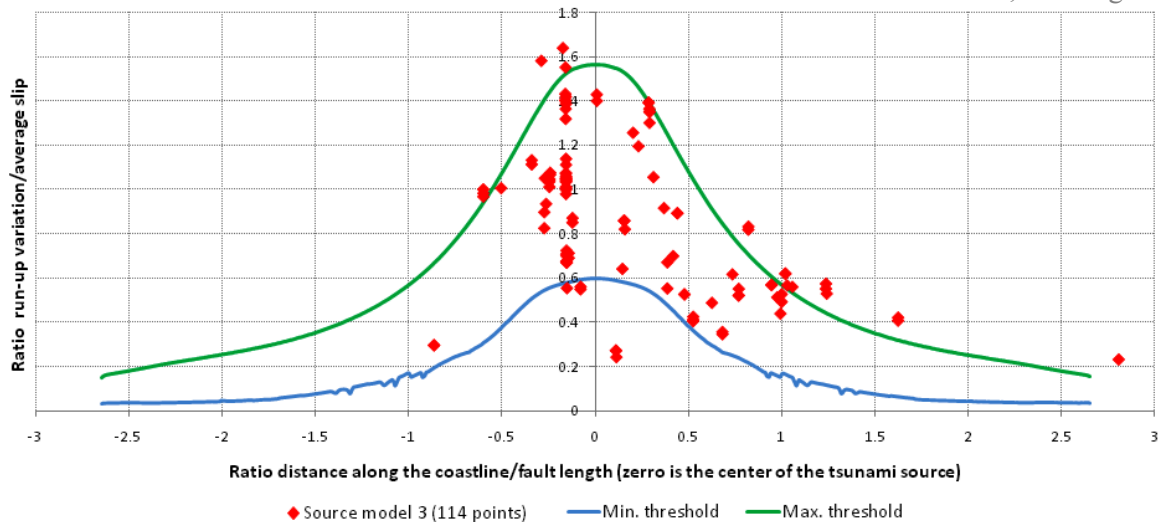


Figure 67: Ratio of run-up variation / average slip of the 2006 Java tsunami (dots)

The overlying data points of tsunami run-up normalized by average slip from source model 3 of the 2006 Java tsunami on the graph in Figure 67 also confirm that the distribution of tsunami amplitudes along the strike direction follows the curves.

From Figure 67 above, the ~87% of the 114 data points are within the ratio of the tsunami run-up of the minimum and maximum threshold. This means in the physical meaning of the slip pattern of the 2006 Java tsunami that the slip difference is between the uniform and proposed distributed slip variation. The scattering data points are also consistent with the tsunami run-up variation curves, which in the middle of the fault length are higher compared to those located in the curve's wings.

The knowledge of distribution patterns of tsunami run-up and its distribution along the coastline is important since the distributed slip at source is strongly linked to the tsunami amplitudes near-shore. This is useful for practical purposes to estimate the variation of tsunami run-up due to the distributed slip source that may occur once those from uniform faults have been numerically estimated.

5.3.3 Tsunamigenic associated with submarine landslide?

In the previous section, the discriminant factor to predict the tsunamigenic, whether the 2006 Java tsunami triggered by the seismic dislocation source or submarine landslide was discussed and estimated. After attempting by trial and error to fit the curves to the datasets of the tsunami run-up using the empirical formula developed by Okal & Synolakis (2004) and checked with curve-fitting tool, the results demonstrated that the best fitting curve to the

datasets with high goodness of fit (high correlation coefficient of R^2) could not be achieved due to the scattered data available.

The discriminant factors, however have been attained as given in Table 9. By visual evaluation of the fitting curve of Figure 58 shows that the curve's peak at the center and flat in both sides seem likely different of those what Okal & Synolakis (2004) produced. Furthermore, the parameters I_2 for both examined datasets are close to the threshold of 10^{-4} . Both factors suggest that the cause of the event does not clearly display whether those solely from the seismic dislocation source or the submarine landslide.

There was the possibility the combination of both seismic dislocation and submarine landslide sources are associated with this event. However, this gets a challenge due to the absence of the tsunami run-up height along Nusakambangan Islands and detail near-shore bathymetry that enable proving the submarine landslide.

The numerical model results from seismic sources, however, give comparable results. The two validation model results in tile 2 in Permisan Cilacap as depicted in Figure 54 – overlaying an inundation mask on the interpreted inundation lines of satellite imagery of SPOT-1 and in Figure 55 – inundation mask on the field observation data – show a fairly good agreement. Yet, the model result gave only the tsunami run-up an average fit of 57% to the field observation data, while 17% of the data points were in the dry area. Such discrepancies might be caused by both inaccuracies of the assimilated terrain model by involving the low-resolution SRTM data and the limitations of the NSWE model, which is unable to represent the vertical flux component ($U_z=0$) due to the steep geometric data in the hilly area.

Another possibility of the extreme run-up at Permisan prison was due to the local run-up amplification by resonant wave interactions phenomena as studied by Stefanakis et al. (2011). The resonant waves are found to occur in both leading elevation and depression waves, where for increasing slope, the amplification factor of run-up by water elevation also increases that could reach extremely high.

5.4 Summary

The findings of the present study consist of three main parts, namely those related to the procedures and elements of study, the simulation model results, and the discussion on the hypotheses and research questions.

In the procedures and elements of study, the specific treatment of the geo-data assimilation by manual digitizing work was inevitably carried out, in which the data has many different resolutions, and both are in the boundary between topography and bathymetry where its coastlines have a complex shape. Further, regarding the detailed DEM data in the study area of Cilacap, which consist of both the DTM and DSM type, their difference should be taken into account in the geometric data input used in the numerical simulations. The selection of such a type should consider the land cover that can only be achieved through a ground check investigation.

The detailed topography measurement in place where the extreme tsunami run-up occurred does not cover the whole area considered due to difficulties in attaining access in dense vegetation and on steep hilly slopes leading to blank data having to be filled using low-resolution data. In addition, to reduce the uncertainties due to the complex coastal features, the tsunami run-up data along the coastline have been selected based on several criteria. The comparison of the original and selected data indicated that the uncertainties factors are sufficiently significant; however, scattering data still exist and convergent data cannot be achieved.

The simulation model results comprise the model reconstruction of the 2006 Java tsunami, the hypothetical model for future hazard, and the synthetic model for the effect of complex ruptures. For the model of the 2006 Java tsunami, six sources have been proposed. The extensive model validation compares the tsunami run-up heights, its distribution along the coastline and the time arrival, maximum inundation in the study area with the field observation data, three tsunami mareograms recordings, and imagery of the SPOT-1 satellite before and after the event, as well as the video snapshots and pictures from an eye witness.

The results demonstrated that the source models of the 2006 Java tsunami imposing the low-rigidity material and higher slip are able to mimic field data and are more comparable to the run-up points than those using normal values. Among them, the distributed multi-fault model gives the best result rather than the single-fault models. In addition, to evaluate whether the source originates from seismic dislocation or submarine landslide, the discriminant values are estimated using the empirical formula. The fitting curves of the data points for both entire and selected tsunami run-up data to give low the goodness of fit. By evaluating the fitting curve's shape seem those are different with the results of previous study. The obtained discriminant parameters are near to the threshold value. Both factors indicate that the cause of such an event was not clear whether those solely from seismic

dislocation or associated with submarine landslide. There was the possibility the cause of the 2006 Java tsunami due to the combination of seismic dislocation associated with the submarine landslide.

Even though low-rigidity source models in general are able to reproduce the 2006 Java tsunami, the run-up height in the study area where the extraordinary run-up occurred only gives an average of ~57% of the extreme run-up heights, while 17% of the data points are located in the dry area. Such discrepancies might be caused by both inaccuracies of the assimilated terrain model that involve low-resolution data and the limitations of the NSWE model, which is unable to represent the vertical flux component due to the steep slopes in hilly areas.

The hypothetical model for future tsunami hazard in the study area of Cilacap has also been done in the present study. The tsunami sources are based on the plausible maximum of certain magnitudes given in the Java subduction zone, which combine the 16 epicenters, three proposed earthquake magnitudes, and three conditions of mitigation measures. Based on the model results, in general tsunami inundation is concentrated in four clusters, namely the upstream river of Donan, the surroundings of the fishing port, the river mouth of Serayu and its surrounding low-land up to ~15 km further east, and the river of Jetis. The effectiveness of the proposed greenbelt at reducing the effects of a tsunami is ~7.5%, while the sand dunes are able to reduce the tsunami inundation by up to 27%.

The synthetic model for the effect of complex ruptures produces eleven graphs, which are constructed from the significant factors involved, namely the tsunami run-up heights and its distribution along the coastline from both uniform and proposed distributed slip, coastal and fault length, rigidity material, and geometric data input. The result is that the variation run-up along the coastline follows Gaussian curves, with those at the center having a ratio value varying between ~0.6–1.55 and those at the edges of the curve's wings being less than 0.2. The ratio between uniformly proposed distributed slip is in the range of ~1–2.5 along the coastline whose length is four times that of the fault. In addition, the rigidity material also has a significant role in the tsunami amplitudes near-shore. The rigidity value ratio of 2, 3, and 4 times will reduce the tsunami amplitudes on average by 61%, 47%, and 37% respectively. It is interesting to note that the significant different geometric data input of about 27% only shows tiny deviation of tsunami amplitudes of 2.4% and 1.5% for distributed and uniformly slips, respectively.

The data plot of the ratio of tsunami run-up from different rigidities on the dimensionless graph of the rigidity ratio versus tsunami run-up from the synthetic model shows the consistency of the rigidity ratio of the 2006 Java tsunami, whose value of about 40% lies within the threshold value of 33–60%. This finding confirms the hypotheses that the rigidity material has an important role in the tsunami run-up heights. Furthermore, to estimate the fault dimension, there are options for selecting the scaling formula, i.e. reverse or all event regressions. Even though both fault area and slip values have a significant difference, the tsunami run-up deviation along the coastline has a moderate effect.

The distribution of the tsunami run-up along the coastline for the 2006 Java tsunami was examined using two dimensionless graphs. They show that ~83% of data points were under the proposed curve indicating that the level of slip difference of such an event is below the proposed ratio values. Further, the data point distribution is consistent and more or less follows the curve's shape.

The data points of the ratio of run-up variation are also consistent when they are overlaid on the dimensionless graph of run-up variation. The ~87% of data points are within the ratio of run-up variation threshold. The distribution patterns of tsunami run-up also follow the curve.

The knowledge of both the trend and ratio value of tsunami run-up and its distribution pattern along the coastline mentioned earlier is important for practical purposes since when designing a tsunami hazard model; its source is assumed to be uniform rectangular faults, even though this is not the case in reality. And the proposed graphs might be used to estimate the maximum variation run-up and its distribution along the coastline due to the rupture complexities, once they have been estimated by uniform rectangular slip source. Hence, the safety factors in the design of the hazard map using the model due to the heterogeneity of slip distribution can be predicted quantitatively.

Chapter 6 - Conclusions & Recommendations

“I love those who can smile in trouble, who can gather strength from distress, and grow brave by reflection.” (Leonardo da Vinci, 1452-1519 AD)

The main objective of this study is to carry out a validation of a numerical simulation for the 2006 Java tsunami that agrees with the observed run-up data by considering various tsunami sources and using high-resolution geometric data. To achieve this goal, several task groups have been proposed in the research design of the present study, which will aim at the improvement of geo-data, and the construction of a 2006 Java tsunami model, a hypothetical model for future tsunami hazard, and a synthetic model of complex ruptures. This chapter delivers the conclusions and recommendations as the outcomes after elaborating and working through the task groups above.

6.1 Conclusions

The conclusions to be drawn based on the findings consist of three main parts, i.e. those related to the procedures and elements of the study, the simulation model results, and the discussion on the hypotheses and research questions.

6.1.1 Procedures and elements of study

The specific treatment of the geo-data assimilation by manual digitizing work was inevitably carried out for those that have different resolutions and are located in the boundary between the topography and bathymetry data where the coastline has a complex shape.

Further, regarding the detailed DEM data in the study area of Cilacap, which consists of both the DTM and DSM data types, the differences between the two datasets should be taken into account when inputting the geometric data in the numerical simulations. The selection of data should take into consideration the land cover, which can only be achieved through a ground check investigation.

In addition, to reduce the uncertainties due to complex coastal features, the tsunami run-up data along the coastline have been selected based on several criteria. The comparison of the original and selected data indicated that the uncertainty factors are sufficiently significant; however, scattering data still exist and convergent data cannot be achieved.

6.1.2 Simulation model results

For the model of the 2006 Java tsunami, six sources have been proposed. The results demonstrated that the source models of the 2006 Java tsunami employing low-rigidity material and higher slip are able to mimic field data and are more comparable to the run-up points than those using normal values. The distributed slip of multi-fault model gives the better results than the uniform slip of single-fault model.

In addition, to evaluate whether the source originated from seismic dislocation or submarine landslide, the discriminant values are estimated using the empirical formula. The fitting of curves to the data points of both entire and selected data to give the low goodness of fit. By evaluating the fitting curve's shape and the discriminant parameter, which is near to the threshold value giving an uncertain conclusion of what the cause of the event, whether those solely from seismic dislocation or associated with submarine landslide. There was the possibility the cause of the event is a seismic dislocation associated with the submarine landslide. However, this gets challenge due to the lack of the tsunami run-up data along the coastline of Nusakambangan Island as well as the detail bathymetry near-shore.

Even though low-rigidity source models in general are able to reproduce the 2006 Java tsunami, the run-up height in the study area where extraordinary run-up occurred only gives an average of ~57% of the extreme run-up heights, while 17% of the data points are located in the dry area. Such discrepancies might be caused by both inaccuracies of the assimilated terrain model that involve low-resolution data and the limitations of the NSWE model, which is unable to represent the vertical flux component due to the steep slopes in hilly areas.

The hypothetic model for future tsunami hazard in the study area of Cilacap is based on the plausible maximum of certain magnitudes given in the Java subduction zone. Based on the model results, in general tsunami inundation is concentrated into four clusters, namely the upstream river of Donan, the surroundings of the fishing port, the mouth of the Serayu River and its surrounding lowlands up to ~15 km further east, and the river of Jetis. The effectiveness of the proposed greenbelt at reducing the effects of a tsunami is ~7.5%, while the sand dunes are able to reduce tsunami inundation by up to 27%.

The synthetic model for the effect of complex ruptures produces graphs constructed from the significant factors involved. The result is that the variation run-up along the coastline follows Gaussian curves, with those at the center having a ratio value of tsunami run-up normalized by average slip varying across the range ~0.6–1.55 and those at the edges

of the curve's wings being less than 0.2. The ratio between tsunami run-up resulting from uniform slip and distributed slip is in the range of ~ 1 – 2.5 along the coastline, whose length is four times that of the fault.

In addition, the rigidity material also has a significant role in the tsunami amplitudes near-shore. The rigidity value ratio of 2, 3, and 4 times will reduce the tsunami amplitudes on average by 61%, 47%, and 37%, respectively. It is interesting to note that the significantly different geometric data input of about 27% only shows a small deviation of tsunami amplitudes of 2.4% and 1.5% for distributed and uniform slips, respectively.

6.1.3 Hypotheses and research questions

The results of the 2006 Java tsunami simulation suggested that low-rigidity material and higher slip has an important role in the tsunami run-up heights along the coastline. The rigidity of 10 GPa, which is 3–4 times lower than the normal gives results comparable to both the selected tsunami run-up datasets and for three tsunami marigrams. Furthermore, those that use multi-faults models are better than the single-fault model. The data plot of the ratio of tsunami run-up from different rigidities on the dimensionless graph of the rigidity ratio versus tsunami run-up from the synthetic model shows the consistency of the rigidity ratio of the 2006 Java tsunami, whose value of about 40% lies within the threshold value of 33–60%.

Furthermore, there are options for selecting the scaling formula to estimate the fault dimension, i.e. reverse or all event regressions. Even though both fault area and slip values show significant differences, the tsunami run-up deviation along the coastline has a moderate effect. The distribution of the tsunami run-up along the coastline for the 2006 Java tsunami was examined using two dimensionless graphs. They show that $\sim 83\%$ of data points have a factor ratio from 0.5 to 2.2 under the proposed curve, indicating that the level of slip difference of such an event is below the proposed ratio values. Further, the data point distribution is consistent and more or less follows the curve's shape. The data points of the ratio of run-up variation are also consistent when they are overlaid on the dimensionless graph of run-up variation. The $\sim 87\%$ of data points are within the ratio of run-up variation threshold. The distribution patterns of tsunami run-up also follow the curve.

The discriminant factors are investigated and estimated to check the cause of the event. The obtained parameter I_2 for both examined datasets are close to the threshold of 10^{-4} , suggesting that the cause of the event is not clearly pronounced whether those solely from the seismic dislocation source or associated with submarine landslide. By visual evaluation of fitting curve shows that the curve's peak at the center and flat in both sides seem likely

different curve shape as what Okal & Synolakis (2004) produced. There was the possibility the combination of both seismic dislocation and submarine landslide sources are associated with this event. However, this gets a challenge due to the absence of the tsunami run-up height along Nusakambangan Islands and detail near-shore bathymetry that enable proving the submarine landslide.

6.2 Recommendations

Recommendations are proposed for further research into changing the methodology and academic and engineering concepts or for practical purposes. The recommendations are outlined in the two sub-chapters, namely that for future research and another for practices.

6.2.1 Recommendations for future research

To avoid the specific treatment of the geo-data assimilation by a lot of manual digitizing work, the area between topography and bathymetry data – the area in which usually such a problem occurs – should be fulfilled by using the near-shore bathymetry data both, from field measurements and other sources such as C-Map data. In the present study, however, such alternatives have not been used due to limited sources and time constraints.

In regard to the DTM-DSM data, the basic grid resolution available in the project is 5 m. However, the present study used numerical simulation with a spatial grid of ~23 m for model validation in tiles 2 and 3. For future research, the author recommends using a finer spatial grid of, e.g., ~ 5 m to obtain the more detailed inundation model. However, additional ground investigation is needed to distinguish the various types of land cover such as vegetation and housing. This information will be useful for further analysis and in considering the hydraulic resistance of data input in the numerical model.

The 2006 Java tsunami was not so clear whether the cause of the event solely from a seismic dislocation or associated with the submarine landslide. Recent studies conducted by Brune et al. (2009a, 2009b, and 2010) by investigating new bathymetry data in the Sunda Arc found some novel and remarkable mass movements in the 12 locations, and one of the them is located in Java's subduction zone. Therefore, the tsunamigenic earthquake associated with landslide in the study area cannot be ruled out. The author recommends for future research that a model be constructed that considers a tsunamigenic combination of both a seismic and landslide source for the Java 2006 tsunami model.

One of the reasons for the inability of the numerical simulation to reproduce the extreme run-up of the 2006 Java tsunami is that the NSWE model is unable to represent the

vertical flux component due to the steep slopes in the hilly area. The author suggests that future research such conduct the numerical modeling in this area using the 3D model (Honda & Tomita, 2008; Choi et al., 2008; Shuto & Fujima, 2009).

The hypothetic model for future tsunami hazard in the study area of Cilacap uses mitigation measures, i.e. the greenbelt of “Waru” trees and the sand dunes, the condition of which is assumed to remain static throughout the entire simulation, which in reality will not be the case. For future research, therefore, the model should consider the dynamic obstacles that interact with the hydraulic flow. Further, the present study assumes that the greenbelt of “Waru” trees will withstand the tsunami regardless of tsunami height. However, a study was carried out to measure the effect of tsunamis on coastal vegetation in Japan and Thailand, which determined that they only have a limited capacity to withstand a tsunami, which is based on its height (Shuto, 1987; Yanagisawa et al., 2009). Therefore, further research dealing with the material strength and its effectiveness of greenbelt to reduce the tsunami is highly demanded.

The synthetic model for the effect of complex ruptures in the present study uses similar earthquakes of magnitude M_W 7.8, source parameters and depths, with a limited amount of geometric data at a fixed distance from the epicenter to the land as well as a relatively coarse spatial grid of 1000 m. For future research, the author suggests increasing number of the variation parameters above, especially those that may play a significant role in the tsunami run-up heights, such as earthquake magnitude, variable distance of the epicenter to the land, and spatial grid in the numerical simulation. The author also recommends varying the coastline shape, e.g., saw tooth or triangle, rectangular, arc, etc.

The present study checked the consistency of the source model of the 2006 Java tsunami with the dimensionless graphs resulting from the synthetic model. The results of this are the factor ratio of the uniformly distributed slips and run-up variation with their distribution along the coastline. For future research, the author recommends conducting similar studies on the events of tsunami earthquakes to those enlisted in Chapter 3.

6.2.2 Recommendations for practices

Regarding the specific treatment of the geo-data assimilation by manual digitizing work, the author proposes that GIS software developers consider adding an option in the TIN interpolation properties so that data can be recognized and selected based on type, i.e. bathymetry or topography as well as their resolutions. With this, the filling blank data using manual digitizing work that occurred in the present study, for future work can be avoided.

The hypothetic model for future tsunami hazard in study area of Cilacap uses uniform rectangular tsunami sources, while the results of the synthetic model and the selected source of the 2006 Java tsunami model suggest that the distributed slip has a significant role in the variety of tsunami run-up along the coastline, with a factor ratio between 0.5 and 2.2. Therefore, for practical purposes the inundation map resulting from the hypothetic model for future tsunami hazard in the present study should consider such a factor ratio.

Based on the model results, the effectiveness of the proposed greenbelt at reducing the effects of a tsunami is $\sim 7.5\%$, while the sand dunes are able to reduce tsunami inundation by up to 27%. These results suggest the mitigation measures by utilizing the artificial greenbelt and sand dunes are insufficient, hence the mitigation programs of vertical and horizontal evacuation is highly demanded.

6.3 Summary

The main objective of this study is to carry out a validation of a numerical simulation for the 2006 Java tsunami that agrees with the observed run-up data by considering various tsunami sources and using high-resolution geometric data. To fulfill such a goal, several task groups have been designed and worked through in the present study.

In the procedures and elements of the study, several issues emerged and were assessed. These include the specific treatment of geo-data assimilation, the differences between DEM data types, and field data selection.

From simulation model results for the 2006 Java tsunami, it was seen that the higher slip and low-rigidity material of tsunami sources is able to resemble field data, and the distributed slip of multi-fault model gives the better result than the uniform slip of single-fault model. The cause of such an event was not so clear, whether those due to solely a seismic dislocation or associated with submarine landslide. There was the possibility the combination sources causing the event. The deficiency of tsunami run-up heights resulting from the numerical simulation seems to be due to the inaccuracies geometric data input or limitations of the NSWE model.

To determine the future tsunami hazard in the study area, the hypothetic model based on several scenarios has been conducted. It revealed tsunami inundation concentrated in certain locations consisting of four clusters. The farthest and biggest inundation is in the mouth of the Serayu River and its surrounding lowlands up to ~ 15 km further east. The

effectiveness of the proposed mitigation measures varies by up to ~27% in terms of inundation area.

Based on the synthetic model for the effect of complex ruptures, the ratio of tsunami run-up resulting from uniform slip and distributed slip is in the range ~1-2.5 along the coastline, whose length is four times that of the fault. The variation run-up along the coastline follow Gaussian curves, with those at the center being the maximum with a ratio of tsunami run-up normalized by averaged slip varying ~0.6–1.55. The rigidity value ratio of 2, 3, and 4 times will reduce the tsunami amplitudes on average by 61%, 47%, and 37%, respectively. While, the significant different geometric data input of about 27% only showed a small deviation of tsunami amplitudes of 2.4% and 1.5% for distributed and uniform slips, respectively.

The three tests of the 2006 Java tsunami, namely the ratio of rigidities, the ratio of uniformly distributed slips, and the variation of run-up by using dimensionless graphs resulting from the synthetic model showed consistent trends.

Some recommendations for future research and practice have been proposed. They deal with the use of extensive near-shore data, re-modeling the 2006 Java tsunami by modifying the spatial grid or tsunami sources, as well as the requirement of the 3D model for inundation in steep slopes. Further analysis is also proposed for the use of mitigation measures of the hypothetical model for future tsunami hazard and to increase the variety of the relevant parameters for the synthetic model.

For practical use, the recommendations are related to the enhancement of the GIS software properties for geo-data editing and assimilation, while the inundation maps resulting from the hypothetical model should consider the factor of heterogeneous slip, the ratio of which was proposed in the present study. Furthermore, based on the model results, the proposed tsunami countermeasures are insufficient, thus mitigation programs of vertical and horizontal evacuation are highly demanded.

Bibliography

- Abe, K., 1989. Quantification of tsunamigenic earthquakes by the M_t scale. *Tectonics*, 166, pp.27-34.
- Abercrombie, R., Antolik, M., Felzer, K. & Ekstroem, G., 2001. The 1994 Java Tsunami Earthquake: Slip over a Subducting Seamount. *Geophysical Research*, 106(B4), pp.6595-6607.
- Abidin, H.Z., Andreas, H., Kao, T., Ito, T., Meilano, I., Kimata, F., Natawidjaya, D.H. & Harjono, H., 2009. Crustal deformation studies in Java (Indonesia) using GPS. *Journal of Earthquake and Tsunami*, 3(2), pp.77-88.
- Abidin, Z.H. & Kato, T., 2007. Why Many Victims: Lessons from the July 2006 South Java Tsunami Earthquake. *Advances in Geosciences*, 13, pp.249-263.
- Ahmad, R. & Kongko, W., 2008. Report of bathymetry survey of Cilacap phase 2 (in Bahasa Indonesia), BPDP-BPPT.
- Ahmad, R. & Harmiawan, Y., 2009. Report of bathymetry survey of Cilacap phase 3 (in Bahasa Indonesia), BPDP-BPPT.
- Ahmad, R. Harmiawan, Y. & Nugroho, S., 2009. Report of topography survey of Cilacap phase 3 (in Bahasa Indonesia), BPDP-BPPT.
- Aida, I., 1978. Reliability of a tsunami source model derived from fault parameters. *J. Phys. Earth*, 26, pp.57-73.
- Aki, K., 1966. Generation and Propagation of G Waves from the Niigata Earthquake of June 16, 1964, Part 2. Estimation of Earthquake Moment, Released Energy, and Stress-Strain Drop from the G Wave Spectrum. *Bulletin of the Earthquake Research Institute*, 44, pp.73-88.
- Aki, K. & Richards, P.G., 2002. *Quantitative Seismology*, University Science Books.
- Amante, C. & Eakins, B.W., 2009. Etopo1 1 Arc-minute Global Relief Model: Procedures, Data Sources and Analysis. Available at: <http://www.ngdc.noaa.gov/mgg/global/relief/ETOPO1/docs/ETOPO1.pdf>.
- Ammon, C., Kanamori, H., Lay, T. & Velasco, A., 2006. The 17 July 2006 Java Tsunami Earthquake. *Geophysical Research Letters*, 33(L24308), pp.1-5.
- Arcement, G.J. & Schneider, V.R., 1984. Guide for Selecting Manning's Roughness Coefficients for Natural Channels and Flood Plains, USGS Water-Supply.
- Babeyko, A.Y., 2007. Rupture Generator v.1.1., Potsdam, Germany.
- Beckers, J. & Lay, T., 1995. Very broadband seismic analysis of the 1992 Flores, Indonesia, earthquake (M_w -7.9). *Journal of Geophysical Research*, 100, pp.18,179-18,193.

- Behrens, J., Androsov, A., Babeyko, A.Y.; Harig, S., Klaschka, F. & Mentrup, L., 2010. A new multi-sensor approach to simulation assisted tsunami early warning. *Nat. Hazards Earth Syst. Sci.*, 10, pp.1085-1100.
- Bernard, E.N., 2005. *Developing Tsunami-Resilient Communities*, Springer.
- Bilek, S., 2011. The 25 October 2010 Sumatera tsunami earthquake: Slip in a slow patch *Geophysical Research Letters*, 38, 1-20.
- Bilek, S., 2007. The Seismogenic Zone of Subduction Thrust Faults. In T. Dixon & C. Moore, eds. Columbia University Press, pp. 123-146.
- Bilek, S.L., 2002. Tsunami Earthquakes Possibility Widespread Manifestations of Frictional Conditional Stability. *Geophysical Research Letters*, 29(14), pp.18-1 - 18-4.
- Bilek, S.L. & Engdahl, E.R., 2007. Rupture Characterization and Aftershock Relocations for the 1994 and 2006 Tsunami Earthquakes in the Java Subduction Zone. *Geophysical Research Letters*, 34, p.L20311.
- Bilek, S.L. & Lay, T., 1999. Rigidity Variations with Depth along Interplate Megathrust Faults in Subduction Zones. *Nature*, 400, pp.443-446.
- Bock, Y., Prawirodirdjo, L., Genrich, J.F., Stevens, C.W., McCaffrey, R., Subarya, C., Puntodewo, S.S.O. & Calais, E., 2003. Crustal motion in Indonesia from Global Positioning System measurements. *Journal of Geophysical Research B: Solid Earth*, 108(8), pp.ETG 3-1- ETG 3-21.
- Borrero, J.C., McAdoo, B., Jaffe, B., Dengler, L., Gelfenbaum, G., Higman, B., Hidayat, R., Moore, A., Kongko, W., Lukijanto, Peters, R., Prasetya, G., Titov, V. & Yulianto, E., 2010. Field Survey of the March 28, 2005 Nias-Simeulue Earthquake and Tsunami. *Pure and Applied Geophysics*, pp.1-14.
- Brune, N.J., 1968. Seismic Moment, Seismicity, and Rate of Slip along Major Fault Zones. *Journal of Geophysical Research*, 73, pp.777-784.
- Brune, S., Babeyko, A. Y., Gaedicke, C. & Ladage, S., 2009a. Hazard assessment of underwater landslide-generated tsunamis: a case study in the Padang region, Indonesia. *Natural Hazards*. pp.1-14
- Brune, S., Ladage, S., Babeyko, A. Y., Mueller, C., Kopp, H. & Sobolev, S. V., 2009b. Submarine landslides at the eastern Sunda margin: observations and tsunami impact assessment. *Natural Hazards*. pp.1-16
- Brune, S., Babeyko, A. Y., Ladage, S. & Sobolev, S., 2010. Landslide tsunami hazard in the Indonesian Sunda Arc. *Natural Hazards Earth System Sciences*. 10, pp.589-604
- Bryant, E., 2008. *Tsunami: The Underrated Hazard*, Springer

- CEA-France, 2007. South of Java Earthquake and Tsunami, July 17, 2006, Available at: http://www-dase.cea.fr/actu/dossiers_scientifiques/2006-07-17/index_en.html#Tsunami.
- Choi, B. H., Pelinovsky, E., Kim, D. C., Didenkulova, I. & Woo, S.-B., 2008. Two- and three-dimensional computation of solitary wave run-up on non-plane beach. *Nonlin. Processes Geophys.*, 15, 489–502
- CGIAR-CSI, 2008. SRTM 90m DEM Digital Elevation Database. Available at: <http://srtm.csi.cgiar.org/>.
- Cousins, J. Palmer, N. Tejakusuma, I., Power, W.; Reese, S. & Nugrahadi, S., 2006. South Java Tsunami of 17th July 2006, Reconnaissance Report, GNS New Zealand.
- Dao, M.H. & Tkalich, P., 2007. Tsunami propagation modelling - a sensitivity study. *Natural Hazards a*, 7, pp.741-754.
- DCRC - Univ. Tohoku - Japan, 2007. Modeling a tsunami generated by the July 17, 2006 Earthquake , South of Java, Available at: http://www.tsunami.civil.tohoku.ac.jp/hokusai2/disaster/06_Java/July17_Java.html.
- DPPK-Cilacap, 2007. Potensi Unggulan Daerah dan Peluang Investasi Cilacap (Investment Opportunities), Dinas Perindustrian Perdagangan dan Koperasi, Kab.Cilacap (in Bahasa Indonesia).
- Dziewonski, A.M. & Anderson, D.L., 1981. Preliminary reference Earth model. *Physics of the Earth and Planetary Interiors*, 25(4), pp.297-356.
- Fritz, H., Kongko, W., Moore, A., McAdoo, B., Goff, J., Harbitz, C., Uslu, B., Kalligeris, N., Suteja, D., Kalsum, K., Titov, V., Gusman, A., Latief, H., Santoso, E., Sujoko, S., Djulkarnaen, D., Sunendar, H. & Synolakis, C., 2007. Extreme run-up from the 17 July 2006 Java Tsunami. *Geophysical Research Letters*, 34(L12602), pp.1-5.
- Fujii, Y. & Satake, K., 2006. Source of the July 2006 Java Tsunami Estimated from Tide Gauge Records. *Geophysical Research Letters*, 33(L23417), pp.1-5.
- Fukao, Y., 1979. Tsunami Earthquakes and Subduction Processes near Deep-Sea Trenches. *Geophysics Researches Letters*, 84, pp.2,303-2314.
- GEBCO, 2008. The GEBCO_08 Grid, version 20090202, <http://www.gebco.net>,
- Geist, E.L., 2002. Complex earthquake rupture and local tsunamis. *Journal of Geophysical Research B: Solid Earth*, 107(5), pp.ESE 2-1 - ESE 2-16.
- Geist, E.L., 1998. Local tsunamis and earthquake source parameters. *Advances in Geosciences*, 39, pp.118-209.
- Geist, E. L., 2005. Rapid tsunami models and earthquake source parameters: far-field and local applications. *ISSET Journal of Earthquake Technology*. 42 (4), pp.127-136

- Geist, E., Bilek, S., Arcas, D. & Titov, V., 2006. Differences in Tsunami Generation Between the December 26, 2004 and March 28, 2005 Sumatra Earthquakes. *Earth Planets Space*, 58, pp.185-193.
- Geist, E.L. & Dmowska, R., 1999. Local tsunamis and distributed slip at the source. *Pure and Applied Geophysics*, 154(3-4), pp.485-512.
- Geller, R.J., 1976. Scaling relations for earthquake source parameters and magnitudes. *Bulletin of the Seismological Society of America*, 66(5), pp.1501-1523.
- Gusman, A. R., Tanioka, Y., Matsumoto, H. & Iwasaki, S. I., 2009. Analysis of the Tsunami generated by the great 1977 Sumba earthquake that occurred in Indonesia. *Bulletin of the Seismological Society of America*, 99(4), pp.2169-2179.
- Gutenberg, B., 1945a. Amplitudes of p, pp, and s and magnitude of shallow earthquakes. *Bulletin - Seismological Society of America*, 35, pp.57-69.
- Gutenberg, B., 1945b. Amplitudes of surface waves and magnitudes of shallow earthquakes. *Bulletin - Seismological Society of America*, 35, pp.3-12.
- Gutenberg, B. & Richter, C.F., 1955. Magnitude and energy of earthquake. *Nature*, 4486, p.755.
- Hall, R., 2009. Encyclopedia of Islands. In D. A. Clague, with Rosemary G. Gillespie, eds. Regents of the University of California, pp. 454-460. Available at: http://searg.rhul.ac.uk/pubs/hall_2009_Indonesia%20Islands.pdf.
- Hanifa, R.N., Meilano, I., Sagiya, S., Kimata, F. & Abidin, H.Z., 2007. Numerical Modeling of The 2006 Java Tsunami Earthquake. *Advances in Geosciences*, 13, pp.231-248
- Hamzah, L., Puspito, N.T. & Imamura, F., 2000. Tsunami catalog and zones in Indonesia. *Journal of Natural Disaster Science*, 22(1), pp.25-43.
- Hanks, T.C. & Kanamori, H., 1979. A Moment Magnitude Scale. *Journal of Geophysical Research*, 84(B5), pp.2348-2350.
- Harada, K. & Imamura, F., 2000. Experimental Study on the Resistance by Mangroves under the Unsteady Flow. In *Proceedings of the 1st Congress of APACE*, pp.975-984.
- Harig, S., Chaeroni, Pranowo, W. S. & Behrens, J., 2008. Tsunami simulations on several scales. *Ocean Dynamics*, 58, pp.429-440.
- Hidayat, D., Barker, J.S. & Satake, K., 1995. Modeling the Seismic Source and Tsunami Generation of the December 12 1992, Flores Island, Indonesia, Earthquake. *Pure Applied Geophysics*, 144, pp.537-554.
- Honda, K., & T. Tomita. 2008. Tsunami estimation including effect of coastal structures and buildings by 3d-model, *Proceedings of 31st International Conference on Coastal Engineering*, ASCE, 1433-1445.

- Ide, S., Imamura, F., Yoshida, Y. & Abe, K., 1993. Source Characteristics of the Nicaraguan Tsunami Earthquake of September 2, 1992. *Geophysical Research Letters*, 20(9), pp.863-866.
- Imamura, F., 2009. Tsunami Modeling: Calculating Inundation and Hazard Maps. In E. N. Bernard & A. R. Robinson, eds. *The Sea. the President and Fellows of Harvard College*, pp. 321-329.
- Imamura, F., Shuto, N., Ide, S., Yoshida, Y. & Abe, K., 1993. Estimate of the Tsunami Source of the 1992 Nicaragua Earthquake from Tsunami Data. *Geophysics Researches Letters*, 20, pp.863-866.
- Imamura, F., Yalciner, A.C. & Ozyurt, G., 2006. *Tsunami Modeling Manual*, Disaster Control Research Center, Tohoku University, Sendai, Japan.
- Intermap Federal Services, I., 2007. *Digital Terrain Model Cilacap*, DLR Germany.
- Italy, TST - University of Bologna, Italy., 2007. The Java Tsunami, July 17 2006: Preliminary Numerical Simulations, Available at: [http://labtinti4.df.unibo.it/tsunami/site/simulation\\$_\\$java.php#case4](http://labtinti4.df.unibo.it/tsunami/site/simulation$_$java.php#case4).
- ITDB/WLD, 2007. *Integrated Tsunami Database for the World Ocean*, ver.6.52 of Dec.31 2007, Tsunami Lab. ICMG SD RAS, Novosibirsk, Russia,
- Jaffe, B.E., Borrero, J.C., Prasetya, G.S., Peters, R., McAdoo, B., Gelfenbaum, G., Morton, R., Ruggiero, P., Higman, B., Dengler, L., Hidayat, R. , Kinsley, E. , Kongko, W., Lukijanto, Moore, A., Titov, V., Yulianto, E., 2006. Northwest Sumatra and Offshore Islands Field Survey after the December 2004 Indian Ocean Tsunami. *Earthquake Spectra*, 22(s3), p.s105-s135.
- Ji, C., 2006, M7.7, Indonesia Earthquake of 17 July 2006, USGS. Available at: <http://earthquake.usgs.gov/earthquakes/eqarchives/poster/2006/20060717.php>
- Joku, G.N., Davies, J.M. & Davies, H.L., 2007. Eyewitness accounts of the impact of the 1998 Aitape tsunami, and of other tsunamis in living memory, in the region from Jayapura, Indonesia, to Vanimo, Papua New Guinea. *Pure and Applied Geophysics*, 164(2-3), pp.433-452.
- Kanamori, H., Rivera, L. & Lee, H., 2010. Historical seismograms for unravelling a mysterious earthquake: The 1907 Sumatera Earthquake, *Geophysical Journal International*, 183, 358-374.
- Kanamori, H., 1972. Mechanism of Tsunami Earthquakes. *Physics of the Earth and Planetary Interiors*, 6(5), pp.346-359.
- Kanamori, H., 1978. Quantification of earthquakes. *Nature*, 271, pp.411-414.
- Kanamori, H., 1977. The energy release in great earthquakes. *Journal of Geophysical Research*, 82 (20), pp.2981-1987.

- Kanamori, H. & Anderson, D.L., 1975. Theoretical Basis of Some Empirical Relations in Seismology. *Bulletin - Seismological Society of America*, 65(5), pp.1073-1095.
- Kanamori, H. & Kikuchi, M., 1993. The 1992 Nicaragua Earthquake: a Slow Tsunami Earthquake Associated with Subducted Sediments. *Nature*, 361, pp.714-716.
- Kawata, Y. et al., 1999. Tsunami in Papua New Guinea was as Intense as First Thought. *EOS, Transactions, American Geophysical Union*, 80(9), pp.101, 104-105.
- Kongko, W., 2008. A Sensitivity Test of Tsunami Modelling Using Various Data: Case Study in Cilacap Indonesia. In *International Conference on Tsunami Warning (ICTW) Bali-Indonesia*.
- Kongko, W. & Leschka, S., 2009. Bathymetry measurements in Indonesia, Part 2: Cilacap, DHI-WASY GmbH Syke Germany.
- Kongko, W., Suranto, S., Chaeroni, C., Aprijanto, A., Zikra, Z. & Sujantoko, S., 2006. Rapid Survey on Java Tsunami 17 July 2006. Available at: http://ioc3.unesco.org/itic/files/tsunami-Java170706_e.pdf.
- Kongko, W., 2010. Report of the 2006 Java tsunami run-up survey in Cilacap phase 4 (in Bahasa Indonesia), BPDP-BPPT.
- Kopp, H., Flueh, E., Petersen, C., Weinrebe, W., Wittwer, A. & Meramex-Scientist, 2006. The Java Margin Revisited: Evidence for Subduction Erosion off Java. *Earth and Planetary Science Letters*, 242, pp.130-142.
- Kopp, H. & Kukowski, N., 2003. Backstop Geometry and Accretionary Mechanics of the Sunda Margin. *Tectonics*, 22(6), pp.11-1 - 11-16.
- Kotani, M., Imamura, F. & Shuto, N., 1998. Tsunami run-up simulation and damage estimation by using GIS (in Japanese). In *Proceedings of Coastal Engineering, JSCE*, 45 (1), pp. 356-360.
- Kurniawan, S., Anaya, A.I. & Widiyantoro, S., with Mori, J. & Mooney, W., Afnimar, 2007. The July 17, 2006 West Java Earthquake and Tsunami. *Annual of Dis. Prev. Res. Inst. Kyoto Univ.*, 50A, pp.143-151.
- Latief, H., Riadi, A. & Zulkarnaen, D., 2006. Preliminary Result of the 2006 West Java Tsunami Simulation. Available at: http://oceanpartners.ucsd.edu/documents/News/2006_West_Java_tsunami.pdf.
- Lauterjung, J., Muench, U., and Rudloff, A., 2010. The challenge of installing a tsunami early warning system in the vicinity of the Sunda Arc, Indonesia. *Natural Hazards and Earth Systems Sciences*, 10, pp.641-646.
- Lavigne, F., Gomes, C., Giffò, M., Wassmer, P., Hoebreck, C., Mardiatno, D., Prioyono, J. & Paris, R., 2007. Field Observations of the 17 July 2006 Tsunami in Java. *Natural Hazards and Earth Systems Sciences*, 7, pp.177-183.

- Lay, T., Ammon, C.J., Kanamori, H., Yamazaki, Y., Cheung, K.F. & Hutko, A., 2011. The 25 October 2010 Mentawai tsunami earthquake (Mw 7.8) and the tsunami hazard presented by shallow megathrust ruptures, *Geophysical Research Letters*, 38, 1-5.
- Lay, T. & Bilek, S., 2007. *Anomalous Earthquake Ruptures at Shallow Depths on Subduction Zone Megathrust*. T. Dixon & C. Moore, eds., Columbia University Press.
- Leschka, S., Kongko, W. & Larsen, O., 2009a. On The Influence of Near-shore Bathymetric Data Quality on Tsunami run-up Modeling, Part I: Bathymetry. In *Proceeding of 5th International Conference on APAC2009*.
- Leschka, S., Kongko, W. & Larsen, O., 2009b. On The Influence of Near-shore Bathymetric Data Quality on Tsunami run-up Modeling, Part II : Modeling. In *Proceeding of 5th International Conference on APAC 2009*.
- Lynett, P.J., Borrero, J.C., Liu, P.L.-F., Synolakis, C.E., 2003. Field Survey and Numerical Simulations: A Review of the 1998 Papua New Guinea Tsunami. *Pure Applied Geophysics*, 160, pp.2119-2146.
- Mansinha, L. & Smylie, D.E., 1971. The Displacement Fields of Inclined Faults. *Bulletin of the Seismological Society of America*, 61(5), pp.1433-1440.
- Manzanares, A., 2008. *Distribution of crustal seismicity and structure in the upper plate of Central Java, Indonesia*. Freie Universitaet Berlin.
- Maramai, A. & Tinti, S., 1997. The 3 June 1994 Java Tsunami: a Post-event Survey of the Coastal Effects. *Natural Hazards*, 15, pp.31-49.
- Marfai, M. A., King, L., Singh, L. P., Mardiatno, D., Sartohadi, J., Hadmoko, D. S., Dewi, A., 2008. Natural hazards in Central Java Province, Indonesia: An overview. *Environmental Geology*, 56(2), pp.335-351.
- Masson, D.G., Parson, L.M., Milson, J., Nichols, G., Sikumbang, N., Dwiyanto, B. & Kallagher, H., 1990. Subduction of Seamounts at the Java Trench: a View with Long-range Sides-can Sonar. *Tectonophysics*, 185(1-2), pp.51-65.
- Matsuyama, M., Walsh, J.P. & Yeh, H., 1999. The Effect of Bathymetry on Tsunami Characteristics at Sissano Lagoon, Papua New Guinea. *Geophysics Researches Letters*, 26, pp.3513-3516.
- Mauch, J. E. & Birch, J. W. Kent, A. (Ed.).1993. *Guide to the successful Thesis and Dissertation*, Marcel Dekker, Inc.
- McCloskey, J., Antonioli, A., Piatanesi, A., Sieh, K., Steacy, S., Nalbant, S.S., Cocco, M., Giunchi, C., Huang, J.D., Dunlop, P., 2007. Near-field propagation of tsunamis from megathrust earthquakes. *Geophysical Research Letters*, 34(14), pp.1-5.
- Moore, A., Goff, J., Mcadoo, B.G., Fritz, H., Gusman, A., Kalligeris, N., Kalsum, N., Susanto, A., Suteja & D., Synolakis, C., 2011. Sedimentary Deposits from the 17 July 2006 Western Java Tsunami, Indonesia: Use of Grain Size Analyses to Assess

Tsunami Flow Depth, Speed, and Traction Carpet Characteristics. *Pure and Applied Geophysics*, 1951–1961,

Mori, J., 2007. The 17 July 2006 Tsunami Earthquake in West Java, Indonesia. *Seismology Research Letters*, 78, pp.201-207.

Newcomb, K.R. & McCann, W.R., 1987. Seismic History and Seismotectonic of the Sunda Arc. *Journal of Geophysical Research*, 92(No. B1), pp.421-439.

Newman, A., Hayes, G., Wei, Y. & Convers, J., 2011. The 25 October 2010 Mentawai tsunami earthquake, from real-time discriminants, finite-fault rupture, and tsunami excitation, *Geophysical Research Letters*, 38, 1-7.

Nicolisky, D., Suleimani, E. & Hansen, R., 2010. Validation and Verification of a Numerical Model for Tsunami Propagation and run-up. *Pure and Applied Geophysics*, -, pp.1-24.

Okada, Y., 1985. Surface Deformation due to Shear and Tensile Faults in a Half-space. *Bulletin of the Seismological Society of America*, 75(4), pp.1135-1154.

Okal, E., 2006. Earthquake: Scaling Laws, Hand-out of Course 1-Tsunami Source and Tsunami Propagation, UNESCO-IOC International Training Course in Tsunami Numerical Modeling, Oostende-Belgium, 5-16 June,

Okal, E.A., 1988. Seismic Parameters Controlling Far-field Tsunami Amplitudes: A Review. *Natural Hazards*, 1, pp.67-96.

Okal, E.A., 2003. T Waves from the 1998 Papua New Guinea Earthquake and its Aftershocks: Timing the Tsunamigenic Slump. *Pure Applied Geophysics*, 160(0033-4553/03/111843-21), pp.1843-1863.

Okal, E. & Synolakis, C., 2004. Source discriminants for near-field tsunamis. *Geophysical Journal International*, 158, pp.899-912.

Papazachos, B. C., Scordilis, E. M., Panagiotopoulos, D. G., Papazachos, C. B., Karakaisis, G. F., 2004. Global relations between seismic fault parameters and moment magnitude of earthquakes. *Tenth Congress Hellenic Geol Soc*, XXXVI, pp.539-540.

Pelayo, A.M. & Wiens, D.A., 1992. Tsunami Earthquakes: Slow Thrust-faulting Events in the Accretionary Wedge. *Geophysics Researches Letters*, 97, pp.15321-15337.

Polet, J. & Kanamori, H., 2000. Shallow Subduction Zone Earthquakes and Their Tsunamigenic Potential. *Geophysics Journal International*, 142, pp.684-702.

Polet, J. & Thio, H.K., 2003. The 1994 Java Earthquake and its Normal Aftershocks. *Geophysical Research Letters*, 30(9), pp.27-1 - 27-4.

Rastogi, B. K. & Jaiswal, R.K., 2006. A Catalog of Tsunamis in the Indian Ocean, *Science of Tsunami Hazards*.

RCS, 2006. Indonesia, Western Java Earthquake Tsunami. Available at:

http://www.ifrc.org/cgi/pdf_appeals.pl?rpts06/IDtseq26070603.pdf.

- Reese, S., Cousins, W. J., Power, W. L., Palmer, N. G., Tejakusuma, I. G., Nugrahadi, S., 2007. Tsunami vulnerability of buildings and people in South Java - Field observations after the July 2006 Java tsunami. *Natural Hazards and Earth System Science*, 7(5), pp.573-589.
- Richter, C.F., 1935. An instrumental earthquake magnitude scale. *Bulletin - Seismological Society of America*, 25 (1), pp.1-32.
- Rudloff, A., Lauterjung, J., Muench, U., and Tinti, S., 2009. The GITEWS project (German-Indonesian tsunami early warning system). *Natural Hazards and Earth System Science*, 9(4), pp.1381-1382.
- Satake, K. & Kanamori, H., 1991. Use of tsunami waveforms for earthquake source study. *Natural Hazards*. 4. pp.193-208
- Satake, K., 1995. Linear and Nonlinear Computations of the 1992 Nicaragua Earthquake Tsunami. *Pageoph*, 144, pp.455-470.
- Satake, K., 1994. Mechanism of the 1992 Nicaragua tsunami earthquake. *Geophysical Researches Letters*, 21(23), pp.2519-2522.
- Satake, K. & Tanioka, Y., 1999. Sources of Tsunami and Tsunamigenic Earthquakes in Subduction Zones. *Pure Applied Geophysics*, 154, pp.467-483.
- Satake, K. & Tanioka, Y., 2003. The July 1998 Papua New Guinea earthquake: Mechanism and quantification of unusual tsunami generation. *Pure and Applied Geophysics*, 160(10-11), pp.2087-2118.
- Satake, K. & Tanioka, Y., 1995. Tsunami Generation of the 1993 Hokkaido Nansei-Oki Earthquake. *Pageoph*, 145 (3/4), pp.803-821.
- Schlurmann, T., Kongko, W., Goseberg, N., Natawidjaja, D.H., & Sieh, K., 2010. Near-Field Tsunami Hazard Map Padang, West Sumatra: Utilizing High Resolution Geospatial Data and Reasonable Source Scenarios. *Proceedings of the International Conference on Coastal Engineering*, No. 32(2010), Shanghai, China. Paper : management.26. Retrieved from <http://journals.tdl.org/ICCE/>, 2011.
- Schlurmann, T. & Siebert, M., 2011. The Capacity Building programs of GITEWS - visions, goals, lessons, and re-iterated needs and demands. *Natural Hazards and Earth System Science*, 11, pp.293–300.
- Shuto, N., 1987. The Effectiveness and Limit of Tsunami Control Forest. *Coastal Engineering in Japan*, 30 No.1, pp.143-153
- Shuto, N. & Fujima, K., 2009. A short history of tsunami research and countermeasures in Japan. *Proceedings of the Japan Academy Series B: Physical and Biological Sciences*, 85(8), pp.267-275.

- Spicak, A., Hanus, V. & Vanek, J., 2007. Earthquake occurrence along the Java trench in front of the onset of the Wadati-Benioff zone: Beginning of a new subduction cycle? *Tectonics*, 26(1), pp.1-16.
- Stefanakis, T.S., Dias, F. & Dutykh, D., 2011. Local Run-Up Amplification by Resonant Wave Interactions. *Physical Review Letters*, 107, 124502-1-124502-5
- Stein, S. & Wysession, M., 2003. *An Introduction to Seismology, Earthquakes, and Earth Structure*, Blackwell Publishing Ltd.
- Strasser, F.O., Arango, M.C. & Bommer, J.J., 2010. Scaling of the Source Dimensions of Interface and Intraslab Subduction-zone Earthquakes with Moment Magnitude. *Seismological Research Letters*, 81 (6), pp.941-950.
- Strunz, G., Post, J., Zosseder, K., Wegscheider, S., Mueck, M., Riedlinger, T., Mehl, H., Dech, S., Birkmann, J., Gebert, G., H. H., Anwar H.Z., Sumaryono, Khomarudin, R.M. & Muhari, A., 2011. Tsunami risk assessment in Indonesia. *Natural Hazards Earth System Sciences*, 11, pp.67-82.
- Suppasri, A., Imamura, F. & Koshimura, S., 2008. Comparison Among the Proposed Models for the 2004 Indian Ocean Tsunami. In *Proceedings of the 2008 Western Pacific Geophysics Meeting*, U35B, Cairns, Australia, 29 July -1 August.
- Synolakis, C.E., 1987. The run-up of Solitary Waves. *Journal of Fluid Mechanics*, 185, pp.523-545.
- Synolakis, C., Bardet, J.-P., Borrero, J., Davies, H., Okal, E., Silver, E., Sweet, S. & Tappin, D., 2002. The Slump Origin of the 1998 Papua New Guinea Tsunami, *Proceeding Royal Society London A*.
- Synolakis, C.E., Imamura, F., Tsuji, Y., Matsutomi, H., Tinti, S., Cook, B., Chandra, Y.P. & Usman, M., 1995. Damage, Conditions of East Java Tsunami of 1994 Analyzed. *EOS*, 76(26), pp.257-264.
- Synolakis, C. & Bernard, E.N., 2006. Tsunami Science before and Beyond Boxing Day 2004. *Philosophical Transactions of the Royal Society*, 364(364), pp.2231-2265.
- Synolakis, C., Bernard, E., Titov, V., Kanoglu, U. & Gonzalez, F. I., 2008. Validation and Verification of Tsunami Numerical Models. *Pure Applied Geophysics*, 165, pp.2197-2228.
- Tanioka, Y., 1999. Analysis of the Far-field Tsunamis Generated by the 1998 Papua New Guinea Earthquake. *Geophysics Research Letters*, 26, pp.3393-3396.
- Tanioka, Y. & Satake, K., 1996. Tsunami generation by horizontal displacement of ocean bottom. *Geophysical Research Letters*, 23(8), pp.861-864.
- Tappin, D.R., Watts, P. & Grilli, S.T., 2008. The Papua New Guinea tsunami of 17 July 1998: anatomy of a catastrophic event. *Natural Hazards and Earth Systems Sciences*, 8, pp.243-266.

- Titov, V. V., Gonzalez, F. I., Bernard, E. N., Eble, M. C., Mofjeld, H. O., Newman, J. C. & Venturato, A. J., 2005. Real-time tsunami forecasting: Challenges and solutions. *Natural Hazards*, 35(1), pp.41-58.
- Tregoning, P., Brunner, F.K., Bock, Y., Puntodewo, S.S.O., McCaffrey, R., Genrich, J.F., Calais, E., Rais, J. & Subarya, C., 1994. First geodetic measurement of convergence across the Java Trench. *Geophysical Research Letters*, 21(19), pp.2135-2138.
- Tsuji, Y., Imamura, F., Matsutomi, H., Synolakis, C.E., Nanang, P.T., Jumadi, Harada, S., Han, S.S., Arai, K.I. & Cook, B., 1995, Field Survey of the East Java Earthquake and Tsunami of June 3, 1994, *Pageoph*, 144, 839-854
- Tsuji, Y., Matsutomi, H., Imamura, F., Takeo, M., Kawata, Y., Matsuyama, M., Takahashi, T. & Sunarjo Harjadi, P., 1995. Damage to Coastal Villages due to the 1992 Flores Island Earthquake Tsunami. *Pure Applied Geophysics*, 144, pp.481-524.
- USGS, 2006. Magnitude 7.7 - SOUTH OF JAVA, INDONESIA-USGS. Available at: <http://earthquake.usgs.gov/earthquakes/eqinthenews/2006/usqgaf/#summary>.
- USGS, 2010. Source Parameters of Earthquake M_W 6.5 above at Java Subduction Zone. Available at: <http://earthquake.usgs.gov/earthquakes/eqarchives/sopar/>.
- Wang, R., Martin, F.L. & Roth, F., 2003. Computation of deformation induced by earthquakes in a multi-layered elastic crust - FORTRAN programs EDGRN/EDCMP. *Computers and Geosciences*, 29(2), pp.195-207.
- Wells, D.L. & Coppersmith, K.J., 1994. New empirical relationships among magnitude, rupture length, rupture width, rupture area, and surface displacement. *Bulletin - Seismological Society of America*, 84(4), pp.974-1002.
- WHO, 2006, August. Central and West Java earthquake and tsunami, situation report no11. Available at: <http://reliefweb.int/rw/RWB.NSF/db900SID/VBOL-6SCJ85?OpenDocument>.
- Wyss, M., 1979. Estimating maximum expectable magnitude of earthquakes from fault dimensions. *Geology*, 7(7), pp.336-340.
- Yanagisawa, H., Koshimura, S., Goto, K., Miyagi, T., Imamura, F., Ruangrassamee, A. & Tanavud, C., 2009. The Reduction Effects of Mangrove Forest on a Tsunami Based on Field Surveys at Pakarang Cape, Thailand and Numerical Analysis. *Estuarine, Coastal, and Shelf Science*, 81, pp.27-37.
- Yeh, H., Imamura, F., Synolakis, C., Tsuji, Y., Liu, P. & Shaozhong, Shi., 1993. The Flores Island tsunamis. *EOS*, 74(33), pp.369-376.
- Zielinski, R., 2007. *New Developments and Challenges in Remote Sensing*. Z. Bochenek, ed. Mill press, Rotterdam, pp. 685-693.

Appendix A – The deformation model

Table 1: List of source parameters of Padang Scenario 2B (Source D.H.Natawidjaja)

The fault number of 1-40.

No	Geo-coordinates		Slip (m)	Angle Parameters (°)			Depth (km)
	Longitude	Latitude		Rake	Strike	Dip	
1	100.3992	-4.6990	0.5	75	325	13	8.5
2	100.2958	-4.5516	0.9	75	325	13	8.5
3	100.1923	-4.4041	1.8	75	325	13	8.5
4	100.0888	-4.2567	2.5	75	325	13	8.5
5	99.9854	-4.1093	3.2	75	325	13	8.5
6	99.8819	-3.9618	3.6	75	325	13	8.5
7	99.7785	-3.8144	3.9	75	325	13	8.5
8	99.6750	-3.6670	4.0	75	325	13	8.5
9	99.5716	-3.5195	4.3	75	325	13	8.5
10	99.4681	-3.3721	3.8	75	325	13	8.5
11	99.3647	-3.2246	3.3	75	325	13	8.5
12	99.2612	-3.0772	2.7	75	325	13	8.5
13	99.1578	-2.9298	2.6	75	325	13	8.5
14	99.0543	-2.7823	2.6	75	325	13	8.5
15	98.9509	-2.6349	3.7	75	325	13	8.5
16	98.8474	-2.4875	4.0	75	325	13	8.5
17	98.7440	-2.3400	4.3	75	325	13	8.5
18	98.6405	-2.1926	4.8	75	325	13	8.5
19	98.5371	-2.0452	5.1	75	325	13	8.5
20	98.4336	-1.8977	5.2	75	325	13	8.5
21	98.3302	-1.7503	5.2	75	325	13	8.5
22	98.2267	-1.6029	4.3	75	325	13	8.5
23	98.1233	-1.4554	3.2	75	325	13	8.5
24	98.0198	-1.3080	1.7	75	325	13	8.5
25	97.9164	-1.1605	0.6	75	325	13	8.5
26	97.8129	-1.0131	0.6	75	325	13	8.5
27	97.7095	-0.8657	0.6	75	325	13	8.5
28	100.6466	-4.7458	0.5	75	325	13	13.0
29	100.5432	-4.5984	1.4	75	325	13	13.0
30	100.4397	-4.4510	2.4	75	325	13	13.0
31	100.3363	-4.3035	3.5	75	325	13	13.0
32	100.2328	-4.1561	4.4	75	325	13	13.0
33	100.1294	-4.0087	5.4	75	325	13	13.0
34	100.0259	-3.8612	6.0	75	325	13	13.0
35	99.9225	-3.7138	7.0	75	325	13	13.0
36	99.8190	-3.5664	7.4	75	325	13	13.0
37	99.7156	-3.4189	7.6	75	325	13	13.0
38	99.6121	-3.2715	7.2	75	325	13	13.0
39	99.5086	-3.1241	6.2	75	325	13	13.0
40	99.4052	-2.9766	5.6	75	325	13	13.0

To be continued

Appendix A

Table 1: List of source parameters of Padang Scenario 2B (Source D.H.Natawidjaja)

The fault number of 41-80.

No	Geo-coordinates		Slip (m)	Angle Parameters (°)			Depth (km)
	Longitude	Latitude		Rake	Strike	Dip	
41	99.3017	-2.8292	4.9	75	325	13	13.0
42	99.1983	-2.6818	5.0	75	325	13	13.0
43	99.0948	-2.5343	6.7	75	325	13	13.0
44	98.9914	-2.3869	7.4	75	325	13	13.0
45	98.8879	-2.2394	8.4	75	325	13	13.0
46	98.7845	-2.0920	8.9	75	325	13	13.0
47	98.6810	-1.9446	9.1	75	325	13	13.0
48	98.5776	-1.7971	9.4	75	325	13	13.0
49	98.4741	-1.6497	9.4	75	325	13	13.0
50	98.3707	-1.5023	8.5	75	325	13	13.0
51	98.2672	-1.3548	6.7	75	325	13	13.0
52	98.1638	-1.2074	4.0	75	325	13	13.0
53	98.0603	-1.0600	1.8	75	325	13	13.0
54	97.9569	-0.9125	1.3	75	325	13	13.0
55	97.8534	-0.7651	1.9	75	325	13	13.0
56	100.8940	-4.7927	0.5	75	325	13	17.5
57	100.7906	-4.6453	1.5	75	325	13	17.5
58	100.6871	-4.4978	2.4	75	325	13	17.5
59	100.5837	-4.3504	3.8	75	325	13	17.5
60	100.4802	-4.2030	4.9	75	325	13	17.5
61	100.3768	-4.0555	6.2	75	325	13	17.5
62	100.2733	-3.9081	7.0	75	325	13	17.5
63	100.1699	-3.7606	7.8	75	325	13	17.5
64	100.0664	-3.6132	8.9	75	325	13	17.5
65	99.9630	-3.4658	9.4	75	325	13	17.5
66	99.8595	-3.3183	9.7	75	325	13	17.5
67	99.7561	-3.1709	9.3	75	325	13	17.5
68	99.6526	-3.0235	8.2	75	325	13	17.5
69	99.5492	-2.8760	7.6	75	325	13	17.5
70	99.4457	-2.7286	7.0	75	325	13	17.5
71	99.3423	-2.5812	7.0	75	325	13	17.5
72	99.2388	-2.4337	9.1	75	325	13	17.5
73	99.1354	-2.2863	10.2	75	325	13	17.5
74	99.0319	-2.1389	11.2	75	325	13	17.5
75	98.9284	-1.9914	12.0	75	325	13	17.5
76	98.8250	-1.8440	12.0	75	325	13	17.5
77	98.7215	-1.6965	12.0	75	325	13	17.5
78	98.6181	-1.5491	12.3	75	325	13	17.5
79	98.5146	-1.4017	11.5	75	325	13	17.5
80	98.4112	-1.2542	9.1	75	325	13	17.5

To be continued

Appendix A

Table 1: List of source parameters of Padang Scenario 2B (Source D.H.Natawidjaja)

The fault number of 81-120.

No	Geo-coordinates		Slip (m)	Angle Parameters (°)			Depth (km)
	Longitude	Latitude		Rake	Strike	Dip	
81	98.3077	-1.1068	6.0	75	325	13	17.5
82	98.2043	-0.9594	3.1	75	325	13	17.5
83	98.1008	-0.8119	2.5	75	325	13	17.5
84	97.9974	-0.6645	3.8	75	325	13	17.5
85	101.1414	-4.8395	0.5	75	325	13	22.0
86	101.0380	-4.6921	1.0	75	325	13	22.0
87	100.9345	-4.5447	2.0	75	325	13	22.0
88	100.8311	-4.3972	3.5	75	325	13	22.0
89	100.7276	-4.2498	4.9	75	325	13	22.0
90	100.6242	-4.1024	6.0	75	325	13	22.0
91	100.5207	-3.9549	7.4	75	325	13	22.0
92	100.4173	-3.8075	8.2	75	325	13	22.0
93	100.3138	-3.6601	8.4	75	325	13	22.0
94	100.2104	-3.5126	8.7	75	325	13	22.0
95	100.1069	-3.3652	8.5	75	325	13	22.0
96	100.0035	-3.2178	9.3	75	325	13	22.0
97	99.9000	-3.0703	10.1	75	325	13	22.0
98	99.7966	-2.9229	9.4	75	325	13	22.0
99	99.6931	-2.7754	8.6	75	325	13	22.0
100	99.5897	-2.6280	8.0	75	325	13	22.0
101	99.4862	-2.4806	8.0	75	325	13	22.0
102	99.3828	-2.3331	10.7	75	325	13	22.0
103	99.2793	-2.1857	11.7	75	325	13	22.0
104	99.1759	-2.0383	12.5	75	325	13	22.0
105	99.0724	-1.8908	13.3	75	325	13	22.0
106	98.9690	-1.7434	13.6	75	325	13	22.0
107	98.8655	-1.5960	13.6	75	325	13	22.0
108	98.7621	-1.4485	13.9	75	325	13	22.0
109	98.6586	-1.3011	13.6	75	325	13	22.0
110	98.5552	-1.1537	11.5	75	325	13	22.0
111	98.4517	-1.0062	8.0	75	325	13	22.0
112	98.3482	-0.8588	5.0	75	325	13	22.0
113	98.2448	-0.7113	4.4	75	325	13	22.0
114	98.1413	-0.5639	5.6	75	325	13	22.0
115	101.2854	-4.7390	0.5	75	325	13	26.5
116	101.1819	-4.5915	1.5	75	325	13	26.5
117	101.0785	-4.4441	2.6	75	325	13	26.5
118	100.9750	-4.2966	4.0	75	325	13	26.5
119	100.8716	-4.1492	4.9	75	325	13	26.5
120	100.7681	-4.0018	5.8	75	325	13	26.5

To be continued

Appendix A

Table 1: List of source parameters of Padang Scenario 2B (Source D.H.Natawidjaja)

The fault number of 121-160.

No	Geo-coordinates		Slip (m)	Angle Parameters (°)			Depth (km)
	Longitude	Latitude		Rake	Strike	Dip	
121	100.6647	-3.8543	7.1	75	325	13	26.5
122	100.5612	-3.7069	7.6	75	325	13	26.5
123	100.4578	-3.5595	7.5	75	325	13	26.5
124	100.3543	-3.4120	6.8	75	325	13	26.5
125	100.2509	-3.2646	6.5	75	325	13	26.5
126	100.1474	-3.1172	7.3	75	325	13	26.5
127	100.0440	-2.9697	9.1	75	325	13	26.5
128	99.9405	-2.8223	10.1	75	325	13	26.5
129	99.8371	-2.6749	9.3	75	325	13	26.5
130	99.7336	-2.5274	8.4	75	325	13	26.5
131	99.6302	-2.3800	8.2	75	325	13	26.5
132	99.5267	-2.2325	9.9	75	325	13	26.5
133	99.4233	-2.0851	11.2	75	325	13	26.5
134	99.3198	-1.9377	12.6	75	325	13	26.5
135	99.2164	-1.7902	13.6	75	325	13	26.5
136	99.1129	-1.6428	14.2	75	325	13	26.5
137	99.0095	-1.4954	14.4	75	325	13	26.5
138	98.9060	-1.3479	14.6	75	325	13	26.5
139	98.8026	-1.2005	14.8	75	325	13	26.5
140	98.6991	-1.0531	13.4	75	325	13	26.5
141	98.5957	-0.9056	10.1	75	325	13	26.5
142	98.4922	-0.7582	7.0	75	325	13	26.5
143	98.3888	-0.6108	6.3	75	325	13	26.5
144	98.2853	-0.4633	7.5	75	325	13	26.5
145	101.4293	-4.6384	0.5	75	325	13	31.0
146	101.3259	-4.4909	1.5	75	325	13	31.0
147	101.2224	-4.3435	2.0	75	325	13	31.0
148	101.1190	-4.1961	2.4	75	325	13	31.0
149	101.0155	-4.0486	3.5	75	325	13	31.0
150	100.9121	-3.9012	4.5	75	325	13	31.0
151	100.8086	-3.7537	5.7	75	325	13	31.0
152	100.7052	-3.6063	7.0	75	325	13	31.0
153	100.6017	-3.4589	6.3	75	325	13	31.0
154	100.4983	-3.3114	6.5	75	325	13	31.0
155	100.3948	-3.1640	6.1	75	325	13	31.0
156	100.2914	-3.0166	7.3	75	325	13	31.0
157	100.1879	-2.8691	10.0	75	325	13	31.0
158	100.0845	-2.7217	10.8	75	325	13	31.0
159	99.9810	-2.5743	10.2	75	325	13	31.0
160	99.8776	-2.4268	8.9	75	325	13	31.0

To be continued

Appendix A

Table 1: List of source parameters of Padang Scenario 2B (Source D.H.Natawidjaja)

The fault number of 161-200.

No	Geo-coordinates		Slip (m)	Angle Parameters (°)			Depth (km)
	Longitude	Latitude		Rake	Strike	Dip	
161	99.7741	-2.2794	7.5	75	325	13	31.0
162	99.6707	-2.1320	9.9	75	325	13	31.0
163	99.5672	-1.9845	11.8	75	325	13	31.0
164	99.4638	-1.8371	13.3	75	325	13	31.0
165	99.3603	-1.6897	13.0	75	325	13	31.0
166	99.2569	-1.5422	13.1	75	325	13	31.0
167	99.1534	-1.3948	14.0	75	325	13	31.0
168	99.0500	-1.2473	14.7	75	325	13	31.0
169	98.9465	-1.0999	14.9	75	325	13	31.0
170	98.8431	-0.9525	13.2	75	325	13	31.0
171	98.7396	-0.8050	10.2	75	325	13	31.0
172	98.6362	-0.6576	6.9	75	325	13	31.0
173	98.5327	-0.5102	5.6	75	325	13	31.0
174	98.4293	-0.3627	7.4	75	325	13	31.0
175	101.5733	-4.5378	0.5	75	325	13	35.5
176	101.4698	-4.3903	1.0	75	325	13	35.5
177	101.3664	-4.2429	1.2	75	325	13	35.5
178	101.2629	-4.0955	1.9	75	325	13	35.5
179	101.1595	-3.9480	2.4	75	325	13	35.5
180	101.0560	-3.8006	3.5	75	325	13	35.5
181	100.9526	-3.6532	5.5	75	325	13	35.5
182	100.8491	-3.5057	7.0	75	325	13	35.5
183	100.7457	-3.3583	7.6	75	325	13	35.5
184	100.6422	-3.2109	7.9	75	325	13	35.5
185	100.5388	-3.0634	8.6	75	325	13	35.5
186	100.4353	-2.9160	8.5	75	325	13	35.5
187	100.3319	-2.7685	10.4	75	325	13	35.5
188	100.2284	-2.6211	11.2	75	325	13	35.5
189	100.1250	-2.4737	10.9	75	325	13	35.5
190	100.0215	-2.3262	9.8	75	325	13	35.5
191	99.9181	-2.1788	9.0	75	325	13	35.5
192	99.8146	-2.0314	11.1	75	325	13	35.5
193	99.7112	-1.8839	11.3	75	325	13	35.5
194	99.6077	-1.7365	12.0	75	325	13	35.5
195	99.5043	-1.5891	11.7	75	325	13	35.5
196	99.4008	-1.4416	11.9	75	325	13	35.5
197	99.2974	-1.2942	12.6	75	325	13	35.5
198	99.1939	-1.1468	13.3	75	325	13	35.5
199	99.0905	-0.9993	13.3	75	325	13	35.5
200	98.9870	-0.8519	11.4	75	325	13	35.5

To be continued

Appendix A

Table 1: List of source parameters of Padang Scenario 2B (Source D.H.Natawidjaja)

The fault number of 201-240.

No	Geo-coordinates		Slip (m)	Angle Parameters (°)			Depth (km)
	Longitude	Latitude		Rake	Strike	Dip	
201	98.8836	-0.7044	7.6	75	325	13	35.5
202	98.7801	-0.5570	3.8	75	325	13	35.5
203	98.6767	-0.4096	1.8	75	325	13	35.5
204	98.5732	-0.2621	2.8	75	325	13	35.5
205	101.7173	-4.4372	0.5	75	325	13	40.0
206	101.6138	-4.2897	0.9	75	325	13	40.0
207	101.5104	-4.1423	1.3	75	325	13	40.0
208	101.4069	-3.9949	1.7	75	325	13	40.0
209	101.3035	-3.8474	2.2	75	325	13	40.0
210	101.2000	-3.7000	3.5	75	325	13	40.0
211	101.0965	-3.5526	4.2	75	325	13	40.0
212	100.9931	-3.4051	6.9	75	325	13	40.0
213	100.8896	-3.2577	8.2	75	325	13	40.0
214	100.7862	-3.1103	9.6	75	325	13	40.0
215	100.6827	-2.9628	9.1	75	325	13	40.0
216	100.5793	-2.8154	9.2	75	325	13	40.0
217	100.4758	-2.6680	9.5	75	325	13	40.0
218	100.3724	-2.5205	10.7	75	325	13	40.0
219	100.2689	-2.3731	11.1	75	325	13	40.0
220	100.1655	-2.2256	11.0	75	325	13	40.0
221	100.0620	-2.0782	10.4	75	325	13	40.0
222	99.9586	-1.9308	12.0	75	325	13	40.0
223	99.8551	-1.7833	11.2	75	325	13	40.0
224	99.7517	-1.6359	10.6	75	325	13	40.0
225	99.6482	-1.4885	10.3	75	325	13	40.0
226	99.5448	-1.3410	10.2	75	325	13	40.0
227	99.4413	-1.1936	10.8	75	325	13	40.0
228	99.3379	-1.0462	11.4	75	325	13	40.0
229	99.2344	-0.8987	11.3	75	325	13	40.0
230	99.1310	-0.7513	10.0	75	325	13	40.0
231	99.0275	-0.6039	6.2	75	325	13	40.0
232	98.9241	-0.4564	2.5	75	325	13	40.0
233	101.8612	-4.3366	0.5	75	325	13	44.5
234	101.7578	-4.1892	1.3	75	325	13	44.5
235	101.6543	-4.0417	1.3	75	325	13	44.5
236	101.5509	-3.8943	2.9	75	325	13	44.5
237	101.4474	-3.7469	3.5	75	325	13	44.5
238	101.3440	-3.5994	4.4	75	325	13	44.5
239	101.2405	-3.4520	5.1	75	325	13	44.5
240	101.1371	-3.3045	6.9	75	325	13	44.5

To be continued

Appendix A

Table 1: List of source parameters of Padang Scenario 2B (Source D.H.Natawidjaja)

The fault number of 241-280.

No	Geo-coordinates		Slip (m)	Angle Parameters (°)			Depth (km)
	Longitude	Latitude		Rake	Strike	Dip	
241	101.0336	-3.1571	7.8	75	325	13	44.5
242	100.9302	-3.0097	8.5	75	325	13	44.5
243	100.8267	-2.8622	8.5	75	325	13	44.5
244	100.7232	-2.7148	9.0	75	325	13	44.5
245	100.6198	-2.5674	9.0	75	325	13	44.5
246	100.5163	-2.4199	9.7	75	325	13	44.5
247	100.4129	-2.2725	11.8	75	325	13	44.5
248	100.3094	-2.1251	11.3	75	325	13	44.5
249	100.2060	-1.9776	11.2	75	325	13	44.5
250	100.1025	-1.8302	13.5	75	325	13	44.5
251	99.9991	-1.6828	11.9	75	325	13	44.5
252	99.8956	-1.5353	10.2	75	325	13	44.5
253	99.7922	-1.3879	10.0	75	325	13	44.5
254	99.6887	-1.2404	9.3	75	325	13	44.5
75	99.5853	-1.0930	9.9	75	325	13	44.5
256	99.4818	-0.9456	10.4	75	325	13	44.5
257	99.3784	-0.7981	11.1	75	325	13	44.5
258	99.2749	-0.6507	9.8	75	325	13	44.5
259	99.1715	-0.5033	6.8	75	325	13	44.5
260	99.0680	-0.3558	3.1	75	325	13	44.5
261	98.9646	-0.2084	0.6	75	325	13	44.5
262	102.0052	-4.2360	0.4	75	325	13	49.0
263	101.9017	-4.0886	1.2	75	325	13	49.0
264	101.7983	-3.9411	1.7	75	325	13	49.0
265	101.6948	-3.7937	2.4	75	325	13	49.0
266	101.5914	-3.6463	3.6	75	325	13	49.0
267	101.4879	-3.4988	4.3	75	325	13	49.0
268	101.3845	-3.3514	5.1	75	325	13	49.0
269	101.2810	-3.2040	6.3	75	325	13	49.0
270	101.1776	-3.0565	7.1	75	325	13	49.0
271	101.0741	-2.9091	7.2	75	325	13	49.0
272	100.9707	-2.7616	7.6	75	325	13	49.0
273	100.8672	-2.6142	8.4	75	325	13	49.0
274	100.7638	-2.4668	8.6	75	325	13	49.0
275	100.6603	-2.3193	9.8	75	325	13	49.0
276	100.5569	-2.1719	10.5	75	325	13	49.0
277	100.4534	-2.0245	11.2	75	325	13	49.0
278	100.3500	-1.8770	11.2	75	325	13	49.0
279	100.2465	-1.7296	13.5	75	325	13	49.0
280	100.1430	-1.5822	12.9	75	325	13	49.0

To be continued

Appendix A

Table 1: List of source parameters of Padang Scenario 2B (Source D.H.Natawidjaja)

The fault number of 280-320.

No	Geo-coordinates		Slip (m)	Angle Parameters (°)			Depth (km)
	Longitude	Latitude		Rake	Strike	Dip	
281	100.0396	-1.4347	11.1	75	325	13	49.0
282	99.9361	-1.2873	9.8	75	325	13	49.0
283	99.8327	-1.1399	8.6	75	325	13	49.0
284	99.7292	-0.9924	9.2	75	325	13	49.0
285	99.6258	-0.8450	9.8	75	325	13	49.0
286	99.5223	-0.6976	10.4	75	325	13	49.0
287	99.4189	-0.5501	9.8	75	325	13	49.0
288	99.3154	-0.4027	8.0	75	325	13	49.0
289	99.2120	-0.752	4.9	75	325	13	49.0
290	99.1085	-0.1078	2.5	75	325	13	49.0
291	102.1491	-4.1354	0.4	75	325	13	53.5
292	102.0457	-3.9880	1.1	75	325	13	53.5
293	101.9422	-3.8405	1.9	75	325	13	53.5
294	101.8388	-3.6931	2.6	75	325	13	53.5
295	101.7353	-3.5457	3.4	75	325	13	53.5
296	101.6319	-3.3982	4.1	75	325	13	53.5
297	101.5284	-3.2508	4.6	75	325	13	53.5
298	101.4250	-3.1034	5.1	75	325	13	53.5
299	101.3215	-2.9559	5.6	75	325	13	53.5
300	101.2181	-2.8085	5.8	75	325	13	53.5
301	101.1146	-2.6611	6.3	75	325	13	53.5
302	101.0112	-2.5136	7.2	75	325	13	53.5
303	100.9077	-2.3662	7.7	75	325	13	53.5
304	100.8043	-2.2188	8.7	75	325	13	53.5
305	100.7008	-2.0713	9.2	75	325	13	53.5
306	100.5974	-1.9239	9.2	75	325	13	53.5
307	100.4939	-1.7764	9.7	75	325	13	53.5
308	100.3905	-1.6290	11.7	75	325	13	53.5
309	100.2870	-1.4816	11.1	75	325	13	53.5
310	100.1836	-1.3341	9.8	75	325	13	53.5
311	100.0801	-1.1867	8.6	75	325	13	53.5
312	99.9767	-1.0393	7.4	75	325	13	53.5
313	99.8732	-0.8918	8.0	75	325	13	53.5
314	99.7697	-0.7444	8.6	75	325	13	53.5
315	99.6663	-0.5970	9.2	75	325	13	53.5
316	99.5628	-0.4495	9.2	75	325	13	53.5
317	99.4594	-0.3021	8.0	75	325	13	53.5
318	99.3559	-0.1547	6.1	75	325	13	53.5
319	99.2525	-0.0072	3.7	75	325	13	53.5
320	102.2931	-4.0348	0.5	75	325	13	58.0

To be continued

Appendix A

Table 1: List of source parameters of Padang Scenario 2B (Source D.H.Natawidjaja)

The fault number of 321-348.

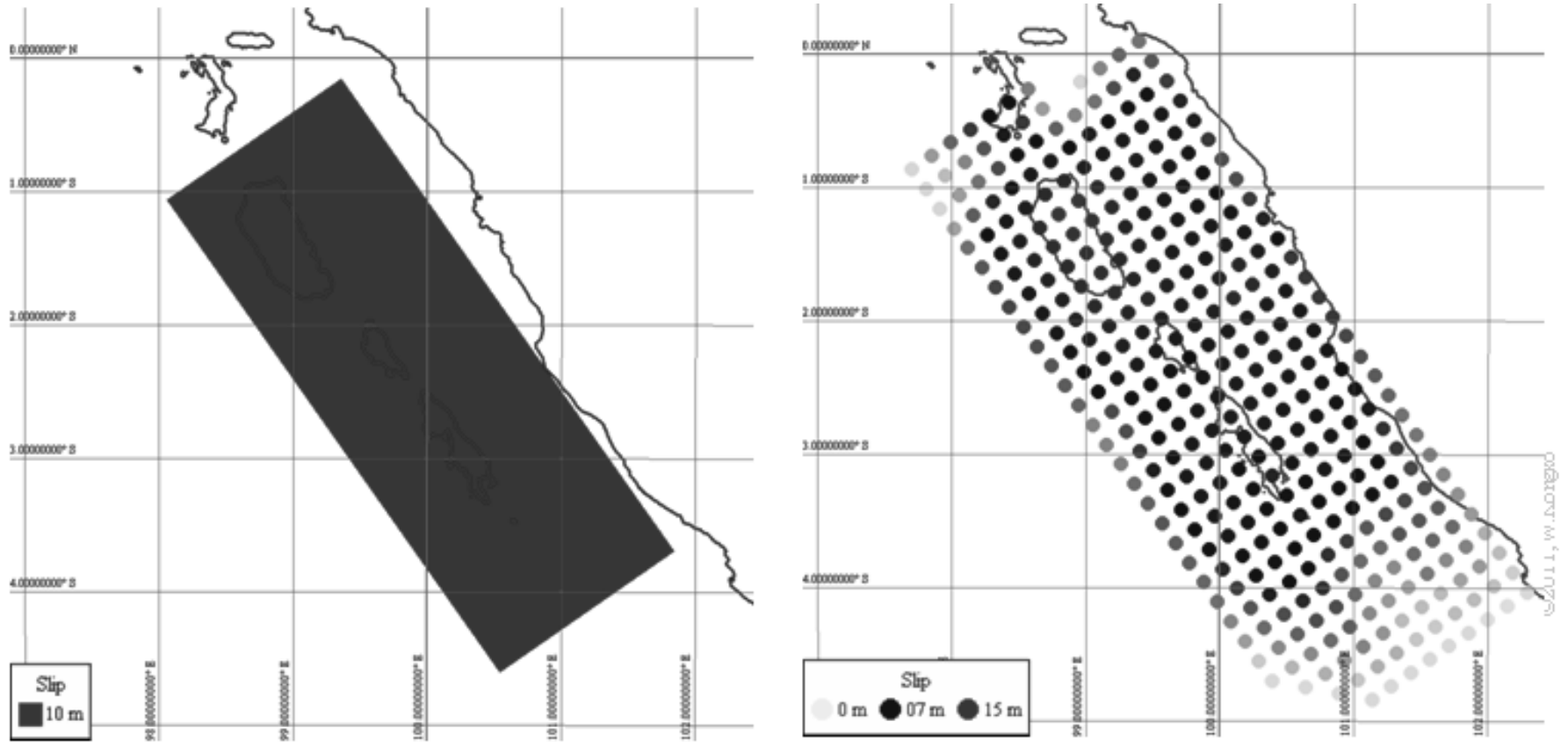
No	Geo-coordinates		Slip (m)	Angle Parameters (°)			Depth (km)
	Longitude	Latitude		Rake	Strike	Dip	
321	102.1896	-3.8874	0.8	75	325	13	58.0
322	102.0862	-3.7400	1.2	75	325	13	58.0
323	101.9827	-3.5925	1.5	75	325	13	58.0
324	101.8793	-3.4451	1.9	75	325	13	58.0
325	101.7758	-3.2976	2.1	75	325	13	58.0
326	101.6724	-3.1502	2.5	75	325	13	58.0
327	101.5689	-3.0028	2.7	75	325	13	58.0
328	101.4655	-2.8553	3.0	75	325	13	58.0
329	101.3620	-2.7079	3.1	75	325	13	58.0
330	101.2586	-2.5605	3.7	75	325	13	58.0
331	101.1551	-2.4130	4.1	75	325	13	58.0
332	101.0517	-2.2656	4.6	75	325	13	58.0
333	100.9482	-2.1182	5.1	75	325	13	58.0
334	100.8448	-1.9707	5.6	75	325	13	58.0
335	100.7413	-1.8233	5.6	75	325	13	58.0
336	100.6379	-1.6759	5.6	75	325	13	58.0
337	100.5344	-1.5284	5.6	75	325	13	58.0
338	100.4310	-1.3810	6.8	75	325	13	58.0
339	100.3275	-1.2335	6.1	75	325	13	58.0
340	100.2241	-1.0861	5.5	75	325	13	58.0
341	100.1206	-0.9387	4.9	75	325	13	58.0
342	100.0172	-0.7912	4.9	75	325	13	58.0
343	99.9137	-0.6438	5.6	75	325	13	58.0
344	99.8103	-0.4964	6.2	75	325	13	58.0
345	99.7068	-0.3489	6.1	75	325	13	58.0
346	99.6034	-0.2015	5.5	75	325	13	58.0
347	99.4999	-0.0541	4.3	75	325	13	58.0
348	99.3965	0.0934	3.1	75	325	13	58.0

Table 2: List of source parameters of Padang Single-fault

No	Geo-coordinates		Slip (m)	Angle Parameters (°)			Depth (km)
	Longitude	Latitude		Rake	Strike	Dip	
1	99.9480	-2.3786	10.0	75	325	13	8.5

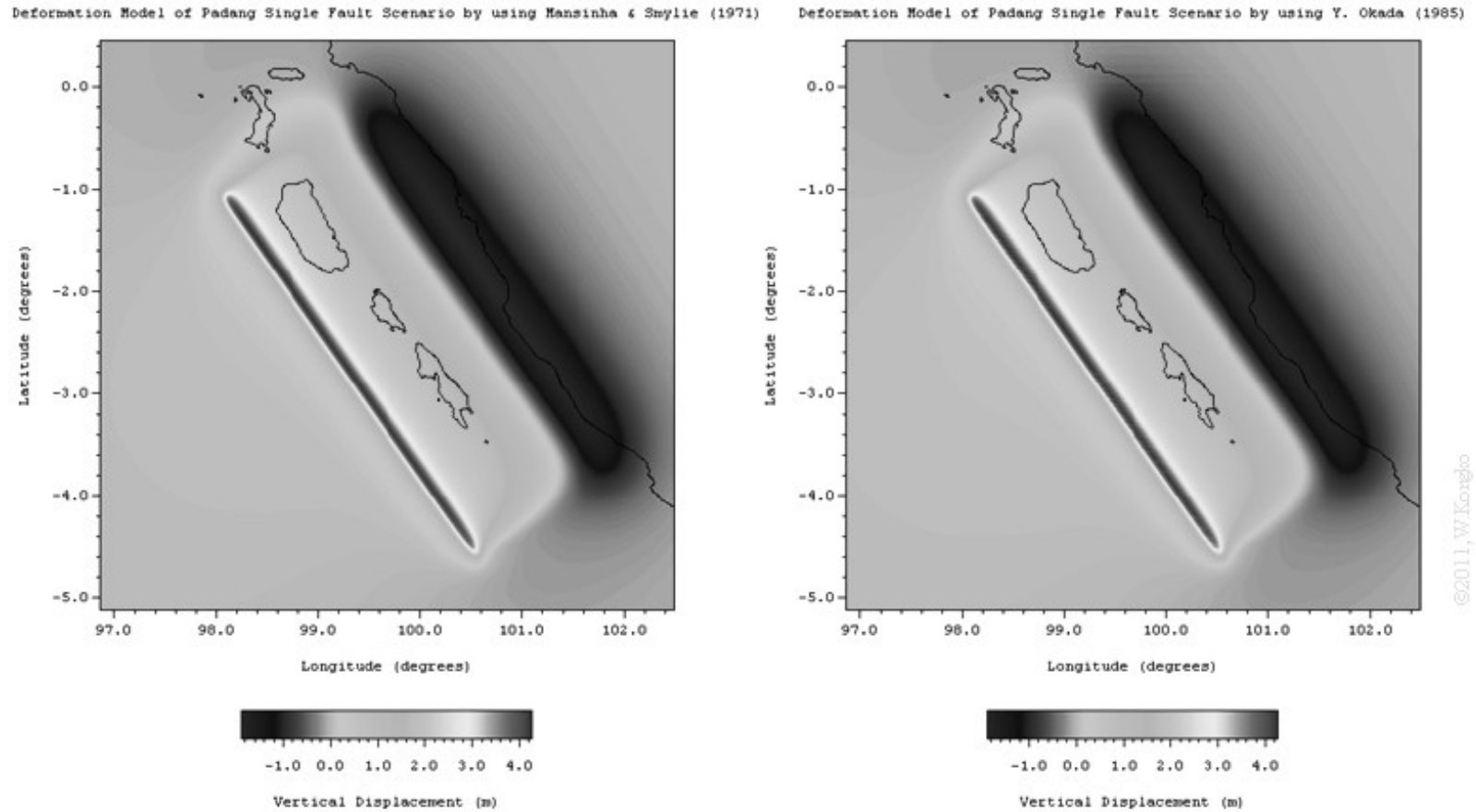
Appendix A

Figure 1: Source model of Padang: single-fault model (left) and multi fault model (right)



Appendix A

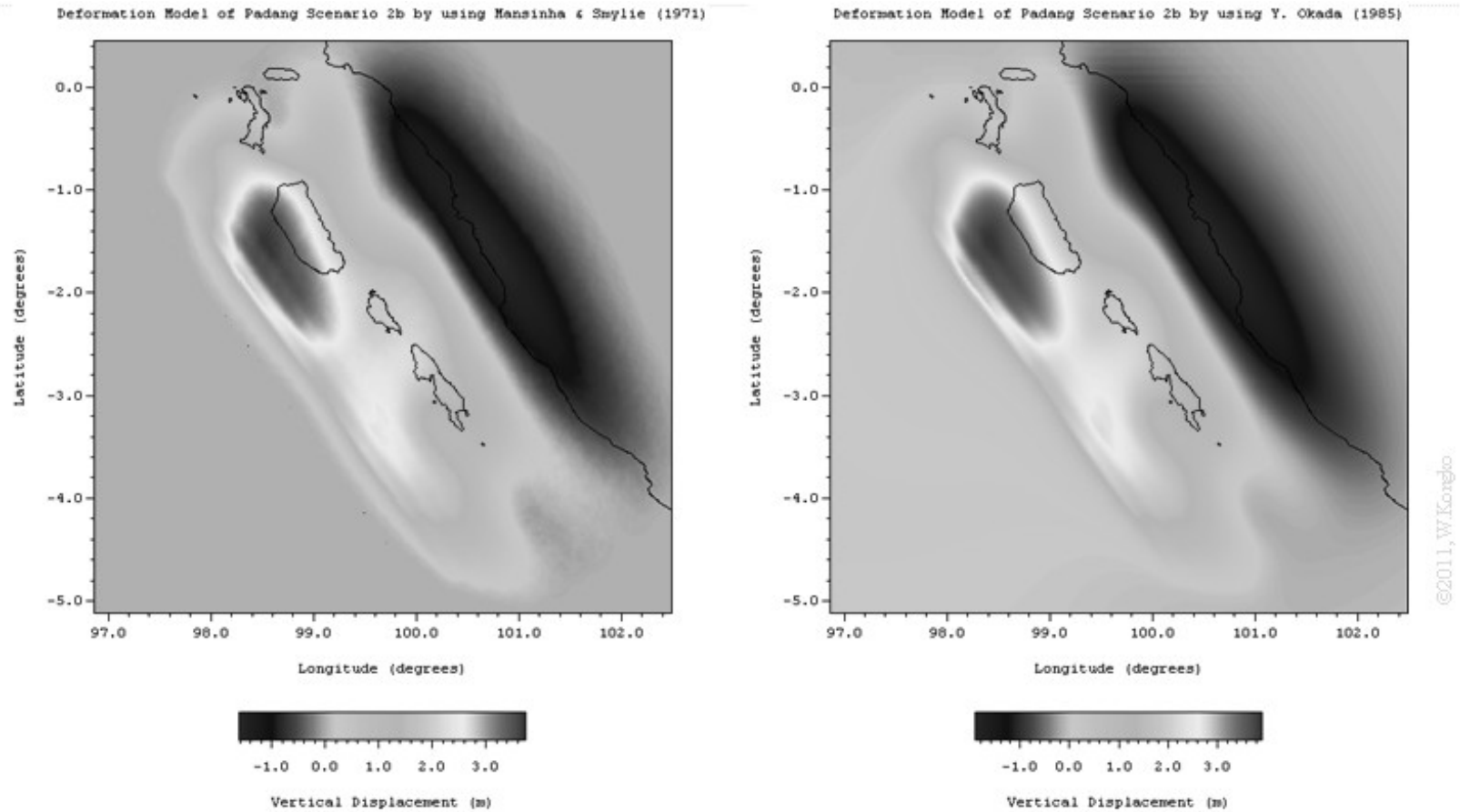
Figure 2: The comparison of deformation model by using M&S and Okada for single-fault model



Both deformation models above are compared by using the statistical method, namely the root mean squared deviation (RMSD) and normalized root mean squared deviation (NRMSD). The amount of data (n) is 260,604, RMSD is 0.05 m, NRMSD is 0.8%, maximum value is 4.25 m, and minimum value is -1.85 m.

Appendix A

Figure 3: The comparison of deformation model by using M&S and Okada for multi fault model



Both deformation models above are compared by using the statistical method, namely the root mean squared deviation (RMSD) and normalized root mean squared deviation (NRMSD). The amount of data (n) is 260,604, RMSD is 0.29 m, NRMSD is 5.2%, maximum value is 3.9 m, and minimum value is -1.6 m.

Appendix B – The scaling laws

Equation*	Slip Type†	Number of Events	Coefficients and Standard Errors		Standard Deviation <i>s</i>	Correlation Coefficient <i>r</i>	Magnitude Range	Length/Width Range (km)
			<i>a</i> (<i>sa</i>)	<i>b</i> (<i>sb</i>)				
$M = a + b * \log(\text{SRL})$	SS	43	5.16(0.13)	1.12(0.08)	0.28	0.91	5.6 to 8.1	1.3 to 432
	R	19	5.00(0.22)	1.22(0.16)	0.28	0.88	5.4 to 7.4	3.3 to 85
	N	15	4.86(0.34)	1.32(0.26)	0.34	0.81	5.2 to 7.3	2.5 to 41
	All	77	5.08(0.10)	1.16(0.07)	0.28	0.89	5.2 to 8.1	1.3 to 432
$\log(\text{SRL}) = a + b * M$	SS	43	-3.55(0.37)	0.74(0.05)	0.23	0.91	5.6 to 8.1	1.3 to 432
	R	19	-2.86(0.55)	0.63(0.08)	0.20	0.88	5.4 to 7.4	3.3 to 85
	N	15	-2.01(0.65)	0.50(0.10)	0.21	0.81	5.2 to 7.3	2.5 to 41
	All	77	-3.22(0.27)	0.69(0.04)	0.22	0.89	5.2 to 8.1	1.3 to 432
$M = a + b * \log(\text{RLD})$	SS	93	4.33(0.06)	1.49(0.05)	0.24	0.96	4.8 to 8.1	1.5 to 350
	R	50	4.49(0.11)	1.49(0.09)	0.26	0.93	4.8 to 7.6	1.1 to 80
	N	24	4.34(0.23)	1.54(0.18)	0.31	0.88	5.2 to 7.3	3.8 to 63
	All	167	4.38(0.06)	1.49(0.04)	0.26	0.94	4.8 to 8.1	1.1 to 350
$\log(\text{RLD}) = a + b * M$	SS	93	-2.57(0.12)	0.62(0.02)	0.15	0.96	4.8 to 8.1	1.5 to 350
	R	50	-2.42(0.21)	0.58(0.03)	0.16	0.93	4.8 to 7.6	1.1 to 80
	N	24	-1.88(0.37)	0.50(0.06)	0.17	0.88	5.2 to 7.3	3.8 to 63
	All	167	-2.44(0.11)	0.59(0.02)	0.16	0.94	4.8 to 8.1	1.1 to 350
$M = a + b * \log(\text{RW})$	SS	87	3.80(0.17)	2.59(0.18)	0.45	0.84	4.8 to 8.1	1.5 to 350
	R	43	4.37(0.16)	1.95(0.15)	0.32	0.90	4.8 to 7.6	1.1 to 80
	N	23	4.04(0.29)	2.11(0.28)	0.31	0.86	5.2 to 7.3	3.8 to 63
	All	153	4.06(0.11)	2.25(0.12)	0.41	0.84	4.8 to 8.1	1.1 to 350
$\log(\text{RW}) = a + b * M$	SS	87	-0.76(0.12)	0.27(0.02)	0.14	0.84	4.8 to 8.1	1.5 to 350
	R	43	-1.61(0.20)	0.41(0.03)	0.15	0.90	4.8 to 7.6	1.1 to 80
	N	23	-1.14(0.28)	0.35(0.05)	0.12	0.86	5.2 to 7.3	3.8 to 63
	All	153	-1.01(0.10)	0.32(0.02)	0.15	0.84	4.8 to 8.1	1.1 to 350
$M = a + b * \log(\text{RA})$	SS	83	3.98(0.07)	1.02(0.03)	0.23	0.96	4.8 to 7.9	3 to 5,184
	R	43	4.33(0.12)	0.90(0.05)	0.25	0.94	4.8 to 7.6	2.2 to 2,400
	N	22	3.93(0.23)	1.02(0.10)	0.25	0.92	5.2 to 7.3	19 to 900
	All	148	4.07(0.06)	0.98(0.03)	0.24	0.95	4.8 to 7.9	2.2 to 5,184
$\log(\text{RA}) = a + b * M$	SS	83	-3.42(0.18)	0.90(0.03)	0.22	0.96	4.8 to 7.9	3 to 5,184
	R	43	-3.99(0.36)	0.98(0.06)	0.26	0.94	4.8 to 7.6	2.2 to 2,400
	N	22	-2.87(0.50)	0.82(0.08)	0.22	0.92	5.2 to 7.3	19 to 900
	All	148	-3.49(0.16)	0.91(0.03)	0.24	0.95	4.8 to 7.9	2.2 to 5,184

*SRL—surface rupture length (km); RLD—subsurface rupture length (km); RW—down-dip rupture width (km), RA—rupture area (km²).

†SS—strike slip; R—reverse; N—normal.

©1994, Wells and Coppersmith

Appendix C – Field measurements

A. The 1th phase of bathymetry survey in Cilacap region

(Project's briefly info & technical specification)

1. Project's name	Bathymetry measurements in Indonesia, Part 2: Cilacap
2. Principal project	IFM Geomar, GITEWS, DHI
3. Objectives	<ul style="list-style-type: none"> • Mapping of topographical sea-floor of Cilacap near-shore region, • Implementing the shallow water mapping technology by using system of multi-beam of 180 kHz, • Implementing the high accuracy navigation technology of GPS RTK system.
4. Period of survey	9 – 25 of March, 2008
5. Location of survey (approx. boundaries)	Near-shore of Cilacap, Teluk Penyu bay outward until depths of approximately -25m, eastward until Serayu river.
6. Method of data acquisition	<ol style="list-style-type: none"> 1. <u>Position system</u>: GPS navigation, Inertial navigation of vessel (speed, position, rotation, pitching, rolling, yawing), Integrated navigation system of Octopus F180 (RTK), HYPACK navigation software. 2. <u>Echo-sounding</u>: Multi-beam system with angle 150°, ELAC SEABEAM 1050D (Freq.180 kHz, and so), HYDROSTAR acquisition software, Sound Velocity Profile (SVP) by using CTD48M. 3. <u>Reference point</u>: GPS RTK (real time kinematic) system, GPS in land pairing with F180 system in the vessel. 4. <u>Beam calibration</u>: Rolling, pitching, and yawing of vessel by using HYDROSTAR software for processing. 5. <u>Offset survey vessel</u>: Pre-installation process of equipments in the vessel, based on the vessel dimensions. Installation the transducer, GPS antennas, and altitude reference. 6. <u>Data analysis</u>: Data filtering by using HDPedit software, data correction from errors due to offset, tide, and SVP, Plotting the result by using HDPpost software and finally produces the xyz data format.
7. Photo gallery (very selected pictures):	<p>The followings are the selected pictures that have been taken during the uploading equipment to the survey vessel, when assembling and installation transducer, and the sampling data activities (continued to next page).</p>

Photo gallery of the 1st phase of bathymetry survey (continuing from preceding page)



A7.1 Survey equipments unloading at vessel



A7.2 GPS RTK measurement



A7.3 Transducer system assembling



A7.4 Mounting the F180 at portside-hull



A7.5 Navigation & Acquisition PC system



A7.6 Sampling of SVP during cruise/survey

Note: The detail information is provided in the technical report of survey (Kongko & Leschka, 2009).

Appendix C

B. The 2nd phase of bathymetry survey in Cilacap region

(Project's briefly info & technical specification)

1. Project's name	Bathymetry survey of Cilacap, phase 2
2. Principal project	GITEWS, BPPT
3. Objectives	<ul style="list-style-type: none"> • Measuring topographical sea-floor of Cilacap near-shore region, rivers, channels, port surroundings, and the area that was not covered in the previous work (in general water depth < 5m), • Implementing the simple technology of depth-finder of GPSMAP 178C Garmin.
4. Period of survey	20 – 24 of November, 2008
5. Location of survey (approx. boundaries)	Teluk Penyu bay of Cilacap less than 2 km from the coastline, in the rivers, main city channels, and port & surroundings.
6. Method of data acquisition	<ol style="list-style-type: none"> 1. <u>Position system</u>: GPS navigation system GPSMAP 178C (RTCM 104). 2. <u>Echo-sounding</u>: Single-beam transducer mounted at portside hull using frequency of 50/200 kHz. 3. <u>Reference point</u>: No GPS RTK (real time kinematic) system. 4. <u>Beam calibration</u>: No rolling, pitching, and yawing of vessel correction. 5. <u>Data analysis</u>: Data filtering by neglecting the spike data, data correction from errors due to tide. Plotting the result by using Mapsource of Garmin software and finally produces the xyz data format.
7. Photo gallery:	 <p style="text-align: center;">B7.1 Small boat for bathymetry survey</p>

Note: The detail information is provided in the technical report of survey (Ahmad & Kongko, 2008).

Appendix C

C. The 3rd phase of bathymetry survey in Cilacap region

(Project's briefly info & technical specification)

1. Project's name	Bathymetry survey of Cilacap, phase 3
2. Principal project	GITEWS, BPPT
3. Objectives	<ul style="list-style-type: none"> • Measuring topographical sea-floor of Cilacap near-shore region, especially the area off Permisian-Nusakambangan Cilacap, • Implementing the simple technology of depth-finder of GPSMAP 178C Garmin.
4. Period of survey	21 – 29 of July, 2009
5. Location of survey (approx. boundaries)	Area off Permisian-Nusakambangan Cilacap until 5 km, and 2 km to the east and west, so that within the area of 20 sq.km.
6. Method of data acquisition	<ol style="list-style-type: none"> 1. <u>Position system</u>: GPS navigation system GPSMAP 178C (RTCM 104). 2. <u>Echo-sounding</u>: Single-beam transducer mounted at portside hull using frequency of 50/200 kHz. 3. <u>Reference point</u>: No GPS RTK (real time kinematic) system. 4. <u>Beam calibration</u>: No rolling, pitching, and yawing of vessel correction. 5. <u>Data analysis</u>: Data filtering by neglecting the spike data, data correction from errors due to tide. Plotting the result by using Mapsource of Garmin software and finally produces the xyz data format.
7. Photo gallery:	 <p style="text-align: center;">C7.1 Boat measuring bathymetry in the channel</p>

Note: The detail information is provided in the technical report of survey (Ahmad & Harmiawan, 2009).

Appendix C

D. The 3rd phase of topography & ground check survey in Permisan- Cilacap

(Project's briefly info & technical specification)

1. Project's name	Topography & Ground-check survey of Cilacap, phase 3
2. Principal project	GITEWS, BPPT
3. Objectives	<ul style="list-style-type: none"> • Measuring the ground level at Permisan-Nusakambangan Cilacap, • Ground check the tsunami run-up points and collect the ground features (land cover, ground steepness, etc).
4. Period of survey	22 – 29 of July, 2009
5. Location of survey (approx. boundaries)	Within the area of Permisan-Nusakambangan Cilacap (the valley that surrounded by hills with area of about 1.5 sq. km.
6. Method of data acquisition	<ol style="list-style-type: none"> 1. <u>Topography survey</u>: Total Station set of Topcon GTS 233S, Tripod, reflector-prism, measuring tape, leveling staff, etc; measuring the ground level from coastline to inland with transect-fashion. Each data set to be referenced to the mean sea level (MSL) hourly. The ground level measurement first is using local coordinates. The data set then converted to UTM coordinates reference and corrected with the DGPS system that its fixed station is located in Cilacap city. 2. <u>Ground-check</u>: Handheld GPS Etrex Vista HCx Garmin; re-routing the points of the 2006 tsunami run-up by using GPS, marking the locations, and recording the ground features.
7. Photo gallery:	<p>The followings are the selected pictures that have been taken during the topography survey and ground-checking the points of the 2006 tsunami run-up heights in Permisan-Nusakambangan, Cilacap.</p> <div style="display: flex; justify-content: space-around;"> <div style="text-align: center;">  <p>D7.1 Surveyor and his assistant are measuring the ground level by using Total Station</p> </div> <div style="text-align: center;">  <p>D7.2 The one of the 2006 tsunami run-up point in the valley in front of the hill</p> </div> </div>
(Continued to next page)	

Photo gallery of the 3rd phase of topography & ground-check survey (continuing from preceding page)



D7.3 Re-marking of the 2006 tsunami run-up in the steep slope hill



D7.4 Re-marking of the 2006 tsunami flow-depth near to the tree/bush



D7.5 Re-marking of the 2006 tsunami run-up in the steep slope cliff



D7.6 The tsunami run-up climbing the hills and reached the sewer system in the prison area

Note: The detail information is provided in the technical report of survey (Ahmad et al., 2009).

Appendix C

E. The 4th phase of the 2006 tsunami run-up survey in Cilacap

(Project's summary)

1. Project's name	The 2006 Java tsunami run-up survey in Cilacap, phase 4
2. Principal project	GITEWS, BPPT
3. Objectives	<ul style="list-style-type: none"> • Collecting the points of maximum inundation of the 2006 Java tsunami through interview, • Collecting the relevant data related to the 2006 Java tsunami, such as time arrival, wave counts, directions, land covers, etc.
4. Period of survey	16 – 17 of April, 2010
5. Location of survey (approx. boundaries)	Two areas: riverside of Serayu & low-land of Widarapayung, and eastern part of Cilacap, all include 11 villages, where experiencing the 2006 Java tsunami.
6. Method of data acquisition	<ol style="list-style-type: none"> 1. <u>Interview</u>: blind-cross interviews of the survivors in the affected area of the 2006 Java tsunami. The questions list; the respondent's data, respondent response & perception during the event, the maximum points of tsunami, time arrival, wave counts, wave direction, 2. <u>Marking/collecting</u>: using handheld GPS marking the points of interest positions, collecting the land cover data / vegetation's type, rivers/channels if available, infrastructures damage, etc.

7. Photo gallery:

The followings are the selected pictures that have been taken during the survey:



E7.1 Interview survivor/farmer at Jetis village (W137), one of the maximum run-up points



E7.2 Pilot project of public housings of "tsunami-proof" (W14)

(Continued to next page)

Photo gallery of the 4th phase of the 2006 Java tsunami run-up (continuing from preceding page)



E7.3 Evacuation route signature at Widarapayung (W144)



E7.4 Interview survivor/farmer in the low-land of riverside Serayu W158)

Appendix D – Observation data

A. Historical earthquake (1977-2007), MS > 5.0, depth < 40 km (ITDB/WLD, 2007), (List number of 1-60)

No	Time						Epicenter		Depth (km)	Ms	No	Time						Epicenter		Depth (km)	Ms
	Year	Mon	Day	Hour	Min	Sec	Lat	Lon				Year	Mon	Day	Hour	Min	Sec	Lat	Lon		
1	1977	1	29	0	0	0	-9.2	111.24	33	5	31	1982	10	29	0	0	0	-8.09	107.18	33	5.1
2	1977	8	14	0	0	0	-7.76	107.56	33	5.6	32	1983	1	25	0	0	0	-6.33	104.06	33	5
3	1977	9	7	0	0	0	-10.07	115.51	33	5	33	1983	2	20	0	0	0	-9.5	108.24	33	5
4	1977	9	14	0	0	0	-10.98	113.48	24	5.3	34	1983	2	26	0	0	0	-11.21	115.56	33	5
5	1977	1	26	0	0	0	-8.21	115.19	33	5.1	35	1983	3	5	0	0	0	-10.73	115.03	33	5.3
6	1978	9	2	0	0	0	-5.83	105.55	33	5.1	36	1983	5	2	0	0	0	-8.66	106.35	33	5.3
7	1978	9	12	0	0	0	-7.76	106.8	33	5.1	37	1983	7	29	0	0	0	-6.72	105.59	33	5.4
8	1978	5	30	0	0	0	-8.29	106.16	33	5	38	1983	9	29	0	0	0	-11.17	115.37	33	5.5
9	1979	4	29	0	0	0	-7.84	104.97	35	5	39	1983	10	2	0	0	0	-8.14	105.54	33	5
10	1979	5	14	0	0	0	-7.66	111.19	37	5	40	1983	10	18	0	0	0	-11.52	115.2	9	5.4
11	1979	5	21	16	31	0	-8.2	115.9	33	5.3	41	1983	10	20	0	0	0	-11.87	115.03	33	5
12	1979	5	30	0	0	0	-8.2	115.94	25	6	42	1983	11	15	0	0	0	-11.28	115.32	33	5.4
13	1979	6	21	0	0	0	-8.44	115.9	33	5	43	1983	12	1	0	0	0	-9.47	115.22	33	5
14	1979	7	24	0	0	0	-11.14	107.7	31	6.9	44	1984	1	26	0	0	0	-9.41	112.93	33	5.1
15	1979	10	10	0	0	0	-7.21	106.03	33	5.9	45	1984	2	2	0	0	0	-9.9	115.05	33	5.4
16	1979	10	20	0	0	0	-8.25	115.84	38	6.1	46	1984	4	6	0	0	0	-10.46	110.59	33	5
17	1979	10	20	1	41	0	-8.3	116	33	6.3	47	1984	6	8	0	0	0	-9.78	114.21	33	5
18	1979	12	17	0	0	0	-8.39	115.88	33	6.3	48	1984	6	8	0	0	0	-5.79	104.16	33	6
19	1979	12	17	19	58	0	-8.4	115.9	33	6.6	49	1984	7	21	0	0	0	-8.21	106.22	33	5.1
20	1980	7	23	0	0	0	-7.56	106.38	33	5.3	50	1984	8	3	0	0	0	-7.85	114.75	38	5
21	1980	8	13	0	0	0	-7.87	112.05	33	5	51	1984	8	11	0	0	0	-11.04	113.74	33	5.3
22	1980	3	20	0	0	0	-7.03	106.16	33	5.3	52	1984	8	19	0	0	0	-8.51	106.14	33	5
23	1981	3	1	0	0	0	-9.45	107.74	33	5	53	1984	8	19	0	0	0	-8.49	106.15	33	5.1
24	1981	10	23	0	0	0	-8.78	106.44	33	5.5	54	1984	10	3	0	0	0	-6	105.65	33	5
25	1981	10	23	0	0	0	-8.81	106.45	33	5.6	55	1984	11	20	0	0	0	-7.55	106.52	33	5.1
26	1981	2	5	0	0	0	-10.68	107.96	33	5.6	56	1985	1	22	0	0	0	-5.9	104.56	33	5.5
27	1982	2	10	0	0	0	-6.86	106.93	39	5.5	57	1985	1	31	0	0	0	-6.49	104.26	33	5
28	1982	3	22	0	0	0	-8.63	106	34	5	58	1985	2	2	0	0	0	-10.56	114.96	33	5.3
29	1982	7	23	0	0	0	-10.79	111.71	34	5.1	59	1985	2	16	0	0	0	-8.53	115.75	33	5.1
30	1982	8	7	0	0	0	-11.14	115.41	33	6.4	60	1985	3	15	0	0	0	-10.09	111.98	33	5

A. Historical earthquake (1977-2007), MS > 5.0, depth < 40 km (ITDB/WLD, 2007) (Continuing from preceding page)

(List number of 61-120)

No	Time						Epicenter		Depth	Ms	No	Time						Epicenter		Depth	Ms
	Year	Mon	Day	Hour	Min	Sec	Lat	Lon	(km)			Year	Mon	Day	Hour	Min	Sec	Lat	Lon	(km)	
61	1985	4	2	0	0	0	-7.76	107.97	33	5.1	91	1988	6	25	0	0	0	-8.71	106.34	33	5
62	1985	4	23	0	0	0	-8.74	111.33	33	5.4	92	1988	7	14	0	0	0	-8.48	112.59	33	5.3
63	1985	4	28	0	0	0	-9.1	112.01	33	5	93	1988	8	17	0	0	0	-7.69	107.15	27	6
64	1985	6	5	0	0	0	-7.3	104.82	33	5.1	94	1988	10	9	0	0	0	-9.67	108.75	25	5.1
65	1985	8	9	0	0	0	-5.43	104.82	33	5	95	1988	12	30	0	0	0	-8.71	106.12	28	5
66	1985	9	9	0	0	0	-9.78	114.1	33	5.1	96	1988	1	28	0	0	0	-11.47	114.79	33	5
67	1985	9	11	0	0	0	-11.14	112.21	33	5	97	1989	3	8	0	0	0	-6.01	105.36	33	5.3
68	1985	10	1	0	0	0	-11.55	114.79	33	5.1	98	1989	6	7	0	0	0	-8.95	106.54	33	5
69	1985	10	25	0	0	0	-9.2	105.59	10	5.4	99	1989	6	17	0	0	0	-9.64	108.87	28	5
70	1985	11	20	0	0	0	-10.44	111.81	33	5	100	1989	8	4	0	0	0	-6.83	106.12	33	5.1
71	1985	12	27	0	0	0	-5.76	104.19	24	6.5	101	1989	9	12	0	0	0	-9.01	110.5	33	5.3
72	1985	12	28	0	0	0	-5.8	104.28	33	6	102	1989	10	31	0	0	0	-9.3	112.05	33	5.4
73	1985	12	29	0	0	0	-5.94	104.23	33	5.3	103	1989	10	31	0	0	0	-9.21	111.96	33	5.3
74	1985	12	31	0	0	0	-5.77	104.29	33	5	104	1989	11	17	0	0	0	-8.7	106.35	23	5
75	1986	3	20	0	0	0	-6.1	105.33	33	5	105	1990	1	5	0	0	0	-8.8	106.44	29	5.8
76	1986	5	12	0	0	0	-6.96	112.01	33	5	106	1990	3	26	0	0	0	-5.66	112.87	33	5
77	1986	5	22	0	0	0	-8.21	105.61	21	5	107	1990	4	6	0	0	0	-6.81	105.14	33	5.5
78	1986	9	14	0	0	0	-6.07	105.52	33	5	108	1990	4	10	0	0	0	-10.52	109.59	39	5.3
79	1986	2	5	0	0	0	-5.84	104.27	33	5	109	1990	4	13	0	0	0	-7.12	106.69	33	5
80	1987	2	26	0	0	0	-6.11	104.76	33	5.1	110	1990	5	21	0	0	0	-8.13	109.04	27	5.5
81	1987	3	2	0	0	0	-6.71	104.6	33	5	111	1990	6	18	0	0	0	-8.81	111.23	33	5
82	1987	7	1	0	0	0	-9.19	107.06	30	5	112	1990	7	4	0	0	0	-10.96	110.01	33	5.1
83	1987	8	10	0	0	0	-6.21	104.88	33	5.4	113	1990	7	6	0	16	0	-6.9	108.1	14	5.8
84	1987	10	9	0	0	0	-7.87	105.25	30	5.5	114	1990	7	6	0	16	0	-6.9	108.12	13	5.8
85	1987	10	22	0	0	0	-5.72	104.23	22	5.1	115	1990	7	15	0	0	0	-6.58	104.99	33	5
86	1987	11	5	0	0	0	-5.96	105.53	33	5	116	1990	8	26	0	0	0	-9.19	110.76	33	5.3
87	1987	11	10	0	0	0	-5.64	113.35	34	5	117	1990	8	26	0	0	0	-9.15	110.76	33	5.3
88	1987	12	14	0	0	0	-9.49	108.22	33	5.4	118	1990	12	9	0	0	0	-8.67	110.58	33	5
89	1988	4	5	0	0	0	-6.73	105.47	33	5	119	1991	1	30	0	0	0	-7.31	106.72	33	5
90	1988	6	25	0	0	0	-8.84	106.25	32	5	120	1991	2	20	0	0	0	-8.57	108.56	33	5

A. Historical earthquake (1977-2007), MS > 5.0, depth < 40 km (ITDB/WLD, 2007) (Continuing from preceding page)

(List number of 121-180)

No	Time						Epicenter		Depth (km)	Ms	No	Time						Epicenter		Depth (km)	Ms
	Year	Mon	Day	Hour	Min	Sec	Lat	Lon				Year	Mon	Day	Hour	Min	Sec	Lat	Lon		
121	1991	2	22	0	0	0	-10.16	113.68	33	5.1	151	1994	6	4	5	54	29	-10.57	113.19	32	5.4
122	1991	3	11	0	0	0	-9.49	115.63	33	5.4	152	1994	6	4	11	18	53	-10.79	113.34	30	5.2
123	1991	6	2	0	0	0	-8.6	111.39	33	5	153	1994	6	4	11	36	36	-10.83	113.22	34	5.6
124	1991	6	7	0	0	0	-9.16	114.12	33	5	154	1994	6	4	12	4	28	-10.7	113.56	28	5.7
125	1991	6	21	0	0	0	-6.01	104.85	33	5.5	155	1994	6	4	14	57	60	-10.56	112.89	33	5.4
126	1991	6	28	0	0	0	-6.64	105.46	33	5.4	156	1994	6	5	1	45	2.2	-10.35	113.4	25	6.1
127	1991	7	5	0	0	0	-9.64	114.59	33	5.8	157	1994	6	4	20	9	35	-10.83	113.2	30	5.7
128	1993	10	13	7	8	36	-8.44	106.82	33	5.1	158	1994	6	5	5	32	34	-10.83	113.45	39	5.2
129	1993	9	11	2	2	19	-8.82	106.21	33	5	159	1994	6	5	5	56	45	-10.72	113.49	33	5.6
130	1994	6	3	21	59	45	-10.54	113.01	33	5.3	160	1994	6	5	6	20	59	-10.02	112.88	32	5.4
131	1994	3	16	0	2	36.2	-7.15	108.54	33	5	161	1994	6	5	17	51	57	-10.65	112.65	39	5.6
132	1994	4	26	4	29	20.9	-9.5	112.88	33	5.2	162	1994	6	5	18	30	15	-10.68	112.42	35	5.2
133	1994	4	26	9	16	49.6	-9.43	112.95	33	5.2	163	1994	6	5	20	11	14	-10.27	114.15	33	5.1
134	1994	7	18	5	24	21.3	-9.74	112.49	33	5.4	164	1994	6	6	1	8	31	-10.81	113.32	34	5.5
135	1994	6	2	18	17	34	-10.48	112.83	18	7.8	165	1994	6	6	2	23	34	-10.93	112.49	33	5
136	1994	6	3	2	55	17.5	-10.35	112.77	23	5.1	166	1994	6	6	2	18	37	-10.52	113.41	21	5.1
137	1994	6	3	10	14	39.4	-10.98	112.74	33	5.1	167	1994	6	6	5	32	55	-10.59	112.62	20	5.5
138	1994	6	3	5	10	7.6	-10.22	113.51	33	5	168	1994	6	6	6	20	21	-11.08	113.08	33	5.2
139	1994	6	3	12	33	22.7	-10.49	113.08	33	5.4	169	1994	6	6	7	40	37	-11	113.2	38	5.3
140	1994	6	3	13	39	24.3	-9.42	114.33	33	5.4	170	1994	6	6	10	14	11	-10.66	112.56	35	5.3
141	1994	6	3	15	18	35.9	-11.74	111.88	33	5.1	171	1994	6	6	12	14	14	-11.03	112.61	33	5
142	1994	6	3	18	54	46.7	-10.66	113.02	33	5.1	172	1994	6	7	4	42	53	-9.66	113.07	33	5.2
143	1994	6	3	16	33	10.5	-9.44	113.04	28	5.3	173	1994	6	8	19	19	58	-10.64	112.67	37	5.1
144	1994	6	3	21	6	59.9	-10.36	112.89	25	6.6	174	1994	6	7	22	0	4.6	-11.07	113.12	33	5.4
145	1994	6	3	21	19	50.1	-10.55	112.87	33	5.3	175	1994	6	9	16	37	47	-10.14	113.62	33	5.8
146	1994	6	3	21	57	30	-10.56	112.8	33	5.2	176	1994	6	10	1	16	50	-11.09	113.15	33	5
147	1994	6	3	23	2	0.6	-10.4	113.59	23	5.6	177	1994	6	10	19	11	17	-10.39	112.73	28	5.3
148	1994	4	26	8	37	47.5	-9.44	113.01	33	5	178	1994	6	10	19	17	52	-10.29	113.5	33	5.4
149	1994	6	3	23	42	31.1	-10.47	112.81	32	5.5	179	1994	6	11	21	59	23	-10.62	112.68	33	5.1
150	1994	6	4	0	57	50.7	-10.78	113.37	11	6.5	180	1994	6	12	1	35	21	-10.46	112.83	33	5.2

A. Historical earthquake (1977-2007), MS > 5.0, depth < 40 km (ITDB/WLD, 2007) (Continuing from preceding page)

(List number of 181-240)

No	Time						Epicenter		Depth	Ms	No	Time						Epicenter		Depth	Ms
	Year	Mon	Day	Hour	Min	Sec	Lat	Lon	(km)			Year	Mon	Day	Hour	Min	Sec	Lat	Lon	(km)	
181	1994	6	12	1	47	19.2	-10.57	112.78	33	5.3	211	1994	7	18	16	33	60	-9.59	112.94	33	5.6
182	1994	6	12	8	3	23.5	-10.83	112.06	33	5	212	1994	7	21	15	52	44	-9.66	112.84	23	5.3
183	1994	6	12	2	14	42.1	-10.84	112.99	33	5.1	213	1994	7	24	21	57	27	-10.65	113.27	34	6
184	1994	6	12	13	53	7.6	-10.61	112.6	34	5.3	214	1994	7	25	0	45	31	-11.06	113.05	10	5
185	1994	6	13	6	49	31.2	-10.77	113.63	27	5	215	1994	7	26	1	46	33	-10.26	113.59	33	5.7
186	1994	6	13	21	4	9.4	-10.28	113.49	23	5.7	216	1994	8	4	1	9	36	-9.86	112.71	23	5.1
187	1994	6	13	21	50	54.7	-10.8	112.89	33	5.1	217	1994	8	6	13	15	31	-10.92	113.6	33	5.4
188	1994	6	13	21	10	6.2	-10.23	113.57	33	5.8	218	1994	8	24	8	53	49	-10.94	112.89	33	5.2
189	1994	6	13	22	48	27.5	-10.33	113.62	25	5.6	219	1994	8	31	12	17	55	-6.74	104.28	33	5
190	1994	6	14	1	48	18.8	-10.55	113.39	30	5.1	220	1994	9	7	18	48	25	-10.7	113.44	33	5
191	1994	6	14	14	54	55.6	-10.53	113.44	25	5.1	221	1994	9	12	11	30	15	-8.91	106.48	33	5.9
192	1994	6	14	2	35	27.9	-10.68	113.31	32	5.1	222	1994	10	4	12	9	40	-6.22	104.89	24	5.6
193	1994	6	14	15	20	51.2	-10.51	113.48	27	5.2	223	1994	11	23	20	42	21	-9.22	106.79	33	5.4
194	1994	6	14	16	0	41.9	-10.49	113.51	33	5.1	224	1995	2	24	6	24	6.8	-8.11	105.72	38	5.1
195	1994	6	15	9	22	57.2	-10.34	113.66	19	6.2	225	1995	5	16	8	40	46	-8.61	106.01	31	5.2
196	1994	6	15	6	18	45.1	-9.44	113.07	28	5.1	226	1996	9	25	21	16	9.7	-9.3	108.72	33	5.7
197	1994	6	15	10	28	50.6	-10.17	113.75	28	6.1	227	1996	11	6	17	4	34	-7.76	106.98	33	5.4
198	1994	6	15	12	10	56.5	-10.5	113.44	24	5.2	228	1996	7	20	23	44	35	-8.65	114.68	33	5.1
199	1994	6	15	13	53	53.1	-10.38	112.44	31	5	229	1996	12	3	21	22	57	-9.79	108.27	33	5.1
200	1994	6	16	12	48	45.7	-10.65	113.47	33	5	230	1997	7	10	13	10	48	-10.75	113.72	33	5.3
201	1994	6	19	3	20	46.2	-9.47	112.76	33	5.3	231	1997	1	10	18	32	42	-5.89	105.58	33	5
202	1994	6	19	12	57	1.3	-10.35	113.48	33	5.3	232	1997	3	17	8	5	48	-6.61	105.51	33	6.4
203	1994	6	19	13	50	38.1	-10.6	113.48	19	5.1	233	1997	7	12	22	49	17	-9.05	110.53	33	5.3
204	1994	6	22	19	11	54.6	-10.56	112.64	33	5.1	234	1998	5	24	2	24	52	-6.54	104.79	33	5.2
205	1994	6	26	6	14	36.3	-10.77	113.31	33	5	235	1998	8	15	3	30	46	-5.93	105.41	33	5
206	1994	6	27	3	33	16.8	-11.02	113.69	33	5.1	236	1998	11	29	22	17	59	-6.18	105.4	33	5
207	1994	6	28	14	45	17.4	-10.85	112.64	33	5.1	237	1998	2	6	21	55	29	-6.01	105.52	33	5
208	1994	7	9	4	48	31	-11.08	112.5	33	5.1	238	1998	12	11	12	53	16	-5.9	104.26	33	5.2
209	1994	7	12	22	40	24.5	-6.2	105.44	33	5	239	1999	9	5	20	57	49	-8.95	106.61	33	5.3
210	1994	6	15	9	50	23	-10.15	113.69	28	5.5	240	1999	2	1	16	35	31	-6.47	104.72	33	5.2

A. Historical earthquake (1977-2007), MS > 5.0, depth < 40 km (ITDB/WLD, 2007) (Continuing from preceding page)

(List number of 241-300)

No	Time						Epicenter		Depth (km)	Ms	No	Time						Epicenter		Depth (km)	Ms
	Year	Mon	Day	Hour	Min	Sec	Lat	Lon				Year	Mon	Day	Hour	Min	Sec	Lat	Lon		
241	1999	2	3	6	35	56.7	-6.19	104.22	33	5.8	271	2002	8	26	14	55	10	-6.72	105.68	33	5.8
242	1999	2	23	5	46	1.5	-8.97	112.67	33	5	272	2002	9	5	0	14	40	-6.23	104.89	33	5.3
243	1999	3	27	8	3	45.1	-9.68	112.79	33	5.7	273	2002	11	29	20	4	48	-5.65	104.04	33	5.2
244	1999	5	24	5	2	48.4	-9.91	109.15	33	5	274	2003	11	24	23	53	57	-7.54	106.26	33	5.2
245	1999	7	13	15	52	46.6	-7.09	107.09	33	5.2	275	2003	6	1	4	39	21	-9.53	108.37	33	5.2
246	1999	8	11	15	28	30.1	-6.01	105.41	33	5.1	276	2003	8	25	22	17	16	-8.94	113.15	33	5.3
247	1999	11	5	17	4	2.1	-11.29	114.31	33	5.3	277	2003	11	20	12	24	33	-10.01	111.03	10	5.8
248	2000	1	15	2	11	58.5	-9.58	111.76	34	5	278	2003	12	3	12	4	4.2	-6.96	106.27	33	5.1
249	2000	3	10	16	22	46.7	-8.68	106.4	33	5.5	279	2004	9	25	16	4	7.1	-7.69	107.97	10	5
250	2000	6	5	17	43	23.9	-7.36	106.65	33	5	280	2004	1	1	20	59	31	-8.31	115.8	33	5.8
251	2000	7	12	1	10	42.2	-6.59	106.71	33	5.2	281	2004	1	13	20	4	25	-8.57	105.88	33	5.2
252	2000	7	31	18	59	42	-6.72	105.44	33	5.1	282	2004	4	2	21	43	48	-6.07	104.03	34	5.2
253	2000	10	25	9	32	23.9	-6.55	105.63	38	6.8	283	2004	11	3	3	7	45	-10.71	112.68	11	5.1
254	2000	1	5	18	26	7.5	-9.19	109.59	33	5.8	284	2005	4	15	4	17	51	-6.08	104.75	26	5.4
255	2000	10	25	17	42	22.6	-7.46	107.82	33	5.3	285	2005	10	3	23	30	29	-7.89	107.03	35	5
256	2001	6	28	3	46	28.1	-6.99	108.28	36	5	286	2005	3	2	1	49	8.4	-9.26	115.28	30	5.3
257	2001	1	4	3	50	11.3	-8.4	108.37	33	5.3	287	2005	10	10	10	55	48	-6.88	105.46	30	5.2
258	2001	1	7	12	55	46.7	-8.7	108.89	33	5.5	288	2006	2	26	13	39	56	-8.66	105.97	34	5.1
259	2001	2	16	23	38	3.7	-6.08	104.68	33	5	289	2006	2	13	10	46	5	-6.35	104.8	31	5.1
260	2001	3	5	21	24	49.2	-9.76	108.82	33	5.1	290	2006	2	20	17	54	6.8	-9.75	107.1	35	5
261	2001	3	12	23	35	8.3	-7.21	106.12	33	5.8	291	2006	3	16	5	43	10	-7.36	106.71	23	5.2
262	2001	3	23	6	55	44.5	-10.49	113.9	33	5.1	292	2006	4	24	20	5	24	-9.39	113.11	37	5
263	2001	4	25	21	2	42.2	-9.18	106.49	33	5.5	293	2006	5	11	23	23	3.1	-11.23	115.98	25	5
264	2001	9	20	2	1	50.7	-11.4	115.05	10	5.6	294	2006	5	12	8	16	57	-5.57	105.39	17	5.5
265	2002	10	28	20	37	52.6	-6.41	104.49	33	5.1	295	2006	5	19	22	19	23	-8.69	105.98	28	5
266	2002	1	15	7	13	0.9	-6.26	105.24	33	6.3	296	2006	5	20	6	15	43	-9.99	112.03	39	5
267	2002	2	17	10	23	0.9	-5.97	104.39	33	5.4	297	2006	5	26	22	53	59	-7.96	110.45	12	6.3
268	2002	3	6	2	11	9.3	-9.2	112.36	33	5.2	298	2006	7	17	8	19	29	-9.25	107.41	34	7.7
269	2002	6	28	0	40	34.9	-6.97	104.02	10	5.3	299	2006	7	17	8	32	28	-9.28	107.35	17	5.6
270	2002	8	13	6	5	37.3	-7.08	104.01	33	5.9	300	2006	7	17	8	38	17	-9.5	107.76	34	5.3

A. Historical earthquake (1977-2007), MS > 5.0, depth < 40 km (ITDB/WLD, 2007) (Continuing from preceding page)

(List number of 301-360)

No	Time						Epicenter		Depth	Ms	No	Time						Epicenter		Depth	Ms
	Year	Mon	Day	Hour	Min	Sec	Lat	Lon	(km)			Year	Mon	Day	Hour	Min	Sec	Lat	Lon	(km)	
301	2006	7	17	8	40	7.5	-9.46	107.71	10	5.2	331	2006	7	17	15	26	23	-9.06	107.93	32	5.3
302	2006	7	17	8	41	17.2	-9.46	107.74	12	5.4	332	2006	7	17	15	28	44	-9.19	107.32	10	5.2
303	2006	7	17	9	0	17.7	-9.68	107.52	24	5.5	333	2006	7	17	15	29	0.1	-9.22	107.31	0	5.3
304	2006	7	17	9	5	17.3	-9.88	107.89	10	5.7	334	2006	7	17	15	30	27	-9.27	108.54	10	5.2
305	2006	7	17	9	13	4.9	-9.09	107.76	10	6.1	335	2006	7	17	15	42	2.6	-9.53	107.71	12	5.5
306	2006	7	17	9	44	11.3	-9.53	107.9	19	5	336	2006	7	17	15	45	60	-9.42	108.32	21	6.1
307	2006	7	17	9	55	7.9	-9.4	107.94	10	5.1	337	2006	7	17	16	9	55	-9.37	108.77	26	5.8
308	2006	7	17	9	55	32.2	-9.45	107.76	10	5.1	338	2006	7	17	16	27	38	-9.5	108.32	15	5.3
309	2006	7	17	10	0	19.7	-9.61	107.73	10	5.2	339	2006	7	17	16	38	39	-9.57	107.66	13	5.4
310	2006	7	17	10	9	6.7	-9.03	107.73	10	5.9	340	2006	7	17	17	40	43	-9.78	108.33	10	5.1
311	2006	7	17	10	26	45.7	-9.75	108.24	35	5.2	341	2006	7	17	19	0	51	-9.41	108.23	10	5
312	2006	7	17	10	34	44.3	-9.3	107.83	27	5.1	342	2006	7	17	19	9	33	-9.09	107.84	21	5.2
313	2006	7	17	10	44	31.9	-9.09	107.68	10	5.5	343	2006	7	17	19	44	11	-9.45	108.64	10	5.1
314	2006	7	17	11	3	14.5	-9.35	107.39	10	5.2	344	2006	7	17	19	49	33	-9.06	107.86	11	5.5
315	2006	7	17	11	7	36.4	-9.51	107.65	35	5.8	345	2006	7	17	20	13	20	-9.33	108.55	26	5.1
316	2006	7	17	11	15	35.6	-9.25	108.53	35	5.2	346	2006	7	17	21	49	4.4	-9.64	107.82	10	5
317	2006	7	17	11	24	44.5	-9.14	107.89	10	5.1	347	2006	7	17	23	24	27	-9.34	108.7	10	5
318	2006	7	17	11	28	48.1	-9.29	108.57	33	5.3	348	2006	7	17	23	36	36	-9.11	107.81	10	5.2
319	2006	7	17	11	40	7.3	-9.51	108.66	33	5	349	2006	7	18	0	15	49	-9.3	108.75	20	5.7
320	2006	7	17	12	52	12.6	-9.01	107.83	23	5.7	350	2006	7	18	1	32	48	-9.18	108.26	34	5
321	2006	7	17	13	2	56.8	-9.04	107.89	10	5.2	351	2006	7	18	2	4	46	-9.7	107.79	10	5
322	2006	7	17	13	4	6.4	-9.53	108.07	6	5.1	352	2006	7	18	2	11	34	-9.02	107.87	10	5
323	2006	7	17	13	39	24.6	-9.99	107.94	13	5	353	2006	7	18	2	59	12	-9.33	108.74	10	5
324	2006	7	17	13	53	48.4	-9.57	108.01	10	5.3	354	2006	7	18	3	1	48	-9.26	108.89	32	5.3
325	2006	7	17	13	55	33.6	-9.11	107.8	25	5.1	355	2006	7	18	3	34	38	-9.29	108.53	10	5.3
326	2006	7	17	13	56	56.2	-9.53	108.02	22	5	356	2006	7	18	4	5	49	-9.2	108.07	10	5.1
327	2006	7	17	14	50	55.7	-9.24	107.14	10	5.1	357	2006	7	18	4	18	23	-9.35	108.78	13	5.6
328	2006	7	17	15	9	14.6	-9.3	108.6	10	5.1	358	2006	7	18	5	6	30	-9.82	108.54	10	5.1
329	2006	7	17	15	20	53.9	-9.38	108.68	12	5.4	359	2006	7	18	6	51	48	-9.69	107.96	33	5.2
330	2006	7	17	15	21	4.7	-9.29	108.71	10	5.2	360	2006	7	18	11	54	12	-9.44	108.09	35	5

A. Historical earthquake (1977-2007), MS > 5.0, depth < 40 km (ITDB/WLD, 2007) (Continuing from preceding page)

(List number of 361-419/the last)

No	Time						Epicenter		Depth (km)	Ms	No	Time						Epicenter		Depth (km)	Ms
	Year	Mon	Day	Hour	Min	Sec	Lat	Lon				Year	Mon	Day	Hour	Min	Sec	Lat	Lon		
361	2006	7	18	14	54	56.5	-9.01	107.74	11	5.4	391	2006	7	25	14	1	26	-9.35	108.46	21	5.1
362	2006	7	18	15	48	31.9	-9.29	107.14	10	5	392	2006	7	25	14	48	28	-9.31	108.52	10	5.2
363	2006	7	18	17	27	58.2	-9.27	107.74	30	5.2	393	2006	7	27	22	55	54	-9.71	107.32	8	5.3
364	2006	7	18	19	11	13.2	-9.47	108.62	34	5.2	394	2006	7	27	23	19	9	-9.6	107.36	11	5.1
365	2006	7	18	19	13	40.1	-9.52	108.69	7	5	395	2006	7	29	9	16	54	-10.11	108.69	34	5.1
366	2006	7	19	1	58	55.1	-9.22	108.37	10	5.5	396	2006	8	7	5	2	48	-9.07	108.05	10	5.1
367	2006	7	19	7	25	6.3	-9.54	107.24	10	5.7	397	2006	8	12	6	55	23	-9.69	107.59	10	5.1
368	2006	7	19	12	1	57.5	-9.84	108.33	10	5	398	2006	8	28	5	22	47	-9.16	107.94	10	5
369	2006	7	19	19	3	54.7	-9.48	108.06	10	5.2	399	2006	8	29	20	59	17	-9.46	108.28	10	5
370	2006	7	19	22	9	23.5	-9.33	108.54	8	5.3	400	2006	8	30	17	39	37	-9.48	107.77	10	5
371	2006	7	19	22	47	3.4	-9.3	107.55	15	5	401	2006	8	30	17	43	58	-9.55	107.73	10	5
372	2006	7	20	1	17	26.5	-9.11	108.03	10	5.1	402	2006	9	4	1	3	50	-9.26	107.54	10	5.1
373	2006	7	20	4	34	7.7	-9.73	107.53	10	5.3	403	2006	9	19	13	58	57	-9.9	107.35	12	5.9
374	2006	7	20	14	36	10.7	-9.51	108.61	26	5.1	404	2006	9	21	18	54	50	-9.05	110.36	25	6
375	2006	7	20	15	38	28	-10.01	108.74	10	5.2	405	2006	9	30	5	50	24	-10.43	105.76	16	5.3
376	2006	7	21	10	11	9.6	-9.18	108	10	5	406	2006	11	17	0	58	2.7	-9.7	108.94	30	5
377	2006	7	22	3	5	11.2	-9.69	108.82	10	5.2	407	2006	12	23	22	59	41	-6.78	105.64	30	5.5
378	2006	7	22	3	21	12.8	-9.33	108.55	5	5.1	408	2006	12	29	6	26	49	-10.7	113.86	10	5.2
379	2006	7	23	6	53	31.2	-10.01	108.68	18	5	409	2007	1	19	2	44	24	-9.97	109.69	25	5.9
380	2006	7	23	17	23	45.7	-9.58	107.43	19	5.1	410	2007	1	31	20	31	30	-7.77	107.15	13	5.8
381	2006	7	23	19	43	4.2	-9.59	107.44	15	5	411	2007	5	16	23	37	43	-6.58	105.22	16	5
382	2006	7	24	0	58	8.1	-9.53	107.47	25	5.1	412	2007	6	26	22	23	3	-10.49	108.15	10	6
383	2006	7	24	1	23	26	-9.71	108.1	10	5.1	413	2007	7	18	19	37	31	-5.95	104.54	30	5.1
384	2006	7	24	11	41	30.2	-9.64	107.61	10	5.2	414	2007	9	11	16	36	9.9	-5.73	105.53	10	5
385	2006	7	24	16	33	57	-9.55	107.67	10	5.1	415	2007	9	24	17	35	26	-5.91	105.57	15	5.2
386	2006	7	24	16	50	0.2	-9.59	107.69	10	5	416	2007	11	9	6	54	7	-6.51	104.56	35	5.1
387	2006	7	24	21	3	16.5	-9.49	107.58	13	5.1	417	2007	11	10	2	43	46	-8.56	107.85	34	5.3
388	2006	7	25	12	34	59.1	-9.26	108.5	10	5.1	418	2007	12	7	10	45	54	-9.98	113.47	10	5.5
389	2006	7	25	12	35	37.1	-9.31	108.4	10	5.2	419	2007	12	17	12	46	15	-10.76	113.36	10	5.4
390	2006	7	25	12	39	23.8	-9.26	108.41	10	5.6											

Appendix D

B. The source parameter of Java earthquakes within period of 1978-2008 (USGS)

Tue May 12 13:35:59 UTC 2009
 FM Format
 Magnitude Range: 6.5 to 10
 Depth Range: 0 to 100
 Date Range: 1978 1 1 to 2008 1 1
 Latitude Range: -20 to -5
 Longitude Range: 100 to 115

DATE		TIME (UTC)			E P I C E N T E R			M O M E N T			P R I N C I P A L A X E S						N O D A L P L A N E S						SRC																																																																																																																																																																																																																																																																																																																																																																																																																																																																																																																																																																																																																																																																																																																																																																																																																																																																																																																																																																																																																																																																																																																																																																																																																																																																																																																																										
YR	MO	DA	HR	MN	SEC	LAT	LONG	SRC	DEPTH	VAL	EX	T	N	P	1	2	3	4	5	6	7	8	9	10	11	12	13	14	15	16	17	18	19	20	21	22	23	24	25	26	27	28	29	30	31	32	33	34	35	36	37	38	39	40	41	42	43	44	45	46	47	48	49	50	51	52	53	54	55	56	57	58	59	60	61	62	63	64	65	66	67	68	69	70	71	72	73	74	75	76	77	78	79	80	81	82	83	84	85	86	87	88	89	90	91	92	93	94	95	96	97	98	99	100	101	102	103	104	105	106	107	108	109	110	111	112	113	114	115	116	117	118	119	120	121	122	123	124	125	126	127	128	129	130	131	132	133	134	135	136	137	138	139	140	141	142	143	144	145	146	147	148	149	150	151	152	153	154	155	156	157	158	159	160	161	162	163	164	165	166	167	168	169	170	171	172	173	174	175	176	177	178	179	180	181	182	183	184	185	186	187	188	189	190	191	192	193	194	195	196	197	198	199	200	201	202	203	204	205	206	207	208	209	210	211	212	213	214	215	216	217	218	219	220	221	222	223	224	225	226	227	228	229	230	231	232	233	234	235	236	237	238	239	240	241	242	243	244	245	246	247	248	249	250	251	252	253	254	255	256	257	258	259	260	261	262	263	264	265	266	267	268	269	270	271	272	273	274	275	276	277	278	279	280	281	282	283	284	285	286	287	288	289	290	291	292	293	294	295	296	297	298	299	300	301	302	303	304	305	306	307	308	309	310	311	312	313	314	315	316	317	318	319	320	321	322	323	324	325	326	327	328	329	330	331	332	333	334	335	336	337	338	339	340	341	342	343	344	345	346	347	348	349	350	351	352	353	354	355	356	357	358	359	360	361	362	363	364	365	366	367	368	369	370	371	372	373	374	375	376	377	378	379	380	381	382	383	384	385	386	387	388	389	390	391	392	393	394	395	396	397	398	399	400	401	402	403	404	405	406	407	408	409	410	411	412	413	414	415	416	417	418	419	420	421	422	423	424	425	426	427	428	429	430	431	432	433	434	435	436	437	438	439	440	441	442	443	444	445	446	447	448	449	450	451	452	453	454	455	456	457	458	459	460	461	462	463	464	465	466	467	468	469	470	471	472	473	474	475	476	477	478	479	480	481	482	483	484	485	486	487	488	489	490	491	492	493	494	495	496	497	498	499	500	501	502	503	504	505	506	507	508	509	510	511	512	513	514	515	516	517	518	519	520	521	522	523	524	525	526	527	528	529	530	531	532	533	534	535	536	537	538	539	540	541	542	543	544	545	546	547	548	549	550	551	552	553	554	555	556	557	558	559	560	561	562	563	564	565	566	567	568	569	570	571	572	573	574	575	576	577	578	579	580	581	582	583	584	585	586	587	588	589	590	591	592	593	594	595	596	597	598	599	600	601	602	603	604	605	606	607	608	609	610	611	612	613	614	615	616	617	618	619	620	621	622	623	624	625	626	627	628	629	630	631	632	633	634	635	636	637	638	639	640	641	642	643	644	645	646	647	648	649	650	651	652	653	654	655	656	657	658	659	660	661	662	663	664	665	666	667	668	669	670	671	672	673	674	675	676	677	678	679	680	681	682	683	684	685	686	687	688	689	690	691	692	693	694	695	696	697	698	699	700	701	702	703	704	705	706	707	708	709	710	711	712	713	714	715	716	717	718	719	720	721	722	723	724	725	726	727	728	729	730	731	732	733	734	735	736	737	738	739	740	741	742	743	744	745	746	747	748	749	750	751	752	753	754	755	756	757	758	759	760	761	762	763	764	765	766	767	768	769	770	771	772	773	774	775	776	777	778	779	780	781	782	783	784	785	786	787	788	789	790	791	792	793	794	795	796	797	798	799	800	801	802	803	804	805	806	807	808	809	810	811	812	813	814	815	816	817	818	819	820	821	822	823	824	825	826	827	828	829	830	831	832	833	834	835	836	837	838	839	840	841	842	843	844	845	846	847	848	849	850	851	852	853	854	855	856	857	858	859	860	861	862	863	864	865	866	867	868	869	870	871	872	873	874	875	876	877	878	879	880	881	882	883	884	885	886	887	888	889	890	891	892	893	894	895	896	897	898	899	900	901	902	903	904	905	906	907	908	909	910	911	912	913	914	915	916	917	918	919	920	921	922	923	924	925	926	927	928	929	930	931	932	933	934	935	936	937	938	939	940	941	942	943	944	945	946	947	948	949	950	951	952	953	954	955	956	957	958	959	960	961	962	963	964	965	966	967	968	969	970	971	972	973	974	975	976	977	978	979	980	981	982	983	984	985	986	987	988	989	990	991	992	993	994	995	996	997	998	999	1000	1001	1002	1003	1004	1005	1006	1007	1008	1009	1010	1011	1012	1013	1014	1015	1016	1017	1018	1019	1020	1021	1022	1023	1024	1025	1026	1027	1028	1029	1030	1031	1032	1033	1034	1035	1036	1037	1038	1039	1040	1041	1042	1043	1044	1045	1046	1047	1048	1049	1050	1051	1052	1053	1054	1055	1056	1057	1058	1059	1060	1061	1062	1063	1064	1065	1066	1067	1068	1069	1070	1071	1072	1073	1074	1075	1076	1077	1078	1079	1080	1081	1082	1083	1084	1085	1086	1087	1088	1089	1090	1091	1092	1093	1094	1095	1096	1097	1098	1099	1100	1101	1102	1103	1104	1105	1106	1107	1108	1109	1110	1111	1112	1113	1114	1115	1116	1117	1118	1119	1120	1121	1122	1123	1124	1125	1126	1127	1128	1129	1130	1131	1132	1133	1134	1135	1136	1137	1138	1139	1140	1141	1142	1143	1144	1145	1146	1147	1148	1149	1150	1151	1152	1153	1154	1155	1156	1157	1158	1159	1160	1161	1162	1163	1164	1165	1166	1167	1168	1169	1170	1171	1172	1173	1174	1175	1176	1177	1178	1179	1180	1181	1182	1183	1184	1185	1186	1187	1188	1189	1190	1191	1192	1193	1194	1195	1196	1197	1198	1199	1200	1201	1202	1203	1204	1205	1206	1207	1208	1209	1210	1211	1212	1213	1214	1215	1216	1217	1218	1219	1220	1221	1222	1223	1224	1225	1226	1227	1228	1229	1230	1231	1232	1233	1234	1235	1236	1237	1238	1239	1240	1241	1242	1243	1244	1245	1246	1247	1248	1249	1250	1251	1252	1253	1254	1255	1256	1257	1258	1259	1260	1261	1262	1263	1264	1265	1266	1267	1268	1269	1270	1271	1272	1273	1274	1275	1276	1277	1278	1279	1280	1281	1282	1283	1284	1285	1286	1287	1288	1289	1290	1291	1292	1293	1294	1295	1296	1297	1298	129

Appendix D

C. The field observation data of tsunami run-up heights

(List number of 1-40)

No.	Location	Position (deg.)		G.lvl (m)	F.depth (m)	Hz.dist. (m)	Tsu.H. (m)	Source
		Lon.	Lat.					
1	Pangandaran East coast	108.658300	-7.701917	3.1	3.5	30	6.6	Tsuii team
2	Pangandaran West, Bima Nusantra Htl	108.656050	-7.699417	2.6	3.0	100	5.7	Tsuii team
3	Pangandaran West	108.654167	-7.696333	2.9	4.6	100	7.6	Tsuii team
4	Batukaras	108.498167	-7.748417	2.5	1.7	50	4.2	Tsuii team
5	Karantirta	108.590467	-7.680133	0.3	2.9	1000	3.2	Tsuii team
6	Cilacap port	109.001117	-7.738050	0.0	2.0	0	2.0	Tsuii team
7	Mangati (Cilacap city)	109.079633	-7.689450	2.3	2.8	300	5.1	Tsuii team
8	Lengkong (Cilacap City)	109.067417	-7.692967	2.0	3.0	300	5.0	Tsuii team
9	Bunton	109.144833	-7.687050	5.7	0.0	150	5.7	Tsuii team
10	Bunton	109.141383	-7.687700	3.5	2.2	700	5.7	Tsuii team
11	Binangun	109.264417	-7.697750	3.3	3.1	200	6.4	Tsuii team
12	Karang Pakis (Nusa Wung)	109.336533	-7.707550	5.7	0.0	300	5.7	Tsuii team
13	Ayah	109.393950	-7.724583	2.5	2.4	50	4.9	Tsuii team
14	Parang Tritis (south of Yogyakarta)	110.333467	-8.025967	2.3	0.6	200	2.8	Tsuii team
15	Pantai Pandansari (Sandakan)	110.253333	-8.000583	5.2	0.0	150	5.2	Tsuii team
16	Pantai Kuwaru	110.226250	-7.990950	7.6	0.0	150	7.6	Tsuii team
17	Pantai Kuwaru	110.226250	-7.990950	5.7	0.3	150	6.0	Tsuii team
18	Pandang Simo	110.217333	-7.987950	4.1	0.0	150	4.1	Tsuii team
19	Galur Pantai Trisik	110.193533	-7.974167	4.1	0.0	100	4.1	Tsuii team
20	Pantai Bugel Peni	110.152917	-7.951667	4.8	0.0	100	4.8	Tsuii team
21	Glagah (Temon City)	110.078033	-7.915383	2.0	0.0	300	2.0	Tsuii team
22	Pantai Congot (Temon City)	110.033967	-7.899867	5.1	0.8	200	5.9	Tsuii team
23	Jatimalang (Pantai Prejo)	109.983300	-7.879083	5.6	0.6	200	6.2	Tsuii team
24	Pantai Keburuhan	109.913117	-7.854167	4.0	1.0	100	5.0	Tsuii team
25	Pantai Keburuhan	109.913117	-7.854167	3.3	0.5	100	3.8	Tsuii team
26	Rowo	109.795083	-7.823217	6.3	0.6	100	6.9	Tsuii team
27	Rowo	109.795083	-7.823217	6.0	0.0	100	6.0	Tsuii team
28	Ambal	109.718133	-7.804783	5.0	0.0	100	5.0	Tsuii team
29	Puring	109.518467	-7.764667	4.5	0.0	100	4.5	Tsuii team
30	Puring	109.518467	-7.764667	4.2	0.0	100	4.2	Tsuii team
31	Pantai Suwuk	109.470283	-7.757333	4.0	2.8	250	6.8	Tsuii team
32	Kapang Bolong	109.466917	-7.757917	5.8	0.0	80	5.8	Tsuii team
33	Teluk Parigi 1	108.656509	-7.703715	2.9	1.1	75	4.0	Fritz team
34	?	108.656770	-7.703830	2.9	1.1	106	4.0	Fritz team
35	?	108.657030	-7.703910	2.9	0.9	137	3.8	Fritz team
36	?	108.657020	-7.703960	2.9	0.6	137	3.5	Fritz team
37	Teluk Parigi 2	108.656610	-7.701500	2.7	1.4	83	4.1	Fritz team
38	Teluk Parigi 3	108.655540	-7.698900	3.0	3.7	31	6.7	Fritz team
39	?	108.655857	-7.698556	2.6	1.5	82	4.1	Fritz team
40	Teluk Parigi 4	108.651704	-7.692872	2.7	1.7	151	4.4	Fritz team

Notes:

- G.lvl = ground level
- F.depth = flow depth
- Hz.dis = horizontal distance from the coastline
- Tsu. H. = tsunami run-up heights (corrected tide)
- “?” = unrecognized or unavailable names/places
- Nills = no data available

Appendix D

C. The field observation data of tsunami run-up heights (Continuing from preceding page)

(List number of 41-80)

No.	Location	Position (deg.)		G.lvl (m)	F.depth (m)	Hz.dist. (m)	Tsu.H. (m)	Source
		Lon.	Lat.					
41	?	108.651785	-7.692711	2.8	1.3	171	4.1	Fritz team
42	?	108.651945	-7.692426	2.9	0.4	208	3.3	Fritz team
43	?	108.652108	-7.692093	2.9	0.3	249	3.2	Fritz team
44	?	108.652152	-7.692040	3.0	0.1	256	3.1	Fritz team
45	Teluk Parigi 5	108.634113	-7.686126	2.2	4.1	132	6.3	Fritz team
46	?	108.634485	-7.685317	2.7	3.7	229	6.4	Fritz team
47	?	108.634756	-7.684965	3.0	1.4	276	4.4	Fritz team
48	?	108.634960	-7.684300	3.8	0.0	353	3.8	Fritz team
49	Teluk Parigi 6	108.652362	-7.707086	3.6	0.0	24	3.6	Fritz team
50	Teluk Pangandaran1	108.658260	-7.702274	3.6	1.9	22	5.5	Fritz team
51	?	108.658260	-7.702274	3.6	2.1	22	5.7	Fritz team
52	?	108.658260	-7.702274	3.6	2.8	22	6.4	Fritz team
53	Teluk Pangandaran2	108.663620	-7.707010	2.5	0.4	78	2.9	Fritz team
54	Teluk Pangandaran3	108.703290	-7.676123	2.5	5.1	30	7.6	Fritz team
55	?	108.704093	-7.676198	2.5	4.0	40	6.5	Fritz team
56	?	108.704213	-7.675144	2.7	2.1	158	4.8	Fritz team
57	?	108.704213	-7.675144	2.7	3.7	158	6.4	Fritz team
58	?	108.704213	-7.675144	2.7	2.3	158	5.0	Fritz team
59	?	108.704327	-7.674616	2.6	3.3	218	5.9	Fritz team
60	?	108.704404	-7.674234	2.6	0.5	261	3.1	Fritz team
61	?	108.704441	-7.673923	2.4	0.2	296	2.6	Fritz team
62	?	108.704487	-7.673637	1.7	0.0	329	1.7	Fritz team
63	Teluk Pangandaran4	108.676885	-7.681919	1.2	3.5	60	4.7	Fritz team
64	?	108.676885	-7.681919	1.2	2.0	60	3.2	Fritz team
65	?	108.675815	-7.680065	2.6	0.0	298	2.6	Fritz team
66	Teluk Pangandaran5	108.662730	-7.692670	2.5	2.4	31	4.9	Fritz team
67	?	108.659708	-7.696522	3.2	1.5	26	4.7	Fritz team
68	Pantai Barat1	108.762506	-7.695993	7.3	0.0	71	7.3	Fritz team
69	Pantai Barat2	108.762510	-7.695680	7.7	0.0	106	7.7	Fritz team
70	Pantai Barat3	108.756207	-7.691182	6.1	0.0	296	6.1	Fritz team
71	Pantai Barat4	108.753140	-7.692120	4.4	3.5	28	7.9	Fritz team
72	?	108.754552	-7.691071	6.2	0.0	223	6.2	Fritz team
73	Cilacap1	108.996640	-7.741660	0.0	1.0	0	1.0	Fritz team
74	Cilacap2	109.015640	-7.750330	2.4	0.0	15	2.4	Fritz team
75	Cilacap3	109.019710	-7.748550	2.3	0.0	26	2.3	Fritz team
76	Cilacap4	109.032830	-7.714450	2.6	0.0	22	2.6	Fritz team
77	Cilacap5	109.080010	-7.689478	2.2	1.8	86	4.0	Fritz team
78	?	109.079107	-7.687101	3.9	0.0	368	3.9	Fritz team
79	Adipala1	109.143650	-7.685890	3.3	0.0	460	3.3	Fritz team
80	Binangun1	109.257890	-7.697220	3.6	3.1	127	6.7	Fritz team

Notes:

- G.lvl = ground level
- F.depth = flow depth
- Hz.dis = horizontal distance from the coastline
- Tsu. H. = tsunami run-up heights (corrected tide)
- “?” = unrecognized or unavailable names/places
- Nills = no data available

Appendix D

C. The field observation data of tsunami run-up heights (Continuing from preceding page)

(List number of 81-120)

No.	Location	Position (deg.)		G.lvl (m)	F.depth (m)	Hz.dist. (m)	Tsu.H. (m)	Source
		Lon.	Lat.					
81	?	109.257890	-7.697220	3.6	2.8	127	6.4	Fritz team
82	?	109.258010	-7.696800	4.3	2.5	174	6.8	Fritz team
83	?	109.258160	-7.695250	4.1	0.0	348	4.1	Fritz team
84	Permisan1	108.882737	-7.745068	10.7	0.0	95	10.7	Fritz team
85	Permisan2	108.882282	-7.744952	13.3	0.0	106	13.3	Fritz team
86	Permisan3	108.882125	-7.745036	16.1	0.0	76	16.1	Fritz team
87	Permisan4	108.881829	-7.745035	14.8	0.0	65	14.8	Fritz team
88	Permisan5	108.881403	-7.744963	10.7	0.0	44	10.7	Fritz team
89	Permisan6	108.881301	-7.744946	11.1	0.0	42	11.1	Fritz team
90	Permisan7	108.880674	-7.744551	4.6	5.7	52	10.3	Fritz team
91	?	108.880957	-7.743884	13.1	0.0	131	13.1	Fritz team
92	?	108.880875	-7.743666	15.2	0.0	149	15.2	Fritz team
93	?	108.880769	-7.743625	14.7	0.0	150	14.7	Fritz team
94	?	108.880677	-7.743599	16.2	0.0	150	16.2	Fritz team
95	Permisan8	108.880501	-7.740683	20.9	0.0	427	20.9	Fritz team
96	?	108.879520	-7.741494	12.8	0.0	320	12.8	Fritz team
97	?	108.879353	-7.741583	14.6	0.0	310	14.6	Fritz team
98	?	108.878952	-7.741255	20.3	0.0	351	20.3	Fritz team
99	?	108.878387	-7.741263	16.0	0.0	365	16.0	Fritz team
100	?	108.878289	-7.741370	17.4	0.0	358	17.4	Fritz team
101	?	108.878407	-7.741769	15.1	0.0	312	15.1	Fritz team
102	?	108.878220	-7.742144	15.9	0.0	283	15.9	Fritz team
103	?	108.878170	-7.742419	15.6	0.0	259	15.6	Fritz team
104	Permisan9	108.877390	-7.742460	3.9	8.2	209	12.1	Fritz team
105	?	108.877070	-7.742600	3.9	7.1	209	11.0	Fritz team
106	?	108.877955	-7.742217	17.0	0.0	224	17.0	Fritz team
107	?	108.877572	-7.742122	15.3	0.0	239	15.3	Fritz team
108	Permisan10	108.876452	-7.740254	15.1	0.0	401	15.1	Fritz team
109	?	108.876252	-7.740432	13.9	0.0	382	13.9	Fritz team
110	?	108.875783	-7.740897	14.9	0.0	335	14.9	Fritz team
111	?	108.874896	-7.741877	19.8	0.0	273	19.8	Fritz team
112	?	108.874889	-7.741844	19.4	0.0	276	19.4	Fritz team
113	Permisan11	108.884555	-7.747274	18.4	0.0	65	18.4	Fritz team
114	Ayah1	109.369610	-7.715030	4.9	1.7	123	6.6	Fritz team
115	Karangbolong1	109.466780	-7.757996	3.0	1.2	66	4.2	Fritz team
116	Ambal1	109.719890	-7.804660	5.8	0.0	44	5.8	Fritz team
117	Pentanahan1	109.582210	-7.775400	4.0	1.1	62	5.1	Fritz team
118	?	109.582330	-7.774920	4.0	0.7	117	4.7	Fritz team
119	?	109.582340	-7.774700	4.4	0.0	141	4.4	Fritz team
120	Karangbot1	109.436130	-7.768110	3.0	0.0	56	3.0	Fritz team

Notes:

- G.lvl = ground level
- F.depth = flow depth
- Hz.dis = horizontal distance from the coastline
- Tsu. H. = tsunami run-up heights (corrected tide)
- “?” = unrecognized or unavailable names/places
- Nills = no data available

Appendix D

C. The field observation data of tsunami run-up heights (Continuing from preceding page)

(List number of 121-160)

No.	Location	Position (deg.)		G.lvl (m)	F.depth (m)	Hz.dist. (m)	Tsu.H. (m)	Source
		Lon.	Lat.					
121	Karangboto2	109.438370	-7.766710	5.5	0.0	44	5.5	Fritz team
122	Ketawang1	109.867588	-7.841252	4.7	0.0	48	4.7	Fritz team
123	Pantai Jatimalang1	109.983441	-7.879410	5.5	0.5	79	6.0	Fritz team
124	?	109.983600	-7.879090	5.7	0.0	119	5.7	Fritz team
125	Pantai Bugel	110.152970	-7.951660	5.2	0.0	51	5.2	Fritz team
126	Cikembulan	108.612867	-7.682600	3.4	4.5	nil	7.9	Fritz team
127	Cikembulan	108.612683	-7.680017	2.2	0.0	408	2.2	Fritz team
128	W of Cikembulan	108.603767	-7.682533	4.6	3.0	nil	7.6	Fritz team
129	W of Cikembulan	108.604567	-7.682667	4.6	3.0	nil	7.6	Fritz team
130	W of Cikembulan	108.604033	-7.681550	6.3	0.0	333	6.3	Fritz team
131	MUARA LAGOON	108.599517	-7.680167	1.6	0.4	nil	2.0	Fritz team
132	MUARA LAGOON	108.600150	-7.680250	3.9	0.9	291	4.7	Fritz team
133	?	108.592167	-7.676733	2.5	0.0	nil	2.5	Fritz team
134	BATU HIU	108.535500	-7.690517	0.3	0.0	272	0.3	Fritz team
135	BATU HIU	108.535350	-7.691833	1.5	1.5	104	3.0	Fritz team
136	Timin	108.511600	-7.701767	2.5	0.0	80	2.5	Fritz team
137	Karang	108.501633	-7.710967	3.9	0.9	147	4.8	Fritz team
138	Batu Karas	108.496517	-7.747683	1.1	0.9	nil	1.9	Fritz team
139	Batu Karas	108.496517	-7.747683	1.1	0.0	300	1.1	Fritz team
140	Batu Karas	108.498067	-7.748600	2.1	1.0	68	3.1	Fritz team
141	CIRAPANTI	108.406683	-7.816483	3.9	2.0	78	5.9	Fritz team
142	Bulak Benda, South West of town	108.476433	-7.802200	3.5	0.0	nil	3.5	Fritz team
143	Bulak Benda, South West of town	108.474967	-7.802800	2.9	0.0	358	2.9	Fritz team
144	Bulak Benda, South West of town	108.476517	-7.804683	4.6	3.2	90	7.8	Fritz team
145	Bulak Benda	108.483917	-7.793917	1.4	0.7	550	2.1	Fritz team
146	Bulak Benda	108.485633	-7.794783	2.2	1.8	340	4.0	Fritz team
147	Bulak Benda	108.485183	-7.795117	2.8	1.4	340	4.2	Fritz team
148	Singkil	108.332267	-7.812967	5.5	0.0	306	5.5	Fritz team
149	Singkil	108.332267	-7.813567	5.4	0.4	nil	5.8	Fritz team
150	Singkil	108.332383	-7.813700	5.3	0.9	nil	6.2	Fritz team
151	Singkil	108.332367	-7.814117	4.9	0.9	nil	5.8	Fritz team
152	Sukamenak	108.316417	-7.811683	4.5	1.8	194	6.3	Fritz team
153	Cipatujah	108.013933	-7.748183	4.8	0.0	168	4.8	Fritz team
154	Cipatujah	108.008717	-7.744333	2.2	0.8	314	3.0	Fritz team
155	Pameungpeuk	107.695983	-7.668850	3.4	0.5	39	3.9	Fritz team
156	Pameungpeuk	107.689300	-7.663983	1.1	0.0	47	1.1	Fritz team
157	Pameungpeuk	107.689217	-7.663500	-0.2	0.0	nil	-0.2	Fritz team
158	Pantai Baron	110.548917	-8.128306	2.3	0.0	51	2.3	Kongko team
159	Pantai Baron	110.548389	-8.128500	1.3	1.1	53	2.4	Kongko team
160	Pantai Kukup	110.554806	-8.133528	1.1	0.0	80	1.1	Kongko team

Notes:

- G.lvl = ground level
- F.depth = flow depth
- Hz.dis = horizontal distance from the coastline
- Tsu. H. = tsunami run-up heights (corrected tide)
- “?” = unrecognized or unavailable names/places
- Nills = no data available

Appendix D

C. The field observation data of tsunami run-up heights (Continuing from preceding page)

(List number of 161-200)

No.	Location	Position (deg.)		G.lvl (m)	F.depth (m)	Hz.dist. (m)	Tsu.H. (m)	Source
		Lon.	Lat.					
161	Pantai Krakal	110.599028	-8.145167	3.3	0.0	9	3.3	Kongko team
162	Sundak	110.607333	-8.146750	4.0	0.0	23	4.0	Kongko team
163	Pantai Drini	110.576889	-8.137861	4.1	0.0	27	4.1	Kongko team
164	Pantai Samas	110.266333	-8.005306	2.3	0.0	24	2.3	Kongko team
165	Pantai Pandansari	110.253556	-8.000611	2.0	0.0	104	2.0	Kongko team
166	Pantai Sadeng	110.799361	-8.190194	1.9	0.0	231	1.9	Kongko team
167	Pantai Tamperan 1	111.074667	-8.226000	1.6	0.0	55	1.6	Kongko team
168	Pantai Tamperan 2	111.074583	-8.224944	1.7	0.2	39	1.9	Kongko team
169	Pantai Sendang Biru	112.684556	-8.432000	1.7	0.0	175	1.7	Kongko team
170	Pantai Pr.kusumo-depok	110.303944	-8.047222	3.4	0.0	80	3.4	Kongko team
171	Pantai Keburuhan	109.913417	-7.880278	2.0	0.3	102	2.3	Kongko team
172	Pantai Suwuk	109.470333	-7.780278	-0.1	1.0	161	0.8	Kongko team
173	Pantai Suwuk	109.470528	-7.780278	-0.6	1.1	250	0.5	Kongko team
174	Pantai Suwuk	109.471083	-7.780278	0.1	0.4	304	0.4	Kongko team
175	Pantai Ayah	109.394111	-7.746944	1.1	0.4	111	1.5	Kongko team
176	Pantai Ayah	109.394639	-7.746944	1.1	0.4	208	1.5	Kongko team
177	Pantai Ayah	109.394917	-7.746944	1.6	0.0	214	1.6	Kongko team
178	Pantai Windoropayung	109.264250	-7.713611	3.0	0.7	73	3.7	Kongko team
179	Pantai Bunton	109.142667	-7.713611	0.0	0.8	296	0.7	Kongko team
180	Cikembulan 1, Ciamis	108.612833	-7.696667	2.1	1.2	190	3.4	Kongko team
181	Cikembulan 1, Ciamis	108.612972	-7.696667	0.4	0.9	325	1.3	Kongko team
182	Cikembulan 2, Ciamis	108.624000	-7.696667	2.5	1.1	227	3.6	Kongko team
183	Pangandaran 1, Ciamis	108.650528	-7.713333	1.6	1.1	112	2.7	Kongko team
184	Pangandaran 2, Ciamis	108.656389	-7.730000	1.6	0.7	81	2.3	Kongko team
185	Pangandaran 2, Ciamis	108.656611	-7.730000	1.3	1.1	107	2.4	Kongko team
186	Cimerak Bulakbenda	108.479627	-7.802587	nil	nil	nil	2.5	Lavigne team
187	?	108.485232	-7.795680	nil	nil	nil	4.0	Lavigne team
188	?	108.496828	-7.738045	nil	nil	121	7.6	Lavigne team
189	?	108.496960	-7.740251	nil	nil	89	10.4	Lavigne team
190	?	108.496965	-7.739338	nil	nil	148	1.6	Lavigne team
191	Pangandaran Batukaras	108.497904	-7.747505	nil	nil	58	5.5	Lavigne team
192	Pangandaran Parigi	108.501205	-7.713291	nil	nil	nil	5.5	Lavigne team
193	Pangandaran Batu Hiu	108.534360	-7.692073	nil	nil	nil	1.4	Lavigne team
194	?	108.534869	-7.690241	nil	nil	nil	1.4	Lavigne team
195	?	108.535763	-7.692217	nil	nil	nil	1.5	Lavigne team
196	?	108.589450	-7.679751	nil	nil	nil	1.2	Lavigne team
197	?	108.591537	-7.680748	nil	nil	nil	2.2	Lavigne team
198	?	108.592467	-7.679651	nil	nil	nil	2.7	Lavigne team
199	?	108.592572	-7.678775	nil	nil	nil	1.5	Lavigne team
200	?	108.592650	-7.679344	nil	nil	nil	2.7	Lavigne team

Notes:

- G.lvl = ground level
- F.depth = flow depth
- Hz.dis = horizontal distance from the coastline
- Tsu. H. = tsunami run-up heights (corrected tide)
- “?” = unrecognized or unavailable names/places
- Nills = no data available

Appendix D

C. The field observation data of tsunami run-up heights (Continuing from preceding page)

(List number of 201-240)

No.	Location	Position (deg.)		G.lvl (m)	F.depth (m)	Hz.dist. (m)	Tsu.H. (m)	Source
		Lon.	Lat.					
201	?	108.592686	-7.674627	nil	nil	nil	2.7	Lavigne team
202	Pangandaran	108.611760	-7.683681	nil	nil	nil	7.8	Lavigne team
203	Pangandaran	108.612160	-7.681975	nil	nil	nil	4.9	Lavigne team
204	Pangandaran Pananjung	108.634635	-7.685624	nil	nil	nil	3.2	Lavigne team
205	?	108.643502	-7.687896	nil	nil	nil	3.9	Lavigne team
206	?	108.643841	-7.688775	nil	nil	nil	6.4	Lavigne team
207	?	108.644094	-7.688876	nil	nil	nil	5.9	Lavigne team
208	?	108.644205	-7.688479	nil	nil	nil	5.6	Lavigne team
209	?	108.644256	-7.687593	nil	nil	nil	1.9	Lavigne team
210	?	108.644564	-7.687568	nil	nil	nil	1.9	Lavigne team
211	?	108.644563	-7.687622	nil	nil	nil	1.7	Lavigne team
212	?	108.644654	-7.689249	nil	nil	nil	5.7	Lavigne team
213	?	108.644701	-7.688897	nil	nil	nil	5.8	Lavigne team
214	?	108.644891	-7.689034	nil	nil	nil	7.4	Lavigne team
215	?	108.644921	-7.688501	nil	nil	nil	6.9	Lavigne team
216	?	108.644961	-7.689531	nil	nil	nil	7.4	Lavigne team
217	?	108.645105	-7.689659	nil	nil	nil	6.1	Lavigne team
218	?	108.645397	-7.689226	nil	nil	nil	6.5	Lavigne team
219	?	108.645859	-7.689346	nil	nil	nil	5.9	Lavigne team
220	?	108.645859	-7.689346	nil	nil	nil	6.0	Lavigne team
221	?	108.654957	-7.703849	nil	nil	nil	4.5	Lavigne team
222	?	108.655700	-7.698900	nil	nil	50	4.1	Lavigne team
223	?	108.655673	-7.705398	nil	nil	nil	6.0	Lavigne team
224	?	108.656015	-7.704162	nil	nil	nil	3.4	Lavigne team
225	?	108.656157	-7.703069	nil	nil	nil	3.8	Lavigne team
226	?	108.656167	-7.704569	nil	nil	nil	5.0	Lavigne team
227	?	108.656496	-7.702402	nil	nil	nil	4.6	Lavigne team
228	?	108.656489	-7.703622	nil	nil	nil	5.2	Lavigne team
229	?	108.656518	-7.703387	nil	nil	nil	4.5	Lavigne team
230	?	108.656594	-7.704463	nil	nil	nil	2.8	Lavigne team
231	?	108.657403	-7.702316	nil	nil	nil	3.8	Lavigne team
232	?	108.658114	-7.703152	nil	nil	nil	2.5	Lavigne team
233	?	108.658355	-7.703885	nil	nil	nil	3.2	Lavigne team
234	?	108.659200	-7.698503	nil	nil	nil	3.0	Lavigne team
235	?	108.665317	-7.685042	nil	nil	nil	3.8	Lavigne team
236	Pangandaran Bulaksetra	108.676098	-7.680102	nil	nil	nil	0.0	Lavigne team
237	Pangandaran Keboncarik	108.694642	-7.675547	nil	nil	273	2.7	Lavigne team
238	?	108.696236	-7.675619	nil	nil	nil	9.2	Lavigne team
239	?	108.696237	-7.675565	nil	nil	nil	8.5	Lavigne team
240	Pangandaran Karang Sari	108.703363	-7.676335	nil	nil	10	8.4	Lavigne team

Notes:

- G.lvl = ground level
- F.depth = flow depth
- Hz.dis = horizontal distance from the coastline
- Tsu. H. = tsunami run-up heights (corrected tide)
- “?” = unrecognized or unavailable names/places
- Nills = no data available

Appendix D

C.The field observation data of tsunami run-up heights (Continuing from preceding page)

(List number of 241-280)

No.	Location	Position (deg.)		G.lvl (m)	F.depth (m)	Hz.dist. (m)	Tsu.H. (m)	Source
		Lon.	Lat.					
241	?	108.703998	-7.676203	nil	nil	nil	3.7	Lavigne team
242	?	108.704651	-7.674317	nil	nil	nil	5.1	Lavigne team
243	?	108.704676	-7.674797	nil	nil	nil	5.2	Lavigne team
244	?	108.704806	-7.674282	nil	nil	nil	4.8	Lavigne team
245	?	108.705094	-7.676164	nil	nil	nil	6.4	Lavigne team
246	?	108.705712	-7.675860	nil	nil	nil	6.8	Lavigne team
247	?	108.706244	-7.676396	nil	nil	nil	7.4	Lavigne team
248	?	108.706714	-7.676606	nil	nil	nil	7.9	Lavigne team
249	Pangandaran Krapyak	108.752345	-7.691752	nil	nil	nil	5.9	Lavigne team
250	?	108.752345	-7.691716	nil	nil	nil	7.1	Lavigne team
251	?	108.753024	-7.690129	nil	nil	nil	6.7	Lavigne team
252	?	108.753138	-7.692588	nil	nil	nil	8.1	Lavigne team
253	?	108.753303	-7.692101	nil	nil	nil	8.5	Lavigne team
254	?	108.753303	-7.692101	nil	nil	18	9.7	Lavigne team
255	?	108.755207	-7.693765	nil	nil	24	6.0	Lavigne team
256	?	108.756961	-7.692690	nil	nil	nil	6.9	Lavigne team
257	?	108.757312	-7.694816	nil	nil	30	5.6	Lavigne team
258	?	108.881720	-7.745194	nil	nil	35	8.2	Lavigne team
259	?	108.881722	-7.744841	nil	nil	73	12.8	Lavigne team
260	?	108.882182	-7.754254	nil	nil	46	11.8	Lavigne team
261	?	108.882184	-7.753955	nil	nil	80	15.7	Lavigne team
262	Nusa Kambangan Permisan	108.882833	-7.745570	nil	nil	38	8.2	Lavigne team
263	Nusa Kambangan Permisan	108.882834	-7.745443	nil	nil	53	8.8	Lavigne team
264	?	109.079185	-7.687238	nil	nil	nil	2.0	Lavigne team
265	?	109.080026	-7.689547	nil	nil	84	2.2	Lavigne team
266	?	109.088700	-7.687308	nil	nil	nil	2.9	Lavigne team
267	?	109.088693	-7.688854	nil	nil	nil	3.7	Lavigne team
268	Cilacap Bunton	109.144050	-7.686818	nil	nil	457	1.9	Lavigne team
269	Cilacap Bunton	109.161694	-7.685023	nil	nil	nil	2.4	Lavigne team
270	Cilacap Bunton	109.183597	-7.692159	nil	nil	nil	5.0	Lavigne team
271	Cilacap Widarapayung	109.260198	-7.697594	nil	nil	nil	1.2	Lavigne team
272	Cilacap Widarapayung	109.262273	-7.697720	nil	nil	nil	3.5	Lavigne team
273	Cilacap Widarapayung	109.263215	-7.695834	nil	nil	nil	3.5	Lavigne team
274	Cilacap Widarapayung	109.263255	-7.694849	nil	nil	nil	1.0	Lavigne team
275	Cilacap Widarapayung	109.264292	-7.698262	nil	nil	nil	5.4	Lavigne team
276	Cilacap Widarapayung	109.264476	-7.695351	nil	nil	nil	1.7	Lavigne team
277	Cilacap Widarapayung	109.264494	-7.697594	nil	nil	nil	5.1	Lavigne team
278	Cilacap Widarapayung	109.264628	-7.698064	nil	nil	nil	4.0	Lavigne team
279	Cilacap Jetis	109.373437	-7.716367	nil	nil	nil	1.5	Lavigne team
280	Kebumen Ayah	109.389871	-7.723663	nil	nil	nil	3.5	Lavigne team

Notes:

- G.lvl = ground level
- F.depth = flow depth
- Hz.dis = horizontal distance from the coastline
- Tsu. H. = tsunami run-up heights (corrected tide)
- “?” = unrecognized or unavailable names/places
- Nills = no data available

Appendix D

C. The field observation data of tsunami run-up heights (Continuing from preceding page)

(List number of 281-320)

No.	Location	Position (deg.)		G.lvl (m)	F.depth (m)	Hz.dist. (m)	Tsu.H. (m)	Source
		Lon.	Lat.					
281	Kebumen Ayah	109.391550	-7.723218	nil	nil	nil	1.5	Lavigne team
282	Kebumen Ayah	109.393878	-7.723705	nil	nil	nil	6.7	Lavigne team
283	Kebumen Ayah	109.394406	-7.725498	nil	nil	nil	3.4	Lavigne team
284	Kebumen Ayah	109.394692	-7.726611	nil	nil	nil	1.0	Lavigne team
285	Kebumen Ayah	109.437904	-7.766241	nil	nil	nil	1.4	Lavigne team
286	Kebumen Ayah	109.466773	-7.758091	nil	nil	nil	5.0	Lavigne team
287	Kebumen Ayah	109.466810	-7.757946	nil	nil	nil	2.0	Lavigne team
288	Kebumen Ayah	109.467390	-7.758075	nil	nil	nil	4.6	Lavigne team
289	Kebumen Ayah	109.467653	-7.758076	nil	nil	nil	5.1	Lavigne team
290	Puring	109.468623	-7.758179	nil	nil	nil	1.4	Lavigne team
291	Puring	109.469343	-7.757006	nil	nil	nil	3.5	Lavigne team
292	Puring	109.469919	-7.755724	nil	nil	nil	2.0	Lavigne team
293	Puring	109.472409	-7.759051	nil	nil	nil	2.5	Lavigne team
294	Puring	109.472540	-7.757876	nil	nil	nil	3.9	Lavigne team
295	Ketawang	109.571434	-7.774362	nil	nil	nil	4.0	Lavigne team
296	Ketawang	109.580344	-7.775070	nil	nil	nil	2.2	Lavigne team
297	Ketawang	109.581259	-7.775471	nil	nil	nil	6.7	Lavigne team
298	Ketawang	109.581821	-7.775310	nil	nil	nil	1.4	Lavigne team
299	Ketawang	109.663418	-7.791798	nil	nil	45	3.8	Lavigne team
300	Purworejo Keburuhan	109.894644	-7.849225	nil	nil	32	6.7	Lavigne team
301	Purworejo Keburuhan	109.894847	-7.847959	nil	nil	137	1.4	Lavigne team
302	Purworejo Keburuhan	109.912988	-7.854093	nil	nil	nil	1.7	Lavigne team
303	Purworejo Keburuhan	109.913219	-7.852438	nil	nil	nil	3.0	Lavigne team
304	Kulon Progo Congot	110.034074	-7.899556	nil	nil	26	1.8	Lavigne team
305	Kulon Progo Congot	110.034074	-7.899556	nil	nil	26	1.6	Lavigne team
306	Glagah	110.077834	-7.915474	nil	nil	nil	4.2	Lavigne team
307	Bugel	110.152682	-7.951693	nil	nil	nil	2.8	Lavigne team
308	Bantul Pandansimo	110.217273	-7.988189	nil	nil	nil	1.5	Lavigne team
309	Samas	110.264596	-8.005497	nil	nil	75	3.7	Lavigne team
310	Parangkusumo	110.324001	-8.023399	nil	nil	nil	4.2	Lavigne team
311	Parangkusumo	110.325996	-8.024099	nil	nil	nil	5.5	Lavigne team
312	Parangkusumo	110.329833	-8.024765	nil	nil	170	4.6	Lavigne team
313	Parangkusumo	110.330079	-8.024133	nil	nil	nil	3.7	Lavigne team
314	Parangkusumo	110.335202	-8.026701	nil	nil	nil	4.2	Lavigne team
315	Parangkusumo	110.335540	-8.025652	nil	nil	nil	5.5	Lavigne team
316	Parangkusumo	110.336604	-8.024197	nil	nil	nil	0.8	Lavigne team
317	Gunung Kidul Baron	110.548897	-8.128496	nil	nil	70	2.9	Lavigne team
318	Krakal	110.603135	-8.145006	nil	nil	54	4.1	Lavigne team
319	Cilacap Selatan, Cilacap	109.009889	-7.742556	2.2	0.6	nil	2.7	K. Fujima/PARI
320	Cilacap Selatan, Cilacap	109.023417	-7.729444	2.6	0.0	81	2.6	K. Fujima/PARI

Notes:

- G.lvl = ground level
- F.depth = flow depth
- Hz.dis = horizontal distance from the coastline
- Tsu. H. = tsunami run-up heights (corrected tide)
- “?” = unrecognized or unavailable names/places
- Nills = no data available

Appendix D

C. The field observation data of tsunami run-up heights (Continuing from preceding page)

(List number of 321-360)

No.	Location	Position (deg.)		G.lvl (m)	F.depth (m)	Hz.dist. (m)	Tsu.H. (m)	Source
		Lon.	Lat.					
321	Cilacap Selatan, Cilacap	?	?	1.6	1.0	nil	2.6	K. Fujima/PARI
322	Cilacap Selatan, Cilacap	?	?	2.3	0.5	nil	2.8	K. Fujima/PARI
323	Menganti, Kesugihan, Cilacap	109.079944	-7.689500	2.2	1.8	94	4.0	K. Fujima/PARI
324	Menganti, Kesugihan, Cilacap	109.079944	-7.689500	2.2	2.8	94	5.0	K. Fujima/PARI
325	Menganti, Kesugihan, Cilacap	109.079500	-7.688000	1.4	0.9	295	2.2	K. Fujima/PARI
326	Menganti, Kesugihan, Cilacap	109.079556	-7.687833	1.4	0.1	295	1.5	K. Fujima/PARI
327	Menganti, Kesugihan, Cilacap	109.079667	-7.687889	1.0	0.3	295	1.3	K. Fujima/PARI
328	Menganti, Kesugihan, Cilacap	109.079444	-7.687972	1.4	0.0	295	1.4	K. Fujima/PARI
329	Widarapayung Wetan, Binangun, Clp	109.264611	-7.697944	3.7	2.9	97	6.5	K. Fujima/PARI
330	Widarapayung Wetan, Binangun, Clp	109.264472	-7.697889	4.4	2.3	97	6.7	K. Fujima/PARI
331	Widarapayung Wetan, Binangun, Clp	109.264583	-7.697306	4.3	1.6	182	5.9	K. Fujima/PARI
332	Widarapayung Wetan, Binangun, Clp	109.264444	-7.696778	1.3	1.4	226	2.7	K. Fujima/PARI
333	Pangandaran, Pangandaran, Ciamis	108.656083	-7.704806	2.1	1.3	71	3.4	K. Fujima/PARI
334	Pangandaran, Pangandaran, Ciamis	108.656583	-7.704556	2.1	1.1	127	3.2	K. Fujima/PARI
335	Pangandaran, Pangandaran, Ciamis	108.656639	-7.704528	1.7	0.5	126	2.1	K. Fujima/PARI
336	Pangandaran, Pangandaran, Ciamis	108.657611	-7.704222	1.9	0.5	225	2.4	K. Fujima/PARI
337	Pangandaran, Pangandaran, Ciamis	108.658361	-7.703806	2.8	0.8	339	3.6	K. Fujima/PARI
338	Pangandaran, Pangandaran, Ciamis	108.652611	-7.693722	3.1	2.0	182	5.1	K. Fujima/PARI
339	Pangandaran, Pangandaran, Ciamis	108.652833	-7.693722	3.0	1.8	182	4.8	K. Fujima/PARI
340	Pangandaran, Pangandaran, Ciamis	108.660611	-7.695444	2.7	0.2	41	2.9	K. Fujima/PARI
341	Pangandaran, Pangandaran, Ciamis	108.660333	-7.695306	2.7	0.3	72	3.0	K. Fujima/PARI
342	Pangandaran, Pangandaran, Ciamis	108.659778	-7.695417	2.8	0.2	126	3.1	K. Fujima/PARI
343	Pangandaran, Pangandaran, Ciamis	108.656833	-7.696139	3.2	0.0	398	3.2	K. Fujima/PARI
344	Pangandaran, Pangandaran, Ciamis	108.655833	-7.695889	3.2	0.3	297	3.5	K. Fujima/PARI
345	Pangandaran, Pangandaran, Ciamis	108.655194	-7.695722	3.1	0.6	215	3.7	K. Fujima/PARI
346	Pangandaran, Pangandaran, Ciamis	108.654667	-7.695694	2.8	0.9	152	3.7	K. Fujima/PARI
347	Pangandaran, Pangandaran, Ciamis	108.654444	-7.695722	2.9	1.5	115	4.4	K. Fujima/PARI
348	Pangandaran, Pangandaran, Ciamis	108.654333	-7.696028	3.0	1.9	115	4.9	K. Fujima/PARI
349	Sukaresik, Pangandaran, Ciamis	108.590500	-7.680056	1.5	0.9	nil	2.4	K. Fujima/PARI
350	Sukaresik, Pangandaran, Ciamis	108.590472	-7.680139	1.8	1.9	nil	3.7	K. Fujima/PARI
351	Ciliang, Parigi, Ciamis	108.535500	-7.691833	2.9	1.0	94	3.9	K. Fujima/PARI
352	Ciliang, Parigi, Ciamis	108.535472	-7.691694	2.7	0.7	94	3.4	K. Fujima/PARI
353	Ciliang, Parigi, Ciamis	108.535556	-7.691583	2.3	0.7	125	3.0	K. Fujima/PARI
354	Ciliang, Parigi, Ciamis	108.541444	-7.690139	4.0	1.3	115	5.3	K. Fujima/PARI
355	Ciliang, Parigi, Ciamis	108.541417	-7.689944	3.8	0.7	115	4.6	K. Fujima/PARI
356	Legokjawa, Cimerak, Ciamis	108.447083	-7.813833	3.6	0.5	182	4.1	K. Fujima/PARI
357	Ciparanti, Cimerak, Ciamis	108.406556	-7.816472	4.7	0.7	121	5.3	K. Fujima/PARI
358	Mandalajaya, Cikalong, Tasikmaraya	108.183722	-7.791833	3.6	0.0	82	3.6	K. Fujima/PARI
359	Cipatujah, Cipatujah, Tasikmaraya	108.054278	-7.762083	4.4	0.7	49	5.1	K. Fujima/PARI
360	Cipatujah, Cipatujah, Tasikmaraya	108.054444	-7.761500	3.7	0.5	107	4.2	K. Fujima/PARI

Notes:

- G.lvl = ground level
- F.depth = flow depth
- Hz.dis = horizontal distance from the coastline
- Tsu. H. = tsunami run-up heights (corrected tide)
- “?” = unrecognized or unavailable names/places
- Nills = no data available

Appendix D

C. The field observation data of tsunami run-up heights (Continuing from preceding page)

(List number of 361-394)

No.	Location	Position (deg.)		G.lvl (m)	F.depth (m)	Hz.dist. (m)	Tsu.H. (m)	Source
		Lon.	Lat.					
361	Cipatujah, Cipatujah, Tasikmaraya	108.054611	-7.761194	3.8	0.0	144	3.8	K. Fujima/PARI
362	Ciheras, Cipatujah, Tasikmaraya	107.944278	-7.731833	1.9	0.0	nil	1.9	K. Fujima/PARI
363	Karyamukti, Cibalong, Garut	107.794750	-7.683306	2.6	0.0	nil	2.6	K. Fujima/PARI
364	Mancaqahar, Pameungpeuk, Garut	107.696389	-7.668944	4.3	0.7	30	4.9	K. Fujima/PARI
365	Mancaqahar, Pameungpeuk, Garut	107.696528	-7.668722	4.2	0.0	50	4.2	K. Fujima/PARI
366	Pangandaran west coast	108.656389	-7.704722	2.6	1.6	104	4.2	H. Matsutomi/PARI
367	Pangandaran west coast	108.656111	-7.700028	3.4	1.3	63	4.7	H. Matsutomi/PARI
368	?	?	?	3.3	0.6	68	3.9	H. Matsutomi/PARI
369	Pangandaran west coast	108.655556	-7.698333	2.7	2.4	79	5.1	H. Matsutomi/PARI
370	?	?	?	2.8	1.5	85	4.2	H. Matsutomi/PARI
371	Pangandaran west coast	108.653889	-7.696389	6.4	0.0	18	6.4	H. Matsutomi/PARI
372	Pangandaran west coast	108.653056	-7.695000	3.8	1.6	100	5.4	H. Matsutomi/PARI
373	?	?	?	3.8	1.1	107	4.9	H. Matsutomi/PARI
374	Pangandaran west coast	108.650583	-7.692611	6.6	0.1	116	6.7	H. Matsutomi/PARI
375	Pangandaran east coast	108.658889	-7.704444	2.7	1.3	30	3.9	H. Matsutomi/PARI
376	Pangandaran east coast	108.660278	-7.696111	2.8	1.1	36	3.9	H. Matsutomi/PARI
377	Pangandaran east coast	108.658889	-7.704444	2.6	1.4	60	4.0	H. Matsutomi/PARI
378	Tasikmalaya Cimanuk	108.336111	-7.815833	7.4	0.0	32	7.4	H. Matsutomi/PARI
379	Tasikmalaya Cimanuk	108.341667	-7.817500	11.4	0.0	27	11.4	H. Matsutomi/PARI
380	Tasikmalaya Kalapagenep	108.292222	-7.810833	5.5	0.0	208	5.5	H. Matsutomi/PARI
381	Cilacap Cilacap	109.020056	-7.751389	2.8	0.0	111	2.8	H. Matsutomi/PARI
382	Cilacap Tegalkatlayu	109.037417	-7.710583	3.3	0.0	23	3.3	H. Matsutomi/PARI
383	Cilacap Mertasinga	109.067333	-7.692806	3.1	0.0	55	3.1	H. Matsutomi/PARI
384	Cilacap Karangkadri	109.084722	-7.689444	6.2	0.0	20	6.2	H. Matsutomi/PARI
385	Cilacap Karangkadri	109.084722	-7.689361	3.3	0.0	74	3.3	H. Matsutomi/PARI
386	?	?	?	3.8	0.0	139	3.8	H. Matsutomi/PARI
387	Cilacap Karangkadri	109.093667	-7.686694	4.3	0.0	31	4.3	H. Matsutomi/PARI
388	Cilacap Karangkadri	109.183889	-7.691389	3.5	0.0	35	3.5	H. Matsutomi/PARI
389	Cilacap Widarapayung kulon	109.263361	-7.698389	5.2	0.0	181	5.2	H. Matsutomi/PARI
390	?	?	?	4.9	0.0	201	4.9	H. Matsutomi/PARI
391	Kebumen Ayah	109.394472	-7.726056	1.3	0.0	210	1.3	H. Matsutomi/PARI
392	Cilacap Sidaup	109.292472	-7.700778	2.3	1.6	111	3.9	H. Matsutomi/PARI
393	?	?	?	2.3	0.9	111	3.2	H. Matsutomi/PARI
394	?	?	?	3.6	0.0	143	3.6	H. Matsutomi/PARI

Notes:

- G.lvl = ground level
- F.depth = flow depth
- Hz.dis = horizontal distance from the coastline
- Tsu. H. = tsunami run-up heights (corrected tide)
- “?” = unrecognized or unavailable names/places
- Nills = no data available

Appendix D

D. The selected field observation data of tsunami run-up heights

(List number of 1-45)

No	Geo-coordinates (deg)		Tsu-rup*) (m)	Hz dist. (m)	Beach slope Hz/Vt	Sources/Authors
	longintude	Latitude				
1	107.689300	-7.663983	1.1	47.0	42	Fritz et al. (2007)
2	107.695983	-7.668850	3.9	39.0	12	Fritz et al. (2007)
3	108.406683	-7.816483	5.9	78.0	20	Fritz et al. (2007)
4	108.476517	-7.804683	7.8	90.0	20	Fritz et al. (2007)
5	108.498067	-7.748600	3.1	68.0	32	Fritz et al. (2007)
6	108.501633	-7.710967	4.8	147.0	38	Fritz et al. (2007)
7	108.511600	-7.701767	2.5	80.0	32	Fritz et al. (2007)
8	108.535350	-7.691833	3.0	104.0	69	Fritz et al. (2007)
9	108.634113	-7.686126	6.3	131.7	61	Fritz et al. (2007)
10	108.651704	-7.692872	4.4	151.3	57	Fritz et al. (2007)
11	108.655540	-7.698900	6.7	30.7	10	Fritz et al. (2007)
12	108.655857	-7.698556	4.1	81.6	31	Fritz et al. (2007)
13	108.656509	-7.703715	4.0	75.1	26	Fritz et al. (2007)
14	108.656610	-7.701500	4.1	82.8	31	Fritz et al. (2007)
15	108.656770	-7.703830	4.0	106.4	37	Fritz et al. (2007)
16	108.657020	-7.703960	3.5	137.3	47	Fritz et al. (2007)
17	108.657030	-7.703910	3.8	136.7	47	Fritz et al. (2007)
18	108.662730	-7.692670	4.9	31.2	12	Fritz et al. (2007)
19	108.663620	-7.707010	2.9	78.4	31	Fritz et al. (2007)
20	108.676885	-7.681919	4.7	60.0	51	Fritz et al. (2007)
21	108.676885	-7.681919	3.2	60.0	51	Fritz et al. (2007)
22	108.703290	-7.676123	7.6	30.1	12	Fritz et al. (2007)
23	108.704093	-7.676198	6.5	40.3	16	Fritz et al. (2007)
24	108.762506	-7.695993	7.3	71.3	10	Fritz et al. (2007)
25	108.762510	-7.695680	7.7	105.8	14	Fritz et al. (2007)
26	108.880769	-7.743625	14.7	149.5	10	Fritz et al. (2007)
27	108.880957	-7.743884	13.1	131.0	10	Fritz et al. (2007)
28	109.019710	-7.748550	2.3	26.0	12	Fritz et al. (2007)
29	109.080010	-7.689478	4.0	86.3	40	Fritz et al. (2007)
30	109.257890	-7.697220	6.7	127.0	35	Fritz et al. (2007)
31	109.257890	-7.697220	6.4	127.0	35	Fritz et al. (2007)
32	109.369610	-7.715030	6.6	123.4	25	Fritz et al. (2007)
33	109.436130	-7.768110	3.0	56.0	19	Fritz et al. (2007)
34	109.466780	-7.757996	4.2	65.6	22	Fritz et al. (2007)
35	109.582210	-7.775400	5.1	61.9	16	Fritz et al. (2007)
36	109.582330	-7.774920	4.7	116.8	30	Fritz et al. (2007)
37	109.582340	-7.774700	4.4	141.1	32	Fritz et al. (2007)
38	109.867588	-7.841252	4.7	48.3	10	Fritz et al. (2007)
39	109.983441	-7.879410	6.0	79.5	14	Fritz et al. (2007)
40	109.983600	-7.879090	5.7	118.8	21	Fritz et al. (2007)
41	110.152970	-7.951660	5.2	51.2	10	Fritz et al. (2007)
42	108.653056	-7.695000	5.4	100.4	28	H.Matsutomi/PARI team
43	108.655556	-7.698333	5.1	78.9	31	H.Matsutomi/PARI team
44	108.656111	-7.700028	4.7	62.9	19	H.Matsutomi/PARI team
45	108.656389	-7.704722	4.2	104.3	42	H.Matsutomi/PARI team

Notes:

The tsunami run-up heights are above mean sea level & already corrected with tide data

Appendix D

D.The selected field observation data of tsunami run-up heights (Continuing from preceding page)

(List number of 46-90)

No	Geo-coordinates (deg)		Tsu-rup* (m)	Hz dist. (m)	Beach slope Hz/Vt	Sources/Authors
	longintude	Latitude				
46	108.658889	-7.704444	3.9	30.0	12	H.Matsutomi/PARI team
47	108.658889	-7.704444	4.0	60.2	24	H.Matsutomi/PARI team
48	108.660278	-7.696111	3.9	35.6	13	H.Matsutomi/PARI team
49	109.020056	-7.751389	2.8	111.4	41	H.Matsutomi/PARI team
50	109.067333	-7.692806	3.1	54.9	18	H.Matsutomi/PARI team
51	109.084722	-7.689361	3.3	73.7	23	H.Matsutomi/PARI team
52	109.183889	-7.691389	3.5	35.0	10	H.Matsutomi/PARI team
53	109.263361	-7.698389	5.2	180.6	35	H.Matsutomi/PARI team
54	109.292472	-7.700778	3.9	111.2	50	H.Matsutomi/PARI team
55	107.696528	-7.668722	4.2	50.3	12	K. Fujima/PARI team
56	108.054278	-7.762083	5.1	49.0	11	K. Fujima/PARI team
57	108.054444	-7.761500	4.2	107.4	29	K. Fujima/PARI team
58	108.054611	-7.761194	3.8	144.2	39	K. Fujima/PARI team
59	108.183722	-7.791833	3.6	82.5	23	K. Fujima/PARI team
60	108.406556	-7.816472	5.3	121.1	26	K. Fujima/PARI team
61	108.535472	-7.691694	3.4	93.9	36	K. Fujima/PARI team
62	108.535500	-7.691833	3.9	93.9	34	K. Fujima/PARI team
63	108.535556	-7.691583	3.0	125.2	57	K. Fujima/PARI team
64	108.541417	-7.689944	4.6	115.0	31	K. Fujima/PARI team
65	108.541444	-7.690139	5.3	115.0	29	K. Fujima/PARI team
66	108.654333	-7.696028	4.9	114.6	40	K. Fujima/PARI team
67	108.654444	-7.695722	4.4	114.6	40	K. Fujima/PARI team
68	108.654667	-7.695694	3.7	151.5	55	K. Fujima/PARI team
69	108.655833	-7.695889	3.5	297.2	95	K. Fujima/PARI team
70	108.656083	-7.704806	3.4	70.6	35	K. Fujima/PARI team
71	108.656583	-7.704556	3.2	126.9	62	K. Fujima/PARI team
72	108.656639	-7.704528	2.1	126.5	78	K. Fujima/PARI team
73	108.659778	-7.695417	3.1	126.0	46	K. Fujima/PARI team
74	108.660333	-7.695306	3.0	72.1	28	K. Fujima/PARI team
75	108.660611	-7.695444	2.9	40.7	16	K. Fujima/PARI team
76	109.023417	-7.729444	2.6	81.1	32	K. Fujima/PARI team
77	109.079944	-7.689500	4.0	94.3	45	K. Fujima/PARI team
78	109.079944	-7.689500	5.0	94.3	45	K. Fujima/PARI team
79	109.264472	-7.697889	6.7	97.4	23	K. Fujima/PARI team
80	109.264611	-7.697944	6.5	97.4	27	K. Fujima/PARI team
81	108.650528	-7.713333	2.7	112.0	69	Kongko et al. (2006)
82	108.656389	-7.730000	2.3	81.0	51	Kongko et al. (2006)
83	108.656611	-7.730000	2.4	107.0	81	Kongko et al. (2006)
84	109.264250	-7.713611	3.7	73.0	25	Kongko et al. (2006)
85	109.394111	-7.746944	1.5	111.0	100	Kongko et al. (2006)
86	109.913417	-7.880278	2.3	102.0	51	Kongko et al. (2006)
87	110.253556	-8.000611	2.0	103.5	53	Kongko et al. (2006)
88	110.266333	-8.005306	2.3	24.0	11	Kongko et al. (2006)
89	110.303944	-8.047222	3.4	80.0	24	Kongko et al. (2006)
90	110.548389	-8.128500	2.4	52.5	41	Kongko et al. (2006)

Notes:

The tsunami run-up heights are above mean sea level & already corrected with tide data

Appendix D

D.The selected field observation data of tsunami run-up heights (Continuing from preceding page)

(List number of 90-114)

No	Geo-coordinates (deg)		Tsu-rup* (m)	Hz dist. (m)	Beach slope Hz/Vt	Sources/Authors
	longintude	Latitude				
91	110.548917	-8.128306	2.3	50.7	22	Kongko et al. (2006)
92	110.554806	-8.133528	1.1	80.0	72	Kongko et al. (2006)
93	111.074583	-8.224944	1.9	39.0	23	Kongko et al. (2006)
94	111.074667	-8.226000	1.6	55.2	34	Kongko et al. (2006)
95	112.684556	-8.432000	1.7	175.2	105	Kongko et al. (2006)
96	108.498167	-7.748417	4.2	50.0	20	Tsuji team
97	108.654167	-7.696333	7.6	100.0	32	Tsuji team
98	108.656050	-7.699417	5.7	100.0	36	Tsuji team
99	109.144833	-7.687050	5.7	150.0	26	Tsuji team
100	109.393950	-7.724583	4.9	50.0	18	Tsuji team
101	109.466917	-7.757917	5.8	80.0	14	Tsuji team
102	109.518467	-7.764667	4.5	100.0	21	Tsuji team
103	109.518467	-7.764667	4.2	100.0	22	Tsuji team
104	109.718133	-7.804783	5.0	100.0	18	Tsuji team
105	109.795083	-7.823217	6.9	100.0	15	Tsuji team
106	109.795083	-7.823217	6.0	100.0	17	Tsuji team
107	109.913117	-7.854167	5.0	100.0	25	Tsuji team
108	109.913117	-7.854167	3.8	100.0	33	Tsuji team
109	110.152917	-7.951667	4.8	100.0	20	Tsuji team
110	110.193533	-7.974167	4.1	100.0	23	Tsuji team
111	110.217333	-7.987950	4.1	150.0	35	Tsuji team
112	110.226250	-7.990950	7.6	150.0	20	Tsuji team
113	110.226250	-7.990950	6.0	150.0	26	Tsuji team
114	110.253333	-8.000583	5.2	150.0	29	Tsuji team

Notes:

The tsunami run-up heights are above mean sea level & already corrected with tide data

Appendix D

E. The maximum tsunami run-up heights at Permisan – Nusakambangan Cilacap

(Data sources from Fritz et al., 2007 and Lavigne et al., 2007)

No	UTM Coordinates		Htsu-rup	source	remarks
	x-utm49s	y-utm49s	(m)		
1	266373.0	9143328.0	12.8	F.Lavigne	hill-slope
2	266429.0	9143320.0	15.7	F.Lavigne	hill-slope
3	266485.5	9143303.2	10.7	H.Fritz	trimline in forest
4	266434.6	9143316.3	13.3	H.Fritz	trimline in forest
5	266418.1	9143306.2	16.1	H.Fritz	trimline in forest
6	266385.0	9143306.0	14.8	H.Fritz	trimline in forest
7	266337.5	9143314.7	10.7	H.Fritz	trimline in forest
8	266326.5	9143315.7	11.1	H.Fritz	trimline in forest
9	266288.4	9143433.9	13.1	H.Fritz	trimline in forest
10	266278.4	9143457.1	15.2	H.Fritz	trimline in forest
11	266267.3	9143462.6	14.7	H.Fritz	trimline in forest
12	266257.3	9143464.7	16.2	H.Fritz	trimline in forest
13	266235.9	9143787.6	20.9	H.Fritz	trimline in forest
14	266128.2	9143697.5	12.8	H.Fritz	trimline in forest
15	266109.5	9143687.4	14.6	H.Fritz	trimline in forest
16	266065.2	9143722.6	20.3	H.Fritz	trimline in forest
17	266003.4	9143722.3	16.0	H.Fritz	trimline in forest
18	265992.4	9143710.1	17.4	H.Fritz	trimline in forest
19	266005.9	9143665.9	15.1	H.Fritz	trimline in forest
20	265985.1	9143624.9	15.9	H.Fritz	trimline in forest
21	265979.7	9143593.9	15.6	H.Fritz	trimline in forest
22	265955.4	9143615.9	17.0	H.Fritz	trimline in forest
23	265913.4	9143626.7	15.3	H.Fritz	trimline in forest
24	265788.8	9143833.0	15.1	H.Fritz	trimline in forest
25	265766.8	9143813.0	13.9	H.Fritz	trimline in forest
26	265715.2	9143760.7	14.9	H.Fritz	trimline in forest
27	265618.6	9143651.8	19.8	H.Fritz	trimline in forest
28	265617.5	9143656.2	19.4	H.Fritz	trimline in forest
29	266687.5	9143060.9	18.4	H.Fritz	trimline in forest

Notes:

- The tsunami run-up heights are above mean sea level & already corrected with tide data
- The tsunami run-up heights are the maximum inundation (or flow-depth is equal to zero)

Appendix D

F. The difference of the tsunami run-up heights at Permisan Cilacap (field observation vs topography measurement)

No.	Data from H.Fritz & F.Lavigne (rapid survey 2006 event aftermath)							Interp. Measu. & corr-SRTM30			Differences			
	x-utm49s	y-utm49s	z(d+h) (m)	d (m)	z(d+h) (m)	data sources	remarks	x-utm49s	y-utm49s	z(d+h) (m)	x-utm49s	y-utm49s	z(d+h) (m)	% Vr. Diff.
	1	2	3	4	6	7	8	9	10	11	12	13	14	15
1	266373.0	9143328.0	12.8	0	12.8	F.Lavigne	hill-slope	266373.0	9143328.0	18.477	0.0	0.0	5.7	18.2%
2	266429.0	9143320.0	15.7	0	15.7	F.Lavigne	hill-slope	266429.0	9143320.0	17.239	0.0	0.0	1.5	4.7%
3	266485.5	9143303.2	10.7	0	10.7	H.Fritz	trimline in forest	266485.5	9143303.2	7.037	0.0	0.0	-3.7	20.7%
4	266434.6	9143316.3	13.3	0	13.3	H.Fritz	trimline in forest	266434.6	9143316.3	15.256	0.0	0.0	2.0	6.8%
5	266418.1	9143306.2	16.1	0	16.1	H.Fritz	trimline in forest	266418.1	9143306.2	9.992	0.0	0.0	-6.1	23.4%
6	266385.0	9143306.0	14.8	0	14.8	H.Fritz	trimline in forest	266385.0	9143306.0	9.699	0.0	0.0	-5.1	20.8%
7	266337.5	9143314.7	10.7	0	10.7	H.Fritz	trimline in forest	266337.5	9143314.7	7.503	0.0	0.0	-3.2	17.6%
8	266326.5	9143315.7	11.1	0	11.1	H.Fritz	trimline in forest	266326.5	9143315.7	5.754	0.0	0.0	-5.3	31.7%
9	266288.4	9143433.9	13.1	0	13.1	H.Fritz	trimline in forest	266288.4	9143433.9	10.428	0.0	0.0	-2.7	11.4%
10	266278.4	9143457.1	15.2	0	15.2	H.Fritz	trimline in forest	266278.4	9143457.1	14.637	0.1	0.0	-0.6	1.9%
11	266267.3	9143462.6	14.7	0	14.7	H.Fritz	trimline in forest	266267.3	9143462.6	13.818	0.0	0.0	-0.9	3.1%
12	266257.3	9143464.7	16.2	0	16.2	H.Fritz	trimline in forest	266257.3	9143464.7	12.349	0.0	0.0	-3.9	13.5%
13	266235.9	9143787.6	20.9	0	20.9	H.Fritz	trimline in forest	266235.9	9143787.6	7.433	0.0	0.0	-13.5	47.5%
14	266128.2	9143697.5	12.8	0	12.8	H.Fritz	trimline in forest	266128.2	9143697.5	2.956	0.0	0.0	-9.8	62.5%
15	266109.5	9143687.4	14.6	0	14.6	H.Fritz	trimline in forest	266109.5	9143687.4	2.648	0.0	0.0	-12.0	69.3%
16	266065.2	9143722.6	20.3	0	20.3	H.Fritz	trimline in forest	266065.2	9143722.6	13.268	0.0	0.0	-7.0	20.9%
17	266003.4	9143722.3	16	0	16	H.Fritz	trimline in forest	266003.4	9143722.3	14.992	0.0	0.0	-1.0	3.3%
18	265992.4	9143710.1	17.4	0	17.4	H.Fritz	trimline in forest	265992.4	9143710.1	15.673	0.0	0.0	-1.7	5.2%
19	266005.9	9143665.9	15.1	0	15.1	H.Fritz	trimline in forest	266005.9	9143665.9	3.977	0.0	0.0	-11.1	58.3%
20	265985.1	9143624.9	15.9	0	15.9	H.Fritz	trimline in forest	265985.1	9143624.9	4.569	0.0	0.0	-11.3	55.4%
21	265979.7	9143593.9	15.6	0	15.6	H.Fritz	trimline in forest	265979.7	9143593.9	2.224	0.0	0.0	-13.4	75.0%
22	265955.4	9143615.9	17	0	17	H.Fritz	trimline in forest	265955.4	9143615.9	4.976	0.0	0.0	-12.0	54.7%
23	265913.4	9143626.7	15.3	0	15.3	H.Fritz	trimline in forest	265913.4	9143626.7	4.537	0.0	0.0	-10.8	54.3%
24	265788.8	9143833.0	15.1	0	15.1	H.Fritz	trimline in forest	265788.8	9143833.0	13.189	0.0	0.0	-1.9	6.8%
25	265766.8	9143813.0	13.9	0	13.9	H.Fritz	trimline in forest	265766.8	9143813.0	13.644	0.0	0.0	-0.3	0.9%
26	265715.2	9143760.7	14.9	0	14.9	H.Fritz	trimline in forest	265715.2	9143760.7	8.309	0.0	0.0	-6.6	28.4%
27	265618.6	9143651.8	19.8	0	19.8	H.Fritz	trimline in forest	265618.6	9143651.8	18.73	0.0	0.0	-1.1	2.8%
28	265617.5	9143656.2	19.4	0	19.4	H.Fritz	trimline in forest	265617.5	9143656.2	19.206	0.0	0.0	-0.2	0.5%
29	266687.5	9143060.9	18.4	0	18.4	H.Fritz	trimline in forest	266687.5	9143060.9	14.671	0.0	0.0	-3.7	11.3%

Notes:

The tsunami run-up heights' difference between field observation and topography measurements in average of 25.2%

Appendix D

G. The difference of the tsunami run-up heights at Permisan Cilacap (adjusted field observation vs topography measurement)

No.	adjusted points' position		z(d+h) (m)	Differences with field observation data					Remark
	x-utm49s	y-utm49s		x-utm49s	y-utm49s	z(d+h)	Vr. Diff.	Hk. Dist	
			(m)			%	(m)		
1	266371	9143316	12.8	2.1	11.9	0.0	0%	12.1 *)	
2	266429	9143317	15.7	0.0	3.0	0.0	0%	3.0	
3	266482	9143313	10.7	3.7	-9.4	0.0	0%	10.1	
4	266435	9143313	13.3	-0.1	3.7	0.0	0%	3.7	
5	266417	9143318	16.1	0.8	-11.9	0.0	0%	12.0 *)	
6	266387	9143317	14.8	-2.3	-11.3	0.0	0%	11.5 *)	
7	266339	9143320	10.7	-1.8	-5.0	0.0	0%	5.3	
8	266330	9143322	11.1	-3.6	-6.2	0.0	0%	7.2	
9	266292	9143435	13.1	-3.9	-1.5	0.0	0%	4.2	
10	266279	9143458	15.2	-0.8	-1.0	0.0	0%	1.3	
11	266269	9143464	14.7	-1.3	-1.6	0.0	0%	2.1	
12	266263	9143472	16.2	-5.2	-7.0	0.0	0%	8.7	
13	266226	9143823	21.0	9.9	-35.9	-0.1	0%	37.2 *)	
14	266111	9143729	12.8	17.0	-31.6	0.0	0%	35.9 *)	
15	266098	9143725	14.6	11.8	-37.8	0.0	0%	39.6 *)	
16	266069	9143735	20.3	-3.5	-12.2	0.0	0%	12.6 *)	
17	266003	9143731	16.0	0.5	-8.8	0.0	0%	8.8	
18	265982	9143713	17.2	10.1	-2.8	0.2	1%	10.5 *)	
19	265978	9143681	15.0	28.1	-15.1	0.1	0%	31.9 *)	
20	265960	9143659	15.9	25.5	-33.7	0.0	0%	42.3 *)	
21	265956	9143654	15.6	23.6	-60.1	0.0	0%	64.6 *)	
22	265951	9143662	17.0	4.3	-46.2	0.0	0%	46.4 *)	
23	265945	9143656	15.4	-31.7	-28.8	-0.1	0%	42.9 *)	
24	265781	9143833	15.0	7.9	0.5	0.1	0%	8.0	
25	265766	9143814	13.9	0.6	-0.6	0.0	0%	0.9	
26	265725	9143780	14.9	-9.7	-19.1	0.0	0%	21.4 *)	
27	265617	9143656	19.4	1.8	-4.6	0.4	1%	4.9	
28	265616	9143652	19.4	1.1	4.2	0.0	0%	4.3	
29	266692	9143062	18.5	-4.4	-1.3	-0.1	0%	4.5	

Notes:

- The points' location are adjusted to fit the tsunami run-up heights (Z) from observation data
- The horizontal differences (Hz. dist.) are obtained between observation data and field measurements
- Denotes of *) are the points that the horizontal differences more than 10 m, the value of the GPS accuracy.

Appendix E – Tsunami sources

A. Tsunami source by Cheng-Ji (2006)

#Total number of fault_segments= 1								#	Lat	Lon.	depth	slip	rake	strike	dip
#Fault_segment= 1 nx(Along-strike)= 21 Dx= 15.00km								21	-9.457	106.585	6.8	25.1	66.62	288.94	10.35
ny(downdip)= 7 Dy= 11.00km								22	-10.241	109.203	8.8	0.7	88.79	288.94	10.35
#Boundary of Fault_segment 1								23	-10.197	109.074	8.8	30.7	97.90	288.94	10.35
Lon	Lat	Depth						24	-10.153	108.945	8.8	76.1	99.93	288.94	10.35
109.205	-10.374	6.2						25	-10.110	108.815	8.8	0.6	79.59	288.94	10.35
106.504	-9.459	6.2						26	-10.066	108.686	8.8	1.0	114.33	288.94	10.35
106.724	-8.828	19.8						27	-10.022	108.557	8.8	64.8	121.81	288.94	10.35
109.425	-9.743	19.8						28	-9.978	108.427	8.8	81.3	105.21	288.94	10.35
109.205	-10.374	6.2						29	-9.934	108.298	8.8	137.6	121.72	288.94	10.35
#	Lat	Lon.	depth	slip	rake	strike	dip	30	-9.891	108.169	8.8	85.8	88.14	288.94	10.35
1	-10.333	109.171	6.8	5.0	121.66	288.94	10.35	31	-9.847	108.040	8.8	30.6	80.38	288.94	10.35
2	-10.289	109.042	6.8	4.3	80.94	288.94	10.35	32	-9.803	107.910	8.8	60.1	113.75	288.94	10.35
3	-10.245	108.913	6.8	48.9	85.43	288.94	10.35	33	-9.759	107.781	8.8	47.0	96.25	288.94	10.35
4	-10.202	108.783	6.8	3.6	101.69	288.94	10.35	34	-9.716	107.652	8.8	21.7	80.83	288.94	10.35
5	-10.158	108.654	6.8	0.9	67.05	288.94	10.35	35	-9.672	107.522	8.8	11.0	112.63	288.94	10.35
6	-10.114	108.525	6.8	1.0	99.45	288.94	10.35	36	-9.628	107.393	8.8	27.9	75.88	288.94	10.35
7	-10.070	108.395	6.8	0.6	71.54	288.94	10.35	37	-9.584	107.264	8.8	6.0	77.66	288.94	10.35
8	-10.026	108.266	6.8	0.0	99.45	288.94	10.35	38	-9.540	107.134	8.8	3.9	83.58	288.94	10.35
9	-9.983	108.137	6.8	2.7	119.63	288.94	10.35	39	-9.497	107.005	8.8	3.2	113.73	288.94	10.35
10	-9.939	108.008	6.8	0.6	114.26	288.94	10.35	40	-9.453	106.876	8.8	29.9	116.11	288.94	10.35
11	-9.895	107.878	6.8	14.5	112.72	288.94	10.35	41	-9.409	106.747	8.8	65.3	72.61	288.94	10.35
12	-9.851	107.749	6.8	31.7	107.27	288.94	10.35	42	-9.365	106.617	8.8	19.6	65.99	288.94	10.35
13	-9.808	107.620	6.8	2.7	85.79	288.94	10.35	43	-10.149	109.235	10.8	20.6	124.43	288.94	10.35
14	-9.764	107.490	6.8	3.4	78.97	288.94	10.35	44	-10.105	109.106	10.8	69.9	122.65	288.94	10.35
15	-9.720	107.361	6.8	68.0	64.89	288.94	10.35	45	-10.061	108.977	10.8	63.1	99.24	288.94	10.35
16	-9.676	107.232	6.8	62.3	65.44	288.94	10.35	46	-10.018	108.847	10.8	0.6	74.09	288.94	10.35
17	-9.632	107.102	6.8	35.3	66.90	288.94	10.35	47	-9.974	108.718	10.8	1.0	117.54	288.94	10.35
18	-9.589	106.973	6.8	1.8	101.94	288.94	10.35	48	-9.930	108.589	10.8	85.5	123.65	288.94	10.35
19	-9.545	106.844	6.8	40.6	81.78	288.94	10.35	49	-9.886	108.459	10.8	167.2	104.57	288.94	10.35
20	-9.501	106.715	6.8	84.2	68.96	288.94	10.35	50	-9.842	108.330	10.8	202.6	122.12	288.94	10.35

Notes:

- The number of sub-faults are $21 \times 7 = 147$
- Each sub-fault has an area of $15 \text{ km} \times 11 \text{ km}$

Appendix E

A. Tsunami source by Cheng-Ji (2006) (Continued from preceding page)

#	Lat	Lon.	depth	slip	rake	strike	dip		#	Lat	Lon.	depth	slip	rake	strike	dip
51	-9.799	108.201	10.8	144.8	81.50	288.94	10.35		83	-9.225	106.811	12.7	11.0	81.95	288.94	10.35
52	-9.755	108.072	10.8	54.0	72.84	288.94	10.35		84	-9.181	106.681	12.7	2.4	123.05	288.94	10.35
53	-9.711	107.942	10.8	79.2	98.66	288.94	10.35		85	-9.965	109.299	14.7	22.4	123.90	288.94	10.35
54	-9.667	107.813	10.8	83.0	80.82	288.94	10.35		86	-9.921	109.170	14.7	48.6	115.46	288.94	10.35
55	-9.623	107.684	10.8	119.1	74.37	288.94	10.35		87	-9.877	109.041	14.7	6.0	83.81	288.94	10.35
56	-9.580	107.554	10.8	95.9	116.25	288.94	10.35		88	-9.833	108.911	14.7	7.2	123.81	288.94	10.35
57	-9.536	107.425	10.8	36.9	102.32	288.94	10.35		89	-9.790	108.782	14.7	0.1	93.41	288.94	10.35
58	-9.492	107.296	10.8	0.3	81.50	288.94	10.35		90	-9.746	108.653	14.7	0.4	69.37	288.94	10.35
59	-9.448	107.166	10.8	8.1	98.41	288.94	10.35		91	-9.702	108.523	14.7	104.2	123.83	288.94	10.35
60	-9.405	107.037	10.8	3.0	116.90	288.94	10.35		92	-9.658	108.394	14.7	46.1	95.97	288.94	10.35
61	-9.361	106.908	10.8	10.7	74.61	288.94	10.35		93	-9.615	108.265	14.7	0.3	89.57	288.94	10.35
62	-9.317	106.779	10.8	57.9	75.39	288.94	10.35		94	-9.571	108.136	14.7	2.1	80.14	288.94	10.35
63	-9.273	106.649	10.8	61.0	64.77	288.94	10.35		95	-9.527	108.006	14.7	30.6	66.23	288.94	10.35
64	-10.057	109.267	12.7	22.0	121.11	288.94	10.35		96	-9.483	107.877	14.7	73.7	87.91	288.94	10.35
65	-10.013	109.138	12.7	74.5	119.75	288.94	10.35		97	-9.439	107.748	14.7	112.9	92.28	288.94	10.35
66	-9.969	109.009	12.7	17.3	124.09	288.94	10.35		98	-9.396	107.618	14.7	74.7	86.52	288.94	10.35
67	-9.925	108.879	12.7	14.4	87.42	288.94	10.35		99	-9.352	107.489	14.7	121.7	64.69	288.94	10.35
68	-9.882	108.750	12.7	3.0	106.36	288.94	10.35		100	-9.308	107.360	14.7	231.2	65.51	288.94	10.35
69	-9.838	108.621	12.7	9.0	101.54	288.94	10.35		101	-9.264	107.231	14.7	96.6	87.02	288.94	10.35
70	-9.794	108.491	12.7	114.9	115.94	288.94	10.35		102	-9.220	107.101	14.7	28.3	122.56	288.94	10.35
71	-9.750	108.362	12.7	91.9	115.95	288.94	10.35		103	-9.177	106.972	14.7	0.8	70.22	288.94	10.35
72	-9.707	108.233	12.7	64.7	100.08	288.94	10.35		104	-9.133	106.843	14.7	8.0	87.52	288.94	10.35
73	-9.663	108.104	12.7	17.3	123.07	288.94	10.35		105	-9.089	106.713	14.7	1.3	96.33	288.94	10.35
74	-9.619	107.974	12.7	57.1	68.21	288.94	10.35		106	-9.873	109.331	16.7	43.3	121.79	288.94	10.35
75	-9.575	107.845	12.7	64.8	79.84	288.94	10.35		107	-9.829	109.202	16.7	87.2	124.50	288.94	10.35
76	-9.531	107.716	12.7	131.0	76.46	288.94	10.35		108	-9.785	109.073	16.7	61.5	87.11	288.94	10.35
77	-9.488	107.586	12.7	112.1	99.52	288.94	10.35		109	-9.741	108.943	16.7	31.5	70.58	288.94	10.35
78	-9.444	107.457	12.7	60.2	97.77	288.94	10.35		110	-9.698	108.814	16.7	0.7	65.18	288.94	10.35
79	-9.400	107.328	12.7	127.0	80.27	288.94	10.35		111	-9.654	108.685	16.7	5.7	87.71	288.94	10.35
80	-9.356	107.198	12.7	63.4	65.01	288.94	10.35		112	-9.610	108.555	16.7	93.5	107.32	288.94	10.35
81	-9.312	107.069	12.7	0.5	94.79	288.94	10.35		113	-9.566	108.426	16.7	93.6	85.39	288.94	10.35
82	-9.269	106.940	12.7	1.5	66.79	288.94	10.35		114	-9.522	108.297	16.7	47.3	74.24	288.94	10.35

Notes:

- The number of sub-faults are $21 \times 7 = 147$
- Each sub-fault has an area of $15 \text{ km} \times 11 \text{ km}$

Appendix E

A. Tsunami source by Cheng-Ji (2006) (Continued from preceding page)

#	Lat	Lon.	depth	slip	rake	strike	dip		#	Lat	Lon.	depth	slip	rake	strike	dip
115	-9.479	108.168	16.7	24.7	124.20	288.94	10.35		141	-9.168	107.553	18.7	0.4	67.81	288.94	10.35
116	-9.435	108.038	16.7	35.6	71.79	288.94	10.35		142	-9.124	107.424	18.7	35.3	124.05	288.94	10.35
117	-9.391	107.909	16.7	25.1	75.28	288.94	10.35		143	-9.080	107.295	18.7	59.2	124.55	288.94	10.35
118	-9.347	107.780	16.7	68.2	107.43	288.94	10.35		144	-9.036	107.165	18.7	15.2	66.83	288.94	10.35
119	-9.304	107.650	16.7	24.7	112.78	288.94	10.35		145	-8.993	107.036	18.7	28.1	76.08	288.94	10.35
120	-9.260	107.521	16.7	0.5	79.87	288.94	10.35		146	-8.949	106.907	18.7	48.1	124.24	288.94	10.35
121	-9.216	107.392	16.7	119.9	75.03	288.94	10.35		147	-8.905	106.777	18.7	42.4	124.43	288.94	10.35
122	-9.172	107.263	16.7	77.1	110.83	288.94	10.35									
123	-9.128	107.133	16.7	31.7	123.83	288.94	10.35									
124	-9.085	107.004	16.7	11.4	66.47	288.94	10.35									
125	-9.041	106.875	16.7	33.8	115.66	288.94	10.35									
126	-8.997	106.745	16.7	39.5	65.16	288.94	10.35									
127	-9.781	109.363	18.7	35.4	111.96	288.94	10.35									
128	-9.737	109.234	18.7	103.1	124.63	288.94	10.35									
129	-9.693	109.105	18.7	101.4	122.71	288.94	10.35									
130	-9.649	108.975	18.7	76.8	68.20	288.94	10.35									
131	-9.606	108.846	18.7	10.7	77.80	288.94	10.35									
132	-9.562	108.717	18.7	1.3	100.73	288.94	10.35									
133	-9.518	108.587	18.7	37.5	124.59	288.94	10.35									
134	-9.474	108.458	18.7	119.0	100.38	288.94	10.35									
135	-9.430	108.329	18.7	79.6	91.57	288.94	10.35									
136	-9.387	108.200	18.7	97.6	109.86	288.94	10.35									
137	-9.343	108.070	18.7	87.7	87.57	288.94	10.35									
138	-9.299	107.941	18.7	15.1	64.75	288.94	10.35									
139	-9.255	107.812	18.7	82.6	71.67	288.94	10.35									
140	-9.211	107.682	18.7	66.1	98.56	288.94	10.35									

Notes:

- The number of sub-faults are $21 \times 7 = 147$
- Each sub-fault has an area of $15 \text{ km} \times 11 \text{ km}$

Appendix E

B. Summary of the tsunami source by RuptGen ver.1.1 for rigidity of 30 GPa

RuptGen v.1.1: Summary file

Fri Jul 9 18:11:48 2010

Name of the plate interface file: pi15150.pi

Total earthquake Mw magnitude = 7.8, seismic moment M0, [Nm] = 6.30957e+20

Grid for surface displacements: longitude: 102 113, latitude: -13 -5, step [arc min]: 2

Maximal uplift, [m]: 1.0358

Maximal depression, [m]: -0.417242

Earthquake consists of 1 ruptures.

Rupture No. 1:

Mw = 7.8, M0 = 6.30957e+20

Epicenter: Lon = 107.989, Lat = -9.405

Central patch: I = 62, J = 4, IDX = 919

Length,[km] = 127.057, Width,[km] = 38.7258, Avg.slip,[m] = 2.00952

Number of ruptured patches: 15

Maximal slip, [m]: 5.59968

Appendix E

C. Summary of the tsunami source by RuptGen ver.1.1 for rigidity of 10 GPa

RuptGen v.1.1: Summary file

Fri Jul 9 18:04:05 2010

Name of the plate interface file: pi15150.pi

Total earthquake Mw magnitude = 7.8, seismic moment M0,[Nm] = 6.30957e+20

Grid for surface displacements: longitude: 102 113, latitude: -13 -5, step [arc min]: 2

Maximal uplift, [m]: 3.10739

Maximal depression, [m]: -1.25173

Earthquake consists of 1 ruptures.

Rupture No. 1:

Mw = 7.8, M0 = 6.30957e+20

Epicenter: Lon = 107.989, Lat = -9.405

Central patch: I = 62, J = 4, IDX = 919

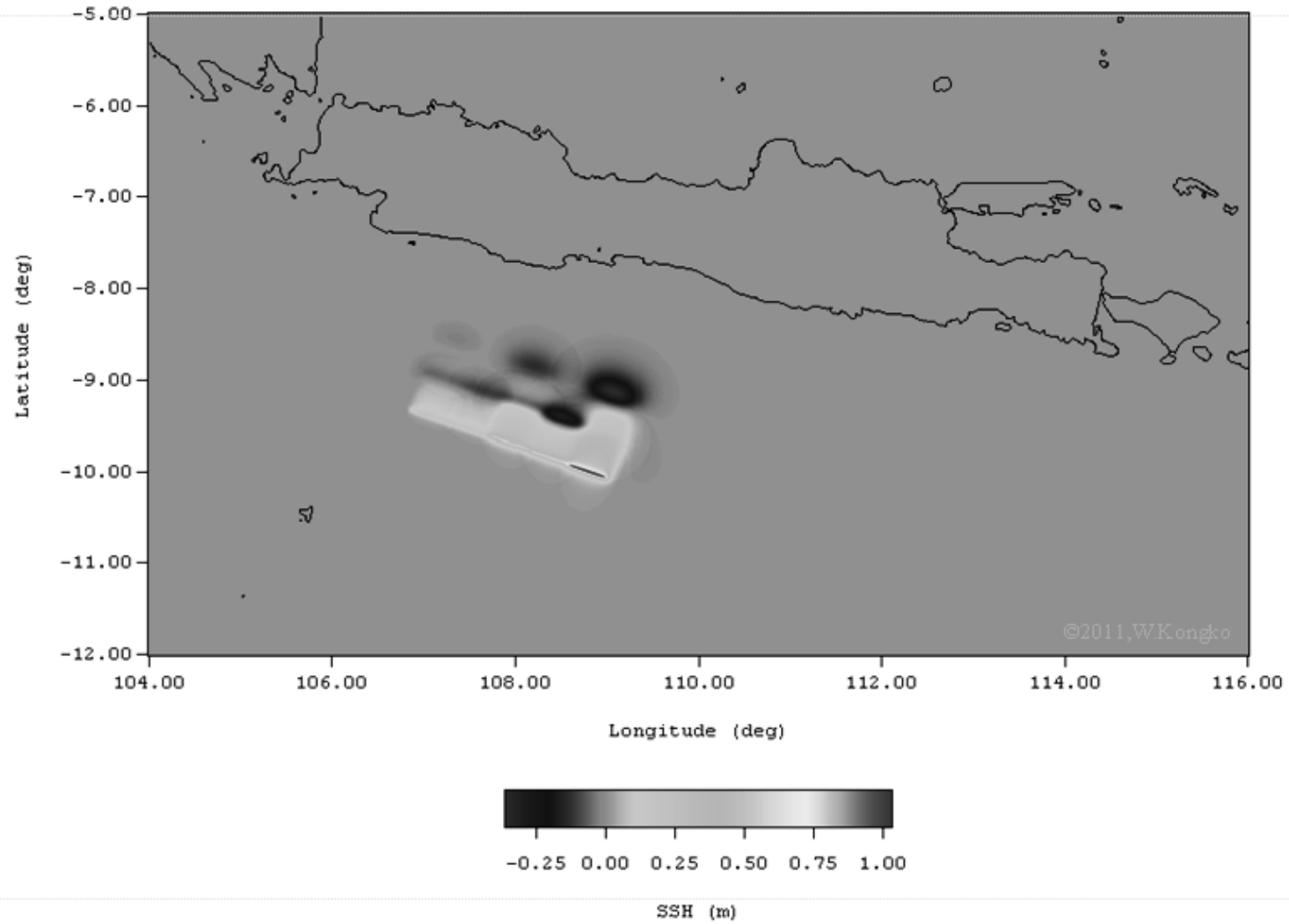
Length,[km] = 127.057, Width,[km] = 38.7258, Avg.slip,[m] = 6.02857

Number of ruptured patches: 15

Maximal slip, [m]: 16.799

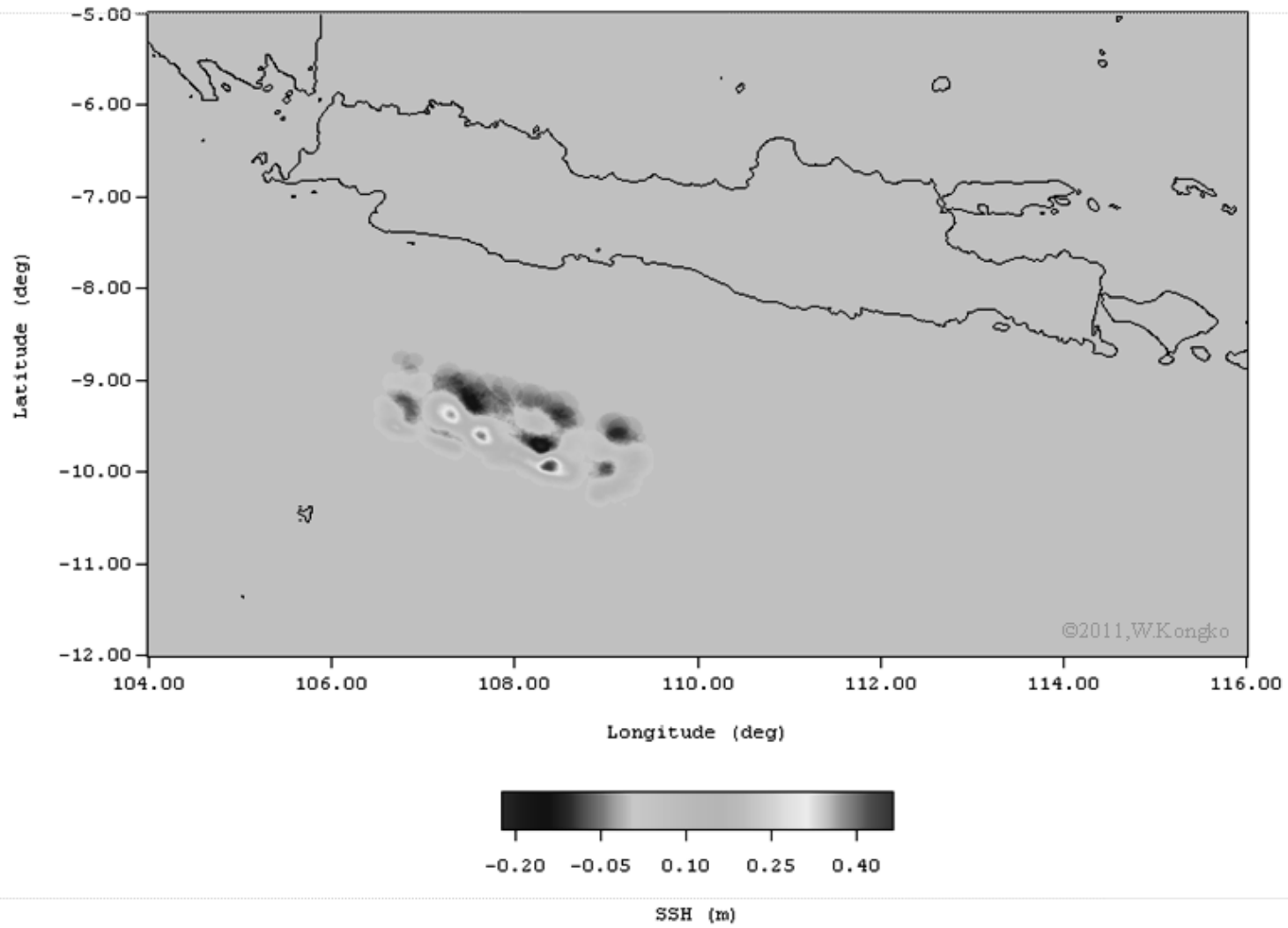
Appendix E

D. Source model of the 2006 Java tsunami (Fujii & Satake, 2006)



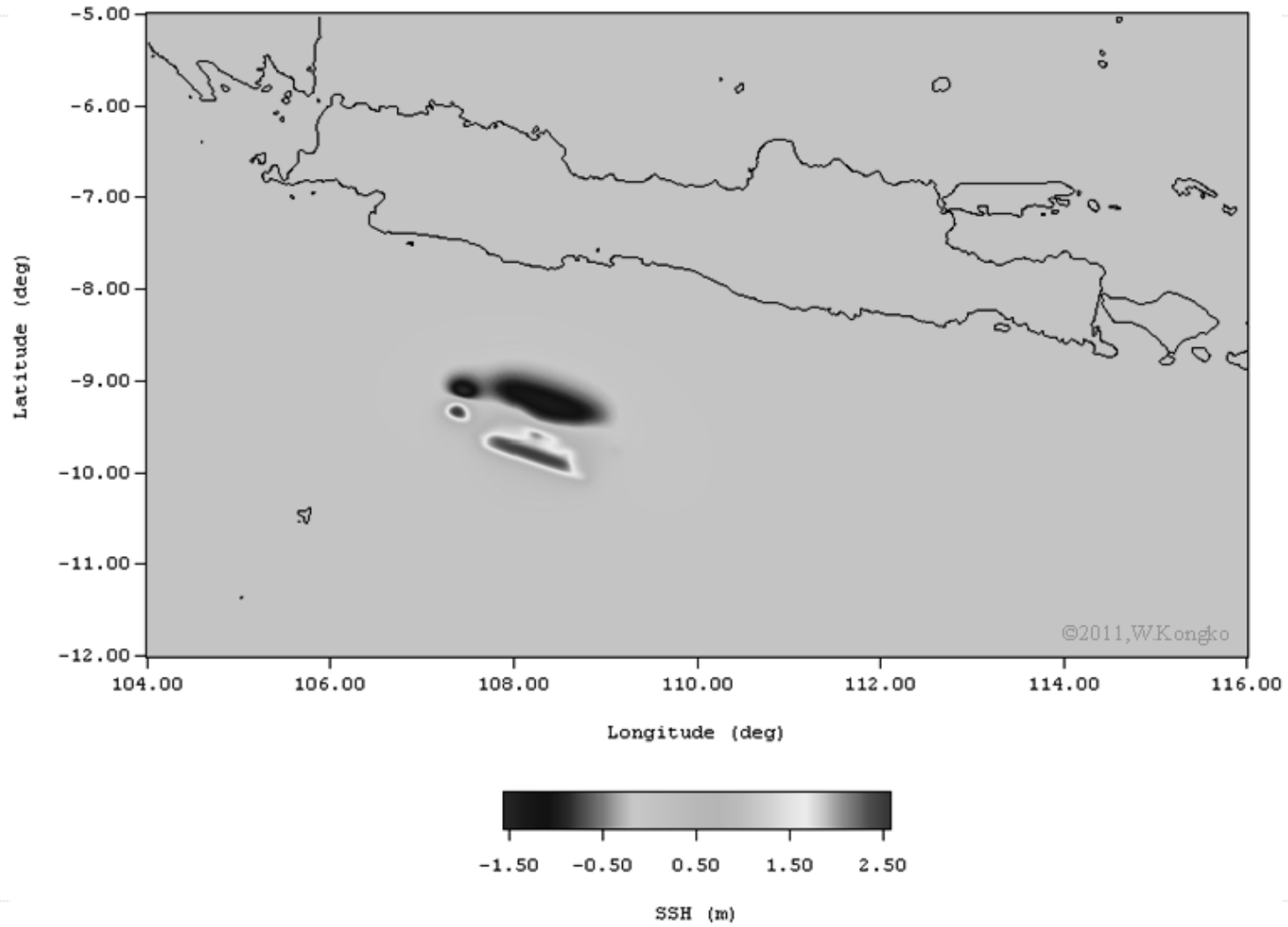
Appendix E

E. Source model of the 2006 Java tsunami (USGS - Ji, 2006)



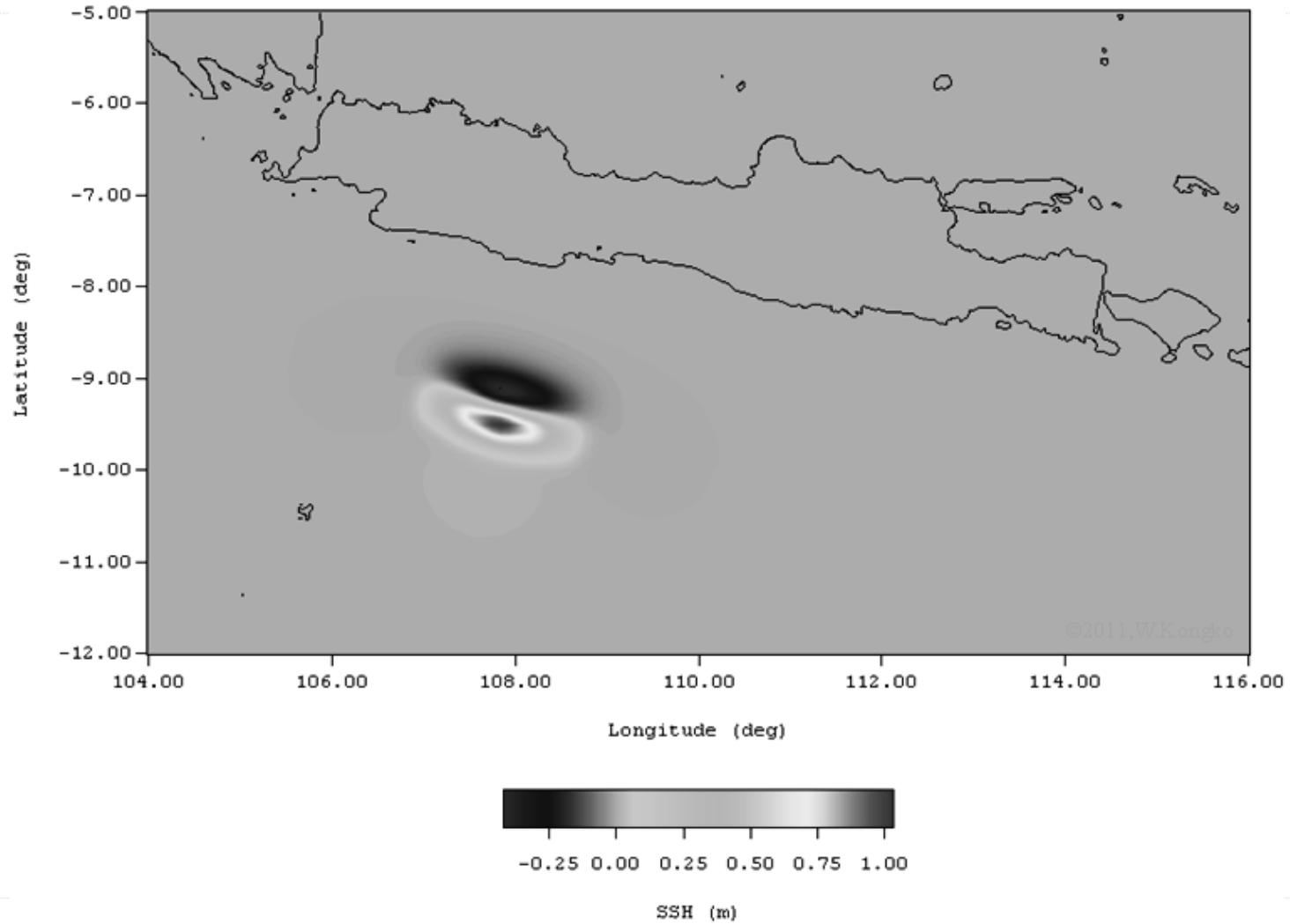
Appendix E

F. Source model of the 2006 Java tsunami (Ammon et al., 2006)



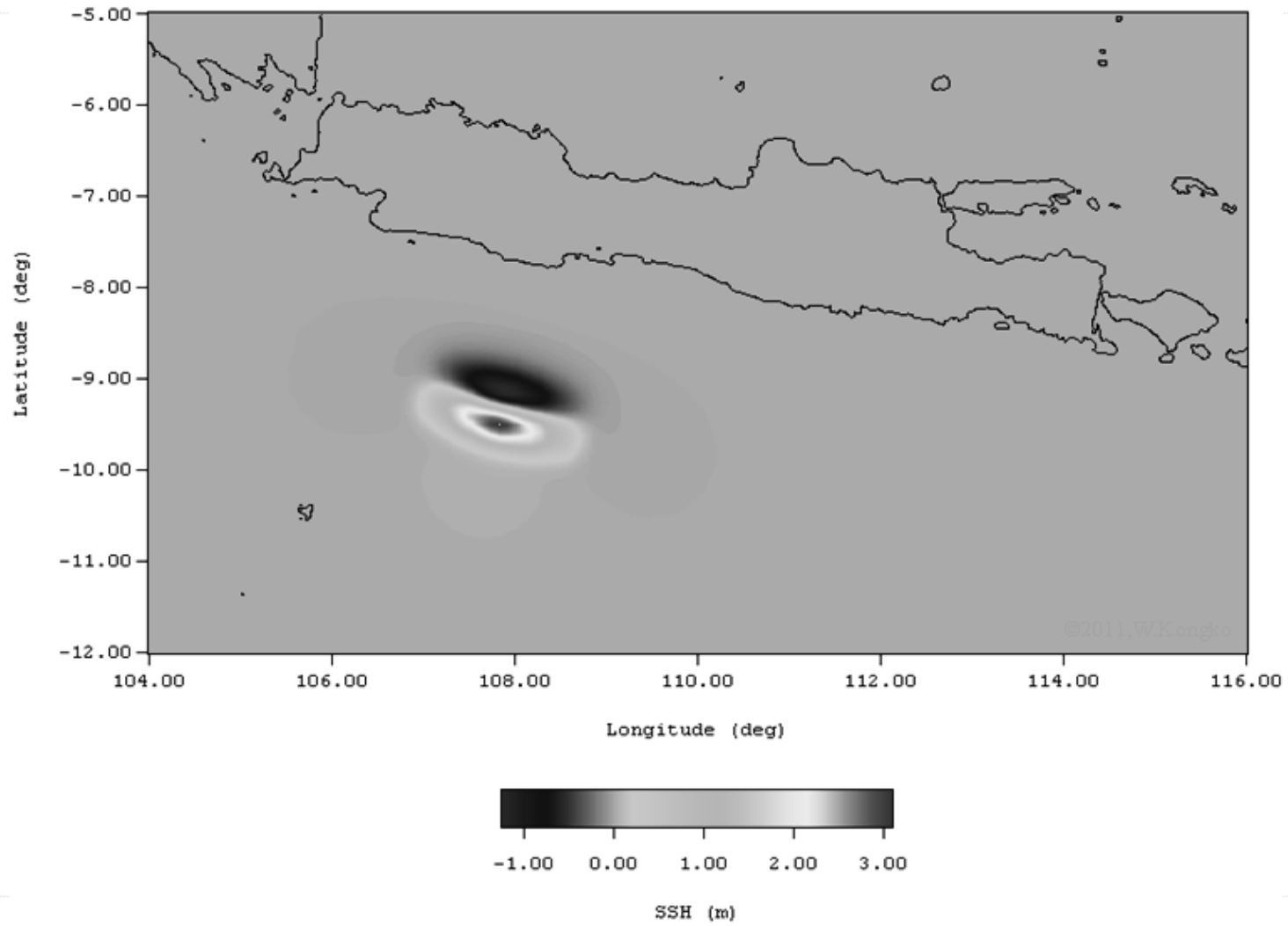
Appendix E

G. Source model of the 2006 Java tsunami with $\mu = 30$ GPa (RuptGen ver.1.1 - GITEWS, 2010)



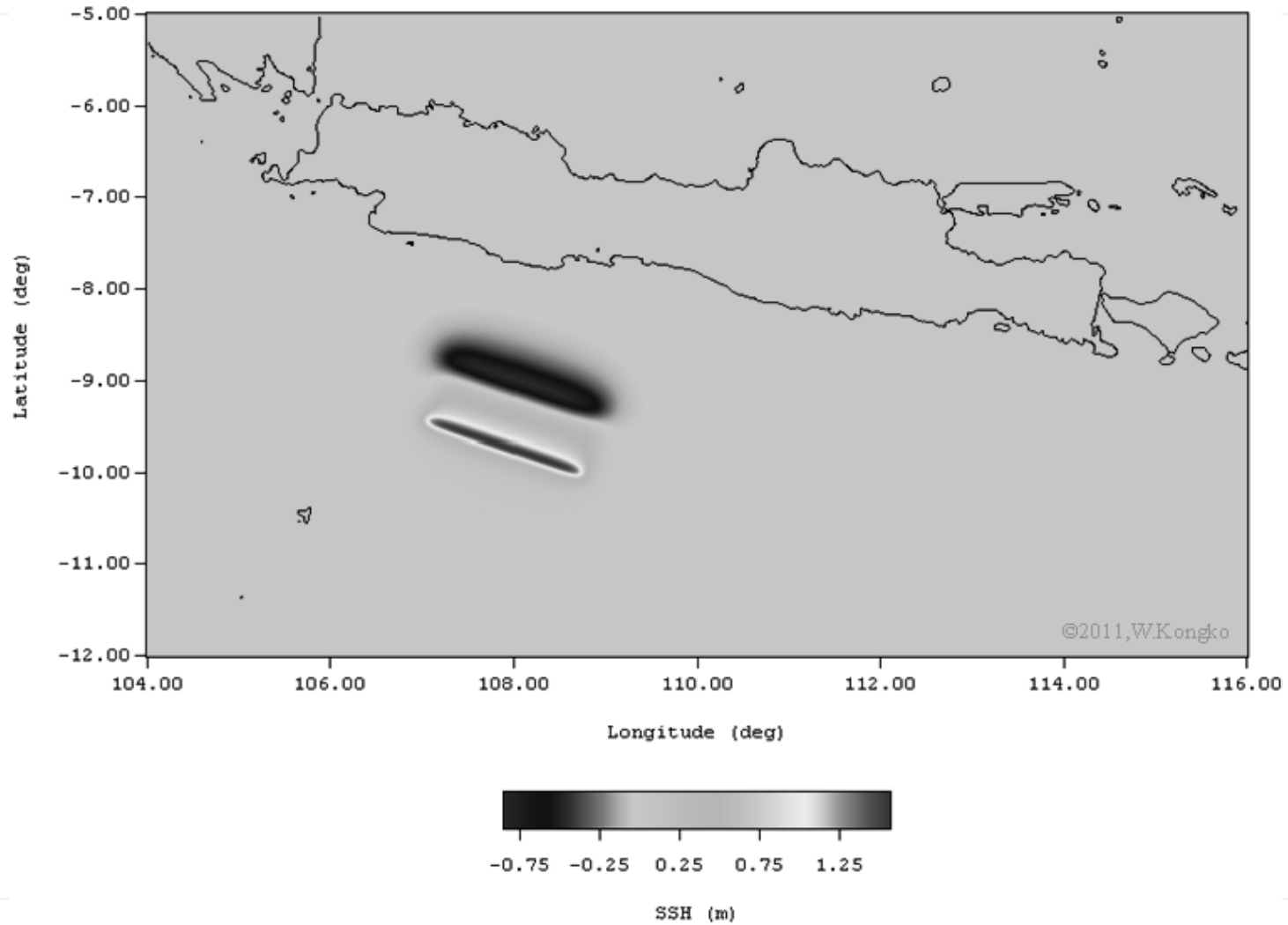
Appendix E

H. Source model of the 2006 Java tsunami with $\mu = 10$ GPa (RuptGen ver.1.1 - GITEWS, 2010)



Appendix E

I. Source model of the 2006 Java tsunami with $\mu = 10$ GPa (Proposed in the present study)



Appendix E

J. Source parameters of hypothetical model for future hazard

Scenario	Epicenter		Depth (km)	Angle		
	Lon.(deg)	Lat.(deg)		Strike	Dip	Rake
1	108.0080	-9.7773	5.0	289°	10°	95°
2	108.4042	-9.9079	5.0	289°	10°	95°
3	108.7991	-10.0380	5.0	289°	10°	95°
4	108.8759	-9.8198	10.0	289°	10°	95°
5	108.4843	-9.6805	10.0	289°	10°	95°
6	108.0923	-9.5494	10.0	289°	10°	95°
7	108.1687	-9.3417	15.0	289°	12°	95°
8	108.5578	-9.4720	15.0	289°	12°	95°
9	108.9554	-9.6059	15.0	289°	12°	95°
10	107.3200	-9.2220	10.0	289°	10°	95°
11	108.6800	-9.2100	25.0	289°	15°	95°
12	110.0032	-10.0197	10.0	280°	10°	95°
13	111.1466	-10.2193	10.0	280°	10°	95°
14	112.8350	-10.4770	10.0	280°	10°	95°
15	109.0468	-9.3349	25.0	289°	15°	95°
16	112.8350	-10.4770	10.0	289°	15°	95°

Notes:

- Hypocenters are assumed in accretionary prism, which its depth < 25 km; closer to Java coastline is deeper (following the Beniof-Wadati curve),
- Strike angles in the west zone of ~110°E, the parameters are set to be 289°. Those in the eastern of ~110°E are set to be 280°E. Slip angles are kept constant values of 95°.

Appendix E

K. Source parameters of hypothetical model for future hazard

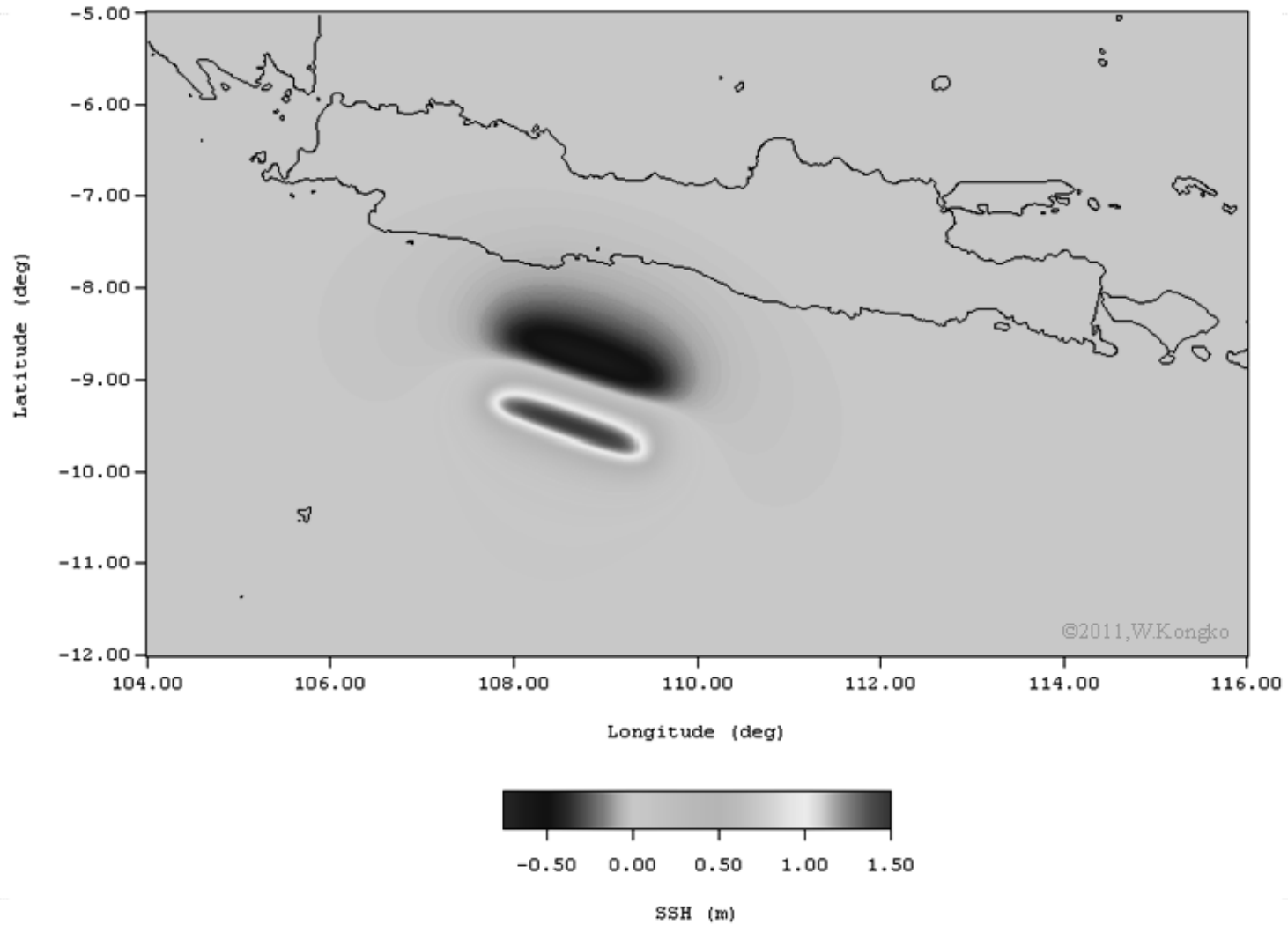
Magnitude	Wells & Coppersmith (1994)				Papazachos et al. (2004)			E. Okal (2006)			Strasser et al. (2010)			Present study (2011)		
	Mw / Mo(Nm)	Event	L (Km)	W (Km)	Slip (m)	L (Km)	W (Km)	Slip (m)	L (Km)	W (Km)	Slip (m)	L (Km)	W (Km)	Slip (m)	L (Km)	W (Km)
7.8	All	197.4	45.9	7.0	125.9	61.4	8.2	95.5	47.7	2.8	127.7	75.5	6.5	200.0	80.0	3.95
6.31E+20	Reverse	127.1	38.7	12.8												
8.0	All	268.9	56.4	8.3	162.2	70.8	11.0	120.2	60.1	3.5	177.8	97.5	7.3	275.0	110.0	4.15
1.26E+21	Reverse	166.0	46.8	16.2												
8.2	All	366.2	69.2	9.9	208.9	81.7	14.7	151.4	75.7	4.4	247.6	125.8	8.1	375.0	150.0	4.46
2.51E+21	Reverse	216.8	56.5	20.5												

Notes:

- The magnitudes scenario refers to the historical data in Sunda trench (USGS, 2006; Tsuji et al., 1995; Gusman et al., 2009),
- Rupture dimensions are proposed by considering empirical studies conducted by prior researchers. Except slips proposed by Okal (2006), others are determined based on the low rigidity of 10 GPa.

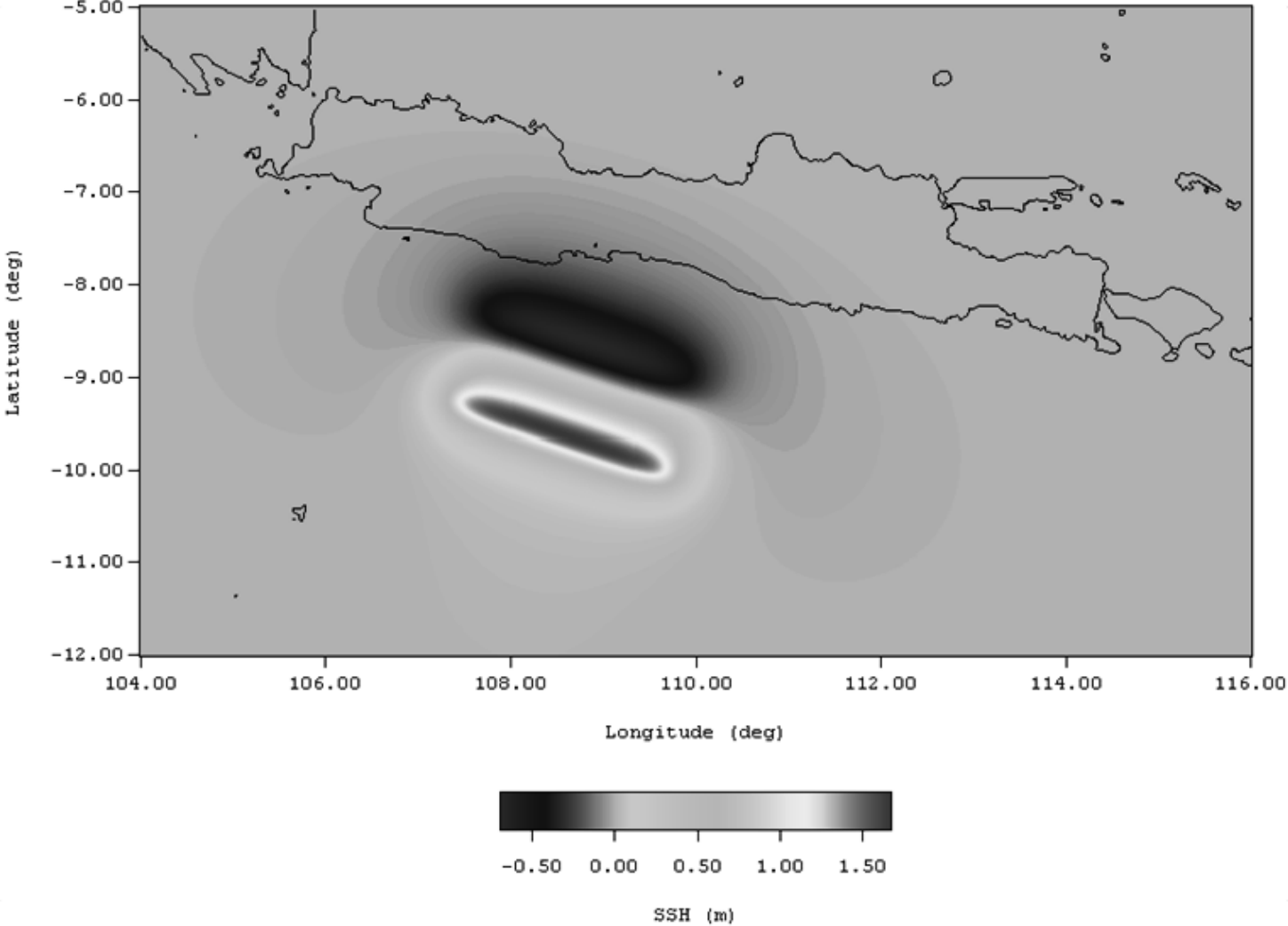
Appendix E

L. Source of hypothetical model for future hazard, M_W 7.8 epicenter at point 11



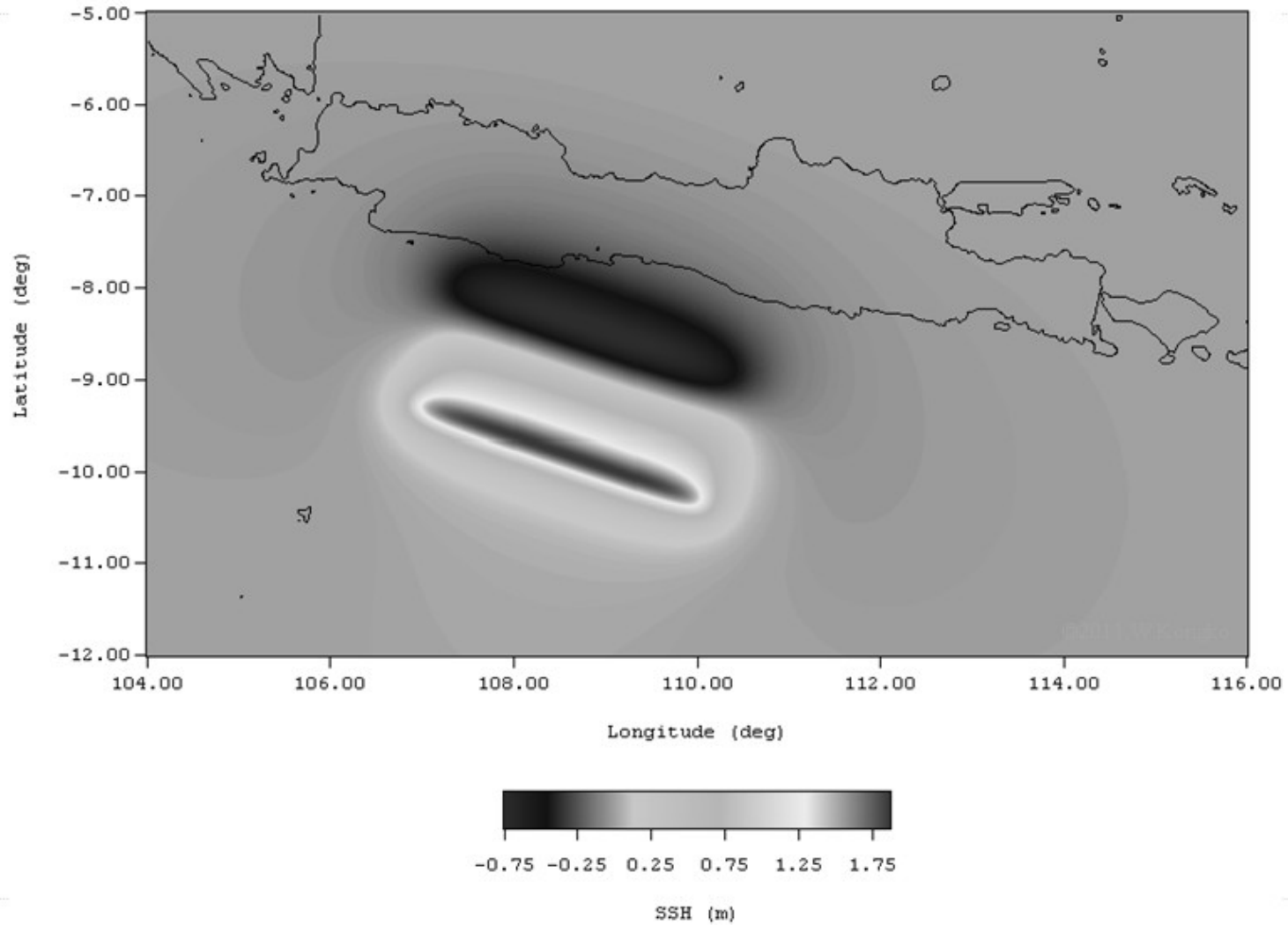
Appendix E

M. Source of hypothetical model for future hazard, M_W 8.0 epicenter at point 11



Appendix E

N. Source of hypothetical model for future hazard, M_W 8.2 epicenter at point 11



Appendix E

O. Source parameters of single-fault of synthetic model ($\mu=10$ GPa-40 GPa)

Magnitude	Wells & Coppersmith (1994)				Papazachos et al. (2004)			Strasser et al. (2010)			Present study (2011)			Rigidity
	Mw / Mo(Nm)	Event	L (Km)	W (Km)	Slip (m)	L (Km)	W (Km)	Slip (m)	L (Km)	W (Km)	Slip (m)	L (Km)	W (Km)	
7.8	All	197.4	45.9	6.96	125.9	61.4	8.17	127.7	75.5	6.54	150	60	6.93	10 Gpa
6.31E+20	Reverse	127.1	38.7	12.82										
7.8	All	197.4	45.9	3.48	125.9	61.4	4.09	127.7	75.5	3.27	150	60	3.47	20 Gpa
6.31E+20	Reverse	127.1	38.7	6.41										
7.8	All	197.4	45.9	2.32	125.9	61.4	2.70	127.7	75.5	2.18	150	60	2.35	30 Gpa
6.31E+20	Reverse	127.1	38.7	4.27										
7.8	All	197.4	45.9	1.74	125.9	61.4	2.10	127.7	75.5	1.63	150	60	1.76	40 Gpa
6.31E+20	Reverse	127.1	38.7	3.21										

Notes:

- The angle parameters of strike, dip, and slip are determined of 270°, 10°, and 90°, respectively,
- Depths are set depends on the uniformly & distributed slip, varying from 5.0 km to 13.7 km.

Appendix E

P. Source parameters of distributed slip (multi-faults) for synthetic model (M_w 7.8, $\mu=10$ GPa)

DOMAIN BOUND & SPACING																			

LON-LEFT : 107.318939																			
LON-RIGHT : 112.062002																			
LAT-TOP : -7.091506																			
LAT-BOTTOM : -10.601064																			
SPACING (min) : 0.540000																			

SOURCE PARAMETER																			

No	Epicenter		Depth	Strike	Dip	Slip	L	W	Slip	No	Epicenter		Depth	Strike	Dip	Slip	L	W	Slip
	Lon	Lat	(km)	(deg)	(deg)	(deg)	(km)	(km)	(m)		Lon	Lat	(km)	(deg)	(deg)	(deg)	(km)	(km)	(m)
1	109.052	-9.658	13.7	270	10	90	10	10	0.0	24	109.781	-9.748	12	270	10	90	10	10	7.1
2	109.143	-9.658	13.7	270	10	90	10	10	0.0	25	109.872	-9.748	12	270	10	90	10	10	5.9
3	109.234	-9.658	13.7	270	10	90	10	10	0.0	26	109.963	-9.748	12	270	10	90	10	10	4.7
4	109.325	-9.658	13.7	270	10	90	10	10	0.0	27	110.054	-9.748	12	270	10	90	10	10	3.6
5	109.417	-9.658	13.7	270	10	90	10	10	0.0	28	110.146	-9.748	12	270	10	90	10	10	2.4
6	109.508	-9.658	13.7	270	10	90	10	10	0.0	29	110.237	-9.748	12	270	10	90	10	10	1.2
7	109.599	-9.658	13.7	270	10	90	10	10	0.0	30	110.328	-9.748	12	270	10	90	10	10	0.0
8	109.690	-9.658	13.7	270	10	90	10	10	0.0	31	109.052	-9.838	10.3	270	10	90	10	10	0.0
9	109.781	-9.658	13.7	270	10	90	10	10	0.0	32	109.143	-9.838	10.3	270	10	90	10	10	26.0
10	109.872	-9.658	13.7	270	10	90	10	10	0.0	33	109.234	-9.838	10.3	270	10	90	10	10	26.0
11	109.963	-9.658	13.7	270	10	90	10	10	0.0	34	109.325	-9.838	10.3	270	10	90	10	10	26.0
12	110.054	-9.658	13.7	270	10	90	10	10	0.0	35	109.417	-9.838	10.3	270	10	90	10	10	23.6
13	110.146	-9.658	13.7	270	10	90	10	10	0.0	36	109.508	-9.838	10.3	270	10	90	10	10	21.3
14	110.237	-9.658	13.7	270	10	90	10	10	0.0	37	109.599	-9.838	10.3	270	10	90	10	10	18.9
15	110.328	-9.658	13.7	270	10	90	10	10	0.0	38	109.690	-9.838	10.3	270	10	90	10	10	16.6
16	109.052	-9.748	12	270	10	90	10	10	0.0	39	109.781	-9.838	10.3	270	10	90	10	10	14.2
17	109.143	-9.748	12	270	10	90	10	10	13.0	40	109.872	-9.838	10.3	270	10	90	10	10	11.8
18	109.234	-9.748	12	270	10	90	10	10	13.0	41	109.963	-9.838	10.3	270	10	90	10	10	9.5
19	109.325	-9.748	12	270	10	90	10	10	13.0	42	110.054	-9.838	10.3	270	10	90	10	10	7.1
20	109.417	-9.748	12	270	10	90	10	10	11.8	43	110.146	-9.838	10.3	270	10	90	10	10	4.7
21	109.508	-9.748	12	270	10	90	10	10	10.6	44	110.237	-9.838	10.3	270	10	90	10	10	2.4
22	109.599	-9.748	12	270	10	90	10	10	9.5	45	110.328	-9.838	10.3	270	10	90	10	10	0.0
23	109.690	-9.748	12	270	10	90	10	10	8.3	46	109.052	-9.928	8.5	270	10	90	10	10	0.0

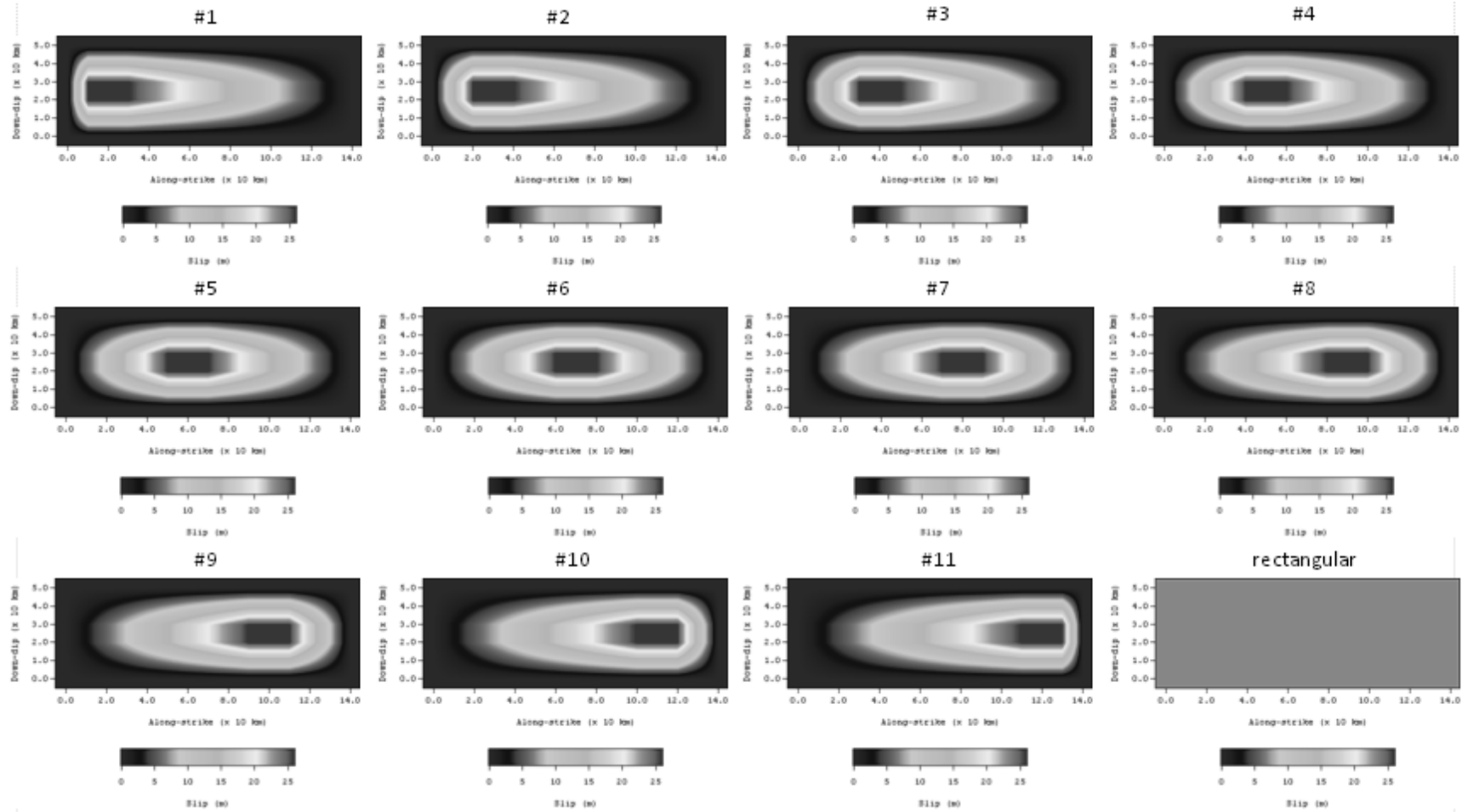
Appendix E

P.Source parameters of distributed slip (multi-faults) for synthetic model (M_w 7.8, $\mu=10$ GPa)

No	Epicenter		Depth (km)	Strike (deg)	Dip (deg)	Slip (deg)	L (km)	W (km)	Slip (m)	No	Epicenter		Depth (km)	Strike (deg)	Dip (deg)	Slip (deg)	L (km)	W (km)	Slip (m)
	Lon	Lat									Lon	Lat							
47	109.143	-9.928	8.5	270	10	90	10	10	26.0	85	109.872	-10.108	5	270	10	90	10	10	0.0
48	109.234	-9.928	8.5	270	10	90	10	10	26.0	86	109.963	-10.108	5	270	10	90	10	10	0.0
49	109.325	-9.928	8.5	270	10	90	10	10	26.0	87	110.054	-10.108	5	270	10	90	10	10	0.0
50	109.417	-9.928	8.5	270	10	90	10	10	23.6	88	110.146	-10.108	5	270	10	90	10	10	0.0
51	109.508	-9.928	8.5	270	10	90	10	10	21.3	89	110.237	-10.108	5	270	10	90	10	10	0.0
52	109.599	-9.928	8.5	270	10	90	10	10	18.9	90	110.328	-10.108	5	270	10	90	10	10	0.0
53	109.690	-9.928	8.5	270	10	90	10	10	16.6										
54	109.781	-9.928	8.5	270	10	90	10	10	14.2										
55	109.872	-9.928	8.5	270	10	90	10	10	11.8										
56	109.963	-9.928	8.5	270	10	90	10	10	9.5										
57	110.054	-9.928	8.5	270	10	90	10	10	7.1										
58	110.146	-9.928	8.5	270	10	90	10	10	4.7										
59	110.237	-9.928	8.5	270	10	90	10	10	2.4										
60	110.328	-9.928	8.5	270	10	90	10	10	0.0										
61	109.052	-10.018	6.8	270	10	90	10	10	0.0										
62	109.143	-10.018	6.8	270	10	90	10	10	13.0										
63	109.234	-10.018	6.8	270	10	90	10	10	13.0										
64	109.325	-10.018	6.8	270	10	90	10	10	13.0										
65	109.417	-10.018	6.8	270	10	90	10	10	11.8										
66	109.508	-10.018	6.8	270	10	90	10	10	10.6										
67	109.599	-10.018	6.8	270	10	90	10	10	9.5										
68	109.690	-10.018	6.8	270	10	90	10	10	8.3										
69	109.781	-10.018	6.8	270	10	90	10	10	7.1										
70	109.872	-10.018	6.8	270	10	90	10	10	5.9										
71	109.963	-10.018	6.8	270	10	90	10	10	4.7										
72	110.054	-10.018	6.8	270	10	90	10	10	3.6										
73	110.146	-10.018	6.8	270	10	90	10	10	2.4										
74	110.237	-10.018	6.8	270	10	90	10	10	1.2										
75	110.328	-10.018	6.8	270	10	90	10	10	0.0										
76	109.052	-10.108	5	270	10	90	10	10	0.0										
77	109.143	-10.108	5	270	10	90	10	10	0.0										
78	109.234	-10.108	5	270	10	90	10	10	0.0										
79	109.325	-10.108	5	270	10	90	10	10	0.0										
80	109.417	-10.108	5	270	10	90	10	10	0.0										
81	109.508	-10.108	5	270	10	90	10	10	0.0										
82	109.599	-10.108	5	270	10	90	10	10	0.0										
83	109.690	-10.108	5	270	10	90	10	10	0.0										
84	109.781	-10.108	5	270	10	90	10	10	0.0										

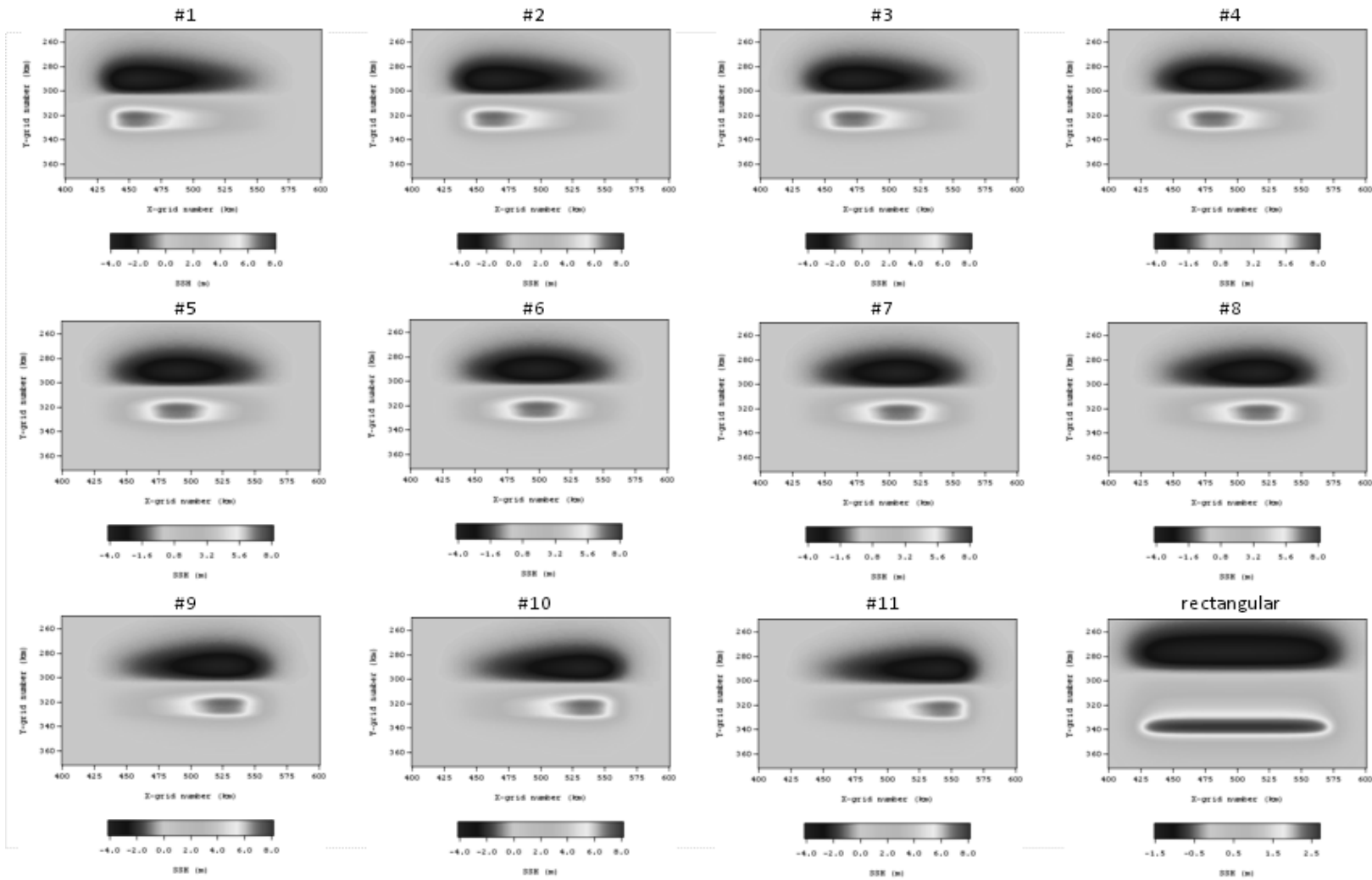
Appendix E

Q. Slip distribution of synthetic model for $\mu=10$ GPa



Appendix E

R. Deformation of synthetic model for $\mu=10$ GPa



Appendix F – Parameters of the model

A. Parameters of the model for the 2006 Java tsunami

Data sources	Domain s' name	Bounding Coordinates (UTM-49S)				Grid Size		Grid Spac.	Time step
		Longitude range		Latitude range		X	Y	(m)	(second)
GEBCO 08	1	-278827	1054045	9444296	8663084	721	423	1851.21	1.00
GEBCO 08 & SRTM	2a	54113	362031	9198116	9094448	500	169	617.07	1.00
GEBCO 08 & SRTM	2b	339931	692895	9155506	9050604	573	171	617.07	1.00
GEBCO 08 & SRTM	3a	94221	351745	9184939	9122615	1253	304	205.69	0.50
GEBCO 08 & SRTM	3b	340624	689269	9146759	9059752	1696	424	205.69	0.50
GEBCO 08 & SRTM	4a1	113728	246192	9172712	9129379	1933	633	68.56	0.30
GEBCO 08 & SRTM	4a1a	124857	171686	9165588	9140082	2050	1117	22.85	0.20
GEBCO 08 & SRTM	4a1b	167480	212618	9147535	9132542	1976	657	22.85	0.20
GEBCO 08 & SRTM	4a1c	201061	246199	9151349	9132563	1976	823	22.85	0.20
GEBCO 08 & SRTM & MEASUREMENTS*)	4a2	232753	349173	9173141	9130221	1699	627	68.56	0.30
GEBCO 08 & SRTM & MEASUREMENTS*)	4a2a	232876	275614	9154777	9138436	1871	716	22.85	0.20
GEBCO 08 & SRTM & MEASUREMENTS*)	4a2b	272806	324709	9154755	9136883	2272	783	22.85	0.20
GEBCO 08 & SRTM & MEASUREMENTS*)	4a2c	309139	349180	9153428	9137156	1753	713	22.85	0.20
GEBCO 08 & SRTM & MEASUREMENTS*)	4b1	346192	535015	9144063	9068849	2755	1098	68.56	0.30
GEBCO 08 & SRTM & MEASUREMENTS*)	4b1a	346221	416202	9142043	9112355	3063	1300	22.85	0.20
GEBCO 08 & SRTM	4b1b	410259	480148	9120120	9090524	3059	1296	22.85	0.20
GEBCO 08 & SRTM	4b1c	470284	535031	9097575	9077623	2834	874	22.85	0.20
GEBCO 08 & SRTM	4b2	527869	686936	9109423	9062114	2321	691	68.56	0.30
GEBCO 08 & SRTM	4b2a	528033	589672	9098174	9069743	2698	1245	22.85	0.20
GEBCO 08 & SRTM	4b2b	584170	639935	9098103	9069604	2441	1248	22.85	0.20
GEBCO 08 & SRTM	4b2c	631114	686856	9081113	9062120	2440	832	22.85	0.20
GEBCO 08 & SRTM & MEASUREMENTS*)	5x1x	262509	269487	9145806	9139757	917	795	7.62	0.10
GEBCO 08 & SRTM & MEASUREMENTS*)	5a1a	277269	300230	9153982	9138213	3015	2071	7.62	0.10
GEBCO 08 & SRTM & MEASUREMENTS*)	6a1a	278312	288302	9153901	9140369	3935	5330	2.54	0.05
GEBCO 08 & SRTM & MEASUREMENTS*)	6x1x	265201	267009	9144218	9141653	713	1011	2.54	0.05

*) Note: Terrain: Intermap SRTM (SRTM-30/90/DTM/DSM) with 30 m, 90 m, 5m resolution, respectively
 Seafloor: Single/Multi Beam Echosouder Measurements

Appendix F

B. Parameters of the model for the hypothetical model of future hazard

Data sources	Domain s' name	Bounding Coordinates (UTM-49S)				Grid Size		Grid Spac.	Time step
		Longitude range		Latitude range		X	Y	(m)	(second)
GEBCO 08	1	-278827	1054045	9444296	8663084	721	423	1851.21	1.00
GEBCO 08 & SRTM	2a	54113	362031	9198116	9094448	500	169	617.07	1.00
GEBCO 08 & SRTM	3a	94221	351745	9184939	9122615	1253	304	205.69	0.50
GEBCO 08 & SRTM & MEASUREMENTS*)	4a2	232753	349173	9173141	9130221	1699	627	68.56	0.30
GEBCO 08 & SRTM & MEASUREMENTS*)	4a2b	272806	324709	9154755	9136883	2272	783	22.85	0.20

*) Note: Terrain: Intermap SRTM (SRTM-30/90/DTM/DSM) with 30 m, 90 m, 5m resolution, respectively
Seafloor: Single/Multi Beam Echosouder Measurements

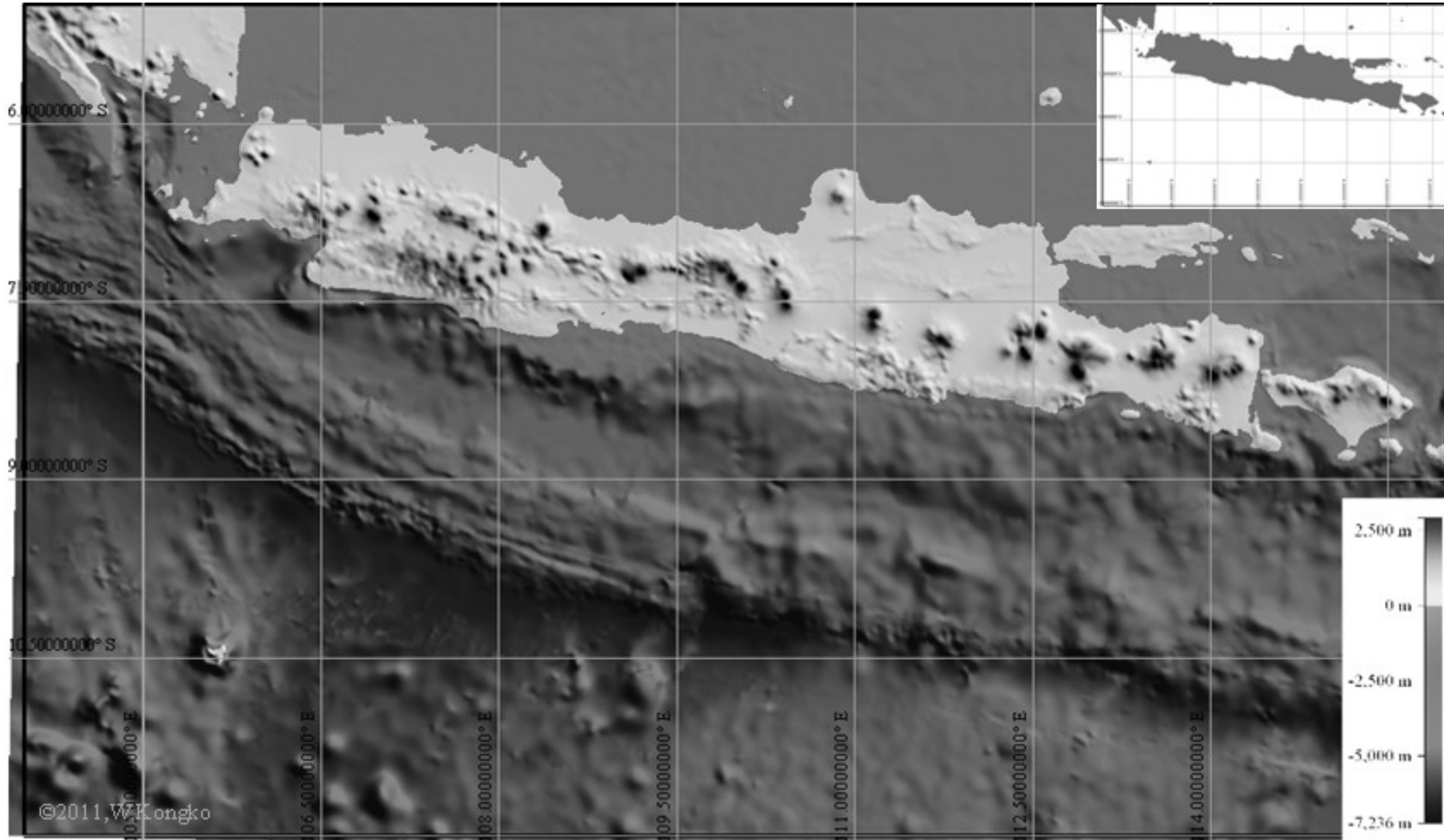
C. Parameters of the synthetic model for complex ruptures

Data sources	Domain s' name	Bounding Coordinates (UTM-49S)				Grid Size		Grid Spac.	Time step
		Longitude range		Latitude range		X	Y	(m)	(second)
Genearted from synthetic moderate line	1	-143463	856536	9217589	8467589	1000	750	1000.00	2.00
Genearted from synthetic maximum line	1	-143463	856536	9217589	8467589	1000	750	1000.00	2.00
Genearted from synthetic minimum line	1	-143463	856536	9217589	8467589	1000	750	1000.00	2.00

*) Note: Geometric data is derived from synthetic lines (moderate, maximum, and minimum)
Laterally (parallel to the coastline), the water depth is similar following the synthetic lines above

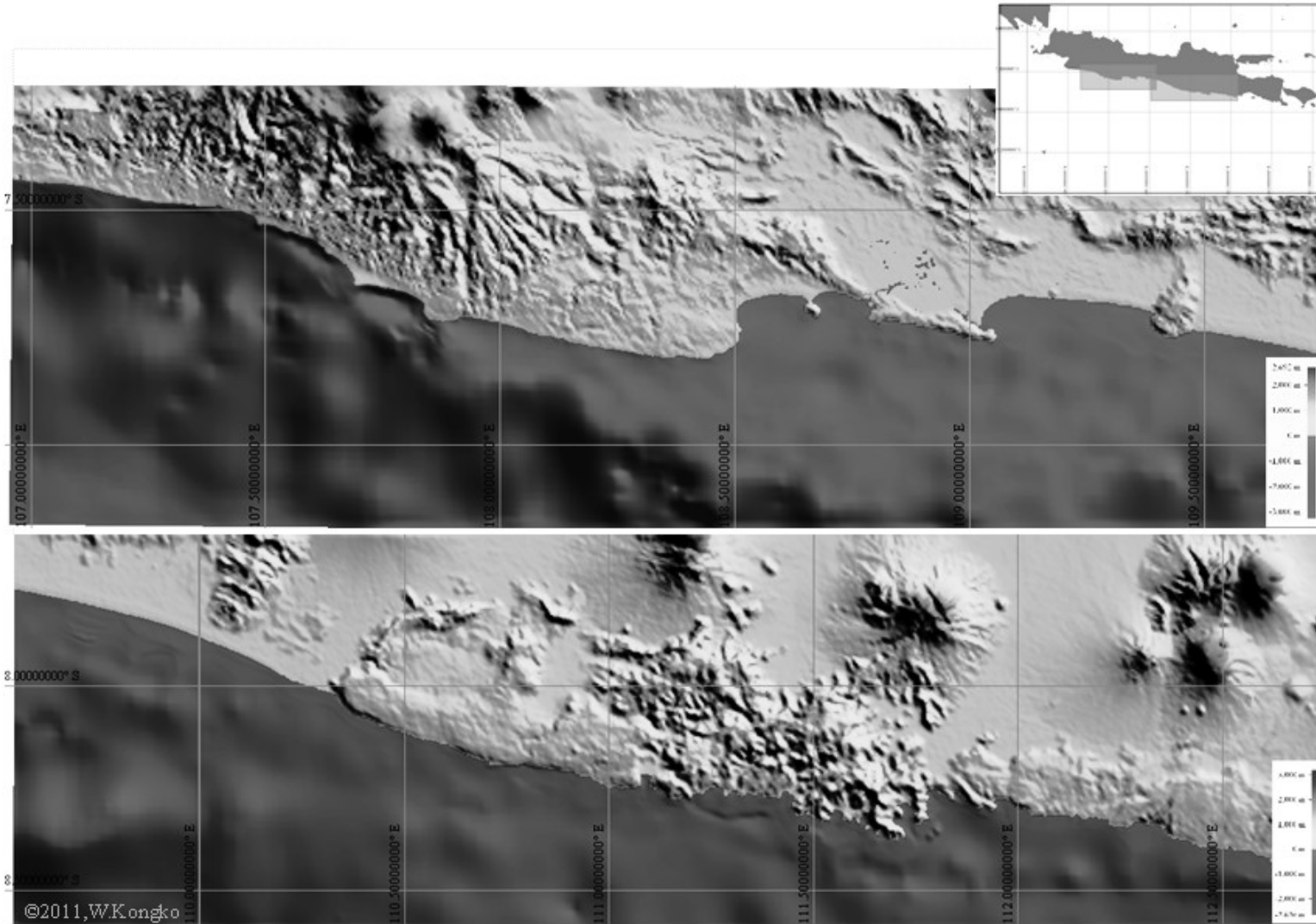
Appendix G – Data assimilation

A. Geometric model of level 1st for domain 1st (see also table parameters of the model in Appendix F section A)



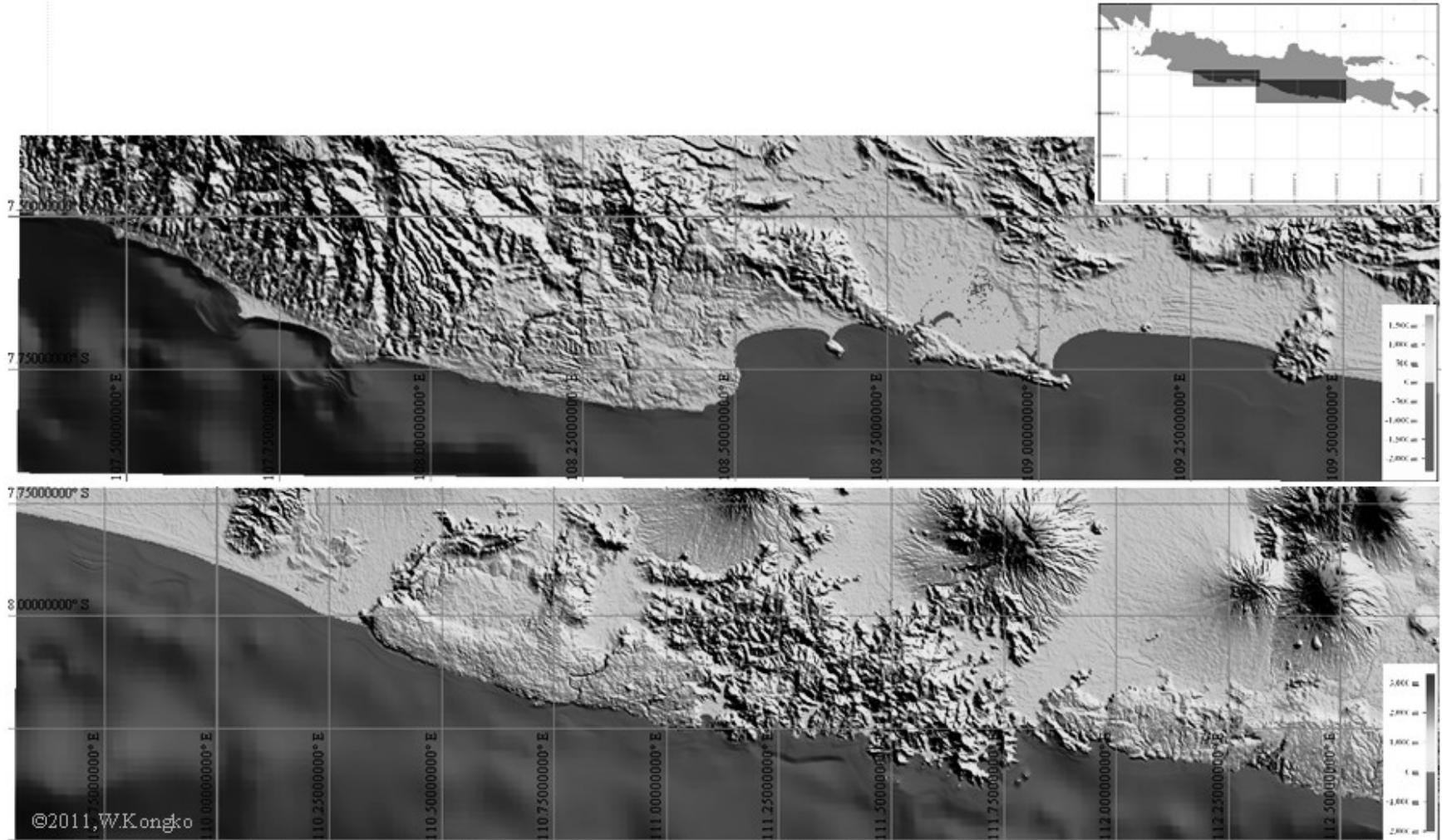
Appendix G

B. Geometric model of level 2nd for domain 2a (top panel) and 2b (bottom panel)



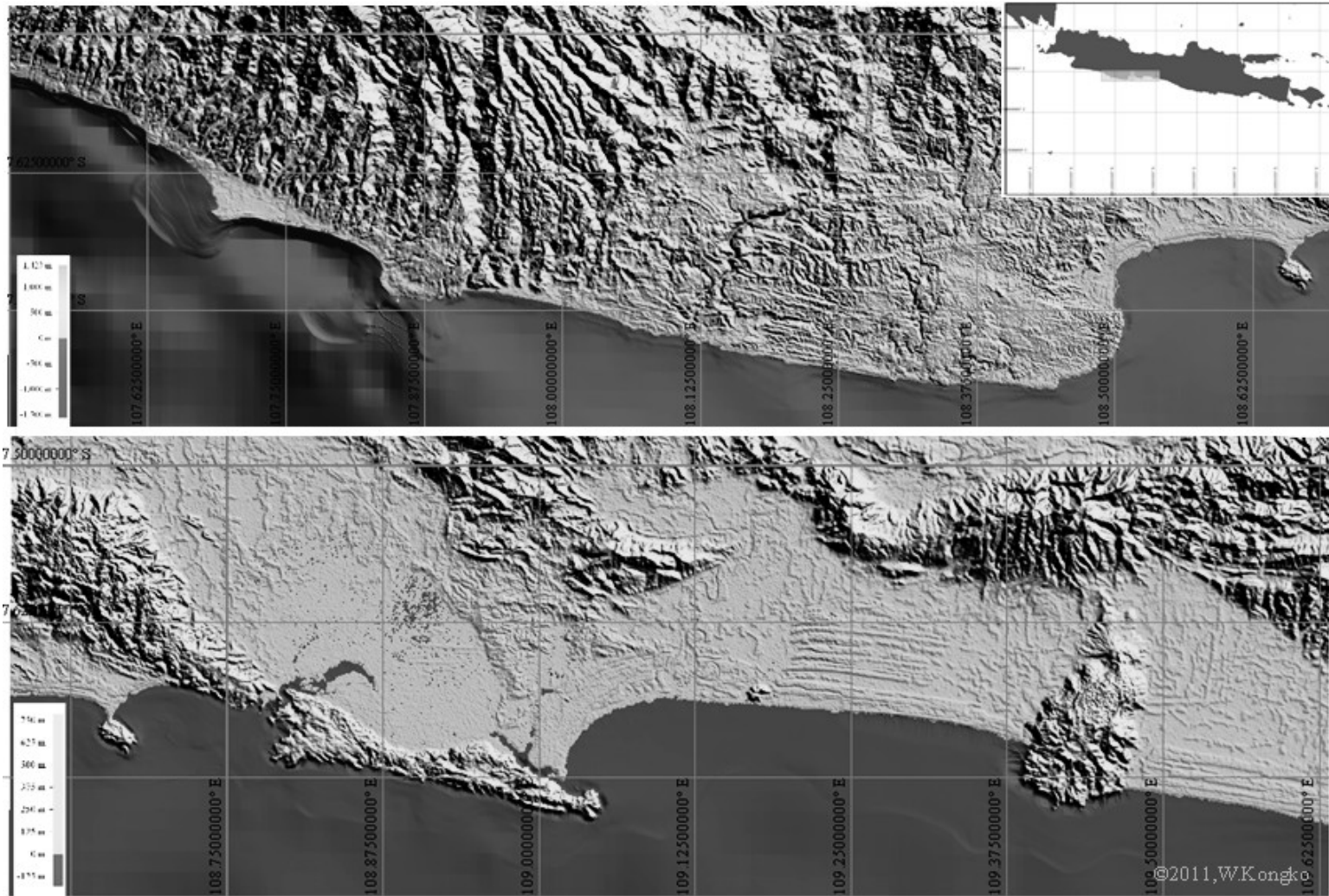
Appendix G

C. Geometric model of level 3rd for domain 3a (top panel) and 3b (bottom panel)



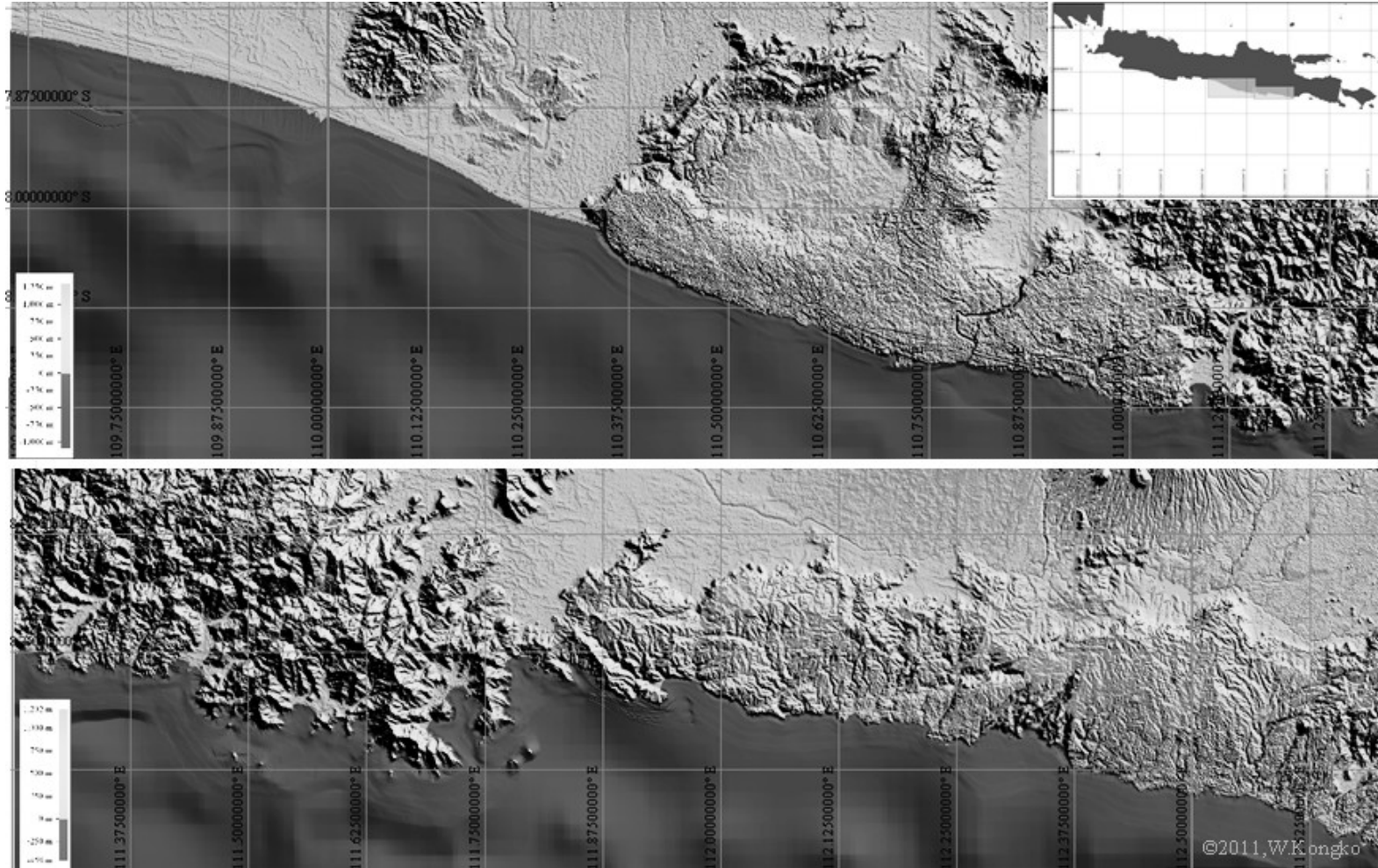
Appendix G

D. Geometric model of level 4th for domain 4a1 (top panel) and 4a2 (bottom panel)



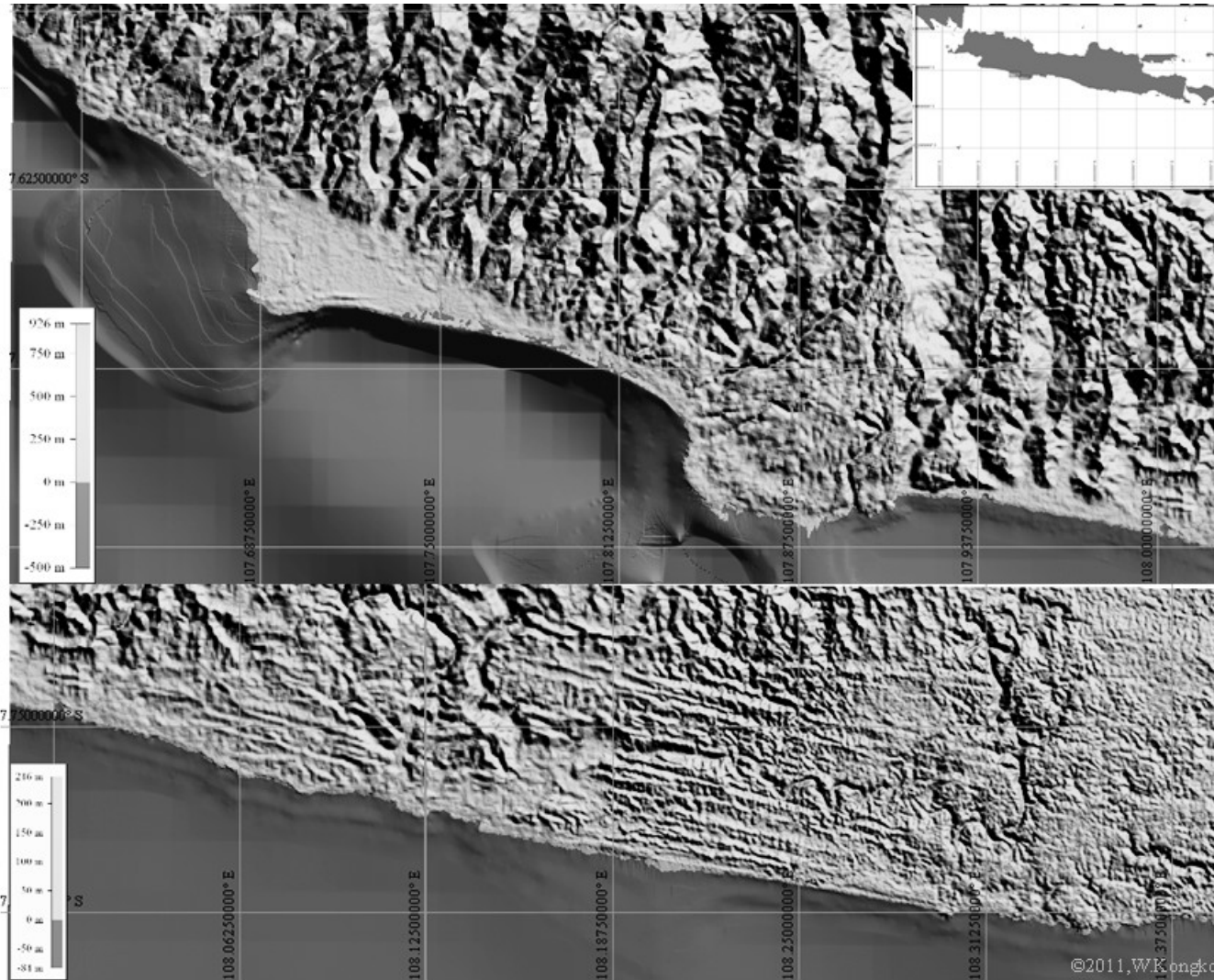
Appendix G

E. Geometric model of level 4th for domain 4b1 (top panel) and 4b2 (bottom panel)



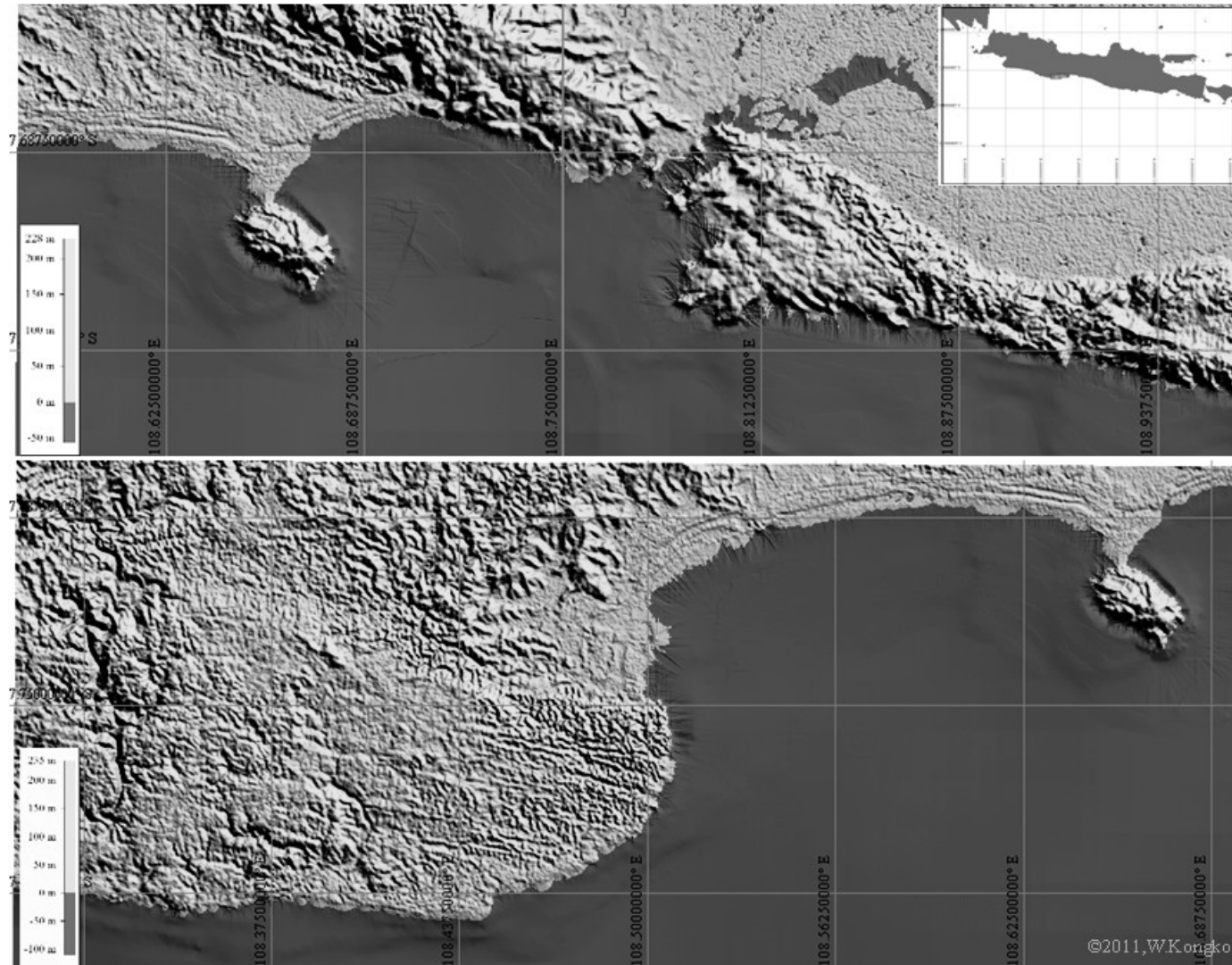
Appendix G

F. Geometric model of level 5th for domain 4a1a (top panel) and 4a1b (bottom panel)



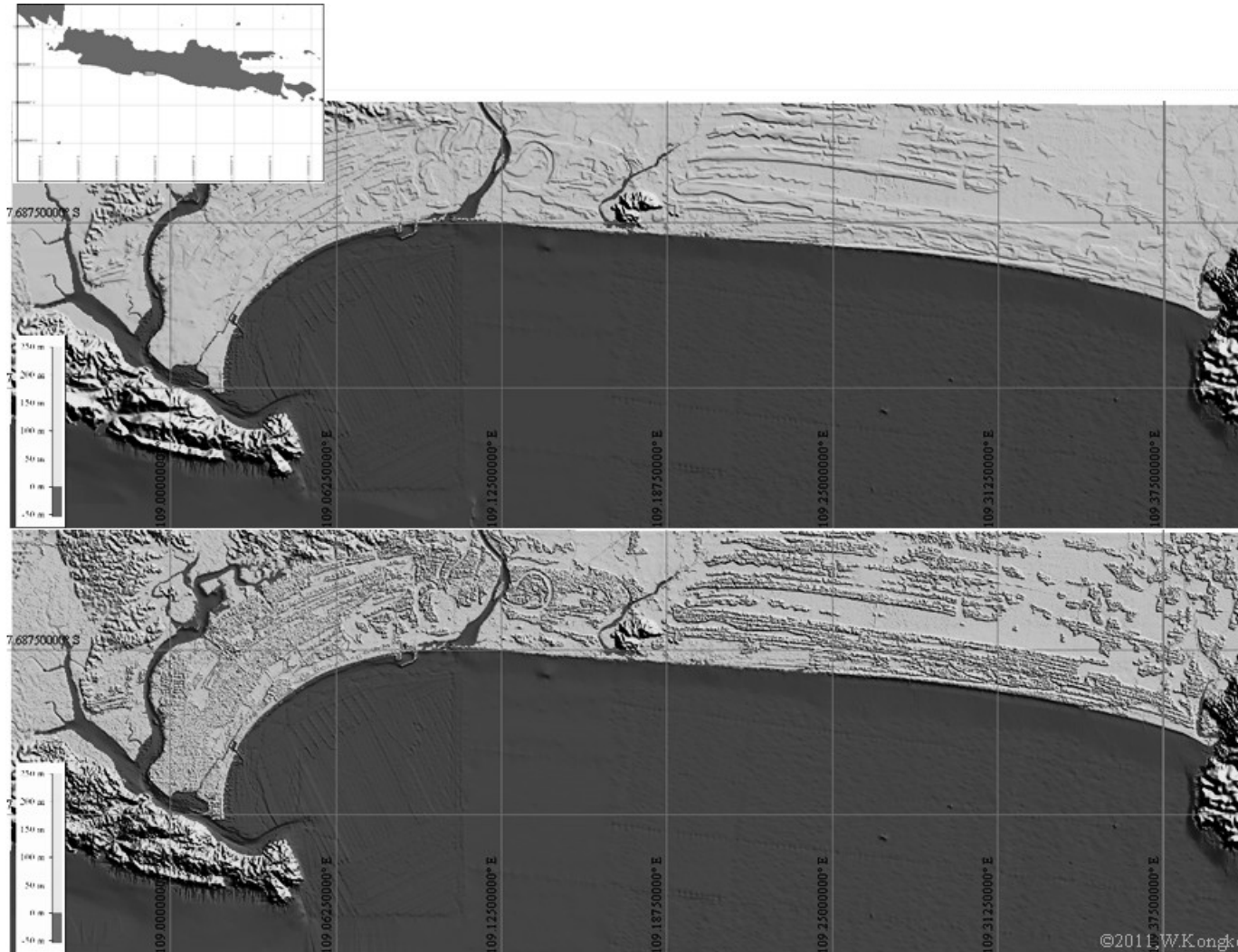
Appendix G

G. Geometric model of level 5th for domain 4a2a (top panel) and 4a1c (bottom panel)



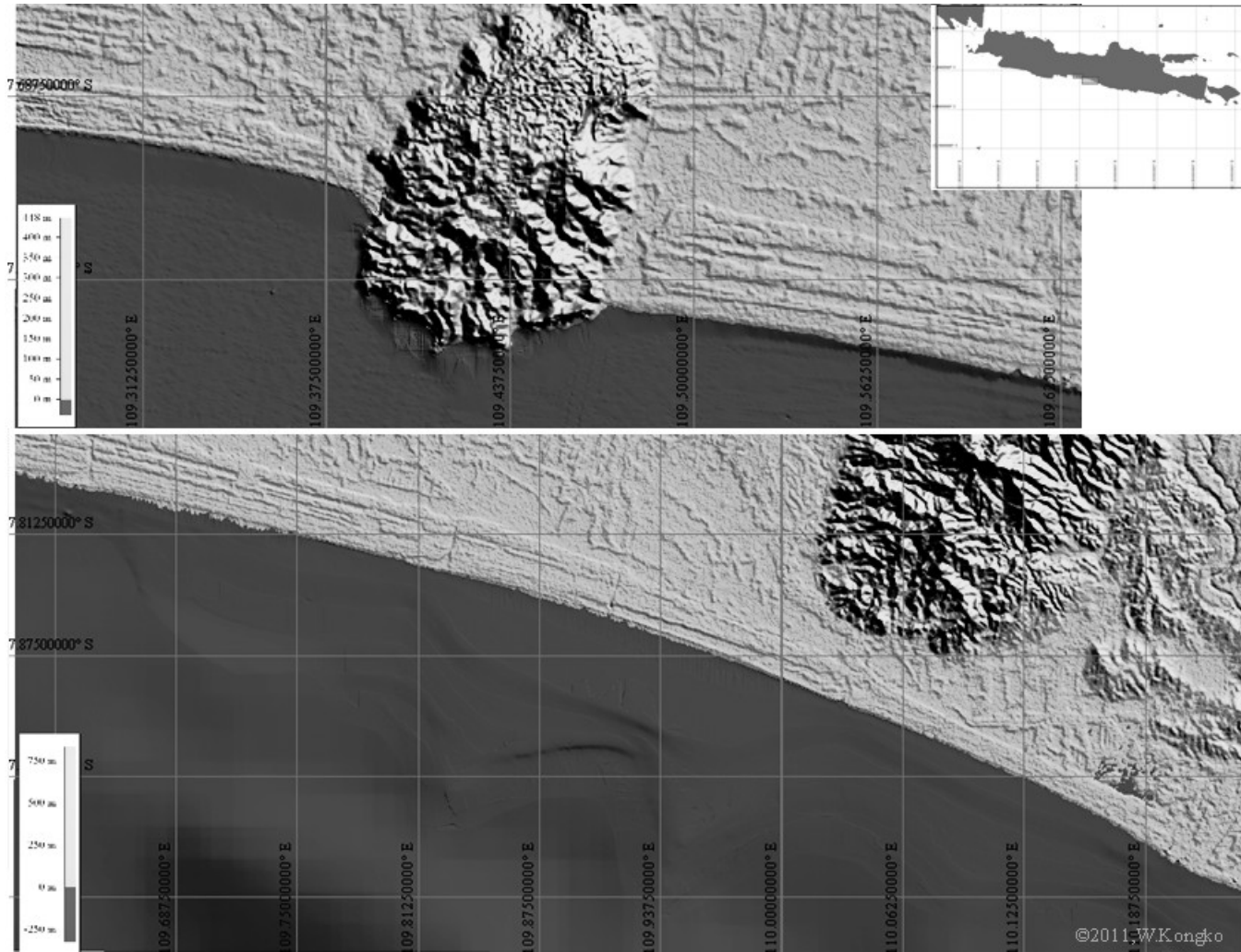
Appendix G

H. Geometric model of level 5th for domain 4a2b –DTM data (top panel) and 4a2b – DSM data (bottom panel)



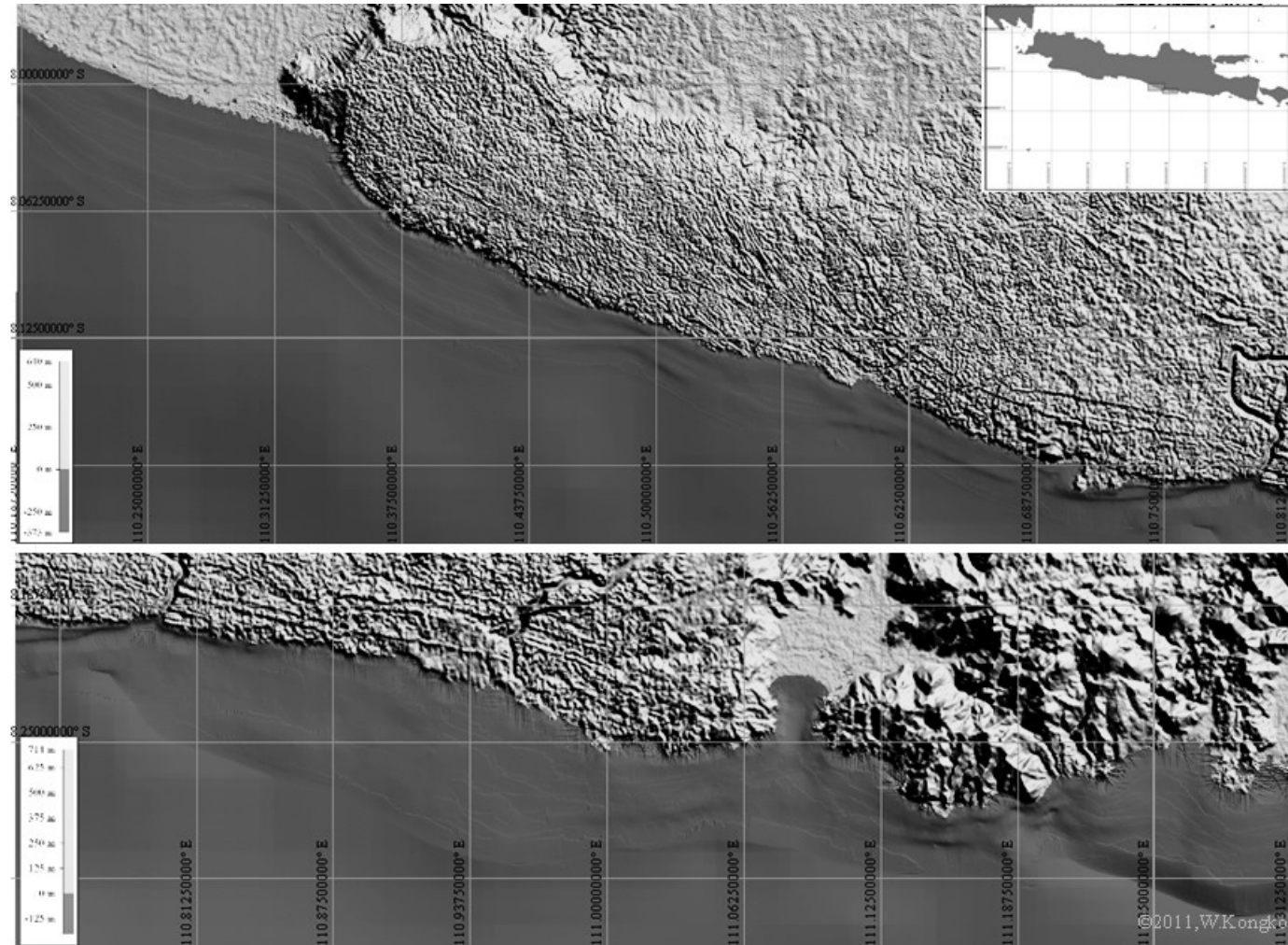
Appendix G

I. Geometric model of level 5th domain 4a2c (top panel) and 4b1a (bottom panel)



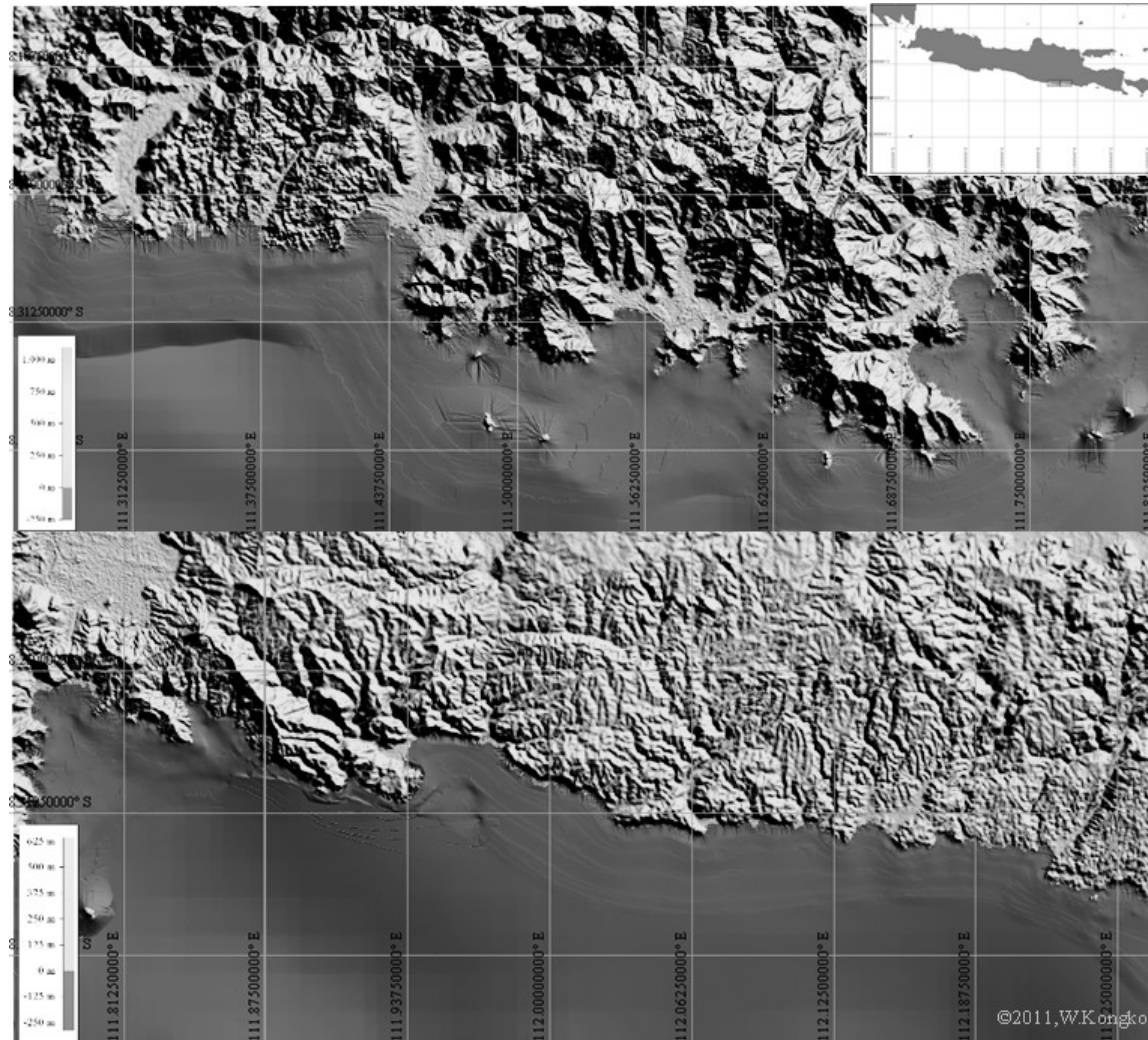
Appendix G

J. Geometric model of level 5th for domain 4b1b (top panel) and 4b1c (bottom panel)



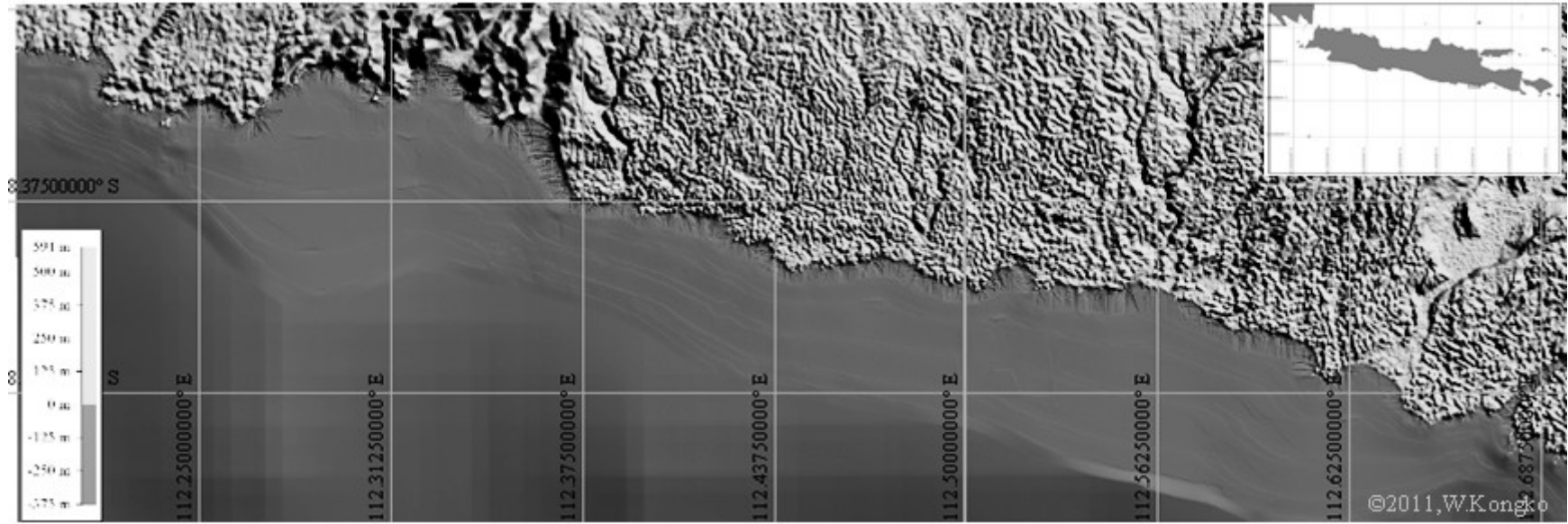
Appendix G

K. Geometric model of level 5th for domain 4b2a (top panel) and 4b2b (bottom panel)



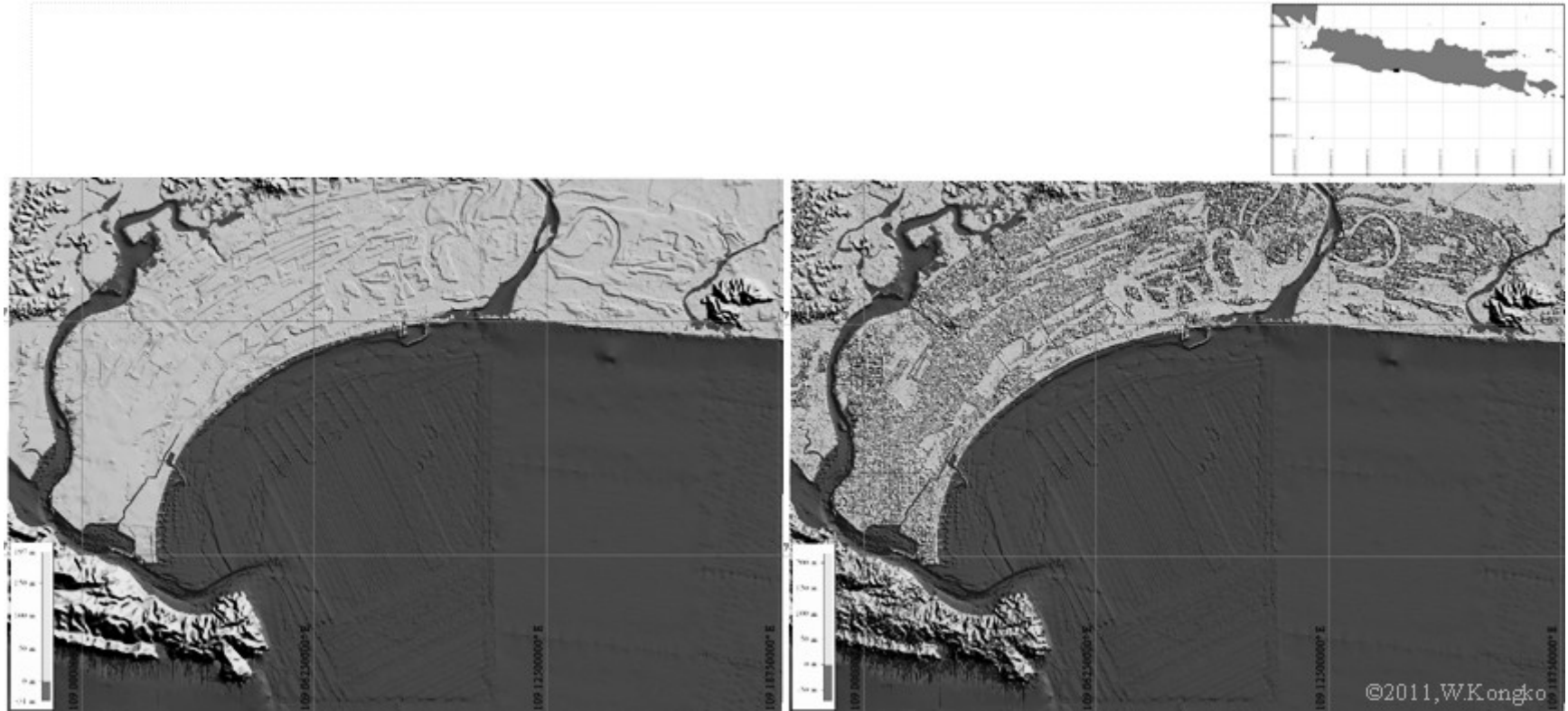
Appendix G

L. Geometric model of level 5th for domain 4b2c



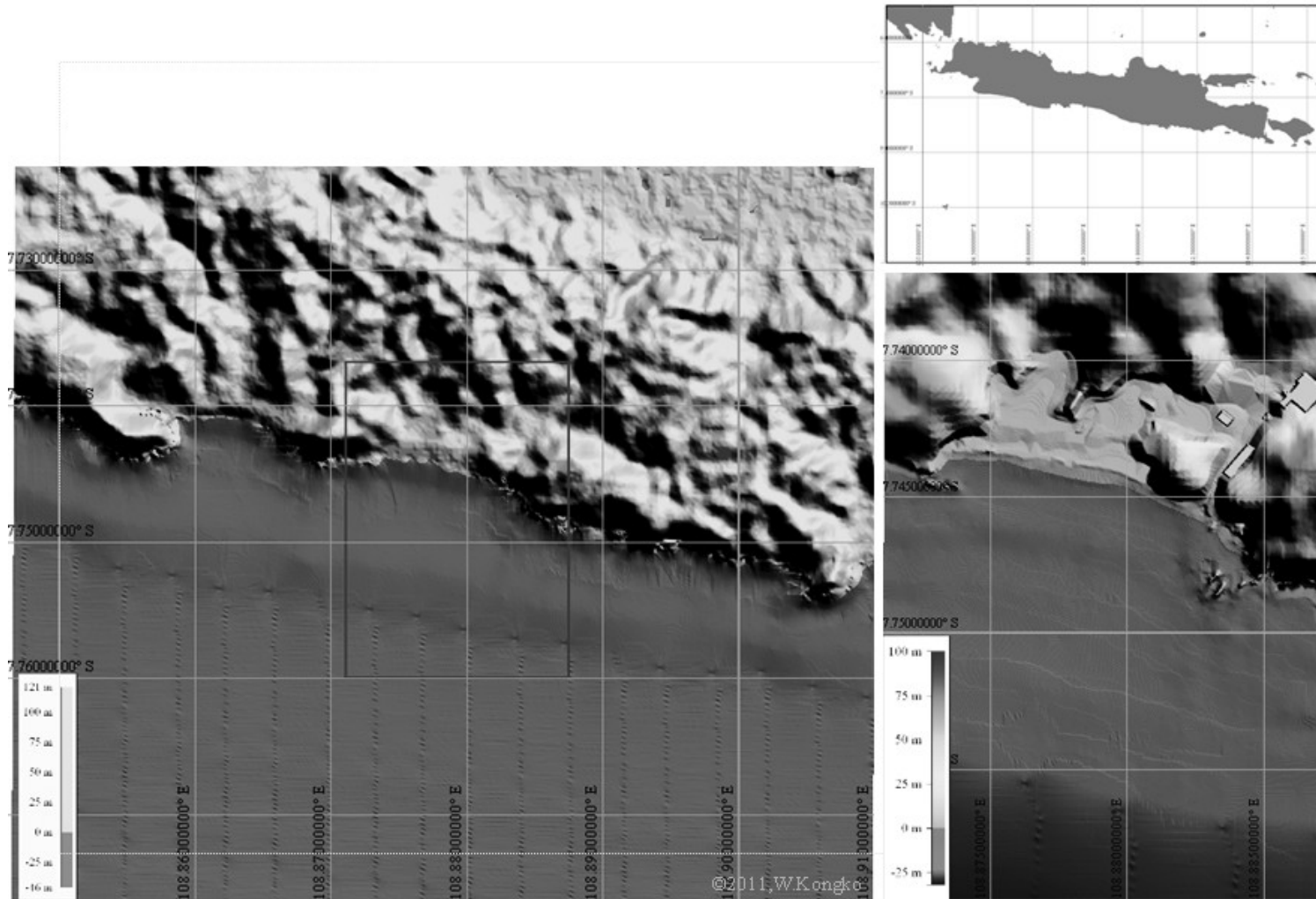
Appendix G

M. Geometric model of level 6th domain 5a1a – DTM data (left panel) and 5a1a – DSM data (right panel)



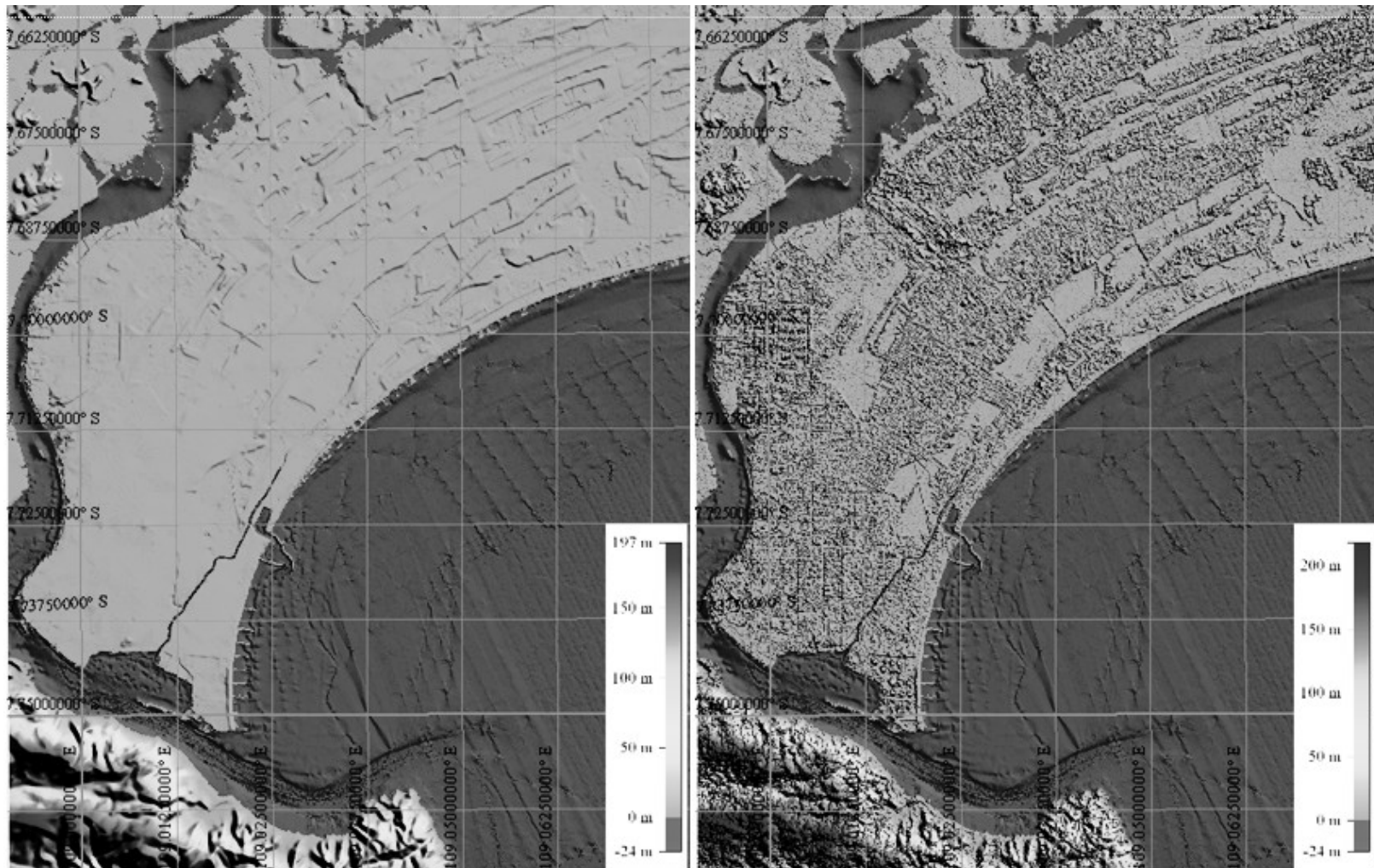
Appendix G

N. Geometric model for domain of level 6th and 7th for domain 5x1x (left panel) and 6x1x (inset)



Appendix G

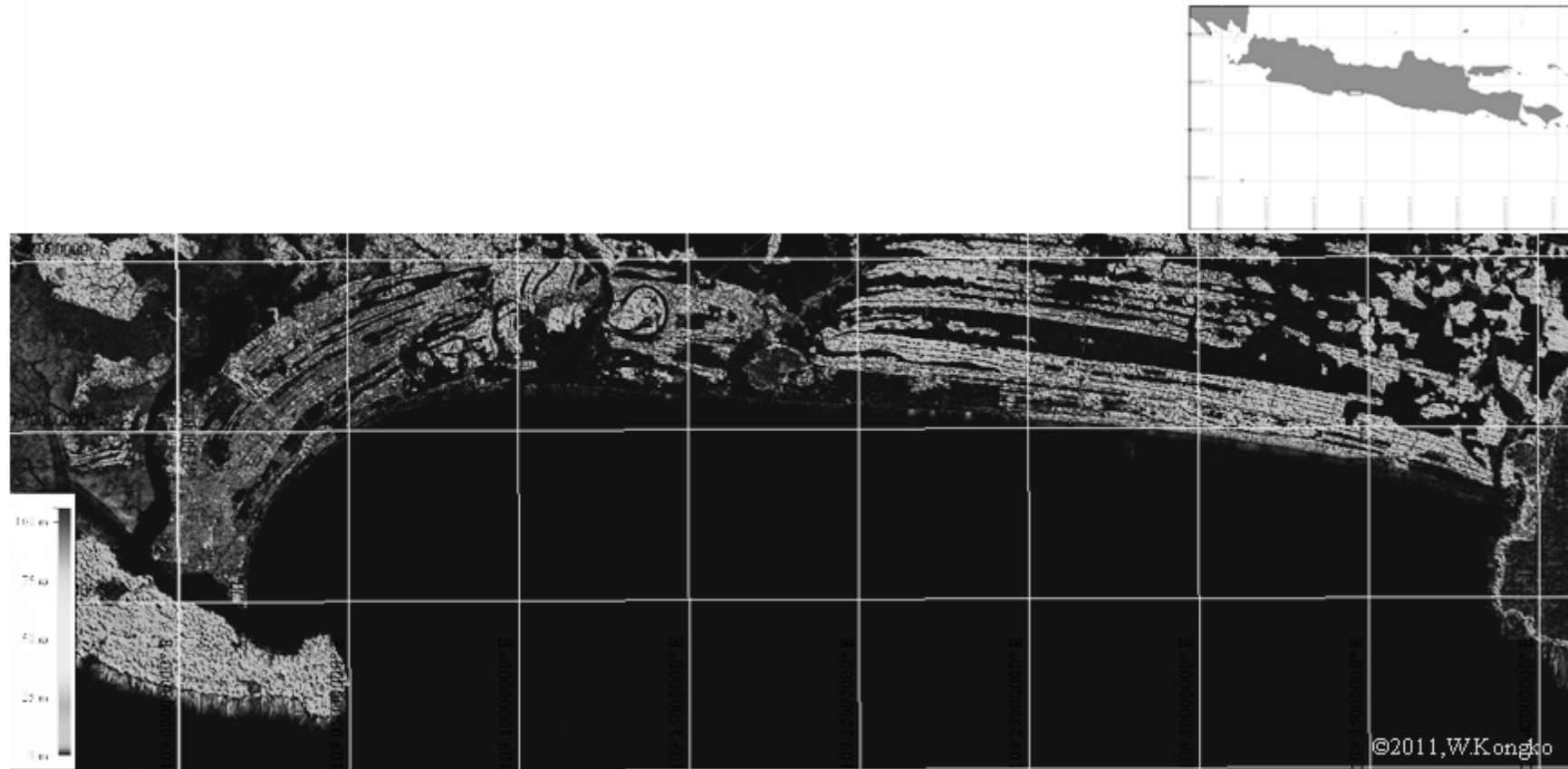
O. Geometric model for domain of level 7th for domain 6a1a – DTM data (left panel) and 6a1a – DSM data (right panel)



©2011, WKongko

Appendix G

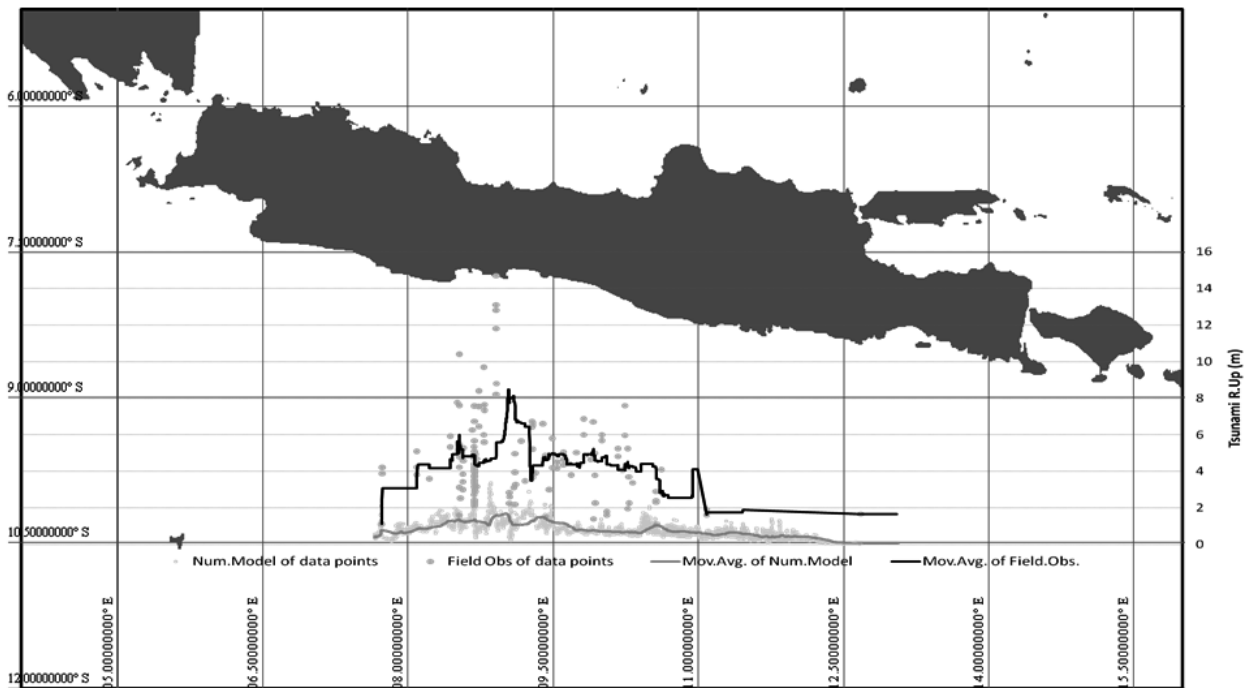
P. The difference of the DSM-DTM data at domain 4a2b



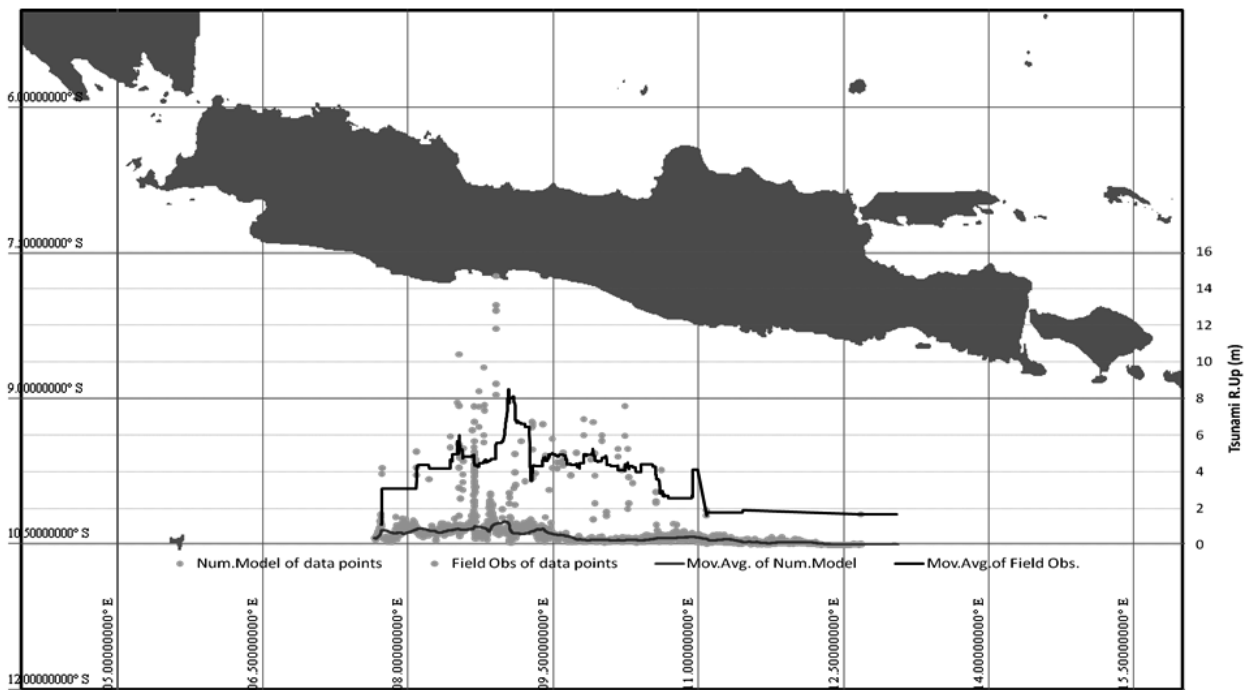
The difference between DSM-DTM data is compared by using the statistical method, namely the root mean squared deviation (RMSD) and normalized root mean squared deviation (NRMSD). The number of data (n) is 1,778,976, RMSD is 2.76 m, NRMSD is 0.9%, maximum value is 250.7 m, and minimum value is -54.2 m.

Appendix H – Simulation results

A. Simulation results for the reconstruction of the 2006 Java tsunami



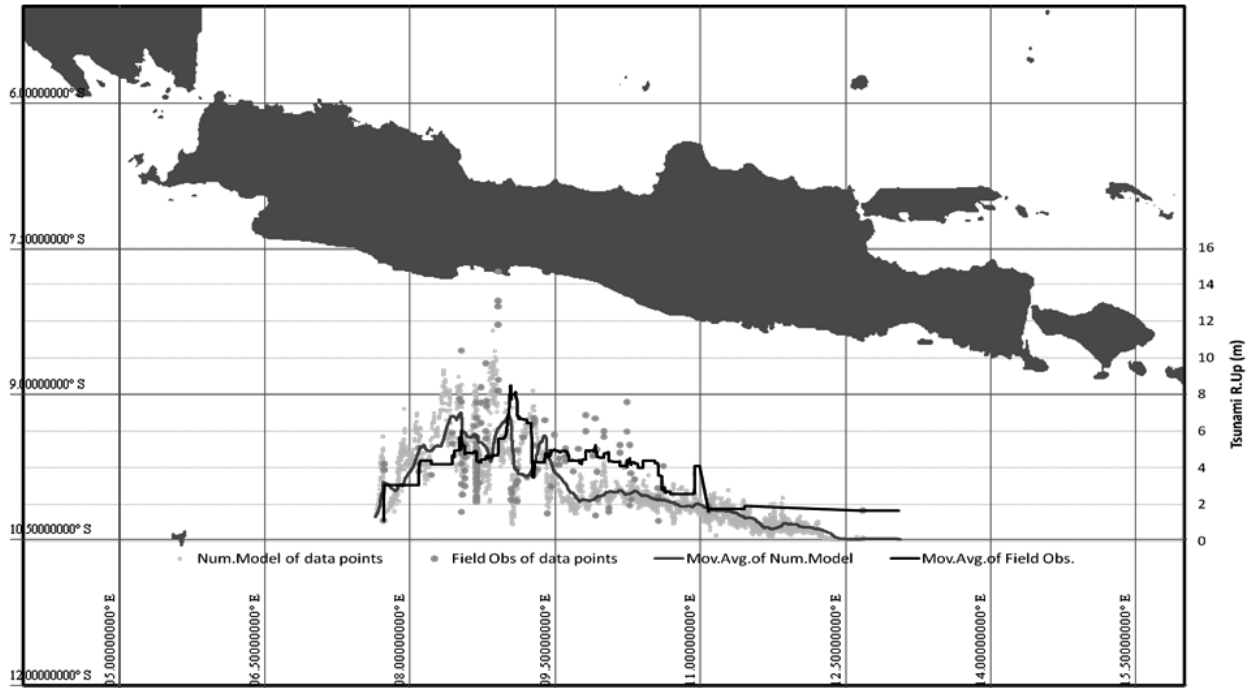
A.1: The field observation data vs. tsunami model based on multi-faults model by Fujii & Satake, 2006



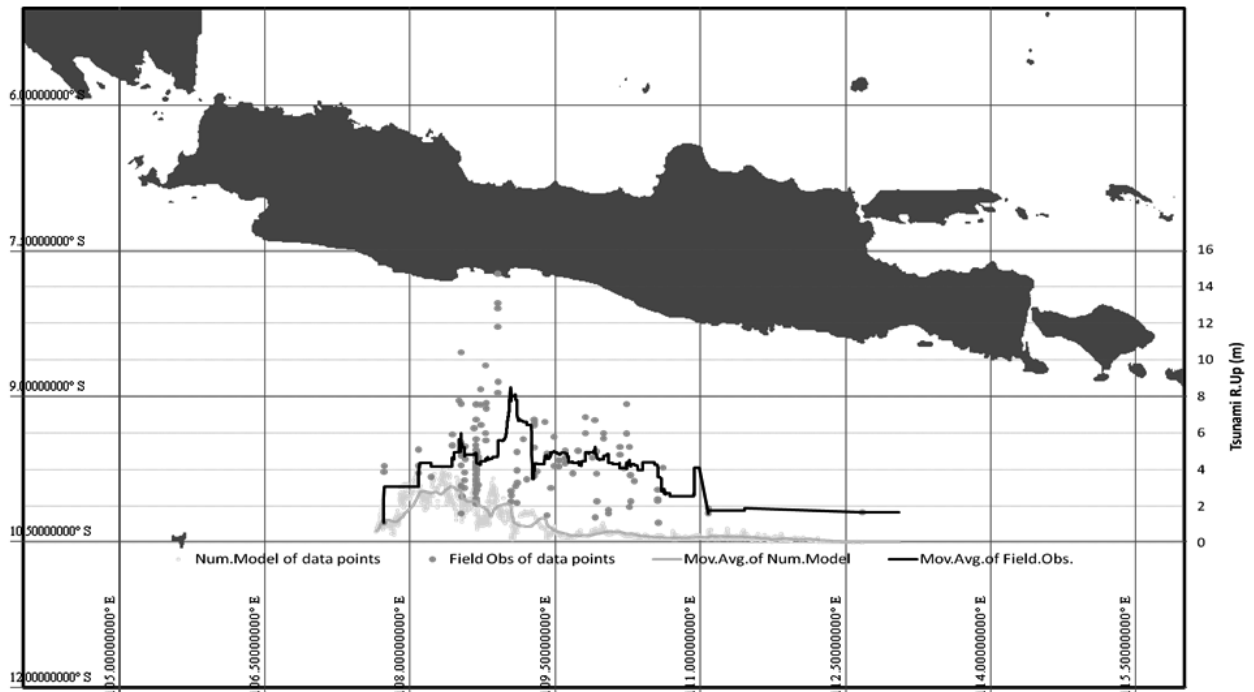
A.2: The field observation data vs. tsunami model based on multi-faults model by Chen-Ji, 2006

Appendix H

A. Simulation results for the reconstruction of the 2006 Java tsunami



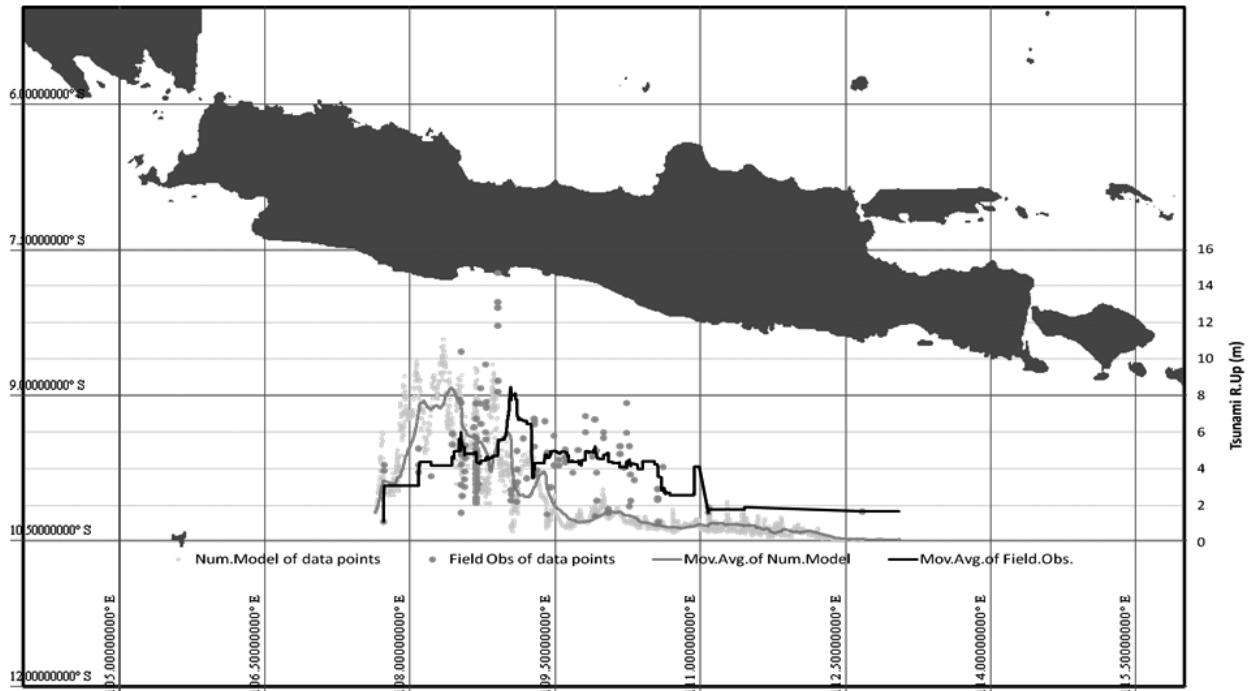
A.3: The field observation data vs. tsunami model based on multi-faults model by Ammon et al., 2006



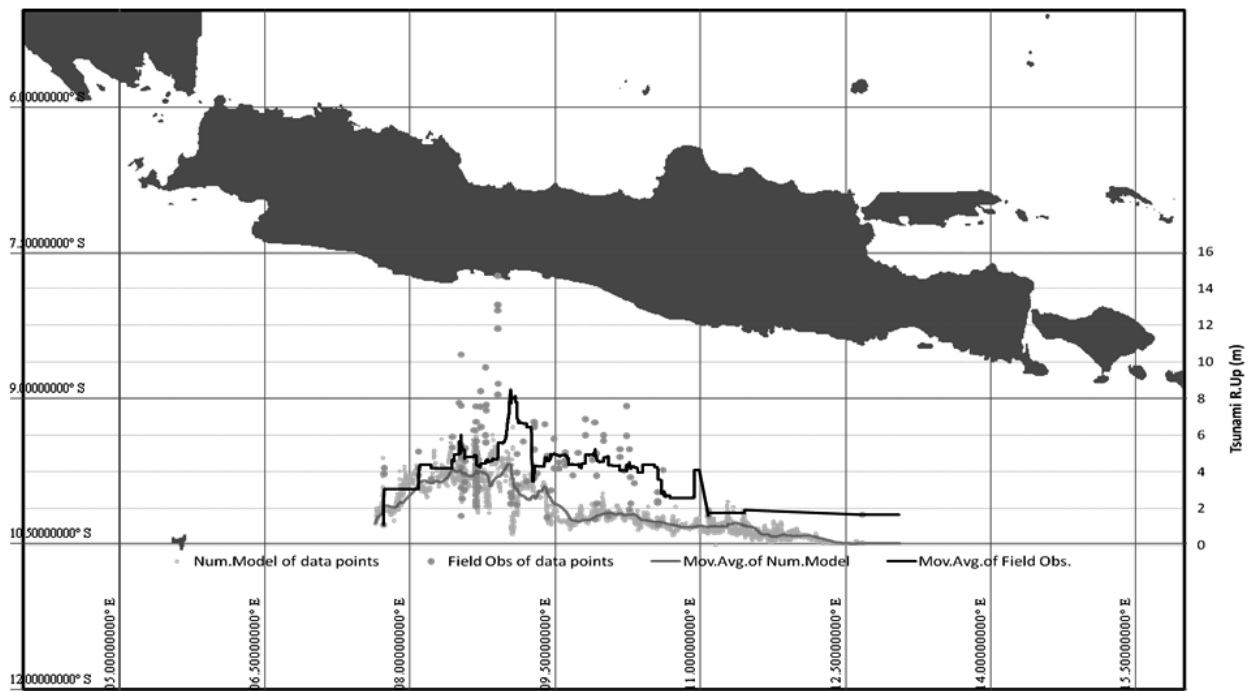
A.4: The field observation data vs. tsunami model based on single-fault model by RuptGen ver. 1.1 (GITEWS, 2010) by using normal rigidity of $\mu=30$ GPa

Appendix H

A. Simulation results for the reconstruction of the 2006 Java tsunami



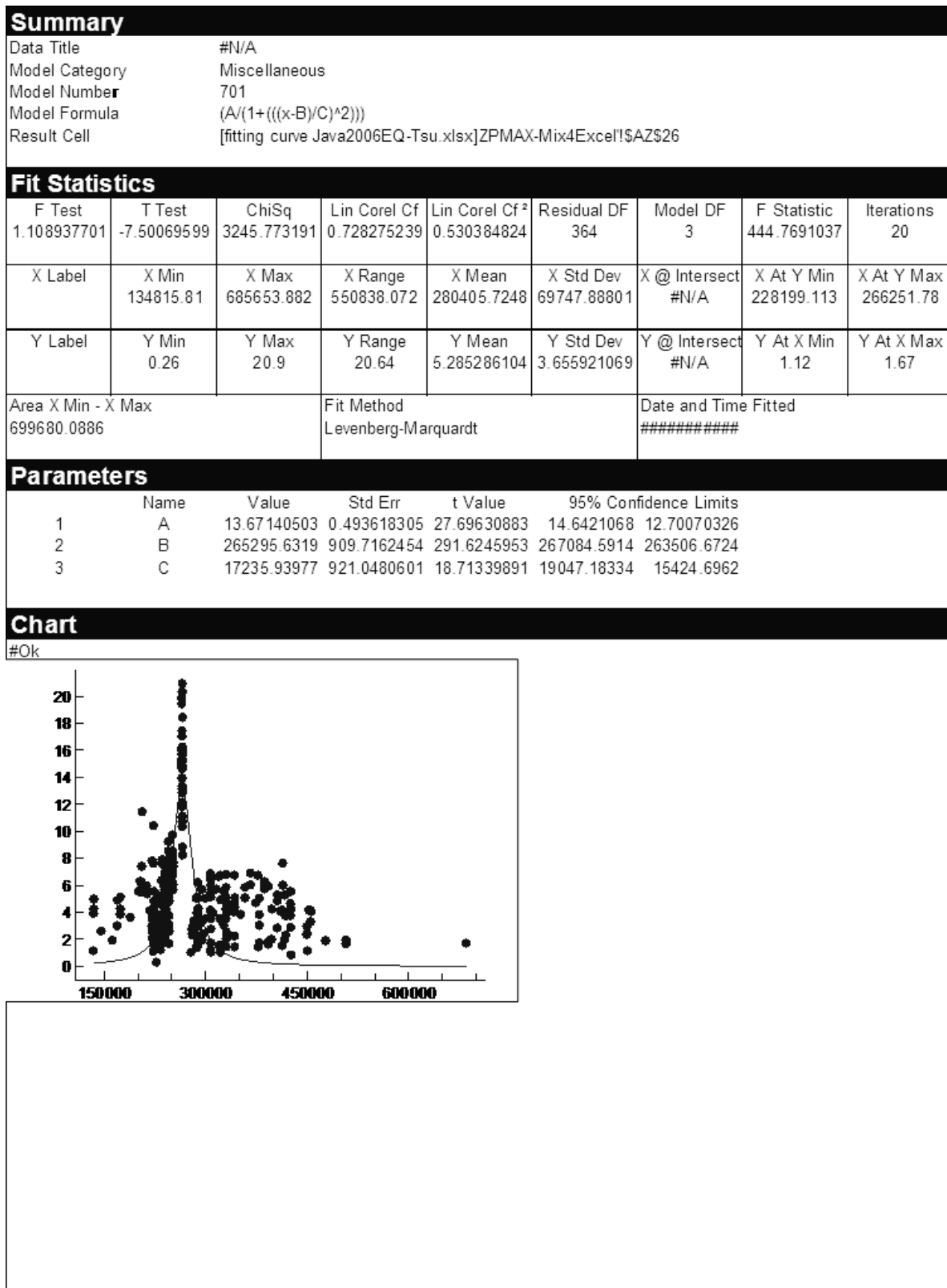
A.5: The field observation data vs. tsunami model based on single-fault model by RuptGen ver. 1.1 (GITEWS, 2010) by using low rigidity of $\mu=10$ GPa



A.6: The field observation data vs. tsunami model based on single-fault model in the present study by using low rigidity of $\mu=10$ GPa

Appendix H

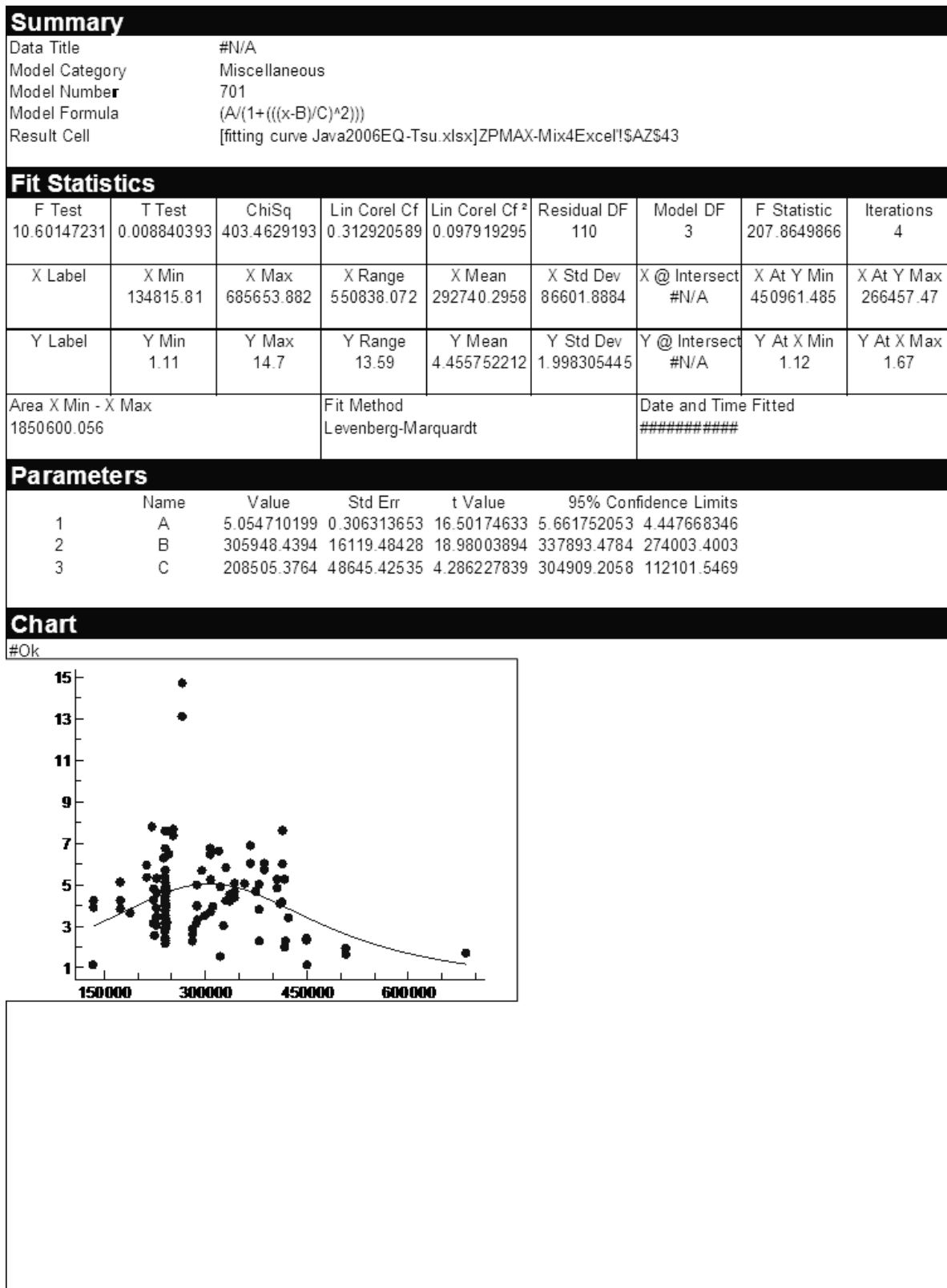
A. Simulation results for the reconstruction of the 2006 Java tsunami



A.7: The summary of the statistical parameters of curve-fitting for entire dataset

Appendix H

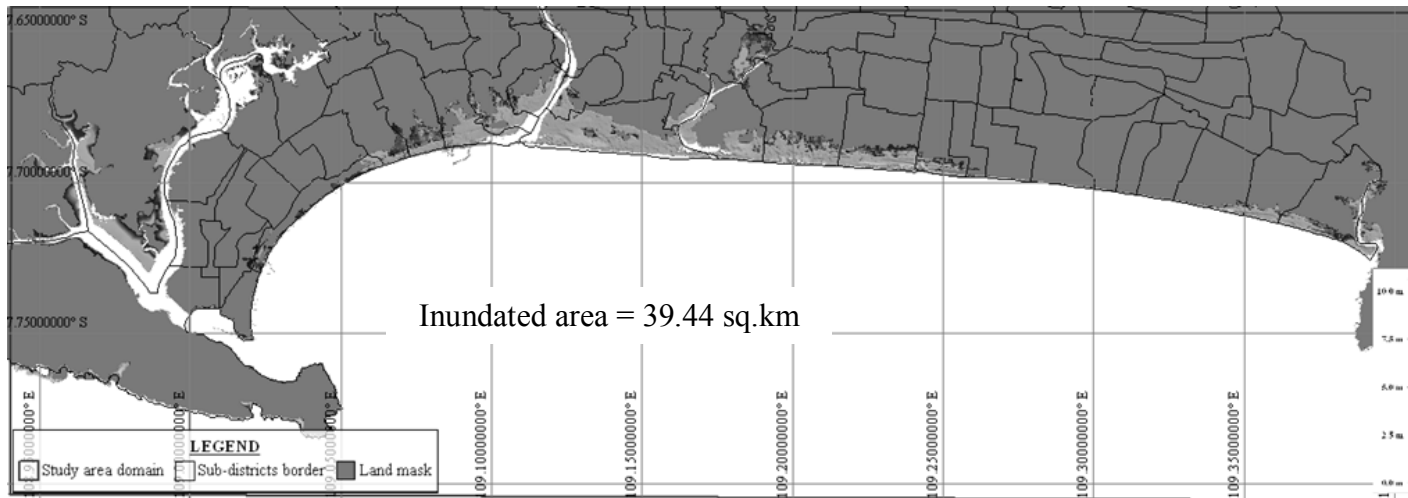
A. Simulation results for the reconstruction of the 2006 Java tsunami



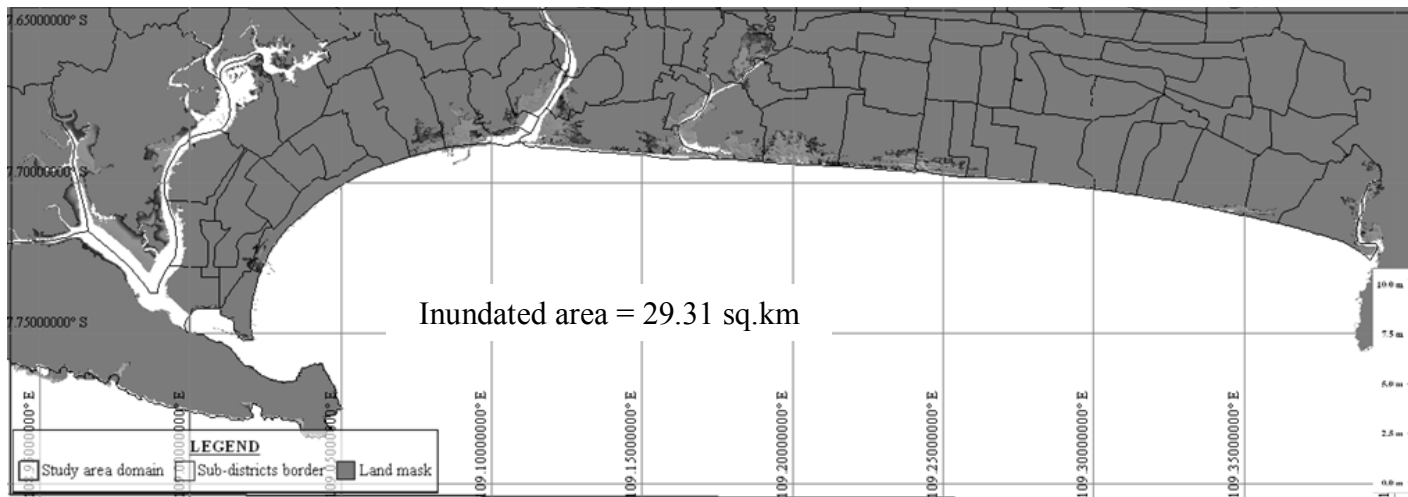
A.8: The summary of the statistical parameters of curve-fitting for pre-selected dataset

Appendix H

B. Simulation results for future hazard



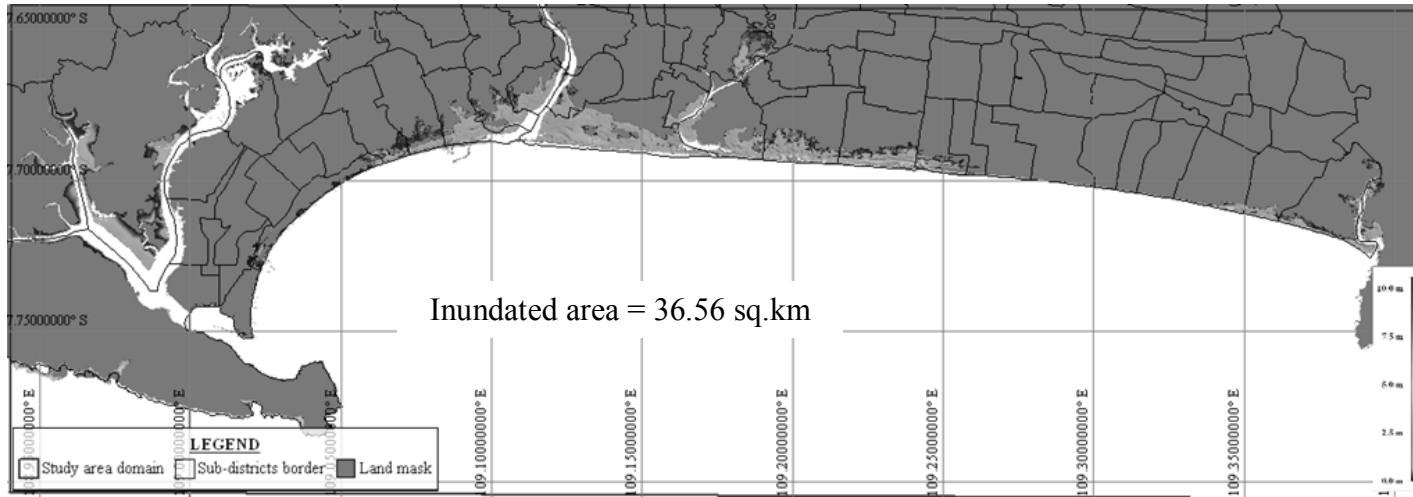
B.1: Inundation model for future hazard (scenario M_w 7.8, without mitigation measures)



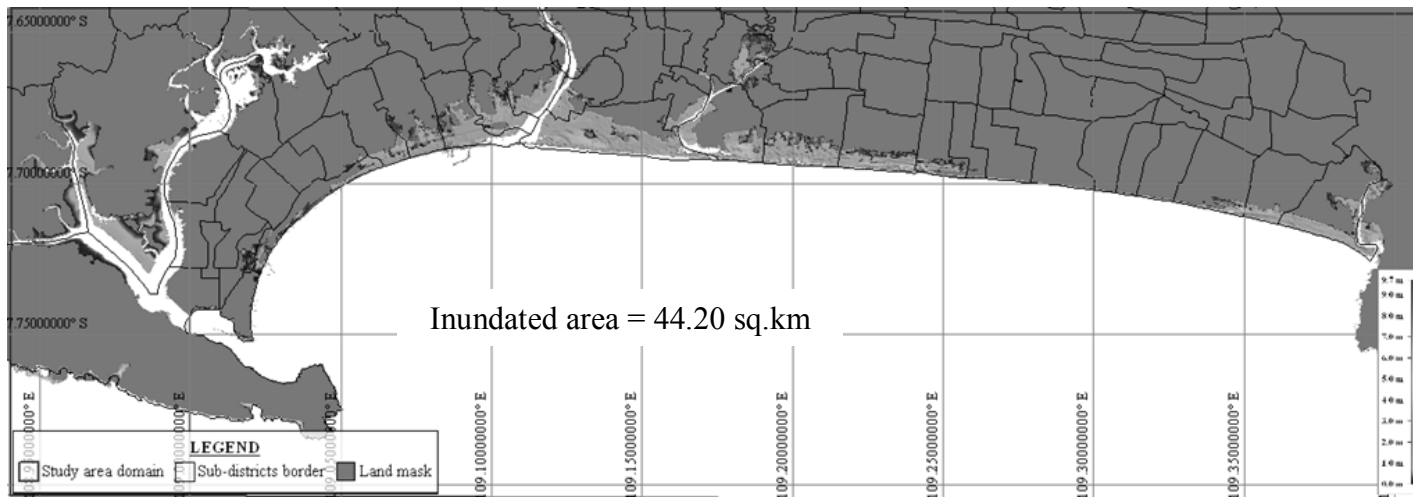
B.2: Inundation model for future hazard (scenario M_w 7.8, with sand dunes $H = 7.5$ m $B = 100$ m)

Appendix H

B. Simulation results for future hazard



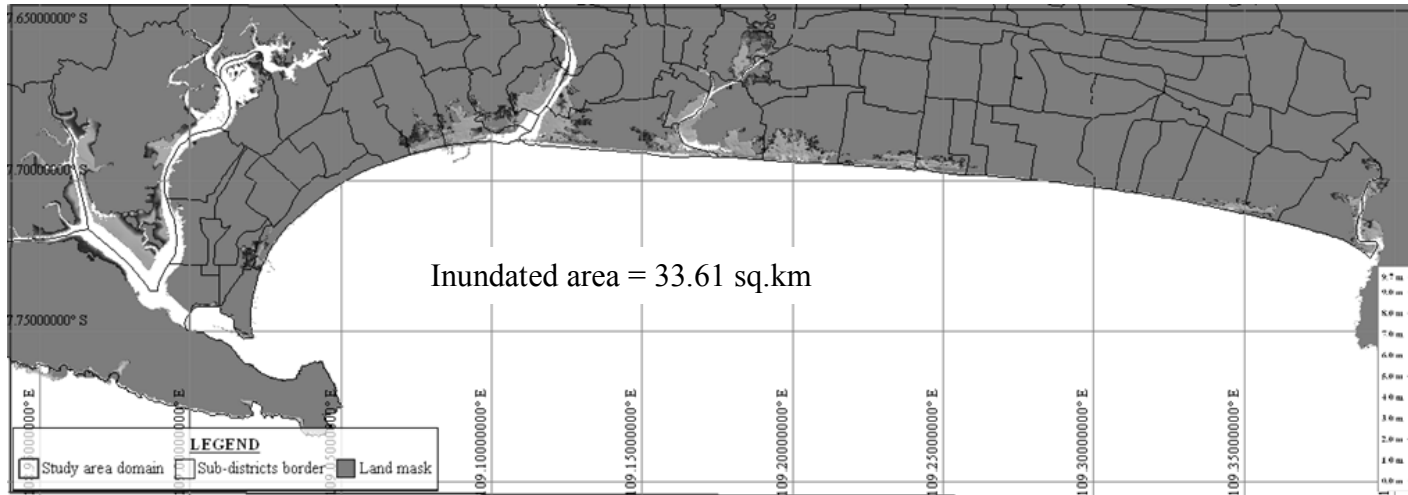
B.3: Inundation model for future hazard (scenario M_W 7.8, with Greenbelt B = 200 m)



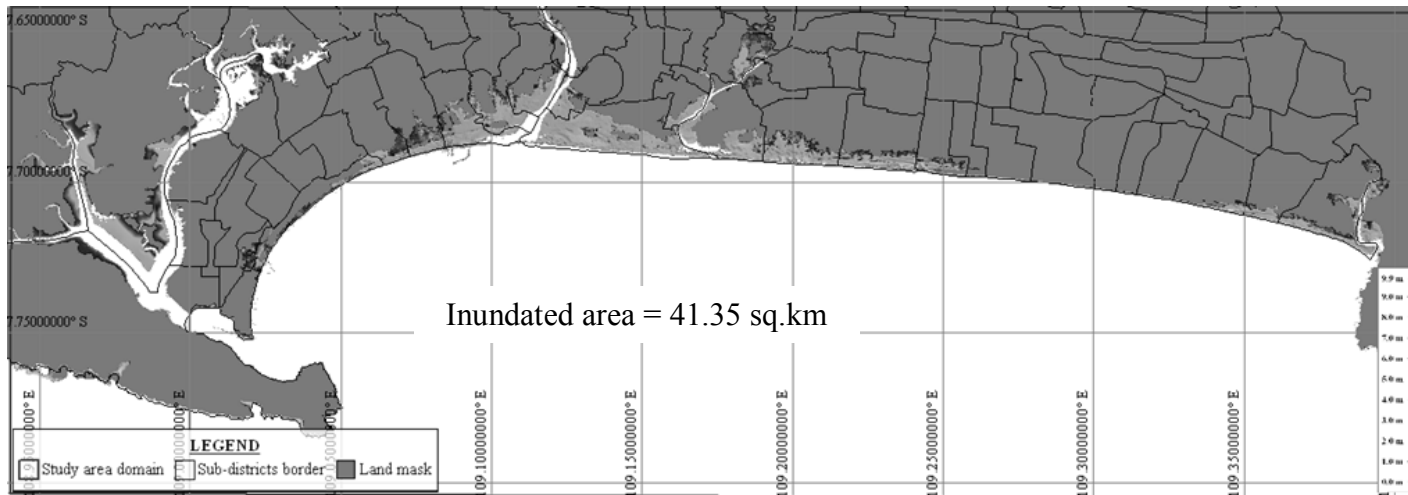
B.4: Inundation model for future hazard (scenario M_W 8.0, without mitigation measures)

Appendix H

B.Simulation results for future hazard



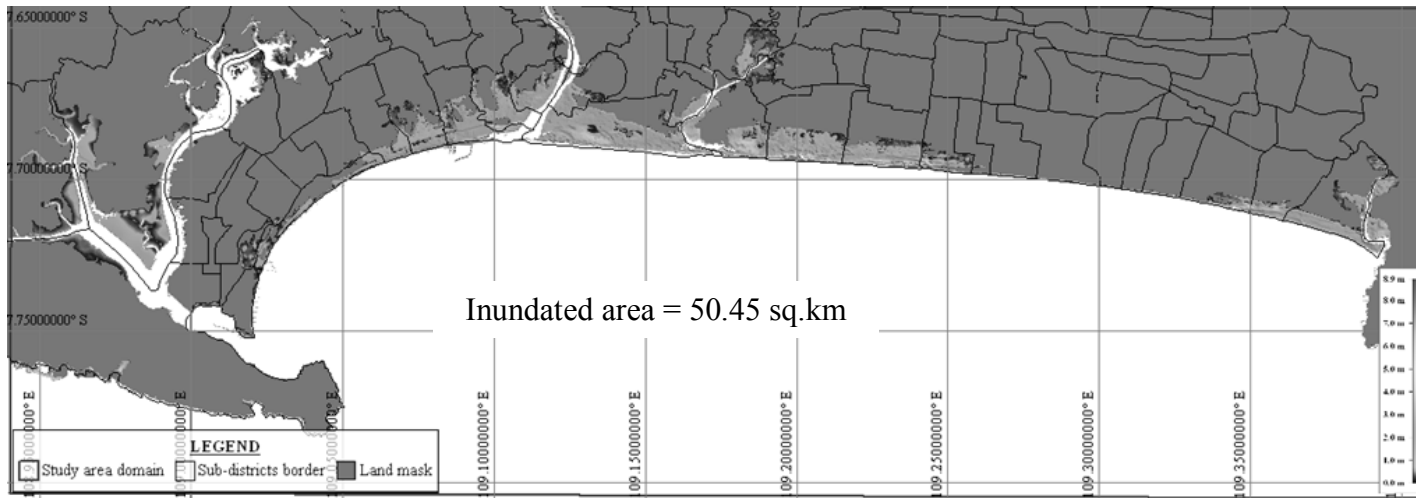
B.5: Inundation model for future hazard (scenario M_w 8.0 with sand dunes $H = 7.5$ m $B = 100$ m)



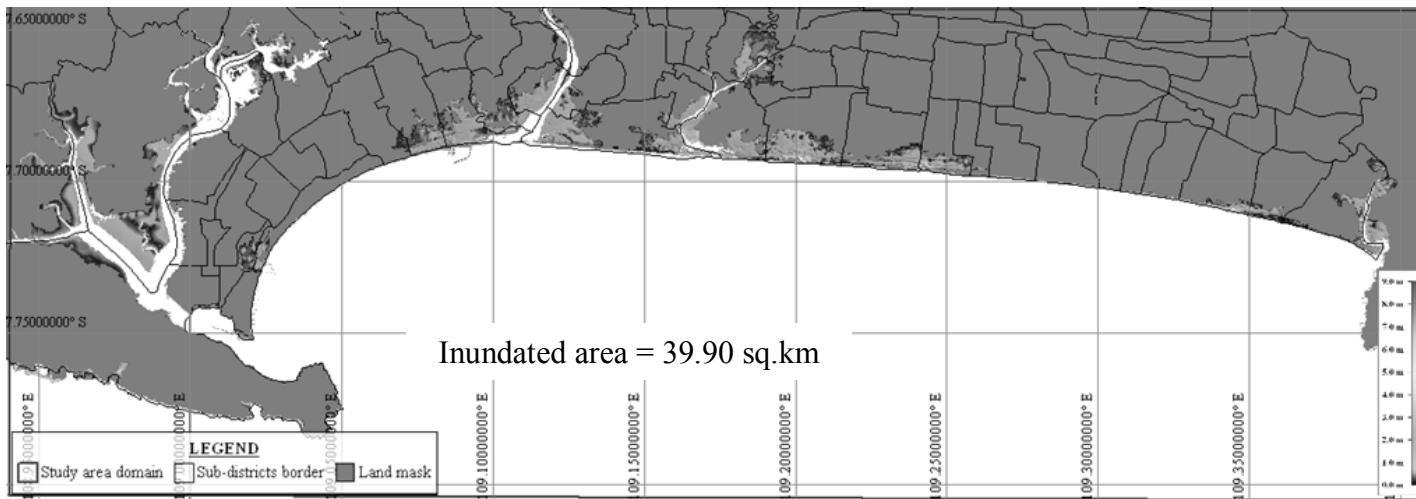
B.6: Inundation model for future hazard (scenario M_w 8.0, with Greenbelt $B = 200$ m)

Appendix H

B.Simulation results for future hazard



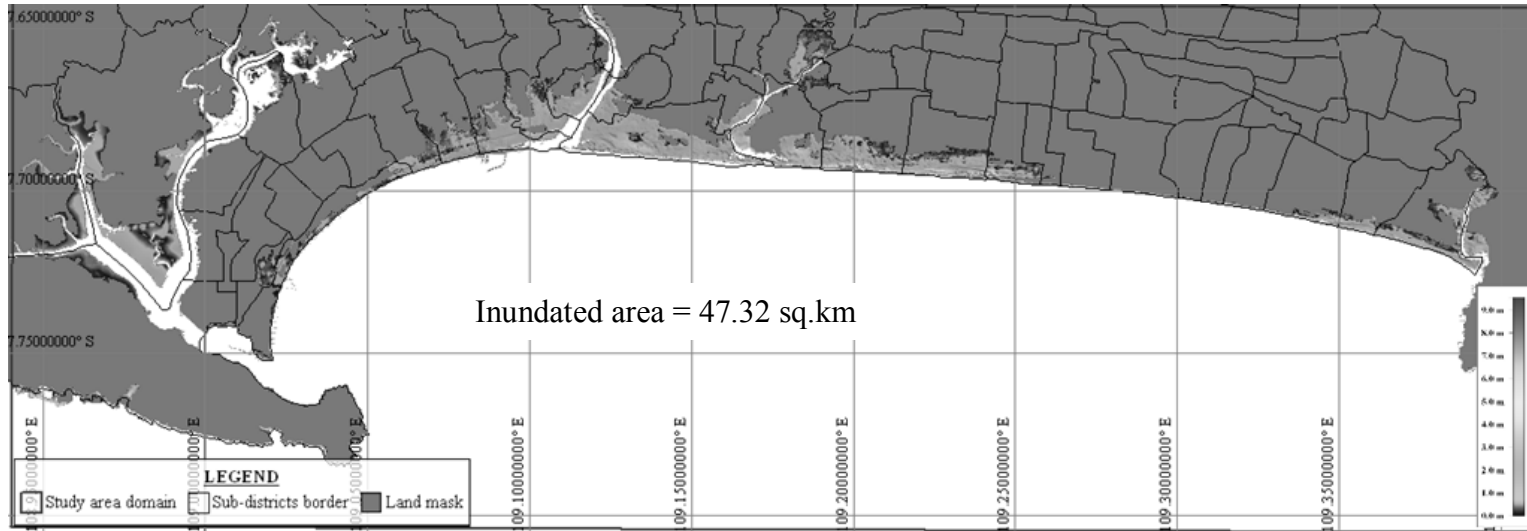
B.7: Inundation model for future hazard (scenario M_W 8.2, without mitigation measures)



B.8: Inundation model for future hazard (scenario M_W 8.2 with sand dunes $H = 7.5$ m $B = 100$ m)

Appendix H

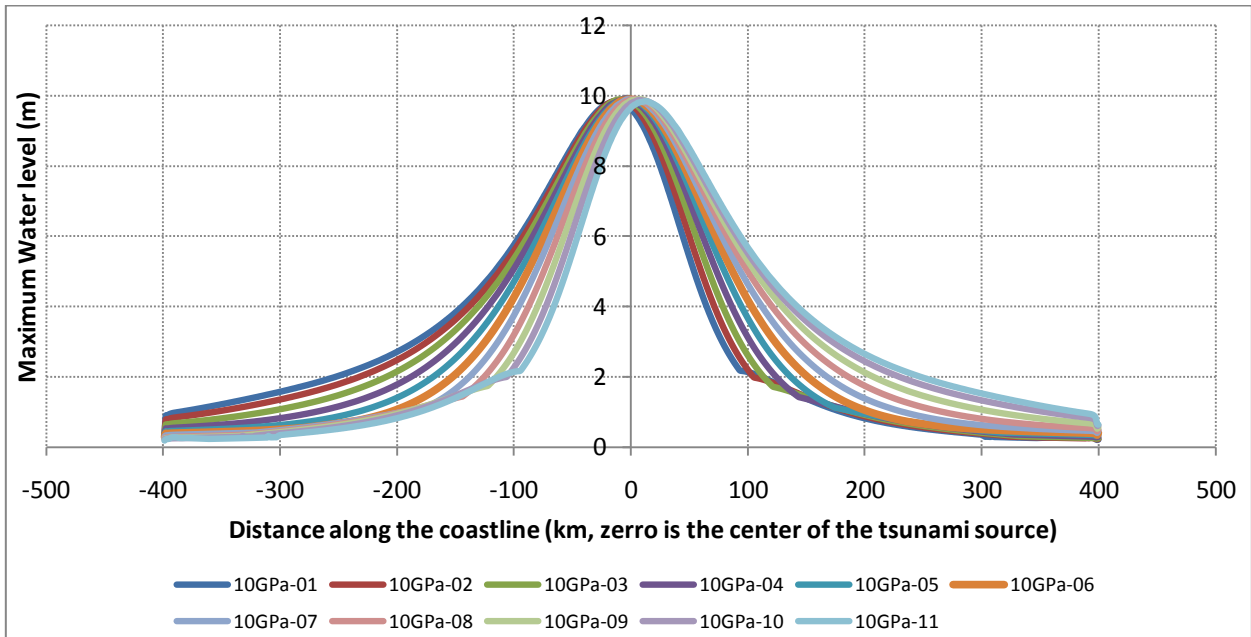
B.Simulation results for future hazard



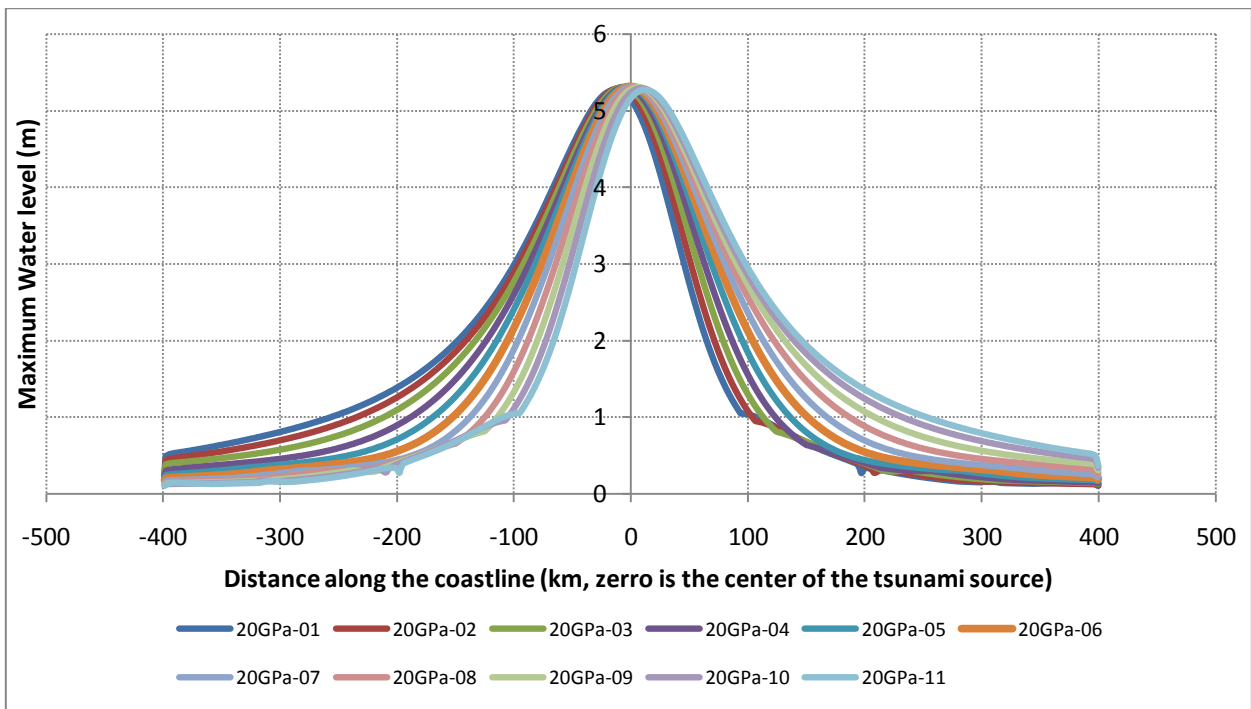
B.9: Inundation model for future hazard (scenario M_W 8.2, with Greenbelt B = 200 m)

Appendix H

C. Simulation results for synthetic model



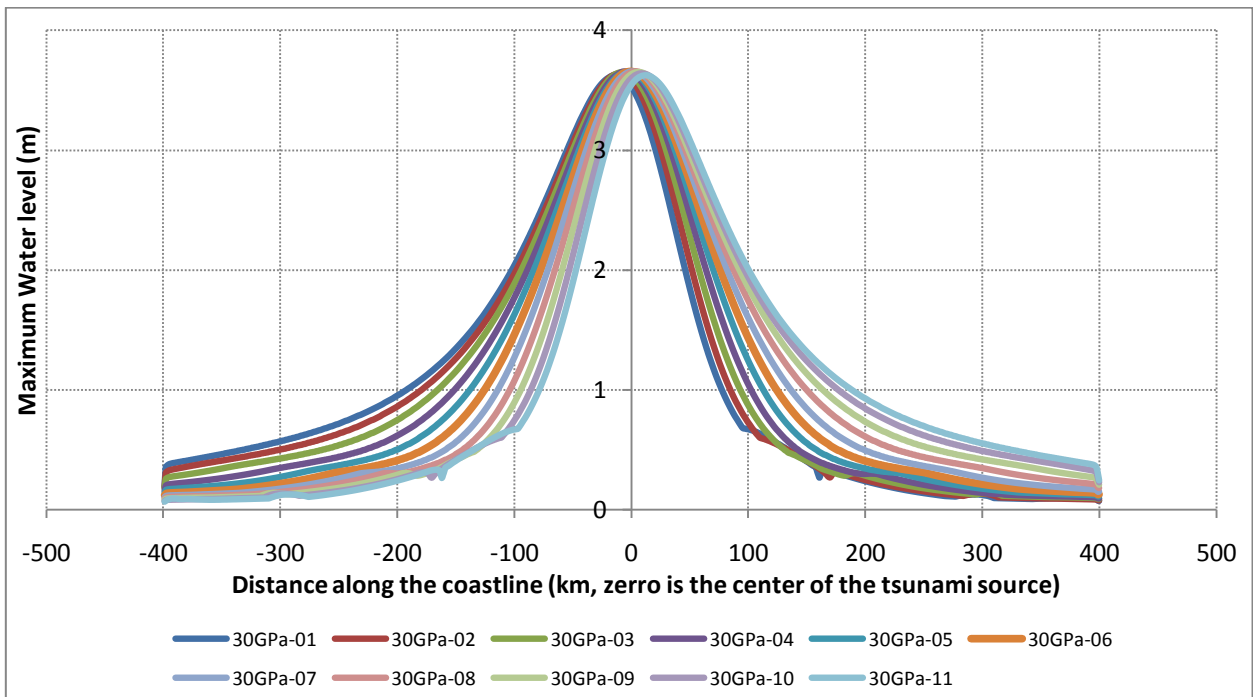
C.1: Maximum run-up distribution along coastline for distributed source ($\mu = 10\text{GPa}$)



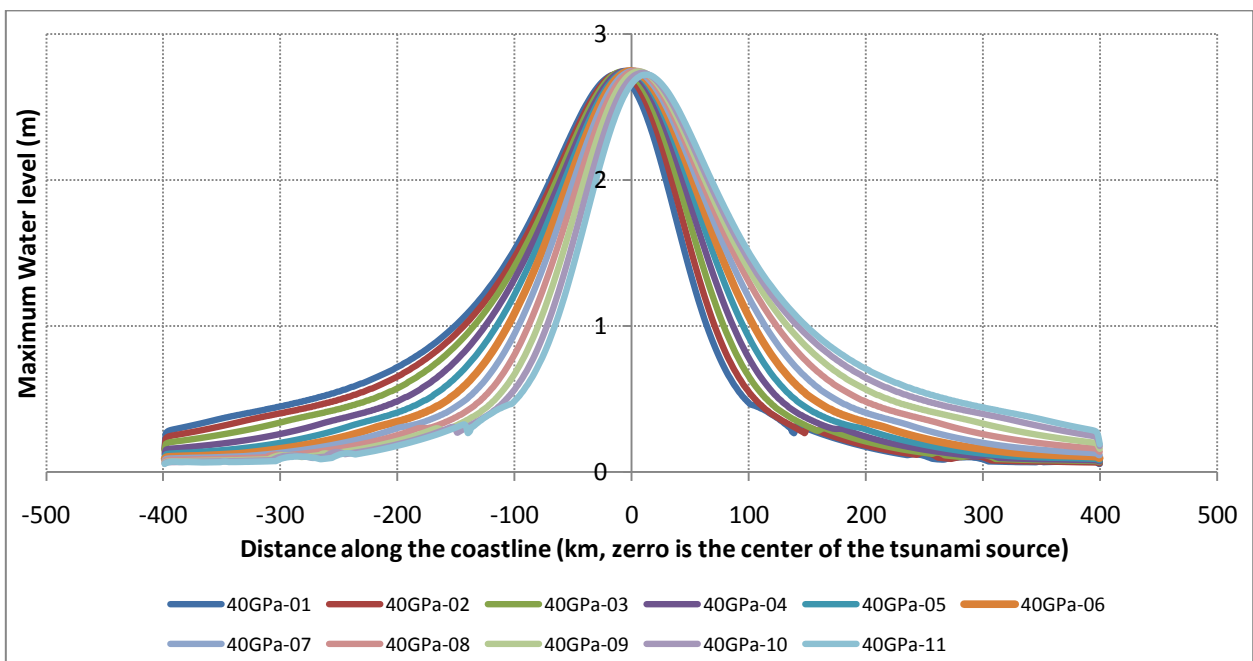
C.2: Maximum run-up distribution along coastline for distributed source ($\mu = 20\text{GPa}$)

Appendix H

C.Simulation results for synthetic model



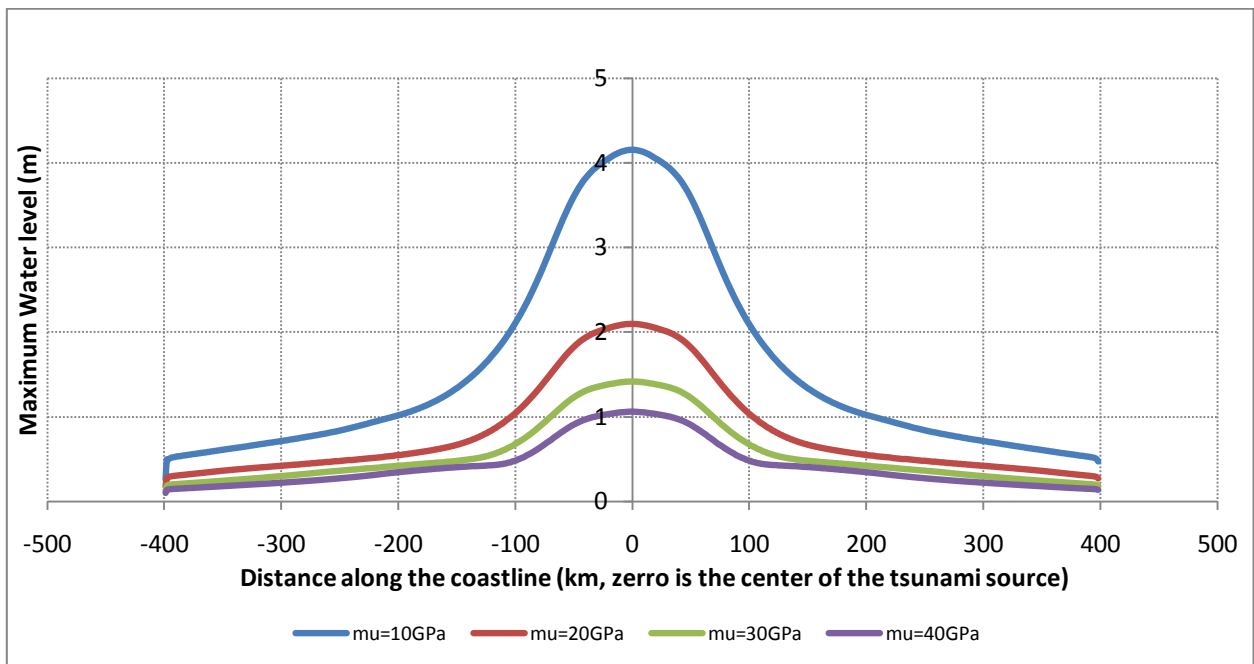
C.3: Maximum run-up distribution along coastline for distributed source ($\mu = 30\text{GPa}$)



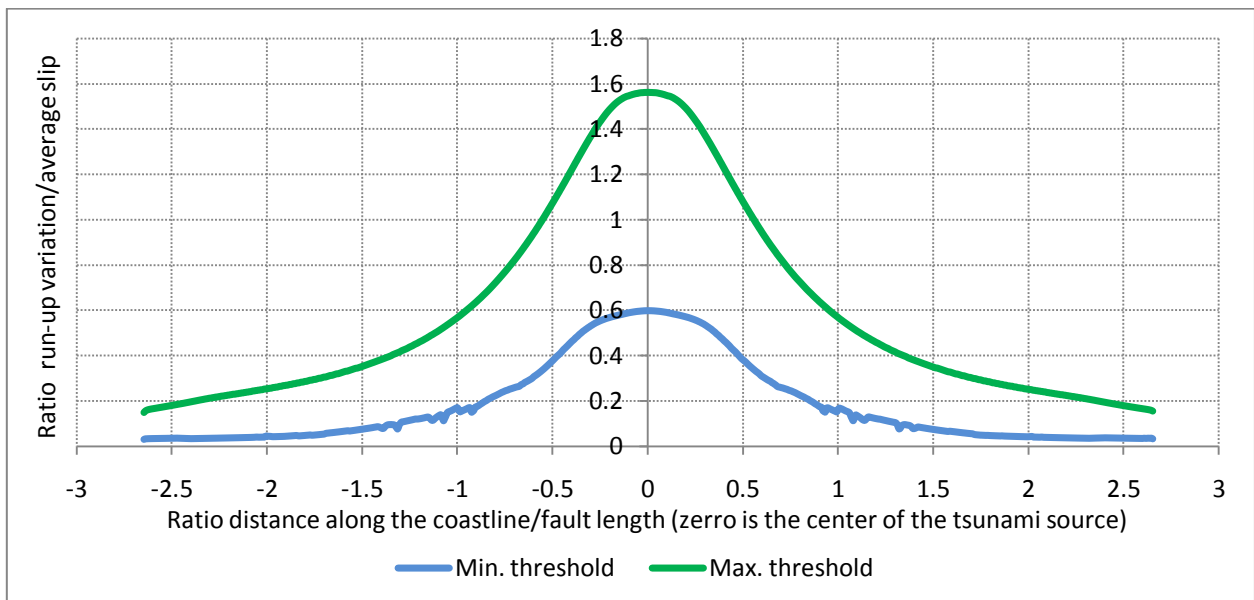
C.4: Maximum run-up distribution along coastline for distributed source ($\mu = 40\text{GPa}$)

Appendix H

C.Simulation results for synthetic model



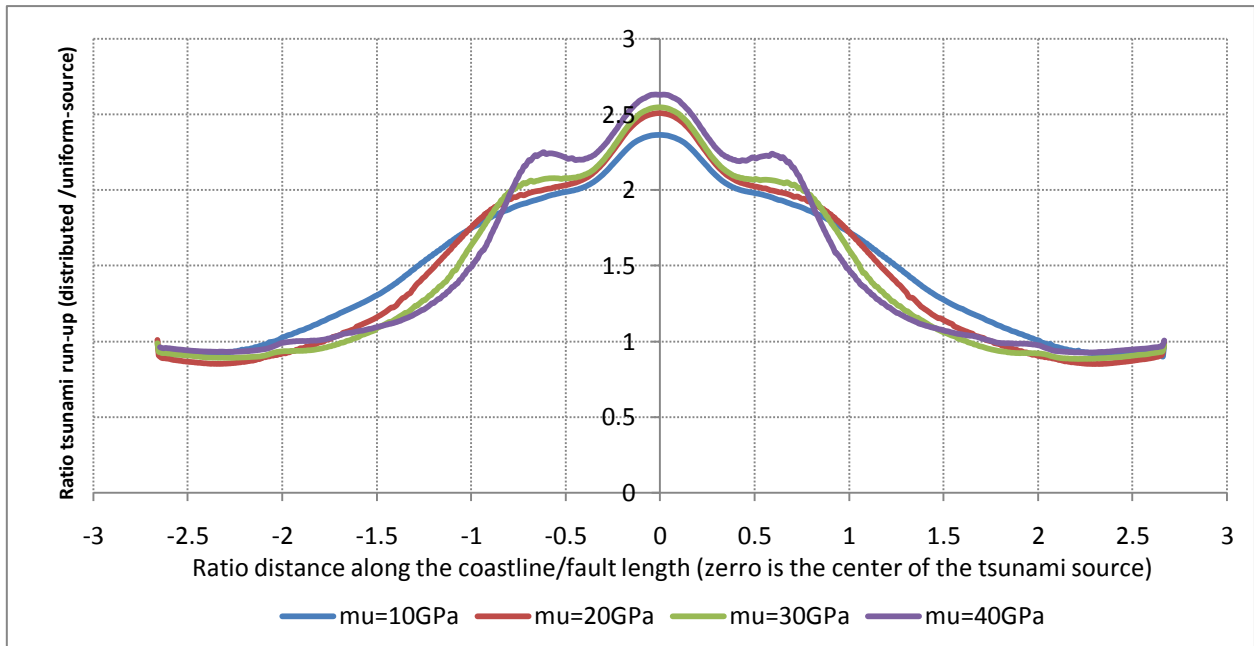
C.5.: Maximum run-up distribution along coastline for uniformly source ($\mu = 10\text{-}40\text{GPa}$)



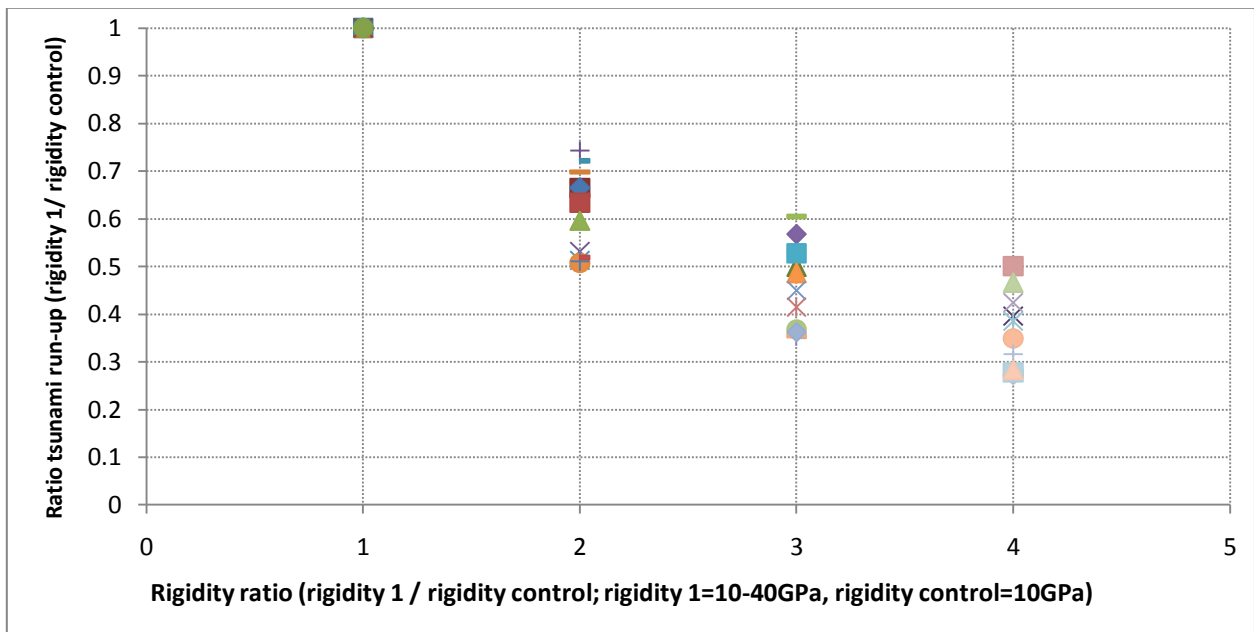
C.6: Ratio of run-up variation threshold vs. ratio distance ($\mu = 10\text{-}40\text{GPa}$)

Appendix H

C.Simulation results for synthetic model



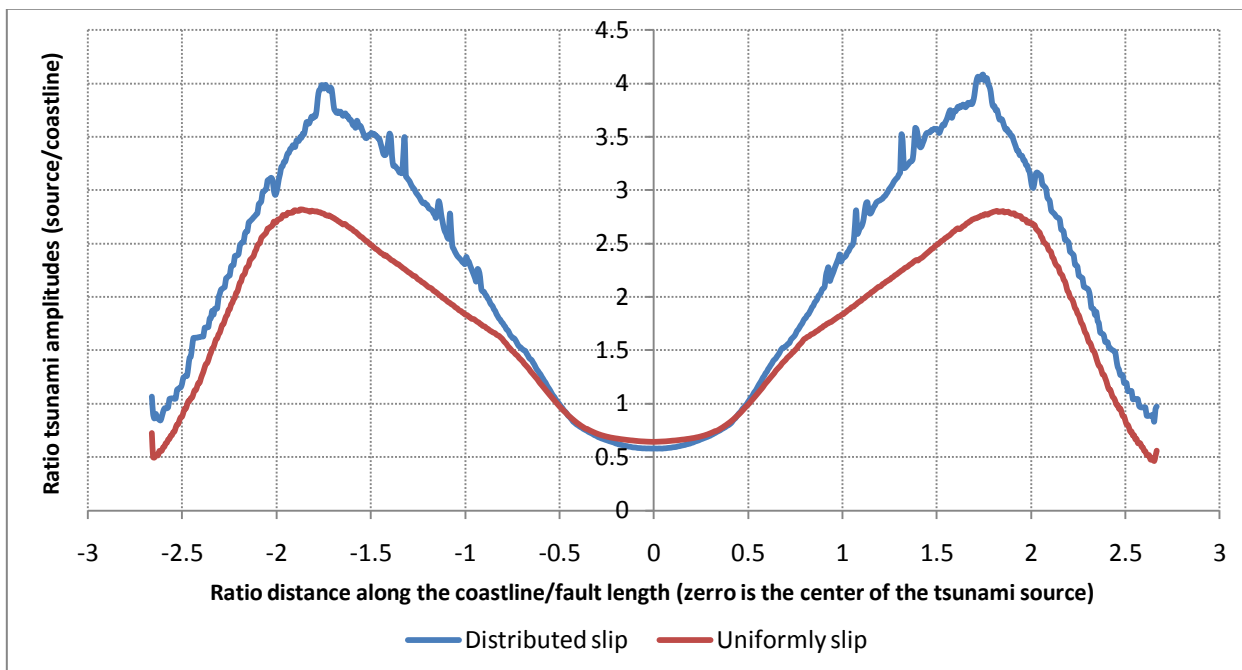
C.7: Ratio of run-up (distributed/uniformly source)



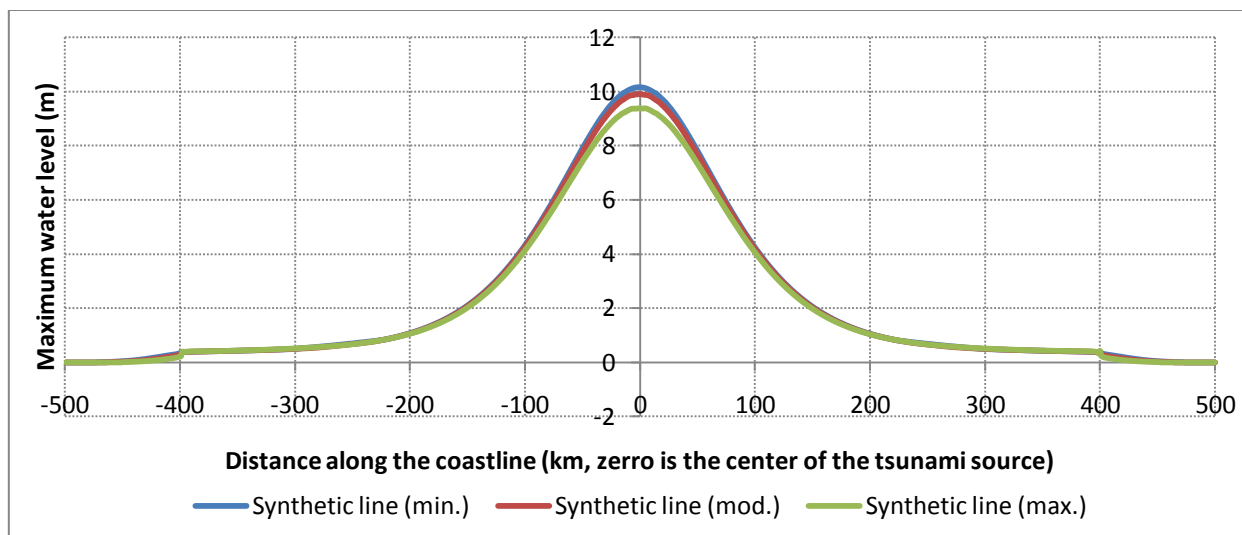
C.8: Ratio of tsunami run-up (rigidity ratio to rigidity of 10GPa)

Appendix H

C.Simulation results for synthetic model



C.9: Ratio of tsunami amplitudes (source/coastline) for distributed/uniformly slip

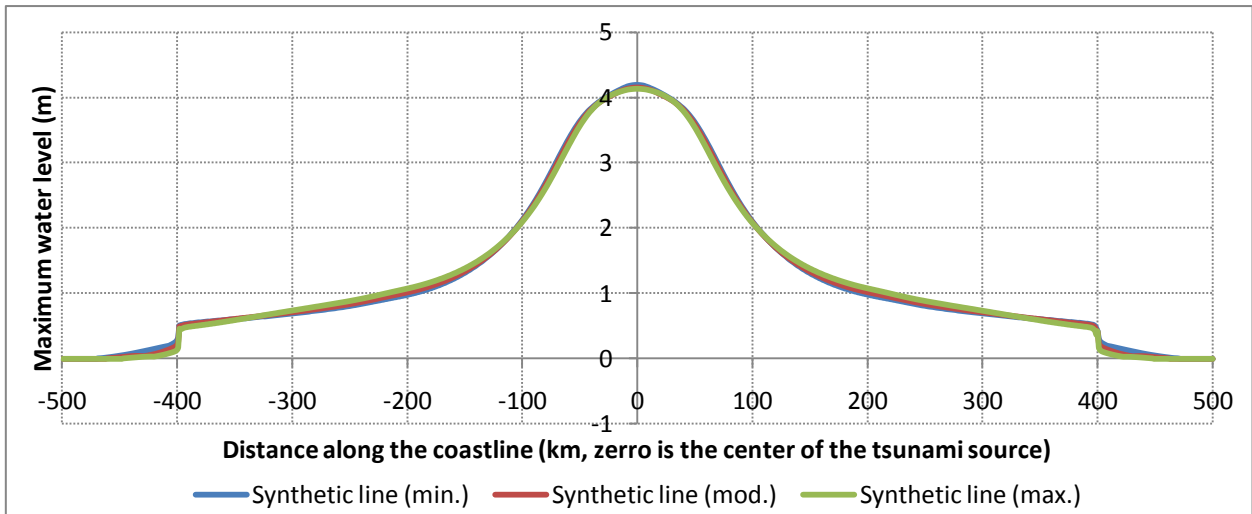


C.10: Tsunami run-up along the coastline under three different geometric data input (distributed slip no.6, M_w 7.8)

The difference tsunami run-up near-shore due to the geometric data input is calculated using the statistical method, namely the root mean squared deviation (RMSD) and normalized root mean squared deviation (NRMSD). The number of data (n) is 1,000, RMSD is 0.24 m, NRMSD is 2.36%, maximum value is 10.16 m, and minimum value is 0.0 m.

Appendix H

C.Simulation results for synthetic model



C.11: Tsunami run-up along the coastline under three different geometric data input (uniformly slip, M_w 7.8)

The difference tsunami run-up near-shore due to the geometric data input is calculated using the statistical method, namely the root mean squared deviation (RMSD) and normalized root mean squared deviation (NRMSD). The number of data (n) is 1,000, RMSD is 0.064 m, NRMSD is 1.53%, maximum value is 4.19 m, and minimum value is 0.0 m.

Appendix I – Definition of Terms

Accretionary Prism: A generally wedge-shaped mass of tectonically deformed sediment at a convergent plate boundary is formed when pelagic sediment, oceanic-floor basalt, and trench-fill turbidite are scraped off the down-going plate during the process of subduction.

Arc: It is a portion of the perimeter of a two-dimensional closed figure lying between two nodes at which two or more arcs intersect. An arc may represent a continuous boundary between two adjoining mapping units. (There are still several meanings, but those above are the most appropriate ones for what is discussed in this thesis).

Arrival Time: The time of the first maximum tsunami waves.

Aseismic: An area that is not subject to earthquakes.

BAKOSURTANAL: Badan Koordinasi Survei dan Pemetaan Nasional, the coordinating agency for surveys and mapping of Indonesia.

Bathymetric: A topographic map of the bottom of a body of water (such as the seafloor), with depths indicated by contours drawn at regular intervals.

BMBF: The Federal Ministry of Education and Research (German: Bundesministerium für Bildung und Forschung, BMBF) is a ministry of the German government. It is headquartered in Bonn, and has an office in Berlin.

BMKG: Badan Meteorologi Klimatologi dan Geofisika Indonesia, the Indonesian Meteorological, Climatological and Geophysical Agency.

C.F.L.: Courant-Friedrichs-Levy. In mathematics, the Courant-Friedrichs-Lewy condition (CFL condition) is a necessary condition for convergence when solving certain partial differential equations numerically.

Catalog of Tsunami: A list or tabulation of tsunami occurrences. It contains the time and geographic coordinates of the events, magnitudes, and other related properties (i.e. run-up height, victims, etc.)

Continental Borderland: An area of the continental margin between the shoreline and the continental slope that is topographically more complex than the continental shelf. It is characterized by ridges and basins, some of which are below the depth of the continental shelf.

Continental Margin: The ocean floor that is between the shoreline and the abyssal ocean floor, including various provinces: the continental shelf, continental borderland, continental slope, and the continental rise.

Appendix I (continued)

Continental Rise: The part of a continental margin that is between the continental slope and the abyssal plain. It is best developed on trailing edges. It is a gentle incline with slopes of 1:40 to 1:2,000, and generally has a smooth topography, although it may contain submarine canyons.

Continental Shelf (i.e. Sunda Shelf): The part of the continental margin between the shoreline and the continental slope (or, when there is no noticeable continental slope, a depth of 200 m). It is characterized by its very gentle slope of 0.1° .

Continental Slope: That part of the continental margin that is between the continental shelf and the continental rise if there is one. It is characterized by its relatively steep slope of 1.5° to 6° .

Convergence Rate: The rate of convergence between plates that are subducting each other. It is usually uses units of mm/year or cm/year.

Convergent plate: A boundary between two plates moving toward each other. It is essentially synonymous with subduction zone, but is used in different contexts (Dennis and Atwater, 1974, p.1034).

DEM: A digital elevation model (DEM) is a digital representation of ground surface topography or terrain. It is also widely known as a digital terrain model (DTM). A DEM can be represented as a raster (a grid of squares) or as a triangular irregular network. It is referenced horizontally either by a Universal Transverse Mercator (UTM) projection or by a geographic coordinate system.

DGPS: The Differential Global Positioning System is an enhancement to the Global Positioning System that uses a network of fixed, ground-based reference stations to broadcast the difference between the positions indicated by the satellite systems and the known fixed positions.

DSM: The digital elevation model, which includes the land cover such as buildings, vegetation, etc. (except, if any specific additional explanations on it). See DEM.

DTM: The digital elevation model, in which the data contains solely terrain or bare soil. The land cover, such as buildings and vegetation by using certain methods are removed. See DEM.

Earthquake Parameters: The parameters related to the earthquake consisting of the azimuth, distance, depth, and magnitude and seismic moment.

Earthquake Tsunami: Simply means a tsunami triggered by an earthquake.

Estimated Time of Arrival (ETA): The time of tsunami arrival at some fixed location, as estimated from modeling the speed and refraction of the tsunami waves as they travel from the source. ETA is estimated with very good precision if the bathymetry and source are well known (less than a couple of minutes).

Appendix I (continued)

Evacuation Map: A drawing or representation that outlines danger zones and designates limits beyond which people must be evacuated to escape harm from tsunami waves.

Fault: A planar fracture or discontinuity in a volume of rock, across which there has been significant displacement. Large faults within the Earth's crust result from the actions of tectonic forces. Energy release associated with rapid movement of active faults is the cause of most earthquakes.

Fault Trench (i.e. Java Trench): A cleft or crack formed on the Earth's surface as a consequence of faulting. It is a smaller-scale feature than a fault trough (rift valley), and is not necessarily related to normal faulting.

FI-LUH: Franzius Institut Leibniz Universitaet Hannover. Its official website is at: <http://www.fi.uni-hannover.de/>

Focal Mechanism: The inelastic deformation in the source region that generates the seismic waves. In the case of a fault-related event, it refers to the orientation of the fault plane that slipped and the slip vector and is also known as a fault-plane solution.

GEBCO: The General Bathymetric Chart of the Oceans is a publicly available bathymetry of the world's oceans. Its official website is at: <http://www.gebco.net/>.

GIS: Geographic information systems or geospatial information systems are sets of tools that capture, store, analyze, manage, and present data linked to location(s). In its simplest terms, GIS is the merging of cartography, statistical analysis, and database technology.

GITEWS: The German-Indonesia Tsunami Early Warning System. The project, which was supported by the German Minister for Education and Research (BMBF), was launched on 14 March, 2005. It aims to design, develop, and implement a tsunami early warning system in Indonesia.

GPS: The Global Positioning System is a space-based global navigation satellite system maintained by the U.S.A. that provides reliable location and time information in all weather and at all times and anywhere on or near the Earth when and where there is an unobstructed line of sight to four or more GPS satellites. It is freely accessible by anyone with a GPS receiver.

Historical Tsunami Data: The historical data of the tsunami, which are available in many forms and at many locations. These forms include published and unpublished catalogs of tsunami occurrences, personal narratives, marigrams, tsunami amplitude, run-up and inundation zone measurements, field investigation reports, newspaper accounts, film, or video records.

Appendix I (continued)

IFRC & RCS: The International Federation of the Red Cross and Red Crescent Societies is a humanitarian institution part of the International Red Cross and Red Crescent Movement along with the ICRC. Founded in 1919 and based in Geneva, Switzerland. It coordinates activities between the national societies in order "to improve the lives of vulnerable people by mobilizing the power of humanity".

InSAR or IfSAR: Interferometric synthetic aperture radar. This is a radar technique used in geodesy and remote sensing. This geodetic method uses two or more synthetic aperture radar (SAR) images to generate maps of surface deformation or digital elevation, using differences in the phase of the waves returning to the satellite or aircraft.

Inundation (Maximum): The maximum horizontal penetration of the tsunami from the shoreline. A maximum inundation is measured for each different coast or harbor affected by the tsunami.

Inundation Area: An area flooded with water by the tsunami.

Inundation Line: Inland limited of wetting, measured horizontally from the mean sea level (MSL) line. The line between living and dead vegetation is sometimes used as a reference. In the field of tsunami science it also means the landward limit of tsunami run-up.

Inundation: The horizontal distance inland, that a tsunami penetrates, generally measured perpendicularly to the shoreline.

IOC: The Intergovernmental Oceanographic Commission, which was established by resolution 2.31 adopted by the General Conference of UNESCO.

ITEWS: The Indonesia Tsunami Early Warning System. The system consists of several types of sensor and belongs to Indonesia's government. It aims to deliver a tsunami warning as early as possible. Tsunami sources are located in the Indian Ocean and the Pacific Ocean.

Leading Wave: The first-arriving wave of a tsunami. In some cases, the leading wave produces an initial depression or drop in sea level, and in other cases, an elevation or rise in sea level.

Lithosphere: The outer part of the Earth, consisting of the crust and upper mantle, which is approximately 100km thick.

Lithospheric Mantle: The outer part of the mantle, above the asthenosphere, which with the crust constitutes tectonic plates.

Magnitude: A number assigned to a quantity by means of which the quantity may be compared with other quantities of the same class.

Appendix I (continued)

Manning's Roughness: A bottom friction scheme, which was proposed by Robert Manning (1816-1897); it was improved and introduced as the Gauckler-Manning formula by Gauckler (1867). It is widely used for hydrodynamics computation and well known as for Manning's roughness formula.

Mareogram (or Marigram): A graphical representation of the rise and fall of the sea level, with time as abscissa and height as the ordinate. It is usually used to measure tides, but may also show tsunamis.

Mean Sea Level: The average height of the sea surface, based on hourly observations of tide height on the open coast or in adjacent waters, which have free access to the sea. These observations are to have been made over a "considerable" period of time (i.e. 19 years).

MERAMEX: MERapi AMphibious EXperiment. A project, which is aim to acquire deeper comprehension about the relation of subduction zone processes and volcanologic arc processes.

Mo: A measure of the strength of an earthquake, particularly of the low-frequency wave motion. The seismic moment is equal to the product of the force and the moment arm of the double-couple system of forces that produces ground displacements equivalent to those produced by the actual earthquake dislocation. The seismic moment is also equal to the product of the rigidity modulus of the Earth material, the fault area, and the average dislocation along the fault surface (Aki & Richards 2002).

Ms: The surface wave magnitude scale is one of the magnitude scales used in seismology to describe the size of an earthquake. It is based on measurements of Rayleigh surface waves that travel primarily along the uppermost layers of the earth.

Mw: An earthquake size calculated from the seismic moment of the earthquake. This measure is the most valid size calculation for earthquakes above Richter or body wave magnitude 7-7.5.

NEIC: The National Earthquake Information Center is part of the United States Geological Survey (USGS), which undertakes mission to determine, as rapidly and as accurately as possible, the location and size of all significant earthquakes that occur worldwide. Its official website can be found at: <http://earthquake.usgs.gov/regional/neic/>.

NESDIS: The National Environmental Satellite, Data, and Information Service was created by NOAA to operate and manage the United States' environmental satellite programs, and manage the data gathered by the NWS and other government agencies and departments.

Appendix I (continued)

NGDC: The National Geophysical Data Center affiliated to the NOAA (U.S.A.) provides scientific stewardship, products and services for geophysical data describing the solid earth, marine, and solar-terrestrial environment, as well as earth observations from space. The website address is <http://www.ngdc.noaa.gov/>.

NOAA: The National Oceanic and Atmospheric Administration is a scientific agency within the United States Department of Commerce focused on the conditions of the oceans and the atmosphere. The address of its website is <http://www.noaa.gov/>.

Post-Tsunami Survey: The survey conducted following tsunamis. It is very important that reconnaissance surveys be organized and carried out quickly and thoroughly after each tsunami occurs in order to collect detailed data valuable for hazard assessment, model validation, and other aspects of tsunami mitigation.

RC Columns: Reinforced concrete columns. It is concrete in which reinforcement bars ("rebars"), reinforcement grids, plates or fibers have been incorporated to strengthen the concrete in tension.

Rigidity (μ): The property of a material to resist applied stress that would tend to distort it. A fluid has zero rigidity.

run-up Distribution: A set of tsunami run-up values measured or observed along a coastline.

run-up: The elevation reached by seawater measured relative to some stated datum such as mean sea level, mean low water, sea level at the time of the tsunami attack, etc., and measured ideally at a point that is a local maximum of the horizontal inundation.

RUPTGEN: The rupture generator software. It is software for calculating the Earth's surface displacement based on the half-space elastic model by Okada. It was developed by GFZ Germany aiming to support the GITEWS project in the establishment of the hazard map regarding the tsunami that originated in Sunda arc.

Seismic: The matters related to the earthquake, whereby seismology is the scientific study of earthquakes and the propagation of elastic waves through the Earth. The field also includes studies of earthquake effects, such as tsunamis as well as diverse seismic sources such as volcanic, tectonic, oceanic, atmospheric, and artificial processes (such as explosions).

Source Parameters: The earthquake's parameter consists of the location (geographic coordinates), depth, event time, magnitudes, and optional moment tensor.

SRTM: The Shuttle Radar Topography Mission is an international research effort that obtained digital elevation models on a near-global scale from 56°S to 60°N, to generate the most complete high-resolution digital topographic database.

Appendix I (continued)

Subduction Zone: A long, narrow belt in which subduction takes place.

Subduction: The process of one lithospheric plate descending beneath another. The term was introduced by André Amstutz (1951). The idea of subduction had earlier roots in Otto Ampherer's concept of a crustal "swallowing zone" (Verschluckungs-zone).

Tectonic: A field of study within geology generally concerned with the structures within the lithosphere of the Earth (or other planets) and particularly with the forces and movements that have operated in a region to create these structures.

Tide Gauge: It is a device for measuring the height (rise and fall) of the tide. The product of the instrument is a continuous graphical record of tide height versus time.

Tide: The rhythmic, alternate rise and fall of the surface (or water level) of the ocean, and of bodies of water connected with the ocean such as estuaries and gulfs, occurring twice a day over most of the Earth and resulting from the gravitational attraction of the moon (and, in lesser degrees, of the sun) acting unequally at different parts of the rotating Earth.

Topographic: The Earth's surface shape and features or those of planets, moons, and asteroids. It is also the description of such surface shapes and features (especially their depiction in maps).

Travel Time: Time required for the first tsunami wave to propagate from its source to a given point on a coastline.

Tsunami Amplitude: The absolute value of the difference between a particular peak or trough of the tsunami and the undisturbed sea level at the time.

Tsunami Earthquake: An earthquake that produces an unusually large tsunami relative to the earthquake magnitude (Kanamori 1972). Tsunami earthquakes are characterized by a very shallow depth, fault dislocations greater than several meters, and fault surfaces smaller than those for normal earthquakes.

Tsunami Generation: Tsunamis are most frequently caused by earthquakes, but can also result from landslides, volcanic eruptions, and very infrequently by meteorites or other impacts upon the ocean surface.

Tsunami Numerical Model: Mathematical descriptions that seek to describe the observed tsunami and its effects.

Tsunami Period: Amount of time that a tsunami wave takes to complete a cycle. Tsunami periods typically range from five minutes to two hours.

Appendix I (continued)

Tsunami Propagation: The way a tsunami travels outward in all directions from the generating area, with the direction of the main energy propagation generally being orthogonal to the direction of the earthquake fracture zone.

Tsunami Simulation: The numerical model of tsunami generation, propagation, and inundation.

Tsunami Source: Point or area of tsunami origin, usually the site of an earthquake, volcanic eruption, or landslide that caused large-scale rapid displacement of water to initiate the tsunami waves.

Tsunami Wave Length: The horizontal distance between similar points on two successive waves measured perpendicular to the crest.

Tsunami: Japanese term meaning wave (“nami”) in a harbor (“tsu”). A series of traveling waves of extremely long length and period, usually generated by disturbances associated with earthquakes occurring below or near the ocean floor.

Tsunamigenic: Adjective used to describe tsunami-generating events: e.g., a tsunamigenic earthquake, a tsunamigenic landslide.

UNU-EHS: United Nations University, Institute for Environment and Human Security. It was established in December 2003, and is part of the United Nations University (UNU) system, a worldwide network of research and training Institutes. Its official website can be found at: <http://www.ehs.unu.edu/>.

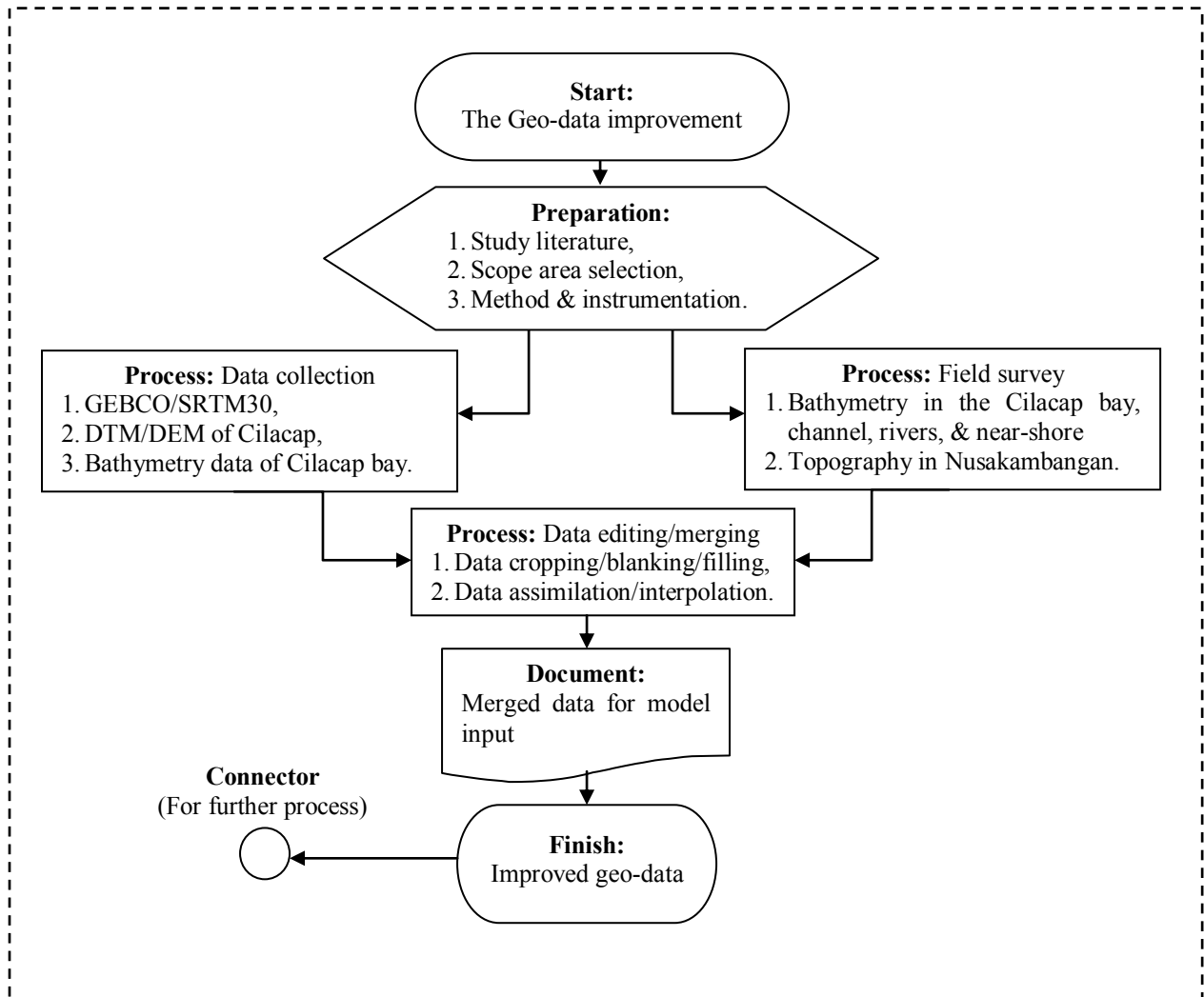
USGS: The United States Geological Survey is a scientific agency of the United States government. The scientists of the USGS study the landscape of the United States, its natural resources, and the natural hazards that threaten it. Its official website is at: <http://www.usgs.gov/>.

WHO: The World Health Organization is a specialized agency of the United Nations (UN) that acts as a coordinating authority on international public health.

WIB: Waktu Indonesia Barat, Indonesian Western Time Zone. This time zone covers the islands of Sumatra, Java, west Kalimantan, and central Kalimantan. It has the +07.00 hours of time difference with UTC.

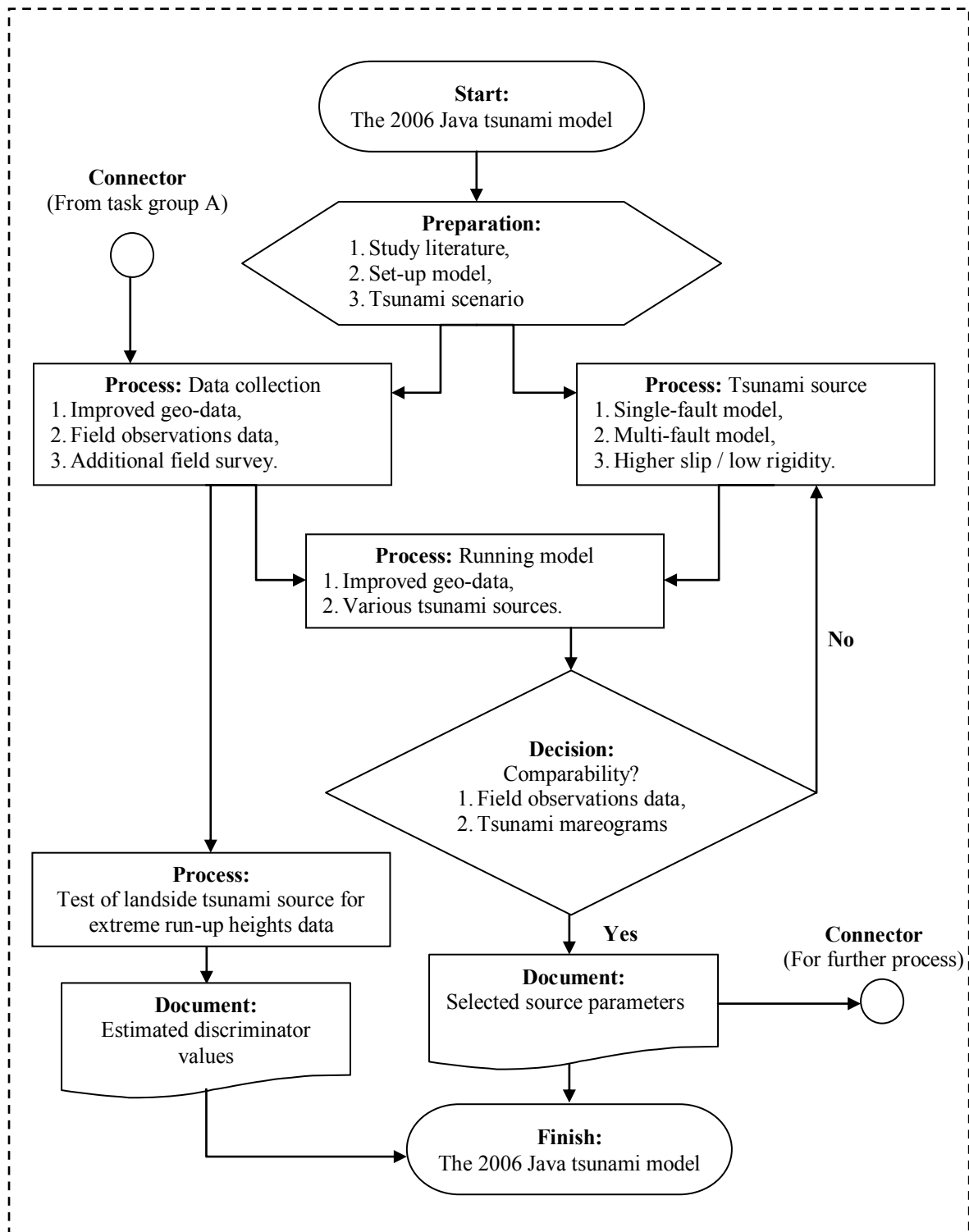
Appendix J – The Flow-chart of Business Processes

A. Geo-data improvement.



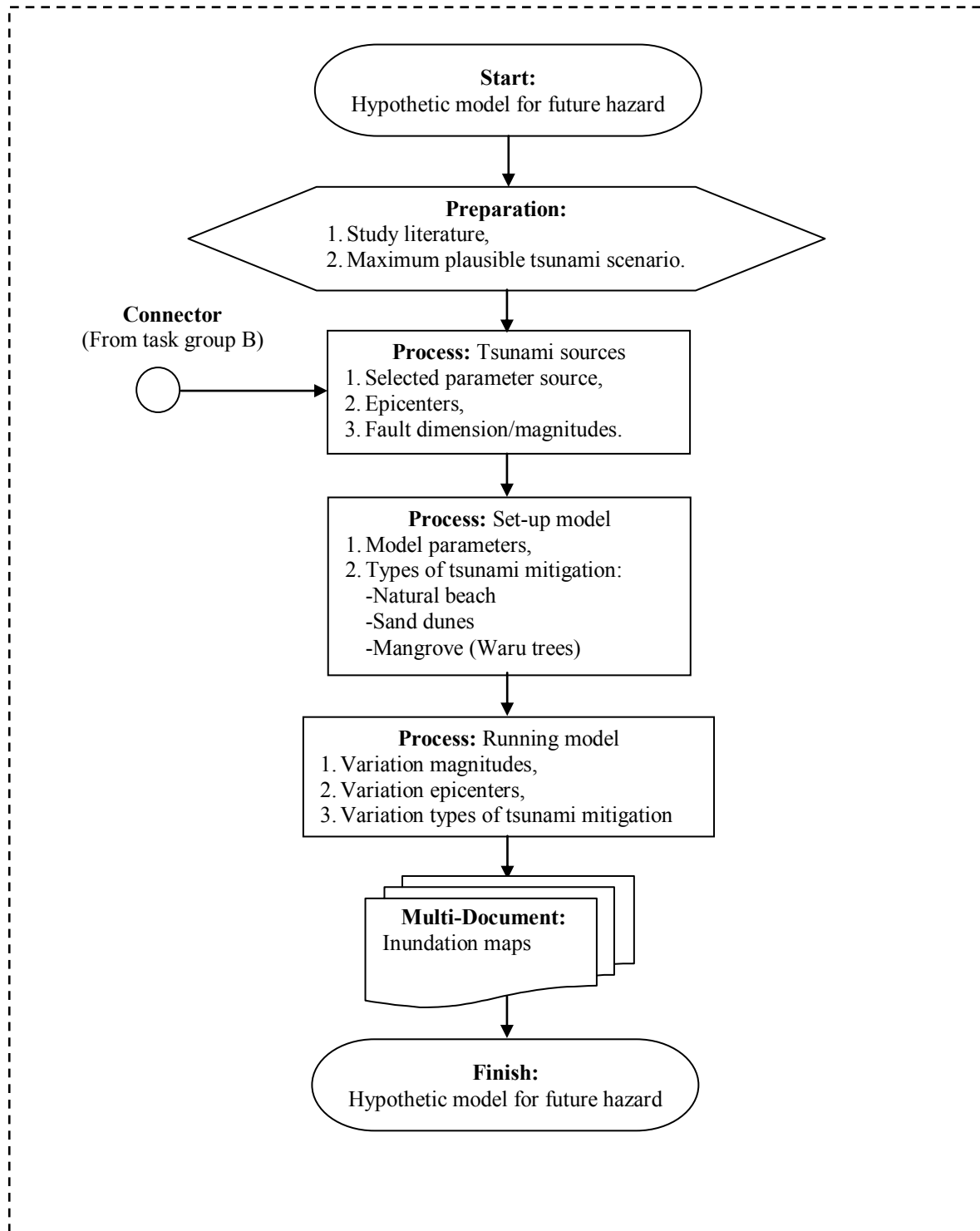
Appendix J

B. Model reconstruction of the 2006 Java tsunami.



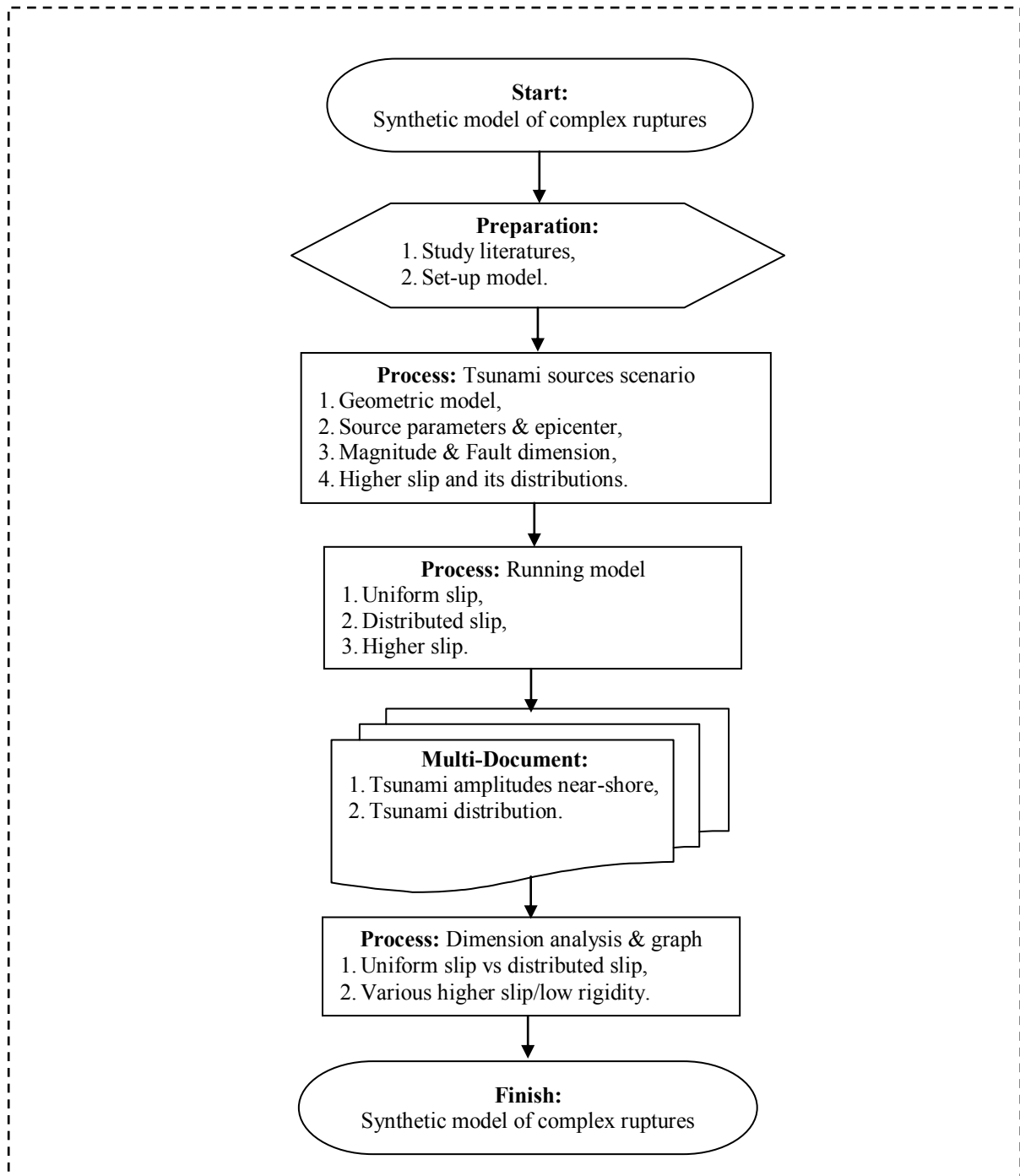
Appendix J

C. Hypothetic model for future hazard.



Appendix J

D. Synthetic model for the effect of complex ruptures to the tsunami run-up heights.



Appendix K – Curriculum Vitae

A. PERSONAL DATA

1. Name : Widjo Kongko
2. Place & date birth : Banyumas, 21 July 1967
3. Nationality : Indonesia
4. Affiliation : BPDP - BPPT
5. Office / E-mail : BPDP - BPPT
Jl. Grafika 2 (komplek Fak.Teknik UGM)
Bulaksumur Yogyakarta 55281 - Indonesia
Ph.:+62 (274) 586239, Fax: +62 (274) 542789
Email: kongko@fi.uni-hannover.de,
widjo.kongko@bppt.go.id, liawid@yahoo.com,



B. EDUCATION

1. Bachelor/Diploma (achieved)
July 1986 – August 1992: Student at Faculty of Civil Engineering, Gadjah Mada University, Indonesia. Thesis title: “Study on Coefficient of Velocity of Long shore Current”
2. Master Degree (achieved)
March 2002 – March 2004: Student at Faculty of Civil & Environmental Engineering, Iwate University, Japan. Thesis title: “Study on Tsunami Energy Dissipation in Mangrove Forest”

C. PROFESSIONAL EXPERIENCES (five selected)

1. 2009: Researcher on Padang Hazard Map: From Source Generation to run-up Using HSRC and Multi-beam Geo-data, Tsunami Model (Last Mile Project).
2. 2008: PhD Researcher on Java Tsunami: Model Using High-Resolved Data & Probable Scenario to Validate run-up Distribution (GITEWS Project).
3. January 2005 – March 2005: Technical Assistant for Engineering Design of Belopa Port, Sulawesi Indonesia.
4. June 2004 – October 2004: Site Engineer for Baron Wave Power Project, in house Project of BPDP BPPT.
5. August 2004 – November 2004: Study of Coastal Abrasion in Saloloang Coast, East Kalimantan Indonesia, join operation BPDP BPPT – Local Government.

E. FIELD WORK EXPERIENCES (ten selected)

1. 2010, 20-28 November: Survey coordinator of Mentawai 25 October 2010 earthquake-tsunami. German-Indonesia Tsunami Survey Team (GITST) funded by GITEWS.
2. 2007 – 2009: Survey Coordinator on Bathymetric and Topographic Campaign Measurement under GITEWS Project Framework.
3. July – August 2006: ITST: Survey on South Java Tsunami 17 July 2006.
4. July, 2 – 11 2006: Tsunami Deposit Survey Supported by IOTWS for Phanga Region, Thailand.
5. May, 28 2006: Rapid Survey on May 27 Yogyakarta Earthquake, Ad hoc. Collaboration RISTEK, UGM, BPPT.
6. April, 4 – 1 2006: The 4th Tsunami Survey in Collaboration with Kent State Univ. USA Post Doctoral Program for Meulaboh-NAD, BPDP BPPT.

Appendix K (continued)

7. November 25 – December 11 2005: The 3rd of Tsunami Survey in Collaboration with IMG Russia for Aceh – Sumatra Utara, BPDP BPPT.
8. March, 28 – April 28 2005: The 2nd of Tsunami Survey with ITST (International Tsunami Survey Tim) for Aceh – Sumatra Utara, BPDP BPPT – multilateral countries cooperation.
9. January, 19 – 30, 2005: The 1st of Tsunami Survey with ITST (International Tsunami Survey Tim) for Aceh – Sumatra Utara, BPDP BPPT – multilateral cooperation.
10. 2004 – 2005: Involve in Oceanographic Surveys in Saloloang-East Kalimantan and Ngobaran Central Java.

F. TRAINING/SHORT COURSES (two selected)

1. January 10 – 23, 2007: Tsunami Inundation Modeling Course, IOC – UNESCO Melbourne, Australia.
2. June 6 – 16 2006: Training on Tsunami Numerical Modeling, IOC – UNESCO Oostende, Belgium.

G. PUBLICATIONS/CONFERENCES (fifteen selected)

1. **Kongko, W.** & Schlurmann, T., 2011. The Java Tsunami Model: Using Highly-Resolved Data To Model The Past Event And To Estimate The Future Hazard. *Proceedings of the International Conference on Coastal Engineering, No. 32(2010), Shanghai, China. Paper: management.26. Retrieved fro <http://journals.tdl.org/ICCE>.*
2. Schlurmann, T.; **Kongko, W.**; Goseberg, N.; Natawidjaja, D.H. & Sieh, K., 2011. Near-Field Tsunami Hazard Map Padang, West Sumatra: Utilizing High Resolution Geospatial Data and Reasonable Source Scenarios. *Proceedings of the International Conference on Coastal Engineering, No. 32(2010), Shanghai, China. Paper: management.26. Retrieved from <http://journals.tdl.org/ICCE>.*
3. Borrero, J.C.; McAdoo, B.; Jaffe, B.; Dengler, L.; Gelfenbaum, G.; Higman, B.; Hidayat, R.; Moore, A.; **Kongko, W.**; Lukijanto; Peters, R.; Prasetya, G.; Titov, V. & Yulianto, E., 2010. Field Survey of the March 28, 2005 Nias-Simeulue Earthquake and Tsunami. *Pure and Applied Geophysics*.
4. Khomarudin, M.R.; Strunz, G.; Ludwig, R.; Zosseder, K.; Post, J.; **Kongko, W.** & Pranowo, W., 2010. Hazard Analysis and Estimation of People Exposure as Contribution to Tsunami Risk Assessment in the West Coast of Sumatra, the South Coast of Java and Bali. *Zeitschrift fuer Geomorphologie, 54, 337-356*.
5. Leschka, S.; **Kongko, W.** & Larsen, O., 2009. On The Influence of Near-shore Bathymetric Data Quality on Tsunami run-up Modeling, Part I: Bathymetry *Proceedings of 5th International Conference on APAC2009*.
6. Leschka, S.; **Kongko, W.** & Larsen, O., 2009. On The Influence of Near-shore Bathymetric Data Quality on Tsunami run-up Modeling, Part II: Modeling *Proceedings of 5th International Conference on APAC2009*.
7. Pranowo, W.S. & **Kongko, W.**, 2009. Modeling of the Bengkulu Minor Tsunami Event, September 12, 2007, West Sumatera, Indonesia: Comparison on Single- and Multi-Segment of Source generation. *Segara, 5 (2), 99-108*.
8. **Kongko, W.**, 14–18 December 2009: Tsunami Model of Cilacap-Indonesia: Inundation and Its Mitigation, AGU Fall Meeting, San Francisco CA-US.
9. **Kongko, W.**, 11–14 August 2009: The July 17, 2006 Java Tsunami: Tsunami Modelling and Its Characteristic Modes Based on the Hilbert-Huang Transformation, AOGS 6th,

Appendix K (continued)

SUNTEC Singapore.

10. **Kongko, W.**, & Schlurmann, T., 19–24 April 2009: The July 17, 2006 Java Tsunami: Tsunami Modelling and the Probable Causes of the Extreme run-up, *EGU2009*, Vienna-Austria.
11. **Kongko, W.**, 22–28 September 2008: Investigation on Colliding Wave of Tsunami run-up in December 26th 2006, Indian Ocean Tsunami, 2nd ITFS, Puglia-Ionian Islands, Italy.
12. Monecke, K.; Finger, W.; Klarer, D.; **Kongko, W.**; McAdoo, B.; Moore, A. & Sudrajat, S., 2008. A 1,000-year sediment record of tsunami recurrence in northern Sumatra. *Nature*, 455, 1232-1234.
13. Fritz, H.; **Kongko, W.**; Moore, A.; McAdoo, B.; Goff, J.; Harbitz, C.; Uslu, B.; Kalligeris, N.; Suteja, D.; Kalsum, K.; Titov, V.; Gusman, A.; Latief, H.; Santoso, E.; Sujoko, S.; Djulkarnaen, D.; Sunendar, H. & Synolakis, C., 2007. Extreme Runup from the 17 July 2006 Java Tsunami. *Geophysical Research Letters*, 34, 1-5.
14. **Kongko, W.**; Suranto, S.; Chaeroni, C.; Aprijanto, A.; Zikra, Z. & Sujantoko, S., 2006. Rapid Survey on Java Tsunami 17 July 2006. Available at: http://ioc3.unesco.org/itic/files/tsunami-java170706_e.pdf.
15. Jaffe, B.; Borrero, J.; Prasetya, G.; Peters, R.; McAdoo, B.; Gelfenbaum, G.; Morton, R.; Ruggiero, P.; Higman, B.; Dengler, L.; Hidayat, R.; Kinsley, E.; **Kongko, W.**; Lukijanto; Moore, A.; Titov, V. & Yulianto, E., 2006. Northwest Sumatra and Offshore Islands Field Survey after the December 2004 Indian Ocean Tsunami. *Earthquake Spectra.*, 22, s105-s135.

Hannover, October 2011



Widjo Kongko

L Previously Published Issues

A list of previously published issues and – if available – the additional electronic document is also available at

<http://www.fi.uni-hannover.de/franzius-mitteilungen.html>. Printed copies are available upon request at:

Issue	Year	Author and Title
99	2012	Kongko, W. South Java Tsunami Model Using Highly Resolved Data And Probable Tsunamigenic Sources
98	2011	Tagungsband des 13. Treffens junger WissenschaftlerInnen an Wasserbauinstituten
97	2011	Goseberg, N. The Run-up of Long Waves – Laboratory-scaled Geophysical Reproduction and Onshore Interaction with Macro-Roughness Elements
96	2008	Spekker, H. Steuerung von Küstenschutzelementen an Tideflüssen als Grundlage für ein Hochwasser- und Risikomanagement
95	2007	Matheja, A., Zimmermann, C., Krabbe, H. Application Architecture and System Technology for LDP (Logistical Data Platform) and FASTCORS (Fast Transport of Containers outside Regular Services) Matheja, A., Schweter, L., Zimmermann, C. Naturmessungen zur Bestimmung schiffsinduzierter Belastungen im Hafen eines Tideflusses Zimmermann, C., Zimmermann, G. Getting Music out of the Waves
94	2007	Matheja, A., Schweter, L., Spekker, H., Zimmermann, C., Pohl, C. Hydrodynamische numerische Simulation von Hochwasserereignissen und von Hochwasserschutzmaßnahmen für ein Tidegebiet Matheja, A., Spekker, H., Zimmermann, C., Brencher, J., Elsner, A. Risiko und Risikominderung in einer Tideregion
93	2007	Scheffermann, J. Instationäre Strömungssimulationen bei Öffnungsvorgängen mit und ohne freier Oberfläche am Beispiel beweglicher Schütze Matheja, A., Zimmermann, C., Bach, F-W., Barcikowski, S., Bunte, J., Haferkamp, J-D., Scheer, C., Reimche, W., Scheffermann, J., Walter, J. Stationäres 3D-Strömungsmesssystem für hochturbulente Strömungszustände unter Tide-, Strömungs- und Welleneinfluss
92	2006	Zimmermann, C., Ohle, N., Elsner, A. Deichüberwachung unter Einsatz der Fernerkundung Paesler, C. Bau, Ausrüstung und Betrieb eines Labordeiches im Naturmaßstab Zimmermann, C., Penchev, V., Scheffermann, J., Shukrieva, S. Evaluation of Reef Breakwater Efficiency from Physical and Numerical Simulations

Continued on next page

Leibniz Universität Hannover
 Franzius-Institut für Wasserbau und Küsteningenieurwesen
 Sekretariat
 Nienburger Str. 4, D-30167 Hannover
 Tel.: +49 511 762-2573
 Fax.: +49 511 762-4002
 Mail: sekretariat@fi.uni-hannover.de

Continued from previous page

Issue	Year	Author and Title
91	2004	Mai, S. Klimafolgenanalyse und Risiko für eine Küstenzone am Beispiel der Jade-Weser-Region
90	2004	Stoschek, O. Sedimentation und Gegenmaßnahmen in tide- und brackwasserbeeinflussten Häfen: eine Analyse mit Hilfe 3-dimensionaler Simulationen Mai, S., Paesler, C., Zimmermann, C. Wellen und Seegang an Küsten und Küstenschutzbauwerken
89	2003	Scheffermann, J., Matheja, A., Zimmermann, C., Linke, T. 5th Framework Programme of the European Commission: Enhancing Access to Research Infrastructures Action. 'Fundamental Hydraulic Research for Coastal Areas by Using Large Scale Facilities of the Hydro-Lab-Cluster North Germany' Stoschek, O., Matheja, A., Zimmermann, C. Entwicklung von Unterwasserstrukturen zur Verminderung von Sedimentation und Baggermengen am Liegeplatz eines Segelschiffes in einem Tidefluss Scheffermann, J., Linke, T. Numerische 3D-Simulationen und physikalische Modellversuche von Ablösezonen und Drehwirbeln im Wasserbau Mai, S., Daemrich, K.-F., Zimmermann, C. Wahrscheinlichkeit des Wellenüberlaufes an der Kaje eines geplanten Containerterminals Ohle, N., Daemrich, K.-F., Zimmermann, C., Möller, J., Schüttrumpf, H., Oumeraci, H. Schräger Wellenauflauf an Seedeichen Ohle, N., Zimmermann, C. Untersuchungen zu den Ursachen von Deckwerksverwerfungen am Nordufer der Elbe
88	2002	Grier, D. Binnenschifffahrt in den Vereinigten Staaten Scheerlinck, E. Elektronische Anbindung von Binnenhäfen und -schiffen an Seehäfen Burkert, P. Telematische Anbindung von Hinterlandverkehren mit Containern im Hamburger Hafen Doerre, H. Logistische Anforderungen an Seehäfen für den Hinterlandtransport auf Binnenwasserstraßen Matheja, A., Zimmermann, C., Miska, M., Bernard, M. BIDIS - Ein integriertes Software-Tool für Betrieb und Management von Binnenhäfen v. Dijk, M. Wirtschaftlichkeit von Binnenschiffstransporten mit schnelleren Schiffseinheiten Linke, T., Scheffermann, J., Zimmermann, C. Grenzen der Geschwindigkeitszunahme infolge hydrodynamischer Belastungen auf Sohle und Deckwerk Abdel-Maksoud, M., Heinke, C. Schnelle Schiffseinheiten - Hydrodynamische Modellierung und ökonomische Aspekte

Continued on next page

Issue	Year	Author and Title
		Heibaum, M., Soyeaux, R. Belastung von Sohle und Deckwerk durch schnellere Binnenschiffe bei Anwendung heutiger Bemessungsansätze
		Willems, C. Flussinformationssysteme im europäischen Vergleich
		Gevers, K. Produktion und Validierung von Inland-ECDIS Karten
		Matheja, A., Zimmermann, C., Miska, M., Bernard, M. Modellierung gemischter Verkehre innerhalb eines Flussinformationssystems
		Vetterlein, H.-U. Verkehrsüberwachung und Verkehrssteuerung auf Binnenwasserstraßen
		Wittmüss, D. Künftige Verkehrsüberwachung und Verkehrssteuerung im modernisierten Verkehrssicherungssystem Nord-Ostsee-Kanal (VSS-NOK)
		Kerstgens, H. Logistische Dienstleistungen einer Reederei für die Erhöhung der Wertschöpfung von Containertransporten mit Binnenschiffen
		Rekers, N. Die Rolle der Häfen als Systemoperateur und Logistikzentren
		Waldmüller, T. Intermodaler Verkehr oder Verkehrschaos
87	2002	Linke, T., Müller, A. Entwicklung eines Einleitungsbauwerkes an einer Binnenwasserstraße
		Matheja, A., Wurpts, A. Bestimmung von Überschwemmungsgrenzen durch Kopplung von hydrodynamischer Simulation und geografischem Informationssystem am Beispiel der Unteraller
		Miska, M. Entwicklung und Implementierung eines integrierten Hafensystems
		Bernard, M. Konzeption und objektorientierte Modellierung eines Simulationsverfahrens auf der Basis zellulärer Automaten für den Verkehrsablauf auf Binnenwasserstraßen
		Mai, S. Seegangsausbreitung in Hever und Heverstrom
		Linke, T., Scheffermann, J., Stockmeyer, M. Numerische Simulation des Strömungsfeldes um Binnenschiffe mittels Computational Fluid Dynamics (CFD)
86	2001	Ohle, N., Dunker, S. Konstruktive Maßnahmen zur Stabilisierung von Deichen
		Stoschek, O., Matheja, A. Simulation von Sedimenttransportprozessen in tidebeeinflussten Hafengebieten
		Zimmermann, C., v. Lieberman, N. Folgen von klimabedingten Wasserstands- und Windänderungen für den Küstenschutz an der Unterweser
		Mai, S. Anwendbarkeit kommerzieller Radar-Wasserstandspegel zur Seegangsmessung
85	2000	Plate, E.-J. Risikoanalyse im Hochwasserschutz, Risk Analysis for Protection and Coastal Defense
		Huber, K. Hochwasserstände an Nord- und Ostseeküsten, High Water-levels at North Sea and Baltic Sea Coasts
		Mai, S., v. Lieberman, N. Belastung der Seedeiche durch Wasserstände und Wellen, Loads on Dikes from Water-levels and Waves
		Jensen, J. Extremereignisse an Nord- und Ostseeküsten - Ermittlung von Bemessungsereignissen, Extreme Events at North Sea and Baltic Sea Coasts - Estimation of Design Criteria
		Starke, W.-D. Schäden und Vorsorgemöglichkeiten im Küsten- und Deichschutz, Damages and Mitigation for Dike Protection and Coastal Defence
		Krause, G. Generalplanung für den Küstenschutz in Niedersachsen, Regional Planning for Coastal Defence in Lower Saxony
		Probst, B. Generalplanung für den Küstenschutz in Schleswig-Holstein, Regional Planning for Coastal Defence in Schleswig-Holstein
		Jorissen, R.-E. Coastal Flood-Risk Management in the Netherlands, Management des Sturmflutrisikos an den Küsten der Niederlande

Continued on next page

Continued from previous page

Issue	Year	Author and Title
		Lastrup, C. Probabilistic Design for Coastal Defence in Denmark, Probabilistische Bemessung im Küstenschutz in Dänemark
		Mai, S., v. Lieberman, N. Risikopotentiale für Nutzflächen und Infrastruktur, Risk Potential for Settlement Areas and Infrastructures
		Hofstede, J., Hamann, M. Wertermittlung sturmflutgefährdeter Gebiete in Schleswig-Holstein, Appraisal for Areas Endangered by Storm Surges in Schleswig Holstein
		Remmers, I. Risiken aus Sicht des Natur- und des Umweltschutzes, Risk to Environmental Protection and Nature Conservation
		Wiedemann, M. Rechtliche Grundlagen für Hochwasser- und Küstenschutz, Legal Basis for Flood Protection and Coastal Defence
		Heiß, G. Katastrophenschutz, Disaster Management
		Kron, W. Occure and Insurance of Natural Disasters, Auftreten und Versicherbarkeit von Elementarereignissen
84	2000	Linke, T., Zimmermann, C., Hüsig, A. Schnelle Schiffe für Combiverkehre und Containertransport
		Mai, S., Zimmermann, C. Konzepte und Techniken im Küstenschutz im Land Niedersachsen
		Matheja, A., Lichy, C. Grundlagen für den Aufbau verteilter agierender Umweltinformationssysteme
83	1999	v. Lieberman, N. Leitbildmodell für den Küstenschutz der Nordseeküste am Beispiel der Vorländer
		Mai, S., v. Lieberman, N. Untersuchungen zum Risikopotential einer Küstenregion
		Mai, S., Zimmermann, C. Safty of Coastal Defense Systems - An Assessment of the Reliability of Coastal Systems in the Event of Rising Water Levels due to Climate Change
82	1998	Matheja, A., Zimmermann, C., v. Lieberman, N., Schwarze, H. Optimierung von Küstensicherungsarbeiten im Küstenvorfeld der Nordseeküste, Untersuchungen zur Wirksamkeit von Lahnungen durch Simulation der Hydromechanisch-Morphodynamischen Wechselwirkungen in physikalischen und numerischen Modellen
		Streich, G., Zimmermann, C., Schwarze, H. Hydraulische Modellversuche für die geplante Hafenerweiterung Altenwerder im Hamburger Hafen - Untersuchungen zur Anordnung und Gestaltung der Kaianlage und der Wendebereiche im Hinblick auf die Schlickfallminimierung im Hafenbereich
81	1998	Kunz, H. Wärmeeinleitung in Tidegewässern und deren Begrenzung durch fach-technische Behördenentscheidungen
80	1997	Dursthoff, W., Mazurkiewicz, B. Soil Water Pipeline Interaction - Review and Resulting Program for Further Investigations
		Schöttler, J. Zur Simulation des Betriebsablaufs auf Binnenwasserstraßen und ihre Anwendung auf den Containertransport mit Binnenschiffen
79	1997	Beyersdorf, J. Verhalten von Luftblasen und Sedimenten in Blasensäulen in Abhängigkeit vom Salzgehalt im Wasser
		Hüsig, A. Wiederherstellung der linearen Durchgängigkeit an Staustufen (Fischaufstiegshilfen) - Stand des Wissens - und hydraulische Modelluntersuchungen für ein naturnahes Parallelgewässer am Schnellen Graben in Hannover
78	1996	Zhan, L. Sekundäre Geschwindigkeitskomponenten im Wellenfeld
		Schulz, N. Aufspülmaßnahmen zum Schutz des Strandes und der Siedlung von Copacabana in Rio de Janeiro

Continued on next page

Continued from previous page

Issue	Year	Author and Title
		Woltering, S. Baggergutentsorgung der Hafengruppe Bremen
		Fiege, M., Hagmeier, H., Schulz, N. Lahnungsbauwerke: Entwicklung, Ausführungsvarianten und Entwässerungssysteme
		Zimmermann, C., Schulz, N. Morphological Effects from Waves and Tides on Artificially Stabilized Forelands in the Wadden Sea
77	1996	Woltering, S. Eine LAGRANGESche Betrachtungsweise des Seeganges
		Deppe, M., Roddewig, K. Entwicklung der Aller als Wasserstraße von Celle bis Verden - Vergangenheit und Perspektive
		Machens, U. Binnenwasserstraßen im Hinblick auf die Erfordernisse von Transportketten
76	1995	Wu, N.-T. Numerische Simulation der Druckschlagbelastung durch brechende Wellen auf senkrechte Bauwerke
		Zimmermann, C., Schwarze, H., Schulz, N., Henkel, S. Modelluntersuchungen zu propellerstrahlinduzierten Strömungen an Schiffs Liegeplätzen mit unterschiedlichen Maßnahmen zum Erosionsschutz
75	1994	Kunz, H. Die Einwirkungen des Meeres und des Menschen auf das Küstengebiet - Küstenschutz und Ökologie: Ein Widerspruch? - Aufgaben und Strategien
		Probst, B. Überlegungen für einen Küstenschutz der Zukunft
		Zander, R. Nationalpark und Küstenschutz als Gemeinschaftsaufgabe von Ökologen und Ingenieuren
		Otto, H.-J. Küstenschutz in Hamburg - Deichbau und Ökologie
		Moutzouris, C.-I., Daniil, E.-I. Oxygenation on a Sloping Beach Under Breaking Waves
		Zimmermann, C., Schöttler, J. Technische und logistische Voraussetzungen und Konzepte für eine Verknüpfung von Binnenschiff und Lkw
		Zimmermann, C., Damian, R.-M., Beyersdorf, J. Air Bubble Sizes in Aqueous NaCl Solutions
		Zimmermann, C. Forschungsvorhaben des Franzius-Instituts im Wasserbau und Küsteningenieurwesen ab 1993 (Stand: März 1994)
		Zimmermann, C. Projektstudien des Franzius-Instituts im Wasserbau und Küsteningenieurwesen ab 1993 (Stand: März 1994)
		Zimmermann, C. Verabschiedung des alten Vorstandes und Vorstellung des neuen Vorstandes der GESELLSCHAFT DER FÖRDERER DES Franzius-Instituts e.V. anlässlich der 31. Mitgliederversammlung und Vortragsveranstaltung am 24. März 1994 in Hannover
74	1993	Zhu, J. Numerische Simulation der Vorlandentwicklung im Tidebereich
		Schröder, D. Chancen und Grenzen der Erhöhung der Verkehrsleistungen auf den Binnenwasserstraßen in Deutschland
		Muller-Zwartepoorte, C.-M. Administrative Maßnahmen und Techniken zur verbesserten Nutzung von Binnenwasserstraßen in den Niederlanden und Europa
		Hecke, R. Chancen, Voraussetzungen und notwendige Anpassungen für den kombinierten Ladungsverkehr im Standort Binnenhafen
		Kaul, S. Neue Antriebe für Binnenschiffe und ihre Bedeutung für die Schifffahrt und die Wasserstraße
73	1992	Preser, F. Belastung horizontaler Rohrkörper in Meeresbodennähe durch Seegang im Übergangsbereich
		Rodiek, W. Der 14 m-Ausbau der Außenweser: Maßnahmen und Berücksichtigung der Umweltverträglichkeitsuntersuchungen

Continued on next page

Continued from previous page

Issue	Year	Author and Title
		Daemrich, K.-F., Osterthun, M., Hirsch, J. Einfluß von Baumaßnahmen auf Strömungs- und Seegangsverhältnisse der Außenweser als Grundlage der Beurteilung zur Umweltverträglichkeit
		Vollstedt, H.-W. Die Erweiterung des Containerterminals Bremerhaven (CT III): Umweltverträglichkeit und notwendige Ersatzmaßnahmen
		Corsmann, M., Elverich, L. Landschaftspflegerische Begleitplanung im Rahmen der Ersatzmaßnahmen für die Erweiterung des Containerterminals Bremerhaven (CT III)
		Zimmermann, C., Osterthun, M., Schwarze, H. Berücksichtigung des Küstenschutzes im Rahmen der Landschaftspflegerischen Begleitplanung für die Erweiterung des Containerterminals Bremerhaven (CT III)
		Hirsch, J. Hydraulische Modellversuche zur Entwicklung umweltrelevanter Planungsalternativen für eine Wasserstraße: Beispiel Mosel bei Fankel
		Liebenstein, H. Ausgleichsmaßnahmen und landschaftspflegerische Begleitplanung beim Ausbau einer Wasserstraße: Beispiel Mosel
		Nestmann, F. Aerodynamische Modelle - eine strömungsmechanische Untersuchungsmethode zur Planung wasserbaulicher Maßnahmen
		Gaumert, T. Anforderungen an Fischaufstiegshilfen in Fließgewässern
		Berkenkamp, G., Zimmermann, C., Schwarze, H. Lösungsvorschläge und Modellversuche für die ökologische Durchgängigkeit zwischen einer Wasserstraße und einem Zufluß am Beispiel der Weser in Nienburg
72	1991	Saathoff, F. Geokunststoffe in Dichtungssystemen - Laboruntersuchungen zum Verhalten von Geotextilien und Kunststoffdichtungsbahnen -
		Wilckens, F. Forschungsförderung im Küsteningenieurwesen
		Kunz, H. Klimaänderungen, Meeresspiegelanstieg, Auswirkungen auf die niedersächsische Küste
		Daemrich, K.-F. Modellversuche zum Wellenüberlauf an Polderwänden
		Osterthun, M., Partenscky, H.-W. Vorlandbildung an Deichen und Sicherungsdämmen Teil 1: Morphologische Analyse der Vorlandentwicklung
		Zhu, J., Partenscky, H.-W. Vorlandbildung an Deichen und Sicherungsdämmen Teil 2: Numerische Modellierung der Vorlandentwicklung
71	1991	Schade, D. Untersuchungen über das Wellenklima an einer Brandungsküste unter Einschluß der Richtungsstruktur des Seegangs, dargestellt am Beispiel der Insel Sylt
70	1990	Brinkmann, B. Ein Beitrag zur Bestimmung des Wasseraustausches zwischen Fluß und Hafen in Tidegebieten
		Klinge, U. Zur Energie von Tidewellen in Ästuaren mit einem Beispiel für die Unterweser
		Römisches, K. Hydromechanische Effekte fahrender Schiffe in Binnenkanälen
69	1989	Bobzin, H. Praktische Naßbagerei
		Mühling, W. Über die Anwendung porenmäßig abgestufter Vliesstoffe beim Ausbau von künstlichen Wasserstraßen
		Lüken, J. Hochwasserschutz in Hamburg. Darstellung der Entwicklung seit der Februarsturmflut 1962
68	1989	Mühling, W. Entwicklung und Stand der Deckwerksbauweisen im Bereich der Wasser- und Schifffahrtsdirektion Mitte
		Bartnik, H. Entwicklung und Stand der Deckwerksbauweisen im Bereich der WSD West
		Paul, W. Deckwerksbauweisen an Rhein, Neckar, Saar

Continued on next page

Issue	Year	Author and Title
		Paul, H.-J. Herstellen von Deckwerken unter ausführungstechnischen Gesichtspunkten
		Möbius, W. Abrollen von Geotextilien unter Wasser
		Saggau, W. Küstenschutzmaßnahmen in der Nordstrander Bucht
		Lastrup, C. Deckwerke an der dänischen Nordseeküste
		de Groot, M.-B. Allgemeine Grundlagen zur Standsicherheit des Untergrundes unter Deckwerken
		Oumeraci, H. Beanspruchung von Betonplattendeckwerken und ihre Berücksichtigung bei der Bemessung
		Richwien, W. Seegang und Bodenmechanik - Geotechnische Versagensmechanismen von Seedeichen
		Köhler, H.-J. Messung von Porenwasserüberdrücken im Untergrund
		Bezuijen, A. Wasserüberdrücke unter Betonsteindeckwerken
		Sparboom, U. Naturmaßstäbliche Untersuchungen an Deckwerken im Großen Wellenkanal
		Heerten, G. Analogiebetrachtungen zu Filtern
		Hallauer, O. Baustoffe für Deckwerke
		Saathoff, F. Prüfungen an Geotextilien
		Schulz, H. Überblick über neue nationale und internationale Empfehlungen
67	1988	Riebensahm, R. Dimensionierung von Container-Terminals in Binnenhäfen - Untersuchung der Einflußfaktoren für die betriebliche Bemessung
		Daemrich, K.-E., Scheffer, H.-J., Schwarze, H., Partenscky, H.-W., Kohlhase, S. Theoretische Vorstudie zur wellendämpfenden Wirkung des Riffs und zum seegangserzeugten Feststofftransport an der Westküste der Insel Sylt
		Brinkmann, B., Schoreder, E. Untersuchung der Abflußverhältnisse an einem im Nieuwe Waterweg geplanten Sturmflutsperrwerk
		Fittschen, T. Modellversuche für den Dollarhafen
		Müller, K.-D. Maßnahmen zur Reduzierung der Walzenströmung am Beispiel der Modellversuche für den Hamburger Hafen
		Osterthun, M. Vorlandbildung an Deichen und Sicherungsdämmen - ein BMFT-Forschungsprojekt -
		Salzmann, H. Planung und Bau des Emstunnels
66	1988	Partenscky, H.-W. Ausrüstungselemente von Binnenschiffs-Schleusen - Bemessung und konstruktive Ausbildung
		Oumeraci, H. Funktionelle Hafenplanung unter Berücksichtigung der Schiffsbewegungen infolge Wellenunruhe im Hafen
		Moutzouris, C.-I. Longshore Sediment Transport Computations: The Wave Power Equation and the Bijker Formula
65	1987	Rupert, D. Kontinuierliche Durchflußermittlung in Tideflüssen zur Bestimmung des Wasserhaushaltsparameters 'Abfluß'
		Ohling, J. Dollarhafen - Leidensweg einer Hafenplanung
		Brinkmann, B. Sedimentation in Hafenbecken
		Ricke, M. Gestaltung von Fischereihäfen
		Schwarze, H. Hydraulisches Tidemodell des See- und Lagunengebietes um Abu Dhabi
		Daemrich, K.-E., Schade, D. Seegangsmessungen vor Sylt mit einem Wellenrichtungsmeßsystem

Continued from previous page

Issue	Year	Author and Title
		Saathoff, F. Filterwirksamkeit gedehnter Geotextilien
		Saathoff, F. Untersuchungen zum Langzeit-Filterverhalten von Geotextilien
		Holtorff, G. Entwicklung natürlicher alluvialer Abflußgerinne
		Müller, J. Verkehrsprobleme im Duisburger Hafen
		Passlack, G. Vom Lehrgebiet Wasserbau zum Franzius-Institut für Wasserbau und Küsten- ingenieurwesen der Universität Hannover (1847 bis 1987)
64	1987	Hartung, W. Über den Einfluß der Komponenten des Wasserverkehrssystems auf die Sicher- heit des Seeschiffsverkehrs
		Saathoff, F. Marktformen und Grundsätzliches zur Wirkungsweise von Geotextilien
		Zanke, U. Sedimenttransportformeln für Bed-Load im Vergleich
63	1986	Xiao, Z. Ein neuer Weg der Fördertechnik für den Rohrleitungstransport von grobkörnigen Feststoffen
62	1986	Partenscky, H.-W. Zum 65. Geburtstag von Professor Dr.-Ing. F.-F. Zitscher
		Kniess, H.-G. Historische Entwicklung der Bauweisen für Auskleidungen von Binnen- wasserstraßen
		Meyer, H. Durchlässige Böschungsbefestigungen am Mittellandkanal - einst und heute
		Mühling, W. Über die Entwicklung der Hartdichtungen beim Ausbau von Kanälen
		Schönian, E. Langzeitverhalten von Asphalt dichtungen im Wasserbau
		Hoffmann, H.-G. Asphalt dichtungen im Wasserbau
		Beckmann, J. Erneuerung der Versiegelung der Oberflächendichtung auf der wasserseitigen Dammfläche der Biggetalsperre
		Saathoff, F., Bassen, R., Kohlhase, S. Anwendungsorientierte Untersuchungen an Deponie- Dichtungssystemen
		Heerten, G. Ein geschlossener Ansatz zur Dimensionierung von Geotextilien für Ufersicher- ungen
		Täubert, U. Das Speicherbecken Geeste - Zwei Millionen Quadratmeter Filtervlies und Asphaltbeton-Dichtung
		Abromeit, H.-U. Maschinelles Unterwassereinbau von geotextilen Filtern
		Knipschild, F.-W. Deponie-Abdichtungen mit Kunststoffdichtungsbahnen - Stand der Tech- nik und Entwicklungen
61	1985	Scheffer, H.-J. Wellenunruhe in Häfen und Schiffsbewegungen -, ein Beitrag für eine integ- rierte Hafenplanung
		Dursthoff, W., Mazurkiewicz, B. Problems Related to Subsea Pipeline-Seabed Interaction
		Daemrich, K.-E., Kahle, W., Partenscky, H.-W. Schutzwirkung von Unterwasserwellen- brechern unter dem Einfluß unregelmäßiger Seegangswellen
		Xi, Y. Pile Berthing Structures in Harbour Engineering
60	1985	Moutzouris, C.I. Coastal Processes Along the Eroding Western Coast of the Island of Sylt, F.R. Germany
		Dieckmann, R. Geomorphologie, Stabilitäts- und Langzeitverhalten von Wattenzugsgebi- eten der Deutschen Bucht
		Schwarze, H. Untersuchung von Baumaßnahmen im Tidegebiet
59	1984	Grett, H.-D. Das Reibungsverhalten von Geotextilien in bindigem und nichtbindigem Boden
		Wilde, P., Kozakiewicz, A. Application of Kalman Filter to Analysis of Vibrations of Struc- tures Due to Waves

Continued on next page

Continued from previous page

Issue	Year	Author and Title
		Burkhardt, O. Bericht über die Arbeiten des Franzius-Instituts in den Jahren 1982 bis 1984
		Partenscky, H.-W. Schleusen und Hebewerke, Überblick und Ausblick
		Passlack, G. Verbau von Hochwasserabflußquerschnitten an der Ems und an der Leine
		Kohlhase, S., Scheffer, H.-J. Modelluntersuchungen für Seehäfen
		Grett, H.-D. Geotextilien im Wasserbau und Eisenbahnbau
		Dieckmann, R. Flächenhafter Küstenschutz
		Nasner, H. Wellenerzeugter Sedimenttransport
		Partenscky, H.-W. Bemessung von Wellenschutz-Bauwerken
		Dursthoff, W. Seegangskräfte auf horizontale Kreiszyylinder
58	1984	Kao, C.-C. Seegangsbelastung auf kreisförmige Rohre in Sohlhöhe
		Tang, F. A Comparison of the Wave Statistics Between the Eastern Part of Taiwan Strait and the North Sea
		Siefert, W. Energiebetrachtungen zum Tideablauf in Flüssen mit einigen Anwendungsbeispielen
		Horn, P. Stoßschutzanlagen an Schleusen und Hebewerken
57	1983	Kohlhase, S. Ozeanographisch-seebauliche Grundlagen der Hafenplanung
		Grabe, W. Kunststoffdichtungsbahnen im Wasserbau
		Kahle, W. Untersuchung des Energiebedarfs beim hydraulischen Feststofftransport von Sanden und Kiesen durch horizontale Rohrleitungen unterschiedlicher äquivalenter Wandrauigkeit
		Grabe, W. Studentische Exkursion im Sommer 1983 zu Wasserbauwerken im westdeutschen Raum und in den Niederlanden
56	1983	Eggert, W.-D. Diffraktion und Wellentransmission an Tauchwänden endlicher Länge. Ein Beitrag zur Bestimmung der Wellendämpfung teildurchlässiger Wellenbrecher
		Partenscky, H.-W. Die Forschungsaktivitäten des Franzius-Instituts in den Jahren 1980 und 1981
		Daemrich, K.-F. Zur Auswertung von Seegangsmessungen am Beispiel von Messungen vor Westerland/Sylt
		Grabe, W. Untersuchungen im Franzius-Institut über die Eigenschaften von Geotextilien
		Passlack, G. Regulierungs- und Ausbaumaßnahmen an Flußläufen
		Grabe, W. Mechanische und hydraulische Eigenschaften von Geotextilien
55	1982	Flügge, G. Transport- und Ausbreitungsmechanismen in Flüssen und Tideästuarien unter besonderer Berücksichtigung der Strömungsturbulenz
		Kahle, W. Hydraulische Einflußgrößen beim Rohrleitungstransport von Sand-Wasser-Gemischen
54	1982	Burkhardt, O. Vorträge im Rahmen der Fachveranstaltung 'Häfen - Planung, Bau, Betrieb' im Haus der Technik, Essen
		Göhren, H. Aufgaben des öffentlichen Bauherrn bei der Abwicklung hafengebäulicher Vorhaben
		Kohlhase, S. Ermittlung ozeanographisch-seebaulicher Grundlagen für die Planung von Seehäfen
		Wiedemann, G. Fragen der Nautik und der Verkehrssicherung für Planung und Betrieb von Häfen und ihren Zufahrten

Continued on next page

Continued from previous page

Issue	Year	Author and Title
		Horn, A. Bodenmechanische und grundbauliche Einflüsse bei der Planung, Konstruktion und Bauausführung von Kaianlagen
		Heyer, E. Konstruktive Gestaltung von Hafenanlagen
		Stückrath, T. Über die Probleme des Unternehmers beim Hafenanbau
		Morisse, M. Der Einfluß der betrieblichen Erfordernisse auf die Hafengestaltung
		Kroh, W. Die Finanzierung von Hafenanbauprojekten durch die Kreditanstalt für Wiederaufbau im Rahmen der finanziellen Zusammenarbeit der Bundesrepublik Deutschland mit Entwicklungsländern
		Hemmer, H.-R. Kosten-Nutzen-Betrachtungen bei Planung und Betrieb von Häfen
		Vetter, A. Die Rolle des Beratenden Ingenieurs bei Planung, Bau und Betrieb von Häfen in Entwicklungsländern
		Meyer, H. Kreuzungsbauwerke am Mittellandkanal
		Mühling, W. Uferauskleidungen beim Ausbau von künstlichen Wasserstraßen am Beispiel des Mittellandkanals
		Zanke, U. Kolke am Pfeiler in richtungskonstanter Strömung und unter Welleneinfluß
53	1981	Tautenhain, E. Der Wellenüberlauf an Seedeichen unter Berücksichtigung des Wellenaufbaus - Ein Beitrag zur Bemessung -
		Keska, J.-K. Förderung von inhomogenen Zwei-Phasen-Gemischen durch Rohrleitungen. Ausgewählte theoretische und praktische Probleme der Meßtechnik, der Mechanik und der Methodik
52	1981	Heerten, G. Geotextilien im Wasserbau - Prüfung, Anwendung, Bewährung -
		Kazanskij, I. Über theoretische und praxisbezogene Aspekte des hydraulischen Feststofftransportes
51	1980	Partenscky, H.-W. Dank an die Gäste und Überleitung zum Festvortrag
		Zitscher, F.-F. Die Bedeutung unseres Wassers im Universum
		Partenscky, H.-W. Dank an Professor Zitscher und Schlußworte
		Lundgren, H. Die zukünftige Rolle natürlicher Wellen in der Küstentechnik (Future Role of Natural Sea States)
		Monkmeyer, D. Wave-Induces in Coastal Protection Works
		Bijker, W. Modern Trends in Coastal Protection Works
		Wilde, P. Problems of Vibration of a Breakwater Structure Due to Wind Waves
		Vischer, D. Durch Felsstürze in Seen erzeugte Wellen
		Price, A.-W. Coastal Engineering - The Impossible Art
		Nougaro, J. Dammbürche
		Führböter, A. Strömungsvorgänge in den wandnahen Grenzschichten beim hydraulischen Feststofftransport
		Hager, M. Maßnahmen zur Bekämpfung von Erosionserscheinungen in Flüssen
		Simons, H. Planung und Bau neuer Seehäfen im Ausland
		Boe, C. Wasserbau und Umweltschutz
		Salzmann, H. Die Entwicklung des deutschen Offshore-Bauens
		Dillo, H.-G. Kleinkraftwerke - ein Beitrag zur Energieversorgung in Entwicklungsländern
		Brühl, H. Einige technische Aspekte bei der Planung und beim Bau des Mehrzweck-Terminals Limón/Costa Rica

Continued on next page

Issue	Year	Author and Title
		Stückrath, T. Bau des Unterwasserrückgabebetunnels für das Kernkraftwerk Buser am Persischen Golf
		Passlack, G. Wasserbauliche Forschungsarbeiten im Franzius-Institut für Wasserbau und Küsteningenieurwesen der Universität Hannover in den Jahren 1977 bis 1979
50	1980	Partenscky, H.-W. Hochschullehrer der Fachgebiete Allgemeiner Wasserbau, Verkehrswasserbau und Küsteningenieurwesen an der Universität Hannover von 1847 bis 1980
		Partenscky, H.-W. Von der Hannoverschen Versuchsanstalt für Grundbau und Wasserbau der Technischen Hochschule Hannover zum Franzius-Institut für Wasserbau und Küsteningenieurwesen der Universität Hannover (1980)
		Partenscky, H.-W. Zum Geleit: Professor Dr.-Ing. Dr.phys. H.-W. Partenscky Direktor des Franzius-Instituts für Wasserbau und Küsteningenieurwesen
		Krolewski, H. Grußwort des 1. Vorsitzenden der Gesellschaft der Förderer des Franzius-Instituts e.V.
		Passlack, G. Entwicklung des Lehr- und Forschungsgebietes Verkehrswasserbau an der Universität Hannover
		Partenscky, H.-W. Neue Erkenntnisse über das Stabilitätsverhalten und den Sedimenttransport in Watt-Prielsystemen
		Heerten, G. Das Franzius-Institut als Prüfinstanz für Geotextilien
		Ross, C. Möglichkeiten und Grenzen eines geregelten Sperrwerksbetriebs zur Beeinflussung der Tidedynamik
		Burkhardt, O. Über die Bestückung eines Kais mit Hafenkranen
		Falldorf, W. Anwendung, Einsatz und Aussagefähigkeit von hydraulischen Tidemodellen
		Lindlar, A. Die Entwicklung von Tidesteueranlagen - Prozeßrechnergesteuerte Nachbildung von Naturtiden im Franzius-Institut der Universität Hannover
		Mahnken, B., Müller, H., Visscher, G. Wärmebilanzmessungen in der Unterweser
		Daemrich, K.-E., Kohlhase, S. Seegangsforschungsprogramme im Franzius-Institut innerhalb des Sonderforschungsbereichs 79
		Schwarze, H. Grundlagen für den Betrieb von hydraulisch-thermischen Modellen
		Bode, E., Zanke, U. Neue Erkenntnisse im Sedimenttransport - Ergebnisse aus der Arbeit des Teilprojektes B5 im SFB 79 -
		Kazanskij, I., Mathias, H.-J. Feststofftransport in Rohrleitungen - Gegenüberstellung von Untersuchungen im Modell und in der Natur
		Passlack, G. Auswirkungen wasserbaulicher Maßnahmen an Binnengewässern im Raum Hannover
		Dursthoff, W. Entwicklung von Primärwandlern zur Nutzung der Seegangenergie
		Barg, G. Salzgehaltsverteilungen in Brackwassergebieten als Grundlage ökologischer Betrachtungen
49	1979	Barg, G. Untersuchungen über Salzgehaltsverteilungen in Brackwassergebieten von Tideflüssen am Beispiel der Unterweser
		Kunz, H. Regelungen für die Abgabe radioaktiver Stoffe aus einem Leichtwasser-Kernkraftwerk vom Druckwassertyp in einen Tidefluß
		Kunz, H. Das Automatische Meßsystem für die Beweissicherung WASSER beim Kernkraftwerk Unterweser
		Kunz, H. Wasserrechtliche Regelungen für die Einleitung von Kühlwässern in einen Tidefluß unter besonderer Berücksichtigung des Einsatzes von automatischen Meßsystemen, dargestellt am Beispiel des Kernkraftwerkes Unterweser

Continued from previous page

Issue	Year	Author and Title
		Zanke, U. Über die Abhängigkeit der Größe des turbulenten Diffusionsaustausches von suspendierten Sedimenten
		Zanke, U. Über die Anwendbarkeit der klassischen Suspensionsverteilungsgleichung über Transportkörpern
		Zanke, U. Konzentrationsverteilung und Kornzusammensetzung der Suspensionsfracht in offenen Gerinnen
		Wundes, R. Entwicklung eines Hybriden Tidemodells
48	1978	Zanke, U. Zusammenhänge zwischen Strömung und Sedimenttransport Teil 2: Berechnung des Sedimenttransportes hinter befestigten Sohlenstrecken - Sonderfall zweidimensionaler Kolk -
		Hinsch, J. Anwendung von Pulswellen beim hydraulischen Feststofftransport
		Elahi, K.-Z. Berechnung von lokalen Gezeitenphänomenen in einem Gebiet mit geringem Beobachtungsmaterial mit Anwendung auf die Sonmiani Bucht (Pakistan)
		Passlack, G. Bauliche Maßnahmen zur Senkung der Hochwasserstände in Hochwasserabflußgebieten von Binnenflüssen
47	1978	Daemrich, K.-F. Diffraktion gebeugter Wellen - Ein Beitrag zur Berechnung der Wellenunruhe in Häfen -
		Daemrich, K.-F., Hillebrand, W., Kohlhase, S., Tautenhain, E. Versuchseinrichtung Wellenbecken für dreidimensionale, vergleichende Untersuchungen mit regelmäßigen Wellen und Wellenspektren
		Zitscher, F.-F. Schadensursachen an Küstenschutzanlagen herkömmlicher Art während der Sturmflut vom 3.1.1976 an der schleswig-holsteinischen Westküste
		Daemrich, K.-F., Kohlhase, S. Diffraktion an halbunendlichen Wellenbrechern - Diagramme der Wellenhöhenverteilung hinter totalreflektierenden linienförmigen Bauwerken -
		Zanke, U. Zusammenhänge zwischen Strömung und Sedimenttransport Teil 1: Berechnung des Sedimenttransportes - allgemeiner Fall -
46	1977	Kunz, H. Schiffsschwall und Sunk in seitlich einer Wasserstraße angeordneten Becken
		Barg, G., Flügge, G., Visscher, G. Experimentelle Bestimmung des Wärmeaustausches an der Gewässeroberfläche
		Zanke, U. Neuer Ansatz zur Berechnung des Transportbeginns von Sedimenten unter Strömungseinfluß
		Hamel, G. Statistische Analyse von Tidewasserständen am Beispiel des Pegels W.shaven 'Seeschleuse'
		Kunz, H. Die Wirkung von Schiffswellen auf Entwässerungsbauwerke an Tideflüssen
		Zanke, U. Berechnung der Sinkgeschwindigkeiten von Sedimenten
		Partenscky, H.-W. Bericht über die Arbeiten des Franzius-Instituts von 1975 bis 1977
		Partenscky, H.-W. Veröffentlichungen von Mitarbeitern des Franzius-Instituts der Technischen Universität Hannover in den Jahren 1975 bis 1977
		Passlack, G. Schwerpunkte der wasserbaulichen Forschungen im Franzius-Institut für Wasserbau und Küsteningenieurwesen (Zeitraum 1975 bis 1977)
		Göhren, H. Perspektiven der Hamburger Hafenplanung
		Visscher, G. Meßprogramm Unterweser
		Flügge, G. Bestimmung des Wärmeaustausches an Wasseroberflächen
		Heerten, G. Problematik der Kühlwasserversorgung an einer Stauhaltungskette
		Schwarze, H. Modelluntersuchungen für die Kühlwasserversorgung der Kernkraftwerke Iran am Persischen Golf

Continued on next page

Continued from previous page

Issue	Year	Author and Title
		Kohlhase, S. Numerisches Modell zur Bestimmung der Wellenunruhe in einem Hafen
		Daemrich, K.-F. Grundsatzuntersuchungen zur Diffraktion an Hafeneinfahrten
		Dursthoff, W. Wellenenergie - nutzbare Energie?
		Partenscky, H.-W. Hydrodynamische Belastung von Pipelines auf der Meeressohle
45	1977	Grcic, J. Einfluß der pulsartigen Strömung bei hydraulischem Feststofftransport
		Berger, U., Kurpiers, J. Automatisierung der graphischen on-line-Darstellung von umfangreichen Meßreihen
		Nasner, H., Partenscky, H.-W. Modellversuche für die Tide-Elbe. Strombaumaßnahmen nach 1962 und ihre Auswirkungen auf die Sturmflutwasserstände
		Nasner, H., Partenscky, H.-W. Sturmfluten in der Elbe und an der deutschen Nordseeküste von 1901 bis zum Januar 1976
		Heerten, G., Partenscky, H.-W. Ein Vergleich der Sturmflut vom 3. Januar 1976 auf der Elbe mit anderen Sturmfluten nach 1962
44	1976	Zanke, U. Über den Einfluß von Kornmaterial, Strömungen und Wasserständen auf die Kenngrößen von Transportkörpern in offenen Gerinnen
		Rupert, D. Zur Bemessung und Konstruktion von Fendern und Dalben
		Zanke, U. Über die Naturähnlichkeit von Geschiebeversuchen bei einer Gewässersohle mit Transportkörpern
		Partenscky, H.-W. Bericht über die Arbeiten des Franzius-Instituts von 1973 bis 1975 und zukünftige Planungen
		Passlack, G. Wasserbauliche Untersuchungen im Franzius-Institut in den Jahren 1973 bis 1975
		Barjenbruch, K.-H. Entwicklung und Stand des Küstenschutzes in Niedersachsen
		Ohling, J. Ausbau der niedersächsischen Seehäfen
		Schwarze, H. Untersuchungen des Franzius-Instituts über die Einleitung von aufgewärmtem Kühlwasser in Gewässer
		Grüne, J. Neue Wellenrinne des Franzius-Instituts - Untersuchungen mit Seegang -
		Renger, E. Grundzüge der Analyse und Berechnung von morphologischen Veränderungen in Wattengebieten
		Wundes, R.-D. Hybride Modelle - Koppelung von numerischen und hydraulischen Modellen
43	1976	Renger, E. Quantitative Analyse der Morphologie von Wateinzugsgebieten und Tidebecken
		Brühl, H. Einfluß von Feinststoffen in Korngemischen auf den hydraulischen Feststofftransport in Rohrleitungen
		Berger, U. MACH-Reflexion als Diffraktionsproblem
42	1975	Henze, R. Beitrag zur Abschätzung der bleibenden Verschiebung kleiner Fundamente auf dicht gelagertem Sandboden
		Hager, M. Untersuchungen über MACH-Reflexion an senkrechter Wand
		Rehling, U. Datenerfassung und -auswertung mit Digitalrechnern bei Wasserstands- und Wellenmessungen
41	1974	Heerten, G. Einfluß von Schiffbau und Umschlagstechnik auf die Gestaltung von Seehäfen
		Niemeyer, H.-D. Wellenerzeugte Strömungen und Sedimenttransport
		Ramacher, H. Der Ausbau von Unter- und Außenweser
40	1974	Nasner, H. Über das Verhalten von Transportkörpern im Tidegebiet

Continued on next page

Continued from previous page

Issue	Year	Author and Title
		Siefert, W. Erste Erfahrungen mit einem neuen Sturmflut-Vorhersageverfahren
		Partenscky, H.-W. Entwicklung und Arbeitslage des Franzius-Instituts für Wasserbau und Küsteningenieurwesen der Technischen Universität Hannover in den Jahren von 1971 bis 1973
		Nasner, H. Dynamisches Verhalten von Transportkörpern. Vergleiche von Messungen in der Natur und im Modell
		Schüttrumpf, R. Maßgebende hydrologische Größen für die Beurteilung von Einleitungen in Tideästuarien
		Schwarze, H. Untersuchungen für die Übertragbarkeit der Ergebnisse aus hydraulisch-thermischen Modellversuchen
		Passlack, G. Entwicklung des Sonderforschungsbereiches 79 der Technischen Universität Hannover
		Rehling, U. Meßwerterfassung an hydraulischen Tidemodellen
		Renger, E. Untersuchungen von Wateinzugsgebieten
		Daemrich, K.-F. Untersuchungen in dreidimensionalen Wellenbecken
		Grüne, J. Entwurf eines Großen Wellenkanals
		Brühl, H. Hydrografische Untersuchungen über die Einleitung von Abwässern in das Seegebiet von Busan/Korea
		Dursthoff, W., Kohlhase, S. Hydrografische Messungen im Seegebiet von Sonmani/Pakistan
		Passlack, G. Mitgliederverzeichnis der Gesellschaft der Förderer des Franzius-Instituts e.V. nach dem Stande vom 1.3.1974
39	1973	Schüttrumpf, R. Über die Bestimmung von Bemessungswellen für den Seebau am Beispiel der südlichen Nordsee
		Liang, N.-K. Über den Einfluß des Windfeldes bei der Wellenvorhersage
38	1973	Ackermann, H. Kriterien und Ansätze für eine integrierte Hafenenwicklungsplanung unter besonderer Berücksichtigung der Probleme in Entwicklungsländern
		Kohlhase, S. Über den Vordrall an Pumpeneinläufen im Wirbelfeld
37	1972	Buchholz, W. Die Entwicklung des Franzius-Instituts von 1949 bis 1971 - Eine Würdigung Professor Hensens -
		Wiedemann, G. Dank und Anerkennung für Herrn Professor Hensen
		Laucht, H. Worte zum Abschied von Professor Dr.-Ing. Dr.-Ing. E.h. W. Hensen
		Peter, H. Worte des Dankes an Herrn Professor Hensen
		Lorenzen, J. Grußworte an Professor Hensen
		Partenscky, H.-W. Entwicklungstendenzen in der Wasserbau-Forschung, Gestern und Heute
		Dillo, H.-G. Planungen, Entwürfe und Bauausführungen im Auslande
		Krolewski, H. Neuere Bauvorhaben im Kraftwerksbau
		Rohde, H. Hydrologische Probleme des Wasserbaus im Küstengebiet
		Kazanskij, I. Wechselwirkung zwischen Makroturbulenz und Feststofftransport in Rohrleitungen
		Kohlhase, S. Elektroanaloge Voruntersuchungen für Kühlwasserkreisläufe
		Schwarze, H. Modelluntersuchungen für die deutschen Tideästuarien

Continued on next page

Continued from previous page

Issue	Year	Author and Title
36	1971	Passlack, G. Kurzbericht über die Arbeiten des Franzius-Instituts von 1969 bis 1971
		Führböter, A. Über die Bedeutung des Lufteinschlages für die Energieumwandlung in Brandungszonen
35	1970	Rohde, H. Eine Studie über die Entwicklung der Elbe als Schifffahrtsstraße
		Spataru, A. Über gleichförmige und ungleichförmige Turbulenz in Freispiegelgerinnen
		Passlack, G. Strömungen im Bodensee
34	1970	Führböter, A. Zur Frage der hydraulischen Förderung von Meerereserzen
		Rocha Felices, A. Wasserableitung aus Flüssen mit Sedimentbewegung
		Stückrath, T. Über die Durchmischung von Süß- und Salzwasser in den Brackwassergebieten von Tideflüssen
33	1969	Rodloff, W. Über Wattwasserläufe
		Schwarz, J. Treibeisdruck auf Pfähle
		Dursthoff, W. Über den quantitativen Wasseraustausch zwischen Fluß und Hafen
32	1969	Wagner, H. Meßprogramm am Gußeisen-Ausbau der U-Bahn-Tunnel in Hamburg
		Ayar, H.-R. On the Hydromechanics of Breakers on Steep Slope
		Schwarze, H. Erweiterung des Anwendungsbereiches der REHBOCKschen Brückenstaugleichung auf Trapezquerschnitte
31	1968	Kontur, G. Die Eisverhältnisse der Donau. Erfahrungen mit Eisbrecher-Schiffen
		Wittmer, H.-G. Modellversuche für die Absperrung der Oste
		Roy, S.-C. Hydraulic Investigations on Behalf of Hooghly Estuary
30	1968	Roy, S.-C. Hydraulische Untersuchungen über das Hooghly Ästuar
		Stückrath, T. Die Bewegung von Großriffeln an der Sohle des Rio Paraná
		Henningsen, D., Mäckel, R. Fossile Holzreste und Baumstämme in Flußablagerungen
		Salzmann, H. Hydraulische und bodentechnische Vorgänge beim Grundsaugen
		Lehmann, U. Der Einfluß von Filterkies und Brunnenrohr auf die Bemessung eines vollkommenen Brunnens
		Dillo, H.-G. Aufgaben deutscher Consultingfirmen im Ausland
		Dursthoff, W. Die Entwicklung der Turbulenzforschung im Hinblick auf ihre Bedeutung im Wasserbau
Kohlhase, S. Analogversuche als Leitmodelle - Elektroanalogversuche und HELE-SHAW-Strömungen -		
Krolewski, H. Wasserbauten der Kraftwirtschaft		
Schwarz, J. Über die physikalischen Vorgänge beim Eisdruck		
Stückrath, T. Die 'Regimetheorie' - Entwicklung und Anwendung -		
Christiansen, H., Schäfer, V. Bericht über die Exkursion des Lehrstuhls für Verkehrswasserbau 1967 nach Ceylon, Indien, Pakistan, Afghanistan und in die Türkei		
30	1968	Siefert, W. Sturmflutvorhersage für den Tidebereich der Elbe aus dem Verlauf der Windstaukurve in Cuxhaven
		Göhren, H. Triftströmungen im Wattenmeer
		Kontur, S. Kinematische Prüfungen des Kapillaranstiegs unter besonderer Berücksichtigung der charakteristischen Eigenschaften des Grundwasser-Strömungsfeldes

Continued on next page

Continued from previous page

Issue	Year	Author and Title
29	1967	Burkhardt, O. Naturmessungen des Strömungswiderstandes von Hubinsel-Beinen im See-gang
		Führböter, A. Zur Mechanik der Strömungsriffel. Ein Ansatz zur Berechnung der Höhe der Transportkörper und ihres Einflusses auf den Feststofftransport
		Krolewski, H. Die Verteilung der Fließgeschwindigkeiten in einem Vorfluter
		Burkhardt, O. Über den Wellendruck auf senkrechte Kreiszyylinder
		Annen, G. Die Bemühungen um das Abflußgesetz aus der Sicht der Praxis
		Gehrig, W. Über die Frage der naturähnlichen Nachbildung der Feststoffbewegung in Mod-ellen
28	1966	Führböter, A. Der Druckschlag durch Brecher auf Deichböschungen
		Hensen, W., Führböter, A. Kunststoff zur Sicherung von Abbruchufern
		Domzig, H. Wasserwirtschaftliche Arbeiten im Vorraum der Landeshauptstadt Hannover
		Roy, N. Hydrodynamic Pressure Oscillation Around a Conduit Gate (Hydrodynamische Druckschwankungen im Bereiche eines Tiefschützes)
27	1966	Führböter, A., Passlack, G., Wittmer, H.-G. Entwicklung des Franzius-Instituts für Grund-und Wasserbau der Technischen Hochschule Hannover
		Wittmer, H.-G. Sedimentologische Probleme des Hafens Quequén, Argentinien
		Sindern, J. Die hydrologischen und morphologischen Aufgaben im Küstenraum, dargestellt an den Aufgaben der Wasser- und Schifahrtsdirektion Kiel
		Dettmers, D. Aus der hydraulischen Feststoffförderung
		Lamprecht, H.-O. Uferschutz mit Betonfertigteilen
		Bischofsberger, W. Wupperdurchstich und Wasserkraftanlage des Klärwerks Wuppertal-Buchenhofen
		Passlack, G. Durchführung von hydrologischen Messungen in der Natur
		Simons, H. Zur Gestaltung abgesenkter Unterwassertunnel
		Krolewski, H. Der Verbau von Abflußquerschnitten. (Eine Betrachtung zur Bemessung von Wehr- und Brückenweiten)
		Gutsche, H.-K. Steuerungsmöglichkeiten bei der Nachbildung wellenerzeugter Sandwan-derungsvorgänge in hydraulischen Modellen des See- und Seehafenbaues
		Führböter, A. Elektrische Geber für elektronische Meßgeräte im wasserbaulichen Versuch-swesen
		Janssen, W. Einige Untersuchungen für die Energieumwandlung an den Auslässen von Kühl- und Triebwasserleitungen sowie an Hochwasserentlastungsanlagen
		Schwarze, H. Modellversuche zur Ermittlung der Einflüsse von baulichen Maßnahmen im Tidegebiet auf die Tide
		Dursthoff, W. Hydrografische und hydrologische Außenarbeiten des Franzius-Instituts
Burkhardt, O. Die studentischen Auslandsexkursionen des Lehrstuhls für Grund- und Wasserbau der Technischen Hochschule Hannover von 1952 bis 1965		
26	1966	Laucht, H. Generalplan für einen Freihafen in Malta
		Aujeszky, L., Kontur, G. Das Problem der künstlichen Niederschlagserzeugung
		Nendza, H. Einflüsse auf die Tragfähigkeit von Zugpfählen mit Fußverbreiterung im Sand-boden
		Rudavsky, A.-B. Energievernichter und Energieverzehrungsmethoden unter Überfall-wehren

Continued on next page

Continued from previous page

Issue	Year	Author and Title
25	1965	Winter, H. Beitrag zur Berechnung der Grundwasserentspannung im Tidegebiet Brösskamp, H. Naßbaggerei und Bodentechnik. Abhängigkeit der Arbeitsvorgänge im Naßbaggerbereich vom Boden. Vorschläge für ein Versuchsprogramm zur Ermittlung fehlender Bodenprüfverfahren Franzius, L. Wirkung und Wirtschaftlichkeit von Rauheckwerken im Hinblick auf den Wellenauflauf
24	1964	Aksoy, S. Über den Kornwiderstand bei offenen Wasserläufen mit beweglicher Sohle Fekete, G. Vergleich verschiedener Binnenwasserstraßen auf Grund der möglichen Tragfähigkeitsausnutzung (TN-Faktor, TK-Faktor) Domzig, H. Schildvortriebsverfahren (Beitrag zum Ausbau der Tunnel) Führböter, A. Modellversuche für das Sturmflutsperrwerk Billwerder Bucht/Hamburg. Untersuchungen über die hydraulischen Belastungen von Toren verschiedener Art Wagner, H. Der moderne Tunnelbau im Schildvortrieb. Bericht über die wissenschaftliche Bearbeitung der Untergrundbahnbauten unter der Innenstadt von Hamburg
23	1963	Löwenberg, H. Einbau, Verdichtung und Verdichtungsprüfung von Sand beim Spülverfahren im Straßenbau Dettmers, D. Folgerungen aus den Versuchen über die Förderung von Sand-Wasser-Gemischen in Rohrleitungen Rogge, T. Über den Bau von Fähranlagen für den rollenden Verkehr Laucht, H. Von den Eigenschaften des Eises
22	1963	Engel, H. Über die Landgewinnung im Wattengebiet Kontur, G. Über die Lagerung hydraulisch geförderter Kohlenstaub-Asche von Kraftwerken Ströhmer, P. Die Abflußkennwerte für die Unterweser und ihre Veränderungen seit 1890. (Ein Beitrag zur Frage der Tidewellenberechnungen.) Aksoy, S. Modellversuche für das Einlaufbauwerk im St.P.s-River/Liberia Hensen, W., Burkhardt, O. Modellversuche für die Aller zwischen Ahlden und Westen
21	1962	Hensen, W. Modellversuche für den Vorhafen der Nordschleuse in Bremerhaven Hensen, W., Dursthoff, W. Modellversuche für die Ausbildung von Saugkrümmern des Kraftwerkes Westfalen der Vereinigten Elektrizitätswerke Westfalen A.G. in Dortmund Hensen, W., Führböter, A. Modellversuche über den Wellenauflauf an den Elbdeichen bei Finkenwerder
20	1961	Hensen, W., Passlack, G. Modellversuche für das Emdener Fahrwasser Gutsche, H.-K. Über den Einfluß von Strandbuhnen auf die Sandwanderung an Flachküsten
19	1961	Freiherr Schenk zu Schweinsberg, W.-R. Beitrag zur Beschreibung des Baugrundverhaltens beim Druckluftvortrieb Weissenbach, A. Der Erdwiderstand vor schmalen Druckflächen
18	1960	Rose, D. Über die quantitative Ermittlung der Gezeiten und Gezeitenströme in Flachwassergebieten mit dem Differenzenverfahren Hensen, W., Schiemenz, F. Eine Fischtreppe in Stromlinienformen. Versuche mit lebenden Fischen und Modellversuche Hensen, W. Das Aufnahmevermögen von Sanden für Mineralölprodukte Hensen, W. Untersuchung der LÜDERSschen Sandfalle Hensen, W., Wittmer, H.-G. Modellversuche für die Abdämmung der Wellier Weserschleife (Staustufe Landesbergen)

Continued on next page

Continued from previous page

Issue	Year	Author and Title
		Hensen, W. Ein einfaches Tide-Steuergerät
		Hensen, W. Über Rauigkeit und Ungleichförmigkeit
17	1960	Dahme, H. Die Sicherung der Nachtschiffahrt auf Binnenschiffahrtsstraßen
		Dillo, H.-G. Sandwanderung in Tideflüssen
		Führböter, A. Einige elektrische Meßverfahren im wasserbaulichen Versuchswesen
		David, K. Die Tragfähigkeit von Ramppfählen im Sandboden. Ein Beitrag zur Ermittlung der Pfahllasten nach erdstatischen Methoden
		Hensen, W. Auswirkung langperiodischer Wellen in Häfen
16	1959	Passlack, G. Über die Berechnung unvollkommener Überfälle bei Sohlenstufen
		Davoudzadeh, E. Beitrag zur Filterausbildung bei der Entwässerung von Feinböden
		Schnoor, E. Leitfaden für das Kubizierungsverfahren
		Krolewski, H. Über das Verhalten von Mineralöl im Boden
		Stehr, E. Berechnungsgrundlagen für Preßluft-Ölsperren
15	1959	Hensen, W. Modellversuche für die Unterweser und ihre Nebenflüsse
		Hensen, W. Modellversuche für die Unterweser und ihre Nebenflüsse
14	1958	Brandenburg, C. Über die Verdichtungsprüfung von Schüttungen aus gleichförmigen Sanden
		Blinde, A. Stufenweiser Ausbau von Klärteichdämmen unter Nutzung des Klärgutes
		Klein, H.-A. Ermittlung des Durchflusses aus Strömungsmessungen im Tidegebiet
		Magens, C. Seegang und Brandung als Grundlage für Planung und Entwurf im Seebau und Küstenschutz
13	1958	Wittmer, H.-G. Tideänderungen durch Einbauten in Tideflüssen
		Führböter, A. Modellversuche für Talsperren-Tiefschütze
		Krabbe, W. Über die Schrumpfung bindiger Böden
12	1957	Zitscher, F.-F. Möglichkeiten und Grenzen in der konstruktiven Anwendung von Asphaltbauweisen bei Küstenschutzwerken
11	1957	Simons, H. Über die Gestaltung von Schiffshebewerken
		Wagner, H. Die Luft-Durchlässigkeit wasserhaltiger Böden - Ein Beitrag zum Untertunnelbau im Druckluftverfahren -
		Griesseier, H., Vollbrecht, K. Zur Problematik der modellmäßigen Darstellung litoraler Prozesse
		Dettmers, D. Ablagerungen in Druckrohrleitungen bei hydraulischer Förderung im Naßbaggerbetrieb
		Friedrich, W., Horst, H. FISCHERs Verfahren zur Aufschlüsselung des regionalen Wasserhaushaltes im Lichte neueren Wissens. Ein Beitrag zur Klärung des Wasserhaushaltsproblems
		Natermann, E. Abschließende Stellungnahme des Verfassers
10	1957	Powell, W. Gebrauch und Mißbrauch von wasserbaulichen Modellen
		Möller-Hartmann, W. Abfluß in offenen Dreiecksgerinnen
		Hensen, W. Modellversuche über den Strandabbruch an den Enden von befestigten Küstenstrecken - Lee-Erosion -
		Menze, G. Über die Tragfähigkeit von Ramppfählen unter Berücksichtigung des Kräfteverlaufes beim Rammen

Continued on next page

Continued from previous page

Issue	Year	Author and Title
9	1956	Hensen, W. Erprobungen von pneumatischen Wellenbrechern im Modell und in der Natur
		Laucht, H. Zustand und Entwicklungsmöglichkeiten des Hamburger Stromspaltungsgebietes der Elbe
		Natermann, E. FISCHERs Verfahren zur Aufschlüsselung des regionalen Wasserhaushaltes im Lichte neueren Wissens
		Simons, H. Bodenmechanische Untersuchungen an den Emsdeichen zwischen Papenburg und Leer
		Hensen, W. Zweite Zusammenstellung der wasserbaulichen Modellversuche, die in der Hannoverschen Versuchsanstalt für Grundbau und Wasserbau, Franzius-Institut der Technischen Hochschule Hannover, durchgeführt worden sind
		Hensen, W. Mitgliederverzeichnis der Gesellschaft der Förderer des Franzius-Instituts e.V. nach dem Stande vom 1.11.1956
8	1955	Schiemann, E. Bericht über die Auslands-Exkursion des Lehrstuhls für Grundbau und Wasserbau der Technischen Hochschule Hannover im Sommer 1956
		Domzig, H. Wellendruck und druckerzeugender Seegang
7	1955	Lamprecht, H.-O. Brandung und Uferveränderungen an der Westküste von Sylt
		Walther, H.-D. Modellversuche für die neue Westmole Helgoland
		Vogl, K.-J. Gründungen in schrumpf- und schwellfähigen Böden
		Giese, H. Über den räumlichen Erdwiderstand
6	1954	Jagau, H. Beitrag zur erdstatischen Berechnung des Fußwiderstandes von Pfählen
		Hensen, W. Modellversuche zur Bestimmung des Einflusses der Form eines Seedeiches auf die Höhe des Wellenauflaufes
		Hensen, W. Modellversuche mit pneumatischen Wellenbrechern
		Hensen, W. Modellversuche für die untere Ems (Text)
		Hensen, W. Modellversuche für die untere Ems (Abbildungen)
5	1954	Hensen, W. Sondermodellversuche für die untere Ems
		Müller, F.-E. Stahlrammpfähle Für Dalbenbau. Ergebnisse Von Großversuchen Im Nord-Ostsee-Kanal Bei Flemhude 1951
		Wiegmann, D. Der Erddruck Auf Verankerte Stahlspundwände, Ermittelt Auf Grund Von Verformungsmessungen Am Bauwerk
4	1953	Menze, G. Probelastungen An Fertigbetonpfählen Und Stahlpfählen
		Hensen, W. Modellversuche Über Den Wellenauflauf An Seedeichen Im Wattengebiet
		Jarlan, G. Der Hafen von Le Havre
		Jarlan, G. Die Ausbildung des Ingenieurs in Frankreich
		Dettmers, D. Beitrag zur Frage der Belüftung von Tiefschützen
3	1953	Helm, K., Möckel, W., Wöltinger, O. Über die gegenseitige Beeinflussung von Schiffen und Kanälen
		Hensen, W. Modellversuche für den Amerika-Hafen in Cuxhaven
		Iribarren, R. Beim Brechen von Wellen unvermutet auftretende heftige Drücke
		Boos, W. Die Messung kleiner Strömungsgeschwindigkeiten im wasserbaulichen Versuchswesen
		Hensen, W. Das Eindringen von Salzwasser in die Gezeitenflüsse und ihre Nebenflüsse, in Seekanäle und in Häfen

Continued on next page

Continued from previous page

Issue	Year	Author and Title
		Steinfeld, K. Über den räumlichen Erdwiderstand
		Petermann, H. Die innere Verformung als Festigkeitsmerkmal von Sand
		Hensen, W. Mitgliederverzeichnis der Gesellschaft der Förderer des Franzius-Instituts e.V. nach dem Stande vom 1.1.1953
2	1952	Seifert, R. Maßstäbe der Modellähnlichkeit grundrißgetreuer Gerinne bei Tiefenverzerrung und Gefällverstärkung
		Hensen, W. Untersuchungen der Standfestigkeit von Rohrfestpunkten
		Schiemenz, F. Versuche mit Glasaalen. Beitrag zur Frage des Hineinleitens wandernder Fische in die untere Mündung einer Fischtreppe
		Hansen, W. Beobachtungen des Windstaus und Triftstroms im Modellkanal
		Natermann, E. Die Entschleierung der Grundwasserganglinie
		Schulz, H. Probleme der gewässerkundlichen Meßtechnik
		Helm, K., Moeckel, W. Einfluß des Wasserquerschnittes von Kanalprofilen auf Absenkung, Vertrimmung und Steuereigenschaften eines großen Tankschiffes
		Hensen, W. Kleine Studien aus dem Tidegebiet Nr. 1: Über die Fortschrittsgeschwindigkeit der Tidewelle in einem Flusse
		Hensen, W. Zusammenstellung der wasserbaulichen Modellversuche, die in der Hannoverschen Versuchsanstalt für Grundbau und Wasserbau, Franzius-Institut der Technischen Hochschule Hannover, seit dem 1. April 1948 durchgeführt worden sind
		Simons, K. Bericht über die Auslands-Exkursion des Lehrstuhls für Grundbau und Wasserbau an der Technischen Hochschule Hannover im Frühjahr 1952
		Hensen, W. Gedanken und Anregungen zu studentischen Exkursionen
1	1952	Streck, A. Die Bewertung des Bodens als Baugrund und Baustoff
		Graupner, A. Die Baugrundkarte von Hildesheim als Beispiel einer Baugrundkartierung
		Steinfeld, K. Über Theorie und Praxis elektroosmotischer Bodenentwässerung
		Schmidbauer, J. Die Fließsand- und Schwimmsanderscheinung
		Paproth, E. Neuere Druckluftgründungen
		Streck, A. Die erdstatische Berechnung der Tragfähigkeit von Pfählen
		Förster, K. Bodenmechanische Erfahrungen bei den Kriegsschäden im Hamburger Hafen
		Petermann, H. Auszug aus dem Vortrag 'Baugrundfragen des Straßenbaues'
		Sichardt, W. Überblick über die Wasserhaltungsverfahren (Anwendungsmöglichkeiten und -grenzen, Fortschritte, Aussichten)
		Schmidbauer, J. Bemessung von Straßen- und Flugplatzdecken
		Streck, A. Aktuelle Fragen des Deichbaues im Bergbauggebiet
		Tübbesing, K. Über die hydrologische Baugrundkarte von Hannover

ISSN 0340-0077

Herausgeber

Leibniz Universität Hannover

Franzius-Institut für Wasserbau und Küsteningenieurwesen

Nienburger Str. 4, 30167 Hannover

Prof. Dr.-Ing. habil. T. Schlurmann

www.fi.uni-hannover.de